TECHNICAL UNIVERSITY OF MUNICH
Department of Informatics

FROM UNDERACTUATION TO QUASI-FULL ACTUATION

A Unifying Control Framework for
Rigid and Elastic Joint Robots

Manuel Keppler

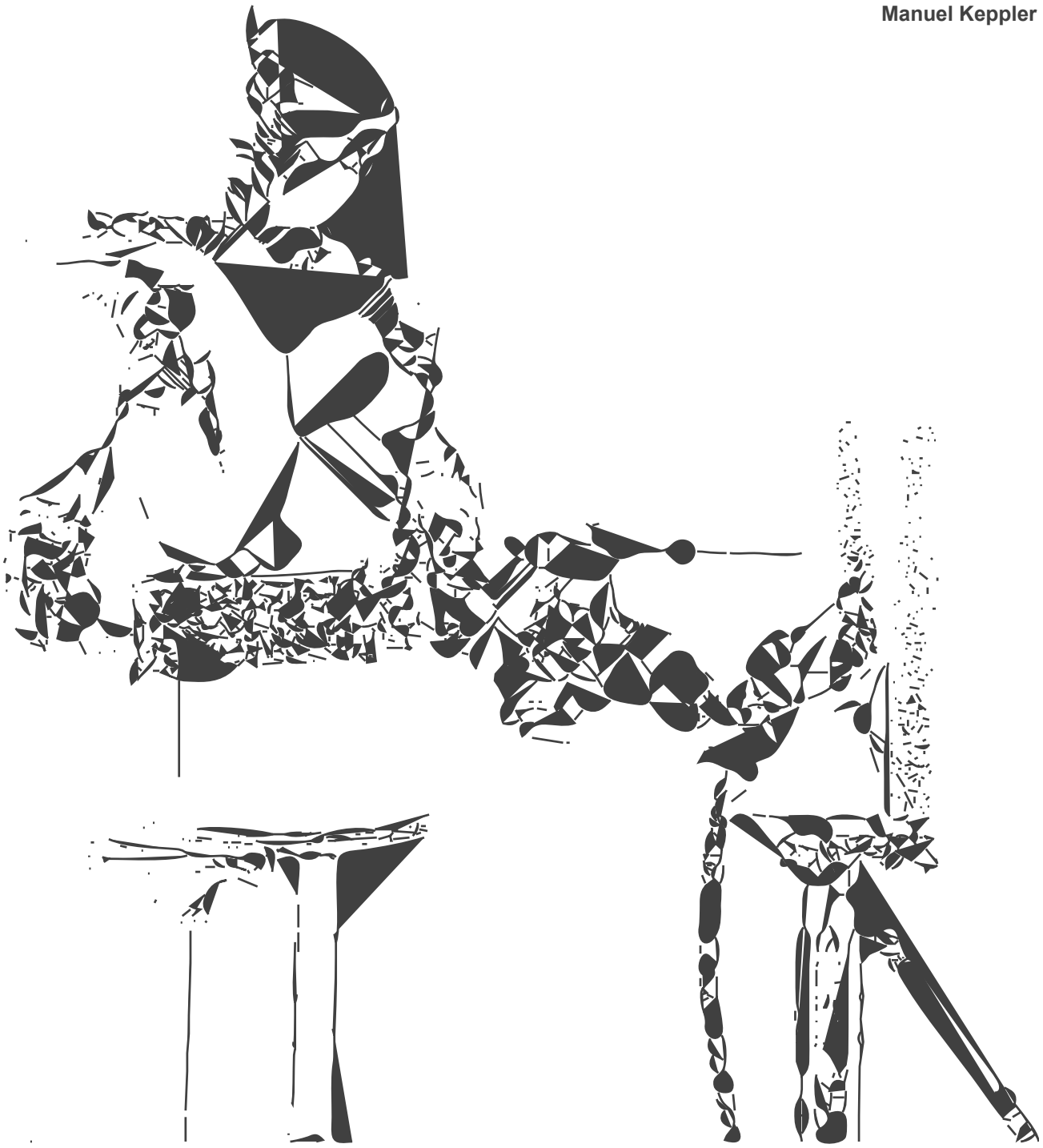

Technische Universität München
TUM School of Computation, Information and Technology

FROM UNDERACTUATION TO QUASI-FULL ACTUATION

A Unifying Control Framework for
Rigid and Elastic Joint Robots

Manuel Keppler

Vollständiger Abdruck der von der TUM School of Computation, Information and Technology der Technischen Universität München zur Erlangung des akademischen Grades eines

Doktors der Ingenieurwissenschaften (Dr.-Ing.)

genehmigten Dissertation.

Vorsitz: Prof. Dr.-Ing. Matthias Althoff

Prüfer*innen der Dissertation: 1. Prof. Dr.-Ing. Alin Albu-Schäffer
2. Prof. Dr. Alessandro De Luca

Die Dissertation wurde am 06.07.2022 bei der Technischen Universität München eingereicht und durch die TUM School of Computation, Information and Technology am 08.02.2023 angenommen.

It is by logic that we prove,
but by intuition that we discover.

– Henri Poincaré

Acknowledgments

This work is based on research conducted at the *Institute of Robotics and Mechatronics* of the *German Aerospace Center* (DLR).

First and foremost, I would like to express my deep and sincere gratitude to Prof. Alin Alin Albu-Schäffer and Dr. Christian Ott for giving me the opportunity to engage in research on robotics and control, and providing valuable guidance throughout that time. I cannot thank them enough for giving me the freedom to choose the theoretical fields of my interest and supporting me to pursue my goals. The experimental part of this thesis would not have been possible without the amazing hardware designed by the Mechatronic Systems department lead by Dr. Markus Grebenstein.

I would like to pay my special regard to Prof. Alessandro De Luca. During my research stay at the *Department of Computer, Control and Management Engineering* (DIAG) at the *Sapienza University* of Rome, his passion and deep knowledge of control theory has been a great source of inspiration. Further, I would like to thank Prof. Leonardo Lanari, Prof. Giuseppe Oriolo, Dr. Claudio Gaz, Dr. Valerio Modugno and Marco Ferro who all contributed to make this stay a fantastic and enriching time.

The past years at the DLR were a wonderful opportunity for me to engage in interesting discussions with many people from very different fields of robotics. I particularly would like to thank Dr. Dominic Lakatos for our exciting discussions on mathematics and control. Moreover, I'm grateful for his advice during my initial years at the DLR. My special thanks goes to Florian Loeffl for his valuable criticism and our fruitful discussions on mechanics and robot design. I would also like to thank all my co-authors for their contributions.

Many thanks go to Dr. Maxim Chalon and Dr. Martin Pfanne for setting up and maintaining the software/computer infrastructure of the anthropomorphic soft robot *David*. At last, I would like to thank everyone involved in the development of this inspiring robot, such as Dr. Markus Grebenstein, Prof. Alin Albu-Schäffer, Thomas Bahls, Dr. Maxime Chalon, Oliver Eiberger, Werner Friedl, Robin Gruber, Prof. Sami Haddadin, Prof. Hannes Höppner, Sebastian Wolf, Dr. Florian Petit, Tilo Wüsthoff, Jens Reinecke, Dr. Bastian Deutschmann, Prof. Gerd Hirzinger.

Some of the research activities associated with this dissertation have been funded by *European Research Council* (ERC) under the European Union's *Horizon 2020* research and innovation programme (grant agreement No. 819358). My research stay in Rome was supported by a *TUM-GS Internationalization Grant*.

Munich, June, 2022 *Manuel Keppler*

Abstract

The quest for animal-like performance in robots has driven the integration of elastic elements in their drive trains, sparking a revolution in robot design. Elastic robots can store and release potential energy, providing distinct advantages over traditional robots, such as enhanced safety in human-robot interaction, resilience to mechanical shocks, improved energy efficiency in cyclic tasks, and dynamic motion capabilities. Exploiting their full potential, however, necessitates novel control methods. This thesis advances the field of nonlinear control for underactuated systems and utilizes the results to push the boundaries of motion and interaction performance of elastic robots. Through real-life experiments and applications, the proposed controllers demonstrate that compliant robots hold promise as groundbreaking robotic technology.

To achieve these objectives, we first derive a simultaneous phase space and input transformation that enables a specific class of underactuated Lagrangian systems to be treated as if fully actuated. These systems can be represented as the interconnection of actuated and underactuated subsystems, with the kinetic energy of each subsystem depending only on its own velocity. Elastic robots are typical representatives. We refer to the transformed system as quasi-fully actuated due to weak constraints on the new inputs. Fundamental aspects of the transforming equations are 1) the same Lagrangian function characterizes both the original and transformed systems, 2) the transformed system establishes a passive mapping between inputs and outputs, and 3) the solutions of both systems are in a one-to-one correspondence, describing the same physical reality. This correspondence allows us to study and control the behavior of the quasi-fully actuated system instead of the underactuated one. Thus, this approach unifies the control design for rigid and elastic joint robots, enabling the direct application of control results inherited from the fully-actuated case while ensuring closed-loop system stability and passivity. Unlike existing methods, the quasi-full actuation concept does not rely on inner control loops or the neglect and cancellation of dynamics. Notably, as joint stiffness values approach infinity, the control equivalent of a rigid robot is recovered.

Building upon the quasi-full actuation concept, we extend energy-based control schemes such as energy shaping and damping injection, Euler-Lagrange controllers, and impedance control. Moreover, we introduce Elastic Structure Preserving (ESP) control, a passivity-based control scheme designed for robots with elastic or viscoelastic joints, guided by the principle of "do as little as possible". The underlying hope is that reducing the system shaping, i.e., having a closed-loop dynamics match in some way the robot's intrinsic structure, will award high performance with little control effort. By minimizing the system shaping, we obtain low-gain designs, which are favorable concerning robustness and facilitate the emergence of natural motions. A comparison with state-of-the-art controllers highlights the minimalistic nature of ESP control. Additionally, we present a synthesis method, based on purely geometric arguments, for achieving time-optimal rest-to-rest motions of an elastic joint with bounded input.

Finally, we showcase the remarkable performance and robustness of the proposed ESP controllers on DLR David, an anthropomorphic robot implemented with variable impedance actuators. Experimental evidence reveals that ESP designs enable safe and compliant interaction with the environment and rigid-robot-level accuracy in free motion. Additionally, we introduce a control framework that allows DLR David to perform commercially relevant tasks, such as pick and place, teleoperation, hammer drilling into a concrete block, and unloading a dishwasher. The successful execution of these tasks provides compelling evidence that compliant robots have a promising future in commercial applications.

Contents

List of Theorems, Propositions, Corollaries

Acronyms

ASR	Articulated Soft Robot.
BAVS	Bidirectional antagonistic variable stiffness.
DLR	Deutsches Zentrum für Luft- und Raumfahrt (German Aerospace Center).
DOF	Degrees of freedom.
EL	Euler-Lagrange.
ESP	Elastic structure preservation/elastic structure preserving.
ESPi	Elastic structure preserving impedance.
FJR	Flexible joint robot.
FSJ	Floating spring joint.
GAS	Global asymptotic stability.
HRI	Human-robot interaction.
ICT	Input and coordinate transformation.
OSP	Output strict passivity.
PBC	Passivity-based control.
QFA	Quasi-Full Actuation/Quasi-Fully Actuated.
RR	Rigid robot.
SEA	Series elastic actuator.
TCP	Tool center point.
VIA	Variable impedance actuator.

List of Symbols

C^∞	The space of (smooth) functions for which all orders of derivatives are continuous.
C^k	The space of k-times continuously differentiable functions.
$D\boldsymbol{f}$	Jacobian matrix of $\boldsymbol{f}$.
δ_{ij}.	Kronecker delta
$\partial_{\boldsymbol{q}}\mathcal{V}$	Partial derivative of $\mathcal{V}$ with respect to $\boldsymbol{q}$.
$\mathcal{H}$	Hamiltonian function (defined by the Legendre transform of the associated Lagrangian).
$\mathcal{T}$	Kinetic energy function.
$\mathcal{L}$	Lagrangian function.
n	Number of degrees of freedom.
n_a	Number of degrees of freedom of the actuated subsystem.
n_u	Number of degrees of freedom of the unactuated subsystem.
$\boldsymbol{\psi}$	Subsystem coupling signal.
ψ_i	ith component of the subsystem coupling signal.
q_i	ith generalized coordinate.
$\boldsymbol{q}$	Set of generalized coordinates $(q_1, \dots, q_n)$.
$\boldsymbol{q}_a$	Set of actuated generalized coordinates $(q_{a1}, \dots, q_{an_a})$.
$\boldsymbol{q}_u$	Set of unactuated generalized coordinates $(q_{u1}, \dots, q_{un_u})$.
$\bar{q}_i$	ith virtual generalized coordinates.
$\bar{\boldsymbol{q}}$	Set of virtual generalized coordinates $(\bar{q}_1, \dots, \bar{q}_n)$.
$\bar{\boldsymbol{q}}_a$	Set of virtual generalized coordinates of the actuated subsystem.
$\bar{\boldsymbol{q}}_u$	Set of virtual generalized coordinates of the unactuated subsystem.
Σ	An Euler-Lagrange system.
Σ_a	Actuated subsystem of Σ.
Σ_u	Unactuated subsystem of Σ.
$\bar{\Sigma}$	Quasi-fully actuated representation of Σ.
$\bar{\Sigma}_a$	Actuated subsystem of $\bar{\Sigma}$.
$\bar{\Sigma}_u$	Unactuated subsystem of $\bar{\Sigma}$.
$\mathcal{V}$	Potential energy function.
$\mathcal{V}_e$	Elastic potential energy function.
$\mathcal{V}_g$	Gravitational potential energy function.
x_i	ith transformed generalized coordinate.
$\boldsymbol{x}$	Set of transformed generalized coordinates.

PROLOGUE

1 Introduction

A Brief History of Compliant Robots

The word "robot" was first used in 1920 in the science fiction play R.U.R. (Rossum's Universal Robots) by the Czech writer Karel Čapek about artificial men—designed to perform unpleasant work—that rebel against their human masters. Robots left fiction and emerged as a tool for production and manufacturing in an industrial environment in the early 1960s. An entire industry was spawned. Initially, these machines were bulky, heavy, and posed a potential risk to the human workforce and, thus, were usually fenced or placed in isolation from humans. Over the last decades, we have seen significant advances in the field of robotics and an ever-increasing surge of its economic potential. With technological advancements and robots becoming more intelligent, new fields of application arise and become economically viable that go beyond the idea of having robots just performing unpleasant tasks. Nowadays, robots are used in many fields, from heavy-duty robots working on assembly lines to lightweight robots in a medical environment and to large-scale manipulators in space. Until recently, a common line of thought in the design phase of robots has been that structural flexibility is to be considered a parasitic effect that must be avoided since it introduces unwanted oscillatory dynamics into the system. However, it was clear that human-friendly robots had to look very different than industrial robots. For a robot that interacts with a human the most critical design concern is safety. Positioning accuracy and speed in task execution come in second. The growing interest in application fields such as service robotics, health care and space robotics sparked the development of a new generation of robots: lightweight manipulators with a load to weight ratio comparable to that of human arms [6]. Such manipulators are required to perform compliant interactions when in contact with an unknown environment while guaranteeing safe interaction with humans [3, 184]. Popular representatives are: LWR III by DLR [66], WAM® Arm by Barrett Technology and MIT, LBR iiwa by KUKA.

[6]: Albu-Schäffer et al. (2007), "A Unified Passivity-based control framework for position, torque and impedance control of flexible joint robots"

[3]: Alami et al. (2006), "Safe and dependable physical human-robot interaction in anthropic domains: State of the art and challenges"

[184]: Tonietti et al. (2005), "Design and control of a variable stiffness actuator for safe and fast physical Human/Robot interaction"

[66]: Hirzinger et al. (2002), "DLR's torque-controlled light weight robot III-are we reaching the technological limits now?"

A major challenge inherent to the control design for a lightweight robot is the flexibility introduced into robot joints. Consequently, the system is underactuated since the number of degrees of freedom is twice the number of actuators, and the matching property between control actions and outputs is lost (noncollocation problem). The situation became worse with the advent of robots with *series elastic actuators* (SEA) [153]; or *variable impedance actuators* (VIA) [190]. In these robots, one deliberately incorporates highly compliant elements into the drive train with a stiffness low enough to exploit these elements as energy storage. This radical paradigm shift in robot design fundamentally increases the mechanical robustness of a robot since the elastic elements low-pass filter impact forces and thereby protect the drive trains. To emphasize this point, let us imagine a rigid joint robot that collides at high speeds with a stiff object. In such a scenario, the impact induces energy too fast for an active controller to prevent damage to the robot's structure and drive trains [54]. Systems with sufficient joint compliance, on the other hand, guarantee enough reaction time to avoid structural damage. Some systems are

[153]: Pratt et al. (1995), "Series elastic actuators"

[190]: Vanderborght et al. (2013), "Variable impedance actuators: A review"

[54]: Grebenstein et al. (2011), "The DLR hand arm system"

even designed to be passively safe—requiring no impact reaction strategies at all. Throughout this work, these kinds of systems are referred to as *articulated soft robots* (ASRs). Some popular representatives of this class are: Waseda Wendy [121] and its successor TwendyOne [78], the anthropomorphic upper body DLR *David* [54], the manipulators ANYpulator [16], Festo BionicSoftArm, the legged systems COMAN [122], ANYmal [74], Robonaut 2 [38], Salto-1P [58].

[121]: Morita et al. (1999), "Development of human symbiotic robot: WENDY"

[78]: Iwata et al. (2009), "Design of human symbiotic robot TWENDY-ONE"

[54]: Grebenstein et al. (2011), "The DLR hand arm system"

[16]: Bodie et al. (2016), "ANYpulator: Design and control of a safe robotic arm"

[122]: Moro et al. (2011), "A human-like walking for the COmpliant huMANoid COMAN based on CoM trajectory reconstruction from kinematic Motion Primitives"

[74]: Hutter et al. (2016), "Anymal-a highly mobile and dynamic quadrupedal robot"

[38]: Diftler et al. (2011), "Robonaut 2 - The first humanoid robot in space"

[58]: Haldane et al. (2017), "Repetitive extreme-acceleration (14-g) spatial jumping with Salto-1P"

Soft robots (SRs) and the subclass of ASRs represent one of the most significant evolutions in robotics in recent times. The growing interest in SRs arises from the unique advantages offered compared to rigidly built robots. Based on rigid mechanisms, traditional industrial robots are fast and precise machines that excel at producing manufactured goods at an incredible throughput. Soft robots cannot compete in this field. The development of SRs instead aims at designing robots destined for safe *human-robot interaction* (HRI) while simultaneously aiming for motion and robustness capabilities matching biological systems. In summary, the key motivations driving the development of ASRs are: safety concerning HRI, mechanical robustness against harsh impacts in unpredictable environments, enhanced dynamic performance and energy efficiency in cyclic tasks, dedicated force/torque sensors become superfluous.

New Technologies bring new Challenges

Naturally, a paradigm shift in technology introduces new challenges. The introduction of a compliant physical structure enables the embodiment of safe and natural behaviors into a robotic system. There is, however, no free lunch.

Compared to rigid robots, we can expect the following drawbacks: (1) the mechanical bandwidth is reduced, (2) higher system complexity, (3) full-state feedback requires additional sensors[1], (4) an increased number of motors, gearboxes, bearings etc. is required in the case of VIA-based systems, (5) achieving good motion tracking accuracy is challenging, (6) the underactuated nature and intrinsic oscillatory dynamics necessitate advanced control concepts. While points (1) to (4) are limitations imposed by physics or the nature of an ASR, issues (5) to (6) can actually be resolved by good control engineering.

1: A compliant joint requires at least two position sensors. A VIA requires usually three position sensors.

The challenges associated with underactuation and unwanted vibrations arising from parasitic elasticities had to be faced already with the advent of lightweight robots. The high interest of the robotics and control community in such systems triggered the development of new control concepts. Spong [170] and Ozgoli [143] provide excellent overviews of the advances in this field. It is, however, important to understand that the challenges concerning the control of ASRs are quite different in some aspects compared to lightweight robots. The joint stiffness of ASRs is lower compared to lightweight robots by more than one magnitude. To put things into perspective, the joint stiffness of a classical industrial robot is around $1 \times 10^6\,\mathrm{N\,m\,rad^{-1}}$ [9, 40]. In a LWR III the mechanical flexibility originates predominantly from the harmonic drive gearboxes and the force/torque sensors resulting in joint stiffness values around 1×10^4 to $2 \times 10^4\,\mathrm{N\,m\,rad^{-1}}$. The most powerful VIAs in DLR *David*'s arms have stiffness range from 50 to $850\,\mathrm{N\,m\,rad^{-1}}$ [194]. Distal joints located in

[170]: Spong (1990), "Control of flexible joint robots: A survey"

[143]: Ozgoli et al. (2006), "A survey on the control of flexible joint robots"

[9]: Alici et al. (2005), "Enhanced stiffness modeling, identification and characterization for robot manipulators"

[40]: Dumas et al. (2011), "Joint stiffness identification of six-revolute industrial serial robots"

[194]: Wolf et al. (2011), "The DLR FSJ: Energy based design of a variable stiffness joint"

the wrist and fingers feature even lower joint stiffness values in the range of 0.5 to 125 $\mathrm{N\,m\,rad^{-1}}$ [47] and 0.3 to 17 $\mathrm{N\,m\,rad^{-1}}$ [46], respectively.

Control of Compliant Robots

Against the backdrop of an ever-increasing surge of the economical potential, the development of robot manipulators with challenging nonlinear dynamics has fueled research in nonlinear control theory. This renewed research led to the development of fundamental control concepts such as computed torque control [187], energy shaping control [178], impedance control [68], operational space control [97], *passivity-based control* (PBC) [6, 98, 144, 165]. It is worth noting that these control strategies were developed for manipulators whose dynamics are modeled by the rigid body equations of motion of open kinematic chains, and rely on the powerful controllability properties of a rigid robot. Further, the equations of motion for a *rigid robot* (RR) can be linearized and decoupled by static nonlinear state feedback (often called computed torque).

It turned out that strategies that assume a rigid model for the manipulator are limited in their performance on real robots since the assumption of perfect rigidity is never truly satisfied. Elasticity in the drive train results in weakly damped oscillatory modes, which impose bandwidth limitations on any control algorithms designed on the assumption of perfect rigidity [168] and may, in fact, cause stability issues for feedback controllers that neglect joint elasticity [177]. The joints experience the highest stress, and the resulting elastic deformation of the joints has a higher significance for control design than do the actual bending modes of the links, which can be of significantly higher frequency than the resonant modes of the joints [177]. This insight set the focus of the control community on *flexible joint robots* (FJRs) that are composed of a chain of rigid links interconnected by elastic joints.

Starting in the 1980s, many attempts have been made to address the aforementioned issues [143, 170]. For a general FJR model, the necessary and sufficient conditions for static feedback linearizability are not satisfied [23] and, thus, no direct analogue of computed torque [13] exists. De Luca [30, 31], however showed that FJR are linearizable by dynamic feedback. In an attempt to make the complexity of the highly nonlinear dynamic model of an elastic joint robot more tractable, Marino and Nicosia [110] exploited its two-time scale property. It turned out that this property allows a reformulation of the dynamic model as a *singularly perturbed* system, where the rigid-body dynamics constitutes the "slow" dynamics and the torque dynamics the "fast" dynamics. Several researchers used the singular perturbation formulation together with composite feedback control [43, 50, 110, 162]. The theoretical justification arises from Tychonov's theorem [95]. However, it is important to understand that the two-time-scale argument is based on the vague assumption that the joint stiffness values are "very large" [110]. Clearly, in the case of ASRs, this assumption is expected to be infringed.

In 1987, Spong [168] introduced the highly influential *reduced model* of a FJR. Throughout this work, the model proposed in [168] will also be referred to as the *Spong model*. It assumes that the angular part of the kinetic energy of each rotor is mainly due to its own rotation and, thus, neglects gyroscopic terms. A structural property of the Spong model that is highly relevant for control purposes is decomposability into the feedback interconnection of two passive

[47]: Friedl et al. (2011), "Wrist and forearm rotation of the DLR hand arm system: Mechanical design, shape analysis and experimental validation"

[46]: Friedl et al. (2011), "FAS A flexible antagonistic spring element for a high performance over"

[187]: Uebel et al. (1992), "Improved computed torque control for industrial robots"

[178]: Takegaki et al. (1981), "A new feedback method for dynamic control of manipulators"

[68]: Hogan (1985), "Impedance control: An approach to manipulation: Part I—Theory"

[97]: Khatib (1987), "A unified approach for motion and force control of robot manipulators: The operational space formulation"

[6]: Albu-Schäffer et al. (2007), "A Unified Passivity-based control framework for position, torque and impedance control of flexible joint robots"

[98]: Koditschek (1984), "Natural motion for robot arms"

[144]: Paden et al. (1988), "Globally asymptotically stable "PD+" controller for robot manipulators"

[165]: Slotine et al. (1988), "Adaptive manipulator control: A case study"

[168]: Spong (1987), "Modeling and control of elastic joint robots"

[177]: Sweet et al. (1984), "Re-definition of the robot motion control problem: Effects of plant dynamics, drive system constraints, and user requirements"

[143]: Ozgoli et al. (2006), "A survey on the control of flexible joint robots"

[170]: Spong (1990), "Control of flexible joint robots: A survey"

[23]: Cesareo et al. (1984), "On the controllability properties of elastic robots"

[13]: Bejczy (1974), *Robot arm dynamics and control*

[30]: De Luca et al. (1995), "Robots with elastic joints are linearizable via dynamic feedback"

[31]: De Luca et al. (1998), "A general algorithm for dynamic feedback linearization of robots with elastic joints"

[110]: Marino et al. (1985), "Singular perturbation techniques in the adaptive control of elastic robots"

[43]: Ficola et al. (1983), "A singular perturbation approach to the control of elastic robots"

[50]: Ghorbel et al. (2000), "Integral manifolds of singularly perturbed Systems with application to rigid-link flexible-joint multibody systems"

[110]: Marino et al. (1985), "Singular perturbation techniques in the adaptive control of elastic robots"

[162]: Siciliano et al. (1988), "A singular perturbation approach to control of lightweight flexible manipulators"

[95]: Khalil (2001), *Nonlinear Systems*

subsystems that represent the rigid body and actuator dynamics. This property is crucial for the developments presented in this work and discussed in detail in Chapter 5. In instances where the joint flexibility is caused by parasitic effects like the gear elasticity or the compliance of a joint torque sensor, the joint stiffness is usually relatively high, and thus the rigid body part gives a good approximation of the dominating dynamics. Consequently, several control approaches for FJRs started with a control law for the rigid body dynamics and used it as the desired torque to be controlled with the elastic actuator dynamics [107, 139]. Inverse dynamics-based control [31] instead allows designing a controller directly for the full flexible robot model without designing first a rigid body controller in an intermediate step. In both cases, the closed-loop system can be rendered stable but will have a significantly different structure than the original open-loop behavior. The works [6, 32, 33, 140] started the development of passivity-based control approaches for elastic joint robots that aim at preserving the intrinsic compliant dynamics. Aiming at a compliance controller, the schemes in [6, 140] utilized a physical interpretation of joint torque feedback as the scaling of motor inertia and implemented the desired compliance on the motor side. While this showed good performance on robots with rather stiff joints, as the DLR light-weight robots [67], it turned out that vibration damping on the motor side in combination with joint torque feedback to scale the motor inertia was not sufficient for highly elastic robots. This observation motivated a series of control developments that culminated in the formulation of the *elastic structure-preserving* (ESP) [86] and *elastic structure-preserving impedance* (ESPi) control schemes [92], which use an idea that is similar to the one presented in [32, 33]. The latter two use the equivalence principle to derive control laws that combine cancellation of gravity effects with motor-side PD terms to achieve set-point regulation. It is interesting to note that using the developed concept of *quasi-full actuation* to cancel the effect of gravity on an ASR produces exactly the controllers reported in [32, 33].

[107]: Loria et al. (1995), "On tracking control of rigid and flexible joints robots"
[139]: Ott et al. (2003), "Decoupling based Cartesian impedance control of flexible joint robots"

[31]: De Luca et al. (1998), "A general algorithm for dynamic feedback linearization of robots with elastic joints"

[6]: Albu-Schäffer et al. (2007), "A Unified Passivity-based control framework for position, torque and impedance control of flexible joint robots"
[32]: De Luca et al. (2011), "A PD-type regulator with exact gravity cancellation for robots with flexible joints"
[33]: De Luca et al. (2010), "Dynamic gravity cancellation in robots with flexible transmissions"
[140]: Ott (2008), *Cartesian Impedance Control of Redundant and Flexible-Joint Robots*
[67]: Hirzinger et al. (2001), "On a new generation of torque controlled light-weight robots"
[86]: Keppler et al. (2018), "Elastic structure preserving (ESP) control for compliantly actuated robots"
[92]: Keppler et al. (2018), "Elastic structure preserving impedance (ESPi) control for compliantly actuated robots"

Goal of this Thesis

The objective of this work is twofold. On the one hand, it aims to advance the field of nonlinear control of underactuated systems, and on the other hand, it aims to demonstrate that ASRs can indeed be considered a viable alternative to classic rigid robots.

The dynamic control of underactuated systems is still an open problem in control. There are still very few general principles for the control of underactuated systems. The crux is that many exciting problems in robotics belong to this class (soft robots, object manipulation, aerial, aquatic, fossorial, and terrestrial locomotion). This work aims at developing a methodology that *unifies* the control design for fully actuated systems and a class of underacted Euler-Lagrange systems, where the following properties characterize the latter: decomposability into a feedback interconnection of two passive subsystems such that one subsystem has one control input per degree of freedom, whereas the other subsystem is entirely free from input forces. Concerning this work, it is worth remarking that most articulated soft robots can be represented in this way. A unified treatment is meant in the following sense: having seen significant advances in nonlinear control of fully actuated systems in the past

decades, this work aims to provide a *bridge* that allows the direct transfer from this rich pool of knowledge to solve underactuated problems.

Given the complex nonlinear and underactuated dynamics of ASRs—paired with a low output control bandwidth—it turned out that designing a control framework that is not only theoretically sound but also delivers in regard to the following points is a highly challenging endeavor:

(**G1**) Sufficient performance and robustness in challenging environments
(**G2**) Safe handling of impacts
(**G3**) Safe physical human-robot interactions
(**G4**) Adjustable interaction behavior
(**G5**) Intuitive closed-loop dynamics

This work aims to develop a control framework that delivers on all these points.

Experience in the lab repeatedly revealed that control approaches that modify (override/shape) the intrinsic rigid robot dynamics to a significant extent tend to show unstable behavior on actual hardware. The higher the joint compliance, the lower the mechanical bandwidth, and the more pronounced this issue becomes. This observation initiated the design of a physically motivated control framework that aims at achieving natural motions, with the hope that minimizing the system shaping, and having a closed-loop dynamics match in some way the intrinsic structure of the robot will award high and robust performance with little control effort.

The results of this endeavor are reported in this work.

Contributions of this Thesis

The major contributions of this work can be summarized as:

- A novel methodology that allows the unified treatment of fully actuated systems and a class of Euler-Lagrange systems. It is demonstrated that by applying a set of coordinate and input transforming equations, the latter can be treated as if fully actuated. Since the new inputs obey some smoothness and weak feedback constraints the term *quasi-full actuation* is coined (Chapter 4 and 5). This equivalent system dynamics formulation literally establishes a *bridge* that enables the direct transfer from the rich pool of classical control methods to solve underactuated problems. It is worth remarking that this transfer is not limited to the control design phase, but extends to techniques used for passivity and Lyapunov-based stability arguments.
- Extensions to fundamental energy-based control methods that were designed for fully actuated system to a class of underactuated Euler-Lagrange systems (Chapter 6), namely: 1) Energy shaping and damping injection, 2) Euler-Lagrange controllers.
- Development of novel passivity-based control schemes tailored for articulated soft robots that aim at natural motions through minimizing the system shaping (Chapter 7). These schemes are summarized under the name *Elastic Structure Preserving* (ESP) control, and can be applied to systems with elastic and visco-elastic actuation elements to achieve *globally asymptotic motion tracking*. The user can directly specify a

desired damping or impedance behavior in terms of the link or end-effector velocities. It is worth noting that the closed-loop stiffness can be increased above the intrinsic one while retaining an output strictly passive closed loop.

- Extensive experimental evaluation demonstrating that the ESP schemes deliver on the design objectives, (**G1**)–(**G5**), set above (Chapter 11). All ESP designs exhibit a physically intuitive closed loop which allows the operator to anticipate the interaction behavior of the robot with its environment. Moreover, all gains have a direct physical interpretation as springs, dampers or inertia shaping factors, which is of immense value during the controller tuning and commissioning stage.
- A performance analysis of articulated soft robots by virtue of the developed theory on quasi-full actuation.
- Introduction of enhanced link-side damping designs based on dynamics extensions that minimize the actuator torque requirements in situations where a robot is subject to impacts. A desirable side effect is the reduction of sensor noise sensitivity compared to design with a fully damped closed loop.
- A comparison of the proposed ESP control schemes with state of the art motion tracking controllers.
- A complete synthesis method for *time-optimal rest-to-rest motions* of an elastic joint system with bounded torque input. The solution is provided in closed form by following purely geometric arguments, and verifies the standard optimality conditions. Further, we introduce the concept of natural motions which are time-optimal solutions to the rest-to-rest motion problem. These are the only rest-to-rest solutions where the minimum-time performance of an elastic joint system matches that of a rigid joint. The insight obtained from the natural motion analysis, can be exploited to optimize the design of an elastic robot joint.
- Designing a software infrastructure for a compliant anthropomorphic robot (DLR *David*) that integrates the control techniques presented in this work to equip the robotic system with the necessary skills to perform complex tasks (Chapter 12) including pick and place, teleoperation, and drill-hammering into a block of concrete.
- The experimental results on DLR *David* demonstrate that articulated soft robots are ripe for the transfer into the commercially space. The ESP schemes are basically tuning knob free and produce a physically intuitive closed loop, which significantly simplifies and accelerates controller commissioning making them an attractive choice for commercial usage.
- This work hopefully spark appreciation of physical intuition and geometric insight for control design.

Figure 1.1: DLR *David*: An articulated soft robot.

Concerning the first point, it is worth remarking that decoupling-based methods allow the adoption of rigid robot controllers to articulated robots as well. These, however, rely on canceling dynamics terms to transform the robot model into a triangular form. A key novelty of the presented methodology is the fact that it enables the adoption without pre-shaping the robot dynamics. The input and coordinate transformations that produces a quasi-fully actuated system representation do not shape the plant dynamics itself just like a standard coordinate transformation. Another important aspect of the new methodology is the fact that in the limiting case of the joint stiffness value approaching infinity, the rigid robot controller is re-obtained, which is not the case for decoupling-based methods.

Thesis Overview

The content of this work is organized in the following way. The relation between the chapters and possible routes of reading are shown in Fig. 1.2.

Chapter 2 covers basic results of analytical mechanics which are required to follow the material treated in this work. The Euler-Lagrange equations are derived from D'Alembert's Principle, and their properties most relevant for the developments in this work are presented. Finally, the implications of underactuation with regard to control design are briefly discussed.

Chapter 3 treats the modeling of articulated soft robots on the basis of the anthropomorphic robot DLR *David*, which is driven by variable impedance actuators in all its joints. Most of the experimental evaluation is performed on this hardware.

Chapter 4 guides the reader through the intuition and thinking that lead to the development of the novel concept of *quasi-full actuation* on the basis of a single elastic joint. The dynamic behavior of the quasi-fully actuated system under feedback control is discussed, and a geometric interpretation of the new coordinates is provided. Finally, a Lagrangian view of articulated soft robots is presented. The established picture serves as inspiration for the developments in Chapter 5.

Chapter 5 contains the central theoretical contribution of this work. All successive developments build on the results developed here. It generalizes the concept of quasi-full actuation presented in Chapter 4 to a *class of underactuated Euler-Lagrange systems*. An Euler-Lagrange structure preserving input and coordinate transformation is derived that enables a class of underactuated Euler-Lagrange systems to be treated as if fully actuated. Finally, the smoothness and feedback constraints on the inputs of the quasi-fully actuated system are discussed and physically motivated.

Chapter 6 reports *extensions* to two fundamental passivity based control methodologies that were originally design for fully actuated systems to a class of underactuated Euler-Lagrange systems: (1) The energy shaping and damping injection technique, (2) the methodology of Euler-Lagrange controllers. Finally, the adoption of impedance control techniques through the quasi-full actuated system representation is demonstrated.

Chapter 7 applies the concept of quasi-full actuation to ASRs to derive several *Elastic Structure-Preserving* (ESP) *control schemes* in a unifying way. These concepts are based on the the idea of preserving the system structure and minimizing the system shaping. Proofs for the passivity and stability results are presented at the end of this chapter. Extensive experimental results demonstrating the remarkable performance of the ESP controllers in challenging practical environment are reported in Chapter 11 and 12. Chapter 7 also applies the concept of quasi-full actuation to extend the ESP control concept to articulated soft robots with *visco-elastic joints*, which results in a dynamic state transformation.

Chapter 8 *compares* several design techniques that guarantee global asymptotic motion tracking for flexible joint robots with the ESP and ESPi designs reported in Chapter 7

Chapter 9 exploits the quasi-fully actuated representation of a SEA-based robot to analyze its *performance limits*. It discusses the challenges associated

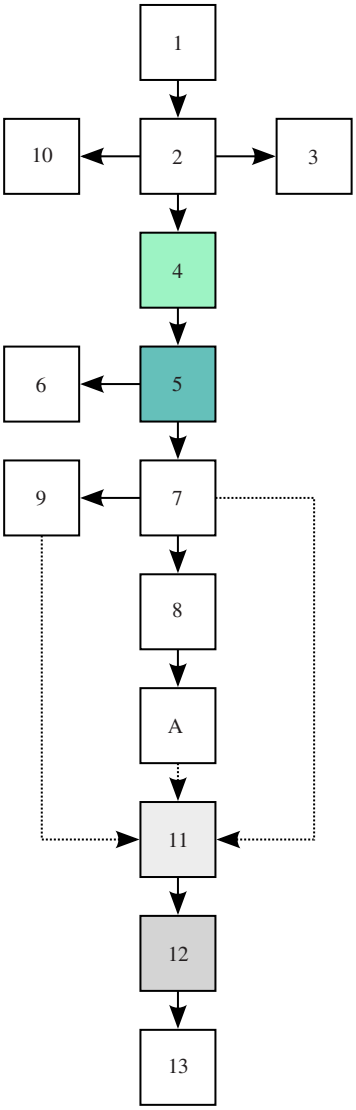

Figure 1.2: Relation between the chapters.

with link-damping injection and the underlying reasons. Based on these insights, *enhanced damping designs* are derived that significantly reduce the actuator torque requirements at the moment of an impact. A positive side effect is the reduction of link position sensor noise amplification.

Chapter 10 presents a complete synthesis method for time-optimal rest-to-rest motions of an elastic joint system with bounded torque input. The solution is provided in closed form by following purely geometric arguments, and verifies the standard optimality conditions. Further, we introduced the concept of natural motions which are time-optimal solutions to the RTR motion problem. These are the only RTR solutions where the minimum-time performance of an elastic joint system matches that of a rigid joint. The insight obtained from the natural motion analysis, can be exploited to optimize the design of an elastic robot joint.

Chapter 11 reports extensive evaluations of the presented control techniques in simulation and on hardware. The focus is set on the experimental evaluation of the ESP control schemes. The results demonstrate the remarkable robustness and performance of this design technique.

Chapter 12 presents a variety of applications in which the ESP control framework is used to facilitate motions on the anthropomorphic robot DLR *David*. These applications demonstrate that the ESP schemes can be used as the core motion control architecture in the software ecosystem of a compliant robot to execute advanced manipulation tasks.

Chapter A introduces a *geometric interpretation* of the transforming equations that produce the quasi-fully actuated representation for systems where the elastic potential function assumes a quadratic form.

Chapter 13 eventually summarizes and concludes the results of this work.

Publications

The research resulted in ten journal articles, eight conferences publications and one invited talk on major conferences in the fields of robotics and control theory. Further, the work associated with ESP control has been featured two times at the *Video Friday* by *IEEE Spectrum*. The first conference paper is awarded with a nomination as *Best Paper Award* Finalist at the *2016 IEEE International Conference on Robotics and Automation (ICRA)*. The novel methodology proposed therein resulted in a patent. Publications listed with "∘" have been developed during the PhD studies, but are not integrated into this monograph.

Journal Publications

- M. Keppler, D. Lakatos, C. Ott, and A. Albu-Schäffer. Elastic structure preserving (esp) control for compliantly actuated robots. *IEEE Transactions on Robotics*, 2018, 34(2), pp.317–335.
- ∘ M. Maier, M. Keppler, C. Ott, and A. Albu-Schäffer. Adaptive air density estimation for precise tracking control and accurate external wrench observation for flying robots. *IEEE Robotics and Automation Letters*, 5(2), 2020, pp.1445–1452.
- R. Mengacci, M. Keppler, M. Pfanne, A. Bicchi, and C. Ott. Elastic structure preserving control for compliant robots driven by agonistic-antagonistic actuators (ESPaa). *IEEE Robotics and Automation Letters*, 6(2), 2021, pp.879–886.

- ∘ N. Mansfeld, M. Keppler, and S. Haddadin. Speed gain in elastic joint robots: An energy conversion-based approach. *IEEE Robotics and Automation Letters*, 6(3), 2021, pp.4600–4607.
- M. Keppler, F. Loeffl, D. Wandinger, C. M. Raschel, and C. Ott. Analyzing the performance limits of articulated soft robots based on the espi framework: Applications to damping and impedance control. *IEEE Robotics and Automation Letters*, 6(4), 2021, pp.7121-7128.
- G. Pollayil, X. Meng, M. Keppler, M. Pfanne, A. Bicchi, C. Ott. Elastic structure preserving impedance control for nonlinearly coupled tendon-driven systems. *IEEE Robotics and Automation Letters*, 2021, 6, pp.1982–1987.
- M. Keppler, C. Ott, and A. Albu-Schäffer. From underactuation to quasi-full actuation: Aiming at a unifying control framework for articulated soft robots. *International Journal of Robust Nonlinear Control.*, 2022, 32(9), pp.5453–5484.
- M. Harder, M. Keppler, X. Meng, C. Ott, H. Höppner, and A. Dietrich. Simultaneous motion tracking and joint stiffness control of bidirectional antagonistic variable-stiffness actuators. *IEEE Robotics and Automation Letters.* 2022, 7(3), pp.6614-6621.
- M. Keppler, C. Raschel, D. Wandinger, A. Stemmer, and C. Ott. Robust stabilization of elastic joint robots by ESP and PID control: Theory and experiments. *IEEE Robotics and Automation Letters.*, 2022, 7(3), pp.8283-8290.
- X. Meng, M. Keppler, C. Ott. Passivity-based motion and force fracking control for constrained Articulated Soft Robots. *IEEE Control Systems Letters.*, 2022, 7, pp.217-222.

Conference Publications

- ⋆ M. Keppler, D. Lakatos, C. Ott, and A. Albu-Schäffer. A passivity-based approach for trajectory tracking and link-side damping of compliantly actuated robots. In *2016 IEEE International Conference on Robotics and Automation (ICRA)*, pp.1079–1086, 2016. (**Award Finalist**[*])
- M. Keppler, D. Lakatos, C. Ott, and A. Albu-Schäffer. A passivity-based controller for motion tracking and damping assignment for compliantly actuated robots. In *2016 IEEE 55th Conference on Decision and Control (CDC)*, pp.1521–1528, 2016.
- M. Keppler, D. Lakatos, C. Ott, and A. Albu-Schäffer. Elastic structure preserving impedance (ESπ)control for compliantly actuated robots. In *2018 IEEE/RSJ International Conference on Intelligent Robots and Systems (IROS)*, 2018, pp.5861–5868.
- M. Keppler, D. Lakatos, A. Werner, F. Loeffl, C. Ott, and A. Albu-Schäffer. Visco-Elastic Structure preserving impedance (VESπ) control for compliantly actuated robots. In *2018 European Control Conference (ECC)*, pp.255–260, 2018.
- A. Werner, B. Henze, M. Keppler, F. Loeffl, S. Leyendecker, and C. Ott. Structure preserving multi-contact balance control for series-elastic and visco-elastic humanoid robots. In *2018 IEEE/RSJ International Conference on Intelligent Robots and Systems (IROS)*, 2018, pp.1233–1240.
- M. Iskandar, C. Ott, O. Eiberger, M. Keppler, A. Albu-Schäffer, and A. Dietrich. Joint-level control of the dlr lightweight robot sara. In *2020 IEEE/RSJ International Conference on Intelligent Robots and Systems (IROS)*, pp.8903–8910, 2020.
- M. Keppler and A. De Luca. On time-optimal control of elastic joints under input constraints. In *2020 59th IEEE Conference on Decision and Control (CDC)*, pp.4149–4156, 2020.
- X. Meng, M. Keppler, and C. Ott. Elastic structure preserving impedance control of bidirectional antagonistic variable stiffness actuation. In *2021 European Control Conference (ECC)*, pp.263–269, 2021.

[*] Finalist for the *Best Paper Award on **Automation** at* 2016 IEEE International Conference on Robotics and Automation (ICRA), May 2016, Stockholm, Sweden

Patent

- M. Keppler, D. Lakatos, C. Ott, Verfahren und Vorrichtung zum Steuern und Regeln von Aktoren, die zum Antrieb eines seriellen, mehrgliedrigen mechanischen Systems dienen, 2016, DE102016005747B3, *Deutsches Patent- und Markenamt*, https://depatisnet.dpma.de/DepatisNet/depatisnet?action=bibdat&docid=DE102016005747B3.

Invited Talks

- M. Keppler, Impedance Control on VSA Robots: Lessons Learned, workshop on "Variable Impedance Robotic Skills: From the Foundations to the Current Challenges and Perspectives", *2022 Robotics: Science and Systems (RSS)*, New York City, USA, 2022.
- M. Keppler, Elastic Structure Preserving Control of Articulated Soft Robots with Elastic and Visco-Elastic Joints. *2018 IEEE/RSJ Int. Conference on Intelligent Robots and Systems (IROS)*, Full-Day Workshop on Soft Robotic Modeling and Control: Bringing Together Articulated Soft Robots and Soft-Bodied Robots, Madrid, Spain, 2018.

Media Coverage

- Featured at IEEE Spectrum Video Friday, 1 Apr 2016
  https://spectrum.ieee.org/video-friday-dogs-that-code-robotic-football-self-driving-bicycle
- Headliner at IEEE Spectrum Video Friday, 27 Jul 2018
  https://spectrum.ieee.org/video-friday-soft-robot-impedance-control-autonomous-rescue-drone-robosimian-skating

A Review of Analytical Mechanics

2

The theoretical development of the laws of motion of bodies is a problem of such interest and importance, that it has engaged the attention of all the most eminent mathematicians, since the invention of dynamics as a mathematical science by Galileo, and especially since the wonderful extension which was given to that science by Newton. Among the successors of those illustrious men, Lagrange has perhaps done more than any other analyst, to give extent and harmony to such deductive researches, by showing that the most varied consequences respecting the motions of systems of bodies may be derived from one radical formula; the beauty of the method so suiting the dignity of the results, as to make of his great work a kind of scientific poem. [59]

– William Rowan Hamilton, 1834

This chapter provides a brief overview of analytical mechanics that should be sufficient to understand the material treated in this thesis. Most results are presented without proof, and proofs are only added when providing particular insights. The style of presenting this material is greatly inspired by the wonderful book [103] by Lanczos. The details on the ideas touched here, are covered in, e.g., [1, 10, 52, 103, 181].

2.1 Generalized Coordinates

In the analytical formulation of mechanics the concept of coordinates play a central role. All the calculations are done in terms of some abstract quantities. In order to make use of the modern mathematical machinery we require the physical world to be translated into the realm of mathematics. We perform this translation with the help of coordinates. The coordinates establish a one-to-one correspondence between the position of points in space and numbers. Setting up three perpendicular axis and introducing three Cartesian coordinates x, y, z (as proposed by Descartes in 1637) is but one way of establishing such correspondence. We may equally well introduce polar coordinates r, θ, φ as indicated in Fig. 2.1. Analytical mechanics requires a generalization of the coordinate concept. It turns out that any set of parameters which can *uniquely* characterize the position of a mechanical system may be chosen as a suitable set of coordinates.

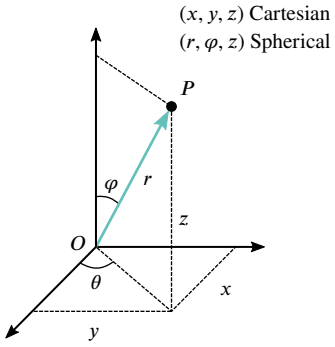

Figure 2.1: Conversion between Cartesian (x, y, z) and spherical (r, θ, φ) coordinates in three dimensions.

Assume that we have a system of N *free* particles. In this case, the configuration of the entire system can be uniquely described with the rectangular coordinates of these particles

$$x_i, y_i, z_i, \quad i = 1, \dots N. \tag{2.1}$$

Note that we require three coordinates for each *free* particle.

The configuration is described equally well, if we express the coordinates x_i, y_i, z_i in terms of some other quantities

$$q_i, \quad i = 1, \dots 3N, \tag{2.2}$$

that are in a one-to-one correspondence to the original coordinates. We call this procedure a *coordinate transformation*. In general, the *transforming equations* appear as

$$\begin{aligned} x_1 &= f_1(q_1, q_2, \dots, q_{3N},), \\ &\vdots \\ z_N &= f_{3N}(q_1, q_2, \dots, q_{3N}). \end{aligned} \tag{2.3}$$

In words, the rectangular particle coordinates are expressed as functions of the $3N$ independent parameters q_i. The variational treatment of mechanics allows great freedom in choosing appropriate coordinates for our problem. Choosing a set of coordinates that "fits" the mechanical problem can significantly simplify the problem. For example, the solutions to the Kepler problem [84, 85]—that arises in orbital mechanics from predicting the orbits of two orbital bodies in a binary system—may be derived more easily by expressing the kinetic and potential energies in terms of the center of mass position and relative distance instead of relying on rectangular coordinates. In [87], we exploited this fact, together with system inherent symmetries, to derive a geometrical method to tackle time-optimal control problems for flexible joints. However, choosing the "right" coordinates requires insightful thinking, but it is time well spent. It is hard to underestimate the value of the freedom of choosing an arbitrary set of coordinates when applying variational methods. The theme of choosing coordinates that "suit" the problem permeates the entire work. In Chapter 4 and 5, we present a control methodology that evolves around introducing virtual coordinates to facilitate an intuitive treatment of some underactuated systems.

[84]: Kepler (1621), *Epitome Astronomiae Copernicanae*
[85]: Kepler (1609), *Astronomia Nova*

[87]: Keppler et al. (2020), "On time-optimal control of elastic joints under input constraints"

In some cases the Lagrangian might be independent of some coordinate. Such coordinate is referred to as *cyclic* or *ignorable*. These coordinates play a fundamental role in physics. Whenever we identify a cyclic coordinate, we know that its associated conjugate momentum is a constant of motion. In general, invariance of the Lagrangian under a symmetry transformation gives rise to a conserved quantity as point out in Noether's Thoerem[128].

[128]: Noethers (1918), "Invariante variationsprobleme"

2.1.1 Kinematic Constraints

The advantage of generalized coordinates becomes even more apparent when dealing with mechanical systems that are subject to *kinematic constraints*, which are mathematical relations between coordinates that express the fact that a system is restrained in its motion. One type of constraint system will be of particular interest in this work, the rigid bodies, where the constraints on the motions of the particles keep their relative distances unchanged. Another important example is the mathematical pendulum as shown in Fig. 2.2, which shares the same dynamics as a revolute joint in robotics.

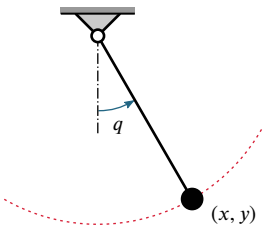

Figure 2.2: A mathematical pendulum.

The position of the point mass can be described with two coordinates x, y. The mass is connected with a massless rod to a pivot. Thus, it stays at a fixed distance from its center of rotation. This implies the condition

$$x^2 + y^2 = l^2. \tag{2.4}$$

As a consequence, we cannot choose the rectangular coordinates independently of each other. We could designate one *master* coordinate and determine

the other dependent coordinate via (2.4). However, this works only locally. Physically speaking; it is obvious that if we are given the x position of the point mass, we can always find two valid y positions—and vice-versa—that don't violate the kinematic constraint. Further, there would be no physical justification to pick one coordinate as the master coordinate over the other. From the physical point of view, it would be more natural to choose the angular position of the rod as a coordinate to describe the mass position. In this case, the two rectangular coordinates would be expressible as a function of this angle. This angle serves as a so-called *generalized coordinate*. Let us consider a mechanical system of N particles that is subject to m independent kinematic constraints. The number of total coordinates required to describe the system configuration is reduced by the number of independent kinematic constraints. The configuration of the entire system can be uniquely described with

$$n = 3N - m \tag{2.5}$$

parameters

$$q_i, \quad i = 1, \dots, n. \tag{2.6}$$

Analogous to (2.3), we may express the rectangular coordinates of all the particles (2.1) as functions of the quantities (2.2):

$$\begin{aligned} x_1 &= f_1(q_1, q_2, \dots, q_n) \\ &\vdots \\ z_N &= f_{3N}(q_1, q_2, \dots, q_n). \end{aligned} \tag{2.7}$$

The number n is system inherent and is the minimum number of coordinates required to uniquely characterize the configuration of a mechanical system. Hence, we refer to such a system as having *n degrees of freedom*. Further, we coin the n parameters (2.6) as the *generalized coordinates*. Albeit having great freedom in choosing the functions (2.7), we require them to be single valued, finite, continuous and differentiable functions of the q_i. Further, the Jacobian of a given combination of n such functions shall be different from zero.[1]

1: More precisely: det $\boldsymbol{Df} \neq 0$ for all valid combinations of the parameters (2.6).

Holonomic and non-holonomic systems

We started our considerations with a system of N particles. It is often necessary to take into account constraints that limit the motion of particles. A rigid body is a classic example; the constraints on the motions of the particles keep their relative distances unchanged. Other examples can be easily envisioned. A particle moving along the surface of a table is constrained in its motion. Whenever the motion of the C-point in its $3N$ dimensional configuration space is restricted, and if the kinematical constraints can be expressed by equations of the form

$$\varphi_i(x_1, \dots, z_N, t), \quad i = 1, \dots, m < 3N \tag{2.8}$$

with φ_i are assumed to be differentiable functions of their arguments, then the constraints are said to be *holonomic*. Often it is more convenient to formulate equations of constraints directly in terms of configuration variables than in terms of positions coordinates of particles. This should become clear from the example below. A constraint that cannot be expressed in the form (2.8) are

referred to a *non-holonomic* constraints. Consider for example a constraint equation containing velocities

$$f_i(x_1, \dots, z_N, \dot{x}_1, \dots, \dot{z}_N, t), \quad i = 1, \dots, m < 3N \tag{2.9}$$

that cannot be brought into the form (2.8) through integration. Unilateral constraints given expressions containing inequalities is another example. Characteristic for a holonomic system with n degrees of freedom is that it can be described by an equal number of n generalized coordinates.

If there are m holonomic constraints in the form (2.8), we can always use these equations to eliminate m of the $3N$ coordinates, and the system is said to have $n = 3N - m$ degrees of freedom. This elimination process of dependent coordinates can also be attacked differently. By introducing independent variables $q_1, \dots, q_n$ and expressing them in terms of the the old coordinates $x_1, \dots, z_N$ through equations of the form

$$\begin{aligned} x_1 &= f_1(q_1, \dots, q_n, t) \\ &\vdots \\ z_N &= f_{3N}(q_1, \dots, q_n, t), \end{aligned} \tag{2.10}$$

that contain the constraints implicitly. This is the standard procedure for modeling the kinematics of rigid robots. For each of the n joints, we introduce one configuration variable q_i, $i = q_1, \dots, q_n$. As it will turn out, the situation becomes slightly more complex when dealing with articulated soft robots since each joint has multiple degrees of freedom.

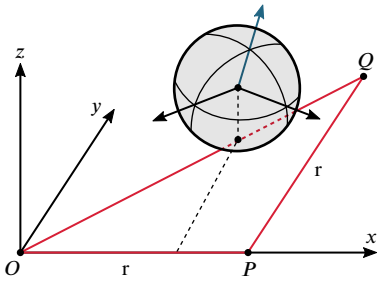

Figure 2.3: A rolling ball as an example for a non-holonomic system.

A popular example of a non-holonomic system is that of an rolling ball on a table without slipping. Since its center is at a constant height above the table its degrees of freedom are reduced from six to five (two rectangular coordinates x, y, three angles α, β, γ). However, if the ball is confined to rolling motions, i.e., no sliding or spinning about its vertical axis, it can only move in two independent directions. The point of contact is always at rest momentarily, and its instantaneous axis of rotations has to go through that point and lie within the plane of the table. This constraint on the instantaneous axis of rotation reduces the number of degrees of freedom from five to two. One could imagine that it would be possible to describe the three angles as a function of the rectangular coordinates. However, this is not the case. This can be demonstrated with the following thought experiment (adopted from [181]). Place the ball at O such that the red arrow aligns with the z axis. Then, roll the ball along the x axis for a distance equal to the balls circumference r, to a point P, where the red arrows aligns again with the z axis. Repeat the procedure in the y direction to a point Q, where the red arrow arrow will be once again aligned with the z axis. Now roll it back along the hypotenuse of the triangle OPQ to its starting location. Since the final path is of length $\sqrt{2}r$, the red will not end up aligned with the z axis. The (x, y) position of the ball has returned its initial value, but it now has a different orientation. Clearly, the two coordinates (x, y) are not sufficient to uniquely specify the balls configuration. In fact, it requires three additional coordinates to specify the orientation. Clearly, it is a non-holonomic system. In the words of [111], we may think intuitively of holonomic and non-holonomic constraints as follows:

- A holonomic constraint is a *constraint on configuration*: it says there are places you cannot go. That is a reduction in degrees freedoms. That's (usually) bad.

[181]: Taylor (2005), *Classical Mechanics*

[111]: Mason (2001), *Mechanics of robotic manipulation*

- A non-holonomic constraint is a *constraint on velocity*: there are directions you cannot go. But you can still get wherever you want. That's (usually) good!

Rheonomic and Scleronomic Systems

The time t is the most characteristic variable in dynamics. We are interested how a systems evolves over time and study the causes of those changes. The coordinates that describe these changes are functions of the time. A decisive question in the analytical treatment of mechanics is the question whether the time appears *explicitly* in the kinetic or potential energies. Consider a 3D mathematical pendulum whose rod length is continuously changing with time. This implies a condition of the form

$$\varphi(x, y, z, t) = 0, \tag{2.11}$$

with (x, y, z) denoting the position of the point mass similarly too planar case in Fig. 2.2. We see that the equation of constraint contain the time as an explicit variable. Constraints are classified according to whether the constraint equations, (2.8), contain the time explicitly (*rheonomous*), or not explicitly (*scleronomous*). Sometimes rheonomous coordinates are called *forced* since the explicit time dependence usually arises from a forced motion.[2] If a system is subject to rheonomic constraints, the elimination of these conditions by a proper choice of curvilinear coordinates will have the consequence that the transforming equations will be of the form (2.10) containing the time explicitly. A similar situation arises even without time-dependent kinematical conditions, if the coordinates chosen belong to a reference system which is in motion [103, p. 32]. Such a scenario is encountered Chapter A, where the new coordinates that belong to a non-inertial. In Chapter 5, we will face implicit coordinate transformating equations containing the time explicitly.

2: Such situations arise frequently in control problems. In the field of ASR control, we frequently encounter the case that the motor position or velocity is assumed as the control input. In other words, it is assumed that the motor control bandwidth is fast enough such that a desired motion can be directly imposed.

Rheonomic constraints can be treated with the tools of analytical mechanics, however certain characteristics are lost which only hold for scleronomic systems. Differentiating (2.10) with respect to time yields

$$\begin{aligned} \dot{x}_1 &= \frac{\partial f_1}{\partial q_1}\dot{q}_1 + \ldots + \frac{\partial f_1}{\partial q_n}\dot{q}_n + \frac{\partial f_1}{\partial t} \\ &\vdots \\ \dot{z}_N &= \frac{\partial f_{3N}}{\partial q_1}\dot{q}_1 + \ldots + \frac{\partial f_{3N}}{\partial q_n}\dot{q}_n + \frac{\partial f_{3N}}{\partial t}. \end{aligned} \tag{2.12}$$

If we substitute (2.12) in the kinetic energy expression for a system of particles, it is evident that it no longer appears as a purely quadratic form of the generalized velocities $\dot{q}_i$. Additional terms which are linear in velocities are obtained, and others that are independent of the velocities altogether. Substituting (2.10) in the definition of the potential energy, it is clear that it will come out as explicitly time dependent. The fundamental difference between a scleronomic and a rheonomic system is that in scleronomic system the total energy (sum of potential and kinetic energy) is conserved over time. Rheonomic systems on the contrary do not satisfy such a conservation law.

2.2 The Configuration Space

The concept of configuration space equips us with a powerful geometric picture. This picture will serve as a great aide in developing the concept of *quasi-full actuation* in Chapter 5. We may think of the three numbers x, y, z as defining a point in a three-dimensional space. Analogously, we may think of the n numbers $q_1, q_2, \dots, q_n$, as the rectangular coordinates of a point $\boldsymbol{P}$ in a n-dimensional space. Further, we can associate the equations

$$\begin{aligned} x &= x(t), \\ y &= y(t), \\ z &= z(t), \end{aligned} \tag{2.13}$$

with the geometric idea of a (parameterized) curve and the motion of a point along that curve with the time as parameter determining its current location. Likewise, we can take on the same view regarding the equations

$$\begin{aligned} q_1 &= q_1(t), \\ q_2 &= q_2(t), \\ &\vdots \\ q_n &= q_n(t). \end{aligned} \tag{2.14}$$

These equations represent the solution of a dynamical system. In the connected geometrical picture, we may think of (2.14) as defining a parameterized curve in a n dimensional space with a point $\boldsymbol{P}$ moving along that curve. At any instant in time, the location of such point $\boldsymbol{P}$ uniquely specifies that configuration of a given system.[3] No matter how complicated the mechanical system, we can always associate its time-evolution with the motion of a single point in a sufficiently high dimensional space, called the *configuration space* or in short form *C-space*, as sketched in Fig. 2.4. For instance, let us consider a double pendulum as shown in Fig. 2.5. Every possible configuration can be uniquely described by two angles q_1 and q_2. Thus, we can correlate its motion with the motion of a point in a two-dimensional configuration space. For the sake of brevity, we shall adopt the following terms from [103]: the location of a mechanical system in the configuration space is referred to as *C-point*, and the curve traced out by that point during the motion will be referred to as the *C-curve*.

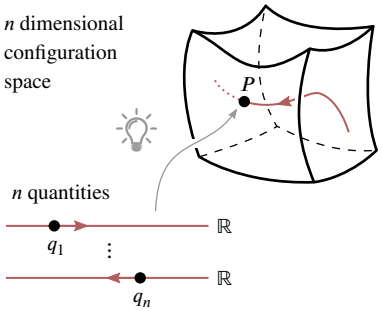

Figure 2.4: Configuration space: a single point $\boldsymbol{P}$ of the configuration space represent the configuration of an entire physical system (adapted from [146, p. 177]).

3: Take note that the states of motion, eg. velocities/momenta are not part of the configuration space. This is in contrast to the phase space, where we also take the states of motion into account.

[103]: Lanczos (2020), *The Variational Principles of Mechanics*

2.2.1 A Topological Point of View

So far our considerations where based on the geometry of an Euclidean space of n dimensions. As it turns out, a more fitting geometric picture can be obtained when switching from analytical geometry to Riemannian geometry (which is a branch of differential geometry).[4] It is important to point out that for the developments in this work our rudimentary picture founded on Euclidean space will serve us well enough. To keep the presentation of results easily, we shall refrain from adopting the language of differential geometry. However, I'm firmly convinced that future generalization would profit from adopting the view of differential geometry. Thus, a brief outlook into the topological point of view on the configuration space is provided in the following. A detailed treatment on the connection between mechanics and differential geometry can,

4: Roughly speaking: Euclidean geometry deals with flat space equipped with a metric, whereas Riemannian geometry deals with curved space equipped with a metric. Nevertheless, Riemannian geometry assumes that curved space resembles Euclidean space at each point infinitesimally (*i. e.*, in the first order approximation).

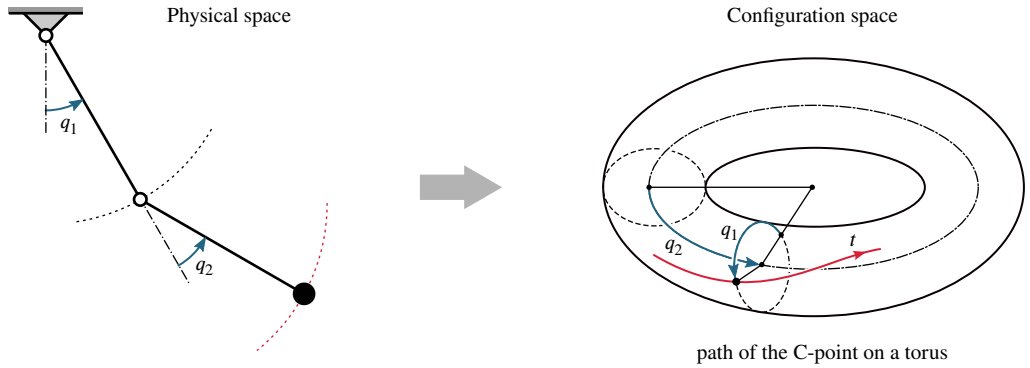

Figure 2.5: Configuration space of a double pendulum.

e.g., be found in [108], where the author approaches the topic from a historical point of view.

[108]: Lützen (1995), "Interactions between mechanics and differential geometry in the 19th century"

Lets us try to obtain a more appropriate picture of the geometrical nature of the configuration space on the basis of the double pendulum. The configuration of the first link is given by the displacement angle q_1 so that the circle S^1 can be associated with the space of all possible configurations. The configuration of the second link is described by the displacement angle q_2. Since both links can move independently from each other the space of all possible configurations is given by the Cartesian product of two circles $S^1 \times S^1$, which is homeomorphic to the torus. This image allows us to rethink our picture of a double pendulum in motion. Instead of imagining two links, subject to kinematic constraints, rotating in physical space, we can associate its the time evolution with the motion of a point on a torus. Every point (q_1, q_2) on the torus represents a configuration of the double pendulum so that any trajectory of the double pendulum correlates to a C-curve on the torus. The torus emerges as the natural geometric structure of a double pendulum representing the space of all admissible configurations that satisfy the kinematic constraints. This structural insight provides a first glimpse into why geometry is an intrinsic part of mechanics and why it might be wise to respect it. In terms of differential geometry, we would think of the configuration space as a *manifold*[5]. The motivation for the geometric treatment of mechanics is well summarized in the following quote by [105].

5: Loosely speaking, we can thing of a manifold as the space where all the configuration variables live.

[105]: Lessig (2012), "A Primer on geometric mechanics"

> "Next to the intuitive appeal, a second characteristic of geometric mechanics is its emphasis on mathematical and physical structure. While Newtonian mechanics is highly descriptive, making it easy to learn and to carry out computations, it does not reveal structure. In geometric mechanics, in contrast, computations are structural arguments which provide insight into the fabric they represent, and this structural insight explains much of the vigor of geometric mechanics."

For an introduction into the geometry of physics, the interested reader is referred to [45]. A detailed mathematical exposition of this matter is presented in [1].

[45]: Frankel (2003), *The Geometry of Physics: An Introduction*

[1]: Abraham et al. (2008), *Foundations of Mechanics*

2.3 Coordinate Transformations

We are free to choose a set of n generalized coordinates

$$q_1, q_2, \dots, q_n \tag{2.15}$$

as long as they uniquely characterize the system. This arbitrariness of coordinates implies that we are free to change from one set of generalized coordinates to another set of n quantities

$$\bar{q}_1, \bar{q}_2, \dots, \bar{q}_n \tag{2.16}$$

as generalized coordinates. However, there must exist a functional relation between these two sets of coordinates of the form:

$$\begin{aligned} \bar{q}_1 &= f_1(q_1, q_2, \dots, q_n, t), \\ &\vdots \\ \bar{q}_n &= f_n(q_1, q_2, \dots, q_n, t). \end{aligned} \tag{2.17}$$

The functions $f_1, f_2, \dots, f_n$ must be single valued, finite, continuous and differentiable functions of the coordinates q_k with an invertible Jacobian. Strictly speaking, we are interested in functions $\boldsymbol{f} : U \to V$, where U and V are open subsets of $\mathbb{R}^n$ that satisfy

- Function $\boldsymbol{f}$ is bijective[6]. This implies that its inverse $\boldsymbol{f}^{-1} : V \to U$ exists.
- Both $\boldsymbol{f}$ and $\boldsymbol{f}^{-1}$ are of class C^1.

6: I.e., onto and one-to-one.

A function $\boldsymbol{f}$ that satisfies these conditions can be thought of defining a change of coordinates. We will rely on the inverse function theorem to identify these functions. Let us consider a transformation in two dimensional space, which allows us to connect an intuitive geometrical picture with this concept. Assume that the quantities q_1, q_2 are plotted as rectangular coordinates of a two-dimensional space and we do so equally for the quantities $\bar{q}_1, \bar{q}_2$. This allows us to draw the following pair of pictures: (1) a collection of lines/curves in the (q_1, q_2) plane, (2) the image of these lines/curves under the transformation $\boldsymbol{f}$. For example, let us consider the mapping

$$f_1(q_1, q_2) = q_2^2 - q_1^2, \tag{2.18}$$
$$f_2(q_1, q_2) = q_1 q_2. \tag{2.19}$$

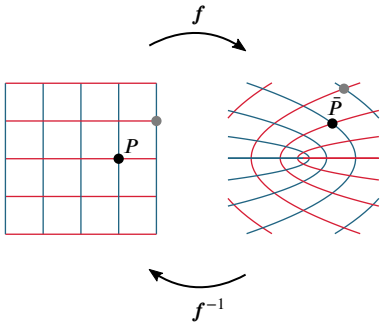

Figure 2.6: A grid in the (q_1, q_2) plane is transformed under $\boldsymbol{f}$ into the $(\bar{q}_1, \bar{q}_2)$ plane.

Figure 2.6 (left) shows the preimage (a Cartesian grid) and Figure 2.6 (right) shows the image of this grid under $\boldsymbol{f}$.

Differentiation of (2.17) yields

$$\begin{aligned} d\bar{q}_1 &= \frac{\partial f_1}{\partial q_1} dq_1 + \dots + \frac{\partial f_1}{\partial q_n} dq_n + \frac{\partial f_1}{\partial t} dt, \\ &\vdots \\ d\bar{q}_n &= \frac{\partial f_n}{\partial q_1} dq_1 + \dots + \frac{\partial f_n}{\partial q_n} dq_n + \frac{\partial f_n}{\partial t} dt. \end{aligned} \tag{2.20}$$

The equations (2.20) are always linear in the velocities. This fact will prove extremely helpful in Chapter 4 since it greatly simplifies expressing the new velocities $\bar{q}_i$ in terms of the old velocities q_i.

When thinking of a coordinate transformations in a n dimensional space it can be easier to think in terms of how individual points in space are mapped. To a single point P of the q-space corresponds a single point $\bar{P}$ of the $\bar{q}$-space. This mapping has several important characteristics besides the requirement of defining a one-to-one correspondence.

- The neighborhood of P is mapped on the neighborhood of $\bar{P}$.
- In general, straight lines in the q-space are no longer straight lines in the $\bar{q}$-space.
- In an infinitesimal region around P straight lines are mapped on straight lines. Parallel lines remain parallel lines, although lengths and angles are not preserved.
- A parallelepiped in the infinitesimal neighborhood of P is mapped on an parallelepiped in the neighborhood of $\bar{P}$. The determinant of the Jacobian of $\boldsymbol{f}$ encodes the ratio of the volume of the new parallelepiped to the volume of the original one.

2.4 Variational Principles of Mechanics

In this work, the Euler-Lagrange equations play a fundamental role for describing the dynamics of a system. To motivate this variational principle based approach of mechanics, we start with the principle of virtual work, and then derive the Euler-Lagrange equations from the D'Alembert's Principle. The section concludes with a brief out view on generalizations of the Lagrangian formalism.

2.4.1 Principle of Virtual Work

A fundamental variational principles in mechanics is the principle of virtual work. A mechanical system is in equilibrium if, and only if, the total virtual work of the impressed forces is zero for any virtual displacement, that is, for any infinitesimal variation of the configuration which is in compliance with the given kinematic constraints. Lagrange presented the virtual work principle in a more efficient form in 1768. With his introduction of generalized coordinates, we can dispense the forces of constraints by limiting the virtual displacements to those that are in harmony with the given constraints. In cases where the impressed force is of *monogenic* nature, i.e. derivable from a single scalar function—the potential energy—the virtual work is equal to the variation of the potential energy. It is well known that a mechanical system with holonomic and scleronomic constrains, and potential energy $\mathcal{V}$ is in a state of equilibrium if the value of the potential energy is stationary with respect to all kinematically permissible variations

$$\delta \mathcal{V} = 0. \tag{2.21}$$

2.4.2 D'Alembert's Principle

Building on previous work by Bernoulli, in 1743, d'Alembert published his Traité de Dynamique where he extended the principle of virtual work to solve various problems in dynamics [26]. By augmenting the impressed forces with

the new “force of inertia" he was able to extent the applicability of the principle of virtual work from statics to dynamics. d’Alembert’s principle states that “the total virtual work, δw, of the effective force, i.e. the sum of impressed and inertial forces, is zero for all reversible variations which satisfy the given kinematic constraints" [103, p. 90]. Suppose, we have a system of N particles. Let $\boldsymbol{r}_i$ be the radius vector, $\delta \boldsymbol{r}_i$ the corresponding virtual displacement, $\boldsymbol{F}_i^a$ the total impressed force[7], and $\boldsymbol{p}_i$ the linear momentum associated with the ith particle. Further, let us assume that the net virtual work of the forces of constraint vanishes. Then d’Alembert’s principle states

7: The expression impressed and applied force will be used synonymously throughout this work.

$$\delta w \equiv \sum_i \left(\boldsymbol{F}_i^a - \dot{\boldsymbol{p}}_i \right) \cdot \delta \boldsymbol{r}_i = 0. \tag{2.22}$$

Hence, by introducing the fictitious force of inertia $-\dot{\boldsymbol{p}}_i$ on particle i for each particle i, (2.22) expresses a balance of forces and we reformulated a problem of dynamics as problem of statics. We can translate this principle into an elegant expression involving virtual displacements of generalized coordinates. Moving from a system of particles to a system of n rigid bodies with n independent generalized coordinates $(q_1, \dots, q_n)$, this translation starts with the transforming equations

$$\boldsymbol{r}_i = \boldsymbol{r}_i(q_1, q_2, \dots, q_n, t). \tag{2.23}$$

The radial coordinates of the particles are no longer all independent, since they are connected through forces of constraint. These forces keep the particles together. In our case, these constraint forces impose $3N - n$ holonomic constraints on the system of particles, which reduce the number of degrees of freedom from $3N$ to n. Through the introduction of generalized coordinates, it is easy rotate and translate rigid bodies merely in such ways that the inner constrained forces, which define the rigid body, do not come into action. Because of this reason, in the variational treatment of mechanics the forces of constraint can be neglected, and only the work of the impressed forces needs to be considered. Any virtual displacement δq_i applied to the system is by definition, in harmony with the kinematic constraints, which allows the action of the constraint to be neglected. This idea is captured in the following postulate which is of central importance in analytical mechanics.[8]

8: For the special case of rigid bodies, this condition can be derived from Newton’s third law.

The net virtual work of the forces of constraint is zero for any virtual displacement which is in harmony with the given kinematic constraints.

In order to continue the translation from $\boldsymbol{r}_i$ to q_i, we make the following observations. The velocities of the particles can by expressed by

$$\boldsymbol{v}_i = \frac{\mathrm{d}}{\mathrm{d}t}\boldsymbol{r}_i = \sum_k \frac{\partial \boldsymbol{r}_i}{\partial q_k}\dot{q}_k + \frac{\partial \boldsymbol{r}_i}{\partial t}. \tag{2.24}$$

Further, the virtual displacement $\delta \boldsymbol{r}_i$ and δq_i are related by

$$\delta \boldsymbol{r}_i = \sum_j \frac{\partial \boldsymbol{r}_i}{\partial q_j}\delta q_j. \tag{2.25}$$

Thus, in terms of the generalized coordinates, the virtual work of the $\boldsymbol{F}_i^a$ becomes

$$\sum_i \boldsymbol{F}_i^a \cdot \delta \boldsymbol{r}_i = \sum_{i,j} \boldsymbol{F}_i^a \cdot \frac{\partial \boldsymbol{r}_i}{\partial q_j} \delta q_j = \sum_j \mathcal{Q}_j \delta q_j, \tag{2.26}$$

where the

$$\mathcal{Q}_j \triangleq \sum_i \boldsymbol{F}_i^a \cdot \frac{\partial \boldsymbol{r}_i}{\partial q_j} \tag{2.27}$$

are called the components of the *generalized force*. The other term involved in (2.22) can be written as

$$\sum_i \dot{\boldsymbol{p}}_i \cdot \delta \boldsymbol{r}_i = \sum_i m_i \ddot{\boldsymbol{r}}_i \cdot \delta \boldsymbol{r}_i = \sum_{i,j} m_i \ddot{\boldsymbol{r}}_i \cdot \frac{\partial \boldsymbol{r}_i}{\partial q_j} \delta q_j. \tag{2.28}$$

Using the product rule, we observe that

$$\sum_i m_i \ddot{\boldsymbol{r}}_i \cdot \frac{\partial \boldsymbol{r}_i}{\partial q_j} = \sum_i \left[\frac{\mathrm{d}}{\mathrm{d}t} \left(m_i \dot{\boldsymbol{r}}_i \cdot \frac{\partial \boldsymbol{r}_i}{\partial q_j} \right) - m_i \dot{\boldsymbol{r}}_i \cdot \frac{\mathrm{d}}{\mathrm{d}t} \left(\frac{\partial \boldsymbol{r}_i}{\partial q_j} \right) \right]. \tag{2.29}$$

In the last term of (2.29), we can interchange the order of differentiation

$$\frac{\mathrm{d}}{\mathrm{d}t} \left(\frac{\partial \boldsymbol{r}_i}{\partial q_j} \right) = \sum_k \frac{\partial^2 \boldsymbol{r}_i}{\partial q_k \partial q_j} \dot{q}_k + \frac{\partial^2 \boldsymbol{r}_i}{\partial t \partial q_j} = \frac{\partial \boldsymbol{v}_i}{\partial q_j}, \tag{2.30}$$

where the last equality follows from (2.24). Further, observe from (2.24) that

$$\frac{\partial \boldsymbol{v}_i}{\partial \dot{q}_j} = \frac{\partial \boldsymbol{r}_i}{\partial q_j}. \tag{2.31}$$

Substituting (2.30) and (2.31) in (2.29) yields

$$\sum_i m_i \ddot{\boldsymbol{r}}_i \cdot \frac{\partial \boldsymbol{v}_i}{\partial \dot{q}_j} = \sum_i \left[\frac{\mathrm{d}}{\mathrm{d}t} \left(m_i \boldsymbol{v}_i \cdot \frac{\partial \boldsymbol{v}_i}{\partial \dot{q}_j} \right) - m_i \boldsymbol{v}_i \cdot \left(\frac{\partial \boldsymbol{v}_i}{\partial q_j} \right) \right]. \tag{2.32}$$

Introducing the kinetic energy $\mathcal{T} \triangleq \frac{1}{2} \sum_i m_i \boldsymbol{v}_i \cdot \boldsymbol{v}_i$ the sum above can be rewritten as

$$\sum_{i,j} m_i \ddot{\boldsymbol{r}}_i \cdot \frac{\partial \boldsymbol{v}_i}{\partial \dot{q}_j} = \sum_i \left[\frac{\mathrm{d}}{\mathrm{d}t} \left(\frac{\partial \mathcal{T}}{\partial \dot{q}_j} \right) - \frac{\partial \mathcal{T}}{\partial q_j} \right]. \tag{2.33}$$

Substituting (2.26), (2.27) and (2.33) in (2.22), then d'Alembert's principle becomes

$$\sum_j \left\{ \frac{\mathrm{d}}{\mathrm{d}t} \left(\frac{\partial \mathcal{T}}{\partial \dot{q}_j} \right) - \frac{\partial \mathcal{T}}{\partial q_j} - \mathcal{Q}_j \right\} \delta q_j = 0. \tag{2.34}$$

Sine we assumed that the coordinates q_j are independent, any virtual displacement δq_j is then independent of δq_k, and we can conclude that (2.34) can only hold if each of the coefficients of vanishes:

$$\frac{\mathrm{d}}{\mathrm{d}t} \left(\frac{\partial \mathcal{T}}{\partial \dot{q}_j} \right) - \frac{\partial \mathcal{T}}{\partial q_j} = \mathcal{Q}_j, \quad j = 1, \ldots, n. \tag{2.35}$$

Suppose, we can split the applied forces into forces that are derivable from a potential function $\mathcal{V}$ and externally applied forces $\boldsymbol{F}_i'$ such that

$$\boldsymbol{F}_i^{(a)} = -\frac{\partial \mathcal{V}}{\partial q_i} + \boldsymbol{F}_i'. \tag{2.36}$$

Using (2.26) it follows that

$$\mathcal{Q}_j = \sum_i \left[-\frac{\partial \mathcal{V}}{\partial q_i}\frac{\partial \boldsymbol{r}_i}{\partial q_j} + \boldsymbol{F}_i'\frac{\partial \boldsymbol{r}_i}{\partial q_j}\right], \tag{2.37}$$

where the first term on the RHS can be identified as the partial derivative of a potential function $\mathcal{V}(\boldsymbol{r}_1, \dots, \boldsymbol{r}_N, t)$ with respect to q_j. Introducing

$$\mathcal{Q}_j \triangleq -\frac{\partial \mathcal{V}}{\partial q_j} + \mathcal{Q}_j', \tag{2.38}$$

with $\mathcal{Q}_j' \triangleq \boldsymbol{F}_i'\frac{\partial \boldsymbol{r}_i}{\partial q_j}$, we can rewrite (2.35) as

Note that the equations of motions (2.39) are not restricted to conservative systems.

$$\frac{\mathrm{d}}{\mathrm{d}t}\left(\frac{\partial \mathcal{T}}{\partial \dot{q}_j}\right) - \frac{\partial \mathcal{T}}{\partial q_j} = -\frac{\partial \mathcal{V}}{\partial q_j} + \mathcal{Q}_j'. \tag{2.39}$$

or defining a new function, the Lagrangian

$$\mathcal{L} \triangleq \mathcal{T} - \mathcal{V}, \tag{2.40}$$

as

$$\frac{\mathrm{d}}{\mathrm{d}t}\left(\frac{\partial \mathcal{L}}{\partial \dot{q}_j}\right) - \frac{\partial \mathcal{L}}{\partial q_j} = \mathcal{Q}_j', \quad j = 1, \dots, n, \tag{2.41}$$

and we have obtained the "Lagrange's equations".[9] Since these equations can be obtained equivalently from a variational principle (as pointed out in Section 10), they are also referred to as "Euler-Lagrange's equation".

9: A detailed derivation can be found in [52, p. 17 ff].

Whenever the generalized forces are derivable from a (generalized) potential function $\mathcal{V}(\boldsymbol{q}, \dot{\boldsymbol{q}})$ according to

$$\mathcal{Q}_j = \frac{\mathrm{d}}{\mathrm{d}t}\frac{\partial \mathcal{V}}{\partial \dot{q}_j} - \frac{\partial \mathcal{V}}{\partial q_j}, \tag{2.42}$$

we can write Lagrange's equations in the form

$$\frac{\mathrm{d}}{\mathrm{d}t}\frac{\partial \mathcal{T}}{\partial \dot{q}_j} - \frac{\partial \mathcal{T}}{\partial q_j} = \frac{\mathrm{d}}{\mathrm{d}t}\frac{\partial \mathcal{V}}{\partial \dot{q}_j} - \frac{\partial \mathcal{V}}{\partial q_j}. \tag{2.43}$$

The n quantities on the LHS can be interpreted as the n components of the force of inertia, the n quantities on the RHS can be identified as the components of the *moving force* or *potential force*. Thus, we can think of (2.43) as the balance between two forces.

Generators of Motion

Above, we have defined the Lagrangian as $\mathcal{L} = \mathcal{T} - \mathcal{V}$. However, for a given set of equations of motions, there is no unique choice of Lagrangian such that the Lagrangian equations (2.41) produce the equations of motion. It is easy to

make up alternative Lagrangians. Suppose that $\mathcal{L}(\boldsymbol{q}, \dot{\boldsymbol{q}}, t)$ is a Lagrangian that leads to the equations of motion and $F(\boldsymbol{q}, t)$ is any differentiable function of the generalized coordinates and time, then the Lagrangian

$$\tilde{\mathcal{L}}(\boldsymbol{q}, \dot{\boldsymbol{q}}, t) = \mathcal{L}(\boldsymbol{q}, \dot{\boldsymbol{q}}, t) + \frac{dF}{dt} \tag{2.44}$$

leads to the same equations of motion. In conclusion, constructing a Lagrangian as in (2.40) always provides a "valid" Lagrangian, but it does not produce the only valid Lagrangian. There are systems which can can be treated by the Lagrangian method, but for which the Lagrangian is not just the excess of kinetic over potential energy. A charged particle in an electric field, electromechanical systems or non-conservative mechanical systems are just a few systems that are often treated with a Lagrangian that does not equal $\mathcal{T} - \mathcal{V}$. The interested reader can consult, e.g, [52, 61, 63]. Naturally, the question arises: what is the definition of the Lagrangian? Throughout this work, we shall use the definition from [181, p. 272] below.

Definition 2.4.1 (The Lagrangian) *For a given system with generalized coordinates $\boldsymbol{q} = (q_1, \dots, q_n)$, a Lagrangian $\mathcal{L}$ is a function $\mathcal{L}(q_1, \dots, q_n, \dot{q}_1, \dots, \dot{q}_n, t)$ of the coordinates and velocities, such that the correct equations of motion for the system are the Lagrangian equations* (2.41).

In other words, given some system, then a Lagrangian is any function $\mathcal{L}$ that generates the corresponding Lagrange's equations of motion. Calculating the Hamiltonian, using the usual definition of $\mathcal{H}$ as the Legendre transformation of $\mathcal{L}$, then it corresponds to the total energy of the system

$$\mathcal{H} = \sum_i \dot{q}_i \frac{\partial \mathcal{L}}{\partial \dot{q}_i} - \mathcal{L} = \mathcal{T} + \mathcal{V} \tag{2.45}$$

if the Lagrangian is defined as in (2.40). In Chapter 5, we face a scenario where the Lagrangian equates to the excess of some virtual kinetic over some virtual potential energy, but nevertheless produces the equations of motions. The corresponding Hamiltonian, however, does not equate to the total energy of the system. In cases where the Lagrangian is not of the form (2.40), or the Hamiltonian is not equal to the total energy, these scalar quantities are often referred to as mathematical Lagrangians (Hamiltonians) or merely generators of the motion in physics [37]. This notion is adopted throughout this work.

2.4.3 Hamilton's Principle

In the previous subsection, we derived Lagrange's equations starting from d'Alembert's principle which makes independent statements at each instant of time during the motion of a system. This principle operates on the instantaneous state of a system and infinitesimal virtual displacements; it requires the vanishing of the virtual work at any time. It it possible to derive Lagrange's equations from a principle of very different nature that considers the entire motion of a system between a given initial point P_1 at a time t_1 and a given end-point P_2 at a time t_2. We can think of this principle working as follows. Unknowing which path is taken by the system, let us start by connecting the two points P_1 and P_2 by any tentative path. All that we require is that our tentative motion starts at time t_1 and ends at time t_2. Next, we compute the

kinetic energy at every moment on the path and subtract the potential energy, and integrate it over the time during the entire path. This time integral is called *action* and has a definite value for our tentative path and any other tentative path that connects P_1 and P_2. For any such conceivable motion it is assumed that the path is transversed in an equal amount of time. We can imagine trying out all possible path and with each path, we associate a certain number, the action. For some paths it will come out bigger and for some smaller. Hamilton's principle tells us, out of all the possible paths by with the C-point could travel from point P_1 to P_2, it will actually travel along that path for which the value of action assumes its smallest[10] value. For monogenic systems, Hamilton's principle can be stated as [52, p.34]:

10: More precisely, Hamilton's principle tells us that the action has a stationary value for the actual path of motion.

The motion of the system from time t_1 to time t_2 is such that the line integral (called the action),

$$I = \int_{t_1}^{t_2} \mathcal{L}\, dt, \tag{2.46}$$

where $\mathcal{L} = \mathcal{T} - \mathcal{V}$, has a stationary value for the actual path of the motion.

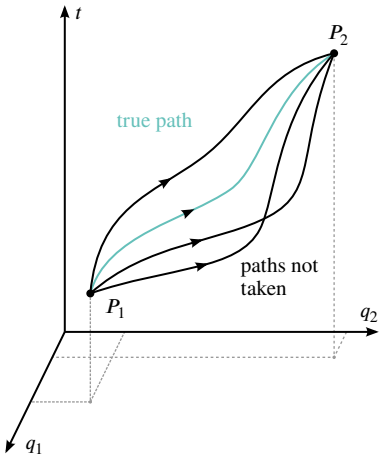

Figure 2.7: As the system evolves, its C-point traces a path through the configuration space. Of all possible paths between two points, the actual path taken has a stationary action.

We can imagine that all possible paths have been tried and for each tentative path the action has a definite value, c.f. Fig. 2.7. Hamilton's principle asserts that for the actual path chosen by nature, the value of this integral is stationary. The meaning attached to "stationary value" of a line integral is that the integral along a given path has the same value within first-order infinitesimals as that along all neighboring paths (i.e., those that differ from it by infinitesimal displacements). In summary, Hamilton's states that the motion of a mechanical system is such that the integral I becomes stationary for prescribed initial and final configurations

$$\delta I = \delta \int_{t_1}^{t_2} \mathcal{L}(\boldsymbol{q}, \dot{\boldsymbol{q}}, t)\, dt = 0. \tag{2.47}$$

It can be shown that Hamilton's principle and d'Alembert's principle are mathematical equivalent for any system that is subject to holonomic constraints and monogenic impressed forces [103, p.114]. D'Alembert's principle, however, is more general since it can equally well be applied to non-holonomic systems.

Calculus of Variations

Hamilton's principle is a necessary and sufficient condition for Lagrange's equations (2.41). The techniques of the calculus of variation allows us to demonstrate that Lagrange's equations indeed follow from Hamilton's principle. We are interested in the following variational problem. Let $f(x, y_1, \dots, y_n, y_1', \dots, y_n')$ be a function with continuous first and second (partial) derivatives with respect to all its arguments, which depends on n continuously differentiable functions $y_1(x), \dots, y_2(x)$ that satisfy the boundary conditions

$$y_i(x_1) = a_i, \quad y_i(x_2) = b_i, \quad i = 1, \dots, n. \tag{2.48}$$

Then, what are the necessary conditions for an extremum of a functional of form

$$J[y_1, \dots, y_2] = \int_{x_1}^{x_2} f(x, y_1, \dots, y_n, y_1', \dots, y_n')\, dx. \tag{2.49}$$

From the geometric point of view, we are searching for an extremum of the functional (2.49) that is defined on the set of smooth curves joining two fixed points in a $(n+1)$-dimensional Euclidean space. The solution to this optimization problem is summarized in the following theorem.

Theorem 2.4.1 (Euler-Lagrange equations [49]) *A necessary condition for the curve*

$$y_i = y_i(x), \quad i = 1, \dots, n$$

to be an extremal of the functional (2.49) *is that the functions* $y_i(x)$ *satisfy the -Lagrange equations*

$$\frac{\partial f}{\partial y_i} - \frac{d}{dx}\frac{\partial f}{\partial y_i'} = 0, \quad i = 1, \dots, n$$

Applying the EL equations to the integral in Hamilton's principle with the transformations

$$\begin{aligned} x &\to t \\ y_i &\to q_i \\ f(y_i, \dot{y}_i, t) &\to \mathcal{L}(q_i, \dot{q}_i, t). \end{aligned}$$

we obtain the Lagrange equations of motion

$$\frac{\mathrm{d}}{\mathrm{d}t}\frac{\partial \mathcal{L}}{\partial \dot{q}_i} - \frac{\partial \mathcal{L}}{\partial q_i} = 0, \quad i = 1, \dots, n$$

for non-monogenic systems with holonomic constraints. Further generalizations of the variational problem (2.49) are possible. The functional f a can be dependent on higher order derivatives $y', y^{(2)}, \dots, y^{(n)}$, see [61]

$$\int_{x_1}^{x_2} f\left(x, y_1, \dots, y_n, y_1', \dots, y_1^{(n)}, \dots, y_n^{(n)}\right) dx,$$

or even on multiple parameters x_j, see [49] for details.

2.5 The Lagrange's Equations

In his monumental treatise on analytical mechanics (*Mécanique Analytique*, [101]), Lagrange reduced the theory and art of solving mechanics problems into general formula [101]. By introducing a scalar quantity expressing the excess of kinetic over potential energy, we can obtain the EL equations (2.41) by applying the *principle of stationary action*. This section reports fundamental properties of these equations that are crucial for the developments in this work. We will focus our attention on systems for which the following properties and assumptions hold. Consider a n degrees of freedom system with the

[101]: Lagrange (1853), *Mécanique Analytique*

generalized coordinates $\boldsymbol{q} \in \mathbb{R}^n$ and applied external forces $\mathcal{Q} \in \mathbb{R}^n$ that is described by the Lagrange's equations

$$\underbrace{\frac{\mathrm{d}}{\mathrm{d}t}\frac{\partial \mathcal{T}}{\partial \dot{q}_i} - \frac{\partial \mathcal{T}}{\partial q_i}}_{\text{inertial}} = \underbrace{\frac{\mathrm{d}}{\mathrm{d}t}\frac{\partial \mathcal{V}}{\partial \dot{q}_i} - \frac{\partial \mathcal{V}}{\partial q_i}}_{\text{monogenic}} + \underbrace{\mathcal{Q}_i}_{\text{non-monogenic}}, \tag{2.50}$$

where the kinetic energy is assumed to be of quadratic form.

Assumption 2.5.1 *The kinetic energy is assumed to be a quadratic form*

$$\mathcal{T}(\boldsymbol{q}, \dot{\boldsymbol{q}}) = \frac{1}{2}\sum_{i,j} m_{ij}(\boldsymbol{q})\dot{q}_i\dot{q}_j = \frac{1}{2}\dot{\boldsymbol{q}}^T\mathcal{M}(\boldsymbol{q})\dot{\boldsymbol{q}}, \tag{2.51}$$

where the (generalized) inertia matrix $\mathcal{M}$ is symmetric and positive definite for any $\boldsymbol{q} \in \mathbb{R}^n$.

We will face two kind of generalized forces throughout this work: *monogenic* forces that are arise from a potential function $\mathcal{V}$ and the *non-monogenic* forces. The latter can be further classified into three types: (1) the control actions $\boldsymbol{u}$, (2) forces that are due to the system's interaction with the environment $\mathcal{Q}'$ and (3) dissipative forces $\mathcal{Q}^d$.[11] In summary, we have that

$$\mathcal{Q} \triangleq \boldsymbol{u} + \mathcal{Q}' + \mathcal{Q}^d. \tag{2.52}$$

11: Note that the control force can be chosen such that it is derivable from a potential, however, in general this will not be the case in this work. The same is true for the dissipative forces, which may, e.g., be obtained from a Rayleigh potential function.

2.5.1 The Force of Inertia

For any system satisfying Assumption 2.5.1, the components of the force of inertia

$$\mathcal{Q}_i^\star \triangleq -\left\{\frac{\mathrm{d}}{\mathrm{d}t}\frac{\partial \mathcal{T}}{\partial \dot{q}_i} - \frac{\partial \mathcal{T}}{\partial q_i}\right\}, \tag{2.53}$$

can be derived as follows. Knowing that

$$\begin{aligned}\frac{\mathrm{d}}{\mathrm{d}t}\frac{\partial \mathcal{T}}{\partial \dot{q}_i} &= \sum_j \left[m_{ij}\ddot{q}_j + \frac{\mathrm{d}}{\mathrm{d}t}m_{ij}\dot{q}_j\right] \\ &= \sum_j m_{ij}\ddot{q}_j + \sum_{k,j}\frac{\partial m_{ij}}{\partial q_i}\dot{q}_k\dot{q}_j\end{aligned} \tag{2.54}$$

and

$$\frac{\partial \mathcal{T}}{\partial q_i} = \frac{1}{2}\sum_{k,j}\frac{\partial m_{kj}}{\partial q_i}\dot{q}_k\dot{q}_j, \tag{2.55}$$

we can apply these changes to (2.53):

$$\mathcal{Q}_i^\star = -\left\{\sum_j m_{ij}\ddot{q}_j + \sum_{k,j}\left[\frac{\partial m_{ij}}{\partial q_k}\dot{q}_k\dot{q}_j - \frac{1}{2}\frac{\partial m_{kj}}{\partial q_i}\dot{q}_k\dot{q}_j\right]\right\} \tag{2.56}$$

By exchanging indices and interchanging the order of summation it follows that[12]

12: Note that $\sum_{k,j}\frac{\partial m_{ij}}{\partial q_k} = \sum_{j,k}\frac{\partial m_{ik}}{\partial q_j} = \sum_{k,j}\frac{\partial m_{ik}}{\partial q_j}$.

$$\sum_{k,j} \frac{\partial m_{ij}}{\partial q_k} \dot{q}_k \dot{q}_j = \frac{1}{2} \sum_{k,j} \left[\frac{\partial m_{ij}}{\partial q_k} + \frac{\partial m_{ik}}{\partial q_j} \right] \dot{q}_k \dot{q}_j. \tag{2.57}$$

Making the substitution (2.56) and (2.57), we get

$$\mathcal{Q}_i^\star = -\left\{ \sum_j m_{ij}(\boldsymbol{q}) \ddot{q}_j + \sum_{k,j} c_{kji}(\boldsymbol{q}) \dot{q}_k \dot{q}_j \right\}, \tag{2.58}$$

where

$$c_{kij} = \frac{1}{2} \left[\frac{\partial m_{ij}}{\partial q_k} + \frac{\partial m_{ik}}{\partial q_j} - \frac{\partial m_{kj}}{\partial q_i} \right] \tag{2.59}$$

are the so called Christoffel symbols of the first kind. Note that for a fixed i, we have that $c_{kji} = c_{ijk}$ [171, p. 207]. In equation (2.58), we can identify two type of terms. The first involves the second time derivative of the generalized coordinates. The second are quadratic in the generalized velocities with the coefficient potentially depending on $\boldsymbol{q}$. The latter are further classified into two types. Terms involving q_i^2, i.e. $k = j$, constitute the centrifugal forces, whiles those involving $q_i q_j$, $k \neq j$, constitute the Coriolis forces. It is common to introduce the matrix $C(\boldsymbol{q}, \dot{\boldsymbol{q}})$ whose components are defined as

$$c_{ij} = \sum_k c_{kij}(\boldsymbol{q}) \dot{q}_k, \tag{2.60}$$

which is called the *Coriolis/centrifugal matrix* in robotics literature. Using this factorization of the Coriolis/centripetal matrix, allows us to rewrite the force of inertia in matrix form:

$$\mathcal{Q}^\star = -\left[\mathcal{M}(\boldsymbol{q}) \ddot{\boldsymbol{q}} + \mathcal{C}(\boldsymbol{q}, \dot{\boldsymbol{q}}) \dot{\boldsymbol{q}} \right]. \tag{2.61}$$

For any system whose kinetic energy can be written in terms of the quadratic form (2.51), we can apply this factorization. The inertia matrix and the Coriolis/centrifugal matrix satisfy the so-called *skew-symmetry* property, which shall be of central importance for the control developments in later chapters.

Lemma 2.5.1 *The matrix C in* (2.61) *satisfies*

$$\dot{\boldsymbol{q}}^T \left(\dot{\mathcal{M}} - 2\mathcal{C} \right) \dot{\boldsymbol{q}} = 0, \ \forall \dot{\boldsymbol{q}} \in \mathbb{R}^n. \tag{2.62}$$

Let the ijth entries of matrix $C(\boldsymbol{q}, \dot{\boldsymbol{q}})$, (2.60)*, be defined via the Christoffel symbols of the first kind as in* (2.59)*, then the matrix*

$$\dot{\mathcal{M}} - 2\mathcal{C}(\boldsymbol{q}, \dot{\boldsymbol{q}}), \quad \forall \boldsymbol{q}, \dot{\boldsymbol{q}} \in \mathbb{R}^n. \tag{2.63}$$

is skew-symmetric. Notice that the skew-symmetry property (2.63) *is equivalent to*

$$\dot{\mathcal{M}}(\boldsymbol{q}) = \mathcal{C}(\boldsymbol{q}, \dot{\boldsymbol{q}}) + C^T(\boldsymbol{q}, \dot{\boldsymbol{q}}). \tag{2.64}$$

A proof is presented in [131].

Remark 2.5.1 Note that (2.62) is always true no matter how $C(\boldsymbol{q}, \dot{\boldsymbol{q}})$ is factorized. This property follows directly from the law of conservation of

energy. However, (2.63) only holds for the factorization applied above, see [131] for details.

2.5.2 Non-Conservative Systems

Unfortunately it is difficult to account for input or dissipative forces in the Lagrange-Hamiltonian variational formulation. In the presence of friction forces or time-dependent input forces, the virtual work of the forces of constraint no longer vanishes. This, however, is a central postulate regarding the treatment of dynamics via d'Alembert's principle. Since the Hamiltonian principle is just an alternative mathematical formulation of d'Alembert's principle, troubles are evident.

For some of the systems in this work, the Lagrange formalism can be extended to include explicitly time-dependent potential functions and have no relation to the physical energy. Let us consider the following types of non-monogenic forces: the control force $\boldsymbol{u}$ and disturbance force $\mathcal{Q}'$ (independent of generalized coordinates and velocities), and Rayleigh dissipation. The former two can be incorporated in a non-conservative potential function

$$\mathcal{V}_{nc}(\boldsymbol{q}, t) = -\left(\boldsymbol{u} + \mathcal{Q}'\right)^{\mathrm{T}} \boldsymbol{q}, \tag{2.65}$$

and the latter can be incorporated in a non-conservative kinetic energy, which is the Rayleigh dissipation function

$$\mathcal{T}_{nc}(\dot{\boldsymbol{q}}) = \int_0^t \mathcal{F}(\dot{\boldsymbol{q}}) dt. \tag{2.66}$$

Then, replacing $\mathcal{L}$ in (2.41) by the non-conservative Lagrangian [133, p. 489]

$$\mathcal{L}_{nc} = \mathcal{L}(\boldsymbol{q}, \dot{\boldsymbol{q}}) + \mathcal{T}_{nc}(\dot{\boldsymbol{q}}) - \mathcal{V}_{nc}(\boldsymbol{q}, t), \tag{2.67}$$

produces the desired Lagrange's equations of motion

$$\frac{\mathrm{d}}{\mathrm{d}t}\frac{\partial \mathcal{L}}{\partial \dot{q}_i} - \frac{\partial \mathcal{L}}{\partial q_i} = u_i + \mathcal{Q}'_i - \frac{\partial \mathcal{F}(\dot{\boldsymbol{q}})}{\partial \dot{q}_i}, \quad i = 1, \ldots, n. \tag{2.68}$$

2.5.3 Equilibrium and Stability Conditions

For a system subject to non-monogenic forces, the condition of *equilibrium* requires that the potential energy is stationary with respect to all kinematically permissible variations, i.e.,

$$\delta \mathcal{V} = \frac{\partial \mathcal{V}}{\partial \boldsymbol{q}} \delta \boldsymbol{q} = 0. \tag{2.69}$$

Since the $\boldsymbol{q}$'s are independent coordinates it must be that

$$\frac{\partial \mathcal{V}}{\partial q_i} = 0, \quad i = 1, \ldots, n. \tag{2.70}$$

There is a crucial connection between the notion of equilibrium and the concept of *stability*. Joseph Lagrange stated already in 1788 that a conservative mechanical system is stable if the potential energy $\mathcal{V}$ assumes a minimum in this position. This result was later proven by Dirichlet [117, p. 76] and is

[117]: Merkin (1997), *Introduction to the Theory of Stability*

now known as the Lagrange-Dirichlet theorem. The following proposition summarizes conditions for the global asymptotic stability (GAS) of fully damped[13] EL systems.

13: The damping due to dissipative forces and represented by the symmetric coefficient matrix $\mathcal{K}_v$ is said to be *full* or *pervasive* if the quadratic form $-\dot{\boldsymbol{q}}^{\mathrm{T}}\mathcal{K}_v\dot{\boldsymbol{q}}$ is negative definite and does not vanish for any non-trivial solution $\boldsymbol{q}(t), t > 0$ of the EL equations (2.41) [157].

Proposition 2.5.2 (GAS with full damping [133, p. 28]) *Let the equilibrium of a fully damped unforced EL system, i.e., with $\mathcal{Q}' = 0$, be $(\boldsymbol{q}, \dot{\boldsymbol{q}}) = (\boldsymbol{q}^*, \boldsymbol{0})$, where $\boldsymbol{q}^*$ is the solution of*

$$\frac{\partial \mathcal{V}(\boldsymbol{q})}{\partial \boldsymbol{q}} = \boldsymbol{0}.$$

The equilibrium is stable if $\boldsymbol{q}^*$ is a strict local minimum of the potential energy function $\mathcal{V}(\boldsymbol{q})$, which is such that

- $\frac{\partial \mathcal{V}}{\partial \boldsymbol{q}}(\boldsymbol{q}) = \boldsymbol{0} \iff \boldsymbol{q} = \boldsymbol{0}$,
- $\frac{\partial^2 \mathcal{V}}{\partial \boldsymbol{q}^2}(\boldsymbol{q}^*) > \epsilon, \boldsymbol{I} > 0$, *for all* $\boldsymbol{q} \in \mathbb{R}^n$.

Furthermore, if $\mathcal{V}(\boldsymbol{q})$ assumes a unique strict and global minimum at $\boldsymbol{q}^*$, then this equilibrium is GAS.

The proof can be established by invoking, e.g., La-Salle's or Krasovskii's Theorem (see Theorems C.1.3 and C.1.1 in Appendix C). An alternative proof that underscores the role of passivity and detectability is provided in [133, p. 28].

Remark 2.5.2 By dropping the condition of $\mathcal{V}$ being radially unbounded, we can conclude only local asymptotic stability. In that case, the proof of Proposition 2.5.2 can be established invoking Barbashin's Theorem (see Theorem C.1.2 in Appendix C). Such an equilibrium condition can be interesting when it comes to ASRs featuring elastic elements with a flattening force-deflection profile, or when it comes to designing impedance controllers with saturation functions; see, e.g., [44].

[44]: Folkertsma et al. (2017), *Energy in Robotics*

Given a block diagonal structure of the inertia matrix, the GAS of an unique equilibrium point can be ensured even when the system is partially damped. The conditions are summarized below.

Proposition 2.5.3 (GAS with partial damping [133, p. 29]) *Consider an unforced underdamped EL system* (2.50) *with a coordinate partition into undamped and damped coordinates:*

$$\boldsymbol{q}_p \triangleq \begin{bmatrix} \boldsymbol{I}_{n_p} & \boldsymbol{0} \end{bmatrix} \boldsymbol{q}, \quad \boldsymbol{q}_c \triangleq \begin{bmatrix} \boldsymbol{0} & \boldsymbol{I}_{n_c} \end{bmatrix} \boldsymbol{q}, \qquad n = n_p + n_c. \tag{2.71}$$

The equilibrium $(\boldsymbol{q}, \dot{\boldsymbol{q}}) = (\boldsymbol{q}_d, \boldsymbol{0})$ is GAS if the potential energy function is proper and has a global and unique minimum at $\boldsymbol{q} = \boldsymbol{q}_d$, and if

(i) $\mathcal{M}(\boldsymbol{q}) \triangleq \operatorname{diag}\left(\boldsymbol{M}_p(\boldsymbol{q}_p), \boldsymbol{M}_c(\boldsymbol{q}_c)\right)$, *where* $\boldsymbol{M}_p(\boldsymbol{q}_p) \in \mathbb{R}^{n_p \times n_p}$ *and* $\boldsymbol{M}_c(\boldsymbol{q}_c) \in \mathbb{R}^{n_c \times n_c}$;

(ii) $\dot{\boldsymbol{q}}^T \frac{\partial \mathcal{F}(\dot{\boldsymbol{q}})}{\partial \dot{\boldsymbol{q}}} \geq \alpha ||\dot{\boldsymbol{q}}_c||^2$ *for some* $\alpha > 0$;

(iii) For each $\boldsymbol{q}_c$, the function $\frac{\partial \mathcal{V}(\boldsymbol{q})}{\partial \boldsymbol{q}_c} = \boldsymbol{0}$ has only isolated zeros in $\boldsymbol{q}_p$.

The motivation for subindices $(.)_p$ and $(.)_c$, which suggest plant and controller, becomes clear in Section 6.3.

2.5.4 Passivity and Interconnection Properties

The notion of *passivity* plays a fundamental role in this work. To understand passivity, we must introduce two functions: the *supply rate* (the rate at which a system exchanges energy) and the *storage function* (a measure for the energy stored in a system). In a passive system the increase in stored energy is at most equal to the energy supplied. A formal definition of passivity is given in Definition C.3.2 in Appendix C. A well known result concerning the passivity of EL systems (2.41) is summarized below.

Proposition 2.5.4 (Passivity of EL systems [133, p. 20]) *The EL system* (2.50) *with* $\mathcal{Q}' = \mathcal{Q}^d = \mathbf{0}$ *defines a passive operator* $\Sigma : \boldsymbol{u} \mapsto \dot{\boldsymbol{q}}$ *with storage function the systems total energy* $\mathcal{H}(\boldsymbol{q}, \dot{\boldsymbol{q}})$*. That is*

$$\mathcal{H}\big(\boldsymbol{q}(t_1), \dot{\boldsymbol{q}}(t_1)\big) \leq \mathcal{H}\big(\boldsymbol{q}(t_0), \dot{\boldsymbol{q}}(t_0)\big) + \int_{t_0}^{t_1} \boldsymbol{u}^T \dot{\boldsymbol{q}} dt \tag{2.72}$$

for all $t_1 > t_0$ *and all bounded* $\boldsymbol{u}$*. Further, this property is strengthened to output strict passivity (OSP) if the system is fully damped.*

This, together with the fact that passivity is invariant under feedback interconnection, lead to the idea of looking for passivity based controllers among the class of EL systems [134, 138]. Defining the control interconnection via the potential forces preserves the EL structure and—importantly—the behavior of the resulting EL system can be obtain by simply adding up the kinetic and potential energies of the plant and controller. This idea is summarized in the proposition below.

Proposition 2.5.5 (Interconnected EL Systems [133, p. 27]) *Consider two EL systems*

$$\Sigma_p : \big\{\mathcal{T}_p(\boldsymbol{q}_p, \dot{\boldsymbol{q}}_p), \mathcal{V}_p(\boldsymbol{q}_p), \mathcal{F}_p(\dot{\boldsymbol{q}}_p)\big\}; \quad \Sigma_c : \big\{\mathcal{T}_c(\boldsymbol{q}_c, \dot{\boldsymbol{q}}_c), \mathcal{V}_c(\boldsymbol{q}), \mathcal{F}_c(\dot{\boldsymbol{q}}_c)\big\}$$

with the generalized coordinates $\boldsymbol{q}_p \in \mathbb{R}^{n_p}$, $\boldsymbol{q}_c \in \mathbb{R}^{n_2}$ *and* $\boldsymbol{q} \triangleq [\boldsymbol{q}_p^T, \boldsymbol{q}_c^T]^T$*, respectively, (notice that the potential energy of* Σ_c *depends on* $\boldsymbol{q}_p$*). Interconnect the systems via:*

$$\boldsymbol{u} = -\frac{\partial \mathcal{V}_c(\boldsymbol{q})}{\partial \boldsymbol{q}_p},$$

where $\boldsymbol{u} \in \mathbb{R}^{n_p}$ *is the input of the subsystem* Σ_p*. See Fig. 2.8. Under these conditions, the closed-loop system is an EL system* $\Sigma : \{\mathcal{T}(\boldsymbol{q}, \dot{\boldsymbol{q}}), \mathcal{V}(\boldsymbol{q}), \mathcal{F}(\dot{\boldsymbol{q}})\}$*, with the EL parameters:*

$$\begin{aligned} \mathcal{T}(\boldsymbol{q}, \dot{\boldsymbol{q}}) &= \mathcal{T}_c(\boldsymbol{q}_c, \dot{\boldsymbol{q}}_c) + \mathcal{T}_p(\boldsymbol{q}_p, \dot{\boldsymbol{q}}_p), \\ \mathcal{V}(\boldsymbol{q}) &= \mathcal{V}_c(\boldsymbol{q}_c, \boldsymbol{q}_p) + \mathcal{V}_p(\boldsymbol{q}_p), \\ \mathcal{F} &= \mathcal{F}_c(\dot{\boldsymbol{q}}_c) + \mathcal{F}_p(\dot{\boldsymbol{q}}_p). \end{aligned}$$

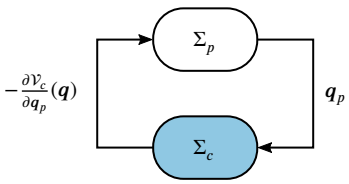

Figure 2.8: Feedback interconnection of two EL systems.

2.5.5 Transformations of Lagrangians

The Lagrange's equations of motion have the remarkable property that the form of the equations remains invariant with respect to transformations of

the generalized coordinates. Due to the importance of this result, we shall prove it. Understanding the proof is important to apprehend the scope of this statement. In particular, it facilitates understanding to which class of transforming equations this statement applies.

Corollary 2.5.6 (Invariance of the Euler-Lagrange equations) *Let $q_1, \dots, q_n$ be a set of independent generalized coordinates for a monogenic system of n degrees of freedom, with a Lagrangian $\mathcal{L}(\boldsymbol{q}, \dot{\boldsymbol{q}}, t)$. Suppose, we transform to another set of generalized coordinates $\bar{\boldsymbol{q}} = (\bar{q}_1, \dots, \bar{q}_n)$ by means of n transforming equations:*

$$q_i = q_i(\bar{\boldsymbol{q}}, t), \quad i = 1, \dots, n. \tag{2.73}$$

Then, the EL equations are invariant under such transformation. If the Lagrangian function is expressed as a function of $(\bar{q}_j, \dot{\bar{q}}_j, t)$ through the transforming equations, then $\mathcal{L}$ satisfies:

$$\frac{\mathrm{d}}{\mathrm{d}t}\frac{\partial \mathcal{L}}{\partial \dot{\bar{q}}_j} - \frac{\partial \mathcal{L}}{\partial \bar{q}_j} = \sum_i \left[Q_i \frac{\partial q_i}{\partial \bar{q}_j} \right]. \tag{2.74}$$

Proof. First, note that deriving (2.73) with respect to time yields

$$\dot{q}_i = \frac{dq_i}{dt} = \sum_j \frac{\partial \bar{q}_i}{\partial q_j}\dot{\bar{q}}_j + \frac{\partial q_i}{\partial t}. \tag{2.75}$$

and that[14]

$$\frac{\mathrm{d}}{\mathrm{d}t}\left(\frac{\partial \mathcal{L}}{\partial \dot{\bar{q}}_j}\right) = \frac{\mathrm{d}}{\mathrm{d}t}\sum_i \left[\frac{\partial \mathcal{L}}{\partial q_i}\frac{\partial q_i}{\partial \dot{\bar{q}}_j} + \frac{\partial \mathcal{L}}{\partial \dot{q}_i}\frac{\partial \dot{q}_i}{\partial \dot{\bar{q}}_j} \right], \tag{2.76}$$

$$\frac{\partial \mathcal{L}}{\partial \bar{q}_j} = \sum_i \left[\frac{\partial \mathcal{L}}{\partial q_i}\frac{\partial q_i}{\partial \bar{q}_j} + \frac{\partial \mathcal{L}}{\partial \dot{q}_i}\frac{\partial \dot{q}_i}{\partial \bar{q}_j} \right]. \tag{2.77}$$

14: Since t is an independent variable we have that $\frac{\partial \mathcal{L}}{\partial t}\frac{\partial t}{\partial \bar{q}_i} = 0$.

Knowing that

$$\frac{\partial q_i}{\partial \dot{\bar{q}}_i} = 0, \tag{2.78}$$

$$dq_i = \sum_j \frac{\partial q_i}{\partial \bar{q}_j} d\bar{q}_j + \frac{\partial q_i}{\partial t}dt, \tag{2.79}$$

$$\frac{dq_i}{dt} = \sum_j \frac{\partial q_i}{\partial \bar{q}_j}\frac{d\bar{q}_j}{dt} + \frac{\partial q_i}{\partial t}, \tag{2.80}$$

$$\dot{q}_i = \sum_j \frac{\partial q_i}{\partial \bar{q}_j}\dot{\bar{q}}_j + \frac{\partial q_i}{\partial t}, \tag{2.81}$$

$$\frac{\partial \dot{q}_i}{\partial \dot{\bar{q}}_j} = \frac{\partial q_i}{\partial q_j}, \tag{2.82}$$

we can apply these changes to (2.76) and obtain:

$$\frac{\mathrm{d}}{\mathrm{d}t}\left(\frac{\partial \mathcal{L}}{\partial \dot{\bar{q}}_j}\right) = \frac{\mathrm{d}}{\mathrm{d}t}\sum_i \left[\frac{\partial \mathcal{L}}{\partial \dot{q}_i}\frac{\partial q_i}{\partial \bar{q}_j} \right] = \sum_i \left[\frac{\mathrm{d}}{\mathrm{d}t}\left(\frac{\partial \mathcal{L}}{\partial \dot{q}_i}\right)\frac{\partial q_i}{\partial \bar{q}_j} + \frac{\partial \mathcal{L}}{\partial \dot{q}_i}\frac{\mathrm{d}}{\mathrm{d}t}\left(\frac{\partial q_i}{\partial \bar{q}_j}\right) \right] \tag{2.83}$$

Given that $\mathcal{L}$ satisfies the EL equations for the set of coordinates $\boldsymbol{q}$, we know

that

$$\frac{\mathrm{d}}{\mathrm{d}t}\left(\frac{\partial \mathcal{L}}{\partial \dot{q}_i}\right) = \frac{\partial \mathcal{L}}{\partial q_i} + \mathcal{Q}_i. \tag{2.84}$$

Using the symmetry of second derivatives (Schwarz's theorem), we may write:

$$\begin{aligned}\frac{\mathrm{d}}{\mathrm{d}t}\left(\frac{\partial q_i}{\partial \bar{q}_j}\right) &= \sum_k \left[\frac{\partial}{\partial \bar{q}_k}\left(\frac{\partial q_i}{\partial \bar{q}_j}\right)\frac{d\bar{q}_k}{dt} + \frac{\partial}{\partial t}\left(\frac{\partial q_i}{\partial \bar{q}_j}\right)\right] \\ &= \sum_k \left[\frac{\partial}{\partial \bar{q}_j}\left(\frac{\partial q_i}{\partial \bar{q}_k}\right)\dot{\bar{q}}_k + \frac{\partial}{\partial \bar{q}_j}\left(\frac{\partial q_i}{\partial t}\right)\right] \\ &= \frac{\partial}{\partial \bar{q}_j}\sum_k \left[\left(\frac{\partial q_i}{\partial \bar{q}_k}\right)\dot{\bar{q}}_k + \left(\frac{\partial q_k}{\partial t}\right)\right] = \frac{\partial \dot{q}_i}{\partial \bar{q}_j}.\end{aligned} \tag{2.85}$$

Equations (2.84) and (2.85) allows us to rewrite (2.83) as

$$\frac{\mathrm{d}}{\mathrm{d}t}\left(\frac{\partial \mathcal{L}}{\partial \dot{\bar{q}}_j}\right) = \sum_i \left[\left(\frac{\partial \mathcal{L}}{\partial q_i} + \mathcal{Q}_i\right)\frac{\partial q_i}{\partial \bar{q}_j} + \frac{\partial \mathcal{L}}{\partial \dot{q}_i}\left(\frac{\partial \dot{q}_i}{\partial \bar{q}_j}\right)\right] \tag{2.86}$$

$$= \sum_i \left[\left(\frac{\partial \mathcal{L}}{\partial q_i}\right)\frac{\partial q_i}{\partial \bar{q}_j} + \frac{\partial \mathcal{L}}{\partial \dot{q}_i}\left(\frac{\partial \dot{q}_i}{\partial \bar{q}_j}\right)\right] + \sum_i \left[\mathcal{Q}_i \frac{\partial q_i}{\partial \bar{q}_j}\right]. \tag{2.87}$$

Now making the substitutions (2.77) and (2.86) results in:

$$\frac{\mathrm{d}}{\mathrm{d}t}\left(\frac{\partial \mathcal{L}}{\partial \dot{\bar{q}}_j}\right) - \frac{\partial \mathcal{L}}{\partial \bar{q}_j} = \sum_i \left[\mathcal{Q}_i \frac{\partial q_i}{\partial \bar{q}_j}\right], \tag{2.88}$$

which proofs that Lagrange's equations are invariant to a point transformation of the form (2.73). ■

Let us denote the components of the transformed generalized external force by

$$\bar{\mathcal{Q}}_i = \sum_i \left[\mathcal{Q}_i \frac{\partial q_i}{\partial \bar{q}_j}\right]. \tag{2.89}$$

Knowing that

$$\frac{\partial \boldsymbol{q}}{\partial \bar{\boldsymbol{q}}} = \boldsymbol{J}^{-1}, \tag{2.90}$$

we can use (2.89) and (2.90) to establish the following relationship between the generalized external forces

$$\bar{\mathcal{Q}} = \boldsymbol{J}^{-\mathrm{T}}\mathcal{Q}, \tag{2.91}$$

where $\mathcal{Q}$ and $\bar{\mathcal{Q}}$ are both column vectors.

Outlook

In Chapter 5, we will face transformations of the form

$$q_i = q_i(\bar{q}, \dot{\bar{q}}, t), \quad i = 1, \ldots, n, \tag{2.92}$$

that do not qualify as point transformations, and it is important to understand that in such case the proof above fails to hold. In particular, (2.78) already fails to hold.

2.5.6 Transforming Inertial and Potential Forces

In the following, let us analyze how the inertial and potential forces transform under a point transformation

$$\bar{\boldsymbol{q}} = \boldsymbol{h}(\boldsymbol{q}); \quad \dot{\bar{\boldsymbol{q}}} = \boldsymbol{J}(\boldsymbol{q})\dot{\boldsymbol{q}}. \tag{2.93}$$

The relationship between the inertia matrices $\mathcal{M}$ and $\bar{\mathcal{M}}$ that are associated with the coordinates $\boldsymbol{q}$ and $\bar{\boldsymbol{q}}$, respectively, can be established by exploiting the *scalar invariance* of the Lagrangian[15] [42] from which follows for the kinetic energy that

$$\tfrac{1}{2}\dot{\boldsymbol{q}}^{\mathrm{T}}\mathcal{M}\dot{\boldsymbol{q}} = \dot{\bar{\boldsymbol{q}}}^{\mathrm{T}}\boldsymbol{J}^{-\mathrm{T}}\mathcal{M}\boldsymbol{J}^{-1}\dot{\bar{\boldsymbol{q}}} = \tfrac{1}{2}\dot{\bar{\boldsymbol{q}}}^{\mathrm{T}}\bar{\mathcal{M}}\dot{\bar{\boldsymbol{q}}}, \tag{2.94}$$

where

$$\bar{\mathcal{M}} = \boldsymbol{J}^{-\mathrm{T}}\mathcal{M}\boldsymbol{J}^{-1}. \tag{2.95}$$

Using the notation introduced above, the force of inertia associated with the $\boldsymbol{q}$'s is given by

$$\mathcal{Q}^{\star} = \frac{\mathrm{d}}{\mathrm{d}t}\left[\frac{\partial \mathcal{T}}{\partial \dot{\boldsymbol{q}}}\right]^{\mathrm{T}} - \left[\frac{\partial \mathcal{T}}{\partial \boldsymbol{q}}\right]^{\mathrm{T}} = \mathcal{M}\ddot{\boldsymbol{q}} + \boldsymbol{\nu}(\boldsymbol{q}, \dot{\boldsymbol{q}}), \tag{2.96}$$

where $\boldsymbol{\nu}$ denotes the Coriolis and centrifugal forces. As pointed out in Corollary 2.5.6, the EL equations transform under (2.93) as

$$\frac{\mathrm{d}}{\mathrm{d}t}\left[\frac{\partial \mathcal{L}}{\partial \dot{\boldsymbol{q}}}\right]^{\mathrm{T}} - \left[\frac{\partial \mathcal{L}}{\partial \boldsymbol{q}}\right]^{\mathrm{T}} = \mathcal{Q} \xrightarrow{(2.93)} \frac{\mathrm{d}}{\mathrm{d}t}\left[\frac{\partial \mathcal{L}}{\partial \dot{\bar{\boldsymbol{q}}}}\right]^{\mathrm{T}} - \left[\frac{\partial \mathcal{L}}{\partial \bar{\boldsymbol{q}}}\right]^{\mathrm{T}} = \bar{\mathcal{Q}}, \tag{2.97}$$

where $\bar{\mathcal{Q}} = \boldsymbol{J}^{-\mathrm{T}}\mathcal{Q}$, and the associated force of inertia is

$$\bar{\mathcal{Q}}^{\star} = \frac{\mathrm{d}}{\mathrm{d}t}\left[\frac{\partial \mathcal{T}}{\partial \dot{\bar{\boldsymbol{q}}}}\right]^{\mathrm{T}} - \left[\frac{\partial \mathcal{T}}{\partial \bar{\boldsymbol{q}}}\right]^{\mathrm{T}}. \tag{2.98}$$

Using the expression for the kinetic energy (2.94), and observing that[16]

$$\frac{\partial}{\partial \bar{q}_i}\left(\frac{dq_j}{dt}\right) = \frac{\mathrm{d}}{\mathrm{d}t}\left(\frac{\partial q_j}{\partial \bar{q}_i}\right), \tag{2.99}$$

$$\begin{aligned}
\frac{\partial \mathcal{T}}{\partial \bar{q}_i} &= \sum_j \left(\frac{\partial \mathcal{T}}{\partial q_j}\frac{\partial q_j}{\partial \bar{q}_i} + \frac{\partial \mathcal{T}}{\partial \dot{q}_j}\frac{\partial \dot{q}_j}{\partial \bar{q}_i}\right) \\
&= \sum_j \left(\frac{\partial \mathcal{T}}{\partial q_j}\frac{\partial q_j}{\partial \bar{q}_i} + \frac{\partial \mathcal{T}}{\partial \dot{q}_j}\frac{\mathrm{d}}{\mathrm{d}t}\frac{\partial q_j}{\partial \bar{q}_i}\right) \\
&= \begin{bmatrix}\frac{\partial \mathcal{T}}{\partial q_1} & \cdots & \frac{\partial \mathcal{T}}{\partial q_n}\end{bmatrix} \cdot \begin{bmatrix}\frac{\partial q_1}{\partial \bar{q}_i} \\ \vdots \\ \frac{\partial q_n}{\partial \bar{q}_i}\end{bmatrix} + \begin{bmatrix}\frac{\partial \mathcal{T}}{\partial \dot{q}_1} & \cdots & \frac{\partial \mathcal{T}}{\partial \dot{q}_n}\end{bmatrix} \cdot \frac{\mathrm{d}}{\mathrm{d}t}\begin{bmatrix}\frac{\partial q_1}{\partial \bar{q}_i} \\ \vdots \\ \frac{\partial q_n}{\partial \bar{q}_i}\end{bmatrix},
\end{aligned} \tag{2.100}$$

15: The Lagrangian behaves like a scalar under a point transformation. In other words, the Lagrangian changes its functional dependence on the coordinates, its value in a given point, however, remains unchanged.

16: The first relation is often exploited in modern derivations of Lagrange's equations of motion. A proof is reported in Appendix D.2.

we can rewrite the components of $\bar{\mathcal{Q}}^\star$ as

$$\begin{aligned}\frac{\mathrm{d}}{\mathrm{d}t}\left(\frac{\partial \mathcal{T}}{\partial \dot{\bar{\boldsymbol{q}}}}\right) =& \left(\dot{\boldsymbol{J}}^{-\mathrm{T}}\mathcal{M}\boldsymbol{J}^{-1} + \boldsymbol{J}^{-\mathrm{T}}\dot{\mathcal{M}}\boldsymbol{J}^{-1} + \boldsymbol{J}^{-\mathrm{T}}\mathcal{M}\dot{\boldsymbol{J}}^{-1}\right)\dot{\bar{\boldsymbol{q}}} + \bar{\mathcal{M}}\ddot{\bar{\boldsymbol{q}}} \\ =& \left(\dot{\boldsymbol{J}}^{-\mathrm{T}}\mathcal{M} + \boldsymbol{J}^{-\mathrm{T}}\dot{\mathcal{M}} - \bar{\mathcal{M}}\dot{\boldsymbol{J}}\right)\dot{\boldsymbol{q}} + \bar{\mathcal{M}}\ddot{\bar{\boldsymbol{q}}},\end{aligned} \tag{2.101}$$

$$\begin{aligned}\frac{\partial \mathcal{T}}{\partial \bar{\boldsymbol{q}}} =& \begin{bmatrix}\frac{\partial \mathcal{T}}{\partial q_1} & \cdots & \frac{\partial \mathcal{T}}{\partial q_n}\end{bmatrix} \cdot \begin{bmatrix}\frac{\partial q_1}{\partial \bar{q}_1} & \cdots & \frac{\partial q_1}{\partial \bar{q}_n} \\ \vdots & \ddots & \vdots \\ \frac{\partial q_n}{\partial \bar{q}_1} & \cdots & \frac{\partial q_n}{\partial \bar{q}_n}\end{bmatrix} + \begin{bmatrix}\frac{\partial \mathcal{T}}{\partial \dot{q}_1} & \cdots & \frac{\partial \mathcal{T}}{\partial \dot{q}_n}\end{bmatrix} \cdot \frac{\mathrm{d}}{\mathrm{d}t}\begin{bmatrix}\frac{\partial q_1}{\partial \bar{q}_1} & \cdots & \frac{\partial q_1}{\partial \bar{q}_n} \\ \vdots & \ddots & \vdots \\ \frac{\partial q_n}{\partial \bar{q}_1} & \cdots & \frac{\partial q_n}{\partial \bar{q}_n}\end{bmatrix} \\ =& \frac{\partial \mathcal{T}}{\partial \boldsymbol{q}}\boldsymbol{J}^{-1} + \frac{\partial \mathcal{T}}{\partial \dot{\boldsymbol{q}}}\dot{\boldsymbol{J}}^{-1}.\end{aligned} \tag{2.102}$$

Making the substitution (2.94) and (2.96), it follows that

$$\boldsymbol{\nu} = \dot{\mathcal{M}}\dot{\boldsymbol{q}} - \left[\frac{\partial \mathcal{T}}{\partial \boldsymbol{q}}\right]^{\mathrm{T}}. \tag{2.103}$$

Denoting the Coriolis and centrifugal force associated with the $\bar{\boldsymbol{q}}$'s by

$$\bar{\boldsymbol{\nu}} = \frac{\mathrm{d}}{\mathrm{d}t}\left[\frac{\partial \mathcal{T}}{\partial \dot{\bar{\boldsymbol{q}}}}\right]^{\mathrm{T}} - \left[\frac{\partial \mathcal{T}}{\partial \bar{\boldsymbol{q}}}\right]^{\mathrm{T}} - \bar{\mathcal{M}}\ddot{\bar{\boldsymbol{q}}}, \tag{2.104}$$

and comparing with (2.103), we get under consideration of (2.101) and (2.102) that[17]

$$\bar{\boldsymbol{\nu}} = \boldsymbol{J}^{-\mathrm{T}}\boldsymbol{\nu} - \bar{\mathcal{M}}\dot{\boldsymbol{J}}\dot{\boldsymbol{q}}. \tag{2.105}$$

17: Note that $\bar{\mathcal{M}}\dot{\boldsymbol{J}}\dot{\boldsymbol{q}} = -\boldsymbol{J}^{-\mathrm{T}}\mathcal{M}\dot{\boldsymbol{J}}^{-1}\dot{\bar{\boldsymbol{q}}}$. This identity is frequently used throughout this work.

Using (2.98), (2.104) and (2.105), we get for the transformed force of inertia

$$\bar{\mathcal{Q}}^\star = \bar{\mathcal{M}}\left(\ddot{\bar{\boldsymbol{q}}} - \dot{\boldsymbol{J}}\dot{\boldsymbol{q}}\right) + \boldsymbol{J}^{-\mathrm{T}}\boldsymbol{\nu}. \tag{2.106}$$

As expected, $\boldsymbol{\nu}$ transforms covariantly under a change of basis. The same is true for the potential force

$$\frac{\partial \mathcal{V}}{\partial \bar{\boldsymbol{q}}} = \frac{\partial \mathcal{V}}{\partial \boldsymbol{q}}\frac{\partial \boldsymbol{q}}{\partial \bar{\boldsymbol{q}}} = \frac{\partial \mathcal{V}}{\partial \boldsymbol{q}}\boldsymbol{J}^{-1}. \tag{2.107}$$

Combining (2.105)–(2.107), we can rewrite the transformed EL equations (2.97) in vector form as

$$\begin{aligned}\frac{\mathrm{d}}{\mathrm{d}t}\left[\frac{\partial \mathcal{L}}{\partial \dot{\bar{\boldsymbol{q}}}}\right]^{\mathrm{T}} - \left[\frac{\partial \mathcal{L}}{\partial \bar{\boldsymbol{q}}}\right]^{\mathrm{T}} =& \frac{\mathrm{d}}{\mathrm{d}t}\left[\frac{\partial \mathcal{T}}{\partial \dot{\bar{\boldsymbol{q}}}}\right]^{\mathrm{T}} - \left[\frac{\partial \mathcal{T}}{\partial \bar{\boldsymbol{q}}}\right]^{\mathrm{T}} + \left[\frac{\partial \mathcal{V}}{\partial \bar{\boldsymbol{q}}}\right]^{\mathrm{T}} \\ =& \bar{\mathcal{M}}\left(\ddot{\bar{\boldsymbol{q}}} - \dot{\boldsymbol{J}}\dot{\boldsymbol{q}}\right) + \boldsymbol{J}^{-\mathrm{T}}\left(\boldsymbol{\nu} + \left[\frac{\partial \mathcal{V}}{\partial \boldsymbol{q}}\right]^{\mathrm{T}}\right) \\ =& \bar{\mathcal{M}}\ddot{\bar{\boldsymbol{q}}} + \bar{\boldsymbol{\nu}} + \boldsymbol{J}^{-\mathrm{T}}\left[\frac{\partial \mathcal{V}}{\partial \boldsymbol{q}}\right]^{\mathrm{T}} = \bar{\mathcal{Q}}.\end{aligned} \tag{2.108}$$

This form of the EL equations is used for developing the motion tracking controllers reported in Chapter 7.

2.5.7 Transforming the Inertia and Coriolis/Centrifugal Matrices

In the following, it will be shown that a point transformation preserves the fundamental properties of the inertia and Coriolis/centrifugal matrices reported in Assumption 2.5.1 and Lemma 2.5.1. Considering (2.105) and the identity

$$\bar{\mathcal{M}}\dot{\boldsymbol{J}}\dot{\boldsymbol{q}} = \boldsymbol{J}^{-\mathrm{T}}\mathcal{M}\dot{\boldsymbol{J}}^{-1}\dot{\tilde{\boldsymbol{q}}}, \tag{2.109}$$

a natural choice for the transformed Coriolis and centrifugal matrix is

$$\bar{C} = \boldsymbol{J}^{-\mathrm{T}}\left(\mathcal{M}\dot{\boldsymbol{J}}^{-1} + C\boldsymbol{J}^{-1}\right), \tag{2.110}$$

where C is defined as in Section 2.5.1. The matrix $\bar{C}$ in (2.110) is of the form commonly used in task space control, c.f. [97]. The following two lemmas summarize properties of the transformed matrices that are crucial for later control developments in this work.

Lemma 2.5.7 *The matrix $\bar{\mathcal{M}}$ is symmetric and positive definite for all $\bar{\boldsymbol{q}} \in \mathbb{R}^n$.*

Exploiting the properties of congruence transformations the proof is straightforward.

Lemma 2.5.8 *No matter how C is defined in* (2.110)*, it is always true that*

$$\dot{\tilde{\boldsymbol{q}}}^T\left(\dot{\mathcal{M}} - 2\bar{C}\right)\dot{\tilde{\boldsymbol{q}}} = \boldsymbol{0},\ \forall \dot{\tilde{\boldsymbol{q}}} \in \mathbb{R}^n. \tag{2.111}$$

If C is defined using the Christoffel symbols, (2.60)*, then the matrix*

$$\dot{\mathcal{M}} - 2\bar{C} \tag{2.112}$$

is skew-symmetric for any $\bar{\boldsymbol{q}}, \dot{\tilde{\boldsymbol{q}}} \in \mathbb{R}^n$. Notice that the skew-symmetry property of (2.112) *is equivalent to*

$$\dot{\mathcal{M}} = \bar{C} + \bar{C}^T. \tag{2.113}$$

Proof. Let us start with proofing the first statement. Introducing

$$\boldsymbol{W} = \dot{\boldsymbol{J}}^{-\mathrm{T}}\mathcal{M}\boldsymbol{J}^{-1} - \boldsymbol{J}^{-\mathrm{T}}\mathcal{M}\dot{\boldsymbol{J}}^{-1}, \tag{2.114}$$

we know that

$$\boldsymbol{W} = -\boldsymbol{W}^{\mathrm{T}} \tag{2.115}$$

$$\dot{\mathcal{M}} = \dot{\boldsymbol{J}}^{-\mathrm{T}}\mathcal{M}\boldsymbol{J}^{-1} + \boldsymbol{J}^{-\mathrm{T}}\dot{\mathcal{M}}\boldsymbol{J}^{-1} + \boldsymbol{J}^{-\mathrm{T}}\mathcal{M}\dot{\boldsymbol{J}}^{-1}, \tag{2.116}$$

$$\bar{C} = \boldsymbol{J}^{-\mathrm{T}}\left(\mathcal{M}\dot{\boldsymbol{J}}^{-1} + C\boldsymbol{J}^{-1}\right), \tag{2.117}$$

$$\bar{C}^{\mathrm{T}} = \left(\dot{\boldsymbol{J}}^{-\mathrm{T}}\mathcal{M} + \boldsymbol{J}^{-\mathrm{T}}C^{\mathrm{T}}\right)\boldsymbol{J}^{-1}, \tag{2.118}$$

and from Lemma 2.5.1 that

$$\dot{\boldsymbol{q}}^{\mathrm{T}}(\dot{\mathcal{M}} - 2C)\dot{\boldsymbol{q}} = \boldsymbol{0},\ \forall \dot{\boldsymbol{q}} \in \mathbb{R}^n. \tag{2.119}$$

Using (2.115)–(2.119), we conclude that

$$\dot{\tilde{\boldsymbol{q}}}^{\mathrm{T}}\big(\dot{\mathcal{M}}-2\bar{\mathcal{C}}\big)\dot{\tilde{\boldsymbol{q}}} = \dot{\tilde{\boldsymbol{q}}}^{\mathrm{T}}\boldsymbol{J}^{-\mathrm{T}}\big(\dot{\mathcal{M}}-2\mathcal{C}\big)\boldsymbol{J}^{-1}\dot{\tilde{\boldsymbol{q}}} + \dot{\tilde{\boldsymbol{q}}}^{\mathrm{T}}\boldsymbol{W}\dot{\tilde{\boldsymbol{q}}} = 0,\ \forall \dot{\tilde{\boldsymbol{q}}} \in \mathbb{R}^n. \quad (2.120)$$

If $\mathcal{C}$ is defined using the Christoffel symbols, it follows from Lemma 2.5.1 that

$$\dot{\mathcal{M}} = \mathcal{C} + \mathcal{C}^{\mathrm{T}}. \quad (2.121)$$

Using (2.116)–(2.118) and (2.121), we have that

$$\dot{\mathcal{M}} - \bar{\mathcal{C}} - \bar{\mathcal{C}}^{\mathrm{T}} = \boldsymbol{J}^{-\mathrm{T}}\big(\dot{\mathcal{M}} - \mathcal{C} - \mathcal{C}^{\mathrm{T}}\big)\boldsymbol{J}^{-1} = \boldsymbol{0}, \quad (2.122)$$

which confirms the second argument and completes the proof. ■

2.6 Underactuation

This chapter provides a short introduction into what defines an underactuated robot and highlights the main challenges when it comes to control of these systems. An excellent introductory source of information on the characteristics and control of underactuation systems are the course notes [182]. Many definitions in this chapter are based on these notes.

[182]: Tedrake (2020), "Online notes for MAT237: Multivariable calculus, 2018-9"

According to Newton's law of motion the dynamics equations of a mechanical system are inherently second order and, in general, of the form:

$$\ddot{\boldsymbol{q}} = \boldsymbol{f}(\boldsymbol{q}, \dot{\boldsymbol{q}}, \boldsymbol{u}, t), \quad (2.123)$$

where $\boldsymbol{q} \in \mathbb{R}^n$ is the position state vector, $\boldsymbol{u} \in \mathbb{R}^m$ is the control input vector and t is time. Exploiting the positive definiteness of the inertia matrix, we may always rewrite the EL (2.41) in the form above. The natural question may arise whether we can command accelerations in arbitrary directions and of arbitrary magnitude. Based on this system intrinsic property, we distinguish two classes of systems.

Definition 2.6.1 (Underactuation [182]) *A system of the form* (2.123) *is said to be fully actuated in a given configuration* $(\boldsymbol{q}, \dot{\boldsymbol{q}})$ *and for a given point in time t if we are able to command an instantaneous acceleration of arbitrary amplitude in an arbitrary direction, i.e. for every* $\ddot{\boldsymbol{q}}$*, we are able to find an input* $\boldsymbol{u}$ *that results in the desired acceleration. Otherwise system* (2.123) *is said to be underactuated in* $(\boldsymbol{q}, \dot{\boldsymbol{q}})$ *and for time t.*

Remark 2.6.1 The Definition 2.6.1 easily transfers to Euler-Lagrange systems. Throughout this work, we shall consider only systems with a positive definite generalized inertia matrix. Considering the EL equations (2.54) and the definition of the non-monogenic forces (2.56) it is straightforward to see that (2.54) is fully actuated if and only if the numbers of inputs and degrees of freedom are equal.

As a direct consequence of this definition; an underactuated system cannot follow arbitrary commanded trajectories. One of the trivial, but in practice quite common cases where it is straightforward to see that a system is underactuated, is for the case $\dim(\boldsymbol{u}) < \dim(\boldsymbol{q})$, i.e., the number of inputs is less

than the number of degrees of freedom. A broad class of robotic systems are affine in the control input:

$$\ddot{\boldsymbol{q}} = \boldsymbol{f}_1(\boldsymbol{q}, \dot{\boldsymbol{q}}, t) + \boldsymbol{f}_2(\boldsymbol{q}, \dot{\boldsymbol{q}}, t)\boldsymbol{u}. \tag{2.124}$$

For this class, we have that if

$$\operatorname{rank}\left(\boldsymbol{f}_2(\boldsymbol{q}, \dot{\boldsymbol{q}}, t)\right) < \dim(\boldsymbol{q}), \tag{2.125}$$

then the system is underactuated. In this text, we are primarily interested in articulated soft robots which are “by design" underactuated. Series elastic actuators are the most basic example of an articulated soft robot. These systems have twice the number of degrees of freedom than control inputs and, thus, are trivially underactuated. For more advanced mechanical realizations, such as a bidirectional antagonistic variable stiffness joint, the situation is similar. We have three degrees of freedom per joint but only two actuators. Apart from a lack of inputs, there are other forms of underactuation. Input and state constraint can significantly complicate control design and can be a cause of underactuation. With regard to our general definition of underactuation it is easy to see that input constraints may render a system underactuated. The motor torque available in a robot joint is limited and intuition suggests that this limits the achievable link acceleration. Regarding state constraints, we have to differ between the holonomic and non-holonomic constraints. Holonomic constraints reduce the configuration space dimensionality. Non-holonomic constraints, however, do not reduce the possible configurations of a robot but impose limitations on how these configurations can be reached. Classical examples are wheeled or fixed-wing robots. Clearly, such systems cannot be accelerated in an arbitrary direction and, thus, are underactuated. In practice, we may encounter systems that are “almost always” fully actuated with the condition of full actuation only being violated at isolated points in the configuration space. A classical example is that of a manipulator under control by end effector forces, which is fully actuated away from joint limits or kinematic singularities. In this work, such systems will be referred to as fully actuated.

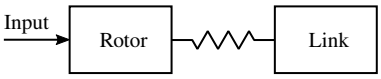

Figure 2.9: A Series Elastic Actuator.

Remark 2.6.2 It is worth noting that whether a system is underactuated may depend on its current state, the time and the choice of coordinates (see manipulator example).

Remark 2.6.3 It is important not to confuse the concept of underactuation with controllability or feedback linearizability. An underactuated system can be controllable (e.g., an inverted pendulum on a cart away from the horizontal [75]). Moreover, an underactuated system can be feedback linearizable (e.g., a robot with SEA).

[75]: Ibáñez et al. (2005), “Lyapunov-based controller for the inverted pendulum cart system”

We adopt the definition by Ortega introduced in [133]:

[133]: Ortega (1998), *Passivity-Based Control of Euler-Lagrange Systems: Mechanical, Electrical, and Electromechanical Applications*

Definition 2.6.2 (Underactuated EL systems) *An EL system is fully actuated if it has equal number of degrees of freedom than available control inputs (that is if $n = n_a$, e.g. if $\mathcal{N} = \boldsymbol{I}_n$). Otherwise, if $n_a < n$, we say that the system is underactuated. In the latter case, $\boldsymbol{q}$ can be partitioned into*

actuated:

$$\boldsymbol{q}_a \triangleq \mathcal{N}\boldsymbol{q} \tag{2.126}$$

and non-actuated components:

$$\boldsymbol{q}_u \triangleq \mathcal{N}^{\perp}\boldsymbol{q}, \tag{2.127}$$

where $\mathcal{N}^{\perp}$ denotes the orthogonal complement of $\mathcal{N}$.

2.6.1 Control Challenges

Assume that we know the full model of the input affine system (2.124), *i.e.* $\boldsymbol{f}_1$ and $\boldsymbol{f}_2$ are known. Further, let $\boldsymbol{f}_2$ be of full rank. In this case, we could apply the following feedback control:

$$\boldsymbol{u} = \boldsymbol{f}_2^{-1}(\boldsymbol{q}, \dot{\boldsymbol{q}}, t)\left(\bar{\boldsymbol{u}} - \boldsymbol{f}_1(\boldsymbol{q}, \dot{\boldsymbol{q}}, t)\right), \tag{2.128}$$

where $\bar{\boldsymbol{u}}$ is our new control input which results in a linear, second-order dynamics

$$\ddot{\boldsymbol{q}} = \bar{\boldsymbol{u}}. \tag{2.129}$$

We say that system (2.124) is "feedback equivalent" to (2.129). By using (2.128), we can reduce the control problem of any fully actuated system to the problem of controlling a linear, decoupled, second-order system. Underactuated systems, however, are not *feedback equivalent* to (2.129). Thus, the control design for underactuated systems, in particular of nonlinear ones, is more challenging.

2.6.2 Underactuation in Robotics

We find underactuation in many interesting robotics problems. Soft robots, legged robots[18] and most swimming and flying robots are underactuated. Even robotic manipulation is an underactuated problem in many situations. In general, rigid robots have one actuator for each joint. However, for any rigid object the robot manipulates that is not firmly attached to the robot, we have to add six degrees of freedom, resulting in underactuation. For (continuously) deformable objects, the situation becomes even worse.

18: As long as the robot is not firmly fixed to the ground.

2.7 Summary

In this chapter, basic concepts of analytical mechanics such as generalized coordinates, configuration space, variational principles have been covered that are essential for the developments in this work. Since transformations play a central role in this work, the transforming properties of the Euler-Lagrange equations have been revisited. A particularly important idea is the invariance of Euler-Lagrange equations under point transformations.

3 Articulated Soft Robots

The design of articulated soft robots is inspired by the vertebrate part of the animal kingdom. To approach the performance of animals, elastic elements are introduced into the drive train to act as energy storage elements. In contrast to soft robots, the soft elements of ASRs, with either constant or variable impedance [73], are concentrated in the joints and interconnect the rigid body segments. In this work, DLR *David* serves as an exemplary ASR platform to demonstrate the performance and practical viability of the proposed control framework. It is important to point out that the presented controllers are formulated in a general form and, thus, applicable to a wide variety of ASRs and not just DLR *David*.

[73]: Huang et al. (2020), "Dynamic simulation of articulated soft robots"

3.1 DLR *David*: A Compliant Anthropomorphic Humanoid

David (formally Hand Arm System) is an anthropomorphic robot system implemented with variable impedance actuators (VIA) in all its joints, which has been developed at the German Aerospace Center (DLR). The robot was first presented in public in 2010. Its design is based on the following objectives: approach human capabilities with regard to robustness, dynamic performance, and dexterity [54]. The system has roughly the size, shape, and weight of an adult human. In total, it features 41 degrees of freedom, 76 brushless DC motors, 165 position sensors. The actuation is realized through three different types of VIAs as shown in Fig. 3.1:

- Floating Spring Joint (FSJ) [194]
- Bidirectional-Antagonist Variable Stiffness Actuator (BAVS) [47, 148]
- Antagonistic Actuator (AA) [55]

The main difference between the first and latter two designs is the relative dimensioning of the motors. The FSJ features a main motor to adjust the joint torque and a smaller motor to adjust the physical joint stiffness. This allows for a clear differentiation between joint torque and joint stiffness adjustment. However, a drawback is that the second motor cannot support the main motor in holding a load. The latter two designs, on the contrary, have two motors of equal size that can share the load. This comes at the cost that the joint stiffness adjustment cannot be separated from the joint torque control. As shown below for the FSJ, the dynamics model can be simplified by assuming the adjuster motor coordinate as a kinematic input. A more detailed introduction of the different joint types can be found in the works listed above.

The actuator performance characteristics of DLR *David* are summarized in Table 3.1. Note that the maximal joint torque can always be reached with the minimal stiffness setting and vice-versa.

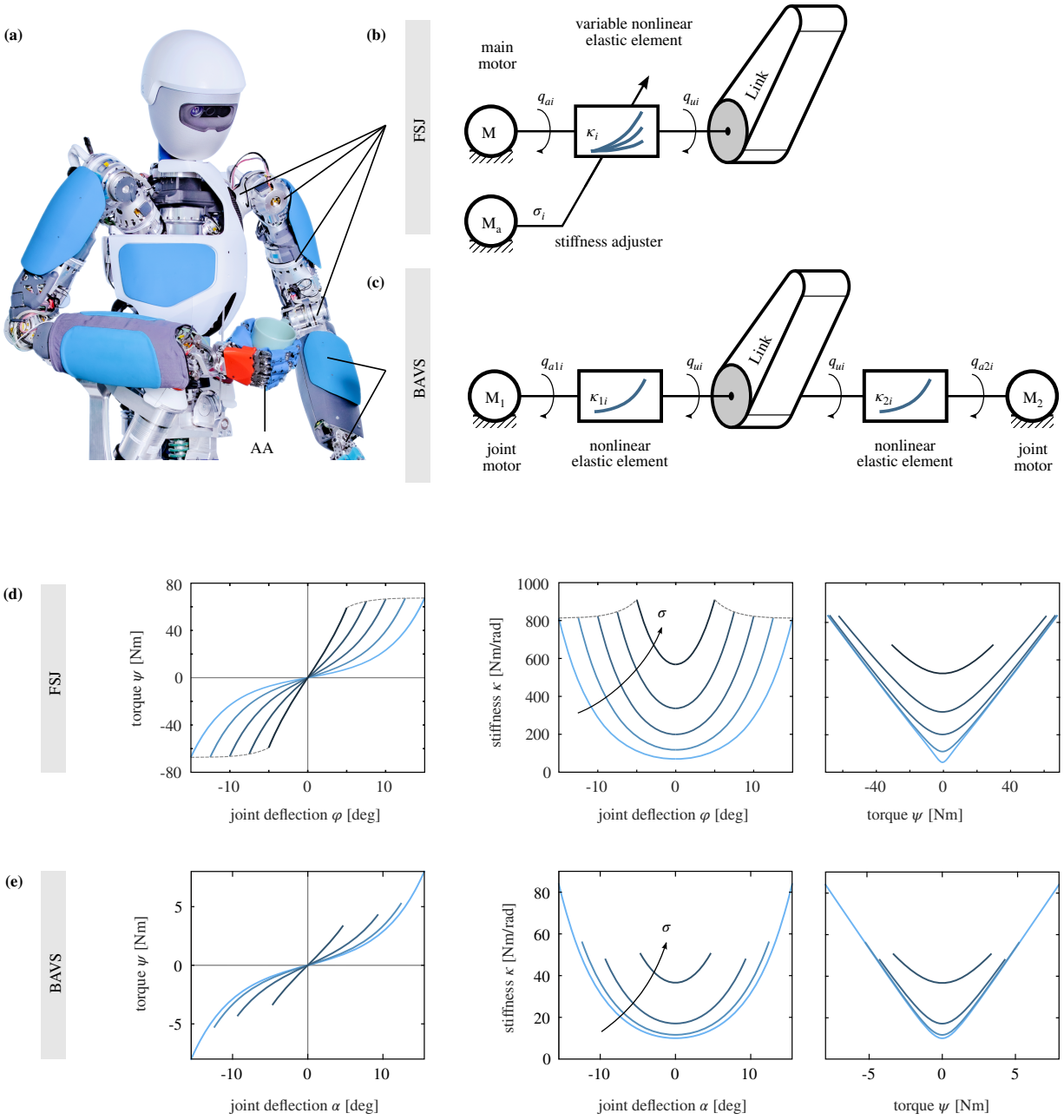

Figure 3.1: (**a**) DLR *David*. (**b**) The first four arm joints, namely the elbow and the three shoulder joints, are implemented by Floating Spring Joints (FSJ) [194]. A simplified working scheme is shown. (**d**) The joint stiffness for various stiffness adjuster positions $\sigma = [\,0, 2.5, 5.0, 7.5, 10\,]$ deg. (**c**) The under arm rotation is realized by a Bidirectional Antagonistic Variable Stiffness (BAVS) joint [47]. (**e**) The corresponding joint stiffness behaviors resulting from different levels of co-contraction of the springs $\sigma = [\,0, 2.5, 5.0, 7.5, 10\,]$ deg.

Table 3.1: Joint performance parameters of DLR *David*.

Joint	Arm (FSJ)	Forearm (BAVS)	Wrist (BAVS)	Fingers (AA) MCP	PIP	DIP
Max. motor velocity [° s^{-1}]	530	960	560	600	960	1280
Max. joint torque [N m]	59–67	3.2–7.6	8	2.73	1.57	0.93
Max. energy storage [J]	5.3	-	-	-	-	-
Max. stiffn. [N m rad^{-1}]	826	84	60	0.3	-	-
Min. stiffn. [N m rad^{-1}]	52.4	10	0.5	17	-	-
Max. deflection [deg]	15	15	21.5	30	-	-
Reflected motor inertia [kg m^2]	0.3117	3.68e-3	4.6e-3	-	-	-
Gear ratios	81	100	100	100	-	-

3.1.1 The Floating Spring Joint

The first four arm joints, namely the elbow and the three shoulder joints, are implemented by FSJs. Each FSJ is a highly integrated joint module including the main and adjuster motor, sensors, springs, harmonic drive, joint bearings and electronics. Throughout this work, the following coordinate notation is used for FSJs:

q_{ui} … ith link coordinate
q_{ai} … ith motor coordinate
σ_i … ith stiffness adjuster coordinate
$\varphi_i = q_{ai} - q_{ui}$ … ith joint deflection coordinate

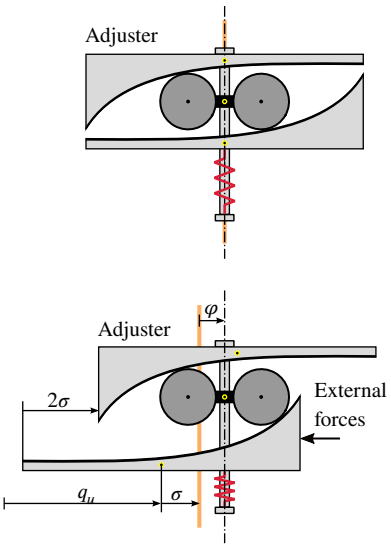

Figure 3.2: The FSJ mechanism. (**top**) Minimal stiffness setting ($\sigma = 0$ deg). (**bottom**) The joint pretension ($\sigma > 0$ deg) increases the joint stiffness.

Let us use the Lagrangian formalism to obtain the dynamics of a single FSJ in absence of gravity. Its kinetic energy is [149]

$$\mathcal{T} = \frac{1}{2}\left(J_a \dot{q}_a^2 + J_\sigma \dot{\sigma}^2 + J_u \dot{q}_u^2\right), \tag{3.1}$$

where J_a is the combined rotor and wave generator inertia reflected to the link side, J_σ is the reflected inertia of the adjuster mechanism and J_u is the link inertia. The potential energy is solely determined by the energy of the linear spring that pushes the two cam discs together, c.f. Fig. 3.2,

$$\mathcal{V} = \frac{1}{2}k\Big[f(\varphi+\sigma) + f(-\varphi-\sigma)\Big]^2, \tag{3.2}$$

with k representing the spring stiffness. The function f describes the geometry of the cam disc path, see Fig. 3.2. Introducing the auxiliary variables $x = -\tilde{x} = \varphi + \sigma$ and observing that

$$\frac{\partial x}{\partial q_u} = -\frac{\partial \tilde{x}}{\partial q_u} = \frac{\partial \varphi}{\partial q_u} = -1, \tag{3.3}$$

$$\frac{\partial x}{\partial q_a} = -\frac{\partial \tilde{x}}{\partial q_a} = \frac{\partial \varphi}{\partial q_a} = 1, \tag{3.4}$$

$$\frac{\partial x}{\partial \sigma} = -\frac{\partial \tilde{x}}{\partial \sigma} = 1, \tag{3.5}$$

we obtain for the generalized elastic forces

$$\frac{\partial \mathcal{V}}{\partial q_u} = -k\Big[f(x) + f(\tilde{x})\Big]\left[\frac{\partial f}{\partial \tilde{x}}(\tilde{x}) - \frac{\partial f}{\partial x}(x)\right] \tag{3.6}$$

$$\frac{\partial \mathcal{V}}{\partial q_a} = -k\Big[f(x) + f(\tilde{x})\Big]\left[\frac{\partial f}{\partial x}(x) - \frac{\partial f}{\partial \tilde{x}}(\tilde{x})\right] \tag{3.7}$$

$$\frac{\partial \mathcal{V}}{\partial \sigma} = -k\Big[f(x) + f(\tilde{x})\Big]\left[\frac{\partial f}{\partial x}(x) - \frac{\partial f}{\partial \tilde{x}}(\tilde{x})\right]. \tag{3.8}$$

Let us further introduce the generalized forces

$$\psi(\varphi, \sigma) \triangleq -\frac{\partial \mathcal{V}}{\partial q_u}. \tag{3.9}$$

Considering the symmetry of ψ with respect to the origin, i.e.

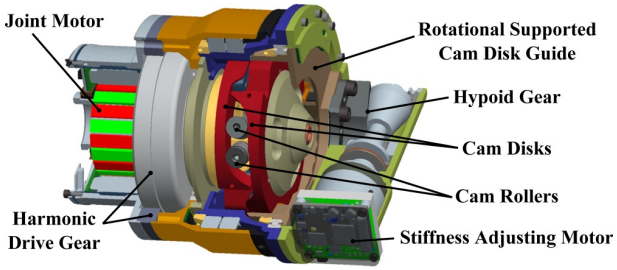

Figure 3.3: Floating spring joint components.

$\psi(\varphi, \sigma) = -\psi(-\varphi, -\sigma)$, we note that

$$\frac{\partial \mathcal{V}}{\partial q_a}(\varphi, \sigma) = \frac{\partial \mathcal{V}}{\partial q_u}(-\varphi, -\sigma) = \psi(\varphi, \sigma). \tag{3.10}$$

Using (3.3)–(3.10) allows us to write the Euler-Lagrange equations of an FSJ as

$$\begin{bmatrix} J_u & 0 & 0 \\ 0 & J_a & 0 \\ 0 & 0 & J_\sigma \end{bmatrix} \begin{bmatrix} \ddot{q}_u \\ \ddot{q}_a \\ \ddot{\sigma} \end{bmatrix} - \begin{bmatrix} \psi(\varphi, \sigma) \\ -\psi(\varphi, \sigma) \\ -\psi(\varphi, \sigma) \end{bmatrix} = \begin{bmatrix} \mathcal{Q}_u \\ \mathcal{Q}_a \\ \mathcal{Q}_\sigma \end{bmatrix}, \tag{3.11}$$

with the applied forces $\mathcal{Q}_u$, $\mathcal{Q}_a = \mathcal{Q}'_a + u_a$ and $\mathcal{Q}_\sigma = \mathcal{Q}'_\sigma + u_\sigma$, where u_a and u_σ are the torque control inputs to the main and adjuster motors, and $\mathcal{Q}'_a, \mathcal{Q}'_\sigma$ denoting external forces. It is common to neglect the dynamics of the adjuster motor and assume the adjuster coordinate σ_i as kinematic control input [8]. This assumption is justified if the adjuster moves slowly such that inertial forces can be neglected and neither the motor velocity or torque limits are violated. For the the scenarios considered in this work, this assumption is met. This allows for a further simplification of the dynamics model to

[8]: Albu-Schäffer et al. (2010), "Dynamic modelling and control of variable stiffness actuators"

$$\begin{bmatrix} J_u & 0 \\ 0 & J_a \end{bmatrix} \begin{bmatrix} \ddot{q}_u \\ \ddot{q}_a \end{bmatrix} - \begin{bmatrix} \psi(\varphi, \sigma) \\ -\psi(\varphi, \sigma) \end{bmatrix} = \begin{bmatrix} \mathcal{Q}_u \\ \mathcal{Q}_a \end{bmatrix}. \tag{3.12}$$

The resulting dynamics assumes the structure of the well known flexible joint model. This model was used for the control implementation on DLR *David* reported in Chapter 11. The torque and stiffness characteristics of the FSJ are reported in Fig. 3.1(b,d). Note that the joint stiffness increases progressively with increasing joint torque. The stiffness adjuster input σ allows a variation of the stiffness characteristics (with increasing values of σ representing increasing join stiffness settings). For the experiments, we shall keep the stiffness setup at a constant setting. In such scenarios, the joint torque can be written as function of the joint deflection only. With some abuse of notation, we may write the simplified FSJ model as:

$$\begin{bmatrix} J_u & 0 \\ 0 & J_a \end{bmatrix} \begin{bmatrix} \ddot{q}_u \\ \ddot{q}_a \end{bmatrix} - \begin{bmatrix} \psi(\varphi) \\ -\psi(\varphi) \end{bmatrix} = \begin{bmatrix} \mathcal{Q}_u \\ \mathcal{Q}_a \end{bmatrix}. \tag{3.13}$$

3.1.2 The Bidirectional Antagonistic Variable Stiffness Joint

The working principle of a BAVS joint is similar to that of an antagonistic actuator: co-contracting the springs changes the joint stiffness, while a synchronized motion changes the net joint torque. The main differences between the antagonist and BAVS joint principle is that in the latter setup each motor

can apply torques in both directions (“push” and “pull"). Throughout this work, the following notation is used for BAVS joints.

- q_{ui} … ith link coordinate
- q_{a1i} … 1st motor coordinate of the ith joint
- q_{a2i} … 2nd motor coordinate of the ith joint
- φ_{1i} … 1st deflection coordinate of the ith joint
- φ_{2i} … 2nd deflection coordinate of the ith joint

The basic working principle of a BAVS joint is shown in Fig. 3.1(c). Each motor is coupled by a nonlinear elastic element to the link. Let $\mathcal{V}_i$ be the potential energy of the ith joint. Introducing

$$\psi_i \triangleq -\frac{\partial \mathcal{V}}{\partial q_{ui}}, \tag{3.14}$$

$$\psi_{a1i} \triangleq \frac{\partial \mathcal{V}}{\partial q_{a1i}}, \tag{3.15}$$

$$\psi_{a2i} \triangleq \frac{\partial \mathcal{V}}{\partial q_{a2i}}, \tag{3.16}$$

and the deflection coordinates $\varphi_{1i} \triangleq q_{ui} - q_{a1i}$ and $\varphi_{2i} \triangleq q_{ui} - q_{a2i}$ allows us to write Euler-Lagrange equations for a BAVS joint as:

$$\begin{bmatrix} J_{ui} & 0 & 0 \\ 0 & J_{a1i} & 0 \\ 0 & 0 & J_{a2i} \end{bmatrix} \begin{bmatrix} \ddot{q}_{ui} \\ \ddot{q}_{a1i} \\ \ddot{q}_{a2i} \end{bmatrix} - \begin{bmatrix} \psi(q_{ui}, \varphi_{1i}, \varphi_{2i}) \\ \psi_{a1i}(\varphi_{a1i}) \\ \psi_{a2i}(\varphi_{a2i}) \end{bmatrix} = \begin{bmatrix} \mathcal{Q}_{ui} \\ \mathcal{Q}_{a1i} \\ \mathcal{Q}_{a2i} \end{bmatrix}. \tag{3.17}$$

For some BAVS joint implementations, e.g. the underarm of DLR *David*, the potential function $\mathcal{V}_i$ of the ith joint can be decomposed in the form:

$$\mathcal{V}_i = \mathcal{U}_{1i}(q_{ui} - q_{a1i}) + \mathcal{U}_{2i}(q_{ui} - q_{a2i}), \tag{3.18}$$

where $\mathcal{U}_{ji}$, $j = 1, 2$, denotes the potential energy of the elastic element that couples the jth motor of the ith joint to the ith link. Given a symmetric motor inertias setup, i.e. $J_{a1i} = J_{a2i} = J_a$ (as used in DLR *David*), we can rewrite

$$\begin{bmatrix} J_{ui} & 0 & 0 \\ 0 & J_a & 0 \\ 0 & 0 & J_a \end{bmatrix} \begin{bmatrix} \ddot{q}_{ui} \\ \ddot{q}_{a1i} \\ \ddot{q}_{a2i} \end{bmatrix} - \begin{bmatrix} \psi_{1i}(\varphi_{1i}) + \psi_{2i}(\varphi_{2i}) \\ \psi_{1i}(\varphi_{1i}) \\ \psi_{2i}(\varphi_{2i}) \end{bmatrix} = \begin{bmatrix} \mathcal{Q}_u \\ \mathcal{Q}_{a1} \\ \mathcal{Q}_{a2} \end{bmatrix}. \tag{3.19}$$

The torque and stiffness characteristics of the BAVS actuator are reported in Fig. 3.1(b,d). Analogous to the FSJ case, the joint stiffness increases progressively with increasing joint torque.

3.2 Modeling of Articulated Soft Robots

An articulated soft robot can be modeled as an underactuated EL system. Let $\boldsymbol{q} \triangleq \left[\boldsymbol{q}_u^{\mathrm{T}}, \boldsymbol{q}_a^{\mathrm{T}}\right]^{\mathrm{T}}$ be the vector of generalized coordinates with $\boldsymbol{q}_u$ and $\boldsymbol{q}_a$ denoting the unactuated link and actuated motor coordinates, respectively. The control inputs are the motor torques at the rotors $\boldsymbol{u}_a \in \mathbb{R}^{n_a}$. Assuming that the rotors can be modeled by uniform cylinders, the gravitational potential energy becomes independent of the motor positions. Further, let $\boldsymbol{B}$ be a constant

diagonal matrix representing the actuator inertias reflected to the link side. In this case, the kinetic and potential energies of an ASR are

$$\mathcal{T}(\boldsymbol{q}_u, \dot{\boldsymbol{q}}) \triangleq \frac{1}{2}\dot{\boldsymbol{q}}^{\mathrm{T}}\mathcal{M}(\boldsymbol{q}_u)\dot{\boldsymbol{q}}, \quad \mathcal{V}(\boldsymbol{q}) \triangleq \mathcal{V}_g(\boldsymbol{q}_u) + \mathcal{V}_e(\boldsymbol{q}), \tag{3.20}$$

where $\mathcal{M} \in \mathbb{R}^n$ is the inertia matrix of the form[1]

$$\mathcal{M}(\boldsymbol{q}_u) \triangleq \begin{bmatrix} \boldsymbol{M}(\boldsymbol{q}_u) & \boldsymbol{S}(\boldsymbol{q}_u) \\ \boldsymbol{S}^{\mathrm{T}}(\boldsymbol{q}_u) & \boldsymbol{B} \end{bmatrix}, \tag{3.21}$$

that satisfies $\mathcal{M}(\boldsymbol{q}_u) = \mathcal{M}^{\mathrm{T}}(\boldsymbol{q}_u) > 0$, submatrix $\boldsymbol{M}$ can be conceived as the "rigid robot" inertia matrix and the functions $\mathcal{V}_g$ and $\mathcal{V}_e$ denote the potential energies due to the gravitational field and the elastic elements. The resulting EL equations are

$$\begin{bmatrix} \boldsymbol{M}(\boldsymbol{q}_u) & \boldsymbol{S}(\boldsymbol{q}_u) \\ \boldsymbol{S}^{\mathrm{T}}(\boldsymbol{q}_u) & \boldsymbol{B} \end{bmatrix} \begin{bmatrix} \ddot{\boldsymbol{q}}_u \\ \ddot{\boldsymbol{q}}_a \end{bmatrix} + \begin{bmatrix} \boldsymbol{C}_{11}(\boldsymbol{q}_u, \dot{\boldsymbol{q}}_u) & \boldsymbol{C}_{12}(\boldsymbol{q}_u, \dot{\boldsymbol{q}}_u) \\ \boldsymbol{C}_{21}(\boldsymbol{q}_u, \dot{\boldsymbol{q}}_u) & \boldsymbol{0} \end{bmatrix} \begin{bmatrix} \dot{\boldsymbol{q}}_u \\ \dot{\boldsymbol{q}}_a \end{bmatrix} + \frac{\partial \mathcal{V}}{\partial \boldsymbol{q}} = \boldsymbol{u} + \mathcal{Q}, \tag{3.22}$$

where control vector is partitioned as $\boldsymbol{u} = [\boldsymbol{0}, \boldsymbol{u}_a^{\mathrm{T}}]^{\mathrm{T}} \in \mathbb{R}^n$ and the Coriolis/centrifugal matrix defined as reported in Section 2.5. We observe that the motor and link dynamics interact via three type of forces: 1) inertial coupling, 2) Coriolis forces 3) forces transmitted through the elastic elements. The primer two are reflected by the presence of the off-diagonal terms in the inertia and Coriolis/centrifugal matrices.

For many ASRs, the elastic forces are more dominant than the inertial ones. Based on this observation, Spong proposed in [168] the following simplifying assumptions:

(A1) The kinetic energy of each rotor is due only to its own rotation. Equivalently, the motion of each rotor is a pure rotation with respect to an inertial frame.
(A2) The rotors/gear inertia is symmetric with respect to the rotor's axis of rotations. Thus, the gravitational potential of the system is independent of the rotor orientation.

These two assumptions are well justified for DLR *David* due to the high gear ratios, see also [54]. Under (A1) and (A2), the expression of the kinetic energy (3.20) simplifies to

$$\mathcal{T} = \frac{1}{2}\left(\dot{\boldsymbol{q}}_u^{\mathrm{T}}\boldsymbol{M}\dot{\boldsymbol{q}}_u + \dot{\boldsymbol{q}}_a^{\mathrm{T}}\boldsymbol{B}\dot{\boldsymbol{q}}_a\right), \tag{3.23}$$

and the corresponding EL equations are given by

$$\begin{aligned} \begin{bmatrix} \boldsymbol{M}(\boldsymbol{q}_u) & \boldsymbol{0} \\ \boldsymbol{0} & \boldsymbol{B} \end{bmatrix} \begin{bmatrix} \ddot{\boldsymbol{q}}_u \\ \ddot{\boldsymbol{q}}_a \end{bmatrix} + \begin{bmatrix} \boldsymbol{C}_{11}(\boldsymbol{q}_u, \dot{\boldsymbol{q}}_u) & \boldsymbol{0} \\ \boldsymbol{0} & \boldsymbol{0} \end{bmatrix} \begin{bmatrix} \dot{\boldsymbol{q}}_u \\ \dot{\boldsymbol{q}}_a \end{bmatrix} + \frac{\partial \mathcal{V}}{\partial \boldsymbol{q}} &= \boldsymbol{u} + \mathcal{Q}, \\ \mathcal{M}(\boldsymbol{q}_u)\ddot{\boldsymbol{q}} + C(\boldsymbol{q}_u, \dot{\boldsymbol{q}}_u)\dot{\boldsymbol{q}} + \frac{\partial \mathcal{V}}{\partial \boldsymbol{q}} &= \boldsymbol{u} + \mathcal{Q}, \end{aligned} \tag{3.24}$$

with the degenerated inertia and Coriolis/centrifugal matrices compared to (3.22).

1: More details on the structure of the inertia matrix can be found in [183].

[168]: Spong (1987), "Modeling and control of elastic joint robots"

3.2.1 Some considerations from the control viewpoint

The inertially decoupled model (3.24) assumes the structure of a flexible joint robot, which has been extensively studied in literature [143, 168]. The main differences are: (1) the elastic potential energy is not necessarily a quadratic form, (2) the number of of actuated coordinates is greater than or equal to the number of unactuated coordinates, i.e. $n_a \geq n_u$. From the control point of view, the main advantage of the model reduction proposed by Spong lies arguably in the fact that the model (3.24) is feedback linearizable [168]. The "full" model, by contrast, is only dynamic feedback linearizable [31]. Many ASR designs can be described by a dynamics model that neglects inertial couplings between the motor and link dynamics, see, e.g. [41, 189] for further examples.

[143]: Ozgoli et al. (2006), "A survey on the control of flexible joint robots"
[168]: Spong (1987), "Modeling and control of elastic joint robots"

[31]: De Luca et al. (1998), "A general algorithm for dynamic feedback linearization of robots with elastic joints"
[41]: Eiberger et al. (2010), "On joint design with intrinsic variable compliance: Derivation of the DLR QA-joint"
[189]: Van Ham et al. (2007), "MACCEPA, the mechanically adjustable compliance and controllable equilibrium position actuator: Design and implementation in a biped robot"

Further effects

Deriving a model for a mechanical system is always a process of abstraction and simplification. In this process, it is critical to identify and model the dynamic effects which are dominant. The implementation of harmonic drives into the actuation units introduces significant friction [186]. The friction in a harmonic drive is highly nonlinear and constituted by four main components: 1) Coulomb friction, 2) velocity-dependent friction, 3) position-dependent friction, and 4) friction from resonance vibration [185]. To ensure that the model (3.24) matches the actual system reasonably well, all the controllers developed for DLR *David* in Chapter 7 are implemented together with a friction compensation algorithm. This ensures, that the motor-side friction can be neglected during the control design.

[186]: Tuttle (1992), "Understanding and modeling the behavior of a harmonic drive gear transmission"
[185]: Tuttle et al. (1996), "A nonlinear model of a harmonic drive gear transmission"

Control bandwidth

On DLR *David*, the torque controller runs at 3 kHz, whereas the underlying current controller runs at 100 kHz [79]. This two-time-scale behavior allows for a cascaded current and torque controller design. Throughout this work, we will consider the actuators as ideal torque sources.

[79]: Jörg et al. (2011), "The computing and communication architecture of the DLR hand arm system"

3.2.2 Euler-Lagrange equations

It is well known that systems described by Euler-Lagrange Equations (EL) posses nice passivity properties that follow directly from energy flow considerations; see, e.g., [191]. In particular, elastic joint robots define a passive operator from applied actuator torques to motor shaft velocities, though it is not passive with respect to the link velocities. Using the kinetic and potential energy functions of an ASR it is straightforward to formulate its Euler-Lagrange equations

[191]: van Schaft (2017), *L2-Gain and Passivity Techniques in Nonlinear Control*

$$\frac{\mathrm{d}}{\mathrm{d}t}\left(\frac{\partial \mathcal{L}}{\partial \dot{\boldsymbol{q}}}(\boldsymbol{q},\dot{\boldsymbol{q}})\right) - \frac{\partial \mathcal{L}}{\partial \boldsymbol{q}}(\boldsymbol{q},\dot{\boldsymbol{q}}) = \mathcal{Q} = \mathcal{N}\boldsymbol{u} - \frac{\partial \mathcal{F}}{\partial \dot{\boldsymbol{q}}}(\dot{\boldsymbol{q}}) + \mathcal{Q}', \tag{3.25}$$

where $\boldsymbol{q} \in \mathbb{R}^n$ denote the generalized coordinates, $\mathcal{L}(\boldsymbol{q},\dot{\boldsymbol{q}}) \triangleq \mathcal{T}(\boldsymbol{q},\dot{\boldsymbol{q}}) - \mathcal{V}(\boldsymbol{q})$ is the Lagrangian with $\mathcal{T}$ and $\mathcal{V}$ representing the kinetic and potential energies, respectively. We consider three types of external forces: control actions ,

A mnemonic: throughout this work index a stands for "actuated" and index u for "unactuated". E.g. n_a denotes the number of actuated coordinates.

interaction of the system with its environment $\mathcal{Q}' \in \mathbb{R}^n$ and dissipation. The control $\boldsymbol{u}_a \in \mathbb{R}^{n_a}$ enters linearly via $\mathcal{N}\boldsymbol{u} \in \mathbb{R}^n$, where $\mathcal{N} \in \mathbb{R}^{n \times n_a}$ denotes a constant input matrix. In some cases the Lagrangian can be adopted to take non-conservative dissipative forces into account. This is in particular the case when the dissipative forces are of the form $-\frac{\partial \mathcal{F}}{\partial \dot{\boldsymbol{q}}}(\dot{\boldsymbol{q}})$, where $\mathcal{F}(\dot{\boldsymbol{q}})$ is the Rayleigh dissipation function which by definition satisfies

$$\dot{\boldsymbol{q}}^{\mathrm{T}} \frac{\partial \mathcal{F}}{\partial \dot{\boldsymbol{q}}} \geq 0 \quad \forall \dot{\boldsymbol{q}} \in \mathbb{R}^n.$$

In this case a non-conservative Lagrangian $\mathcal{L}_{\mathrm{nc}}$ can be formulates that incorporates dissipation

$$\mathcal{L}_{\mathrm{nc}} \triangleq \mathcal{L} + \int_0^t \mathcal{F}(\dot{\boldsymbol{q}}) dt$$

Applying Hamiltonian's principle to this new Lagrangian $\mathcal{L}_{\mathrm{nc}}$ yields (3.25), see [133] for details. In summary, we can characterize the EL equations (3.25) by the EL parameters $\{\mathcal{T}(\boldsymbol{q}, \dot{\boldsymbol{q}}), \mathcal{V}(\boldsymbol{q}), \mathcal{F}(\dot{\boldsymbol{q}}), \mathcal{N}, \mathcal{Q}'\}$. Occasionally, we shall make use of the fact that the LHS of the EL equations (3.25) can be rewritten equivalently in matrix form as:

$$\mathcal{M}(\boldsymbol{q})\ddot{\boldsymbol{q}} + \mathcal{C}(\boldsymbol{q}, \dot{\boldsymbol{q}})\dot{\boldsymbol{q}} + \frac{\partial \mathcal{V}}{\partial \boldsymbol{q}} + \frac{\partial \mathcal{F}}{\partial \dot{\boldsymbol{q}}}(\dot{\boldsymbol{q}}) = \mathcal{Q}, \tag{3.26}$$

with the potential forces $\frac{\partial \mathcal{V}}{\partial \boldsymbol{q}}(\boldsymbol{q})$ constituted by generalized elastic and gravity forces.

THE MAIN CONTRIBUTIONS

From Underactuation to Quasi-Full Actuation

4

A new idea comes suddenly and in a rather intuitive way. But intuition is nothing but the outcome of earlier intellectual experience.

– Albert Einstein

This chapter guides the reader through the intuition and physical reasoning that lead to the development of the novel concept of *quasi full actuation* (QFA) on the basis of simple examples. We start with some physical observations for a series elastic actuator that result in the derivation of input and coordinate transforming equations that allow such system to be treated as if fully actuated. Section 4.1 extends this idea to multi-articulated compliant joints.

In the sense of Tao [180], this chapter should be viewed as the "pre-rigorous" stage building intuition, which is followed by an abstract "rigorous" stage in Chapter 5 generalizing the presented concepts to a class of Euler-Lagrange.

4.1 A Structure Preserving Input and Coordinate Transformation

The proposed approach has strong connections to passivity-based control methods [133, 191], which exploit the robot's intrinsic physical structure. This lies at the core of our idea: exploiting the physical structure of a soft robot to transform it into an easier manageable (controllable) form. This transformation is led by energy considerations. Before continuing, let us recap properties of Euler-Lagrange systems that will be relevant for the following developments. The equilibria of an EL system are determined by the critical points of its potential function. Importantly, given that the potential function has a global and unique minimum, the equilibrium of the EL system is unique and globally stable (as pointed out in Proposition 2.5.2). If suitable[1] damping is present in the system, this equilibrium is asymptotically stable (see again Proposition 2.5.3). These two fundamental properties were first exploited in [178]. Takegaki and Arimoto translated the problem of point regulation of robots into a problem of shaping its potential energy and injecting damping. It can be interpreted as a two-stage approach. First, the potential energy is modified such that the system has a global and unique minimum at the desired equilibrium configuration. Second, the Rayleigh dissipation function is modified to ensure asymptotic convergence.

[133]: Ortega (1998), *Passivity-Based Control of Euler-Lagrange Systems: Mechanical, Electrical, and Electromechanical Applications*
[191]: van Schaft (2017), *L2-Gain and Passivity Techniques in Nonlinear Control*

1: In this chapter, we consider only the case of fully damped closed loops, which is a sufficient but not necessary condition. For certain inertia matrices partial damping is sufficient [152]. A special case is treated in Proposition 2.5.2.

[178]: Takegaki et al. (1981), "A new feedback method for dynamic control of manipulators"

4.1.1 A Rigid Joint

Let us revise the energy shaping concept from Takegaki and Arimoto [178] on the basis of a single robot joint as shown in Fig. 4.1.

Without loss of generality, consider the joint to be represented by a pendulum, constituted by a point mass m on a massless link of unit length, that is driven by an external torque u. Let q be a generalized coordinate representing the link position. The total energy of the system is

$$\mathcal{H} = \underbrace{\tfrac{1}{2}m\dot{q}^2}_{\mathcal{T}(q,\dot{q})} + \underbrace{mg_0(1-\cos q)}_{\mathcal{V}(q)}, \tag{4.1}$$

where g_0 denotes the standard acceleration due to gravity. Let $g(q)$ denote the gravitational force derived from the gravitational potential $\mathcal{V}$, i.e. $g(q) \triangleq \frac{\partial \mathcal{V}}{\partial q}(q)$, then the corresponding Euler-Lagrange equations are

$$m\ddot{q} + g(q) = u. \tag{4.2}$$

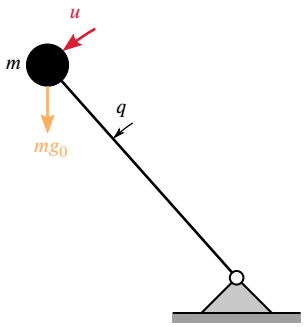

Figure 4.1: A rigid joint with control input u represent a mathematical pendulum. The point mass m on a massless rod reflects the link inertia.

Suppose that we want to asymptotically stabilize the joint at a constant equilibrium $(q, \dot{q}) = (q^*, 0)$, where q^* is the desired equilibrium link position. Then we can do so by modifying the potential energy and Rayleigh function of the system accordingly, while leaving the kinetic energy unchanged. Knowing that a minimum of the potential energy corresponds to a stable equilibrium point, it is clear that the resulting potential function $\mathcal{V}^*$ should have a minimum at $q = q^*$. A basic candidate satisfying this condition is

$$\mathcal{V}^* = \tfrac{1}{2}k_p\tilde{q}^2, \tag{4.3}$$

where $\tilde{q} \triangleq q - q^*$ and $k_p > 0$. In order to render the equilibrium point attractive, we can choose a Rayleigh dissipation function of the form $\mathcal{F}_d(\dot{q}) = \frac{1}{2}k_v\dot{q}^2,\ k_v > 0$. That is, we aim for an EL system characterized by $\{\mathcal{T}(q,\dot{q}), \mathcal{V}^*(q)$ and $\mathcal{F}^*\}$. The corresponding total energy is given by the Hamiltonian

$$\mathcal{H}^* = \underbrace{\tfrac{1}{2}m\dot{q}^2}_{\mathcal{T}(q,\dot{q})} + \underbrace{\tfrac{1}{2}k_p\tilde{q}^2}_{\mathcal{V}^*(q)}. \tag{4.4}$$

Fig. 4.2 shows a visual representation of a system determined by $\mathcal{H}_d$ and $\mathcal{F}^*$.

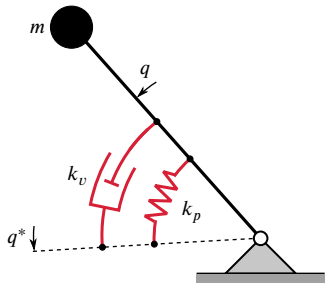

Figure 4.2: A single joint under PD plus gravity cancellation control.

We can easily find a control input for system (4.2) such that its potential function turns into the desired one. It is straightforward to see that

$$u_{PD} = \underbrace{-\frac{\partial V_c}{\partial q}(q)}_{\text{energy shaping}} \underbrace{-\frac{\partial \mathcal{F}_d}{\partial \dot{q}}(\dot{q})}_{\text{damping injection}} = g(q) - k_p\tilde{q} - k_v\dot{q}. \tag{4.5}$$

with the controller potential function

$$\mathcal{V}_c(q) \triangleq \mathcal{V}^*(q) - \mathcal{V}(q), \tag{4.6}$$

produces the desired result. Equation (4.5) represents the popular PD plus gravity cancellation control law. In addition to full-state measurement, the application of this method requires the system to be fully actuated. Applying control input (4.5) to system (4.2), we eventually get the closed-loop model

$$m\ddot{q} + k_v\dot{q} + k_p\tilde{q} = 0, \tag{4.7}$$

as visualized in Fig. 4.2. Clearly, the total energy of the closed loop is given

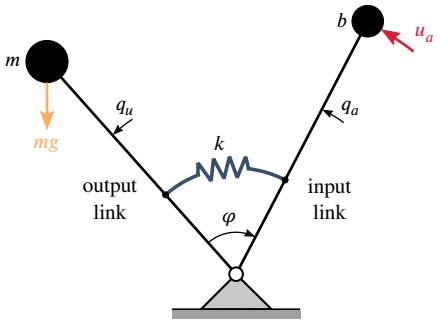

Figure 4.3: An elastic joint represented by two mathematical pendulums. The point masses m and b on massless rods encode the link and reflected motor inertias, respectively. The control input u_a acts on the input link.

by the desired Hamiltonian $\mathcal{H}_d$ in (4.4).

4.1.2 An Elastic Joint

How can we transfer this idea to a series elastic actuator? We start with some initial observations for a single flexible robot joint as shown in Fig. 4.3. Representing the motor inertia by another mathematical pendulum, we can visualize a SEA as indicated in 4.3. To distinguish the two pendulums, we refer to them as *output link* and *input link*. The value of Fig. 4.3 manifests in the fact that it equips us with a simple and intuitive physical picture for all the considerations that are about to come. The unactuated link and actuated motor positions are denoted by q_u and q_a, respectively, where the former is the (noncollocated) output. The link and motor inertias are encoded by the point masses m and b on massless links. Again, without loss of generality, we consider links of unit length. We define the joint deflection as

$$\varphi \triangleq q_a - q_u, \tag{4.8}$$

and the joint stiffness by k. External forces are represented by the vector $\mathcal{Q}' = \left[\mathcal{Q}'_u, \mathcal{Q}'_a\right]^{\mathrm{T}}$. The total energy of the system is

$$\mathcal{H}(q_u, q_a, \dot{q}_u, \dot{q}_a) = \underbrace{\frac{1}{2}\left(m\dot{q}_u^2 + b\dot{q}_a^2\right)}_{\mathcal{T}(\dot{q}_u,\dot{q}_a)} + \underbrace{\frac{1}{2}k(q_a - q_u)^2 + mg(1 - \cos q_u)}_{\mathcal{V}(q_u,q_a)}, \tag{4.9}$$

where $\mathcal{V}$ is the sum of the elastic and gravity potential energies $\mathcal{V}_e$ and $\mathcal{V}_g$. The corresponding Euler-Lagrange equations are

$$\Sigma: \begin{bmatrix} m & 0 \\ 0 & b \end{bmatrix} \begin{bmatrix} \ddot{q}_u \\ \ddot{q}_a \end{bmatrix} + \begin{bmatrix} k & -k \\ -k & k \end{bmatrix} \begin{bmatrix} q_u \\ q_a \end{bmatrix} + \begin{bmatrix} g(q_u) \\ 0 \end{bmatrix} = \begin{bmatrix} 0 \\ u_a \end{bmatrix}. \tag{4.10}$$

Let us continue with some basic physical considerations. Imagine that we had a control input $\bar{u}_u$ that acts directly on the link of system (4.10). This would trivialize the energy shaping and damping injection procedure. However, we only have "indirect" control of the link via the generalized elastic force arising from the potential field $\mathcal{V}_e$

$$\psi(\varphi) = \frac{\partial \mathcal{V}_e(\varphi)}{\partial \varphi} = k\varphi. \tag{4.11}$$

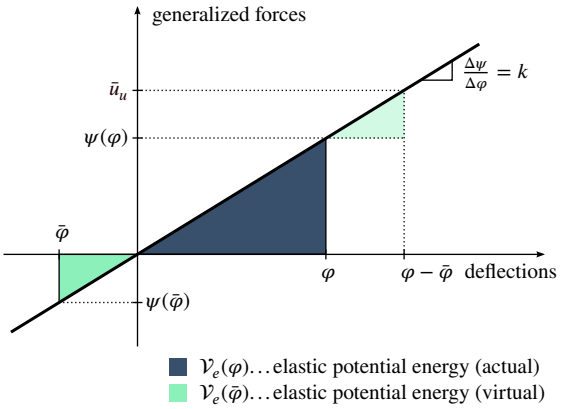

Figure 4.4: State transformations for linear springs: deflection states

We can now express the error between the actual and desired link-side force—analogously to (4.11)—in terms of a generalized force

$$\psi(\bar{\varphi}) \triangleq \psi(\varphi) - \bar{u}_u, \tag{4.12}$$

where $\bar{\varphi}$ represents a *virtual joint* deflection encoding the force error, as visualized in Fig. 4.4. This is the fundamental idea underlying this work; we encode the force error by a virtual joint deflection. The central theme of *duality* is well established in physics and mathematics. In mechanics, many terms are associated into pairs called duals, e.g., force (stress) and deformation (strain) [21]. Here, we introduce a duality between between the force error and a virtual deflection. Using the definition (4.11), we can rewrite (4.12)

$$\bar{\varphi} = \varphi - k^{-1}\bar{u}_u. \tag{4.13}$$

Remark 4.1.1 In (4.12) we are not limited to choosing the same potential function, $\mathcal{V}_e$, for encoding the force error. However, in this work, our goal is to transform the underactuated dynamics into a quasi-fully actuated form while preserving the system structure. For this reason, we choose again potential function $\mathcal{V}_e$.

Introducing new motor coordinates $\bar{q}_a \triangleq \bar{\varphi} + q_u$, in analogous form to (4.8), we can re-formulate (4.13) in terms of motor coordinates

$$\bar{q}_a = q_a - k^{-1}\bar{u}_u. \tag{4.14}$$

Geometrically, the new motor state is formed by shifting the original motor position. The magnitude of the shift is directly proportional to the desired torque $\bar{u}_u$ with the joint compliance k^{-1} being the coefficient of proportionality. Noting that (4.14) has the same form as (4.13), it is clear that Fig. 4.4 serves as visualization of (4.14) as well (simply replace the deflection with the corresponding motor coordinates). Inspired by [86], we use the transforming equations (4.14), to perform a change of coordinates $(q_u, q_a) \to (q_u, \bar{q}_a)$ for system (4.10). Inserting

$$\begin{bmatrix} q_u \\ q_a \end{bmatrix} = \begin{bmatrix} 1 & 0 \\ 0 & 1 \end{bmatrix} \begin{bmatrix} q_u \\ \bar{q}_a \end{bmatrix} + \begin{bmatrix} 0 \\ k^{-1}\bar{u}_u \end{bmatrix} \tag{4.15}$$

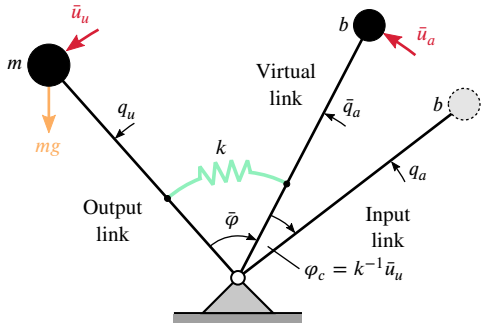

Figure 4.5: A series elastic actuator in its quasi-fully actuated representation.

into (4.10) yields

$$\begin{bmatrix} m & 0 \\ 0 & b \end{bmatrix} \begin{bmatrix} \ddot{q}_u \\ \ddot{\bar{q}}_a \end{bmatrix} + \begin{bmatrix} k & -k \\ -k & k \end{bmatrix} \begin{bmatrix} q_u \\ \bar{q}_a \end{bmatrix} + \begin{bmatrix} g(q_u) \\ 0 \end{bmatrix} = \begin{bmatrix} \bar{u}_u \\ u_a \end{bmatrix} - \begin{bmatrix} 0 \\ \gamma \end{bmatrix} + \mathcal{Q}' \tag{4.16}$$

with $\gamma \triangleq bk^{-1}\ddot{\bar{u}}_u + \bar{u}_u$. Applying the input transformation

$$u_a = \gamma + \bar{u}_a, \tag{4.17}$$

to (4.16), we obtain the "quasi-fully actuated" form

$$\bar{\Sigma}: \begin{bmatrix} m & 0 \\ 0 & b \end{bmatrix} \begin{bmatrix} \ddot{q}_u \\ \ddot{\bar{q}}_a \end{bmatrix} + \begin{bmatrix} k & -k \\ -k & k \end{bmatrix} \begin{bmatrix} q_u \\ \bar{q}_a \end{bmatrix} + \begin{bmatrix} g(q_u) \\ 0 \end{bmatrix} = \begin{bmatrix} \bar{u}_u \\ \bar{u}_a \end{bmatrix} + \mathcal{Q}'. \tag{4.18}$$

Strikingly, by considering q_u and $\bar{q}_a$ as generalized coordinates, the transformed system (4.18) is an EL system with total energy

$$\mathcal{H}(q_u, \bar{q}_a, \dot{q}_u, \dot{\bar{q}}_a) = \underbrace{\tfrac{1}{2}\left(m\dot{q}_u^2 + b\dot{\bar{q}}_a^2\right)}_{\mathcal{T}(\dot{q}_u, \dot{\bar{q}}_a)} + \underbrace{\tfrac{1}{2}k\left(\bar{q}_a - q_u\right)^2 + \mathcal{V}_g(q_u)}_{\mathcal{V}(q_u, \bar{q}_a)},$$

which is visualized in Fig. 4.5. As indicated in Fig. 4.5, the only difference between the dynamics formulation Σ and $\bar{\Sigma}$ is the relative shift of the virtual and actual motor positions for $\bar{u}_u \neq 0$. The EL parameters are $\left\{\mathcal{T}(\dot{q}_u, \dot{\bar{q}}_a), \mathcal{V}(q_u, \bar{q}_a), 0, \mathcal{N}_1\right\}$ with an identity input matrix $\mathcal{N}_1 \triangleq \boldsymbol{I} \in \mathbb{R}^2$ and the new control vector $\bar{\boldsymbol{u}} \triangleq [\bar{u}_u, \bar{u}_a]^{\mathrm{T}}$. Thus, we have transformed the feedback stabilization problem of an underactuated EL system into the feedback stabilization problem of a quasi-fully-actuated EL system. Notice that only the input matrix has changed with all other EL parameters being the *same*. In particular, Σ and $\bar{\Sigma}$ are characterized by the same kinetic and potential energy functions. Consequently, the passivity properties are preserved. System Σ_1 defines an output strictly passive (OSP) map $\mathcal{Q}' \mapsto [\dot{q}_u \ \dot{\bar{q}}_a]^{\mathrm{T}}$. This can be easily shown with $\mathcal{H}$ as storage function.

It is important to point out that our new link-side control input $\bar{u}_u$ obeys some restrictions. From the input transformation (4.17), as visualized in the block-diagram of Fig. 4.6, we know that it must be at least twice differentiable with respect to time.

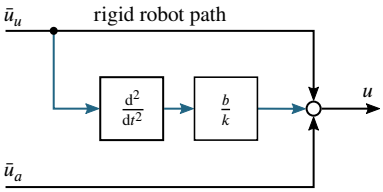

Figure 4.6: Input transformation.

In addition, we must ensure that (4.12) defines a diffeomorphism between the original deflection state φ and the new deflection state $\bar{\varphi}$. In order to simplify the analysis, we assume that $\bar{u}_u$ is solely a function of q_u, $\dot{q}_u$ and t. Further, we assume that $\bar{u}_u$ is a bounded function for bounded q_u, $\dot{q}_u$ and for any $t \in [0, \infty)$. As we will see in the next step, these constraints pose no

obstruction to our goal of adopting the energy shaping technique to solve the regulation problem.

Remark 4.1.2 Note for the special case $\bar{u}_u = 0$, system Σ and $\bar{\Sigma}$ are equivalent, since from (4.14) it follows that $q_a = \bar{q}_a$. In other words, as long as we do not pick a control law for $\bar{u}_u$ the process so far did not change the intrinsic system dynamics at all. Thus, we may conceive (4.17) as a pure input transformation. Only in the second stage, when we design $\bar{u}_u$ and $\bar{u}_a$, we will actually shape the system dynamics.

Considering the quasi-fully actuated system, we could now proceed with applying classical energy shaping and damping injection techniques that have been developed for fully actuated system's such as [178], [98], [136], [164] etc.. However, we want to exploit the duality of the force error and the new deflection state that we introduced in (4.13). Thus, we perform a change of coordinates from the virtual motor space into the virtual deflection space. This has several advantages. First, $\bar{\varphi}$ is directly proportional to the force error. Second, it allows us to exploit the central force field character of the elastic potential [87] to simplify any analysis further down the road. As demonstrated below, this allows separating the potential forces into rigid body and elastic potential forces. This point is absolutely critical for analyzing and controlling the robot arm with respect to the dynamic behavior of its end effector (the unified force and motion control problem in task space). We treat this problem in Chapter 7. Let us continue with applying a coordinate transformation $(q_u, \bar{q}_a) \mapsto (q_u, \bar{\varphi})$ with

[87]: Keppler et al. (2020), "On time-optimal control of elastic joints under input constraints"

$$\begin{bmatrix} q_u \\ \bar{\varphi} \end{bmatrix} = \boldsymbol{T}_2 \begin{bmatrix} q_u \\ \bar{q}_a \end{bmatrix}, \quad \boldsymbol{T}_2 \triangleq \begin{bmatrix} 1 & 0 \\ -1 & 1 \end{bmatrix} \tag{4.19}$$

to system (4.18). Then, the Hamiltonian of $\bar{\Sigma}$ transforms to

$$\begin{aligned} &\mathcal{H}(q_u, q_u + \bar{\varphi}, \dot{q}_u, \dot{q}_u + \dot{\bar{\varphi}}) = \\ &\underbrace{\tfrac{1}{2}\left(m\dot{q}_u^2 + b(\dot{q}_u + \dot{\bar{\varphi}})^2\right)}_{\mathcal{T}(\dot{q}_u, \dot{q}_u + \dot{\bar{\varphi}})} + \underbrace{\tfrac{1}{2}k\bar{\varphi}^2}_{\mathcal{V}_e(\bar{\varphi})} + \mathcal{V}_g(q_u). \end{aligned} \tag{4.20}$$

We can think of this transformation as a separation of the generalized coordinates into rigid, $\bar{q}_u$, and elastic coordinates, $\bar{\varphi}$. We observe that the total potential energy is given by the superposition of a purely rigid and purely elastic potential. The EL parameters expressed in the new coordinates are $\left\{\mathcal{T}(\dot{q}_u, \dot{q}_u + \dot{\bar{\varphi}}), \mathcal{V}(q_u, q_u + \bar{\varphi}), 0, \mathcal{N}_2\right\}$. It is important to remark that only the input matrix has changed to $\mathcal{N}_2 \triangleq \boldsymbol{T}_2^{-\mathrm{T}}\mathcal{N}_1 = \left[\begin{smallmatrix} 1 & 1 \\ 0 & 1 \end{smallmatrix}\right]$. By applying Hamilton's principle to (4.20), we obtain the EL equations

$$\frac{\mathrm{d}}{\mathrm{d}t}\left(\frac{\partial \mathcal{L}}{\partial \dot{q}_u}\right) = -g(q_u) + \sum_{i \in \{u,a\}}^{2} \left(\bar{u}_i + \mathcal{Q}_i'\right), \tag{4.21}$$

$$\frac{\mathrm{d}}{\mathrm{d}t}\left(\frac{\partial \mathcal{L}}{\partial \dot{\bar{\varphi}}}\right) = -k\bar{\varphi} + \bar{u}_a + \mathcal{Q}_a' \tag{4.22}$$

When performing a change of coordinates the virtual work of the generalized forces must be conserved which gives us the last four terms in (4.21). Since the equilibrium of the subsystem (4.21) is independent of $(\bar{q}_a, \dot{\bar{q}}_a)$, it is clear that in order to (asymptotically) stabilize the output at a desired position, it

is sufficient to choose a controller $\bar{u}_u$ with feedback of $q_u, \dot{q}_u$ only. Physically speaking, the LHS of (4.21) describes the rate of change of the *generalized momentum* (also called *canonical momentum*) associated with q_u. Note that we could easily cancel the effect of the gravity field by choosing our rigid input $\bar{u}_u$ accordingly. In this case, the potential function would be independent of the output q_u which would trivializes the energy shaping part of the controller design. In fact, this cancellation would render the output coordinate q_u into a *cyclic coordinate* [52]. Hence its associated conjugate momentum would be conserved and thus become a constant of motion in absence of external forces. In this case (4.21) would describe the motion of the center of mass (q_c), since the LHS describes the rate of change of the generalized momentum associated with the center of mass position. The second EL equation, (4.22), describes the relative motion of the two generalized inertias. We can rewrite (4.21) and (4.22) as

$$\Sigma_3 : \begin{bmatrix} m+b & b \\ b & b \end{bmatrix} \begin{bmatrix} \ddot{q}_u \\ \ddot{\bar{\varphi}} \end{bmatrix} + \begin{bmatrix} 0 & 0 \\ 0 & k \end{bmatrix} \begin{bmatrix} q_u \\ \bar{\varphi} \end{bmatrix} + \begin{bmatrix} g(q_u) \\ 0 \end{bmatrix} = \mathcal{N}_2 \left(\bar{\boldsymbol{u}} + \mathcal{Q}' \right). \quad (4.23)$$

This matrix form can also be obtained straightforwardly by applying the coordinate transformation (4.19) directly to dynamics equations (4.23).

Remark 4.1.3 The implementation of input transformation (4.17) requires the signal $\ddot{\bar{u}}_u$, which can be computed *without differentiation* if $\bar{u}_u$ contains feedback of only q_u and $\dot{q}_u$. This is a fundamental property of the Spong model [168], which is lost in the complete model [126]. To implement the control law (4.17) plus (4.24) requires only position and velocity measurements. However, the fidelity of the model-based calculation of the output acceleration and jerk relies on the availability of an estimation of the external forces and their time derivatives. See Appendix B.2 for a detailed discussion.

4.2 Energy Shaping Control for Series Elastic Joints

We are now in a position where we can adopt the energy shaping technique in a direct manner. Since the noncollocated output is now quasi actuated, we can easily shift the equilibrium of the EL system. We aim for a unique equilibrium at $q_u = q^*$. To this end, we span a virtual spring from the link to its desired position. In addition, we cancel the effect of the gravity field such that the potential energy has a unique minimum at $(q_u, \bar{\varphi}) = (q^*, 0)$. To render this equilibrium attractive we attach a damper to each inertia. The resulting behavior is visualized in Fig. (4.7). This behavior is achieved with the control input

$$\begin{bmatrix} \bar{u}_u \\ \bar{u}_a \end{bmatrix} = \begin{bmatrix} u_{PD} \\ -k_{va}\dot{\bar{q}}_a \end{bmatrix} \quad (4.24)$$

We observe that the first input in (4.24) is simply the rigid joint control law (4.5) (obviously, written in terms of the link coordinate q_u. The second input is used to render the system fully damped. This will be the general pattern for the ASR impedance controllers presented in Chapter 7.

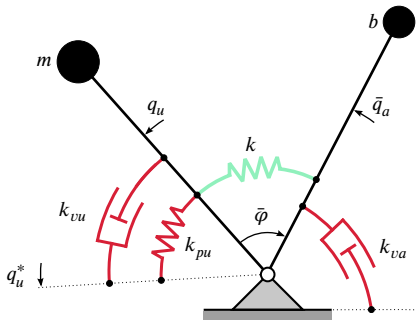

Figure 4.7: A single elastic joint under adopted PD plus gravity cancellation control.

Why does the approach above work? Let us re-derive the controller (4.24), by directly applying the energy shaping machinery, as introduced in [178]. To this end, we express our desired damping behavior in terms of a Rayleigh function.

$$\mathcal{F}_d = \frac{1}{2}\begin{bmatrix}\dot{q}_u\\ \dot{\bar{q}}_a\end{bmatrix}^{\mathrm{T}} \boldsymbol{\mathcal{K}}_v \begin{bmatrix}\dot{q}_u\\ \dot{\bar{q}}_a\end{bmatrix} = \frac{1}{2}\begin{bmatrix}\dot{q}_u\\ \dot{\bar{\varphi}}\end{bmatrix}^{\mathrm{T}} \boldsymbol{T}_2^{-\mathrm{T}} \boldsymbol{\mathcal{K}}_v \boldsymbol{T}_2^{-1} \begin{bmatrix}\dot{q}_u\\ \dot{\bar{\varphi}}\end{bmatrix} \tag{4.25}$$

with the positive gain matrix $\boldsymbol{\mathcal{K}}_v \triangleq \mathrm{diag}\left(k_{vu}, k_{va}\right)$. It is important to note that $\mathcal{N}_2 = \boldsymbol{T}_2^{-\mathrm{T}}$. The desired closed-loop potential energy is given by $\mathcal{V}^* = \mathcal{V}_e(\bar{\varphi}) + \frac{1}{2}k_p\tilde{q}^2$. Our goal is to find a control input $\bar{\boldsymbol{u}}$ such that the closed-loop system is characterized by the EL parameters $\left\{\mathcal{T}(\dot{q}_u, \dot{\bar{q}}_a), \mathcal{V}^*(q_u, \bar{q}_a), \mathcal{F}_d(\dot{q}_u, \dot{\bar{q}}_a)\right\}$. To this end, we choose our input for (4.23) as [178]

$$\mathcal{N}_2\bar{\boldsymbol{u}} = -\begin{bmatrix}\frac{\partial}{\partial q_u}\\ \frac{\partial}{\partial \bar{\varphi}}\end{bmatrix}\mathcal{V}_c(q_u) - \begin{bmatrix}\frac{\partial}{\partial \dot{q}_u}\\ \frac{\partial}{\partial \dot{\bar{\varphi}}}\end{bmatrix}\mathcal{F}_d(\dot{q}_u, \dot{\bar{\varphi}}) \equiv \tag{4.26}$$

$$\bar{\boldsymbol{u}} = -\begin{bmatrix}\frac{\partial \mathcal{V}_c}{\partial q_u}(q_u)\\ 0\end{bmatrix} - \boldsymbol{\mathcal{K}}_v \boldsymbol{T}_2^{-1}\begin{bmatrix}\dot{q}_u\\ \dot{\bar{\varphi}}\end{bmatrix} = \begin{bmatrix}u_{PD}\\ -k_{va}\dot{\bar{q}}_a\end{bmatrix}. \tag{4.27}$$

The potential function $\mathcal{V}_c$ of the controller is defined as in (4.6). The equivalence of (4.26) and (4.27) is due to the fact that we may pre-multiply the LHS and RHS with the inverse of the input matrix $\mathcal{N}_2^{-1}$ since it has full rank. The Hamiltonian of the closed-loop system is given by

$$\mathcal{H}_{cl} = \mathcal{T}(\dot{q}_u, \dot{q}_u + \dot{\bar{\varphi}}) + \mathcal{V}_e(\bar{\varphi}) + \frac{1}{2}k_p\tilde{q}^2, \tag{4.28}$$

where the latter two terms constitute the desired closed-loop potential energy.

4.2.1 Simulation

In this section, we analyze the closed-loop behaviors of the rigid and flexible joint systems that are illustrated in Fig. 4.2 and Fig. 4.7. That is, we consider system (4.2) under control of (4.5) and system (4.10) under control of (4.24). Further, the motor inertia b is shaped to $b^* = \alpha b$, with α representing the motor inertia shaping factor. The system and control parameters are summarized in Table 4.1. The damping parameters are calculated as follows: $k_{vu} = 2\xi\sqrt{m\,k_p}$ and $k_{va} = 2\xi\sqrt{b^*\,k}$. Choosing $\xi = 0.7$ ensures a nice convergence behavior. Both systems are initially at rest with the initial configuration $q_u = \varphi = 0$. The desired output position is $q^* = 0.1$ rad. Fig. 4.8 and Fig. 4.11 show the

m	b	k	k_{pu}	k_{vu}	k_{va}	ξ	α
1	0.2	100	200	19.8	1.98	0.7	0.1
1	0.2	100	200	19.8	6.26	0.7	1
1	0.2	100	200	19.8	19.8	0.7	10

Table 4.1: System and control parameters

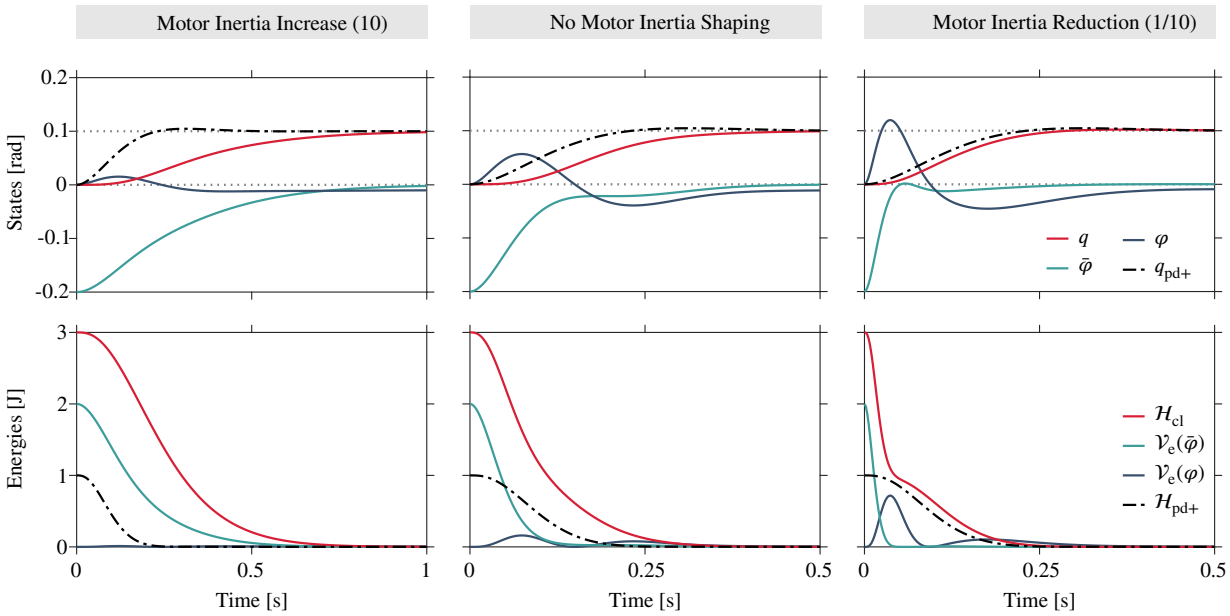

Figure 4.8: Step response of the closed-loop systems illustrated in Fig. 4.2 and Fig. 4.7. The plots illustrate the effect of motor inertia shaping. As anticipated, the link converges to its desired position q^* and $\bar{\varphi}$ converges to zero. The limit value of φ is given by the static equilibrium condition such that the spring torque balances the pull of gravity on the link.

step-responses for different motor inertia values that are due to motor inertia shaping, cf. Table 4.1.

Remark 4.2.1 It makes no difference whether we shape the motor inertia first and then apply the input and state transformation on the shaped system, or, whether we apply the input and coordinate transformation first and then shape the motor inertia utilizing the new motor-side input.

4.3 Dynamics of the QFA System

Note that the points discussed in this section generalize to the multi-joint case which is treated in Chapter 7. However, most aspects of the presented framework can be introduced more intuitively on the basis of a single joint since it provides us with a simple picture of the closed-loop dynamics.

A fundamental aspect of the proposed concept is that it enables damping and stiffness behaviors to be specified directly in terms of the noncollocated output (rigid coordinates). This in turn, allows for an easy adjustment of the output convergence behavior. The tuning reduces to selecting the link-side stiffness and the damping factors. The benefits of controller gains that come with a physical intuition cannot be overestimated for the commissioning and tuning stage of a controller. This intuition is of particular importance when designing controllers for the safe interaction between robots and humans.

It is crucial to understand the effect of the motor inertias on the convergence behavior of the closed-loop system in Fig. 4.7. Physical intuition suggest that reducing motor inertias results in faster motor dynamics and thus smaller springs deflections, $\bar{\boldsymbol{\varphi}}$ during transient. Considering $\bar{\varphi}$'s dual nature to the joint torque error, c.f. (4.12), we conclude that the lower the motor inertia the closer the actual joint torque, $\psi(\varphi)$ approximates the desired joint torque $\bar{u}_u$. This intuition is supported by the simulations results in Fig. 4.8. Notice the increasing convergence rate of $\bar{\varphi}$ from left to right. Naturally, this behavior is also reflected in the decay rate of the potential energy $\mathcal{V}_e(\bar{\varphi})$, (4.20). In other words, for small motor inertia values, the virtual input $\bar{u}_u$ dominates the elastic torque, $\psi(\bar{\varphi})$, such that the dynamic behavior of the flexible joint approaches that of its corresponding rigid joint. This tendency is clearly visible in Fig. 4.8. Notice that not only the variations of q and $q_{\mathrm{PD}+}$ approach each other, but other also the variations of the closed-loop energies of the rigid and elastic joints $\mathcal{H}_{\mathrm{PD}+}$, (4.4), and $\mathcal{H}_{\mathrm{cl}}$, (4.28). In practice, we obviously face limitations regarding to what degree the motor inertia can be lowered, since the control inputs must respect the limits imposed by the respective hardware.

Considering the theoretical limit case of the motor inertia approaching zero, we observe that the last term of the input transformation (4.17) approaches zero. Thus, in the limit case $\boldsymbol{B} \to 0$, the control input (4.17) approaches the rigid joint control law. Interestingly, we observe the same tendency for the limit case $k \to \infty$. In conclusion, for the limit cases $k \to \infty$ and/or $b \to 0$, that would reduce the flexible joint model to the rigid one, the control input (4.17) also reduces to the rigid joint equivalent. The closed-loop behavior in the "almost rigid" case is an important aspect. Clearly, we do want to avoid high-gain designs where the loop gains grow unbounded with increasing stiffness. See [19] for an interesting and detailed discussion.

As a final remark, it is worth noting that the change of coordinates, (4.12), and inputs, (4.17), by itself does not alter the dynamics of the plant. These two transforming equations "merely" allow us to rewrite the system dynamics of underactuated ASRs in a more tractable form by making the transformed dynamics behave as if fully actuated. Only at the moment of picking a control law for the virtual inputs, the system is actually modified.

4.4 The Virtual Coordinates: A Geometric Interpretation

The coordinate transformation (4.36) allows for an elegant geometric interpretation based on the Lagrangian picture of mechanics. Using Fig. 4.3, let us determine the configuration space associated with a series elastic actuator. The configuration of the first pendulum (representing the link inertia) is given by the displacement angle q_u so that the circle S^1 can be associated with the space of all possible configurations. Let the configuration of the second pendulum (representing the motor inertia) be described by the deflection angle φ. We see from the elastic potential energy function $\mathcal{V}_e$, (4.20), that the number of encirclements matter. Moreover precisely, φ can grow unbounded continuously in positive and negative direction suggesting that we view the joint deflection as point on the real number line. Since both links can move independently from each other, the space of all possible configurations is given by product

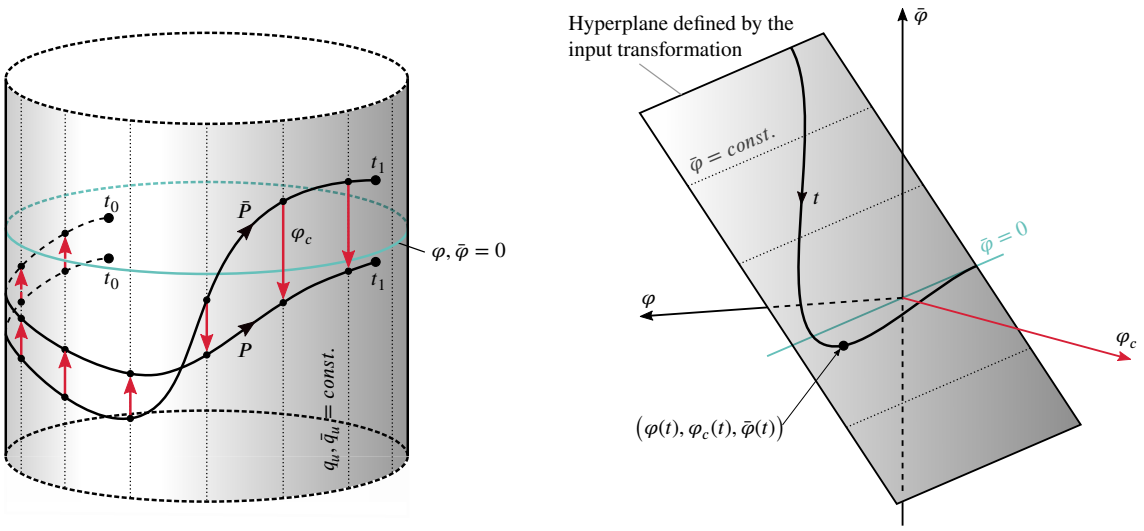

Figure 4.10: (**left**) Time evolution of the C-points associated with Σ and $\bar{\Sigma}$ through the configuration space. (**right**) Alternative geometric interpretation of the coordinate transformation (4.12) as defining a hyperplane in 3D space.

$\mathbb{R} \times S^1$, which is homeomorphic to an cylinder of infinite length, as pointed out in Fig. 4.9.

Considering that Σ and $\bar{\Sigma}$ share the same Lagrangian function, we conclude that the configuration space must be $\mathbb{R} \times S^1$ for both systems. This information allows for an elegant geometric interpretation of the coordinate transformation (4.13). Introducing $\varphi_c \triangleq \bar{u}_u / k$ (see also Fig. 4.5), allows rewriting (4.17) as

$$\varphi - \bar{\varphi} - \varphi_c = 0. \tag{4.29}$$

Let the points P and $\bar{P}$ represent the configuration of Σ and $\bar{\Sigma}$ in $\mathbb{R} \times S^1$. Then, according to (4.29), the trajectories of $\bar{P}$ and P are shifted by φ_c in a direction parallel to the axis of the cylinder, as indicated in Fig. 4.9.

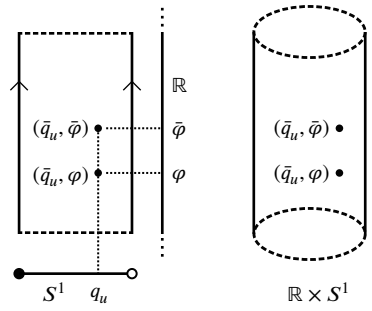

Figure 4.9: Configuration space of a SEA.

Observing that (4.29) defines a hyperplane in $\mathbb{R}^3$ going through the origin as shown in Fig. 4.10, allows for different interpretation. Geometrically speaking, as Σ and $\bar{\Sigma}$ evolve in time, the triplet $\big(\varphi(t), \bar{\varphi}(t), \varphi_c(t)\big)$ traces out a path on that hyperplane. Hence, all solutions of (4.23) evolve on that plane. In general, we wish to design controllers such that the input force error $\bar{\varphi}$ vanishes for $t \to \infty$. In other words, we wish to render the line $\varphi - \varphi_c = 0$ (blue) on the hyperplane (4.29) attractive for $\bar{\Sigma}$. In the Lagrangian picture, this means rendering the subspace $\{0\} \times S^1$ attractive. The controller introduced above achieves this goal as the simulation results in Fig. 4.10 clearly show. Note, that the form of the hyperplane (4.29) is invariant to system parameter variations and applies to any SEA with a linear spring. Projecting this hyperplane into the φ_c, φ-plane allows the evolution of the deflection coordinates to be visualized in a 2D plot. The corresponding isolines are straight since the curvature of the hyperplane is by definition zero at every point. Due to the scaling of the input axis, these isolines are parallel to $\varphi = \varphi_c$ line. Fig. 4.11 shows the time evolution of the point $\big(\varphi(t), \bar{\varphi}(t), \varphi_c(t)\big)$ for the simulation experiments reported above.

Projecting this hyperplane into the φ_c, φ-plane allows the evolution of the deflection coordinates to be visualized in a 2D plot, see Fig. (4.11). These isolines are straight since the curvature of the hyperplane is by definition zero

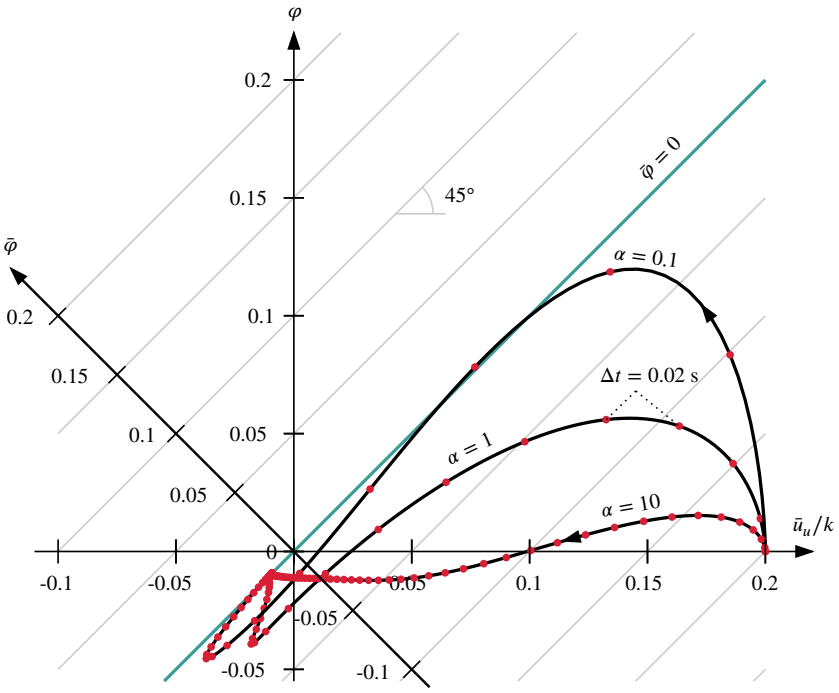

Figure 4.11: A projection of the hyperplane in Fig. 4.10 (right) into the (φ, φ_c)-plane with the gray lines representing its contour lines. The black curves represent the time evolution of the point $(\varphi, \varphi_c, \bar{\varphi})$ for each of the three simulation experiments shown in Fig. 4.8. As the origin of $(\bar{\varphi}, \dot{\bar{q}})$ is globally asymptotically stable, the systems tends to the one-dimensional subspace given by the line $\varphi - \varphi_c = 0$, which is dual to tending to a zero torque error. The effect of scaling the motor inertia on the rate of convergence is clearly visible. The lower the motor inertia, the faster the convergence to the line $\varphi - \varphi_c = 0$.

at every point. Due to the scaling of the input axis, these isolines are parallel to the line $\varphi - \bar{u}_u/k = 0$.

4.5 Extending the Idea of Quasi-Full Actuation

This section sketches out how the QFA concept can be extended to a joint with a nonlinear spring and a multi-articulated joint. Its purpose is mostly to deepen the intuition of the QFA idea and the type of underactuated systems considered throughout this work in order to facilitate understanding of the generalizations of the QFA concept that are developed in the next Chapter.

4.5.1 Nonlinear Springs

Let us assume that the total energy of the system is given by

$$\mathcal{H}(q_u, q_a, \dot{q}_u, \dot{q}_a) = \mathcal{T}(\dot{q}_u, \dot{q}_a) + \mathcal{V}_e(q_a - q_u) + \mathcal{V}_g(q_u), \tag{4.30}$$

with the kinetic energy $\mathcal{T}$ and the gravity potential energy $\mathcal{V}_g$ defined as in (4.9). The EL parameters are $\{\mathcal{T}(\dot{q}_u, \dot{q}_a), \mathcal{V}(q_u, q_a), 0, \mathcal{N}\}$ with $\mathcal{N} \triangleq \left[\begin{smallmatrix} 0 & 0 \\ 0 & 1 \end{smallmatrix}\right]$, input vector $\boldsymbol{u} = [0, u_a]^{\mathrm{T}}$ and $\mathcal{V}$ being the sum of the elastic potential and gravity potential. Applying the EL equations yields the model

$$\Sigma_{q_a}: \begin{bmatrix} m & 0 \\ 0 & b \end{bmatrix} \begin{bmatrix} \ddot{q}_u \\ \ddot{q}_a \end{bmatrix} + \begin{bmatrix} -\psi(q_a - q_u) \\ \psi(q_a - q_u) \end{bmatrix} + \begin{bmatrix} g(q_u) \\ 0 \end{bmatrix} = \begin{bmatrix} 0 \\ u_a \end{bmatrix}. \tag{4.31}$$

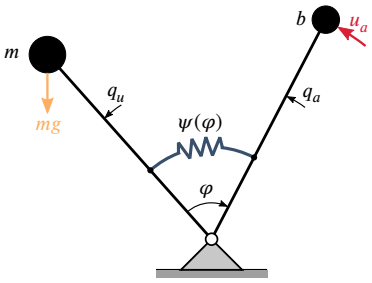

Figure 4.12: An elastic joint with a nonlinear elastic element.

with the generalized elastic force originating from the elastic potential

$$\psi(\varphi) = \frac{\partial \mathcal{V}_e(\varphi)}{\partial \varphi}. \tag{4.32}$$

Applying the coordinate transformation $[q_u, q_a] \to [q_u, \varphi]$ with

$$\begin{bmatrix} q_u \\ \varphi \end{bmatrix} = \boldsymbol{T}_2 \begin{bmatrix} q_u \\ q_a \end{bmatrix}, \quad \boldsymbol{T}_2 \triangleq \begin{bmatrix} 1 & 0 \\ -1 & 1 \end{bmatrix} \tag{4.33}$$

transforms the Hamiltonian (4.30) to

$$\mathcal{H}(q_u, q_u + \varphi, \dot{q}_u, \dot{q}_u + \dot{\varphi}) = \mathcal{T}(\dot{q}_u, \dot{q}_u + \dot{\varphi}) + \mathcal{V}_e(\varphi) + \mathcal{V}_g(q_u). \tag{4.34}$$

Similar to the case in Section 4.1, we can think of this transformation as a separation of the generalized coordinates into rigid and elastic coordinates. The EL parameters are $\{\mathcal{T}(\dot{q}_u, \dot{q}_u + \dot{\varphi}), \mathcal{V}(q_u, q_u + \varphi), 0, \mathcal{N}_\varphi\}$ with an input matrix $\mathcal{N}_\varphi \triangleq \left[\begin{smallmatrix} 0 & 1 \\ 0 & 1 \end{smallmatrix}\right]$. The corresponding EL equations are:

$$\Sigma_\varphi: \begin{bmatrix} m + b & b \\ b & b \end{bmatrix} \begin{bmatrix} \ddot{q}_u \\ \ddot{\varphi} \end{bmatrix} + \begin{bmatrix} -\psi(\varphi) \\ \psi(\varphi) \end{bmatrix} + \begin{bmatrix} g(q_u) \\ 0 \end{bmatrix} = \begin{bmatrix} u_a \\ u_a \end{bmatrix}. \tag{4.35}$$

Again, let $\bar{u}_u$ be the desired link side force. Then, we can express the error between the actual elastic force, $\psi(\varphi)$, and the desired link-side force—analogously to (4.11)—in terms of a generalized elastic forces

$$\psi(\bar{\varphi}) = \frac{\partial \mathcal{V}_e(\bar{\varphi})}{\partial \bar{\varphi}} \triangleq \psi(\varphi) - \bar{u}_u, \tag{4.36}$$

where $\bar{\varphi}$ represents a *virtual joint deflection* that encodes the force error, and thus will also be referred to as deflection error. This equation has the same structure as (4.12), however, with the difference being that $\mathcal{V}_e$ is no longer

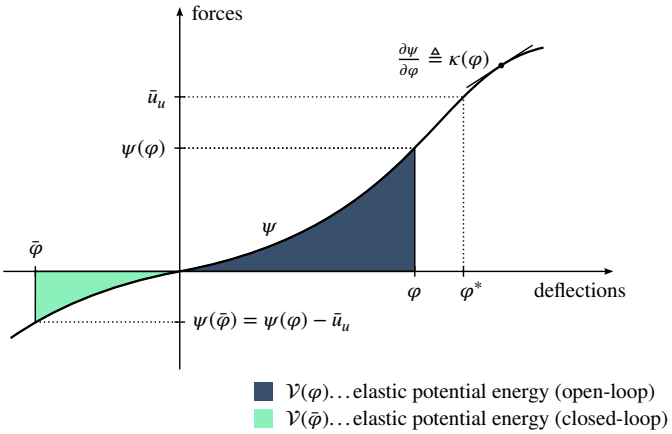

Figure 4.13: Geometric connection between the two deflection coordinates and the desired link-side force. The shaded areas represent the stored elastic potential energies. φ^* can be conceived as desired joint deflection, where the actual joint torque, $\psi(\varphi)$, would match the desired torque, $\bar{u}_u$.

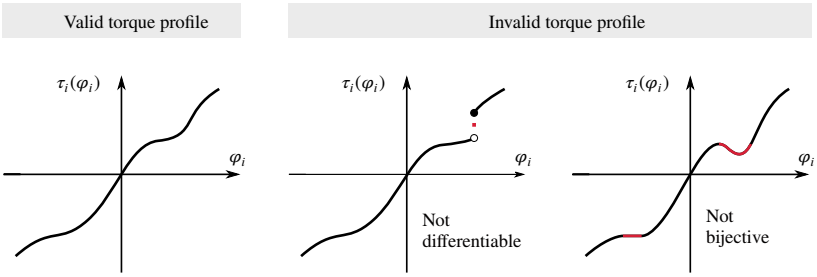

Figure 4.14: Examples of torque characteristics that satisfy and violate the assumption on the elastic potential energy. Only the first function represents a diffeomorphism.

necessarily a quadratic potential function. We must, however, be careful since not any arbitrary potential function $\mathcal{V}_e$ allows this encoding. It is crucial to ensure that the mapping from the force error to the deflection error is bijective. In fact, this mapping must be a C^k, $k \geq 2$, diffeomorphism, c.f. 4.14. In Chapter 5, we will rely on the implicit function theorem to formulate rigorous conditions on the potential function $\mathcal{V}_e$ that guarantee that (4.36), generalized to a multi-DoF system, defines a change of coordinates. For the single joint case, the conditions on $\mathcal{V}_e$ become intuitively clear when connecting a geometrical picture with the mapping between the force error and the deflection error, as shown in Fig. 4.13. Geometrically, the new deflection state is formed by shifting the original deflection state. The magnitude of the shift correlates with the magnitude of the desired torque $\bar{u}_u$.[2] It is straightforward to see that if ψ has a strictly positive slope, i.e.,

$$\kappa(\varphi) \triangleq \frac{\partial \psi}{\partial \varphi}(\varphi) > 0, \tag{4.37}$$

then this mapping is bijective. We conclude that if the potential function $\mathcal{V}_e$ of a given soft joint satisfies (4.37), we can apply the concept of the simultaneous input and state transformation, introduced in Section 4.1, allowing us to treat the joint as quasi-fully actuated. Note that (4.36) no longer defines a hyperplane. The motion of the point $(\varphi, \bar{\varphi}, \bar{u}_u)$ now evolves on a hypersurface in 3D space as illustrated in Fig. 4.15.

2: Notice that the magnitude of the deflection shift is no longer directly proportional to the magnitude of the desired torque as in the linear spring case.

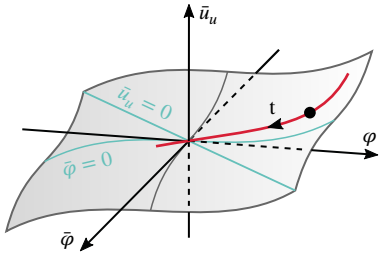

Figure 4.15: Geometric interpretation of the coordinate transforming equation (4.36), which defines a hypersurface in 3D space.

Since (4.36) defines a change of coordinates, given an input $\bar{u}_u$, we can find for any φ a unique $\bar{\varphi}$ and vice versa. This allows us to rewrite the joint dynamics (4.31) in terms of deflection coordinates. Deriving (4.36) with respect to time, we obtain:

$$\kappa(\bar{\varphi})\dot{\bar{\varphi}} = \kappa(\varphi)\dot{\varphi} - \dot{\bar{u}}_u, \tag{4.38}$$

It is worth noting that the velocities always appear linearly in the transforming

equations considered in this work. Deriving (4.36) twice with respect to time, we see that the same is true for the accelerations:

$$\kappa(\bar{\varphi})\ddot{\bar{\varphi}} + \dot{\kappa}(\bar{\varphi})\dot{\bar{\varphi}} = \kappa(\varphi)\ddot{\varphi} + \dot{\kappa}(\varphi)\dot{\varphi} - \ddot{\bar{u}}_u. \tag{4.39}$$

The three transforming equations (4.36), (4.38), (4.39) allow us to rewrite the joint dynamics in terms of the deflection error. In other words, (4.36) qualifies as defining a change of coordinates. After applying this change of coordinates, $(q_u, \varphi) \to (q_u, \bar{\varphi})$, it is possible to find a input transformation of the form $u = u(\bar{u}_u, \bar{u}_a, \dot{\bar{u}}_u, \ddot{\bar{u}}_u, q, \dot{q})$ to obtain the QFA form of Σ:

$$\Sigma_{\bar{\varphi}}: \begin{bmatrix} m+b & b \\ b & b \end{bmatrix} \begin{bmatrix} \ddot{q}_u \\ \ddot{\bar{\varphi}} \end{bmatrix} + \begin{bmatrix} -\psi(\bar{\varphi}) \\ \psi(\bar{\varphi}) \end{bmatrix} + \begin{bmatrix} g(q_u) \\ 0 \end{bmatrix} = \begin{bmatrix} \bar{u}_u + \bar{u}_a \\ \bar{u}_a \end{bmatrix}. \tag{4.40}$$

The general procedure is similar to the one presented in Section 4.1: substitute (4.36), (4.38), (4.39) into (4.35) and compare the resulting dynamics equations with the desired dynamics (4.40). Then choose the control input u_a accordingly to achieve equivalence. A proof detailing the single steps is not presented here as it follows directly from Theorem 5.3.6 developed in Chapter 5.

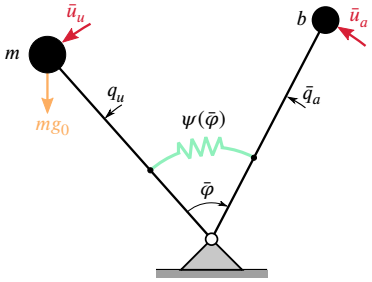

Figure 4.16: The quasi-fully actuated system with the new inputs $\bar{u}_u$ and $\bar{u}_a$.

4.5.2 Bidirectional Antagonistic Variable Stiffness Joint

Let us consider a bidirectional antagonistic variable stiffness (BAVS) joint of the form

$$\Sigma: \begin{bmatrix} m & 0 & 0 \\ 0 & b & 0 \\ 0 & 0 & b \end{bmatrix} \begin{bmatrix} \ddot{q}_u \\ \ddot{q}_{a1} \\ \ddot{q}_{a2} \end{bmatrix} + \begin{bmatrix} \psi_1(q_u, q_a) + \psi_2(q_u, q_a) \\ \psi_1(q_u, q_a) \\ \psi_2(q_u, q_a) \end{bmatrix} + \begin{bmatrix} g(q_u) \\ 0 \\ 0 \end{bmatrix} = \begin{bmatrix} 0 \\ u_{a1} \\ u_{a2} \end{bmatrix}, \tag{4.41}$$

as illustrated in Fig. 4.17 with its QFA representation

$$\bar{\Sigma}: \begin{bmatrix} m & 0 & 0 \\ 0 & b & 0 \\ 0 & 0 & b \end{bmatrix} \begin{bmatrix} \ddot{q}_u \\ \ddot{\bar{q}}_{a,1} \\ \ddot{\bar{q}}_{a,2} \end{bmatrix} + \begin{bmatrix} \psi_1(q_u, \bar{q}_a) + \psi_2(q_u, \bar{q}_a) \\ \psi_1(q_u, \bar{q}_a) \\ \psi_2(q_u, \bar{q}_a) \end{bmatrix} + \begin{bmatrix} g(q_u) \\ 0 \\ 0 \end{bmatrix} = \begin{bmatrix} \bar{u}_u \\ \bar{u}_{a1} \\ \bar{u}_{a2} \end{bmatrix}. \tag{4.42}$$

We need to consider an even more general case where ψ_1 is not the same on the motor and link dynamics. See for example BAVS in DLR David.

Change of coordinates:

$$\psi_1(q_u, q_a) + \psi_2(q_u, q_a) = \psi_1(q_u, \bar{q}_a) + \psi_2(q_u, \bar{q}_a) - \bar{u}_u. \tag{4.43}$$

Since we have only one equation, (4.43), for two unknowns $(\bar{q}_{a1}, \bar{q}_{a2})$, we must impose one additional constraint, e.g.:

$$\psi_c(q_u, q_{a1}, q_{a2}, \bar{q}_{a1}, \bar{q}_{a2}) = 0. \tag{4.44}$$

The constraint equation has to be chosen such that the resulting set of equations /eqref–/eqref satisfies the condition of the implicit function theorem and, thus, guaranteeing a unique solution for $(\bar{q}_{a1}, \bar{q}_{a2})$.

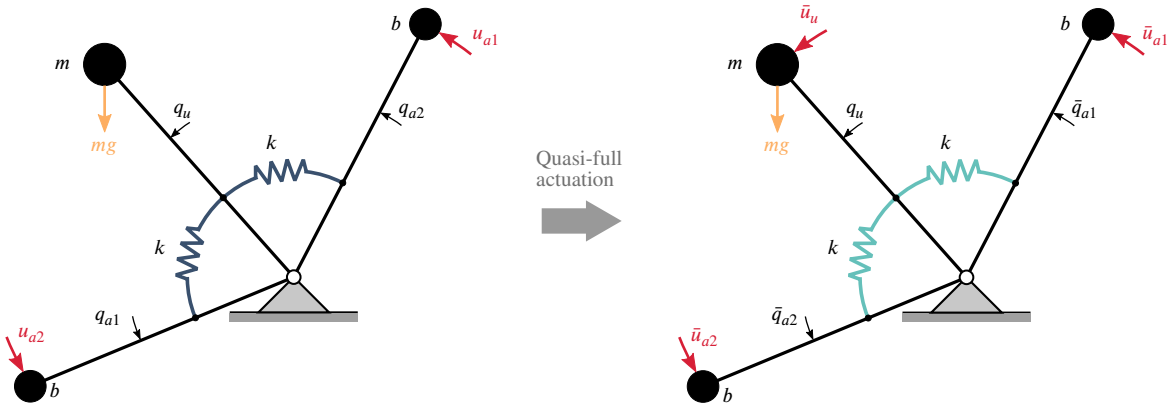

Figure 4.17: A BAVS joint in its original and quasi-fully actuated form. For each input link, one virtual link is introduced.

A Basic Example: Linear Bidirectional Antagonistic Joint

For simplicity, let us consider the case of a bidirectional antagonistic joint with linear[3] spring characteristics as shown in Fig. 4.17. The equations of motion are:

$$\begin{bmatrix} m & 0 & 0 \\ 0 & b & 0 \\ 0 & 0 & b \end{bmatrix} \begin{bmatrix} \ddot{q}_u \\ \ddot{q}_{a1} \\ \ddot{q}_{a2} \end{bmatrix} + \begin{bmatrix} k(q_u - q_{a1}) + k(q_u - q_{a2}) \\ -k(q_u - q_{a1}) \\ -k(q_u - q_{a2}) \end{bmatrix} + \begin{bmatrix} g(q_u) \\ 0 \\ 0 \end{bmatrix} = \begin{bmatrix} 0 \\ u_1 \\ u_a \end{bmatrix}. \quad (4.45)$$

and the corresponding QFA form is given by

$$\begin{bmatrix} m & 0 & 0 \\ 0 & b & 0 \\ 0 & 0 & b \end{bmatrix} \begin{bmatrix} \ddot{\bar{q}}_u \\ \ddot{\bar{q}}_{a1} \\ \ddot{\bar{q}}_{a2} \end{bmatrix} + \begin{bmatrix} k(q_u - \bar{q}_{a1}) + k(q_u - \bar{q}_{a2}) \\ -k(q_u - \bar{q}_{a1}) \\ -k(q_u - \bar{q}_{a2}) \end{bmatrix} + \begin{bmatrix} g(q_u) \\ 0 \\ 0 \end{bmatrix} = \begin{bmatrix} \bar{u}_u \\ \bar{u}_{a1} \\ \bar{u}_{a2} \end{bmatrix}, \quad (4.46)$$

and the required the coordinate transformation (4.43) is:

$$k(q_{a1} - q_u) + k(q_{a2} - q_u) = k(\bar{q}_{a1} - q_u) + k(\bar{q}_{a2} - q_u) - \bar{u}_u, \quad (4.47)$$

which can be further reduced to:

$$q_{a1} + q_{a2} = \bar{q}_{a1} + \bar{q}_{a2} - \bar{u}_u/k. \quad (4.48)$$

With (4.48), we have one equation for two unknowns, $(\bar{q}_{a1}, \bar{q}_{a2})$. Thus an additional constraint equation is required to obtain a system of equations that uniquely defines $(\bar{q}_{a1}, \bar{q}_{a2})$ as a function of (q_{a1}, q_{a2}). Formal conditions are stated by the inverse and implicit function theorems, respectively. Regarding our simple example, it is straightforward to see that

$$q_{a1} - q_{a2} = \bar{q}_{a1} - \bar{q}_{a2} \quad (4.49)$$

is a valid constraint equation candidate. Combining (4.48) and (4.49), we obtain

$$\begin{bmatrix} 1 & 1 \\ 1 & -1 \end{bmatrix} \begin{bmatrix} \bar{q}_{a1} \\ \bar{q}_{a2} \end{bmatrix} = \begin{bmatrix} 1 & 1 \\ 1 & -1 \end{bmatrix} \begin{bmatrix} q_{a1} \\ q_{a2} \end{bmatrix} - \begin{bmatrix} \bar{u}_u/k \\ 0 \end{bmatrix}. \quad (4.50)$$

3: In general, BAVS rely on nonlinear spring characteristics to achieve a variable joint stiffness [14, 195]. However, for the sake of simplicity, linear characteristics are assumed.

Solving (4.50) for the virtual motor coordinates yields

$$\begin{bmatrix} \bar{q}_{a1} \\ \bar{q}_{a2} \end{bmatrix} = \begin{bmatrix} q_{a1} \\ q_{a2} \end{bmatrix} - \frac{1}{2k} \begin{bmatrix} \bar{u}_u \\ \bar{u}_u \end{bmatrix}, \tag{4.51}$$

Substituting (4.45) and (4.51) results in

$$\begin{aligned} &\begin{bmatrix} m & 0 & 0 \\ 0 & b & 0 \\ 0 & 0 & b \end{bmatrix} \begin{bmatrix} \ddot{q}_u \\ \ddot{q}_{a1} \\ \ddot{q}_{a2} \end{bmatrix} + \begin{bmatrix} k(q_u - q_{a1}) + k(q_u - q_{a2}) \\ -k(q_u - q_{a1}) \\ -k(q_u - q_{a2}) \end{bmatrix} + \begin{bmatrix} g(q_u) \\ 0 \\ 0 \end{bmatrix} \\ &= \begin{bmatrix} 0 \\ u_1 \\ u_a \end{bmatrix} - \begin{bmatrix} -\bar{u}_u \\ \frac{1}{2}\left(b/k\ddot{\bar{u}}_u + \bar{u}_u\right) \\ \frac{1}{2}\left(b/k\ddot{\bar{u}}_u + \bar{u}_u\right) \end{bmatrix}. \end{aligned} \tag{4.52}$$

Choosing the input transformation[4]:

$$u_i = \tfrac{1}{2}\left(b/k\ddot{\bar{u}}_u + \bar{u}_u\right) + \bar{u}_{ai}, \tag{4.53}$$

4: As expected from the symmetric nature of the BAVS joint, the link-side torque $\bar{u}_u$ is split in equal parts to the two motors, cf. (4.17).

and making the substitutions (4.52) and (4.53), we obtain the quasi-fully actuated form (4.46), which can be written in matrix form as follows:

$$\mathcal{M}\ddot{\bar{\boldsymbol{q}}} + \mathcal{K}\bar{\boldsymbol{q}} + \boldsymbol{g}(q_u) = \bar{\boldsymbol{u}}. \tag{4.54}$$

with $\bar{\boldsymbol{q}} \triangleq \left[q_u, \bar{q}_{a1}, \bar{q}_{a2}\right]^{\mathrm{T}}$ and

$$\mathcal{M} \triangleq \begin{bmatrix} m & 0 & 0 \\ 0 & b & 0 \\ 0 & 0 & b \end{bmatrix}, \quad \mathcal{K} \triangleq \begin{bmatrix} 2k & -k & -k \\ -k & k & 0 \\ -k & 0 & k \end{bmatrix}, \quad \boldsymbol{g}(q_u) \triangleq \begin{bmatrix} g(q_u) \\ 0 \\ 0 \end{bmatrix}.$$

In order to asymptotically stabilize the system at a desired link position q_u^* in absence of external forces, we can choose, *e. g.*, a simple PD plus gravity cancellation controller:

$$\bar{u}_u = -k_{vu}\dot{q}_u - k_{pu}\tilde{q}_u + g(q_u) \tag{4.55}$$

$$\bar{u}_{a1} = -k_{va1}\dot{\bar{q}}_{a1} \tag{4.56}$$

$$\bar{u}_{a2} = -k_{va2}\dot{\bar{q}}_{a2}, \tag{4.57}$$

with all gains being positive constants and $\tilde{q}_u \triangleq q_u - q_u^*$ denoting the output error. The resulting closed-loop dynamics can be written as

$$\mathcal{M}\ddot{\bar{\boldsymbol{q}}} + \mathcal{K}_v\dot{\bar{\boldsymbol{q}}} + \mathcal{K}\bar{\boldsymbol{q}} + \mathcal{K}_p\tilde{\boldsymbol{q}} = \boldsymbol{0}, \tag{4.58}$$

where $\tilde{\boldsymbol{q}} \triangleq \bar{\boldsymbol{q}} - \boldsymbol{q}^*$, $\boldsymbol{q}^* \triangleq \left[q_u^*, q_u^*, q_u^*\right]^{\mathrm{T}}$ and $\mathcal{K}_p \triangleq \mathrm{diag}(k_{pu}, 0, 0)$. It is straightforward to verify that (4.58) has a unique equilibrium at $\tilde{\boldsymbol{q}} = \boldsymbol{0}$. Note that $\mathcal{K}_v$ is a positive definite matrix. By rewriting (4.58) in terms of error coordinates, the equilibrium is shifted to the origin.

$$\mathcal{M}\ddot{\bar{\boldsymbol{q}}} + \mathcal{K}_v\dot{\bar{\boldsymbol{q}}} + \left(\mathcal{K} + \mathcal{K}_p\right)\tilde{\boldsymbol{q}} + \mathcal{K}\boldsymbol{q}^* = \boldsymbol{0}, \tag{4.59}$$

Using the total energy of the closed-loop dynamics (4.59)

$$\begin{aligned} \mathcal{H} =& \tfrac{1}{2}\left(\dot{\bar{\boldsymbol{q}}}^{\mathrm{T}}\mathcal{M}\dot{\bar{\boldsymbol{q}}} + \bar{\boldsymbol{q}}^{\mathrm{T}}\mathcal{K}\bar{\boldsymbol{q}} + \tilde{\boldsymbol{q}}^{\mathrm{T}}\mathcal{K}_p\tilde{\boldsymbol{q}}\right) \\ =& \tfrac{1}{2}\left(\dot{\bar{\boldsymbol{q}}}^{\mathrm{T}}\mathcal{M}\dot{\bar{\boldsymbol{q}}} + (\tilde{\boldsymbol{q}} + \boldsymbol{q}^*)^{\mathrm{T}}\mathcal{K}(\tilde{\boldsymbol{q}} + \boldsymbol{q}^*) + \tilde{\boldsymbol{q}}^{\mathrm{T}}\mathcal{K}_p\tilde{\boldsymbol{q}}\right), \end{aligned} \tag{4.60}$$

which is a positive and radially unbounded function of $(\tilde{\boldsymbol{q}}, \dot{\tilde{\boldsymbol{q}}})$, as Lyapunov function candidate, we can proof global asymptotic stability of the origin $\tilde{\boldsymbol{q}} = \mathbf{0}$. The time derivative of (4.60), along the solutions of (4.59), is:

$$\dot{\mathcal{H}} = -\dot{\tilde{\boldsymbol{q}}}^{\mathrm{T}} \mathcal{K}_v \dot{\tilde{\boldsymbol{q}}}. \tag{4.61}$$

Invoking La'Salles invariance theorem completes the proof. Since the two sets of motor coordinates, (q_{a1}, q_{a2}) and $(\bar{q}_{a1}, \bar{q}_{a2})$, are in a one-to-one correspondence, the boundedness of the link position and virtual motor coordinates implies boundedness of the original motor coordinates. Evaluating the transforming equations,(4.51), at the equilibrium point $\tilde{\boldsymbol{q}} = \mathbf{0}$, we obtain:

$$\begin{bmatrix} q_{a1} \\ q_{a2} \end{bmatrix} = \begin{bmatrix} q_u^* \\ q_u^* \end{bmatrix} + \frac{1}{2k} \begin{bmatrix} g(q_u^*) \\ g(q_u^*) \end{bmatrix}, \tag{4.62}$$

which denotes the equilibrium point for the motor positions for $t \to \infty$. In the presence of external forces $\mathcal{Q}' \in \mathbb{R}^3$ on the RHS of (4.45), the energy rate of change (4.61) becomes:

$$\dot{\mathcal{H}} = -\dot{\tilde{\boldsymbol{q}}}^{\mathrm{T}} \mathcal{K}_v \dot{\tilde{\boldsymbol{q}}} - \dot{\tilde{\boldsymbol{q}}}^{\mathrm{T}} \mathcal{Q}'. \tag{4.63}$$

Thus, using $\mathcal{H}$ as storage function, we can conclude passivity of the closed-loop system with respect to the power port $\dot{\tilde{\boldsymbol{q}}}^{\mathrm{T}} \mathcal{Q}'$. Further, the closed-loop system can be represented as the negative feedback interconnection of passive subsystems analogously to a SEA joint.

Remark 4.5.1 Due to the symmetric nature of the considered BAVS joint and the particular constraint choice, (4.49), we have at equilibrium that $q_{a1} - q_{a2} = 0$. One of the interesting features of a BAVS joint is the ability to modify the intrinsic stiffness behavior by modulating the pretension of the internal springs, see, e.g., the BAVS actuator of DLR David introduced in Section 3.1.2. In contrast to the simplified example above, this requires in general at least one spring with nonlinear characteristics. In this case, it is possible to design a controller that achieves simultaneous link-side regulation and internal joint stiffness adjustment. By adding a repelling spring between the virtual motor inertias [115] or applying a constant torque offset [114], we can achieve a desired pretension and, thus, a desired stiffness behavior. Since the constraint equation $q_{a1} - q_{a2} = \bar{q}_{a1} - \bar{q}_{a2}$ guarantees that the pretension on the real and virtual system are equal. Thus, achieving a desired pretension on the real system can be simplified to designing a controller for that virtual system that achieves said pretension.

[115]: Mengacci et al. (2021), "Elastic Structure Preserving control for compliant robots driven by agonistic-antagonistic actuators (ESPaa)"

[114]: Meng et al. (2021), "Elastic structure preserving impedance control of bidirectional antagonistic variable stiffness actuation"

4.6 Revisiting the Spong Model

To goal of this section is to offer a physical interpretation for the model reduction proposed by Spong in [168], and to connect geometrical pictures in increasing levels of abstraction with it. The Lagrangian view introduced in the following is fundamental for an intuitive understanding of the developments in Chapter 5.

[168]: Spong (1987), "Modeling and control of elastic joint robots"

First, let us review the model assumptions.

Assumption 4.6.1 (Spong's model [168]) *The system satisfies*

(A1) The kinetic energy of the rotor is due mainly to its own rotation.

In practice, this assumption includes the usual neglecting of motor gyroscopic effects for high-gear actuators [168] and inertial couplings appearing in VIA mechanisms [8]. We further assume.

(A2) The rotor and gear inertias are symmetric about the rotor's axis of rotation such that the gravitational potential and the center of mass position of the system are independent of the angular positions of the rotors.

[8]: Albu-Schäffer et al. (2010), "Dynamic modelling and control of variable stiffness actuators"

In essence, the reduction due to Spong assumes that the kinetic energies of the actuated bodies (motors) are due only to their own spinning. This assumption translates into the fact that the resulting dynamics model has no inertial coupling between the motors and links and leads to a block-diagonal generalized inertia matrix. The motions of the motors and links are only coupled via the forces that are transmitted through the elastic drive train elements. This simplification allows us develop the following geometric view that helps us understanding the dynamics of an articulated soft robot.

(Step 1a) Add each motor mass and inertia to the link it is attached to.
(Step 1b) Calculate the link-side inertia matrix containing these additional inertias and masses.
(Step 1c) The inertia matrix containing the rotor inertias reflected through the gear box is diagonal and constant.
(Step 1d) Since the kinetic energy of each rotor is solely dependent on its own velocity it is invariant to translations. Hence, we can place this rotating inertia anywhere in space. The force transmitted from the rotor to the corresponding link is solely determined by their relative angular position.
(Step 2) The motor dynamics may be equivalently represented through n mathematical pendulums of unit length with point mass values equal in number to the corresponding motor inertias. These pendulums will also be referred to as *virtual links*.
(Step 3) We can think of the motion of an ASR in terms of the motions of two separate subsystems with the transmission of forces solely facilitated through elastic elements.

It is clear that this procedure is generalizable to multi-articulated systems as indicated by Fig. 4.18 (bottom). For each actuator, we introduce a *virtual link* that is interconnected to its corresponding *rigid-body link* via an elastic element. This process is shown for a biantagonistic joints in Fig. 4.18 (bottom).

Let us establish a Lagrangian picture of this abstraction process. Let $\mathcal{C}$ denote the *configuration space*, that is the space of all possible configurations. Then each point in $\mathcal{C}$ encodes a single spatial configuration of the system. Thus, we can represent a system evolving in time by the motion of a single point P through $\mathcal{C}$. The *principle of stationary action* tells us that the path taken by P through $\mathcal{C}$ between times t_0 and t_1 and two fixed points in $\mathcal{C}$ is the one for which the action is stationary. Knowing that we can decompose ASRs into an actuated Σ_a and unactuated subsystem Σ_u (as pointed out in Chapter 5), we can formulate a different picture. Instead of thinking in terms of a single point P moving through $\mathcal{C}$, we can think of two points P_u and P_a—representing

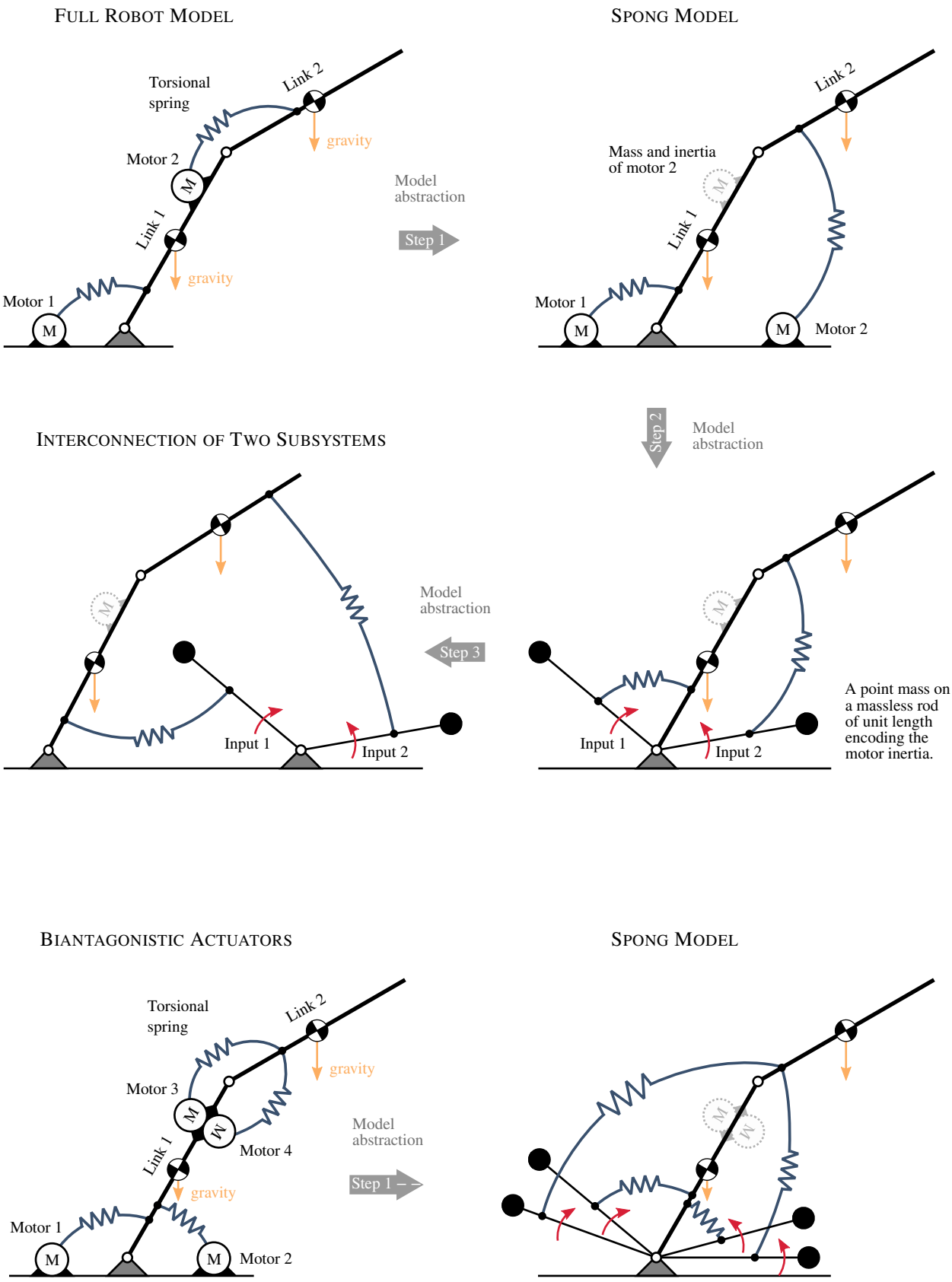

Figure 4.18: Model simplification due to Spong and abstraction thereof. All spring must be considered as pure torsional springs.

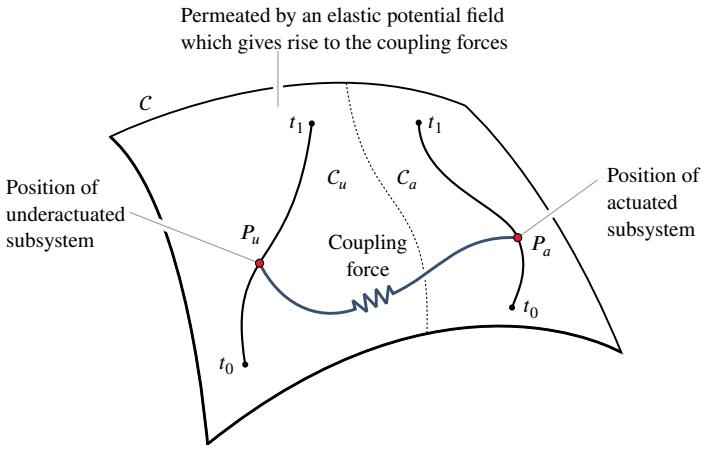

Figure 4.19: Lagrangian picture of the Spong model.

the configurations of Σ_u and Σ_a—moving through the subspaces $\mathcal{C}_u$ and $\mathcal{C}_a$ of $\mathcal{C}$.

The shape of this potential field—and consequently the magnitude and direction of the arising coupling force—is dictated by the relative position of Σ_u and Σ_a. Consequently, the only option to impose a desired motion on the unactuated subsystem Σ_u is to adjust the variation of the coupling force by adjusting the motion of the actuated subsystem accordingly through the input force $\boldsymbol{u}_a$, as indicated in Fig. 4.19 (left).

Chapter 5, which generalizes the concept of quasi-full actuation, shows that it is can be rewarding to adopt this Lagrangian view.

4.7 Summary

Based on a simultaneous change of coordinates ($\boldsymbol{q} \to \bar{\boldsymbol{q}}$) and inputs ($\boldsymbol{u} \to \bar{\boldsymbol{u}}$), this chapter presented a methodology that enables a compliant joint to be treated as if fully actuated. The transformation preserves entirely the Lagrangian structure of the system. Since the virtual inputs on the unactuated subsystem must obey some smoothness and feedback constraints, the transformed system is referred to as quasi-fully actuated. Intuitively, we may think of the virtual coordinates, $\bar{\boldsymbol{q}}$, as encoding the error between the desired and actual link-side control force.

From the control point view, the structural properties of the transformed system that are most notable for control are:

- For each degree of freedom there is one virtual input
- The QFA system (4.18) defines a passive map $\bar{\boldsymbol{u}} \to \dot{\bar{\boldsymbol{q}}}$ with the Hamiltonian associated with $\bar{\Sigma}$ as storage function.

The QFA formulation significantly simplifies the control design for elastic joints since it enables the adoption of classical rigid joint controllers and the associated stability arguments. Such adoption is demonstrated exemplary on the basis of energy shaping and damping injection control in Chapter 6. It is worth recalling that an elastic joint defines a passive operator from applied actuator torques to motor shaft velocities, though it is not passive with respect to the link velocities. The lack of passivity from the input to the output position complicates the design of passivity-based controllers. Considering the second

point above, it is clear that this issue is resolved in the quasi-fully actuated representation of a compliant joint.

Generalizing the Concept of Quasi-Full Actuation

5

All generalizations,
with the possible exception of this one,
are false.

– Kurt Gödel

This chapter contains the central theoretical contribution of this work. The results serve as basis for several later developments. Chapter 4 introduced a transformation allowing compliant joints to be treated as quasi-fully actuated. This chapter treats the generalization of this novel idea to a class of underactuated EL systems that is specified in Section 5.1. The *input and coordinate transformations* (ICT) that produce the quasi-fully actuated representation of an Euler-Lagrange system entirely preserve its structure. The procedure is summarized in a "cook recipe" in Fig. 5.1. Before starting with the main developments, we shall provide some arguments for choosing a variational principle based formulation and why I deem the act of generalization of importance in a field related to mathematics. Although the presented results allow for a rich geometrical interpretation, in an attempt to make them easier accessible, differential geometry methods are avoided whenever possible.

Reasons for a Variational Principle-Based Formulation

Many underactuated systems found in engineering, and ASRs in particular, are nonlinear by nature and, thus, can exhibit extremely complex behaviors. In this regard, the quest for an universal control framework that covers underactuated nonlinear systems in all their facets is likely a hopeless endeavor, and we must specialize the class of systems under consideration. This work focuses on systems where Hamilton's principle can be used to obtain the equations of motion. Hamilton's principle states that the path actually followed by a physical system is that for which the action is stationary. In other words, the action satisfies a variational principle. The solution to this variational problem are the Euler-Lagrange equations. For this reason, systems for which the equations of motion can be obtained from the principle of stationary action shall be referred to as Euler-Lagrange (EL) systems.

The choice for a variational principle based modeling method is motivated due to the following reasons:

- The form of the developed transforming equations and control laws are invariant with regard to the choice of coordinates.
- EL systems cover a big class of contemporary robot systems.
- The modeling is fundamentally linked to the energy of a system.
- We often get a storage or Lyapunov function for "free" using the Hamiltonian associated with an EL system.
- By thinking in terms of energies and flow thereof, we observe that the systems under consideration can be represented as the interconnections of simpler subsystems.
- System symmetries are easily revealed and can potentially be exploited.

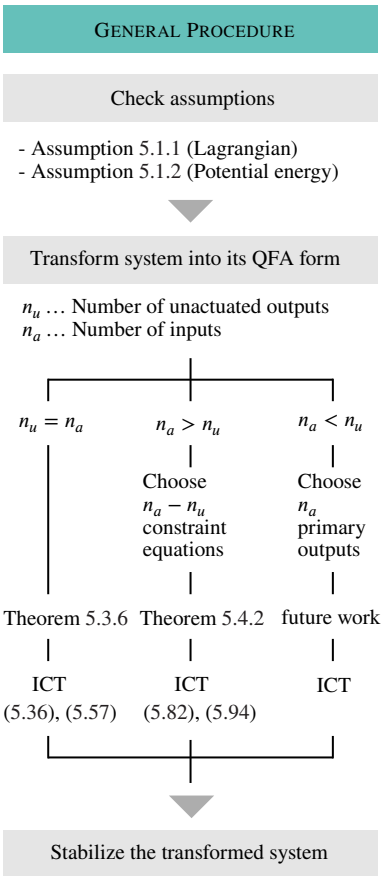

Figure 5.1: Stabilization through the QFA formulation.

Why Aim for a Generalization?

Man muss immer generalisieren.
— C.G.J. Jacobi

Generalization proved to be paramount in the evolution of mathematics and can be defined as "looking for the bigger picture" [179]. Specific results may be useful in themselves, however, characteristically mathematical results are of general nature. When developing a mathematical framework, we can think of going through three phases [62]: (1) specialization, (2) conjecturing, (3) generalization. Phase one consists of solving specific cases. Once we identify connections between specific problems and sense an underlying pattern, even if we cannot articulate it, conjecturing starts. The next main stage is generalization. Based on our experience and intuition obtained from working on specific examples, we formulate a general concept and work on a proof. The same can be said about control theory which can be understood as an applied branch of mathematics.

[179]: Tall (2011), "Looking for the bigger picture"

[62]: Hashemia et al. (2013), "Generalization in the learning of mathematics"

In this sense, Chapter 4 reports the specialization phase. A novel idea was developed and applied to very specific and basic problems. Section 5.2 introduces the central idea underlying all developments in this chapter and represents the conjecturing phase. The generalization phase culminates in the formulation of Theorem 5.3.6 and 5.4.2. The former theorem is actually contained in the latter. However, since the proof of Theorem 5.4.2 is somewhat intricate, it will be rewarding to proof Theorem 5.3.6 first and use it as stepping stone for deriving the latter.

Generalizations that go beyond the presented results, likely require going through the three phases again. In this regard, particular attention should be devoted to finding simple examples that allow a weakening of the assumptions considered in this chapter.

5.1 A Class of Euler-Lagrange Systems

This section specifies the class of underactuated EL systems treated in this chapter. Let $\boldsymbol{q} = (q_1, \dots, q_n)$ be a set of generalized coordinates for a system with a Lagrangian $\mathcal{L}$ and n degrees of freedom that is subject to n generalized external forces $\mathcal{Q} = (\mathcal{Q}_1, \dots, \mathcal{Q}_n)$ such that

$$\Sigma : \frac{\mathrm{d}}{\mathrm{d}t}\frac{\partial \mathcal{L}}{\partial \dot{\boldsymbol{q}}} - \frac{\partial \mathcal{L}}{\partial \boldsymbol{q}} = \mathcal{Q}. \tag{5.1}$$

Two types of external forces will be considered[1]: the control actions, $\boldsymbol{u}$, and external forces, $\mathcal{Q}'$, arising from the system's interaction the environment such that

$$\mathcal{Q} = \mathcal{Q}' + \boldsymbol{u}. \tag{5.2}$$

1: In general, it is possible to extend the theorems presented in this chapter to dynamic systems which are subject to dissipative forces. However, in order to keep things simple and to keep the focus on the central idea, only conservative systems are considered in the following.

Let n_u and $n_a = n - n_u$ be the numbers of unactuated and actuated coordinates, respectively. According to Definition 2.6.1 in Section 2.6, a set of coordinates is called unactuated if the associated accelerations cannot be changed instantaneously to an arbitrary value through an appropriate control action. In contrast, we consider a coordinate to be actuated if the associated acceleration can be instantly assigned to an arbitrary value through the control inputs. Obviously, if we ask for arbitrary instantaneous changes of acceleration, it must be assumed that no bounds on the control signals exist.

Notation: Coordinates, Forces and Subindices

Boldface variables such as $\boldsymbol{q}, \bar{\boldsymbol{q}}$ represent a set of n generalized coordinates, e.g. $\boldsymbol{q} = (q_1, \dots, q_n)$, $\dot{\boldsymbol{q}}, \ddot{\boldsymbol{q}}$ represent the corresponding sets of generalized velocities, and $\mathcal{Q}, \bar{\mathcal{Q}}$ denote the n generalized external forces. The following indices are used consistently throughout this work:

$$(.)_u \dots \text{unactuated},$$
$$(.)_a \dots \text{actuated}.$$

Following this notation, it is convenient to partition the sets of generalized coordinates and forces into subsets with n_u and n_a elements, respectively,

$$\boldsymbol{q} = \left(\boldsymbol{q}_u, \boldsymbol{q}_a\right),\ \mathcal{Q} = \left(\mathcal{Q}_u, \mathcal{Q}_a\right),\ \boldsymbol{u} = \left(\boldsymbol{0}, \boldsymbol{u}_a\right) \text{ and } \mathcal{Q}' = \left(\mathcal{Q}'_u, \mathcal{Q}'_a\right),$$
$$\bar{\boldsymbol{q}} = \left(\bar{\boldsymbol{q}}_u, \bar{\boldsymbol{q}}_a\right),\ \bar{\mathcal{Q}} = \left(\bar{\mathcal{Q}}_u, \bar{\mathcal{Q}}_a\right),\ \bar{\boldsymbol{u}} = \left(\bar{\boldsymbol{u}}_u, \bar{\boldsymbol{u}}_a\right) \text{ and } \bar{\mathcal{Q}}' = \left(\bar{\mathcal{Q}}'_u, \bar{\mathcal{Q}}'_a\right).$$

For the considerations of this chapter, it is helpful to split the EL equations (5.1) into *unactuated* and *actuated subsystems*

$$\Sigma_u : \frac{\mathrm{d}}{\mathrm{d}t}\frac{\partial \mathcal{L}}{\partial \dot{q}_i} - \frac{\partial \mathcal{L}}{\partial q_i} = \mathcal{Q}'_i, \qquad i = 1, \dots, n_u \tag{5.3}$$
$$\Sigma_a : \frac{\mathrm{d}}{\mathrm{d}t}\frac{\partial \mathcal{L}}{\partial \dot{q}_i} - \frac{\partial \mathcal{L}}{\partial q_i} = \mathcal{Q}'_i + u_i, \quad i = n_u + 1, \dots, n. \tag{5.4}$$

In practice, we can assign underactuated EL systems usually to one of the following three categories:

- Class 1: equal number of inputs and unactuated coordinates
- Class 2: more inputs than unactuated coordinates (multi-articulation)
- Class 3: less inputs than unactuated coordinates

This work focuses on Class 1 and 2 systems for which the Lagrangian can be decomposed as follows.

Assumption 5.1.1 *The Lagrangian of* (5.1) *can be decomposed in the form*

$$\mathcal{L}\left(\boldsymbol{q}, \dot{\boldsymbol{q}}\right) = \mathcal{L}_u\left(\boldsymbol{q}_u, \dot{\boldsymbol{q}}_u\right) + \mathcal{L}_a\left(\boldsymbol{q}, \dot{\boldsymbol{q}}_a\right), \tag{5.5}$$

with the sub-Lagrangians of the form

$$\mathcal{L}_u = \mathcal{T}_u(\boldsymbol{q}_u, \dot{\boldsymbol{q}}_u) - \mathcal{V}_u(\boldsymbol{q}_u), \tag{5.6}$$
$$\mathcal{L}_a = \mathcal{T}_a(\boldsymbol{q}_a, \dot{\boldsymbol{q}}_a) - \mathcal{V}_a(\boldsymbol{q}). \tag{5.7}$$

The matrix $\frac{\partial^2 \mathcal{L}}{\partial \dot{\boldsymbol{q}}^2}$ *is invertible.*[2] *The Hamiltonians*

$$\mathcal{H}_u = \sum_i \dot{q}_i \frac{\partial \mathcal{L}_u}{\partial \dot{q}_i} - \mathcal{L}_u, \ i = 1, \dots, n_u \tag{5.8}$$
$$\mathcal{H}_a = \sum_i \dot{q}_i \frac{\partial \mathcal{L}_a}{\partial \dot{q}_i} - \mathcal{L}_a, \ i = n_u + 1, \dots, n \tag{5.9}$$

are bounded from below.

2: This is called the *Hessian condition*. Since the Lagrange's equations are of second order, it must be satisfied to ensure that the system's acceleration can be calculated from its state, as discussed in [80, p. 69]. For dealing with systems that violate this condition (in the Hamiltonian formalism) see [39].

This assumption is central for all derivations in this chapter. It is satisfied by EL systems with a positive definite and block-diagonal generalized inertia

matrix. We can think of Assumption 5.1.1 as expressing the fact that Σ is constituted by two subsystems Σ_u and Σ_a with the kinetic energies of each subsystem being only due to its own velocity. Both subsystems only interact via a coupling force originating from the potential field $\mathcal{V}$. We will sharpen this point of view below in Proposition 5.1.1.

Remark 5.1.1 For some systems, Assumption 5.1.1 introduces ambiguity in terms of what part of the potential energy is assigned to which sub-Lagrangian. Clearly, the equations of motion are independent of the choice made. It is important to underline that the extended phase space transformation, introduced in this chapter, is also invariant to the particular choice being made in this regard. Without loss of generality, let us assume that $\mathcal{V}$ is a superposition of multiple potential functions. Then, according to Assumption 5.1.2, we have the following rules for splitting $\mathcal{V}$ into $\mathcal{V}_u$ and $\mathcal{V}_a$:

- Any potential function that is a function of the configuration, $\boldsymbol{q}$, must be assigned to $\mathcal{L}_a$.
- Any potential function that is only a function of the actuated coordinates, $\boldsymbol{q}_a$, must be assigned to $\mathcal{L}_a$.
- Any potential function that is only a function of the unactuated states, $\boldsymbol{q}_u$, can be assigned to either $\mathcal{L}_u$ or $\mathcal{L}_a$.

The following properties follow from Assumption 5.1.1 immediately.

3: See Theorem D.3.2 in Appendix D.

Property 1. Considering Assumption 5.1.1, Schur's determinant identity[3] asserts that the matrices

$$\frac{\partial^2 \mathcal{L}_k}{\partial \dot{\boldsymbol{q}}_k^2},\ k = (u, a), \tag{5.10}$$

are invertible.

Property 2. From Assumption 5.1.1, it follows that the subsystem coupling forces are comprised of potential forces only, that is

$$\boldsymbol{\psi} = \frac{\partial \mathcal{L}_a}{\partial \boldsymbol{q}_u} = -\frac{\partial \mathcal{V}}{\partial \boldsymbol{q}_u}. \tag{5.11}$$

Let us further assume the following.

Assumption 5.1.2 *The potential energy function $\mathcal{V}$ is of class C^k, $k \geq 3$. Moreover, for $n_u = n_a$ (monoarticulation) at least one of the following two conditions is satisfied*[4]

(i) $|\partial_{\boldsymbol{q}_a} \boldsymbol{\psi}(\boldsymbol{q})| > 0,\ \forall \boldsymbol{q} \in \mathbb{R}^n,$
$\|\dot{\boldsymbol{q}}_a\| \to \infty$ *implies* $|\partial_{\boldsymbol{q}_a} \boldsymbol{\psi}(\boldsymbol{q}) \dot{\boldsymbol{q}}_a| \to \infty,\ \forall \boldsymbol{q} \in \mathbb{R}^n,$
$\|\boldsymbol{q}_a\| \to \infty$ *implies* $\|\boldsymbol{\psi}(\boldsymbol{q})\| \to \infty,\ \forall \boldsymbol{q}_u \in \mathbb{R}^{n_u}$

(ii) $|\partial_{\boldsymbol{q}_a} \boldsymbol{\psi}(\boldsymbol{q})| \geq c > 0, \forall \boldsymbol{q} \in \mathbb{R}^n,$

for some positive constant c.

4: Suppose that $\sigma_m(\partial_{\boldsymbol{q}_a} \boldsymbol{\psi}) \geq k$. Then, noting that $\|\boldsymbol{U}\boldsymbol{x}\|_2 = \|\boldsymbol{x}\|_2$ for an unitary matrix $\boldsymbol{U}$, we can this property and singular value decomposition to show that $\|\partial_{\boldsymbol{q}_a} \boldsymbol{\psi} \ddot{\boldsymbol{q}}_a\| \geq k \|\ddot{\boldsymbol{q}}_a\|$.

From Assumption 5.1.2, we can immediately derive the following statements which shall prove useful for proofing Lemma 5.3.1 and 5.4.1 below.

Property 3. For the case $n_u = n_a$, Assumption 5.1.2 implies the following:

(P1) $\|\dot{\boldsymbol{q}}_a\| \to \infty$ implies $|\partial_{\boldsymbol{q}_a}\boldsymbol{\psi}(\boldsymbol{q})\dot{\boldsymbol{q}}_a| \to \infty, \forall \boldsymbol{q} \in \mathbb{R}^n$,

Moreover, let c be some positive constant, then depending on whether (i) or (ii) holds, we either have that

(P2) $\det\{\partial_{\boldsymbol{q}_a}\boldsymbol{\psi}(\boldsymbol{q})\} \neq 0, \forall \boldsymbol{q} \in \mathbb{R}^n$,

or

(P3) $|\det\{\partial_{\boldsymbol{q}_a}\boldsymbol{\psi}(\boldsymbol{q})\}| \geq \sigma_m\{\partial_{\boldsymbol{q}_a}\boldsymbol{\psi}(\boldsymbol{q})\}^{n_u} = c > 0, \forall \boldsymbol{q} \in \mathbb{R}^n$.

Proof of (P1). For any unitary matrix $\boldsymbol{U}$, we have that $\|\boldsymbol{U}\boldsymbol{x}\| = \|\boldsymbol{x}\|$. Thus, we can show that for some matrix $\boldsymbol{A}$ with $\sigma_m(\boldsymbol{A}) > 0$ it follows that $\|\boldsymbol{A}\| \geq \sigma_m(\boldsymbol{A})\|\boldsymbol{x}\|$, which can be shown exploiting the spectral norm property $\|\boldsymbol{A}\|_2 = \sqrt{\lambda_m(\boldsymbol{A}^*\boldsymbol{A})} = \sigma_m(\boldsymbol{A})$. Using this property, then $(P1)$ follows trivially. ■

Proof of (P2) and (P3). Knowing that for some $n \times n$ square matrix $\boldsymbol{A}$ that $|\det(\boldsymbol{A})| = \prod_i^n \sigma_i(\boldsymbol{A})$ the properties (P2) and (P3) follow immediately. ■

Remark 5.1.2 The corresponding conditions for the multiarticulation case ($n_a > n_u$) are summarized in Assumption 5.4.2.

Since all further developments rely on this fundamental assumption, let us try to obtain an intuitive understanding. Suppose that Assumption 5.1.1 is satisfied, then the EL system (5.1) can be decomposed into two interconnected passive subsystems. This important property is summarized in the following proposition.[5]

Proposition 5.1.1 (Passive subsystem decomposition [133, p. 25]) *Assume that the Lagrangian* (5.1) *can be decomposed in the form* (5.5)*. Then the EL system* (5.1) *can be represented as the negative feedback interconnection of two passive subsystems as indicated by Fig. 5.2*

$$\Sigma_u : (\boldsymbol{\psi} + \mathcal{Q}_u) \mapsto \dot{\boldsymbol{q}}_u, \tag{5.12}$$

$$\Sigma_a : \begin{bmatrix} \mathcal{Q}_a \\ -\dot{\boldsymbol{q}}_u \end{bmatrix} \mapsto \begin{bmatrix} \dot{\boldsymbol{q}}_a \\ \boldsymbol{\psi} \end{bmatrix}, \tag{5.13}$$

with storage functions (5.8) *and* (5.9)*, respectively, where*

$$\boldsymbol{\psi} \triangleq \frac{\partial \mathcal{L}_a}{\partial \boldsymbol{q}_u}(\boldsymbol{q}, \dot{\boldsymbol{q}}_a), \tag{5.14}$$

is the subsystem coupling signal.

With the insight from Proposition 5.1.1, it is clear that Assumption 5.1.2 poses a condition on the partial derivative of the coupling signal. Since $\boldsymbol{\psi}$ has the dimension of a generalized force, the partial Jacobian $\partial_{\boldsymbol{q}_a}\boldsymbol{\psi}$ denotes the partial stiffness matrix of the coupling forces. Loosely speaking, we can think of condition (ii) in Assumption 5.1.2 as some form of "controllability" condition. Appendix B provides a geometric interpretation of Assumption 5.1.2 by revealing its connection to the conditions for differential flatness of (5.1). At this point it should be clear why the exact procedure of splitting $\mathcal{V}$ into $\mathcal{V}_u$ and $\mathcal{V}_a$ is of no concern. Independent of the choice that we make in this regard (in

5: Notice that the storage functions in Proposition 5.1.1 are given by $\mathcal{H}_u$ and $\mathcal{H}_a$, whereas in Proposition 2.10 in [133, p. 25] the Lagrangians $\mathcal{L}_u$ and $\mathcal{L}_a$ were used instead. Without further assumptions, the latter choice can be problematic since a storage function is required by definition to be bounded from below.

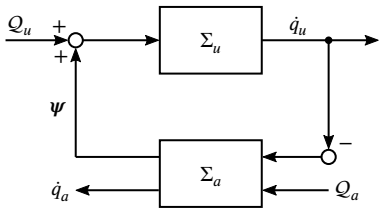

Figure 5.2: Passive decomposition of an EL system.

compliance with Assumption 5.1.1), the subsystem coupling force remains invariant.

Notation: $[.]_q$ vs. $[.]_{\bar{q}}$

The considerations of this chapter involve going from one set of generalized coordinates $\boldsymbol{q}$ to a new set $\bar{\boldsymbol{q}}$ by transformation equations of the form $\bar{q}_i = \bar{q}_i(\boldsymbol{q}, \dot{\boldsymbol{q}}, t)$ and $\dot{\bar{q}}_i = \dot{\bar{q}}_i(\boldsymbol{q}, \dot{\boldsymbol{q}}, t)$. We shall use the following notation convention to improve the readability of the text. The subindices $[.]_q$ and $[.]_{\bar{q}}$ indicate that the term in brackets is a function that is evaluated in terms of the $(\boldsymbol{q}, \dot{\boldsymbol{q}})$'s and $(\bar{\boldsymbol{q}}, \dot{\bar{\boldsymbol{q}}})$'s, respectively. For example, given some Lagrangian function $\mathcal{L} : \mathbb{R}^n \times \mathbb{R}^n \times \mathbb{R}^+ \to \mathbb{R}^n$, we have that:

$$\left[\mathcal{L}\right]_q \triangleq \mathcal{L}(\boldsymbol{q}, \dot{\boldsymbol{q}}, t); \quad \left[\mathcal{L}\right]_{\bar{q}} \triangleq \mathcal{L}(\bar{\boldsymbol{q}}, \dot{\bar{\boldsymbol{q}}}, t).$$

It is important to notice that $[.]_{\bar{q}}$ does not indicate that the expression $[.]$ is evaluated in terms of the $\bar{\boldsymbol{q}}'s$ through the transforming equations, indeed we have in general that $\left[\mathcal{L}\right]_{\bar{q}} \neq \left[\mathcal{L}\right]_q = \mathcal{L}\left(\boldsymbol{q}(\bar{\boldsymbol{q}}), \dot{\boldsymbol{q}}(\bar{\boldsymbol{q}}), t\right)$. The same notation rules are applied to partial derivatives of a function

$$\left[\frac{\partial \mathcal{L}}{\partial \bar{\boldsymbol{q}}}\right]_{\bar{q}} \triangleq \frac{\partial}{\partial \bar{\boldsymbol{q}}}\left[\mathcal{L}\right]_{\bar{q}} = \frac{\partial}{\partial \bar{\boldsymbol{q}}}\left[\mathcal{L}\left(\bar{\boldsymbol{q}}, \dot{\bar{\boldsymbol{q}}}\right)\right], \tag{5.15}$$

$$\left[\frac{\partial \mathcal{L}}{\partial \boldsymbol{q}}\right]_{\bar{q}} \triangleq \frac{\partial}{\partial \boldsymbol{q}}\left[\mathcal{L}\right]_{\bar{q}} = \frac{\partial}{\partial \boldsymbol{q}}\left[\mathcal{L}\left(\bar{\boldsymbol{q}}(\boldsymbol{q}, t), \dot{\bar{\boldsymbol{q}}}(\boldsymbol{q}, \dot{\boldsymbol{q}}, t)\right)\right]. \tag{5.16}$$

In situations where the meaning of the partial derivatives is clear from the context, the brackets are occasionally omitted. In cases where no brackets are used, the terms are to be evaluated in standard fashion, i.e:

$$\frac{\partial \mathcal{L}}{\partial \boldsymbol{q}} = \left[\frac{\partial \mathcal{L}}{\partial \boldsymbol{q}}\right]_q, \quad \frac{\partial \mathcal{L}}{\partial \bar{\boldsymbol{q}}} = \left[\frac{\partial \mathcal{L}}{\partial \bar{\boldsymbol{q}}}\right]_{\bar{q}}. \tag{5.17}$$

5.2 A Thought Experiment

[103]: Lanczos (2020), *The Variational Principles of Mechanics*

D'Alembert's principle states that "the total virtual work of the effective force, i.e. the sum of impressed and inertial forces, is zero for all reversible variations which satisfy the given kinematical constraints" [103]. Let us consider a system Σ of n rigid bodies with n independent generalized coordinates $(q_1, \ldots, q_n)$. Transforming d'Alembert's principle into an expression involving generalized coordinates, it can be formulated as follows:

$$\delta W = \sum_i^n \left(\mathcal{Q}_i^\star + \mathcal{Q}_i\right) \delta q_i = 0, \tag{5.18}$$

where W denotes the work, $\mathcal{Q}^\star$ the force of inertia, and $\mathcal{Q}$ the sum of the impressed forces. Any virtual displacement δq_i is independent of δq_k $(i \neq k)$, and thus, for (5.18) to hold requires the vanishing of all the individual coefficients, that is

$$\mathcal{Q}_i^\star + \mathcal{Q}_i = 0, \quad i = 1, \ldots, n. \tag{5.19}$$

This equation can be interpreted as follows; a mechanical system moves in a way such that the force of inertia, arising from the motion, balances the resultant of the impressed forces. This balance holds at any point in time as the C-point P of the system traces out a curve in its n-dimensional configuration space, as visualized in Fig. 5.3. A similar balance of forces can be established in the analytical treatment [52, p. 20]:

$$\frac{\mathrm{d}}{\mathrm{d}t}\frac{\partial \mathcal{T}}{\partial \dot{q}_i} - \frac{\partial \mathcal{T}}{\partial q_i} = Q_i \quad i = 1, \dots, n \tag{5.20}$$

where the two terms on the left hand side can be identified with $-Q_i^\star$. For the case considered in this chapter, where the generalized forces are derivable from a single scalar potential function $\mathcal{V}$, these equations take on the form

$$\Sigma_u : \frac{\mathrm{d}}{\mathrm{d}t}\frac{\partial \mathcal{T}_u}{\partial \dot{\boldsymbol{q}}_u} - \frac{\partial \mathcal{T}_u}{\partial \boldsymbol{q}_u} = -\frac{\partial \mathcal{V}}{\partial \boldsymbol{q}_u}, \tag{5.21}$$

$$\Sigma_a : \frac{\mathrm{d}}{\mathrm{d}t}\frac{\partial \mathcal{T}_a}{\partial \dot{\boldsymbol{q}}_a} - \frac{\partial \mathcal{T}_a}{\partial \boldsymbol{q}_a} = -\frac{\partial \mathcal{V}}{\partial \boldsymbol{q}_a} + \boldsymbol{u}_a(t). \tag{5.22}$$

where Σ_u and Σ_a can be interpreted as unactuated and actuated subsystems of Σ. For simplicity, the generalized external forces are neglected and the case $n_u = n_a$ is assumed. The quantities on the LHS are the generalized inertial forces, and the quantities on the RHS can be interpreted as the *moving forces* [103].

Let us establish a Lagrangian picture of the subsystem decomposition (5.21)–(5.22). Let $\mathcal{C}$ denote the *configuration space*, that is the space of all possible configurations. Then each point in $\mathcal{C}$ encodes a single spatial configuration of the system. Thus, we can represent a system evolving in time by the motion of a single point P through $\mathcal{C}$. The *principle of stationary action* tells us that the path taken by P through $\mathcal{C}$ between times t_0 and t_1 and two fixed points in $\mathcal{C}$ is the one for which the action is stationary. Knowing that we can decompose Σ into an actuated and unactuated subsystem, we can formulate a different picture. Instead of thinking in terms of a single point P moving through $\mathcal{C}$, we can think of two points P_u and P_a—representing the configurations of Σ_u and Σ_a—moving through two distinct subspaces of $\mathcal{C}$. The only source of interaction between both subsystems are the forces arising from the potential field $\mathcal{V}$ that permeates $\mathcal{C}$. Figure 5.4 connects a geometric picture with our observations so far. Considering that $\mathcal{V}$ is a function of $\boldsymbol{q}$, it is clear that the moving force experienced by Σ_u ($\partial_{\boldsymbol{q}_u}\mathcal{V}$) is not only dependent on its own position, but also on that of Σ_a, and vice versa. The only option to impose a desired motion on the unactuated subsystem Σ_u is by adjusting the motion of the actuated subsystem through the input force $\boldsymbol{u}_a$ for ultimately achieving the appropriate variation of the coupling force. Intuitively, by adjusting the trajectory of P_a through $\boldsymbol{u}_a$, we can "steer" the point P_u in its subspace $\mathcal{C}_u$, as indicated in Fig. 5.5. A naturally arising question: given some sufficiently smooth trajectory $\boldsymbol{q}_u^*(t) : [t_0, t_1] \to \mathbb{R}^{n_u}$ for Σ_u does there exist a trajectory $\boldsymbol{q}_a^*(t) : [t_0, t_1] \to \mathbb{R}^{n_a}$ for Σ_a facilitating this motion. If such a trajectory for Σ_a existed, we would also want to know whether it was unique. [6] In the following, we are interested in a different but closely related question.

According to d'Alembert's principle, any two sets of forces are dynamically equivalent if they do the same virtual work. Exploiting this fact, we can decompose the moving force arising from the potential field $\mathcal{V}$ into an

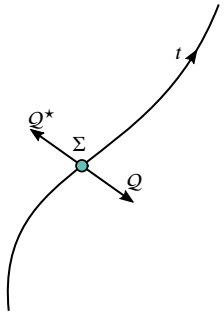

Figure 5.3: Geometrical picture: the C-point of system Σ traces out a curve in its n dimensional configuration space. This curve is determined by the balance of the inertial and moving force.

6: It turns out that this is indeed the case for $n_u = n_a = n/2$. The fact that the input force can be written in terms of the $\boldsymbol{q}_u$ (outputs), and their time derivatives, is closely connected with the concept of *differential flatness*. A more detailed discussion of this connection is provided in Section B.1 of Appendix B.

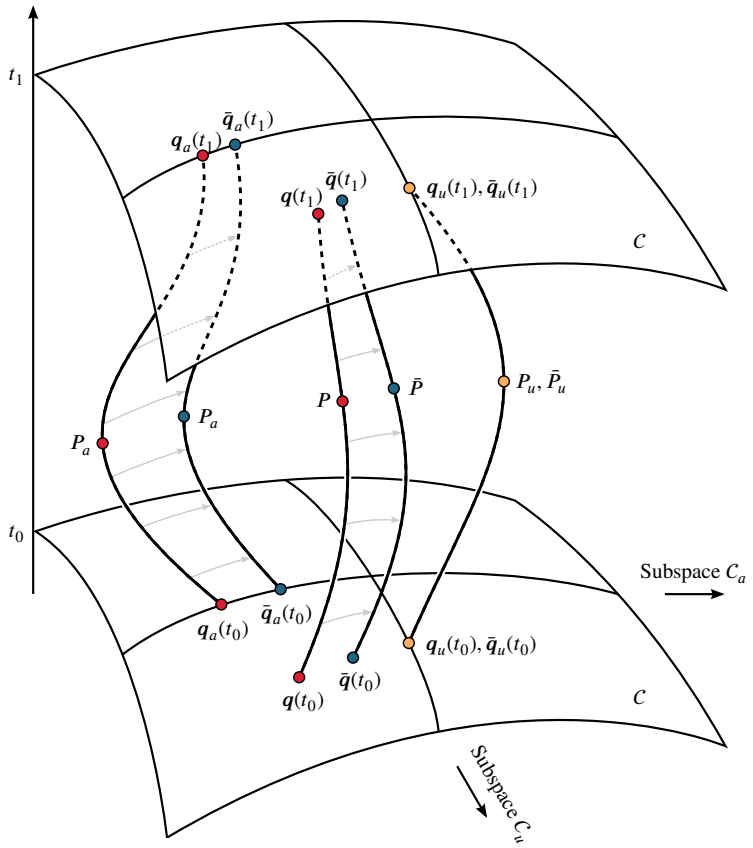

Figure 5.4: Time evolution of a trajectory started at the point $(\boldsymbol{q}(t_0))$, governed by the Lagrangian $\mathcal{L}$, is transformed according to (5.25). The time evolution of the transformed trajectory is governed by the same Hamiltonian. It is worth noting that all subsystems move through the same potential field $\mathcal{V}$. It is just that subsystem $\bar{\Sigma}_a$ moves along a C-curve that is "shifted" compared to the Σ_a C-curve, where Σ_u and $\bar{\Sigma}_u$ move along the "same" curves. The relative position of both subsystems dictates the magnitude and direction of the coupling force. In the new representation, the coupling force $\partial_{\bar{q}_u}\mathcal{V}$ encodes the error between the desired moving force and the actual moving force on $\bar{\Sigma}_u$.

undesired and desired component

$$-\partial_{\boldsymbol{q}_u}\mathcal{V}(\boldsymbol{q}) = \text{undesired moving force} + \text{desired moving force}. \tag{5.23}$$

The fact that the two sides of (5.23) are dynamically equivalent with regard to the motion of subsystem Σ_u invites for the following thought experiment. Suppose that $\bar{\boldsymbol{u}}_u$ encodes the desired moving force on Σ_u. Let us start with the following question: given some evolution of the moving force $\partial_{\boldsymbol{q}_u}\mathcal{V}$ on Σ_u does there exist an imaginary trajectory $\bar{\boldsymbol{q}}_a(t)$ for Σ_a, which is possibly different from the actual one $\boldsymbol{q}_a$, such that at all times

$$-\frac{\partial \mathcal{V}}{\partial \boldsymbol{q}_u}(\boldsymbol{q}_u, \bar{\boldsymbol{q}}_a) = \text{ undesired moving force}. \tag{5.24}$$

If such a trajectory $\bar{\boldsymbol{q}}_a$ for Σ_a existed, we would also want to know whether it was unique. In other words, and in harmony with the idea in Chapter 4, we ask whether the coupling force error (undesired moving force) can be encoded through a new set of generalized coordinates that describe the position of the (shifted) unactuated subsystem $\bar{\Sigma}_a$, as indicate in Fig. 5.5, such that

$$-\frac{\partial \mathcal{V}}{\partial \boldsymbol{q}_u}(\boldsymbol{q}_u, \bar{\boldsymbol{q}}_a) = -\frac{\partial \mathcal{V}}{\partial \boldsymbol{q}_u}(\boldsymbol{q}_u, \boldsymbol{q}_a) - \bar{\boldsymbol{u}}_u. \tag{5.25}$$

Section 5.3 below answers this question affirmatively, and establishes sufficient conditions on the signal $\bar{\boldsymbol{u}}_u$ such that (5.25) univocally defines a trajectory $\bar{\boldsymbol{q}}_a(t)$. In conclusion, balancing the inertial force on Σ_u, c.f (5.21), with the

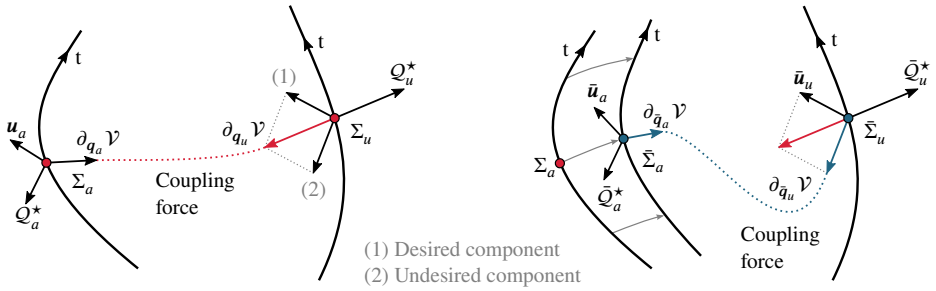

Figure 5.5: Balance of inertial and impressed forces. (**Right**) The actuated system Σ is shifted from its actual trajectory $\boldsymbol{q}_a$ to a virtual trajectory $\bar{\boldsymbol{q}}_a(t)$ so that the virtual coupling force $\partial_{\boldsymbol{q}_u}\mathcal{V}(\boldsymbol{q}_u, \bar{\boldsymbol{q}}_a)$ encodes the undesired component of the actual coupling force $\partial_{\boldsymbol{q}_u}\mathcal{V}(\boldsymbol{q}_u, \boldsymbol{q}_a)$.

impressed forces on the RHS of (5.23) such that

$$\bar{\Sigma}_u : \frac{\mathrm{d}}{\mathrm{d}t}\frac{\partial \mathcal{T}_u}{\partial \dot{\boldsymbol{q}}_u} - \frac{\partial \mathcal{T}_u}{\partial \boldsymbol{q}_u} = -\frac{\partial \mathcal{V}}{\partial \boldsymbol{q}_u} + \bar{\boldsymbol{u}}_u(t), \tag{5.26}$$

then $\bar{\Sigma}_u$ will follow the "same" trajectory as Σ_u. Noticing the resemblance of (5.21) and (5.26), suggests the following. Given that we can choose an arbitrary smooth variation for $\bar{\boldsymbol{u}}_u(t)$, we may treat the impressed force as a control input on $\bar{\Sigma}_u$. This makes $\bar{\Sigma}_u$ appear as if fully actuated.

The catch is, we started our thought experiment with a system constituted by two subsystems, Σ_u and Σ_a. Clearly, we derived an equivalent representation for the former only and we must extend our considerations to include the latter. Proposition 5.1.1 motivates us to aim for a dynamics of the form

$$\bar{\Sigma}_a : \frac{\mathrm{d}}{\mathrm{d}t}\frac{\partial \mathcal{T}_a}{\partial \dot{\bar{\boldsymbol{q}}}_a} - \frac{\partial \mathcal{T}_a}{\partial \bar{\boldsymbol{q}}_a} = -\frac{\partial \mathcal{V}}{\partial \bar{\boldsymbol{q}}_a} + \bar{\boldsymbol{u}}_a(t). \tag{5.27}$$

such that $\bar{\Sigma}_u$ and $\bar{\Sigma}_a$ can be interpreted as the feedback interconnection of two passive EL subsystems, with $\bar{\Sigma}_a$ being subject to the control forces $\bar{\boldsymbol{u}}_a$. In Section 5.3 it is shown, that is indeed possible to find some control signal $\boldsymbol{u}_a$ such that Σ_a assumes the desired dynamics $\bar{\Sigma}_a$. Given that we can choose arbitrary smooth variations $\bar{\boldsymbol{u}}_u(t)$ and $\bar{\boldsymbol{u}}_a(t)$, we may treat these impressed forces as control inputs on $\bar{\Sigma}_u$ and $\bar{\Sigma}_a$. This makes $\bar{\Sigma}_u$ appear as if fully actuated. Remarkably, the Lagrangian with the new EL equations is still the old one.

The presented idea is formalized in Section 5.3, which culminates in the formulation of Theorem 5.3.6. Section 5.4 reports a further generalization to the case, where the sub-configuration space of Σ_a has more dimensions than the sub-configuration space of Σ_u. Interestingly, this dimension imbalance implies the loss of differential flatness when considering $\boldsymbol{q}_u$ as the outputs, which introduces new challenges as the assumption above on the unique existence of a $\bar{\boldsymbol{q}}_a(t)$ trajectory matching some variation of $\bar{\boldsymbol{u}}_u$ is violated. A solution to this case is summarized in Theorem 5.4.2.

5.3 Mono-Articulated Systems

The goal of this section is to put the idea from Section 5.2, of transforming an underactuated EL system into its QFA form, on a firm mathematical footing. In the following, we treat systems satisfying Assumption 5.1.1 and 5.1.2 and having an equal number of unactuated and actuated coordinates. The main result is summarized below in Theorem 5.3.6.

5.3.1 A Nonpoint Transformation

We recall that the subsystem coupling force is of the form

$$\boldsymbol{\psi}: \begin{cases} \mathbb{R}^n & \to & \mathbb{R}^{n_u} \\ \boldsymbol{q} & \mapsto & -\partial_{\boldsymbol{q}_u}\mathcal{V}(\boldsymbol{q}) \end{cases}. \tag{5.28}$$

Inspired by the force decomposition (5.25), let us consider a change of coordinates from one set of coordinates $\boldsymbol{q}$ to a new set $\bar{\boldsymbol{q}}$ by a simultaneous (time-dependent) transformation of the generalized coordinates and velocities of the form [7]:

7: Throughout this text, we shall often make use of (5.29a) and (5.29c) to rewrite (5.29b) as $\boldsymbol{\psi}(\boldsymbol{q}) = \boldsymbol{\psi}(\bar{\boldsymbol{q}}) + \bar{\boldsymbol{u}}_u(\bar{\boldsymbol{q}}_u, \dot{\bar{\boldsymbol{q}}}_u, t)$

$$\bar{\boldsymbol{q}}_u = \boldsymbol{q}_u, \tag{5.29a}$$
$$\boldsymbol{\psi}(\bar{\boldsymbol{q}}) = \boldsymbol{\psi}(\boldsymbol{q}) - \bar{\boldsymbol{u}}_u(\boldsymbol{q}_u, \dot{\boldsymbol{q}}_u, t), \tag{5.29b}$$
$$\dot{\bar{\boldsymbol{q}}}_u = \dot{\boldsymbol{q}}_u, \tag{5.29c}$$
$$\dot{\boldsymbol{\psi}}(\bar{\boldsymbol{q}}) = \dot{\boldsymbol{\psi}}(\boldsymbol{q}) - \dot{\bar{\boldsymbol{u}}}_u(\boldsymbol{q}_u, \dot{\boldsymbol{q}}_u, t), \tag{5.29d}$$
$$t = t. \tag{5.29e}$$

where the mapping $\bar{\boldsymbol{u}}_u: \mathbb{R}^{n_u} \times \mathbb{R}^{n_u} \times \mathbb{R} \to \mathbb{R}^{n_u}$ is of class C^k, $k \geq 2$ and satisfying the following.

Assumption 5.3.1 *For any bounded $\boldsymbol{x}, \boldsymbol{y} \in \mathbb{R}^{n_u}$, there exists a positive constant c, independent of $t \in \mathbb{R}$, such that $\|\bar{\boldsymbol{u}}_u(\boldsymbol{x}, \boldsymbol{y}, t)\| \leq c$.*

In harmony with our thought experiment in Section 5.2; c.f. (5.25)–(5.23), we can interpret (5.29b) as follows; the excess of the moving force $\boldsymbol{\psi}(\boldsymbol{q})$ over the desired one $\bar{\boldsymbol{u}}_u$ (RHS) is encoded in terms of the moving force $\boldsymbol{\psi}(\bar{\boldsymbol{q}})$, which acts on the virtual unactuated subsystem $\bar{\Sigma}_u$ (LHS), as indicated in Fig. 5.5. This interpretation will become clear below. Knowing from (5.3) that

$$\ddot{\boldsymbol{q}}_u = \left[\frac{\partial^2 \mathcal{L}_u}{\partial \dot{\boldsymbol{q}}_u^2}\right]^{-1} \left\{ \frac{\partial \mathcal{L}}{\partial \boldsymbol{q}_u} - \left[\frac{\partial^2 \mathcal{L}_u}{\partial \boldsymbol{q}_u \partial \dot{\boldsymbol{q}}_u}\right] \dot{\boldsymbol{q}}_u + \mathcal{Q}'_u \right\}, \tag{5.30}$$

and according to the chain rule that

$$\dot{\bar{\boldsymbol{u}}}_u = \frac{\partial \bar{\boldsymbol{u}}_u}{\partial \boldsymbol{q}_u}\dot{\boldsymbol{q}}_u + \frac{\partial \bar{\boldsymbol{u}}_u}{\partial \dot{\boldsymbol{q}}_u}\ddot{\boldsymbol{q}}_u + \frac{\partial \bar{\boldsymbol{u}}_u}{\partial t}, \tag{5.31}$$

we can express $\dot{\bar{\boldsymbol{u}}}_u$ in terms of only the generalized positions, velocities, external forces $(\boldsymbol{q}_u, \dot{\boldsymbol{q}}_u, \mathcal{Q}'_u)$ and time t by making the substitution (5.30) and (5.31)

$$\begin{aligned} \dot{\bar{\boldsymbol{u}}}(\boldsymbol{q}_u, \dot{\boldsymbol{q}}_u, t) &= \frac{\partial \bar{\boldsymbol{u}}_u}{\partial \boldsymbol{q}_u}\dot{\boldsymbol{q}}_u + \frac{\partial \bar{\boldsymbol{u}}_u}{\partial \dot{\boldsymbol{q}}_u}\left[\frac{\partial^2 \mathcal{L}_u}{\partial \dot{\boldsymbol{q}}_u^2}\right]^{-1} \left\{ \frac{\partial \mathcal{L}}{\partial \boldsymbol{q}_u} - \left[\frac{\partial^2 \mathcal{L}_u}{\partial \boldsymbol{q}_u \partial \dot{\boldsymbol{q}}_u}\right] \dot{\boldsymbol{q}}_u + \mathcal{Q}'_u \right\} + \frac{\partial \bar{\boldsymbol{u}}_u}{\partial t} \\ &\triangleq \boldsymbol{\delta}(\boldsymbol{q}, \dot{\boldsymbol{q}}_u, t, \mathcal{Q}'_u) \end{aligned} \tag{5.32}$$

such that (5.29d) can rewritten as

$$\dot{\boldsymbol{\psi}}(\bar{\boldsymbol{q}}) = \dot{\boldsymbol{\psi}}(\boldsymbol{q}) - \boldsymbol{\delta}(\boldsymbol{q}, \dot{\boldsymbol{q}}_u, t, \mathcal{Q}'_u). \tag{5.33}$$

From (5.33), it is clear that the external force $\mathcal{Q}'_u$ acting on the unactuated subsystem enters the transforming equation (5.29d) through (5.32). In the following, we will show that (5.29) defines a coordinate transformation $(\boldsymbol{q}, \dot{\boldsymbol{q}}) \to (\bar{\boldsymbol{q}}, \dot{\bar{\boldsymbol{q}}})$.

To this end, we shall proceed in two steps: 1) rewrite the RHS of (5.29d) in terms of only the generalized coordinates and velocities $\boldsymbol{q}, \dot{\boldsymbol{q}}$ and time t using (5.33), 2) show the existence of a diffeomorphism between the extended phase spaces of the original and virtual systems, as summarized in Lemmma 5.3.1. To rewrite the transforming equations (5.29) in compact form, it is convenient to introduce the mappings:

$$\boldsymbol{\alpha}: \begin{cases} \mathbb{R}^n \times \mathbb{R}^n \times \mathbb{R} & \to & \mathbb{R}^{2n+1} \\ (\boldsymbol{q}, \dot{\boldsymbol{q}}, t) & \mapsto & \begin{bmatrix} \boldsymbol{q}_u \\ \boldsymbol{\psi}(\boldsymbol{q}) \\ \dot{\boldsymbol{q}}_u \\ \dot{\boldsymbol{\psi}}(\boldsymbol{q}) \\ t \end{bmatrix} \end{cases},$$

$$\boldsymbol{\beta}: \begin{cases} \mathbb{R}^n \times \mathbb{R}^n \times \mathbb{R} & \to & \mathbb{R}^{2n+1} \\ (\boldsymbol{q}, \dot{\boldsymbol{q}}, t) & \mapsto & \begin{bmatrix} \boldsymbol{q}_u \\ \boldsymbol{\psi}(\boldsymbol{q}) - \bar{\boldsymbol{u}}(\boldsymbol{q}_u, \dot{\boldsymbol{q}}_u, t) \\ \dot{\boldsymbol{q}}_u \\ \dot{\boldsymbol{\psi}}(\boldsymbol{q}) - \boldsymbol{\delta}(\boldsymbol{q}, \dot{\boldsymbol{q}}_u, t, \mathcal{Q}'_u) \\ t \end{bmatrix} \end{cases},$$

$$\boldsymbol{\gamma}: \begin{cases} \mathbb{R}^n \times \mathbb{R}^n \times \mathbb{R} & \to & \mathbb{R}^{2n+1} \\ (\boldsymbol{q}, \dot{\boldsymbol{q}}, t) & \mapsto & \begin{bmatrix} \boldsymbol{q}_u \\ \boldsymbol{\psi}(\boldsymbol{q}) + \bar{\boldsymbol{u}}(\boldsymbol{q}_u, \dot{\boldsymbol{q}}_u, t) \\ \dot{\boldsymbol{q}}_u \\ \dot{\boldsymbol{\psi}}(\boldsymbol{q}) + \boldsymbol{\delta}(\boldsymbol{q}, \dot{\boldsymbol{q}}_u, t, \mathcal{Q}'_u) \\ t \end{bmatrix} \end{cases}.$$

Let

$$\begin{aligned} \boldsymbol{x} &= (\boldsymbol{q}, \dot{\boldsymbol{q}}, t) \in X, \quad \text{where } X = \mathbb{R}^n \times \mathbb{R}^n \times \mathbb{R}, \\ \bar{\boldsymbol{x}} &= (\bar{\boldsymbol{q}}, \dot{\bar{\boldsymbol{q}}}, t) \in \bar{X}, \quad \text{where } \bar{X} = \mathbb{R}^n \times \mathbb{R}^n \times \mathbb{R}, \end{aligned}$$

then using the definitions above, we can rewrite (5.29a)–(5.29e) as

$$\boldsymbol{\beta}(\boldsymbol{x}) = \boldsymbol{\alpha}(\bar{\boldsymbol{x}}), \tag{5.34}$$

or, by making use of the equivalence $(\boldsymbol{q}_u, \dot{\boldsymbol{q}}_u) = (\bar{\boldsymbol{q}}_u, \dot{\bar{\boldsymbol{q}}}_u)$, as

$$\boldsymbol{\alpha}(\boldsymbol{x}) = \boldsymbol{\gamma}(\bar{\boldsymbol{x}}). \tag{5.35}$$

We are now in a position to formulate the main results of this section.

Lemma 5.3.1 (A one-to-one correspondence) *The mapping*

$$\boldsymbol{\pi}: \begin{cases} \boldsymbol{X} & \to & \bar{\boldsymbol{X}} \\ \boldsymbol{x} & \mapsto & \boldsymbol{\alpha}^{-1} \circ \boldsymbol{\beta}(\boldsymbol{x}) \end{cases}, \tag{5.36}$$

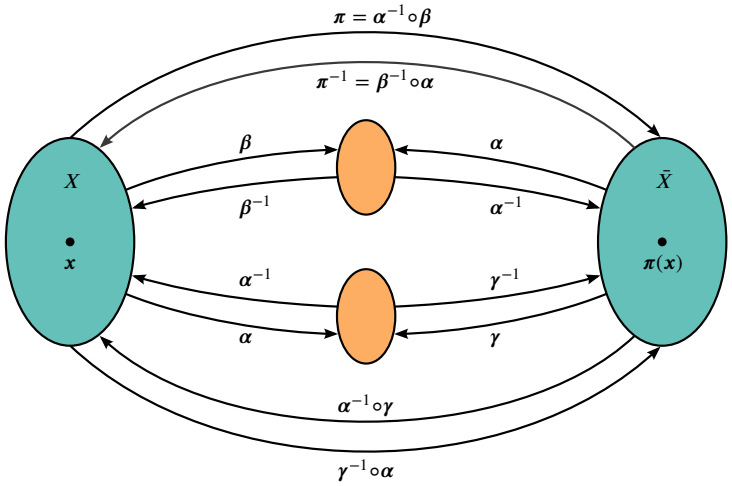

Figure 5.6: Extended state space transformation: the diffeomorphism π defining the one-to-one correspondence between the sets X and $\bar{X}$ is a composition of diffeomorphisms.

is a C^1 diffeomorphism, and thus defines a change of coordinates

$$\begin{aligned} \bar{q}_i &= \bar{q}_i(q, \dot{q}, t), \quad i = 1, \dots, n \\ \dot{\bar{q}}_i &= \dot{\bar{q}}_i(q, \dot{q}, t), \quad i = 1, \dots, n \end{aligned} \tag{5.37}$$

with $|D\pi(x)| = |D\alpha(\bar{x})|^{-1} |D\alpha(x)|$.[8]

8: This determinant can be interpreted

The proof of Lemma 5.3.1 relies on the following global inverse function theorems that go back to Hadamard [56], and a standard property of proper functions summarized in Lemma 5.3.2. The cases where either condition (i) or (ii) of Assumption 5.1.2 hold will be treated independently. The connections between the central mappings are sketched in Fig. 5.6.

[56]: Hadamard (1906), "Sur les transformations ponctuelles"

Lemma 5.3.2 (DeMarco [35]) *A continuous function $f : \mathbb{R}^n \to \mathbb{R}^n$ is proper if and only if it is coercive, namely $\|f(x)\| \to \infty$, as $\|x\| \to \infty$.*

Theorem 5.3.3 (Gordon [53]) *A C^1 map $f : \mathbb{R}^n \to \mathbb{R}^n$ is a C^1 diffeomorphism if and only if f is proper and the Jacobian determinant Df never vanishes.*

Theorem 5.3.4 (Miller [119], Ortega [130]) *Assume that $f : \mathbb{R}^n \to \mathbb{R}^n$ is continuously differentiable on $\mathbb{R}^n$ and that $\|Df(x)^{-1}\| \leq c$ for all $x \in \mathbb{R}^n$. Then f is a homeomorphism of $\mathbb{R}^n$ onto $\mathbb{R}^n$* .

The following properties of diffeomorphism are repeatably exploited in the proof of Lemma 5.3.1.

- Let $f : A \to B$ and $g : B \to C$ be diffeomorphisms, then $g \circ f : A \to C$ is a diffeomorphism [82, p. 301].
- Let A be open in $\mathbb{R}^n$ and $f : A \to \mathbb{R}^n$ be a diffeomorphism. Then f^{-1} is a diffeomorphism from $f(A)$ onto A [82, p. 300].
- Let the C^k map $f : \mathbb{R}^n \to \mathbb{R}^n$ be a global homeomorphism, then f is a global C^k diffeomorphism by the usual local inverse function theorem.

[82]: Kass et al. (2011), *Geometrical Foundations of Asymptotic Inference*

Finally, the following result will be used to verify the critical inverse Jacobian condition in Theorem 5.3.4.

Lemma 5.3.5 *Let $\boldsymbol{A}$ in $\mathbb{C}^{n\times n}$ be nonsingular. By [160], we have*

$$\|\boldsymbol{A}\|_2 \geq \sigma_m(\boldsymbol{A}) \geq \frac{1}{|\boldsymbol{A}|}\left(\frac{n}{n-1}\right)^{(n-1)/2}. \tag{5.38}$$

[160]: Yi-Sheng et al. (1997), "A note on a lower bound for the smallest singular value"

It is worth remarking that the result by Yi-Sheng [160] is a minor modification of Theorem 1 by Hong [71].

Proof of Lemma 5.3.1 using Theorem 5.3.3. The following proof considers the case where condition (i) in Assumption 5.1.2 is satisfied. The proof consists of three steps: 1) show that $\boldsymbol{\alpha}$ and $\boldsymbol{\beta}$ are diffeomorphisms using Theorem 5.3.3. 2) conclude that the composition $\boldsymbol{\pi}$ is a diffeomorphism, 3) establish lower bound for $|\boldsymbol{\pi}|$.[9] Note that from the properties of the potential function $\mathcal{V}$ follows that $\boldsymbol{\alpha}$ and $\boldsymbol{\beta}$ are continuously differentiable; thus also compositions of these two functions.

Step 1: Assumption 5.1.2 with condition (i) implies that $\boldsymbol{\alpha}$ is a coercive map; thus, according to Lemma 5.3.2, it is proper. Invoking Theorem 5.3.3 and further knowing that the determinant of $\boldsymbol{\alpha}$ never vanishes since $|D\boldsymbol{\alpha}| = |\frac{\partial \boldsymbol{\psi}}{\partial \boldsymbol{q}_a}|^2$, as detailed below in (5.39), we conclude that $\boldsymbol{\alpha}$ is a diffeomorphism. Considering that $\boldsymbol{\alpha}$ is proper and that $\bar{\boldsymbol{u}}_u$ satisfies Assumption 5.3.1, it is clear that $\boldsymbol{\beta}$ is also a proper map satisfying Theorem 5.3.3. Since $\boldsymbol{\alpha}$ is a diffeomorphism it implies that $\boldsymbol{\alpha}^{-1}$ is a diffeomorphism [82, p. 301].

Step 2: Given that the composition of diffeomorphisms is a diffeomorphism [82, p. 300], we conclude that $\boldsymbol{f} = \boldsymbol{\alpha}^{-1}\circ\boldsymbol{\beta}$ is a diffeomorphism.

Step 3: An argument is provided in the proof below, see (5.45). ■

9: Note that for the case where condition (ii) in Assumption 5.1.2 is satisfied the proof of step 1) is trivial invoking Theorem 5.3.4.

[82]: Kass et al. (2011), *Geometrical Foundations of Asymptotic Inference*

Proof of Lemma 5.3.1 using Theorem 5.3.4. The following proof considers the case where condition (ii) in Assumption 5.1.2 is satisfied and consists of three steps: 1) show that $\boldsymbol{\alpha}$ and $\boldsymbol{\beta}$ are diffeomorphisms using Theorem 5.3.4, 2) conclude that the composition $\boldsymbol{\pi}$ is a diffeomorphism, 3) establish the desired expression for $|D\boldsymbol{\pi}|$.

Step 1: Knowing that

$$D\boldsymbol{\alpha}(\boldsymbol{x}) = \frac{\partial \alpha_i}{\partial x_j} = \left[\begin{array}{ccc|cc} \frac{\partial \boldsymbol{q}_u}{\partial \boldsymbol{q}_u} & \frac{\partial \boldsymbol{q}_u}{\partial \boldsymbol{q}_a} & \frac{\partial \boldsymbol{q}_u}{\partial \dot{\boldsymbol{q}}_u} & \frac{\partial \boldsymbol{q}_u}{\partial \dot{\boldsymbol{q}}_a} & \frac{\partial \boldsymbol{q}_u}{\partial t} \\ \frac{\partial \boldsymbol{\psi}}{\partial \boldsymbol{q}_u} & \frac{\partial \boldsymbol{\psi}}{\partial \boldsymbol{q}_a} & \frac{\partial \boldsymbol{\psi}}{\partial \dot{\boldsymbol{q}}_u} & \frac{\partial \boldsymbol{\psi}}{\partial \dot{\boldsymbol{q}}_a} & \frac{\partial \boldsymbol{\psi}}{\partial t} \\ \hline \frac{\partial \dot{\boldsymbol{q}}_u}{\partial \boldsymbol{q}_u} & \frac{\partial \dot{\boldsymbol{q}}_u}{\partial \boldsymbol{q}_a} & \frac{\partial \dot{\boldsymbol{q}}_u}{\partial \dot{\boldsymbol{q}}_u} & \frac{\partial \dot{\boldsymbol{q}}_u}{\partial \dot{\boldsymbol{q}}_a} & \frac{\partial \dot{\boldsymbol{q}}_u}{\partial t} \\ \frac{\partial \dot{\boldsymbol{\psi}}}{\partial \boldsymbol{q}_u} & \frac{\partial \dot{\boldsymbol{\psi}}}{\partial \boldsymbol{q}_a} & \frac{\partial \dot{\boldsymbol{\psi}}}{\partial \dot{\boldsymbol{q}}_u} & \frac{\partial \dot{\boldsymbol{\psi}}}{\partial \dot{\boldsymbol{q}}_a} & \frac{\partial \dot{\boldsymbol{\psi}}}{\partial t} \\ \hline \frac{\partial t}{\partial \boldsymbol{q}_u} & \frac{\partial t}{\partial \boldsymbol{q}_a} & \frac{\partial t}{\partial \dot{\boldsymbol{q}}_u} & \frac{\partial t}{\partial \dot{\boldsymbol{q}}_u} & \frac{\partial t}{\partial t} \end{array}\right],$$

considering that $\frac{\partial \dot{\boldsymbol{\psi}}}{\partial \dot{\boldsymbol{q}}_k} = \frac{\partial \boldsymbol{\psi}}{\partial \boldsymbol{q}_k}$, $k = u, a$, due to the velocity-independence of $\boldsymbol{\psi}$ and using Schur's determinant identity[10], we get

10: See Theorem D.3.2 in Appendix D.

$$|D\boldsymbol{\alpha}(\boldsymbol{x})| = \left|\begin{array}{ccc} \boldsymbol{I} & \boldsymbol{0} & \boldsymbol{0} \\ \frac{\partial \boldsymbol{\psi}}{\partial \boldsymbol{q}_u} & \frac{\partial \boldsymbol{\psi}}{\partial \boldsymbol{q}_a} & \boldsymbol{0} \\ \boldsymbol{0} & \boldsymbol{0} & 1 \end{array}\right| \left|\begin{array}{cc} \boldsymbol{I} & \boldsymbol{0} \\ \frac{\partial \boldsymbol{\psi}}{\partial \boldsymbol{q}_u} & \frac{\partial \boldsymbol{\psi}}{\partial \boldsymbol{q}_a} \end{array}\right| = \left|\begin{array}{cc} \boldsymbol{I} & \boldsymbol{0} \\ \frac{\partial \boldsymbol{\psi}}{\partial \boldsymbol{q}_u} & \frac{\partial \boldsymbol{\psi}}{\partial \boldsymbol{q}_a} \end{array}\right|^2 = \left|\frac{\partial \boldsymbol{\psi}}{\partial \boldsymbol{q}_a}\right|^2, \tag{5.39}$$

where the last equality can be shown through repeated cofactor expansion along the first row. Proceeding analogously to the steps above, and further

considering that $\partial_{\dot{\boldsymbol{q}}_a}\boldsymbol{\delta} = \mathbf{0}$, we obtain

$$D\boldsymbol{\beta}(\boldsymbol{x}) = \frac{\partial \beta_i}{\partial x_j} = \left[\begin{array}{cc|cc|c} \frac{\partial \boldsymbol{q}_u}{\partial \boldsymbol{q}_u} & \frac{\partial \boldsymbol{q}_u}{\partial \boldsymbol{q}_a} & \frac{\partial \boldsymbol{q}_u}{\partial \dot{\boldsymbol{q}}_u} & \frac{\partial \boldsymbol{q}_u}{\partial \dot{\boldsymbol{q}}_a} & \frac{\partial \boldsymbol{q}_u}{\partial t} \\ \partial_{\boldsymbol{q}_u}(\boldsymbol{\psi} - \bar{\boldsymbol{u}}_u) & \frac{\partial \boldsymbol{\psi}}{\partial \boldsymbol{q}_a} & \partial_{\dot{\boldsymbol{q}}_u}(\boldsymbol{\psi} - \bar{\boldsymbol{u}}_u) & \frac{\partial \boldsymbol{\psi}}{\partial \dot{\boldsymbol{q}}_a} & \partial_t(\boldsymbol{\psi} - \bar{\boldsymbol{u}}_u) \\ \hline \frac{\partial \dot{\boldsymbol{q}}_u}{\partial \boldsymbol{q}_u} & \frac{\partial \dot{\boldsymbol{q}}_u}{\partial \boldsymbol{q}_a} & \frac{\partial \dot{\boldsymbol{q}}_u}{\partial \dot{\boldsymbol{q}}_u} & \frac{\partial \dot{\boldsymbol{q}}_u}{\partial \dot{\boldsymbol{q}}_a} & \frac{\partial \dot{\boldsymbol{q}}_u}{\partial t} \\ \partial_{\boldsymbol{q}_u}(\dot{\boldsymbol{\psi}} - \boldsymbol{\delta}) & \partial_{\boldsymbol{q}_a}(\dot{\boldsymbol{\psi}} - \boldsymbol{\delta}) & \partial_{\dot{\boldsymbol{q}}_u}(\dot{\boldsymbol{\psi}} - \boldsymbol{\delta}) & \partial_{\dot{\boldsymbol{q}}_a}(\dot{\boldsymbol{\psi}} - \boldsymbol{\delta}) & \partial_t(\dot{\boldsymbol{\psi}} - \boldsymbol{\delta}) \\ \hline \frac{\partial t}{\partial \boldsymbol{q}_u} & \frac{\partial t}{\partial \boldsymbol{q}_a} & \frac{\partial t}{\partial \dot{\boldsymbol{q}}_u} & \frac{\partial t}{\partial \dot{\boldsymbol{q}}_a} & \frac{\partial t}{\partial t} \end{array}\right],$$

and[11]

11: A detailed argument of this step is provided Appendix B.3.

$$|D\boldsymbol{\beta}(\boldsymbol{x})| = \left|\begin{array}{cc} \frac{\partial \boldsymbol{\psi}}{\partial \boldsymbol{q}_a} & \partial_t(\dot{\boldsymbol{\psi}} - \boldsymbol{\delta}) \\ \mathbf{0} & 1 \end{array}\right| \left|\begin{array}{ccc} \boldsymbol{I} & \mathbf{0} & \mathbf{0} \\ \partial_{\boldsymbol{q}_u}(\boldsymbol{\psi} - \bar{\boldsymbol{u}}_u) & \frac{\partial \boldsymbol{\psi}}{\partial \boldsymbol{q}_a} & \mathbf{0} \\ \mathbf{0} & \mathbf{0} & 1 \end{array}\right| = \left|\frac{\partial \boldsymbol{\psi}}{\partial \boldsymbol{q}_a}\right|^2. \tag{5.40}$$

Considering condition (ii) of Assumption 5.1.2, we know that

$$|D\boldsymbol{\alpha}(\boldsymbol{x})| \geq c^2 > 0, \text{ and } |D\boldsymbol{\beta}(\boldsymbol{x})| \geq c^2 > 0, \quad \forall \boldsymbol{x} \in X. \tag{5.41}$$

To show that $\|D\boldsymbol{\alpha}^{-1}\|$ is bounded from above it is sufficient to show that $\sigma_m(D\boldsymbol{\alpha})^{-1} \leq k < \infty$.[12] To this end, let us establish a lower bound for the smallest singular values using Lemma 5.3.5 and (5.41)

12: Note that $\|\boldsymbol{A}\| = \sigma_M(\boldsymbol{A})$ implies that $\|\boldsymbol{A}^{-1}\| \leq \sigma_m(\boldsymbol{A})^{-1}$.

$$\sigma_m(D\boldsymbol{\alpha}) > |D\boldsymbol{\alpha}| \left(\frac{n-1}{n}\right)^{(n-1)/2} \geq \frac{c^2}{\sqrt{e}}. \tag{5.42}$$

A proof for the last inequality is provided below. Considering (5.41) and (5.42), and knowing that $c \neq 0$ and $\sigma_m(D\boldsymbol{\alpha}) \neq 0$, we conclude the desired result

$$\sigma_m(D\boldsymbol{\alpha})^{-1} \leq \frac{\sqrt{e}}{c^2}. \tag{5.43}$$

We leave it to the reader to verify that inequality (5.43) equally holds for $\sigma_m(D\boldsymbol{\beta})^{-1}$.

In summary, $\boldsymbol{\alpha}$ and $\boldsymbol{\beta}$ satisfy the desired conditions of Theorem 5.3.4, which concludes the proof that $\boldsymbol{\alpha}$ and $\boldsymbol{\beta}$ are diffeomorphisms.
Step 2: Given that the composition of diffeomorphisms is a diffeomorphism [82, p. 300], we conclude that $\boldsymbol{\pi} = \boldsymbol{\alpha}^{-1} \circ \boldsymbol{\beta}$ is a diffeomorphism.

[82]: Kass et al. (2011), *Geometrical Foundations of Asymptotic Inference*

Step 3: The result above and the chain rule tell us that the composition $\boldsymbol{\pi}$ is differentiable on X, and that the Jacobian matrices corresponding to $\boldsymbol{\pi}, \boldsymbol{\alpha}$ and $\boldsymbol{\beta}$ are related as follows

$$D\boldsymbol{\pi}(\boldsymbol{x}) = D\boldsymbol{\alpha}^{-1}\big(\boldsymbol{\beta}(\boldsymbol{x})\big) D\boldsymbol{\beta}(\boldsymbol{x}). \tag{5.44}$$

According to the inverse function theorem $D\boldsymbol{\alpha}^{-1}\big(\boldsymbol{\beta}(\boldsymbol{x})\big) = D\boldsymbol{\alpha}(\bar{\boldsymbol{x}})^{-1}$ and we conclude from (5.44) that[13]

13: Recall that for some invertible matrix $\boldsymbol{A}$, we have that $|\boldsymbol{A}^{-1}| = |\boldsymbol{A}|^{-1}$.

$$|D\boldsymbol{\pi}(\boldsymbol{x})| = |D\boldsymbol{\alpha}(\bar{\boldsymbol{x}})|^{-1} |D\boldsymbol{\beta}(\boldsymbol{x})| = |D\boldsymbol{\alpha}(\bar{\boldsymbol{x}})|^{-1} |D\boldsymbol{\alpha}(\boldsymbol{x})|, \tag{5.45}$$

which completes the proof. ■

Supplementary Limit Analysis for Proof of Lemma 5.3.1

This section establishes the lower bound for the function

$$\rho(n) = \left(\frac{n-1}{n}\right)^{\frac{n-1}{2}}, \quad n \in \mathbb{N}_{>0}, \tag{5.46}$$

that was considered in (5.42) without proof; see Fig. 5.7 for a graphical representation. We shall proceed in three steps: 1) proof that $\rho(n)$ is a strictly monotonously decreasing function on the interval $\mathbb{R}_{>0}$, 2) show that $\lim_{n\to\infty} \rho(n) = e^{-1/2}$, 3) conclude that $\rho(n) \geq e^{-1/2}$, $n \in \mathbb{N}_{>0}$.

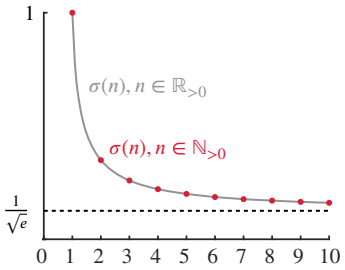

Figure 5.7: Evaluation of $\sigma(n)$.

Step 1: The derivative of (5.46) is

$$\rho'(n) = \frac{1}{2n}\left(\frac{n-1}{n}\right)^{\frac{n-1}{2}}\left[n\log\left(\frac{n-1}{n}\right) + 1\right]. \tag{5.47}$$

It is easy to see that the sign of ρ' equals the sign of the last term inside the [.] brackets for all $n \in \mathbb{N}$. Observing that

$$\frac{d}{dx}\left[x\log\left(\frac{x-1}{x}\right)\right] = \frac{1}{x-1} + \log\left(\frac{x-1}{x}\right) \tag{5.48}$$

is strictly greater zero for $x > 1$, and that

$$\lim_{x\to\infty} x\log\left(\frac{x-1}{x}\right) = -1. \tag{5.49}$$

A proof for this limit is shown below in Step 2.

The first equality is trivially satisfied, and the latter follows immediately from the inequality[14]

$$\left[\frac{x-1}{x}\right]^x = \left[1-\frac{1}{x}\right]^x \leq \left[1+\frac{1}{x}\right]^x < e, \quad x \in \mathbb{R}.$$

14: Note that e is the unique real number satisfying $(1+1/x)^x < e < (1+1/x)^{x+1}$ for all positive x.

We conclude that the sign-determining term in (5.47) is strictly negative; thus $\sigma(n)$ is strictly monotonously decreasing. Moreover since $\mathbb{N}_{>0}$ is a subset of $\mathbb{R}_{>0}$, σ evaluated on the interval $\mathbb{N}_{>0}$ must also be strictly monotonously decreasing.

Step 2: Making use of the following limit laws

$$\lim_{x\to a} b^{f(x)} = b^{\lim_{x\to a} f(x)}, \quad \text{exponential law for limits (EL)},$$

$$\lim_{x\to a} \frac{f(x)}{g(x)} = \frac{\lim_{x\to a} f(x)}{\lim_{x\to a} g(x)} \text{ for } \lim_{x\to a} g(x) \neq 0, \quad \text{quotient law for limits (QL)},$$

$$\lim_{x\to a} f(x)^n = \left[\lim_{x\to a} f(x)\right]^n, \quad \text{power law for limits (PL)},$$

$$\lim_{x\to a}\left[f(x)g(x)\right] = \lim_{x\to a} f(x) \cdot \lim_{x\to a} g(x), \quad \text{product law for limits (ML)},$$

we get

$$\begin{aligned}\lim_{n\to\infty}\rho(n) &\overset{\text{QL}}{=} \frac{\lim\limits_{n\to\infty}\left(\frac{n-1}{n}\right)^{n/2}}{\lim\limits_{n\to\infty}\left(\frac{n-1}{n}\right)^{1/2}} \overset{\text{PL}}{=} \frac{\lim\limits_{n\to\infty}\left(\frac{n-1}{n}\right)^{n/2}}{\left[\lim\limits_{n\to\infty}\left(\frac{n-1}{n}\right)\right]^{1/2}} \\ &= \lim_{n\to\infty}\left(\frac{n-1}{n}\right)^{n/2} = \lim_{n\to\infty}\left\{\exp\left[\log\left(\frac{n-1}{n}\right)^{n/2}\right]\right\} \\ &= \lim_{n\to\infty}\left\{\exp\left[\frac{n}{2}\log\left(\frac{n-1}{n}\right)\right]\right\} \overset{\text{EL}}{=} \exp\left\{\lim_{n\to\infty}\left[\frac{n}{2}\log\left(\frac{n-1}{n}\right)\right]\right\} \\ &\overset{\text{ML}}{=} \exp\left\{\frac{1}{2}\lim_{n\to\infty}\frac{\log\left(\frac{n-1}{n}\right)}{\frac{1}{n}}\right\}.\end{aligned}$$

Knowing that

$$\lim_{n\to\infty}\log\frac{n-1}{n}=0; \quad \lim_{n\to\infty}\frac{1}{n}=0,$$

we can apply L'Hopital's rule such that

$$\lim_{n\to\infty}\frac{\log\left(\frac{n-1}{n}\right)}{\frac{1}{n}} = \lim_{n\to\infty}\frac{\frac{n}{n-1}\frac{n-(n-1)}{n^2}}{-\frac{1}{n^2}} = \lim_{n\to\infty}\frac{\frac{1}{n(n-1)}}{-\frac{1}{n^2}} = \lim_{n\to\infty}\frac{n}{1-n} = -1.$$

Combing the results above, we eventually get

$$\lim_{n\to\infty}\rho(n)=\frac{1}{\sqrt{e}}.$$

Step 3: Considering the results above, we conclude that

$$\rho : \mathbb{N}_{>0} \to (e^{-1/2}, 1]. \tag{5.50}$$

Remark 5.3.1 From (5.36), we see that the computation of the mapping $\boldsymbol{\pi}^{-1}: \bar{X} \to X$ requires knowledge of the inverse $\boldsymbol{\beta}^{-1}$. However, considering (5.35) and the existence of $\boldsymbol{\alpha}^{-1}$, it is clear that we can establish a mapping from the elements of $\bar{X}$ to the unique elements of X through

$$\boldsymbol{x} = \boldsymbol{\alpha}^{-1}\circ\boldsymbol{\gamma}(\bar{\boldsymbol{x}}). \tag{5.51}$$

Proceeding mutatis mutandis to the proof of Lemma 5.3.1, it is straightforward to show that (5.51) is a $\mathcal{C}^1$ diffeomorphism. Thus, using (5.51) instead of $\boldsymbol{x} = \boldsymbol{\pi}^{-1}(\bar{\boldsymbol{x}})$, we can avoid the computation of $\boldsymbol{\beta}^{-1}$ and limit the computational effort to the calculation of only $\boldsymbol{\alpha}^{-1}$ for establishing a mapping from $\bar{X}$ to X.

5.3.2 Main Result

The following Theorem formalizes the idea presented in the thought experiment of Section 5.2. It is convenient to introduce the "partial" Jacobians

$$\boldsymbol{X}(\boldsymbol{q}) \triangleq \frac{\partial^2 \mathcal{L}_a}{\partial \boldsymbol{q}_u^2}(\boldsymbol{q}); \quad \boldsymbol{Y}(\boldsymbol{q}) \triangleq \frac{\partial^2 \mathcal{L}_a}{\partial \boldsymbol{q}_a \partial \boldsymbol{q}_u}(\boldsymbol{q}). \tag{5.52}$$

and the auxiliary functions

$$\boldsymbol{A}(\boldsymbol{q}, \bar{\boldsymbol{q}}) \triangleq \left[\boldsymbol{Y}\right]_q^{-1} \left[\boldsymbol{Y}\right]_{\bar{q}}, \tag{5.53}$$

$$\boldsymbol{R}(\boldsymbol{q}, \bar{\boldsymbol{q}}) \triangleq \left[\frac{\partial^2 \mathcal{L}_a}{\partial \dot{\bar{\boldsymbol{q}}}_a^2}\right]_{\bar{q}} \boldsymbol{A}^{-1}(\boldsymbol{q}, \bar{\boldsymbol{q}}) \left[\frac{\partial^2 \mathcal{L}_a}{\partial \dot{\boldsymbol{q}}_a^2}\right]_q^{-1}, \tag{5.54}$$

$$\boldsymbol{\mu}_1(\boldsymbol{q}, \bar{\boldsymbol{q}}, \dot{\boldsymbol{q}}_u, \mathcal{Q}'_u, t) \triangleq \left[\boldsymbol{Y}\right]_q^{-1} \left\{ \left(\left[\boldsymbol{X}\right]_{\bar{q}} - \left[\boldsymbol{X}\right]_q \right) \dot{\bar{\boldsymbol{q}}}_u + \dot{\bar{\boldsymbol{u}}}_u \right\}, \tag{5.55}$$

$$\boldsymbol{\mu}_2(\boldsymbol{q}, \bar{\boldsymbol{q}}, \dot{\boldsymbol{q}}, \dot{\bar{\boldsymbol{q}}}, \mathcal{Q}'_u, \dot{\mathcal{Q}}'_u, t) \triangleq \left[\frac{\partial^2 \mathcal{L}_a}{\partial \dot{\boldsymbol{q}}_a^2}\right]_q \left(\dot{\boldsymbol{A}} \dot{\bar{\boldsymbol{q}}}_a + \dot{\boldsymbol{\mu}}_1\right) + \left[\frac{\partial^2 \mathcal{L}_a}{\partial \boldsymbol{q}_a \partial \dot{\boldsymbol{q}}_a}\right]_q \dot{\boldsymbol{q}}_a. \tag{5.56}$$

Theorem 5.3.6 (Quasi-Full Actuation—Monoarticulation) *Suppose that the Euler-Lagrange system* (5.1) *satisfies Assumption 5.1.1 and 5.1.2, and let* $n_u = n_a$. *Consider the phase space transformation* $(\boldsymbol{q}, \dot{\boldsymbol{q}}, t) \to (\bar{\boldsymbol{q}}, \dot{\bar{\boldsymbol{q}}}, t)$ *defined by the diffeomorphism* $\boldsymbol{\pi}$ *in* (5.36), *with* $\bar{\boldsymbol{u}}_u$ *satisfying Assumption 5.3.1, and the following change of control inputs* $\boldsymbol{u} \to \bar{\boldsymbol{u}}$

$$\boldsymbol{u}_a = \boldsymbol{R}^{-1} \left\{ \left[\frac{\partial \mathcal{L}_a}{\partial \bar{\boldsymbol{q}}_a}\right]_{\bar{q}} - \left[\frac{\partial^2 \mathcal{L}_a}{\partial \bar{\boldsymbol{q}}_a \partial \dot{\bar{\boldsymbol{q}}}_a}\right]_{\bar{q}} \dot{\bar{\boldsymbol{q}}}_a + \bar{\boldsymbol{u}}_a \right\} + \boldsymbol{\mu}_2 - \left[\frac{\partial \mathcal{L}_a}{\partial \boldsymbol{q}_a}\right]_q, \tag{5.57}$$

then the equations of motion (5.1) *in the new sets of generalized coordinates and inputs are of the Lagrangian form*

$$\bar{\Sigma}: \frac{\mathrm{d}}{\mathrm{d}t} \left[\frac{\partial \mathcal{L}}{\partial \dot{\bar{\boldsymbol{q}}}}\right]_{\bar{q}} - \left[\frac{\partial \mathcal{L}}{\partial \bar{\boldsymbol{q}}}\right]_{\bar{q}} = \bar{\mathcal{Q}}, \tag{5.58}$$

where $\bar{\mathcal{Q}} = col\left(\bar{\boldsymbol{u}}_u + \mathcal{Q}'_u, \bar{\boldsymbol{u}}_a + \boldsymbol{R}\mathcal{Q}'_a\right)$.

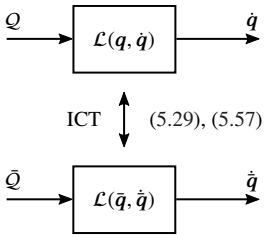

Figure 5.8: The transformation fully preserves the EL structure.

Proof. The proof is based on two central arguments. First, Lemma 5.3.1 tells us that the mapping $\boldsymbol{\pi}$, (5.36), is a diffeomorphism between the two sets of generalized coordinates and velocities $(\boldsymbol{q}, \dot{\boldsymbol{q}}, t)$ and $(\bar{\boldsymbol{q}}, \dot{\bar{\boldsymbol{q}}}, t)$ including the time. Second, we will show that applying simultaneously the transformations $\bar{\boldsymbol{x}} = \boldsymbol{\pi}(\boldsymbol{x})$ and (5.57) to the EL equations (5.1) produces the desired EL equations (5.58).

For ease of reference the central transforming equations (5.29b) and (5.29d) are repeated:

$$\left[\frac{\partial \mathcal{L}_a}{\partial \boldsymbol{q}_u}\right]_q = \left[\frac{\partial \mathcal{L}_a}{\partial \bar{\boldsymbol{q}}_u}\right]_{\bar{q}} + \bar{\boldsymbol{u}}_u, \tag{5.59}$$

$$\frac{\mathrm{d}}{\mathrm{d}t} \left[\frac{\partial \mathcal{L}_a}{\partial \boldsymbol{q}_u}\right]_q = \frac{\mathrm{d}}{\mathrm{d}t} \left[\frac{\partial \mathcal{L}_a}{\partial \bar{\boldsymbol{q}}_u}\right]_{\bar{q}} + \dot{\bar{\boldsymbol{u}}}_u. \tag{5.60}$$

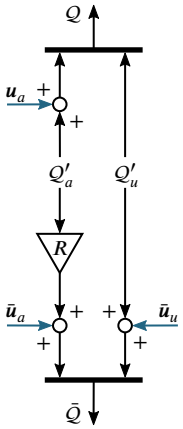

Figure 5.9: Relation between the generalized external forces.

Equation (5.60) gives us an explicit relation between the generalized velocities $\dot{\boldsymbol{q}}_a$ and $\dot{\bar{\boldsymbol{q}}}_a$. From Assumption 5.1.1, it follows that

$$\frac{\mathrm{d}}{\mathrm{d}t}\left[\frac{\partial \mathcal{L}_a}{\partial \boldsymbol{q}_u}\right]_q = \left[\frac{\partial^2 \mathcal{L}_a}{\partial \boldsymbol{q}_u^2}\right]_q \dot{\boldsymbol{q}}_u + \left[\frac{\partial^2 \mathcal{L}_a}{\partial \boldsymbol{q}_a \partial \boldsymbol{q}_u}\right]_q \dot{\boldsymbol{q}}_a, \tag{5.61}$$

$$\frac{\mathrm{d}}{\mathrm{d}t}\left[\frac{\partial \mathcal{L}_a}{\partial \bar{\boldsymbol{q}}_u}\right]_{\bar{q}} = \left[\frac{\partial^2 \mathcal{L}_a}{\partial \bar{\boldsymbol{q}}_u^2}\right]_{\bar{q}} \dot{\bar{\boldsymbol{q}}}_u + \left[\frac{\partial^2 \mathcal{L}_a}{\partial \bar{\boldsymbol{q}}_a \partial \bar{\boldsymbol{q}}_u}\right]_{\bar{q}} \dot{\bar{\boldsymbol{q}}}_a. \tag{5.62}$$

Using (5.52) and making the substitutions (5.60)–(5.62), we obtain

$$\boldsymbol{Y}(\boldsymbol{q})\dot{\boldsymbol{q}}_a = \boldsymbol{Y}(\bar{\boldsymbol{q}})\dot{\bar{\boldsymbol{q}}}_a + \left[\boldsymbol{X}(\bar{\boldsymbol{q}}) - \boldsymbol{X}(\boldsymbol{q})\right]\dot{\bar{\boldsymbol{q}}}_u + \dot{\boldsymbol{u}}_u \tag{5.63}$$

Using the definitions (5.53) and (5.55), and exploiting Assumption (5.1.2), we can rewrite (5.63) as

$$\dot{\boldsymbol{q}}_a = \boldsymbol{A}\dot{\bar{\boldsymbol{q}}}_a + \boldsymbol{\mu}_1, \tag{5.64}$$

which reveals the linear dependence of the velocities $\dot{\boldsymbol{q}}_a$ and $\dot{\bar{\boldsymbol{q}}}_a$. We can now use (5.36) and (5.64) to transform the EL equations (5.1) into the desired form (5.58). Splitting (5.1) into its components, we get:

$$\frac{\mathrm{d}}{\mathrm{d}t}\left[\frac{\partial \mathcal{L}_u}{\partial \dot{\boldsymbol{q}}_u}\right]_q - \left[\frac{\partial \mathcal{L}_u}{\partial \boldsymbol{q}_u}\right]_q - \left[\frac{\partial \mathcal{L}_a}{\partial \boldsymbol{q}_u}\right]_q = \mathcal{Q}_u, \tag{5.65}$$

$$\frac{\mathrm{d}}{\mathrm{d}t}\left[\frac{\partial \mathcal{L}_a}{\partial \dot{\boldsymbol{q}}_a}\right]_q - \left[\frac{\partial \mathcal{L}_a}{\partial \boldsymbol{q}_a}\right]_q = \mathcal{Q}_a. \tag{5.66}$$

Knowing that the sub-Lagrangian $\mathcal{L}_u$ in (5.65) is a function of only the $\boldsymbol{q}_u$'s and $\dot{\boldsymbol{q}}_u$'s, and considering that $\boldsymbol{q}_u \equiv \bar{\boldsymbol{q}}_u$ according to (5.36), it follows immediately

$$\frac{\mathrm{d}}{\mathrm{d}t}\left[\frac{\partial \mathcal{L}_u}{\partial \dot{\boldsymbol{q}}_u}\right]_q - \left[\frac{\partial \mathcal{L}_u}{\partial \boldsymbol{q}_u}\right]_q \equiv \frac{\mathrm{d}}{\mathrm{d}t}\left[\frac{\partial \mathcal{L}_u}{\partial \dot{\bar{\boldsymbol{q}}}_u}\right]_{\bar{q}} - \left[\frac{\partial \mathcal{L}_u}{\partial \bar{\boldsymbol{q}}_u}\right]_{\bar{q}}. \tag{5.67}$$

Making the substitutions (5.67), (5.59) and (5.65) gives the important result

$$\frac{\mathrm{d}}{\mathrm{d}t}\left[\frac{\partial \mathcal{L}_u}{\partial \dot{\boldsymbol{q}}_u}\right]_{\bar{q}} - \left[\frac{\partial \mathcal{L}_u}{\partial \boldsymbol{q}_u}\right]_{\bar{q}} - \left[\frac{\partial \mathcal{L}_a}{\partial \bar{\boldsymbol{q}}_u}\right]_{\bar{q}} = \bar{\boldsymbol{u}}_u + \mathcal{Q}_u = \bar{\mathcal{Q}}_u, \tag{5.68}$$

Considering that

$$\frac{\mathrm{d}}{\mathrm{d}t}\left[\frac{\partial \mathcal{L}_a}{\partial \dot{\boldsymbol{q}}_a}\right]_q = \left[\frac{\partial^2 \mathcal{L}_a}{\partial \dot{\boldsymbol{q}}_a^2}\right]_q \ddot{\boldsymbol{q}}_a + \left[\frac{\partial^2 \mathcal{L}_a}{\partial \boldsymbol{q}_a \partial \dot{\boldsymbol{q}}_a}\right]_q \dot{\boldsymbol{q}}_a, \tag{5.69}$$

we can make the substitution (5.64) and (5.69) and obtain:

$$\begin{aligned}\frac{\mathrm{d}}{\mathrm{d}t}\left[\frac{\partial \mathcal{L}_a}{\partial \dot{\boldsymbol{q}}_a}\right]_q &= \left[\frac{\partial^2 \mathcal{L}_a}{\partial \dot{\boldsymbol{q}}_a^2}\right]_q \frac{\mathrm{d}}{\mathrm{d}t}\left(\boldsymbol{A}\dot{\bar{\boldsymbol{q}}}_a + \boldsymbol{\mu}_1\right) + \left[\frac{\partial^2 \mathcal{L}_a}{\partial \boldsymbol{q}_a \partial \dot{\boldsymbol{q}}_a}\right]_q \left(\boldsymbol{A}\dot{\bar{\boldsymbol{q}}}_a + \boldsymbol{\mu}_1\right) \\ &= \left[\frac{\partial^2 \mathcal{L}_a}{\partial \dot{\boldsymbol{q}}_a^2}\right]_a \boldsymbol{A}\ddot{\bar{\boldsymbol{q}}}_a + \boldsymbol{\mu}_2,\end{aligned} \tag{5.70}$$

where the last equality is due to (5.64) and the definition of $\boldsymbol{\mu}_2$ in (5.56). Notice that we can always rewrite the functions $\boldsymbol{A}, \boldsymbol{\mu}_1, \boldsymbol{\mu}_2$ as functions of time t and the original coordinates $\boldsymbol{q}$ only by applying the diffeomorphism sin (5.36). Inserting (5.70) into (5.66) and pre-multiplying both sides with $\boldsymbol{R}$ from the

left, we obtain after rearranging terms:

$$\left[\frac{\partial^2 \mathcal{L}_a}{\partial \dot{\bar{q}}_a^2}\right]_{\bar{q}} \ddot{\bar{q}}_a = \boldsymbol{R}\left(\mathcal{Q}_a + \left[\frac{\partial \mathcal{L}_a}{\partial \boldsymbol{q}_a}\right]_a - \boldsymbol{\mu}_2\right). \tag{5.71}$$

Finally, introducing

$$\mathcal{Q}_a = \mathcal{Q}'_a - \left[\frac{\partial \mathcal{L}_a}{\partial \boldsymbol{q}_a}\right]_q + \boldsymbol{\mu}_2 + \boldsymbol{R}^{-1}\left(\left[\frac{\partial \mathcal{L}_a}{\partial \bar{\boldsymbol{q}}_a}\right]_{\bar{q}} - \left[\frac{\partial^2 \mathcal{L}_a}{\partial \bar{\boldsymbol{q}}_a \partial \dot{\bar{\boldsymbol{q}}}_a}\right]_{\bar{q}} \dot{\bar{\boldsymbol{q}}}_a + \bar{\boldsymbol{u}}_a\right), \tag{5.72}$$

and making the substitutions (5.71) and (5.72) gives:

$$\left[\frac{\partial^2 \mathcal{L}_a}{\partial \dot{\bar{q}}_a^2}\right]_{\bar{q}} \ddot{\bar{q}}_a + \left[\frac{\partial^2 \mathcal{L}_a}{\partial \bar{\boldsymbol{q}}_a \partial \dot{\bar{\boldsymbol{q}}}_a}\right]_{\bar{q}} \dot{\bar{\boldsymbol{q}}}_a - \left[\frac{\partial \mathcal{L}_a}{\partial \bar{\boldsymbol{q}}_a}\right]_{\bar{q}} = \bar{\boldsymbol{u}}_a + \boldsymbol{R}\mathcal{Q}'_a = \bar{\mathcal{Q}}_a. \tag{5.73}$$

Considering that (5.69) holds equally when written in terms of the $\bar{\boldsymbol{q}}$'s, we can use this fact to rewrite (5.73) in the desired form

$$\frac{\mathrm{d}}{\mathrm{d}t}\left[\frac{\partial \mathcal{L}_a}{\partial \dot{\bar{\boldsymbol{q}}}_a}\right]_{\bar{q}} - \left[\frac{\partial \mathcal{L}_a}{\partial \bar{\boldsymbol{q}}_a}\right]_{\bar{q}} = \bar{\mathcal{Q}}_a. \tag{5.74}$$

It is clear that (5.68) and (5.74) constitute the EL equations

$$\frac{\mathrm{d}}{\mathrm{d}t}\left[\frac{\partial \mathcal{L}}{\partial \dot{\bar{\boldsymbol{q}}}}\right]_{\bar{q}} - \left[\frac{\partial \mathcal{L}}{\partial \bar{\boldsymbol{q}}}\right]_{\bar{q}} = \bar{\mathcal{Q}}, \tag{5.75}$$

which completes the proof. ■

Following the geometrical interpretation of the thought experiment in Section 5.2, we may think of the first n_u transforming equations (5.36) as defining the trajectory $\bar{\boldsymbol{q}}_a$ of the shifted subsystem $\bar{\Sigma}_a$ such that the virtual subsystem coupling forces $\frac{\partial \mathcal{L}_a}{\partial \boldsymbol{q}_u}(\bar{\boldsymbol{q}})$ encodes the difference of the actual $\frac{\partial \mathcal{L}_a}{\partial \boldsymbol{q}_u}(\boldsymbol{q})$ and desired moving force $\bar{\boldsymbol{u}}_u$ acting on Σ_u.

5.4 Multi-Articulated Systems

Let us extend the results from Section 5.3 to the case where the number of actuated coordinates is strictly greater than the number of unactuated coordinates, i.e., $n_a > n_u$.

5.4.1 A Nonpoint Transformation

In the multiarticulation case ($n_a > n_u$), the equations (5.29) no longer define a change of coordinates since we have $2n_u$ equations for $n = n_u + n_a$ unknowns. We can remedy this issue by introducing an additional $m = n_a - n_u$ constraint equations.[15] For the further analysis, it is convenient to introduce

15: As an alternative to introducing m constraint equations, we could also impose the equivalence $q_{ai} = \bar{q}_{ai}$ for m different coordinates. This case is not treated in this work and will be subject to future investigations.

the mappings

$$\boldsymbol{\psi}' : \begin{cases} \mathbb{R}^n & \to & \mathbb{R}^{n_u+m} \\ \boldsymbol{q} & \mapsto & \begin{bmatrix} \boldsymbol{\psi}(\boldsymbol{q}) \\ \boldsymbol{h}(\boldsymbol{q}) \end{bmatrix} \end{cases}, \tag{5.76}$$

$$\bar{\boldsymbol{u}}' : \begin{cases} \mathbb{R}^{n_u} \times \mathbb{R}^{n_u} \times \mathbb{R} & \to & \mathbb{R}^{n_u+m} \\ (\boldsymbol{q}_u, \dot{\boldsymbol{q}}_u, t) & \mapsto & \begin{bmatrix} \bar{\boldsymbol{u}}_u(\boldsymbol{q}_u, \dot{\boldsymbol{q}}_u, t) \\ \boldsymbol{v}_u(\boldsymbol{q}_u, \dot{\boldsymbol{q}}_u, t) \end{bmatrix} \end{cases}. \tag{5.77}$$

where the mappings $\bar{\boldsymbol{u}}_u$, $\boldsymbol{v}_u$ and $\boldsymbol{h}$ are such that the compositions $\bar{\boldsymbol{u}}'$ and $\boldsymbol{\psi}'$ are of class C^p, $p \geq 2$, and satisfy the following.

Assumption 5.4.1 *For any bounded $\boldsymbol{x}, \boldsymbol{y} \in \mathbb{R}^{n_u}$, there exists a positive constant c, independent of $t \in \mathbb{R}$, such that $\|\bar{\boldsymbol{u}}'_u(\boldsymbol{x}, \boldsymbol{y}, t)\| \leq c$.*

Assumption 5.4.2 *The C^k, $k \geq 3$, potential energy function $\mathcal{V}$ and the C^l, $l \geq 2$, mapping $\boldsymbol{h} : \mathbb{R}^n \to \mathbb{R}^{n_u+m}$ are such that for $n_a > n_u$ at least one of the following two conditions is satisfied*

(i) $|\partial_{\boldsymbol{q}_a} \boldsymbol{\psi}'(\boldsymbol{q})| > 0$ *and* $\|\boldsymbol{q}_a\| \to \infty$ *implies* $|\boldsymbol{\psi}'(\boldsymbol{q})| \to \infty$, *(necessary)*
(ii) $|[\partial_{\boldsymbol{q}_a} \boldsymbol{\psi}'(\boldsymbol{q})]^{-1}| \leq c < \infty$ *and* $\boldsymbol{\psi}'(\boldsymbol{0}) = \boldsymbol{0}$, *(sufficient)*

for some positive constant c.

Then, analogously to the monoarticulated case, we can define a phase space transformation $(\boldsymbol{q}, \dot{\boldsymbol{q}}, t) \to (\bar{\boldsymbol{q}}, \dot{\bar{\boldsymbol{q}}}, t)$ by the following set of $2n+1$ equations:

$$\bar{\boldsymbol{q}}_u = \boldsymbol{q}_u, \tag{5.78a}$$
$$\boldsymbol{\psi}'(\bar{\boldsymbol{q}}) = \boldsymbol{\psi}'(\boldsymbol{q}) - \bar{\boldsymbol{u}}'_u(\boldsymbol{q}_u, \dot{\boldsymbol{q}}_u, t), \tag{5.78b}$$
$$\dot{\bar{\boldsymbol{q}}}_u = \dot{\boldsymbol{q}}_u, \tag{5.78c}$$
$$\dot{\boldsymbol{\psi}}'(\bar{\boldsymbol{q}}) = \dot{\boldsymbol{\psi}}'(\boldsymbol{q}) - \dot{\bar{\boldsymbol{u}}}'_u(\boldsymbol{q}_u, \dot{\boldsymbol{q}}_u, t), \tag{5.78d}$$
$$t = t. \tag{5.78e}$$

Note that (5.78b) and (5.78d) implicitly define the new positions and velocities $\bar{\boldsymbol{q}}_a$ and $\dot{\bar{\boldsymbol{q}}}_a$. Following the procedure in Section 5.3, we can express $\dot{\bar{\boldsymbol{u}}}'_u$ in terms of only the generalized positions and velocities $(\boldsymbol{q}_u, \dot{\boldsymbol{q}}_u)$ and time t by making use of (5.30). Knowing that

$$\dot{\bar{\boldsymbol{u}}}'_u = \frac{\partial \bar{\boldsymbol{u}}'_u}{\partial \boldsymbol{q}_u} \dot{\boldsymbol{q}}_u + \frac{\partial \bar{\boldsymbol{u}}'_u}{\partial \dot{\boldsymbol{q}}_u} \ddot{\boldsymbol{q}}_u + \frac{\partial \bar{\boldsymbol{u}}'_u}{\partial t}, \tag{5.79}$$

we can make the substitution (5.30) and (5.79) to obtain

$$\begin{aligned} \dot{\bar{\boldsymbol{u}}}'_u &= \frac{\partial \bar{\boldsymbol{u}}'_u}{\partial \boldsymbol{q}_u} \dot{\boldsymbol{q}}_u + \frac{\partial \bar{\boldsymbol{u}}'_u}{\partial \dot{\boldsymbol{q}}_u} \left[\frac{\partial^2 \mathcal{L}_u}{\partial \dot{\boldsymbol{q}}_u^2} \right]^{-1} \left\{ \frac{\partial \mathcal{L}}{\partial \boldsymbol{q}_u} - \left[\frac{\partial^2 \mathcal{L}_u}{\partial \boldsymbol{q}_u \partial \dot{\boldsymbol{q}}_u} \right] \dot{\boldsymbol{q}}_u + \mathcal{Q}'_u \right\} + \frac{\partial \bar{\boldsymbol{u}}'_u}{\partial t} \\ &\triangleq \boldsymbol{\delta}'(\boldsymbol{q}, \dot{\boldsymbol{q}}_u, \mathcal{Q}'_u, t) \end{aligned} \tag{5.80}$$

such that (5.78b) can be rewritten as

$$\dot{\boldsymbol{\psi}}'(\bar{\boldsymbol{q}}) = \dot{\boldsymbol{\psi}}'(\boldsymbol{q}) - \boldsymbol{\delta}'(\boldsymbol{q}, \dot{\boldsymbol{q}}_u, \mathcal{Q}'_u, t). \tag{5.81}$$

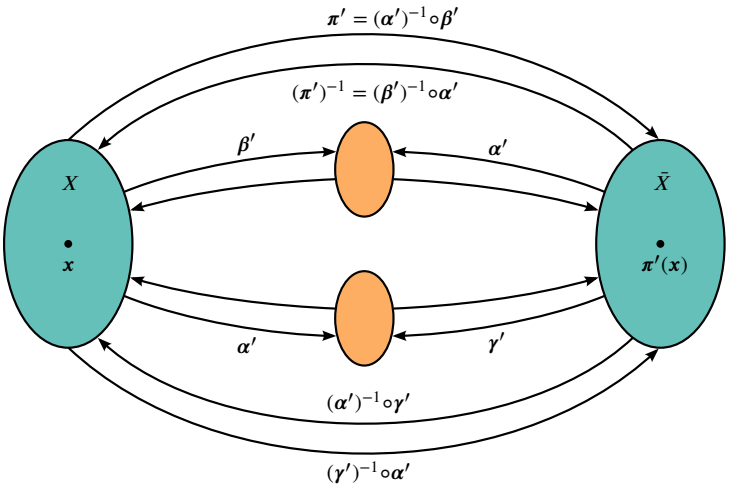

Figure 5.10: Extended state space transformation: the diffeomorphism $\boldsymbol{\pi}$, which is a composition of diffeomorphisms, defines the one-to-one correspondence between the sets X and $\bar{X}$. Treating time as another coordinate, we can interpret $\boldsymbol{\pi}$ as defining a volume-preserving transformation of the extended phase space. In the extended state space, the time coordinate is related to the new independent variable through the identity phase.

To rewrite the transforming equations (5.78a)–(5.78e) in compact form, it is convenient to introduce the mappings:

$$\boldsymbol{\alpha}' : \begin{cases} \mathbb{R}^n \times \mathbb{R}^n \times \mathbb{R} & \to & \mathbb{R}^{2n+1} \\ (\boldsymbol{q}, \dot{\boldsymbol{q}}, t) & \mapsto & \begin{bmatrix} \boldsymbol{q}_u \\ \boldsymbol{\psi}'(\boldsymbol{q}) \\ \dot{\boldsymbol{q}}_u \\ \dot{\boldsymbol{\psi}}'(\boldsymbol{q}) \\ t \end{bmatrix} \end{cases},$$

$$\boldsymbol{\beta}' : \begin{cases} \mathbb{R}^n \times \mathbb{R}^n \times \mathbb{R} & \to & \mathbb{R}^{2n+1} \\ (\boldsymbol{q}, \dot{\boldsymbol{q}}, t) & \mapsto & \begin{bmatrix} \boldsymbol{q}_u \\ \boldsymbol{\psi}'(\boldsymbol{q}) - \bar{\boldsymbol{u}}(\boldsymbol{q}_u, \dot{\boldsymbol{q}}_u, t) \\ \dot{\boldsymbol{q}}_u \\ \dot{\boldsymbol{\psi}}'(\boldsymbol{q}) - \boldsymbol{\delta}'(\boldsymbol{q}, \dot{\boldsymbol{q}}_u, \mathcal{Q}'_u, t) \\ t \end{bmatrix} \end{cases},$$

$$\boldsymbol{\gamma}' : \begin{cases} \mathbb{R}^n \times \mathbb{R}^n \times \mathbb{R} & \to & \mathbb{R}^{2n+1} \\ (\boldsymbol{q}, \dot{\boldsymbol{q}}, t) & \mapsto & \begin{bmatrix} \boldsymbol{q}_u \\ \boldsymbol{\psi}'(\boldsymbol{q}) + \bar{\boldsymbol{u}}'(\boldsymbol{q}_u, \dot{\boldsymbol{q}}_u, t) \\ \dot{\boldsymbol{q}}_u \\ \dot{\boldsymbol{\psi}}'(\boldsymbol{q}) + \boldsymbol{\delta}'(\boldsymbol{q}, \dot{\boldsymbol{q}}_u, \mathcal{Q}'_u, t) \\ t \end{bmatrix} \end{cases}.$$

Then, we can define a diffeomorphism between the two sets of generalized coordinates and velocities as follows.

Lemma 5.4.1 (A one-to-one correspondence) *The mapping*

$$\boldsymbol{\pi}' : \begin{cases} \boldsymbol{X} & \to & \bar{\boldsymbol{X}} \\ \boldsymbol{x} & \mapsto & (\boldsymbol{\alpha}')^{-1} \circ \boldsymbol{\beta}'(\boldsymbol{x}) \end{cases}, \tag{5.82}$$

is a C^1 diffeomorphism, and thus defines a change of coordinates

$$\begin{aligned}\bar{q}_i &= \bar{q}_i(\boldsymbol{q}, \dot{\boldsymbol{q}}, t),\\ \dot{\bar{q}}_i &= \dot{\bar{q}}_i(\boldsymbol{q}, \dot{\boldsymbol{q}}, t),\end{aligned} \tag{5.83}$$

with $|D\boldsymbol{\pi}'(\boldsymbol{x})| = |D\boldsymbol{\alpha}'(\bar{\boldsymbol{x}})|^{-1}|D\boldsymbol{\alpha}'(\boldsymbol{x})|$.

Assumption 5.4.2 is unique to the multiarticulation case and will be central to the proof of Lemma 5.4.1. Considering its central role let us verify the existence of functions $\boldsymbol{h}$ and $\boldsymbol{\nu}_u$ satisfying Assumption 5.4.2 before continuing with the actual proof. We shall rely on a proof by example. To this end, without loss of generality, let us consider

$$\nu_{ui} = 0, \text{ and } h_i = \begin{cases} 0 & \text{for } i = 1, \dots, n_u, \\ q_{ai} & \text{for } i = n_{n_u+1}, \dots, n_a, \end{cases}. \tag{5.84}$$

The following arguments follow directly from the properties of potential function $\mathcal{V}$ summarized in Assumption 5.1.2. Given that all singular values of $\partial_{\boldsymbol{q}_a}\boldsymbol{\psi}(\boldsymbol{q})$ are strictly positive, we conclude that s has full row rank.[16] Hence, by reordering of the q_{ai} and thus of the $\bar{q}_{ai}$, we can always obtain a partitioning of $\partial_{q_a}\boldsymbol{\psi}$ such that the left $n_u \times n_u$ submatrix

16: Note that given some (complex) matrix $\boldsymbol{A}$, then $\operatorname{rank}(\boldsymbol{A}) = \operatorname{rank}(\boldsymbol{U}\boldsymbol{\Sigma}\boldsymbol{V}^*) = \operatorname{rank}(\boldsymbol{\Sigma})$.

$$\left[\frac{\partial\boldsymbol{\psi}}{\partial\dot{q}_{a1}} \cdots \frac{\partial\boldsymbol{\psi}}{\partial\dot{q}_{an_u}} \cdots \frac{\partial\boldsymbol{\psi}}{\partial\dot{q}_{an_u+1}} \cdots \frac{\partial\boldsymbol{\psi}}{\partial\dot{q}_{an_a}}\right] \tag{5.85}$$

$$\left[\begin{array}{ccc|ccc} \frac{\partial\boldsymbol{\psi}}{\partial q_{a1}} & \cdots & \frac{\partial\boldsymbol{\psi}}{\partial q_{an_u}} & \frac{\partial\boldsymbol{\psi}}{\partial q_{an_u+1}} & \cdots & \frac{\partial\boldsymbol{\psi}}{\partial q_{an_a}} \end{array}\right] \tag{5.86}$$

is invertible. In this case, we get for $\partial_{\boldsymbol{q}_a}\boldsymbol{\psi}'$

$$\left[\begin{array}{ccc|ccc} \frac{\partial\boldsymbol{\psi}}{\partial q_{a1}} & \cdots & \frac{\partial\boldsymbol{\psi}}{\partial q_{an_u}} & \frac{\partial\boldsymbol{\psi}}{\partial q_{an_u+1}} & \cdots & \frac{\partial\boldsymbol{\psi}}{\partial q_{an_a}} \\ \hline \multicolumn{3}{c|}{\boldsymbol{0}} & \multicolumn{3}{c}{\boldsymbol{I}} \end{array}\right]. \tag{5.87}$$

Considering Schur's determinant identity, it is clear that $\partial_{q_a}\boldsymbol{\psi}'$ is full rank as desired. Moreover, its determinant is $|\partial_{q_a}\boldsymbol{\psi}|$, and thus similar to the monoarticulation case. Follow analogously the steps of proof of Property 3, it is straightforward to show that choice of h_i and ν_i, as in (5.84), always satisfies Assumption 5.4.2.

Remark 5.4.1 This particular choice of results in a set of constraint equations that considers only a subset of generalized coordinates, and is by no means the most appropriate for every system. In fact, making the substitution (5.78b) and (5.84) yields $q_{ak} = \bar{q}_{ak}, k = n_u + 1, \dots, n_a$. In most scenarios there is no physical justification for this unequal treatment of the actuated coordinates. The example above shall only serve as a proof that there always exist constraint equations such that Lemma 5.4.1 holds. A "smart" choice for the constraint equations, however, requires physical insight into the structure of the considered system. For example, in [60, 115, 151], we introduce physically motivated constraint equations tailored to elastic tendon-driven fingers and bi-antagonistic variable stiffness actuators, respectively. In the former and latter case, the introduced constraint equations translate into the joint pretensions of the original and virtual system being equal. In [114], we choose pure kinematic constraints that aim at simplifying the solving of the coordinate transformation.

[60]: Harder et al. (2022), "Simultaneous motion tracking and joint stiffness control of bidirectional antagonistic variable-stiffness actuators"

[115]: Mengacci et al. (2021), "Elastic Structure Preserving control for compliant robots driven by agonistic-antagonistic actuators (ESPaa)"

[151]: Pollayil et al. (2021), "Elastic structure preserving impedance controlfor nonlinearly coupled tendon-driven systems"

[114]: Meng et al. (2021), "Elastic structure preserving impedance control of bidirectional antagonistic variable stiffness actuation"

Proof of Lemma 5.4.1 using Theorem 5.3.4. We can proceed analogously to the proof of Lemma 5.3.1 and shall focus on the case where condition (ii) in Assumption 5.1.2 is satisfied only. The proof consists of three steps: 1) show that $\boldsymbol{\alpha}'$ and $\boldsymbol{\beta}'$ are diffeomorphisms using Theorem 5.3.4, 2) conclude that the composition $\boldsymbol{\pi}'$ is a diffeomorphism, 3) establish the desired expression for $|D\boldsymbol{\pi}'|$.
Step 1: Knowing that

$$D\boldsymbol{\alpha}'(\boldsymbol{x}) = \frac{\partial \alpha_i'}{\partial x_j} = \left[\begin{array}{cc|ccc} \frac{\partial \boldsymbol{q}_u}{\partial \boldsymbol{q}_u} & \frac{\partial \boldsymbol{q}_u}{\partial \boldsymbol{q}_a} & \frac{\partial \boldsymbol{q}_u}{\partial \dot{\boldsymbol{q}}_u} & \frac{\partial \boldsymbol{q}_u}{\partial \dot{\boldsymbol{q}}_a} & \frac{\partial \boldsymbol{q}_u}{\partial t} \\ \frac{\partial \boldsymbol{\psi}'}{\partial \boldsymbol{q}_u} & \frac{\partial \boldsymbol{\psi}'}{\partial \boldsymbol{q}_a} & \frac{\partial \boldsymbol{\psi}'}{\partial \dot{\boldsymbol{q}}_u} & \frac{\partial \boldsymbol{\psi}'}{\partial \dot{\boldsymbol{q}}_a} & \frac{\partial \boldsymbol{\psi}'}{\partial t} \\ \hline \frac{\partial \dot{\boldsymbol{q}}_u}{\partial \boldsymbol{q}_u} & \frac{\partial \dot{\boldsymbol{q}}_u}{\partial \boldsymbol{q}_a} & \frac{\partial \dot{\boldsymbol{q}}_u}{\partial \dot{\boldsymbol{q}}_u} & \frac{\partial \dot{\boldsymbol{q}}_u}{\partial \dot{\boldsymbol{q}}_a} & \frac{\partial \dot{\boldsymbol{q}}_u}{\partial t} \\ \frac{\partial \dot{\boldsymbol{\psi}}'}{\partial \boldsymbol{q}_u} & \frac{\partial \dot{\boldsymbol{\psi}}'}{\partial \boldsymbol{q}_a} & \frac{\partial \dot{\boldsymbol{\psi}}'}{\partial \dot{\boldsymbol{q}}_u} & \frac{\partial \dot{\boldsymbol{\psi}}'}{\partial \dot{\boldsymbol{q}}_a} & \frac{\partial \dot{\boldsymbol{\psi}}'}{\partial t} \\ \hline \frac{\partial t}{\partial \boldsymbol{q}_u} & \frac{\partial t}{\partial \boldsymbol{q}_a} & \frac{\partial t}{\partial \dot{\boldsymbol{q}}_u} & \frac{\partial t}{\partial \dot{\boldsymbol{q}}_u} & \frac{\partial t}{\partial t} \end{array}\right],$$

considering that $\frac{\partial \dot{\boldsymbol{\psi}}'}{\partial \dot{\boldsymbol{q}}_k} = \frac{\partial \boldsymbol{\psi}'}{\partial \boldsymbol{q}_k}$, $k = u, a$, and using Schur's determinant identity[17], we get

17: See Theorem D.3.2 in Appendix D.

$$|D\boldsymbol{\alpha}(\boldsymbol{x})| = \begin{vmatrix} \boldsymbol{I} & \boldsymbol{0} & \boldsymbol{0} \\ \frac{\partial \boldsymbol{\psi}'}{\partial \boldsymbol{q}_u} & \frac{\partial \boldsymbol{\psi}'}{\partial \boldsymbol{q}_a} & \boldsymbol{0} \\ \boldsymbol{0} & \boldsymbol{0} & 1 \end{vmatrix} \begin{vmatrix} \boldsymbol{I} & \boldsymbol{0} \\ \frac{\partial \boldsymbol{\psi}'}{\partial \boldsymbol{q}_u} & \frac{\partial \boldsymbol{\psi}'}{\partial \boldsymbol{q}_a} \end{vmatrix} = \begin{vmatrix} \boldsymbol{I} & \boldsymbol{0} \\ \frac{\partial \boldsymbol{\psi}'}{\partial \boldsymbol{q}_u} & \frac{\partial \boldsymbol{\psi}'}{\partial \boldsymbol{q}_a} \end{vmatrix}^2 = \left| \frac{\partial \boldsymbol{\psi}'}{\partial \boldsymbol{q}_a} \right|^2, \quad (5.88)$$

where the last equality can be shown through repeated cofactor expansion along the first row. Proceeding analogously to the steps above, and further considering that $\partial_{\dot{\boldsymbol{q}}_a} \boldsymbol{\delta}' = \boldsymbol{0}$, we obtain

$$D\boldsymbol{\beta}'(\boldsymbol{x}) = \left[\begin{array}{cc|ccc} \frac{\partial \boldsymbol{q}_u}{\partial \boldsymbol{q}_u} & \frac{\partial \boldsymbol{q}_u}{\partial \boldsymbol{q}_a} & \frac{\partial \boldsymbol{q}_u}{\partial \dot{\boldsymbol{q}}_u} & \frac{\partial \boldsymbol{q}_u}{\partial \dot{\boldsymbol{q}}_a} & \frac{\partial \boldsymbol{q}_u}{\partial t} \\ \partial_{\boldsymbol{q}_u}(\boldsymbol{\psi}' - \bar{\boldsymbol{u}}_u') & \frac{\partial \boldsymbol{\psi}'}{\partial \boldsymbol{q}_a} & \partial_{\dot{\boldsymbol{q}}_u}(\boldsymbol{\psi}' - \bar{\boldsymbol{u}}_u') & \frac{\partial \boldsymbol{\psi}'}{\partial \dot{\boldsymbol{q}}_a} & \partial_t(\boldsymbol{\psi}' - \bar{\boldsymbol{u}}_u') \\ \hline \frac{\partial \dot{\boldsymbol{q}}_u}{\partial \boldsymbol{q}_u} & \frac{\partial \dot{\boldsymbol{q}}_u}{\partial \boldsymbol{q}_a} & \frac{\partial \dot{\boldsymbol{q}}_u}{\partial \dot{\boldsymbol{q}}_u} & \frac{\partial \dot{\boldsymbol{q}}_u}{\partial \dot{\boldsymbol{q}}_a} & \frac{\partial \dot{\boldsymbol{q}}_u}{\partial t} \\ \partial_{\boldsymbol{q}_u}(\dot{\boldsymbol{\psi}}' - \boldsymbol{\delta}') & \partial_{\boldsymbol{q}_a}(\dot{\boldsymbol{\psi}}' - \boldsymbol{\delta}') & \partial_{\dot{\boldsymbol{q}}_u}(\dot{\boldsymbol{\psi}}' - \boldsymbol{\delta}') & \partial_{\dot{\boldsymbol{q}}_a}(\dot{\boldsymbol{\psi}}' - \boldsymbol{\delta}') & \partial_t(\dot{\boldsymbol{\psi}} - \boldsymbol{\delta}) \\ \hline \frac{\partial t}{\partial \boldsymbol{q}_u} & \frac{\partial t}{\partial \boldsymbol{q}_a} & \frac{\partial t}{\partial \dot{\boldsymbol{q}}_u} & \frac{\partial t}{\partial \dot{\boldsymbol{q}}_a} & \frac{\partial t}{\partial t} \end{array}\right],$$

and eventually conclude that[18]

18: Note that we can proceed analogously to the argument in Appendix B.3.

$$|D\boldsymbol{\beta}'(\boldsymbol{x})| = \begin{vmatrix} \frac{\partial \boldsymbol{\psi}'}{\partial \boldsymbol{q}_a} & \partial_t(\dot{\boldsymbol{\psi}}' - \boldsymbol{\delta}') \\ \boldsymbol{0} & 1 \end{vmatrix} \begin{vmatrix} \boldsymbol{I} & \boldsymbol{0} & \boldsymbol{0} \\ \partial_{\boldsymbol{q}_u}(\boldsymbol{\psi}' - \bar{\boldsymbol{u}}_u') & \frac{\partial \boldsymbol{\psi}'}{\partial \boldsymbol{q}_a} & \boldsymbol{0} \\ \boldsymbol{0} & \boldsymbol{0} & 1 \end{vmatrix} = \left| \frac{\partial \boldsymbol{\psi}'}{\partial \boldsymbol{q}_a} \right|^2. \quad (5.89)$$

Considering condition (ii) of Assumption 5.1.2, we know that

$$|D\boldsymbol{\alpha}'(\boldsymbol{x})| \geq c^2 > 0, \text{ and } |D\boldsymbol{\beta}'(\boldsymbol{x})| \geq c^2 > 0, \quad \forall \boldsymbol{x} \in X. \quad (5.90)$$

We leave it to the reader to verify that $\boldsymbol{\alpha}'$ and $\boldsymbol{\beta}'$ satisfy the desired conditions of Theorem 5.3.4, which concludes the proof that $\boldsymbol{\alpha}'$ and $\boldsymbol{\beta}'$ are diffeomorphisms.
Step 2: Given that the composition of diffeomorphisms is a diffeomorphism [82, p. 300], we conclude that $\boldsymbol{\pi}' = (\boldsymbol{\alpha}')^{-1} \circ \boldsymbol{\beta}'$ is a diffeomorphism.
Step 3: The result above and the chain rule tell us that the composition $\boldsymbol{\pi}'$, (5.36), is differentiable on X, and that the Jacobian matrices corresponding to

[82]: Kass et al. (2011), *Geometrical Foundations of Asymptotic Inference*

$\boldsymbol{\pi}'$, $\boldsymbol{\alpha}'$ and $\boldsymbol{\beta}'$ are related as follows

$$D\boldsymbol{\pi}'(\boldsymbol{x}) = D\left[(\boldsymbol{\alpha}')^{-1}\right]\left(\boldsymbol{\beta}'(\boldsymbol{x})\right) \cdot D\boldsymbol{\beta}'(\boldsymbol{x}). \tag{5.91}$$

Knowing from the inverse function theorem that $D\left[(\boldsymbol{\alpha}')^{-1}\right]\left(\boldsymbol{\beta}'(\boldsymbol{x})\right) = D\boldsymbol{\alpha}'(\bar{\boldsymbol{x}})^{-1}$, we conclude from (5.91) that[19]

$$|D\boldsymbol{\pi}'(\boldsymbol{x})| = |D\boldsymbol{\alpha}'(\bar{\boldsymbol{x}})|^{-1}\,|D\boldsymbol{\beta}'(\boldsymbol{x})| = |D\boldsymbol{\alpha}'(\bar{\boldsymbol{x}})|^{-1}|D\boldsymbol{\alpha}'(\boldsymbol{x})|, \tag{5.92}$$

which completes the proof. ■

19: Recall that $|\boldsymbol{A}\boldsymbol{B}| = |\boldsymbol{A}||\boldsymbol{B}|$ and for some invertible matrix $\boldsymbol{A}$, we have that $|\boldsymbol{A}^{-1}| = |\boldsymbol{A}|^{-1}$.

5.4.2 Main Result

The following Theorem extends the concept of quasi-full actuation, presented in Section Section 5.3, to the multiarticulation case. It is convenient to introduce the "partial" Jacobians and the auxiliary functions

$$\boldsymbol{X}'(\boldsymbol{q}) \triangleq \frac{\partial \boldsymbol{\psi}'}{\partial \boldsymbol{q}_u}(\boldsymbol{q}); \quad \boldsymbol{Y}'(\boldsymbol{q}) \triangleq \frac{\partial \boldsymbol{\psi}'}{\partial \boldsymbol{q}_a}(\boldsymbol{q}), \tag{5.93a}$$

$$\boldsymbol{A}'(\boldsymbol{q}, \bar{\boldsymbol{q}}) \triangleq \left[\boldsymbol{Y}'\right]_q^{-1}\left[\boldsymbol{Y}'\right]_{\bar{q}}, \tag{5.93b}$$

$$\boldsymbol{R}'(\boldsymbol{q}, \bar{\boldsymbol{q}}) \triangleq \left[\frac{\partial^2 \mathcal{L}_a}{\partial \dot{\bar{\boldsymbol{q}}}_a^2}\right]_{\bar{q}} (\boldsymbol{A}')^{-1}(\boldsymbol{q}, \bar{\boldsymbol{q}}) \left[\frac{\partial^2 \mathcal{L}_a}{\partial \dot{\boldsymbol{q}}_a^2}\right]_q^{-1}, \tag{5.93c}$$

$$\boldsymbol{\mu}_1'(\boldsymbol{q}, \bar{\boldsymbol{q}}, \dot{\boldsymbol{q}}_u, \mathcal{Q}_u', t) \triangleq \left[\boldsymbol{Y}'\right]_q^{-1}\left\{\left(\left[\boldsymbol{X}'\right]_{\bar{q}} - \left[\boldsymbol{X}'\right]_q\right)\dot{\bar{\boldsymbol{q}}}_u + \dot{\bar{\boldsymbol{u}}}_u\right\}, \tag{5.93d}$$

$$\boldsymbol{\mu}_2'(\boldsymbol{q}, \bar{\boldsymbol{q}}, \dot{\boldsymbol{q}}, \dot{\bar{\boldsymbol{q}}}, \mathcal{Q}_u', \dot{\mathcal{Q}}_u', t) \triangleq \left[\frac{\partial^2 \mathcal{L}_a}{\partial \dot{\boldsymbol{q}}_a^2}\right]_q \left(\dot{\boldsymbol{A}}'\dot{\bar{\boldsymbol{q}}}_a + \dot{\boldsymbol{\mu}}_1'\right) + \left[\frac{\partial^2 \mathcal{L}_a}{\partial \boldsymbol{q}_a \partial \dot{\boldsymbol{q}}_a}\right]_q \dot{\boldsymbol{q}}_a. \tag{5.93e}$$

Theorem 5.4.2 (Quasi-Full Actuation—Multiarticulation) *Suppose that the Euler-Lagrange system* (5.1) *satisfies Assumption 5.1.1 and 5.4.2 and* $n_a > n_u$. *Consider the phase space transformation* $(\boldsymbol{q}, \dot{\boldsymbol{q}}, t) \to (\bar{\boldsymbol{q}}, \dot{\bar{\boldsymbol{q}}}, t)$ *defined by the diffeomorphism* $\boldsymbol{\pi}$ *in* (5.82), *with* $\bar{\boldsymbol{u}}_u$ *satisfying Assumption 5.4.1, and the following change of control inputs* $\boldsymbol{u} \to \bar{\boldsymbol{u}}$

$$\boldsymbol{u}_a = (\boldsymbol{R}')^{-1}\left\{\left[\frac{\partial \mathcal{L}_a}{\partial \bar{\boldsymbol{q}}_a}\right]_{\bar{q}} - \left[\frac{\partial^2 \mathcal{L}_a}{\partial \bar{\boldsymbol{q}}_a \partial \dot{\bar{\boldsymbol{q}}}_a}\right]_{\bar{q}} \dot{\bar{\boldsymbol{q}}}_a + \bar{\boldsymbol{u}}_a'\right\} + \boldsymbol{\mu}_2' - \left[\frac{\partial \mathcal{L}_a}{\partial \boldsymbol{q}_a}\right]_q, \tag{5.94}$$

then the equations of motion (5.1) *in the new sets of coordinates and inputs are in the Lagrangian form*

$$\bar{\Sigma}: \frac{\mathrm{d}}{\mathrm{d}t}\left[\frac{\partial \mathcal{L}}{\partial \dot{\bar{\boldsymbol{q}}}}\right]_{\bar{q}} - \left[\frac{\partial \mathcal{L}}{\partial \bar{\boldsymbol{q}}}\right]_{\bar{q}} = \bar{\mathcal{Q}}, \tag{5.95}$$

where $\bar{\mathcal{Q}} = col(\bar{\boldsymbol{u}}_u + \mathcal{Q}_u', \bar{\boldsymbol{u}}_a + \boldsymbol{R}'\mathcal{Q}_a')$.

Proof. For ease of reference, the transforming equation (5.78b) is repeated

$$\frac{\partial \mathcal{L}_a}{\partial \boldsymbol{q}_u} = \frac{\partial \mathcal{L}_a}{\partial \bar{\boldsymbol{q}}_u} + \bar{\boldsymbol{u}}_u(\boldsymbol{q}_u, \dot{\boldsymbol{q}}_u, t). \tag{5.96}$$

From Assumption 5.1.1, we know that

$$\partial_{\dot{\boldsymbol{q}}_u}\mathcal{L} = \partial_{\dot{\boldsymbol{q}}_u}\mathcal{L}_u, \tag{5.97}$$

$$\partial_{\dot{\boldsymbol{q}}_a}\mathcal{L} = \partial_{\dot{\boldsymbol{q}}_a}\mathcal{L}_a, \tag{5.98}$$

$$\partial_{\boldsymbol{q}_a}\mathcal{L} = \partial_{\boldsymbol{q}_a}\mathcal{L}_a. \tag{5.99}$$

and according to (5.78a), which implies that $\boldsymbol{q}_u = \bar{\boldsymbol{q}}_u$, we further know that

$$\frac{\mathrm{d}}{\mathrm{d}t}\left[\frac{\partial\mathcal{L}_u}{\partial\dot{\boldsymbol{q}}_u}\right]_q - \left[\frac{\partial\mathcal{L}_u}{\partial\boldsymbol{q}_u}\right]_q = \frac{\mathrm{d}}{\mathrm{d}t}\left[\frac{\partial\mathcal{L}_u}{\partial\dot{\bar{\boldsymbol{q}}}_u}\right]_{\bar{q}} - \left[\frac{\partial\mathcal{L}_u}{\partial\bar{\boldsymbol{q}}_u}\right]_{\bar{q}}, \tag{5.100}$$

Considering (5.97)–(5.100) it is evident that the EL equations of the unactuated subsystem, (5.1), can be written as

$$\frac{\mathrm{d}}{\mathrm{d}t}\left[\frac{\partial\mathcal{L}_u}{\partial\dot{\bar{\boldsymbol{q}}}_u}\right]_{\bar{q}} - \left[\frac{\partial\mathcal{L}_u}{\partial\bar{\boldsymbol{q}}_u}\right]_{\bar{q}} - \left[\frac{\partial\mathcal{L}_a}{\partial\bar{\boldsymbol{q}}_u}\right]_{\bar{q}} = \bar{\mathcal{Q}}_u. \tag{5.101}$$

Recalling that $\bar{\mathcal{Q}}_u = \mathcal{Q}'_u + \bar{\boldsymbol{u}}_u$, we see that (5.101) represent the first n_u equations of the desired EL equations (5.95). Let us continue with expanding the transforming equations (5.78e) as

$$\frac{\partial\boldsymbol{\psi}'}{\partial\boldsymbol{q}_u}\dot{\boldsymbol{q}}_u + \frac{\partial\boldsymbol{\psi}'}{\partial\boldsymbol{q}_a}\dot{\boldsymbol{q}}_a = \frac{\partial\boldsymbol{\psi}'}{\partial\bar{\boldsymbol{q}}_u}\dot{\bar{\boldsymbol{q}}}_u + \frac{\partial\boldsymbol{\psi}'}{\partial\bar{\boldsymbol{q}}_a}\dot{\bar{\boldsymbol{q}}}_a + \dot{\bar{\boldsymbol{u}}}'_u(\boldsymbol{q}_u, \dot{\boldsymbol{q}}_u, t). \tag{5.102}$$

Using (5.93a)–(5.93d), we can solve (5.102) for $\dot{\boldsymbol{q}}_a$:

$$\dot{\boldsymbol{q}}_a = \boldsymbol{A}'(\boldsymbol{q}, \dot{\boldsymbol{q}}_u, t)\dot{\bar{\boldsymbol{q}}}_a + \boldsymbol{\mu}'_1 \tag{5.103}$$

Further knowing that

$$\frac{\mathrm{d}}{\mathrm{d}t}\frac{\partial\mathcal{L}_a}{\partial\dot{\boldsymbol{q}}_a} = \frac{\partial^2\mathcal{L}_a}{\partial\dot{\boldsymbol{q}}_a^2}\ddot{\boldsymbol{q}}_a + \frac{\partial^2\mathcal{L}_a}{\partial\boldsymbol{q}_a\partial\dot{\boldsymbol{q}}_a}\dot{\boldsymbol{q}}_a, \tag{5.104}$$

we can make the substitutions (5.103) and (5.104) to obtain

$$\frac{\mathrm{d}}{\mathrm{d}t}\frac{\partial\mathcal{L}_a}{\partial\dot{\boldsymbol{q}}_a} = \left[\frac{\partial^2\mathcal{L}_a}{\partial\dot{\boldsymbol{q}}_a^2}\right]_q\left\{\boldsymbol{A}'\ddot{\bar{\boldsymbol{q}}}_a + \dot{\boldsymbol{A}}'\dot{\bar{\boldsymbol{q}}}_a + \dot{\boldsymbol{\mu}}'_1\right\} + \frac{\partial^2\mathcal{L}_a}{\partial\boldsymbol{q}_a\partial\dot{\boldsymbol{q}}_a}\left\{\boldsymbol{A}'\dot{\bar{\boldsymbol{q}}}_a + \boldsymbol{\mu}'_1\right\}. \tag{5.105}$$

Next, using (5.93e) and (5.105), we can rewrite (5.104) as

$$\frac{\mathrm{d}}{\mathrm{d}t}\left[\frac{\partial\mathcal{L}_a}{\partial\dot{\boldsymbol{q}}_a}\right] = \left[\frac{\partial^2\mathcal{L}_a}{\partial\dot{\boldsymbol{q}}_a^2}\right]_q\boldsymbol{A}'\ddot{\bar{\boldsymbol{q}}}_a + \boldsymbol{\mu}_2. \tag{5.106}$$

Inserting (5.106) into (5.1) and multiplying both sides with $\boldsymbol{R}'$ from the left, we obtain after rearranging some terms

$$\left[\frac{\partial^2\mathcal{L}_a}{\partial\dot{\bar{\boldsymbol{q}}}_a^2}\right]_{\bar{q}}\ddot{\bar{\boldsymbol{q}}}_a = \boldsymbol{R}'\left\{\left[\frac{\partial\mathcal{L}_a}{\partial\boldsymbol{q}_a}\right]_q - \boldsymbol{\mu}'_2 + \mathcal{Q}_a\right\}. \tag{5.107}$$

Finally, applying the input transformation (5.94) to (5.107) gives

$$\left[\frac{\partial^2\mathcal{L}_a}{\partial\dot{\bar{\boldsymbol{q}}}_a^2}\right]_{\bar{q}}\ddot{\bar{\boldsymbol{q}}}_a + \left[\frac{\partial^2\mathcal{L}_a}{\partial\dot{\bar{\boldsymbol{q}}}_a\partial\bar{\boldsymbol{q}}_a}\right]_q\dot{\bar{\boldsymbol{q}}}_a - \left[\frac{\partial\mathcal{L}_a}{\partial\bar{\boldsymbol{q}}_a}\right]_{\bar{q}} = \bar{\boldsymbol{u}}_a + \boldsymbol{R}'\mathcal{Q}'_a. \tag{5.108}$$

Considering that (5.104) must equally hold when written in terms of the $\bar{\boldsymbol{q}}'s$,

we conclude that (5.108) is equivalent to the desired result

$$\frac{\mathrm{d}}{\mathrm{d}t}\left[\frac{\partial^2 \mathcal{L}_a}{\partial \dot{\bar{q}}_a^2}\right]_{\bar{q}} - \left[\frac{\partial \mathcal{L}_a}{\partial \bar{q}_a}\right]_{\bar{q}} = \bar{Q}_a. \tag{5.109}$$

Considering (5.97)–(5.98), it is clear that (5.101) and (5.109) constitute the EL equations

$$\frac{\mathrm{d}}{\mathrm{d}t}\left[\frac{\partial \mathcal{L}}{\partial \dot{\bar{q}}}\right]_{\bar{q}} - \left[\frac{\partial \mathcal{L}}{\partial \bar{q}}\right]_{\bar{q}} = \bar{Q}, \tag{5.110}$$

which completes the proof. ■

Choosing the Constraint Equations: An Example

Consider an EL system with n_u unactuated coordinates $\boldsymbol{q}_u$ and $2n_u$ actuated coordinates $\boldsymbol{q}_a$, with the latter being split into two subsets of each n_u coordinates such that $\boldsymbol{q}_a = (\boldsymbol{q}_{a1}, \boldsymbol{q}_{a2})$. Suppose that the Lagrangian can be decomposed in the form[20]

20: Practical cases where such decomposition can be found include (bi-)antagonistic variable stiffness joints; see, e.g., 3.1.2.

$$\mathcal{L}(\boldsymbol{q}, \dot{\boldsymbol{q}}) = \mathcal{L}_u(\boldsymbol{q}_u, \dot{\boldsymbol{q}}_u) + \mathcal{L}_{a1}(\boldsymbol{q}_u, \boldsymbol{q}_{a1}, \dot{\boldsymbol{q}}_{a1}) + \mathcal{L}_{a2}(\boldsymbol{q}_u, \boldsymbol{q}_{a2}, \dot{\boldsymbol{q}}_{a2}), \tag{5.111}$$

where $\boldsymbol{q} = (\boldsymbol{q}_u, \boldsymbol{q}_a)$, and the subsystem coupling forces

$$\boldsymbol{\psi}_1 = \frac{\partial \mathcal{L}_{a1}}{\partial \boldsymbol{q}_u}; \quad \boldsymbol{\psi}_2 = \frac{\partial \mathcal{L}_{a2}}{\partial \boldsymbol{q}_u}, \tag{5.112}$$

satisfy

$$\left|\frac{\partial \boldsymbol{\psi}_1}{\partial \boldsymbol{q}_{a1}}^{-1}\right| \geq c_1 > 1, \quad \left|\frac{\partial \boldsymbol{\psi}_2}{\partial \boldsymbol{q}_{a2}}^{-1}\right| \geq c_2 > 0. \tag{5.113}$$

Then, we can choose

$$\boldsymbol{h}: \boldsymbol{q} \mapsto \boldsymbol{\psi}_1(\boldsymbol{q}) - \boldsymbol{\psi}_2(\boldsymbol{q}), \tag{5.114}$$

$$\boldsymbol{v}_u: (\boldsymbol{q}_u, \dot{\boldsymbol{q}}_u, t) \mapsto \boldsymbol{0}, \tag{5.115}$$

such that $\boldsymbol{\psi}'$, as in (5.76), satisfies condition (ii) of Assumption 5.4.2, which is straightforward to show. Knowing from (5.111) and (5.112) that

$$\boldsymbol{\psi}' = \begin{bmatrix} \boldsymbol{\psi} \\ \boldsymbol{h} \end{bmatrix} = \begin{bmatrix} \boldsymbol{\psi}_1 + \boldsymbol{\psi}_2 \\ \boldsymbol{\psi}_1 - \boldsymbol{\psi}_2 \end{bmatrix}, \tag{5.116}$$

we get for the partial Jacobian

$$\frac{\partial \boldsymbol{\psi}'(\boldsymbol{q})}{\partial \boldsymbol{q}_a} = \begin{bmatrix} \frac{\partial \boldsymbol{\psi}_1}{\partial \boldsymbol{q}_{a1}} & \frac{\partial \boldsymbol{\psi}_2}{\partial \boldsymbol{q}_{a2}} \\ \frac{\partial \boldsymbol{\psi}_1}{\partial \boldsymbol{q}_{a1}} & -\frac{\partial \boldsymbol{\psi}_2}{\partial \boldsymbol{q}_{a2}} \end{bmatrix} \tag{5.117}$$

and its associated determinant using Schur's determinant identity

$$\left|\frac{\partial \boldsymbol{\psi}'(\boldsymbol{q})}{\partial \boldsymbol{q}_a}\right| = \left|\frac{\partial \boldsymbol{\psi}_1}{\partial \boldsymbol{q}_{a1}}\right| \left| -\frac{\partial \boldsymbol{\psi}_2}{\partial \boldsymbol{q}_{a2}} - \frac{\partial \boldsymbol{\psi}_1}{\partial \boldsymbol{q}_{a1}} \left[\frac{\partial \boldsymbol{\psi}_1}{\partial \boldsymbol{q}_{a1}}\right]^{-1} \frac{\partial \boldsymbol{\psi}_2}{\partial \boldsymbol{q}_{a2}} \right| \tag{5.118}$$

such that

$$\left|\frac{\partial \boldsymbol{\psi}'(\boldsymbol{q})}{\partial \boldsymbol{q}_a}\right| \geq \quad 2^{n_u} c_1 c_2 > 0, \text{ for } n_u \text{ even} \tag{5.119}$$

$$\left|\frac{\partial \boldsymbol{\psi}'(\boldsymbol{q})}{\partial \boldsymbol{q}_a}\right| \leq -2^{n_u} c_1 c_2 < 0, \text{ for } n_u \text{ uneven} \tag{5.120}$$

as desired. The constraint equations of (5.78b), for the considered $\boldsymbol{h}$ and $\boldsymbol{v}_u$ in (5.114)–(5.115), evaluate to $\boldsymbol{h}(\boldsymbol{q}) = \boldsymbol{h}(\bar{\boldsymbol{q}})$, and can be interpreted as demanding that the internal actuator pretension of the open (real) and closed loop (virtual) system to be equal. Constraint equations of this form were used in the work [115] for extending the ESP control concept to bidirectional antagonistic variable stiffness actuators [148]. It is worth remarking that the constraint equations introduced above are all but one possible choice. In general, a "smart" choice for the constraint equations requires physical insight insight into the structure of the considered system. For example, an alternative choice for $\boldsymbol{h}$, that aims at simplifying the solving of the transforming equations for the unknown $\bar{\boldsymbol{q}}_a$'s, can be found in [114].

[115]: Mengacci et al. (2021), "Elastic Structure Preserving control for compliant robots driven by agonistic-antagonistic actuators (ESPaa)"

[148]: Petit et al. (2010), "Bidirectional antagonistic variable stiffness actuation: Analysis, design & implementation"

[114]: Meng et al. (2021), "Elastic structure preserving impedance control of bidirectional antagonistic variable stiffness actuation"

5.5 Passivity of the Transformed System

The QFA formulation is the basis for many control developments in this work. This section summarizes the properties of the transformed systems $\bar{\Sigma}$, (5.58) and (5.95), that are key to these developments. For simplicity, we shall focus on the case of monoarticualted systems.

5.5.1 Passive Subsystem Decomposition

Since the transforming equations (5.78) and (5.94) fully preserve the EL structure of Σ, the passive subsystem decomposition property (c.f. Proposition 5.1.1) is preserved as well. The transformed system $\bar{\Sigma}$, (5.95), has the following important property.

Corollary 5.5.1 (QFA: Passive Subsystem Decomposition) *Suppose that the Euler Lagrange system Σ, (5.1), satisfies the conditions of Theorem 5.3.6. Then, it can be represented as the negative feedback interconnection of the two passive subsystems Σ_u and Σ_a, as pointed out in Proposition 5.1.1 and shown in Fig. 5.11. Further, the same feedback decomposition holds for the associated QFA system $\bar{\Sigma}$, (5.95),*

$$\bar{\Sigma}_u : \left(\boldsymbol{\psi} + \bar{Q}_u\right) \mapsto \dot{\bar{\boldsymbol{q}}}_u \tag{5.121}$$

$$\bar{\Sigma}_a : \begin{bmatrix} \bar{Q}_a \\ -\dot{\bar{\boldsymbol{q}}}_u \end{bmatrix} \mapsto \begin{bmatrix} \dot{\bar{\boldsymbol{q}}}_a \\ \boldsymbol{\psi} \end{bmatrix} \tag{5.122}$$

with storage functions $\mathcal{L}_u(\bar{\boldsymbol{q}}_u, \dot{\bar{\boldsymbol{q}}}_u)$ and $\mathcal{L}_a(\bar{\boldsymbol{q}}, \dot{\bar{\boldsymbol{q}}}_a)$, respectively, where

$$\boldsymbol{\psi}(\bar{\boldsymbol{q}}) = \frac{\partial \mathcal{L}_a}{\partial \bar{\boldsymbol{q}}_u}(\bar{\boldsymbol{q}}) \frac{\partial \mathcal{V}_a}{\partial \bar{\boldsymbol{q}}_u}(\bar{\boldsymbol{q}}) \tag{5.123}$$

is the subsystem coupling signal.

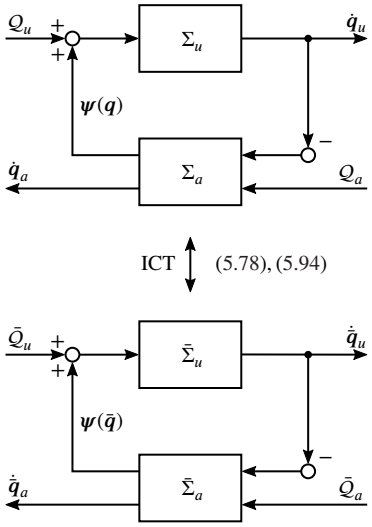

Figure 5.11: Analogous to the original system, the QFA form can be represented as the feedback interconnection of an EL system.

Proof. Using Assumption 5.1.1, let us split the EL equations (5.95) associated with $\bar{\Sigma}$ into the EL equations of the subsystems $\bar{\Sigma}_u$ and $\bar{\Sigma}_a$

$$\bar{\Sigma}_u : \frac{\mathrm{d}}{\mathrm{d}t}\frac{\partial \mathcal{L}_u}{\partial \dot{\bar{q}}_{ui}} - \frac{\partial}{\partial \bar{q}_{ui}}\left(\mathcal{L}_u + \mathcal{L}_a\right) = \mathcal{Q}_{ui}, \qquad i = 1, \dots, n_u, \tag{5.124}$$

$$\bar{\Sigma}_a : \frac{\mathrm{d}}{\mathrm{d}t}\frac{\partial \mathcal{L}_a}{\partial \dot{\bar{q}}_{aj}} - \frac{\partial \mathcal{L}_a}{\partial \bar{q}_{aj}} = \mathcal{Q}_{aj}, \qquad j = 1, \dots, n_a. \tag{5.125}$$

The total time derivative of $\mathcal{L}_u$ is

$$\frac{\mathrm{d}}{\mathrm{d}t}\mathcal{L}_u = \sum_i \left[\frac{\partial \mathcal{L}_u}{\partial \dot{\bar{q}}_{ui}}\ddot{\bar{q}}_{ui} + \frac{\partial \mathcal{L}_u}{\partial \bar{q}_{ui}}\dot{\bar{q}}_{ui} + \frac{\partial \mathcal{L}_u}{\partial t}\right]. \tag{5.126}$$

Making use of (5.124), and the time-independence of $\mathcal{L}_u$, we can rewrite (5.126) as

$$\frac{\mathrm{d}}{\mathrm{d}t}\mathcal{L}_u = \sum_i \left[\left\{\frac{\mathrm{d}}{\mathrm{d}t}\frac{\partial \mathcal{L}_u}{\partial \dot{\bar{q}}_{ui}} - \frac{\partial \mathcal{L}_a}{\partial \bar{q}_{ui}} - \mathcal{Q}_{ui}\right\}\dot{\bar{q}}_{ui} + \frac{\partial \mathcal{L}_u}{\partial \dot{\bar{q}}_{ui}}\ddot{\bar{q}}_{ui}\right] \tag{5.127}$$

It follows that

$$\frac{\mathrm{d}}{\mathrm{d}t}\sum_i \left[\frac{\partial \mathcal{L}_u}{\partial \dot{\bar{q}}_{ui}}\dot{\bar{q}}_{ui} - \mathcal{L}_u\right] = \sum_i \left[\mathcal{Q}_{ui} + \frac{\partial \mathcal{L}_a}{\partial \bar{q}_{ui}}\right]\dot{\bar{q}}_{ui} \tag{5.128}$$

Identifying the LHS above with $\frac{\mathrm{d}}{\mathrm{d}t}\mathcal{H}_u$, where $\mathcal{H}_u \triangleq \sum_i \frac{\partial \mathcal{L}_u}{\partial \dot{\bar{q}}_{ui}}\dot{\bar{q}}_{ui} - \mathcal{L}_u$, we obtain

$$\frac{\mathrm{d}}{\mathrm{d}t}\mathcal{H}_u = \sum_i \left[\mathcal{Q}_{ui} + \frac{\partial \mathcal{L}_a}{\partial \bar{q}_{ui}}\right]\dot{\bar{q}}_{ui}. \tag{5.129}$$

From (5.129) follows that Σ_u defines a passive operator $\mathcal{Q}_u + \boldsymbol{\psi} \mapsto \dot{\bar{\boldsymbol{q}}}_u$. Let us proceed analogous to the procedure above for subsystem $\bar{\Sigma}_a$. Knowing that

$$\frac{\mathrm{d}}{\mathrm{d}t}\mathcal{L}_a = \sum_j \left[\frac{\partial \mathcal{L}_a}{\partial \dot{\bar{q}}_{aj}}\ddot{\bar{q}}_{aj} + \frac{\partial \mathcal{L}_a}{\partial \bar{q}_{aj}}\dot{\bar{q}}_{aj}\right] + \frac{\partial \mathcal{L}_a}{\partial t} + \sum_i \frac{\partial \mathcal{L}_a}{\partial \bar{q}_{ui}}\dot{\bar{q}}_{ui}, \tag{5.130}$$

we can make use of (5.125) and the time-independence of $\mathcal{L}_a$ to rewrite (5.130)

$$\frac{\mathrm{d}}{\mathrm{d}t}\mathcal{L}_a = \sum_j \left[\frac{\partial \mathcal{L}_a}{\partial \dot{\bar{q}}_{ai}}\ddot{\bar{q}}_{ai} + \left\{\frac{\mathrm{d}}{\mathrm{d}t}\frac{\partial \mathcal{L}_a}{\partial \dot{\bar{q}}_{aj}} - \mathcal{Q}_{aj}\right\}\dot{\bar{q}}_{aj}\right] + \sum_i \frac{\partial \mathcal{L}_a}{\partial \bar{q}_{ui}}\dot{\bar{q}}_{ui}. \tag{5.131}$$

Introducing $\mathcal{H}_a \triangleq \sum_j \frac{\partial \mathcal{L}_a}{\partial \dot{\bar{q}}_{aj}}\dot{\bar{q}}_{aj} - \mathcal{L}_a$, it follows that

$$\frac{\mathrm{d}}{\mathrm{d}t}\mathcal{H}_a = \sum_j \mathcal{Q}_{aj}\dot{\bar{q}}_{aj} - \sum_i \frac{\partial \mathcal{L}_a}{\partial \bar{q}_{ui}}\dot{\bar{q}}_{ui}, \tag{5.132}$$

and we conclude that Σ_a defines a passive operator $(\mathcal{Q}_a, \boldsymbol{\psi}) \mapsto (\dot{\bar{\boldsymbol{q}}}_a, -\dot{\bar{\boldsymbol{q}}}_u)$. Considering (5.129) and (5.132), it is clear that Σ can be represented as the negative feedback interconnection of the two passive subsystems $\bar{\Sigma}_u$ and Σ_a. ■

5.5.2 Collocation of Input and Output

Let us consider the Euler Lagrange system Σ in (5.1). Suppose that the position of the underactuated subsystem $\boldsymbol{q}_u$ is the output. Then, it is clear that the

mapping from associated velocities $\dot{\boldsymbol{q}}_u$ to the inputs $\boldsymbol{u}_a$ is not passive; see, e.g., [168]. This form of non-collocation of input and output impedes the direct application of passivity-based control laws in many cases and complicates the control problem. Crucially, the passive mapping between input and output is recovered in the QFA representation. Indeed, the transformed systems defines a passive mapping $\bar{\boldsymbol{u}} \to \dot{\bar{\boldsymbol{q}}}$. This result is summarized in Corollary 6.1.2 in Chapter 6.

[168]: Spong (1987), "Modeling and control of elastic joint robots"

5.6 Further Generalizations

This sections sketches two generalizations of Theorem 5.3.6: 1) a relaxation of the feedback condition on the virtual inputs in Assumption 5.3.1 and 2) a more general coordinate transformation that yields a QFA representation with a Lagrangian different from the original one.

5.6.1 Relaxing the Feedback Condition on the Virtual Input

In order to reduce the complexity of the proofs concerning Theorem 5.3.6 and Theorem 5.4.2, it was assumed that $\bar{\boldsymbol{u}}_u$ contains feedback of only the position and velocity of subsystem Σ_u. It is important to understand that this is no necessary condition, and that we can allow $\bar{\boldsymbol{u}}_u$ to contain position and velocity feedback of the entire system $\bar{\Sigma}$, i.e., $(\bar{\boldsymbol{q}}, \dot{\bar{\boldsymbol{q}}})$, under the conditions sketched below. Revisiting the proofs of Theorem 5.3.6 and Theorems 5.4.2, we see that the argument for the one-to-one correspond is based on the global inverse function theorems in Theorem 5.3.3 and 5.3.4. In summary, we are free to choose $\bar{\boldsymbol{u}}_u$ as long as the transforming equations (5.29a)–(5.29e) and (5.78a)–(5.78e) respectively establish a one-to-one correspond between the $\boldsymbol{q}$'s and $\bar{\boldsymbol{q}}$'s.

5.6.2 A Shaped and Time-Dependent Lagrangian

The transformation procedure introduced in this chapter does not require the QFA representation $\bar{\Sigma}$ to be characterized by the same Lagrangian as the original system Σ. We may think of many practical scenarios where it is desirable to *shape* the Lagrangian of the original system. A popular application of such technique would be the modification of the interaction behavior of an system by shaping its potential energy function. Moreover, for solving motion tracking problems it can be helpful to aim for an explicitly time-dependent potential energy function, as demonstrated in Chapter 7 for ASRs. In this section, we shall focus on the monoarticulation case. Now, let us replace the n_u transforming equations in (5.29b) and (5.29d) with

$$\left[\frac{\partial \bar{\mathcal{V}}_a}{\partial \bar{\boldsymbol{q}}_u}\right]_{\bar{q}} = \left[\frac{\partial \mathcal{V}_a}{\partial \boldsymbol{q}_u}\right]_{q} - \bar{\boldsymbol{u}}_u(\boldsymbol{q}_u, \dot{\boldsymbol{q}}_u, t), \tag{5.133}$$

and the time derivative of (5.133), where the Lagrangian $\bar{\mathcal{L}}$ is such that it be decomposed, similar to the original one, of the form

$$\bar{\mathcal{L}}(\bar{\boldsymbol{q}}, \dot{\bar{\boldsymbol{q}}}, t) \quad = \mathcal{L}_u(\bar{\boldsymbol{q}}_u, \dot{\bar{\boldsymbol{q}}}_u) + \bar{\mathcal{L}}_a(\bar{\boldsymbol{q}}, \dot{\bar{\boldsymbol{q}}}_a, t), \tag{5.134}$$

$$\bar{\mathcal{L}}_a(\bar{\boldsymbol{q}}, \dot{\bar{\boldsymbol{q}}}_a, t) = \bar{\mathcal{T}}_a(\bar{\boldsymbol{q}}_a, \dot{\bar{\boldsymbol{q}}}_a) + \bar{\mathcal{V}}(\bar{\boldsymbol{q}}, t). \tag{5.135}$$

Note that $\mathcal{L}$ and $\bar{\mathcal{L}}$ differ in terms of the sub-Lagrangian associated with the actuated subsystem, while the kinetic energy function connected with the unactuated subsystem is preserved. Suppose that the new potential function shares the properties of the original one, as summarized in Assumption 5.1.2. Then, the updated transforming equations define a phase space transformation, and, we can find an input transformation, similar to the one in Section 5.3, such that the Lagrange's equations (5.1) are transformed as follows:

$$\left(\frac{\mathrm{d}}{\mathrm{d}t}\frac{\partial}{\partial \dot{\boldsymbol{q}}} - \frac{\partial}{\partial \boldsymbol{q}}\right)\mathcal{L}(\boldsymbol{q},\dot{\boldsymbol{q}},t) + \mathcal{Q} \xrightarrow{\text{ICT}} \left(\frac{\mathrm{d}}{\mathrm{d}t}\frac{\partial}{\partial \dot{\bar{\boldsymbol{q}}}} - \frac{\partial}{\partial \bar{\boldsymbol{q}}}\right)\bar{\mathcal{L}}(\bar{\boldsymbol{q}},\dot{\bar{\boldsymbol{q}}}) + \bar{\mathcal{Q}},$$

Remark 5.6.1 The additional freedom in modifying the potential energy allows for greater freedom in designing the motion and/or interaction behavior of Σ. Further, by replacing the kinetic energy function $\mathcal{T}_a$ with $\bar{\mathcal{T}}_a$, we have greater freedom in shaping the transient behavior of Σ. The latter point is exploited for the design of the so-called ESP+ controllers in Section 7. It is important to point out that shaping the system's natural behavior to a significant extent usually comes at the price of increased actuator requirements and reduced closed-loop robustness. The possibility to achieve a time-dependent potential energy function is exploited in Section 7; we demonstrate that the motion tracking problem for ASRs can be solved elegantly by aiming for a transformed transformed (QFA) system that is characterized by an explicitly time-dependent potential function that gives rise to an explicitly time-dependent subsystem coupling force. The time variation of this coupling force can then be chosen to facilitate the nominal motion of the unactuated subsystems $\bar{\Sigma}_u$. Finally, the additional virtual input on $\bar{\Sigma}_u$ can be used to render the desired trajectory attractive.

Main Result

In the following, we consider EL systems of the form (5.1) satisfying Assumption 5.1.1 and Assumption 5.1.2 with $n_u = n_a$.[21] The goal of this section is to consider coordinate transforming equations of the form[22]

$$\bar{\boldsymbol{q}}_u = \boldsymbol{q}_u, \tag{5.136a}$$

$$\left[\frac{\partial \bar{\mathcal{V}}_a}{\partial \bar{\boldsymbol{q}}_u}\right]_{\bar{q}} = \left[\frac{\partial \mathcal{V}_a}{\partial \boldsymbol{q}_u}\right]_{q} - \bar{\boldsymbol{u}}_u(\boldsymbol{q}_u,\dot{\boldsymbol{q}}_u,t), \tag{5.136b}$$

$$\dot{\bar{\boldsymbol{q}}}_u = \dot{\boldsymbol{q}}_u, \tag{5.136c}$$

$$\frac{\mathrm{d}}{\mathrm{d}t}\left[\frac{\partial \bar{\mathcal{V}}_a}{\partial \bar{\boldsymbol{q}}_u}\right]_{\bar{q}} = \frac{\mathrm{d}}{\mathrm{d}t}\left[\frac{\partial \mathcal{V}_a}{\partial \boldsymbol{q}_u}\right]_{q} - \dot{\bar{\boldsymbol{u}}}_u(\boldsymbol{q}_u,\dot{\boldsymbol{q}}_u,t), \tag{5.136d}$$

$$t = t, \tag{5.136e}$$

where the mapping $\bar{\boldsymbol{u}}_u$ is of class $\mathcal{C}^k$, $k \geq 2$, and satisfies Assumption 5.3.1. The Lagrangian $\bar{\mathcal{L}}$, as defined in (5.134)–(5.135), and the associated potential function $\bar{\mathcal{V}}$ are assumed to satisfy Assumption 5.1.1 and Assumption 5.1.2, respectively.

21: Note that the result below is easily modified to consider the multiarticulation case ($n_a > n_u$) using the techniques from Section 5.4.

22: For the derivations below, we shall repeatably make use of the fact that (5.136b) can be written equivalently as $\left[\frac{\partial \mathcal{L}_a}{\partial \boldsymbol{q}_u}\right]_{q} = \left[\frac{\partial \bar{\mathcal{L}}_a}{\partial \bar{\boldsymbol{q}}_u}\right]_{\bar{q}} + \bar{\boldsymbol{u}}_u(\bar{\boldsymbol{q}}_u,\dot{\bar{\boldsymbol{q}}}_u,t)$.

It is convenient to introduce the definitions

$$\bar{\boldsymbol{X}}(\boldsymbol{q}^0) = \frac{\partial^2 \bar{\mathcal{L}}_a}{\partial \boldsymbol{q}_u^2}(\boldsymbol{q}^0); \quad \bar{\boldsymbol{Y}}(\boldsymbol{q}^0) = \frac{\partial^2 \bar{\mathcal{L}}_a}{\partial \bar{\boldsymbol{q}}_a \partial \bar{\boldsymbol{q}}_u}(\boldsymbol{q}^0). \tag{5.137}$$

Next, the following assumptions guarantees a one-to-one correspondence between $\boldsymbol{q}$'s and $\bar{\boldsymbol{q}}$'s.

Assumption 5.6.1 *The Lagrangian $\bar{\mathcal{L}}_a$ is such that the matrices $\left[\bar{\boldsymbol{Y}}\right]_{\bar{q}}$ and $\left[\frac{\partial^2 \bar{\mathcal{L}}_a}{\partial \dot{\bar{\boldsymbol{q}}}_a^2}\right]_{\bar{q}}$ are full rank for any $\bar{\boldsymbol{q}}, \dot{\bar{\boldsymbol{q}}} \in \mathbb{R}^n$ and $t \in \mathbb{R}^+$.*

The proof that (5.136) defines a unique change of coordinates can be established proceeding mutatis mutandis to the proof of Theorem 5.3.6 by invoking the implicit function theorem. This suggest the following result

Theorem 5.6.1 (QFA: Modified Lagrangian) *Suppose that the EL system* (5.1) *satisfies Assumption 5.1.1 and Assumption 5.6.1. Then, there exists an input transformation, see* (5.155) *below, such that the EL equations* (5.1) *transform under the coordinate transformation* (5.136) *to*

$$\frac{\mathrm{d}}{\mathrm{d}t}\left[\frac{\partial \bar{\mathcal{L}}}{\partial \dot{\bar{\boldsymbol{q}}}}\right]_{\bar{q}} - \left[\frac{\partial \bar{\mathcal{L}}}{\partial \bar{\boldsymbol{q}}}\right]_{\bar{q}} = \bar{\mathcal{Q}}. \tag{5.138}$$

Proof. Knowing that

$$\left[\frac{\partial \mathcal{L}_a}{\partial \boldsymbol{q}_u}\right]_q = \left[\frac{\partial \mathcal{V}}{\partial \boldsymbol{q}_u}\right]_q, \tag{5.139}$$

$$\left[\frac{\partial \bar{\mathcal{L}}_a}{\partial \bar{\boldsymbol{q}}_u}\right]_{\bar{q}} = \left[\frac{\partial \bar{\mathcal{V}}}{\partial \bar{\boldsymbol{q}}_u}\right]_{\bar{q}}, \tag{5.140}$$

we can expand (5.136d) to

$$\left[\boldsymbol{X}\right]_q \dot{\boldsymbol{q}}_u + \left[\boldsymbol{Y}\right]_q \dot{\boldsymbol{q}}_a = \left[\bar{\boldsymbol{X}}\right]_{\bar{q}} \dot{\bar{\boldsymbol{q}}}_u + \left[\bar{\boldsymbol{Y}}\right]_{\bar{q}} \dot{\bar{\boldsymbol{q}}}_a + \frac{\partial}{\partial t}\left[\frac{\partial \bar{\mathcal{V}}}{\partial \bar{\boldsymbol{q}}_u}\right]_{\bar{q}}^{\mathrm{T}} + \dot{\bar{\boldsymbol{u}}}_u. \tag{5.141}$$

Let us introduce

$$\bar{\boldsymbol{A}} = \left[\boldsymbol{Y}\right]_q^{-1}\left[\bar{\boldsymbol{Y}}\right]_{\bar{q}}, \tag{5.142}$$

$$\bar{\boldsymbol{\mu}}_1 = \left[\boldsymbol{Y}\right]_q^{-1}\left\{\left(\left[\bar{\boldsymbol{X}}\right]_{\bar{q}} - \left[\boldsymbol{X}\right]_q\right)\dot{\bar{\boldsymbol{q}}}_u + \dot{\bar{\boldsymbol{u}}}_u + \frac{\partial}{\partial t}\left[\frac{\partial \bar{\mathcal{V}}}{\partial \bar{\boldsymbol{q}}_u}\right]^{\mathrm{T}}\right\}, \tag{5.143}$$

$$\bar{\boldsymbol{\mu}}_2 = \left[\frac{\partial^2 \mathcal{L}_a}{\partial \dot{\boldsymbol{q}}_a^2}\right]\left(\dot{\bar{\boldsymbol{A}}}\dot{\bar{\boldsymbol{q}}}_a + \dot{\bar{\boldsymbol{\mu}}}_1\right) + \left[\frac{\partial^2 \mathcal{L}_a}{\partial \boldsymbol{q}_a \partial \dot{\boldsymbol{q}}_a}\right]_q\left(\bar{\boldsymbol{A}}\dot{\bar{\boldsymbol{q}}}_a + \bar{\boldsymbol{\mu}}_1\right), \tag{5.144}$$

then, we can rewrite (5.141) compactly as

$$\dot{\boldsymbol{q}}_a = \bar{\boldsymbol{A}}\dot{\bar{\boldsymbol{q}}}_a + \bar{\boldsymbol{\mu}}_1. \tag{5.145}$$

Next, using (5.136) and (5.145), we can apply a phase space transformation $(\boldsymbol{q}, \dot{\boldsymbol{q}}, t) \to (\bar{\boldsymbol{q}}, \dot{\bar{\boldsymbol{q}}}, t)$ to the EL equations (5.1). Splitting (5.1) into the subdynamics (5.65) and (5.66), and applying the transforming equations (5.136)

to (5.65), we get

$$\frac{\mathrm{d}}{\mathrm{d}t}\left[\frac{\partial \mathcal{L}_u}{\partial \dot{\bar{q}}_u}\right]_{\bar{q}}^{\mathrm{T}} - \left[\frac{\partial \mathcal{L}_u}{\partial \bar{q}_u}\right]_{\bar{q}}^{\mathrm{T}} - \left[\frac{\partial \bar{\mathcal{L}}_a}{\partial \bar{q}_u}\right]_{\bar{q}}^{\mathrm{T}} = \mathcal{Q}_u + \bar{\boldsymbol{u}}_u. \tag{5.146}$$

Further knowing that

$$\frac{\mathrm{d}}{\mathrm{d}t}\left[\frac{\partial \mathcal{L}_a}{\partial \dot{\boldsymbol{q}}_a}\right]_q = \left[\frac{\partial^2 \mathcal{L}_a}{\partial \dot{\boldsymbol{q}}_a^2}\right]_q \ddot{\boldsymbol{q}}_a + \left[\frac{\partial^2 \mathcal{L}_a}{\partial \boldsymbol{q}_a \partial \dot{\boldsymbol{q}}_a}\right]_q \dot{\boldsymbol{q}}_a, \tag{5.147}$$

we can make the substitutions (5.144), (5.145) and (5.147) to obtain

$$\frac{\mathrm{d}}{\mathrm{d}t}\left[\frac{\partial \mathcal{L}_a}{\partial \dot{\boldsymbol{q}}_a}\right]_q = \left[\frac{\partial^2 \mathcal{L}_a}{\partial \dot{\boldsymbol{q}}_a^2}\right]_q \bar{\boldsymbol{A}} \ddot{\bar{\boldsymbol{q}}}_a + \bar{\boldsymbol{\mu}}_2. \tag{5.148}$$

Inserting (5.148) in (5.66) and pre-multiplying both sides with

$$\bar{\boldsymbol{R}} = \left[\frac{\partial^2 \bar{\mathcal{L}}_a}{\partial \dot{\bar{q}}_a^2}\right]_{\bar{q}} \bar{\boldsymbol{A}}^{-1} \left[\frac{\partial^2 \mathcal{L}_a}{\partial \dot{\boldsymbol{q}}_a^2}\right]_q^{-1}, \tag{5.149}$$

gives

$$\left[\frac{\partial^2 \bar{\mathcal{L}}_a}{\partial \dot{\bar{q}}_a^2}\right]_{\bar{q}} \ddot{\bar{\boldsymbol{q}}}_a = \bar{\boldsymbol{R}} \left\{ \left[\frac{\partial \mathcal{L}_a}{\partial \boldsymbol{q}_a}\right]_q^{\mathrm{T}} - \bar{\boldsymbol{\mu}}_2 + \mathcal{Q}_a \right\}. \tag{5.150}$$

Finally, introducing

$$\bar{\mathcal{Q}}'_a = \bar{\boldsymbol{R}} \mathcal{Q}'_a, \tag{5.151}$$
$$\bar{\mathcal{Q}}_a = \bar{\boldsymbol{u}}_a + \bar{\mathcal{Q}}'_a, \tag{5.152}$$
$$\bar{\mathcal{Q}}' = \left(\mathcal{Q}'_u, \bar{\mathcal{Q}}'_a\right), \tag{5.153}$$
$$\bar{\mathcal{Q}} = \bar{\boldsymbol{u}} + \bar{\mathcal{Q}}', \tag{5.154}$$

and applying the input transformation

$$\boldsymbol{u}_a = \bar{\boldsymbol{\mu}}_2 - \left[\frac{\partial \mathcal{L}_a}{\partial \boldsymbol{q}_a}\right]_q + \bar{\boldsymbol{R}}^{-1} \left\{ \left[\frac{\partial \bar{\mathcal{L}}_a}{\partial \bar{q}_a}\right]_{\bar{q}} - \left[\frac{\partial^2 \bar{\mathcal{L}}_a}{\partial \bar{q}_a \partial \dot{\bar{q}}_a}\right]_{\bar{q}} \dot{\bar{\boldsymbol{q}}}_a + \bar{\boldsymbol{u}}_a \right\}, \tag{5.155}$$

to (5.150) yields

$$\left[\frac{\partial^2 \bar{\mathcal{L}}_a}{\partial \dot{\bar{q}}_a^2}\right]_{\bar{q}} \ddot{\bar{\boldsymbol{q}}}_a + \left[\frac{\partial^2 \bar{\mathcal{L}}_a}{\partial \bar{q}_a \partial \dot{\bar{q}}_a}\right]_{\bar{q}} \dot{\bar{\boldsymbol{q}}}_a - \left[\frac{\partial \bar{\mathcal{L}}_a}{\partial \bar{q}_a}\right]_{\bar{q}} = \bar{\mathcal{Q}}_a. \tag{5.156}$$

Noticing that the set of equations (5.146) and (5.156) is equivalent to the desired EL equations (5.138) concludes the proof. ■

Remark 5.6.2 Comparing (5.155) with (5.57) and (5.94), reveals the structural similarity between all input transformations. The former differs from the latter only in the presence of an additional time-derivative term in the definition of $\boldsymbol{\mu}_1$.

5.7 On the Phase Space Transformation

This sections discusses the proposed coordinate transformations from the viewpoint of classical mechanics. First, we shall assume an absence of generalized external forces. In the Lagrangian formulation of mechanics one set of coordinate $\boldsymbol{q}$ is naturally transformed to a new set $\bar{\boldsymbol{q}}$ by transforming equations of the form

$$\bar{q}_i = \bar{q}_i(\boldsymbol{q}, t), \quad i = 1, \dots, n. \tag{5.157}$$

For example, the change from polar to Cartesian coordinates has the general form (5.157). Such transformations are known as *point transformations* since the configuration space is mapped onto itself.

The transformation defined by (5.29a)–(5.29e) is of a different kind; it must be understood as a simultaneous transformation of generalized coordinates and velocities, and, in absence of external generalized forces, has the general form

$$\bar{q}_i = \bar{q}_i(\boldsymbol{q}, \dot{\boldsymbol{q}}, t), \tag{5.158}$$

$$\dot{\bar{q}}_i = \dot{\bar{q}}_i(\boldsymbol{q}, \dot{\boldsymbol{q}}, t), \tag{5.159}$$

with $\dot{\bar{q}}_i = \frac{\mathrm{d}}{\mathrm{d}t}\bar{q}_i$ and $\dot{\bar{q}}_i = dt/\dot{\bar{q}}_i$. Crucially, the new coordinates are defined not only in terms of the original coordinates but also in terms of the original velocities. Equations (5.157) may be interpreted as defining a *point transformation* of *configuration space*. Analogously, we may think of (5.29a)–(5.29e) as defining a *point transformation* of *phase space*. The proposed transformation must not be confused with point transformations of phase space in the Hamiltonian formulation, where the concept of coordinate transformations is naturally extended to include simultaneous transformations of the independent coordinates and momenta $\boldsymbol{q}, \boldsymbol{p}$ to a new set $\bar{\boldsymbol{q}}, \bar{\boldsymbol{p}}$ through *canonical transformations* [52] of the form

A canonical transformation is a change of canonical coordinates $(\boldsymbol{q}, \boldsymbol{p}, t) \to (\bar{\boldsymbol{q}}, \bar{\boldsymbol{p}}, t)$ that preserves the form of Hamilton's equations.
[52]: Goldstein et al. (2001), *Classical Mechanics*

$$\bar{p}_i = \bar{p}_i(\boldsymbol{q}, \boldsymbol{p}, t), \quad i = 1, \dots, n, \tag{5.160}$$

$$\bar{q}_i = \bar{q}_i(\boldsymbol{q}, \boldsymbol{p}, t), \quad i = 1, \dots, n. \tag{5.161}$$

At this point is unclear whether the proposed transformations can be considered as a canonical transformation for $\mathcal{Q}' = \boldsymbol{0}$.

We recall that in the presence of generalized external forces $\mathcal{Q}_u$, these forces enter the velocity transforming equation such that

$$\dot{\bar{q}}_i = \dot{\bar{q}}_i(\boldsymbol{q}, \dot{\boldsymbol{q}}, t, \mathcal{Q}_u). \tag{5.162}$$

Clear, by assuming $\mathcal{Q}_u$ as a function of $\boldsymbol{q}, \dot{\boldsymbol{q}}, t$, we can avoid this issue. The author is not aware of transforming equation of the form (5.162) in the literature of classical mechanics or physics. Consequently, it is unclear how the proposed transformations, which include in addition to a change of generalized coordinates a change of generalized external forces $(\mathcal{Q}', \boldsymbol{u}) \to (\bar{\mathcal{Q}}', \bar{\boldsymbol{u}})$, can be interpreted from the viewpoint of classical mechanics. It is worth remarking that generalized external forces are rarely considered in the classical Lagrangian (Hamiltonian) formulation. Chapter A reports a first attempt to connect the theoretical developments of this chapter with "standard" methods of classical mechanics. For a system satisfying the Spong model, it is shown

that the QFA representation arises naturally by describing the motion of the actuated subsystem from a non-inertial reference frame.

Finally, we are interested whether the new coordinates $\bar{\boldsymbol{q}}$ are well-behaved. For simplicity, let us focus on the monoarticulation case. We recall that the considered phase space transformation is defined by the diffeomorphism $\boldsymbol{\pi}$, and that the connected Jacobian determinant is given by $|D\boldsymbol{\pi}(\boldsymbol{x})| = |D\boldsymbol{\alpha}(\bar{\boldsymbol{x}})|^{-1}|D\boldsymbol{\alpha}(\boldsymbol{x})|$, as pointed out in Lemma 5.3.1. Knowing that $\bar{\boldsymbol{u}} \equiv \boldsymbol{0}$ implies $\boldsymbol{q} \equiv \bar{\boldsymbol{q}}$ (and $\mathcal{Q}' \equiv \bar{\mathcal{Q}}'$), it is evident that the extended phase space volume is preserved in this case, as the Jacobian $D\boldsymbol{\pi}(\boldsymbol{x})$ degenerates to the identity matrix. Note that the absolute value of the Jacobian determinant at $\boldsymbol{x}$ gives us the factor by which the function $\boldsymbol{\pi}$ expands or shrinks the extended phase space volume near $\boldsymbol{x}$ [176].[23] This motivates the following hypothesis: the scaling of extended phase space volume elements in X is relate to the difference in the origin distance of the two subsystems Σ_a and $\bar{\Sigma}_a$, i.e., $\|\boldsymbol{q}_a - \bar{\boldsymbol{q}}_a\|$.

[176]: Sussman et al. (2015), *Structure and Interpretation of Classical Mechanics*

23: This must not be confused with *Liouville's tehorem* which states that phase-space volume is preserved by the phase space flow.

5.7.1 Some Energy Considerations

In Section 5.4, it has been shown that Σ in (5.1) and $\bar{\Sigma}$ in (5.95) are equivalent representations of any EL system satisfying the conditions of Theorem 5.4.2. Both sets of EL equations are characterized by the same $\mathcal{L}$. However, depending on the representation the Lagrangian is either evaluated in terms of the $\boldsymbol{q}$'s or in terms of the $\bar{\boldsymbol{q}}$'s. As indicated above, the proposed coordinate transformations do not qualify as "classical" point [103] or canonical transformation [52], as encountered in the Lagrangian or Hamiltonian formulation of mechanics. Thus, there is no reason to think a priori that the principle of *scalar invariance* [42] holds for the Lagrangian/Hamiltonian. Consequently, we cannot expect the Lagrangians/Hamiltonians connected with the systems Σ and $\bar{\Sigma}$ to evaluate to the same values for $\bar{\boldsymbol{u}}_u \neq \boldsymbol{0}$. Indeed, we see that the difference

[103]: Lanczos (2020), *The Variational Principles of Mechanics*

[52]: Goldstein et al. (2001), *Classical Mechanics*

[42]: Ferrario et al. (2008), "Transformation properties of the Lagrange function"

$$\mathcal{L}(\boldsymbol{q}, \dot{\boldsymbol{q}}) - \mathcal{L}(\bar{\boldsymbol{q}}, \dot{\bar{\boldsymbol{q}}}) = \mathcal{L}_a(\boldsymbol{q}, \dot{\boldsymbol{q}}_a) - \mathcal{L}_a(\bar{\boldsymbol{q}}, \dot{\bar{\boldsymbol{q}}}_a) \neq 0, \tag{5.163}$$

is nonzero in general, where $(\bar{\boldsymbol{q}}, \dot{\bar{\boldsymbol{q}}})$ should obviously be evaluated by means of the transforming equations. Computing the Hamiltonian, using the usual definition of $\mathcal{H}$ as the Legendre transformation of $\mathcal{L}$, i.e.

$$\mathcal{H} = \sum_i \dot{q}_i \frac{\partial \mathcal{L}}{\partial \dot{q}_i} - \mathcal{L} = \mathcal{T} + \mathcal{V}, \tag{5.164}$$

then it corresponds to the total energy[24] of the system, and it is clear that the original system Σ and the transformed system $\bar{\Sigma}$ share the same Hamiltonian. However, we have in general that

24: The exact conditions when this is the case are reported in [181]. Within the scope of this work, we can safely assume that these conditions are met since it is assumed that the relation between the $\boldsymbol{q}$'s and the Cartesian coordinates of the particles constituting the rigid bodies are time-independent.

$$\Delta\mathcal{H} = \mathcal{H}(\boldsymbol{q}, \dot{\boldsymbol{q}}) - \mathcal{H}(\bar{\boldsymbol{q}}, \dot{\bar{\boldsymbol{q}}}) \neq 0 \tag{5.165}$$

with the energy discrepancy $\Delta\mathcal{H}$ satisfying according to Assumption 5.1.1

$$\begin{aligned} \Delta\mathcal{H} =& \mathcal{T}(\boldsymbol{q}, \dot{\boldsymbol{q}}) + \mathcal{V}(\boldsymbol{q}) - \mathcal{T}(\bar{\boldsymbol{q}}, \dot{\bar{\boldsymbol{q}}}) - \mathcal{V}(\bar{\boldsymbol{q}}) \\ =& \mathcal{T}_a(\boldsymbol{q}, \dot{\boldsymbol{q}}_a) - \mathcal{T}_a(\bar{\boldsymbol{q}}, \dot{\bar{\boldsymbol{q}}}_a) + \mathcal{V}(\boldsymbol{q}) - \mathcal{V}(\bar{\boldsymbol{q}}), \end{aligned} \tag{5.166}$$

where $(\bar{\boldsymbol{q}}, \dot{\bar{\boldsymbol{q}}})$ should be evaluated by means of the coordinate transforming equations. Clearly, $\Delta\mathcal{H}$ is identically zero if $\bar{\boldsymbol{u}}_u = \boldsymbol{0}$ and $\dot{\bar{\boldsymbol{u}}}_u = \boldsymbol{0}$. In this case, the coordinate transformation degenerates to $(\boldsymbol{q}, \dot{\boldsymbol{q}}) = (\bar{\boldsymbol{q}}, \dot{\bar{\boldsymbol{q}}})$. Note that this

is not the only case where $\Delta\mathcal{H} = 0$. In fact, it is easy to see that there are infinitely many choices for non-zero $\bar{\boldsymbol{u}}_u$ and $\dot{\bar{\boldsymbol{u}}}_u$ such that $\Delta\mathcal{H} = 0$.

In conclusion, the Lagrangian and Hamiltonian associated with $\bar{\Sigma}$ have no relation to "real" energies. Regarding the QFA formulation, we must treat $\mathcal{L}$ ($\mathcal{H}$) as a mathematical Lagrangian (Hamiltonian) or generator of the motion in the sense of [37]. The concept of the Lagrangian (Hamiltonian) as a generator of motion is commonly found e.g, in the context of quantum mechanics [37]. The work [63] treats extensively a range of applications of the Lagrange formalism that goes beyond the case where the Lagrangian is just the excess of kinetic over potential energy. Given a second order system, Havas discusses the necessary and sufficient conditions for the existence of a Lagrangian such that the corresponding EL equations produce the equations of motions. In future work, it seems worth to investigate whether the theory presented in this chapter can be connected with the theory on higher order Lagrangians [25] for classical mechanics; see generally [61].

[37]: Dekker (1981), "Classical and quantum mechanics of the damped harmonic oscillator"

[63]: Havas (1957), "The range of application of the lagrange formalism — I"

25: Suppose that $\bar{\boldsymbol{u}}_u$ contains feedback of the velocities $\dot{\bar{\boldsymbol{q}}}_u$, then we have the interesting case that, when expressing $\mathcal{L}(\bar{\boldsymbol{q}}, \dot{\bar{\boldsymbol{q}}})$ in terms of the $\boldsymbol{q}$ coordinates through the transforming equations, the resulting Lagrangian $\mathcal{L}$ would be a function of the link accelerations $\ddot{\bar{\boldsymbol{q}}}_u$.

[61]: Harmanni (2016), "Higher Order Lagrangians for classical mechanics and scalar fields"

Note that avoiding the "model-based" computation of $\ddot{\boldsymbol{q}}_u$, as disscussed in Section B.2 in Appendix B, results in a coordinate transformation of the form $\dot{\bar{q}}_i = \dot{\bar{q}}_i(\boldsymbol{q}, \dot{\boldsymbol{q}}, \ddot{\boldsymbol{q}}, t$. Now, expressing $\mathcal{L}(\bar{\boldsymbol{q}}, \dot{\bar{\boldsymbol{q}}})$ in terms of the $\boldsymbol{q}$ coordinates through the transforming equations yields a Lagrangian of the form $\mathcal{L}(\bar{\boldsymbol{q}}, \dot{\bar{\boldsymbol{q}}}, \ddot{\bar{\boldsymbol{q}}}, t)$. For Lagrangians of this form, the necessary conditions for a stationary value of the action are provided by the "extended" Euler-Lagrange equations [49]. It it appears worth investigating whether the concept of quasi-full actuation can be treated in this framework.

5.8 Conclusions

Let us summarize the results obtained in this chapter. Guided by a brief thought experiment and physical considerations, an alternative dynamics representation for a class of underactuated EL systems was derived. Applying the coordinate and input transformations (5.94) and (5.78) to the EL equations (5.1), i.e.,

$$\Sigma: \ \frac{\mathrm{d}}{\mathrm{d}t}\frac{\partial \mathcal{L}}{\partial \dot{\boldsymbol{q}}}(\boldsymbol{q}, \dot{\boldsymbol{q}}) - \frac{\partial \mathcal{L}}{\partial \boldsymbol{q}}(\boldsymbol{q}, \dot{\boldsymbol{q}}) = \mathcal{Q},$$

results in the *equivalent* EL equations

$$\bar{\Sigma}: \ \frac{\mathrm{d}}{\mathrm{d}t}\frac{\partial \mathcal{L}}{\partial \dot{\bar{\boldsymbol{q}}}}(\bar{\boldsymbol{q}}, \dot{\bar{\boldsymbol{q}}}) - \frac{\partial \mathcal{L}}{\partial \bar{\boldsymbol{q}}}(\bar{\boldsymbol{q}}, \dot{\bar{\boldsymbol{q}}}) = \bar{\mathcal{Q}},$$

with $\bar{\mathcal{Q}}$ containing the transformed disturbance forces $\bar{\mathcal{Q}}'$ and the virtual control inputs $\bar{\boldsymbol{u}}$. The structural properties of the transformed system that are most notable for control are:

- The proposed transformation entirely preserves the structure of the EL equations. Moreover, the Lagrangian associated with the new equations is still the original one.[26]
- For each degree of freedom there is a virtual input.
- The QFA system (4.18) defines a passive mapping $\bar{\boldsymbol{u}} \to \dot{\bar{\boldsymbol{q}}}$. Thus, the familiar collocation between input and output variables is "restored", which simplifies the design of control laws. Notably, the interaction port of the unactuated subsystem is preserved, i.e., $\dot{\boldsymbol{q}}_u^{\mathrm{T}}\mathcal{Q}'_u = \dot{\bar{\boldsymbol{q}}}_u^{\mathrm{T}}\bar{\mathcal{Q}}'_u$.
- System $\bar{\Sigma}$ can be represented as the negative feedback interconnection of two passive subsystems.
- Considering that $\bar{\boldsymbol{u}} \equiv \boldsymbol{0}$ implies that $\boldsymbol{q} \equiv \bar{\boldsymbol{q}}$ and $\boldsymbol{u} \equiv \boldsymbol{0}$, it is clear that the proposed transformation itself does alter the plant dynamics. Only at the moment of making a choice for the virtual control inputs, we actually modify the system dynamics.[27]

26: Of course, this is not necessarily the case for the generalizations reported in Section 4.5.

27: This central property is lost for the generalizations discussed in 4.5.

Since the virtual inputs on the unactuated subsystem $\bar{\Sigma}_u$ cannot be chosen fully independently, the transformed system is being referred to as quasi-fully

actuated. Of course, at heart the system remains underactuated as no transformation can change this fundamental physical property. On the first sight, this property is concealed in the QFA formulation. However, the underactuation manifests in the smoothness condition on the virtual input $\bar{\boldsymbol{u}}_u$ and the fact that we can not realize arbitrary feedback laws. In particular, the smoothness constraint expresses the fact that we cannot command an instantaneous acceleration of arbitrary direction and amplitude—which is the defining property of underactuated systems as pointed out in Section 2.6. Yet, as long as the control input satisfies the imposed restrictions, we can treat the transformed system as fully actuated and, theoretically, we may command any sufficiently smooth configuration space trajectory.[28]

28: More precisely, the desired trajectory must be four times continuously differentiable.

Is the New Representation Worth the Effort?

The movements associated with the proposed virtual motor coordinates elude direct observation, the forces associated with the virtual inputs elude direct measurements. Their introduction, however, enables rewriting the EL dynamics in an easier tractable form. Easier tractable in the sense, that from the control point of view it is fundamentally easier to cope with a fully actuated than an underactuated system. In this regard, we should think of the virtual coordinates and inputs simply as a tool simplifying the control design for the considered class of underactuated systems.

A key aspect of the transforming equations is that the original and transformed systems are characterized by the same Lagrangian (Hamiltonian) function. This aspect facilitates intuitive and physically motivated design approaches. Since Σ and $\bar{\Sigma}$ share the same Lagrangian function, both systems also share exactly the same physical properties. The "picture" that we have of Σ's dynamic behavior can be immediately transferred to $\bar{\Sigma}$, we only have to imagine some additional input forces at hand. This property invites control approaches that shape the natural dynamics to a minimal extend. Using the virtual inputs, we can "add" to $\bar{\Sigma}$ whatever is "missing" in Σ. Following nature's *principle of least action*, we may refer to this design philosophy as: *Do as little as possible*. A control design for articulated soft robots following this line of thought is presented in Chapter 7.[29]

29: Loosely speaking, in its most basic iteration the control objectives are: 1) achieve pervasive damping, 2) remove gravity's influence on the links and 3) stabilize the desired equilibrium configuration.

Energy-Based Control of Underactuated Euler-Lagrange Systems

6

There is a fact, or if you wish, a law, governing natural phenomena that are known to date. There is no known exception to this law–it is exact so far we know. The law is called conservation of energy; it states that there is a certain quantity, which we call energy that does not change in manifold changes which nature undergoes. That is a most abstract idea, because it is a mathematical principle; it says that there is a numerical quantity, which does not change when something happens. It is not a description of a mechanism, or anything concrete; it is just a strange fact that we can calculate some number, and when we finish watching nature go through her tricks and calculate the number again, it is the same.

—Richard P. Feynman

The safe and controlled interaction of a robotic system with its environment plays an ever-increasing role. At its most fundamental level, this physical interaction is dictated by the exchange of energy. Putting energy and the exchange of energy at the center of the thought process facilitates the design of control strategies that govern the interaction of a robot with its environment. More importantly, it leads to more insightful and physically intuitive concepts than purely signal-driven design concepts [166, 174]. Some popular representatives of this paradigm/school of thought are: (a) energy shaping and damping injection [178], (b) Euler-Lagrange controllers [133], (c) impedance control [68–70], (d) interconnection and damping assignment passivity-based control (IDA-PBC) [132, 136]. The concepts (b) and (d) can be summarized under the general idea of *control by interconnection*; see [135] for an in-depth treatment. As pointed out by Hogan [68–70], classic position and force control are inadequate for physical interaction tasks since they are insufficient to control the work exchanged between a manipulator and its environment. In contrast, the energy-based techniques (a-d) are excellent candidates when interaction with the physical world is at the center. They enable modulating and controlling the dynamic behavior of the robot while simultaneously commanding a desired position.

Energy-based control concepts that exhibit a physically intuitive closed loop enable the operator to anticipate the interaction behavior of the robot with the environment (i.e., another physical system). Loosely speaking, the interaction between two physical systems that are visualizable in terms of real physical elements is fundamentally easier to comprehend and anticipate than the interaction between a set of (partial) differential equations and the environment. In addition, having a physical intuitive closed-loop behavior provides—to some extent—a feeling for the extent of system shaping imposed by a particular control design. This enables the operator to provide an ad-hoc estimate of the maximal achievable gains. This fact can hardly be overestimated when it comes to the commissioning stage since physical intuition is of immense value for tuning a controller. Without a doubt, extensive hands-on experience regarding robot control design will foster appreciation of these aspects. In the words of Hogan [68]: "no controller can make the manipulator appear to the environment as anything other than a physical system". From

[166]: Slotine (1989), "Putting Physics Back in Control"
[174]: Stramigioli (2015), "Energy-Aware Robotics"
[178]: Takegaki et al. (1981), "A new feedback method for dynamic control of manipulators"
[133]: Ortega (1998), *Passivity-Based Control of Euler-Lagrange Systems: Mechanical, Electrical, and Electromechanical Applications*
[68]: Hogan (1985), "Impedance control: An approach to manipulation: Part I—Theory"
[69]: Hogan (1985), "Impedance control: An approach to manipulation: Part II—Implementation"
[70]: Hogan (1985), "Impedance control: An approach to manipulation: Part III—Applications"
[132]: Ortega et al. (2002), "Stabilization of a class of underactuated mechanical systems via interconnection and damping assignment"
[136]: Ortega et al. (2002), "Interconnection and damping assignment passivity-based control of port-controlled Hamiltonian systems"
[135]: Ortega et al. (2008), "Control by interconnection and standard passivity-based control of port-Hamiltonian systems"

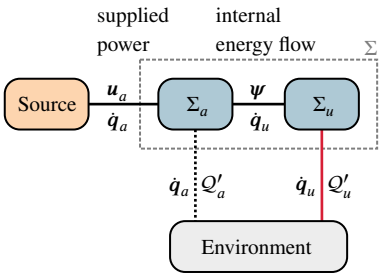

Figure 6.1: Energy flows. Note that the physical power port of the unactuated subsystem is preserved, i.e., $\dot{\boldsymbol{q}}_u^{\mathrm{T}}\mathcal{Q}'_u = \dot{\bar{\boldsymbol{q}}}_u^{\mathrm{T}}\mathcal{Q}'_u$.

this point of view, it seems obvious to make the manipulator appear to the environment as a physical system that we can actually "understand" in its interaction behavior. The combination of these positive aspects makes energy-based methods an appealing choice for interaction control. To be clear; when dealing with a robot moving freely in space or a robot that operates in a predictable environment (e.g., manipulators in automotive manufacturing that are caged away from humans), the above arguments lose much of their appeal, and standard position or force control techniques are acceptable options in many situations. The limitations of these classic control methodologies primarily arise when a robot operates in an unpredictable, and thus to some degree non-modellable, environment. This chapter considers the class of EL systems specified in Chapter 5, and it is assumed that the non-actuated subsystem Σ_u is the primary agent that interacts with the environment. Controlling the work exchanged between Σ_u and its environment while simultaneously regulating it to a desired position, will be our primary concern in the following. See Fig. 6.1 for an overview of the energy flows governing the interaction behavior.

With the advent of articulated soft robots [54, 74, 153, 190], the situation changed fundamentally when it comes to interaction control. In these systems, one deliberately incorporates highly compliant elements into the drive train with a stiffness that is low enough such that these elements can be exploited as energy storage [17]. By nature, these systems are underactuated, which is a structural obstacle that impedes the direct adoption of classic rigid robot impedance control. The control concepts developed in this chapter are not limited in their scope of application to ASRs, but applicable to all EL systems satisfying considered assumptions. However, since this work is primarily concerned with the application of the presented concepts to ASRs, several control aspects are discussed in the "language" of soft robots. The sets of unactuated generalized coordinates $\boldsymbol{q}_u$ and $\bar{\boldsymbol{q}}_u$ will be synonymously referred to as link coordinates, and the sets of actuated generalized coordinates $\boldsymbol{q}_a$ and $\bar{\boldsymbol{q}}_a$ will be referred to as (virtual) motor coordinates, respectively. Correspondingly, the subsystems Σ_u and $\bar{\Sigma}_u$ encode the rigid body dynamics of an ASR, and the subsystems Σ_a and $\bar{\Sigma}_a$ encode the (virtual) motor dynamics.

In principle, energy-based techniques such as (a) and (b) can be directly applied to underactuated systems. However, for such systems, we face clear limitations regarding the achievable closed-loop potential energy. In particular, the achievable closed-loop stiffness and damping behavior are severely limited, which impairs the ability to shape the interaction behavior [133]. This chapter introduces extensions to the two methodologies (a) and (b) that relax these limitations. The results are summarized in Proposition 6.2.1 and Proposition 6.3.1. Furthermore, an extension of impedance control (c) to a class of underactuated EL systems is presented in Proposition 6.4.1. The most significant limitation with the presented extensions is the necessity of the virtual input to be twice differentiable with respect to time, which translates into a smoothness constraint on the achievable link-side potential energy and damping functions. However, as argued in Section 5.8, this limitation arises naturally from the physical limitations of an underactuated robot and is not inherent to the presented concepts. A unique feature of the presented extensions of (a) and (c) is that they enable the closed-loop dynamics to be rendered fully damped by specifying a desired damping behavior directly in terms of the non-actuated output coordinates. This is in strong contrast to state of the art approaches [2, 6, 7, 133, 141, 178, 183]. Injecting damping on the non-actuated outputs, however, is critical for highly compliant systems due to

[54]: Grebenstein et al. (2011), "The DLR hand arm system"
[74]: Hutter et al. (2016), "Anymal-a highly mobile and dynamic quadrupedal robot"
[153]: Pratt et al. (1995), "Series elastic actuators"
[190]: Vanderborght et al. (2013), "Variable impedance actuators: A review"

[17]: Braun et al. (2011), "Exploiting variable stiffness in explosive movement tasks"

[2]: Ailon et al. (1993), "An observer-based set-point controller for robot manipulators with flexible joints"
[6]: Albu-Schäffer et al. (2007), "A Unified Passivity-based control framework for position, torque and impedance control of flexible joint robots"
[7]: Albu-Schäffer et al. (2012), "Constructive energy shaping control for a class of Euler-Lagrange Systems"
[133]: Ortega (1998), *Passivity-Based Control of Euler-Lagrange Systems: Mechanical, Electrical, and Electromechanical Applications*
[141]: Ott et al. (2004), "A passivity based cartesian impedance controller for flexible joint robots-part I: Torque feedback and gravity compensation"
[178]: Takegaki et al. (1981), "A new feedback method for dynamic control of manipulators"
[183]: Tomei (1991), "A simple PD controller for robots with elastic joints"

the intrinsic oscillatory nature of their dynamics [89, 102] as demonstrated in https://www.youtube.com/watch?v=PATvv47QfQs. Note that in certain scenarios indirect damping of the links can be sufficient if the energy dissipation propagates efficiently through the closed-system to the unactuated subsystem $\bar{\Sigma}_u$, see for example the developments Section 9.

The main contribution of this chapter is the development of a series of globally asymptotically stable feedback passivity-based regulation controllers for a class of underactuated EL systems (see Chapter 5.1). Central to all developments is the link-side power port $(\bar{\boldsymbol{u}}_u, \dot{\bar{\boldsymbol{q}}}_u)$ that has been established through the QFA formulation in Chapter 5, and the passivity properties of the quasi-fully actuated EL system (as will be pointed out in Corollary 6.1.2).

The energy based control developments of this chapter are guided by the three design principles summarized in Fig. 6.2. The main results of this chapter are listed below:

- Corollary 6.1.2 reveals a crucial passivity property of the QFA system.
- Proposition 6.2.1 reports an extension of the energy shaping and damping injection concept.
- Proposition 6.3.1 reports an extension of Euler Lagrange controllers.
- Proposition 6.4.1 reports an extension of the impedance control concept.

[89]: Keppler et al. (2016), "A passivity-based approach for trajectory tracking and link-side damping of compliantly actuated robots"
[102]: Lakatos et al. (2014), "Nonlinear oscillations for cyclic movements in human and robotic arms"

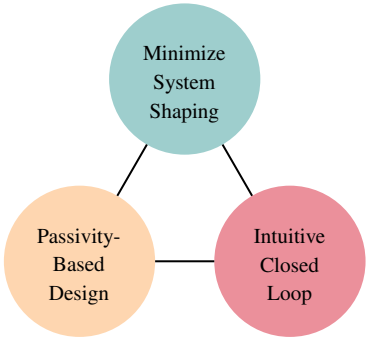

Figure 6.2: Guiding design principles.

Remark 6.0.1 The works [4, 7], which solve the regulation problem for a similar class of EL systems as introduced in Chapter 5 by energy shaping and damping injection, are most closely related to impedance controller presented in this chapter. Compared to [7], the presented approach: 1) requires significantly weaker assumptions on potential function connected with the Lagrange equations; in particular, the existence of the constants α_1, α_2 and α_4 associated with the inequalities (7) and (8) in [7] are not required, 2) the damping injection and potential energy shaping is not limited by relying on only collocated feedback (motor positions and velocities); instead, direct link-side potential shaping and damping injection is possible, 3) explicitly time-dependent forces can be added to the link dynamics; enables, e.g., the implementation of (asymptotically stable) task-space motion tracking, as demonstrated in [91]. 4) using Theorem 5.4.2 allows the consideration of multiarticulated systems.

[4]: Albu-Schäffer et al. (2005), "Constructive energy shaping based impedance control for a class of underactuated Euler-Lagrange systems"
[7]: Albu-Schäffer et al. (2012), "Constructive energy shaping control for a class of Euler-Lagrange Systems"

[91]: Keppler et al. (2021), "Analyzing the performance limits of articulated soft robots based on the ESPi framework: Applications to damping and impedance control"

6.1 Energy Exchange with the Physical World

This section reports several important properties of EL systems that are fundamental for the control developments in this chapter. The energy a system exchanges with its environment will play a pivotal role and can be analyzed by taking the time derivative of its total energy. Using the notion of passivity, see Definition C.3.2 in Appendix C, we can establish the following key statement concerning the energy balance of EL systems.

Proposition 6.1.1 (Passivity of EL Systems) *Let $\mathcal{L}(\boldsymbol{q}, \dot{\boldsymbol{q}})$ be a Lagrangian of the EL system* (5.1)*, and assume that the Hamiltonian $\mathcal{H} = \sum_i \dot{q}_i \frac{\partial \mathcal{L}}{\partial \dot{q}_i} - \mathcal{L}$ is bounded from below. Then* (5.1) *is a passive system with respect to the*

supply rate, $\mathcal{Q}^T\dot{\boldsymbol{q}}$, and $\mathcal{H}$ as storage function. The energy balance

$$\underbrace{\mathcal{H}\big(\boldsymbol{q}(t_1),\dot{\boldsymbol{q}}(t_1)\big)}_{\text{stored energy}} = \underbrace{\mathcal{H}\big(\boldsymbol{q}(t_0),\dot{\boldsymbol{q}}(t_0)\big)}_{\text{initial energy}} + \underbrace{\int_{t_0}^{t_1}\sum_i \mathcal{Q}_i\dot{q}_i dt}_{\text{supplied energy}}, \tag{6.1}$$

holds for any $t_1 \geq t_0$ and any bounded $\mathcal{Q}$. The statement can be strengthened to output strict passivity (OSP) if the system is fully damped. Suppose the generalized forces can be decomposed as $\mathcal{Q} = \mathcal{Q}^r - \mathcal{Q}^d$, with the dissipation forces, $\mathcal{Q}^d$, satisfying $\sum_i \mathcal{Q}^d\dot{q}_i \geq \sum_i \alpha_i\dot{q}_i^2$, $\alpha_i > 0$, then the energy balance

$$\underbrace{\mathcal{H}\big(\boldsymbol{q}(t_1),\dot{\boldsymbol{q}}(t_1)\big)}_{\text{stored energy}} \leq \underbrace{\mathcal{H}\big(\boldsymbol{q}(t_0),\dot{\boldsymbol{q}}(t_0)\big)}_{\text{initial energy}} + \underbrace{\int_{t_0}^{t_1}\sum_i \left(\mathcal{Q}_i^r\dot{q}_i - \alpha_i\dot{q}_i^2\right)\dot{q}_i dt}_{\text{supplied/dissipated energy}}, \tag{6.2}$$

holds for any $t_1 \geq t_0$ and any bounded $\mathcal{Q}$.

Proof. The total time derivative of $\mathcal{L}$ is

$$\frac{d\mathcal{L}}{dt} = \sum_i \left[\frac{\partial\mathcal{L}}{\partial q_i}\frac{\partial q_i}{\partial t} + \frac{\partial\mathcal{L}}{\partial\dot{q}_i}\frac{d\dot{q}_i}{dt}\right] + \frac{\partial\mathcal{L}}{\partial t}. \tag{6.3}$$

Making use of the EL equations (5.1)

$$\frac{\partial\mathcal{L}}{\partial q_i} = \frac{\mathrm{d}}{\mathrm{d}t}\frac{\partial\mathcal{L}}{\partial\dot{q}_i} - \mathcal{Q}_i,$$

and the time-independence of $\mathcal{L}$, we can rewrite (6.3) as

$$\frac{d\mathcal{L}}{dt} = \sum_i \left[\frac{\mathrm{d}}{\mathrm{d}t}\frac{\partial\mathcal{L}}{\partial\dot{q}_i} - \mathcal{Q}_i\right]\dot{q}_i + \sum_j \frac{\partial\mathcal{L}}{\partial\dot{q}_i}\frac{d\dot{q}_i}{dt} \tag{6.4}$$

or

$$\frac{d\mathcal{L}}{dt} = \sum_i \frac{\mathrm{d}}{\mathrm{d}t}\left[\dot{q}_i\frac{\partial\mathcal{L}}{\partial\dot{q}_i}\right] - \sum_i \mathcal{Q}_i\dot{q}_i. \tag{6.5}$$

It follows that

$$\frac{\mathrm{d}}{\mathrm{d}t}\sum_i \left[\dot{q}_i\frac{\partial\mathcal{L}}{\partial\dot{q}_i} - \mathcal{L}\right] = \sum_i \mathcal{Q}_i\dot{q}_i. \tag{6.6}$$

Identifying the LHS of (6.6) with $\frac{\mathrm{d}}{\mathrm{d}t}\mathcal{H}$, and integrating (6.6) from t_0 to t_1 establishes the energy balance

$$\mathcal{H}\big(\boldsymbol{q}(t_1),\dot{\boldsymbol{q}}(t_1)\big) - \mathcal{H}\big(\boldsymbol{q}(t_0),\dot{\boldsymbol{q}}(t_0)\big) = \int_{t_0}^{t_1}\sum_i \mathcal{Q}_i\dot{q}_i dt. \tag{6.7}$$

which completes the first part of the proof. If the EL system (5.1) is fully damped, then the supply rate on the RHS of (6.7) can be expanded to

$$\int_{t_0}^{t_1}\sum_i \left(\mathcal{Q}_i^r\dot{q}_i - \mathcal{Q}_i^d\dot{q}_i\right)dt \leq \int_{t_0}^{t_1}\sum_i \left(\mathcal{Q}_i^r\dot{q}_i - \alpha_i\dot{q}_i^2\right)dt, \tag{6.8}$$

and output strict passivity follows immediately after making the substitutions (6.7) and (6.8). ∎

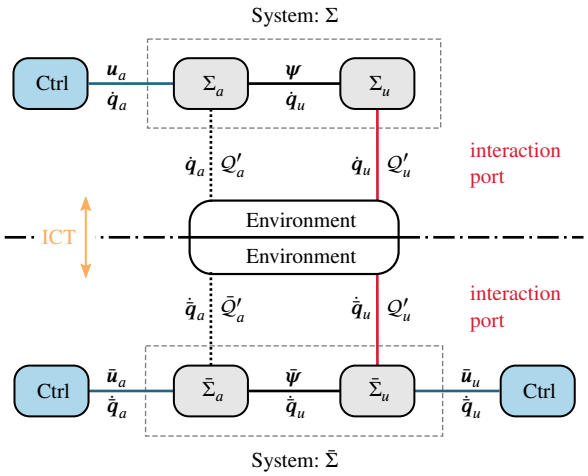

Figure 6.3: Comparing the internal and external power flows of the EL system Σ and its associated QFA form Σ̄.

6.1.1 Systems with a Block Diagonal Inertia Matrix

Let us apply the result above to the class of EL systems specified in Section 5.1. Then, we obtain for system Σ, (5.1), the energy balance:

$$\mathcal{H}\big(\boldsymbol{q}(T),\dot{\boldsymbol{q}}(T)\big) = \mathcal{H}\big(\boldsymbol{q}(0),\dot{\boldsymbol{q}}(0)\big) + \underbrace{\int_0^T \left(\dot{\boldsymbol{q}}_u^{\mathrm{T}}\boldsymbol{Q}'_u + \dot{\boldsymbol{q}}_a^{\mathrm{T}}\boldsymbol{Q}'_a\right) dt}_{\text{natural exchange}} + \underbrace{\int_0^T \dot{\boldsymbol{q}}_a^{\mathrm{T}}\boldsymbol{u}_a dt}_{\text{supplied}}. \tag{6.9}$$

Proceeding mutatis mutandis for the virtual system Σ̄, we get the following fundamental property of the QFA formulation.

Corollary 6.1.2 (Passivity of QFA EL Systems) *Let $\mathcal{L}(\bar{\boldsymbol{q}},\dot{\bar{\boldsymbol{q}}})$ be the Lagrangian of the QFA system Σ̄, (5.95), associated with the EL system Σ. Suppose that the Hamiltonian $\big[\mathcal{H}\big]_{\bar{q}} = \sum_i \dot{\bar{q}}_i \left[\frac{\partial \mathcal{L}}{\partial \dot{\bar{q}}_i}\right]_{\bar{q}} - \big[\mathcal{L}\big]_{\bar{q}}$ is bounded from below, then Σ̄ is passive with respect to the supply rate, $\bar{Q}^T\dot{\bar{q}}$, and $\mathcal{H}$ as storage function. The energy balance (as visualized in Fig. 6.3)*

$$\mathcal{H}\big(\bar{\boldsymbol{q}}(T),\dot{\bar{\boldsymbol{q}}}(T)\big) = \mathcal{H}\big(\bar{\boldsymbol{q}}(0),\dot{\bar{\boldsymbol{q}}}(0)\big) + \underbrace{\int_0^T \left(\dot{\bar{\boldsymbol{q}}}_u^{T}\boldsymbol{Q}'_u + \dot{\bar{\boldsymbol{q}}}_a^{T}\bar{\boldsymbol{Q}}'_a\right) dt}_{\textit{natural exchange}} + \underbrace{\int_0^T \left(\dot{\bar{\boldsymbol{q}}}_u^{T}\bar{\boldsymbol{u}}_u + \dot{\bar{\boldsymbol{q}}}_a^{T}\bar{\boldsymbol{u}}_a\right) dt}_{\textit{supplied}}. \tag{6.10}$$

holds for any $t_1 \geq t_0$ and any bounded $\bar{Q}$. The statement can be strengthened to output strict passivity (OSP) if the system is fully damped, c.f. Proposition 6.1.1.

This result follows directly from Proposition 6.1.1. In each of the energy balances (6.9) and (6.10), we can identify two types of power flows. The first two terms on the RHS of (6.9) and (6.10) represent the respective system's natural exchange of energy with the environment. The remaining terms on the RHS represent the artificial supply rate imposed by a particular controller. All power flows are visualized in Fig. 6.3. Even though the Hamiltonian $\mathcal{H}$, in general, does not evaluate to the same values for Σ and Σ̄ as pointed out in Section 5.5, we can conclude that $\mathcal{H}$ qualifies as a storage function for either

system. Corollary 6.1.2 asserts that $\bar{\Sigma}$ is passive according to Definition C.3.2 in Appendix C since it is dissipative with respect to the supply rate $\bar{Q}^{\mathrm{T}}\dot{\bar{q}}$. A critical aspect of transforming equations (ICT) is the fact that the power port $\dot{q}_u^{\mathrm{T}}Q_u$ is preserved since $q_u \equiv \bar{q}_u$ and $Q_u \equiv \bar{Q}_u$. Comparing (6.9) and (6.10) reveals that this power port appears in both energy balances. For ASRs, this port uniquely determines the interaction behavior of the robot with its environment and, thus, it will be at the center of our attention in Chapter 7. In the following, it will be assumed that the non-actuated subsystem Σ_u is the primary agent interacting with the environment. Thus, when it comes to the work exchanged with the environment, we shall focus on the port $(\bar{q}_u, Q'_u)$.

6.2 Energy Shaping and Damping Injection Control: An Extension

This section introduces an extension of the energy shaping and damping injection concept from Takegaki and Arimoto [178] to the class of underactuated EL systems specified in Section 5.1. The two-stage character is preserved. First, the potential energy is modified such that the system has a global and unique minimum at the desired equilibrium configuration. Second, damping is injected to ensure asymptotic convergence. Starting with the transformed system $\bar{\Sigma}_u$, we can make use of the virtual input vector $\bar{u}$ to adopt the idea of Takegaki and Arimoto. The resulting controller is summarized in the proposition below.

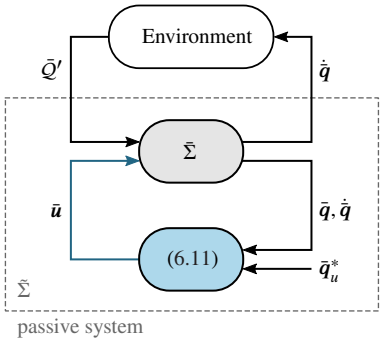

Figure 6.4: Feedback system resulting from the energy shaping and damping injection extension procedure.

Proposition 6.2.1 (Energy Shaping and Damping Injection) *Suppose the EL system* Σ, (5.1) *satisfies the conditions of Theorem 5.4.2. Let the virtual control inputs,* (5.94)*, be given by:*

$$\bar{u} = -\frac{\partial \mathcal{V}_c}{\partial \bar{q}}(\bar{q}) - \mathcal{K}_v \dot{\bar{q}}, \tag{6.11}$$

and let $\mathcal{V}_c$ *be a potential function of class* C^k*,* $k \geq 3$*. Further, let us assume the following:*

(i) $\mathcal{V}_c(\bar{q}) \triangleq \mathcal{V}_{cu}(\bar{q}_u) + \mathcal{V}_{ca}(\bar{q}_a)$*,*
(ii) $\mathcal{V}^*(\bar{q}) \triangleq \mathcal{V} + \mathcal{V}_c$ *has a unique global minimum at* $\bar{q} = \bar{q}^*$ *(constant) and is radially unbounded with respect to the error* $\tilde{q} = \bar{q} - \bar{q}^*$*,*
(iii) $\mathcal{K}_v \triangleq \mathrm{diag}(K_{vu}, K_{va})$ *is symmetric, positive definite with* $K_{vu} \in \mathbb{R}^{n_u \times n_u}$ *and* $K_{va} \in \mathbb{R}^{n_a \times n_a}$*.*

Then, in absence of external forces, i.e. $Q' = 0$*, the equilibrium* $(\bar{q}, \dot{\bar{q}}) = (\bar{q}^*, 0)$ *of the QFA system* $\bar{\Sigma}$ *is globally asymptotically stable. The corresponding globally asymptotic equilibrium of* Σ *is given according to Lemma 5.4.1.*

Proof. Conditions (i) and (ii) guarantee that condition (i) of Theorem 5.4.2 is satisfied. Suppose that condition (ii) of Theorem 5.4.2 is satisfied as well. The proof concludes with an argument that this assumption was indeed justified. In this case, Theorem 5.4.2 asserts that we can transform the EL system Σ into its QFA form $\bar{\Sigma}$. Applying the control input (6.11) to $\bar{\Sigma}$, (5.95), we get

the following equations of motion:

$$\Sigma^*: \frac{\mathrm{d}}{\mathrm{d}t}\frac{\partial \mathcal{T}}{\partial \dot{\bar{\boldsymbol{q}}}} - \frac{\partial \mathcal{T}}{\partial \bar{\boldsymbol{q}}} = \bar{\boldsymbol{u}} + \mathcal{Q}' - \frac{\partial \mathcal{V}}{\partial \bar{\boldsymbol{q}}} = -\frac{\partial \mathcal{V}^*}{\partial \bar{\boldsymbol{q}}} - \mathcal{K}_v \dot{\bar{\boldsymbol{q}}} + \mathcal{Q}', \tag{6.12}$$

with the potential function turning out to be the desired one, $\mathcal{V}^*$. Introducing the Lagrangian $\mathcal{L}^* = \mathcal{T} - \mathcal{V}^*$ and the generalized force $\mathcal{Q}^* \triangleq \mathcal{Q}' - \mathcal{K}_v \dot{\bar{\boldsymbol{q}}}$, we can rewrite (6.12) as

$$\Sigma^*: \frac{\mathrm{d}}{\mathrm{d}t}\frac{\partial \mathcal{L}^*}{\partial \dot{\bar{\boldsymbol{q}}}} - \frac{\partial \mathcal{L}^*}{\partial \bar{\boldsymbol{q}}} = \mathcal{Q}^*. \tag{6.13}$$

When studying the stability of an EL system with a Lagrangian that does not explicitly depend on time, it is convenient to assume that at the equilibrium position is located at the origin. This can be assumed without loss of generality since it is sufficient to place the coordinate origin at this position. Suppose that $\bar{\boldsymbol{q}}^* \neq \boldsymbol{0}$, then we can transform to another set of generalized coordinates $\tilde{\boldsymbol{q}}$ via the transforming equations

$$\bar{\boldsymbol{q}} = \bar{\boldsymbol{q}}(\tilde{\boldsymbol{q}}) = \tilde{\boldsymbol{q}} + \bar{\boldsymbol{q}}^*, \tag{6.14}$$

such that, according to Corollary 2.5.6 EL equations (6.13), become

$$\frac{\mathrm{d}}{\mathrm{d}t}\frac{\partial \mathcal{L}^*}{\partial \dot{\tilde{\boldsymbol{q}}}} - \frac{\partial \mathcal{L}^*}{\partial \tilde{\boldsymbol{q}}} = \mathcal{Q}^*, \tag{6.15}$$

where the Lagrangian is expressed as a function of $(\tilde{\boldsymbol{q}}, \dot{\tilde{\boldsymbol{q}}})$ through the transforming equations, (6.14), and its time derivatives, i.e., $\mathcal{L}^* = \mathcal{L}^*\big(\bar{\boldsymbol{q}}(\tilde{\boldsymbol{q}}), \dot{\bar{\boldsymbol{q}}}(\dot{\tilde{\boldsymbol{q}}})\big)$. Introducing a new Lagrangian function

$$\tilde{\mathcal{L}}\big(\tilde{\boldsymbol{q}}, \dot{\tilde{\boldsymbol{q}}}\big) \triangleq \mathcal{L}^*\big(\bar{\boldsymbol{q}}(\tilde{\boldsymbol{q}}), \dot{\bar{\boldsymbol{q}}}(\dot{\tilde{\boldsymbol{q}}})\big), \tag{6.16}$$

constituted by the kinetic energy $\tilde{\mathcal{T}} \triangleq \mathcal{T}\big(\bar{\boldsymbol{q}}(\tilde{\boldsymbol{q}}), \dot{\bar{\boldsymbol{q}}}(\dot{\tilde{\boldsymbol{q}}})\big)$ and potential energy $\tilde{\mathcal{V}} \triangleq \mathcal{V}^*\big(\bar{\boldsymbol{q}}(\tilde{\boldsymbol{q}})\big)$, and making the substitution (6.15) and (6.16), we get

$$\tilde{\Sigma}: \frac{\mathrm{d}}{\mathrm{d}t}\frac{\partial \tilde{\mathcal{L}}}{\partial \dot{\tilde{\boldsymbol{q}}}} - \frac{\partial \tilde{\mathcal{L}}}{\partial \tilde{\boldsymbol{q}}} = \mathcal{Q}^*. \tag{6.17}$$

As desired, the transformed system has an unique equilibrium at the origin, which follows directly from condition (ii) and (6.14). Further, $\tilde{\mathcal{V}}$ is radially unbounded w.r.t. $\tilde{\boldsymbol{q}}$. Since there is a one-to-one correspondence between the solutions of (6.13) and (6.17), we can study the behavior of (6.17) instead. Proceeding analogous to the proof of Proposition 6.1.1, it is clear that

$$\frac{d\tilde{\mathcal{L}}}{dt} = \ldots = \sum_i \frac{\mathrm{d}}{\mathrm{d}t}\left[\dot{\tilde{q}}_i \frac{\partial \tilde{\mathcal{L}}}{\partial \dot{\tilde{q}}_i}\right] + \sum_i \mathcal{Q}_i^* \dot{\tilde{q}}_i, \tag{6.18}$$

or after rearranging terms

$$\frac{\mathrm{d}}{\mathrm{d}t}\sum_i \left[\dot{q}_i \frac{\partial \tilde{\mathcal{L}}}{\partial \dot{q}_i} - \tilde{\mathcal{L}}\right] = \sum_i \mathcal{Q}_i^* \dot{\tilde{q}}_i. \tag{6.19}$$

Introducing the Hamiltonian $\tilde{\mathcal{H}} = \sum_i \dot{\tilde{q}}_i \frac{\partial \tilde{\mathcal{L}}}{\partial \dot{\tilde{q}}_i} - \tilde{\mathcal{L}}$, we can rewrite (6.19) as

$$\dot{\tilde{\mathcal{H}}} = -\dot{\tilde{\boldsymbol{q}}}^{\mathrm{T}} \mathcal{K}_v \dot{\tilde{\boldsymbol{q}}} + \dot{\tilde{\boldsymbol{q}}}^{\mathrm{T}} \mathcal{Q}'. \tag{6.20}$$

We are now in position to establish GAS of the origin $(\bar{\boldsymbol{q}}, \dot{\bar{\boldsymbol{q}}}) = \boldsymbol{0}$ of $\tilde{\Sigma}$,

for $\mathcal{Q}' = \mathbf{0}$, by invoking Krasovskii's Theorem (C.1.3). Since $\tilde{\mathcal{H}}$ is continuously differentiable, radially unbounded w.r.t $(\tilde{\boldsymbol{q}}, \dot{\tilde{\boldsymbol{q}}})$ and positive definite it qualifies as Lyapunov function V. The radial unboundedness of $\tilde{\mathcal{H}}$ follows from condition (ii) and the fact that $\tilde{\mathcal{T}}(\tilde{\boldsymbol{q}}, \dot{\tilde{\boldsymbol{q}}}) \to \infty$ as $||\dot{\boldsymbol{q}}|| \to \infty$. To find $S = \left\{(\tilde{\boldsymbol{q}}, \dot{\tilde{\boldsymbol{q}}}) \in \mathbb{R}^{2n} | \dot{V} = 0\right\}$, note that $\dot{V} = 0 \;\Rightarrow\; \dot{\tilde{\boldsymbol{q}}} = \mathbf{0}$, and thus $S = \left\{(\tilde{\boldsymbol{q}}, \dot{\tilde{\boldsymbol{q}}}) \in \mathbb{R}^{2n} | \dot{\tilde{\boldsymbol{q}}} = \mathbf{0}\right\}$. Let $(\tilde{\boldsymbol{q}}(t), \dot{\tilde{\boldsymbol{q}}}(t) = \mathbf{0})$ be a solution that belongs to S, then

$$\dot{\tilde{\boldsymbol{q}}} \;\Rightarrow\; \ddot{\tilde{\boldsymbol{q}}} = \mathbf{0} \overset{(2.57)}{\Rightarrow} \frac{\mathrm{d}}{\mathrm{d}t}\frac{\partial \tilde{\mathcal{T}}}{\partial \dot{\tilde{\boldsymbol{q}}}} - \frac{\partial \tilde{\mathcal{T}}}{\partial \tilde{\boldsymbol{q}}} = \mathbf{0} \overset{(6.17)}{\Rightarrow} \frac{\mathrm{d}}{\mathrm{d}t}\frac{\partial \tilde{\mathcal{V}}}{\partial \dot{\tilde{\boldsymbol{q}}}} - \frac{\partial \tilde{\mathcal{V}}}{\partial \tilde{\boldsymbol{q}}} = \mathbf{0} \;\Rightarrow\; \frac{\partial \tilde{\mathcal{V}}}{\partial \tilde{\boldsymbol{q}}} = \mathbf{0}. \tag{6.21}$$

The last implication is due to Assumption 5.1.1. In conclusion, the only solution $\left(\bar{\boldsymbol{q}}(t), \dot{\bar{\boldsymbol{q}}}(t) = \mathbf{0}\right)$ that can stay identically in S is defined by $\frac{\partial \tilde{\mathcal{V}}}{\partial \tilde{\boldsymbol{q}}} = \mathbf{0}$ which has the unique solution $\tilde{\boldsymbol{q}} = \mathbf{0}$. Therefore, the origin of (6.17) is GAS, which again, implies GAS of the equilibrium, $\bar{\boldsymbol{q}} = \bar{\boldsymbol{q}}^*$, of (6.13). To complete the proof, we have yet to show that condition (ii) of Theorem 5.4.2 is indeed satisfied during the transient. GAS implies that for any bounded initial state the solution $\left(\bar{\boldsymbol{q}}(t), \dot{\bar{\boldsymbol{q}}}(t)\right)$ remains bounded. Since $\bar{\boldsymbol{u}}_u$, (6.11), is a C^{k-1}, $k \geq 3$, function of $\left(\bar{\boldsymbol{q}}(t), \dot{\bar{\boldsymbol{q}}}(t)\right)$ by assumption, it follows that $\dot{\bar{\boldsymbol{u}}}_u, \ddot{\bar{\boldsymbol{u}}}_u$ are continuous functions. Considering that $\dot{\bar{\boldsymbol{u}}}_u, \ddot{\bar{\boldsymbol{u}}}_u$ can be written as functions of the bounded solution $\left(\bar{\boldsymbol{q}}(t), \dot{\bar{\boldsymbol{q}}}(t)\right)$, as pointed out in Section B.2 in Appendix B, we can conclude that $\dot{\bar{\boldsymbol{u}}}_u, \ddot{\bar{\boldsymbol{u}}}_u$ remain bounded. This guarantees that condition (ii) of Theorem 5.4.2 is satisfied. It remains to be shown that the solution $\left(\boldsymbol{q}_a(t), \dot{\boldsymbol{q}}_a(t)\right)$ of subsystem Σ_a remains bounded. Considering that the solutions of Σ and $\bar{\Sigma}$ are in a one-to-one correspondence through the transforming equations, and further considering the continuity of the transforming equations implies boundedness of the Σ_a solution. ■

Despite the conditions stated in Proposition 6.2.1 regarding the closed-loop potential function $\mathcal{V}^*$, we have great freedom in shaping the transient and interaction behaviors of $\bar{\Sigma}_u$ and $\bar{\Sigma}_a$. Let us decompose the potential function:

$$\mathcal{V}(\bar{\boldsymbol{q}}) = \mathcal{V}_1(\bar{\boldsymbol{q}}) + \mathcal{V}_2(\bar{\boldsymbol{q}}_u) + \mathcal{V}_3(\bar{\boldsymbol{q}}_a). \tag{6.22}$$

Proposition 6.2.1 allows arbitrary shaping or canceling of the potential fields $\mathcal{V}_2$ and $\mathcal{V}_3$, more importantly, we can add arbitrary smooth potential fields that exclusively interact with either $\bar{\Sigma}_u$ or $\bar{\Sigma}_a$. Only when it comes to shaping the potential function $\mathcal{V}_1$, we have to make sure that the final potential function, $\mathcal{V}^*$, complies with the conditions of Proposition 6.2.1. From the robustness point of view, it is favorable to superimpose physical with artificial (controller) potential fields rather than replacing physical potential fields with a desired one, since the latter operation can be expected to be susceptible to model uncertainties. Furthermore, it is widely believed that dominating instead of canceling nonlinear terms enhances robustness of the closed-loop system vis-avis parametric uncertainties [133]. In this regard, the following potential function candidate, which is adapted from [178], is particularly interesting

$$\mathcal{V}^*(\bar{\boldsymbol{q}}) = \mathcal{V}(\bar{\boldsymbol{q}}) - \mathcal{V}(\bar{\boldsymbol{q}}^*) - \left[\frac{\partial \mathcal{V}}{\partial \bar{\boldsymbol{q}}}\right](\bar{\boldsymbol{q}} - \bar{\boldsymbol{q}}^*) + \tfrac{1}{2}\tilde{\boldsymbol{q}}^{\mathrm{T}}\mathcal{K}\tilde{\boldsymbol{q}}, \tag{6.23}$$

where a $\mathcal{K}$ is a suitable block-diagonal, symmetric and positive definite matrix. This potential function is realized by linear position feedback plus constant

[133]: Ortega (1998), *Passivity-Based Control of Euler-Lagrange Systems: Mechanical, Electrical, and Electromechanical Applications*

[178]: Takegaki et al. (1981), "A new feedback method for dynamic control of manipulators"

bias, that is

$$\bar{\boldsymbol{u}} = \frac{\partial \mathcal{V}}{\partial \bar{\boldsymbol{q}}}(\bar{\boldsymbol{q}}^*) - \mathcal{K}(\bar{\boldsymbol{q}} - \bar{\boldsymbol{q}}^*). \tag{6.24}$$

Although $\bar{\boldsymbol{u}}$ takes on a simple form, the actual control input $\boldsymbol{u}$, (5.94), is in general a highly nonlinear state feedback control law. Note that the last term in (6.23) can easily be replaced by a more general potential function that is radially unbounded w.r.t $\bar{\boldsymbol{q}} - \bar{\boldsymbol{q}}^*$, sufficiently smooth and satisfies condition (i).

6.2.1 Possible Generalizations

Condition (i) of Proposition 6.2.1 imposes limitations on the desired potential function $\mathcal{V}^*$. Choosing a desired potential $\mathcal{V}^* = \mathcal{V} - \mathcal{V}_1$ would violate condition (i) above. From the physical point of view this seems intuitive. After all, the interaction between the subsystems $\bar{\Sigma}_u$ and $\bar{\Sigma}_a$ is solely dictated by the force arising from the potential field $\mathcal{V}_1$. If it was possible to completely cancel this potential field, it would be possible to fully decouple the two subsystems. Obviously, this is physically impossible. It is, however, possible to modify the potential field $\mathcal{V}_1$. Below, we sketch two ways for achieving this goal that are in harmony with the framework presented in Chapter 5.

First, we can use Theorem 5.6.1 to consider transforming equations that yield a QFA system that is characterized by a new Lagrangian $\tilde{\mathcal{L}}$

$$\tilde{\mathcal{L}} = \mathcal{T}(\bar{\boldsymbol{q}}, \dot{\bar{\boldsymbol{q}}}) - \tilde{\mathcal{V}}(\bar{\boldsymbol{q}}). \tag{6.25}$$

By choosing a potential function $\tilde{\mathcal{V}}$ different from the intrinsic one, $\mathcal{V}$, allows us to impose a new interaction behavior between $\bar{\Sigma}_a$ and $\bar{\Sigma}_u$, and consequently with respect to the environment. Such alternative approach would shift the potential energy shaping part to the stage at which the coordinate transforming equations are formulated. In essence, the first n_u equations of (5.36), i.e.,

$$\frac{\partial \mathcal{V}}{\partial \boldsymbol{q}_u} = \frac{\partial \mathcal{V}}{\partial \bar{\boldsymbol{q}}} + \bar{\boldsymbol{u}}_u, \tag{6.26}$$

are replaced with

$$\frac{\partial \mathcal{V}}{\partial \boldsymbol{q}_u} = \frac{\partial \tilde{\mathcal{V}}}{\partial \bar{\boldsymbol{q}}_u} + \bar{\boldsymbol{u}}_u. \tag{6.27}$$

In other words, the potential energy shaping is directly incorporated into the ICT equations as discussed in Section 5.6.

Second, we could extend Proposition 6.2.1 to allow for increased freedom in choosing $\mathcal{V}_c$. In particular, Assumption (i) of Proposition 6.2.1 can be replaced with the more general assumption that

$$\frac{\partial^2 \mathcal{V}}{\partial \bar{\boldsymbol{q}}_a \partial \bar{\boldsymbol{q}}_u}(\bar{\boldsymbol{q}}) + \frac{\partial^2 \mathcal{V}_c}{\partial \bar{\boldsymbol{q}}_a \partial \bar{\boldsymbol{q}}_u}(\bar{\boldsymbol{q}}),$$

is non-singular at any position of the configuration space, which guarantees that the resulting coordinate transforming equations have (locally) a unique solution. A global statement requires that the matrix above satisfies conditions as stated in Assumption 5.1.2. Notice that such extension Proposition 6.2.1,

would result in $\bar{\boldsymbol{u}}_u$ of (6.11) containing feedback of $\bar{\boldsymbol{q}}_a$ which is not within the scope of the central theorems presented in Chapter 5.

6.2.2 Discussion

[178]: Takegaki et al. (1981), "A new feedback method for dynamic control of manipulators"

The energy shaping and damping injection concept [178] was introduced for fully actuated systems. Proposition 6.2.1 can be considered as an extension of this concept to the class of underactuated EL systems specified in Section 5.1. Compared to the original method, the new scheme introduces Condition (i) and (iii) in Proposition 6.2.1, which imposes limitations on the achievable closed-loop potential energy function and damping behavior. It is worth investigation whether this limitation connected with the presented framework, or whether this limitation arise from the physical properties of the considered class of EL system. Clearly, the potential energy function of such systems cannot be arbitrarily modified through control. For example, it is physically impossible to cancel the subsystem coupling potential since this would imply a vanishing of the subsystem coupling force between Σ_u and Σ_a. This becomes immediately clear from (5.29b); substituting $\bar{\boldsymbol{u}}_u = \frac{\partial \bar{\mathcal{L}}_a}{\partial \bar{\boldsymbol{q}}_u}(\bar{\boldsymbol{q}})$ gives $\frac{\partial \mathcal{L}_a}{\partial \boldsymbol{q}_u}(\boldsymbol{q}) = \boldsymbol{0}$. Conditions (i) and (iii) of Proposition 6.2.1, however, are stronger than necessary and possible relaxations are discussed above. In summary, Proposition 6.2.1, allows specifying a closed-loop potential energy and a damping behavior directly in terms of the non-collocated link-velocities (outputs). The resulting feedback system is shown in Fig. 6.4.

6.3 Euler-Lagrange Controllers: An Extension

The previous section revealed that damping injection on subsystem Σ_u relies on the jerk $\boldsymbol{q}_u^{(3)}$. Even though these signals can be computed via the system model (as pointed out in Section B.2 of Appendix B), it is often not a desirable procedure since it is prone to model uncertainties. Further, if Σ_u is subject to harsh impacts direct damping injection on $\bar{\Sigma}_u$ can easily cause input saturation. Chapter B.2 reveals the underlying physical reasons and discusses the general issues connected with the reliance on jerk signals in a feedback loop.

This section presents an energy-based approach that obviates the need of jerk signals. The availability of the link-side interconnection port $(\dot{\boldsymbol{q}}_u, \bar{\boldsymbol{u}}_u)$ on the QFA form introduced in Chapter 5, motivates the adoption of Euler Lagrange controllers to the QFA system $\bar{\Sigma}$. Motivated by the availability of the link-side interconnection port $(\dot{\boldsymbol{q}}_u, \bar{\boldsymbol{u}}_1)$, an extension of Euler-Lagrange controllers is developed in the following. The development of EL controllers was motivated by the following two observations. First, passivity is invariant under feedback interconnection (as pointed out in Proposition C.3.1 in Appendix C.3). Second, choosing PBC among the class of EL systems, one can define a feedback interconnection that preserves the EL structure—and, importantly—the new Lagrangian and storage functions are obtained by simply adding up the corresponding functions of the plant and the controller (as pointed out in Proposition 2.5.5). The following proposition can be considered as an extension of Proposition 3.6 from [133].

[133]: Ortega (1998), *Passivity-Based Control of Euler-Lagrange Systems: Mechanical, Electrical, and Electromechanical Applications*

Proposition 6.3.1 (Euler-Lagrange Controller) *Consider an EL system* (5.1)*, in absence of external forces, i.e.* $\mathcal{Q}' = \mathbf{0}$*, that satisfies the conditions of 5.4.2. Let the virtual control input be an EL controller:*

$$\bar{\boldsymbol{u}} = -\frac{\partial \mathcal{V}_c}{\partial \bar{\boldsymbol{q}}}(\boldsymbol{q}_c, \bar{\boldsymbol{q}}), \tag{6.28}$$

with the Lagrangian $\mathcal{L}_c(\bar{\boldsymbol{q}}, \boldsymbol{q}_c, \dot{\boldsymbol{q}}_c)$ *and the controller dynamics:*

$$\Sigma_c : \boldsymbol{M}_c(\boldsymbol{q}_c)\ddot{\boldsymbol{q}}_c + \boldsymbol{C}_c(\boldsymbol{q}_c, \dot{\boldsymbol{q}}_c)\dot{\boldsymbol{q}}_c + \frac{\partial \mathcal{V}_c(\boldsymbol{q}_c, \bar{\boldsymbol{q}})}{\partial \boldsymbol{q}_c} + \frac{\partial \mathcal{F}_c(\dot{\boldsymbol{q}}_c)}{\partial \dot{\boldsymbol{q}}_c} = \mathbf{0}, \tag{6.29}$$

with the controller coordinates $\boldsymbol{q}_c \in \mathbb{R}^{n_c}$*. Further, assume that the potential energy function* $\mathcal{V}_c(\boldsymbol{q}_c, \bar{\boldsymbol{q}})$ *and dissipation function* $\mathcal{F}_c(\dot{\boldsymbol{q}}_c)$ *are at least twice continuously differentiable. Let* $\boldsymbol{q}_u^*$ *be the constant desired value of* Σ_u*. Then, the closed-loop system is GAS at an equilibrium* $\hat{\boldsymbol{q}} = (\bar{\boldsymbol{q}}^*, \boldsymbol{q}_c^*)$*, such that* $\boldsymbol{q}_u^* = [\boldsymbol{I}_{n_u}, \mathbf{0}_{n_a+n_c}]\hat{\boldsymbol{q}}$ *with the partitioning* $\bar{\boldsymbol{q}}^* \triangleq \left[\boldsymbol{q}_u^*, \boldsymbol{q}_v^*\right]$*, and the EL controller* (6.28) *solves the state feedback global stabilization problem above, if*

(i) (Energy shaping) $\tilde{\mathcal{V}} \triangleq \mathcal{V} + \mathcal{V}_c$*, with* $\mathcal{V}_c(\boldsymbol{q}_c, \bar{\boldsymbol{q}}) \triangleq \mathcal{V}_{c1}(\boldsymbol{q}_c, \bar{\boldsymbol{q}}_u) + \mathcal{V}_{c2}(\boldsymbol{q}_c, \bar{\boldsymbol{q}}_a)$*, is proper and has a global and unique minimum at* $\bar{\boldsymbol{q}} = \bar{\boldsymbol{q}}^*$

(ii) (Damping injection) $\mathcal{F}_c(\dot{\boldsymbol{q}}_c)$ *satisfies:*

$$\dot{\boldsymbol{q}}_c^T \frac{\partial \mathcal{F}_c}{\partial \dot{\boldsymbol{q}}_c}(\dot{\boldsymbol{q}}_c) \geq \alpha ||\dot{\boldsymbol{q}}_c||^2,$$

for some $\alpha > 0$*.*

(iii) (Dissipation propagation) For each trajectory such that $\boldsymbol{q}_c \equiv$ *const. and* $\frac{\partial \mathcal{V}_c}{\partial \boldsymbol{q}_c}(\boldsymbol{q}_c, \bar{\boldsymbol{q}}) = \mathbf{0}$*, we have that* $\bar{\boldsymbol{q}} \equiv$ *const..*

Proof. The proof is based on Proposition 2.5.3 and Proposition 2.5.5. Condition (i) above guarantees that condition (i) of Theorem 5.4.2 is satisfied. Suppose that condition (iii) of Theorem 5.4.2 is satisfied. The proof concludes with a statement that this assumption was indeed justified. Then, Theorem 5.4.2 asserts that we can transform the EL system Σ into its QFA form $\bar{\Sigma}$, (5.95). Input (6.28) interconnects the two EL systems $\bar{\Sigma}$ and Σ_c such that the resulting closed-loop system is again an EL system (as pointed out in Proposition 2.5.5) with the Lagrangian

$$\tilde{\mathcal{L}}(\bar{\boldsymbol{q}}, \boldsymbol{q}_c, \dot{\bar{\boldsymbol{q}}}, \dot{\boldsymbol{q}}_c) = \mathcal{L}(\bar{\boldsymbol{q}}, \dot{\bar{\boldsymbol{q}}}) + \mathcal{L}_c(\bar{\boldsymbol{q}}, \boldsymbol{q}_c, \dot{\boldsymbol{q}}_c), \tag{6.30}$$

and with the kinetic and potential energy functions

$$\tilde{\mathcal{T}} \triangleq \mathcal{T}(\bar{\boldsymbol{q}}, \dot{\bar{\boldsymbol{q}}}) + \mathcal{T}_c(\boldsymbol{q}_c, \dot{\boldsymbol{q}}_c);\ \tilde{\mathcal{V}} \triangleq \mathcal{V}(\bar{\boldsymbol{q}}) + \mathcal{V}_c(\bar{\boldsymbol{q}}, \boldsymbol{q}_c). \tag{6.31}$$

The generalized inertia matrix associated with $\tilde{\mathcal{L}}$ is block diagonal (c.f. Proposition 5.1.1) and satisfies condition (i) of Proposition 2.5.3. Observing that condition (iii) above implies that $\dot{\bar{\boldsymbol{q}}} \neq \mathbf{0}$ and $\frac{\partial \mathcal{V}}{\partial \boldsymbol{q}_c}(\boldsymbol{q}, \bar{\boldsymbol{q}}) = \mathbf{0}$ cannot occur simultaneously, we can conclude that condition (iii) of Proposition 2.5.3 is satisfied. The boundedness of $\bar{\boldsymbol{u}}_u$ up to its second time derivative and boundedness of the solutions $\left(\boldsymbol{q}_a(t), \dot{\boldsymbol{q}}_a(t)\right)$ of Σ_a can be shown analog to the proof of Proposition 6.2.1, which completes the proof. ■

6.3.1 Passivity Analysis

In the following, it will be shown that the closed-loop system obtained from the control law (6.28) can be represented by three passive subsystems in feedback interconnection. The closed-loop dynamics are given by the EL equations associated with the Lagrangian $\tilde{\mathcal{L}}$, (6.30). Exploiting the fact that $\tilde{\mathcal{L}}$ is composed of two sub-Lagrangians, we can split the associated Hamiltonian as follows

$$\tilde{\mathcal{H}} = \sum_{i}^{n} \dot{q}_i \frac{\partial \tilde{\mathcal{L}}}{\partial \dot{q}_i} + \sum_{j}^{n_c} \dot{q}_{cj} \frac{\partial \tilde{\mathcal{L}}}{\partial \dot{q}_{cj}} - \tilde{\mathcal{L}} = \underbrace{\sum_{i}^{n} \dot{q}_i \frac{\partial \mathcal{L}}{\partial \dot{q}_i} - \mathcal{L}}_{\mathcal{H}} + \underbrace{\sum_{j}^{n_c} \dot{q}_{cj} \frac{\partial \mathcal{L}_c}{\partial \dot{q}_{cj}} - \mathcal{L}_c}_{\mathcal{H}_c}, \tag{6.32}$$

where $\mathcal{H}$ and $\mathcal{H}_c$ are the Hamiltonians of the EL systems Σ and Σ_c, respectively. The corresponding EL equations of these subsystems are

$$\bar{\Sigma}: \ \frac{\mathrm{d}}{\mathrm{d}t}\frac{\partial \mathcal{T}}{\partial \dot{\bar{q}}_i} - \frac{\partial \mathcal{T}}{\partial \bar{q}_i} = -\frac{\partial \mathcal{V}}{\partial \bar{q}} + \bar{\mathcal{Q}}, \quad i = 1, \dots, n \tag{6.33}$$

$$\Sigma_c: \ \frac{\mathrm{d}}{\mathrm{d}t}\frac{\partial \mathcal{L}_c}{\partial \dot{q}_{cj}} - \frac{\partial \mathcal{L}_c}{\partial q_{cj}} = \mathcal{Q}_{cj}, \quad j = 1, \dots, n_c \tag{6.34}$$

with $\mathcal{Q}_{cj} = -\frac{\partial \mathcal{Q}_{cj}}{\partial \dot{q}_{cj}}$. Using (6.28) and (6.31), we can rewrite (6.33)–(6.34)

$$\bar{\Sigma}: \ \frac{\mathrm{d}}{\mathrm{d}t}\frac{\partial \tilde{\mathcal{L}}}{\partial \dot{\bar{q}}_i} - \frac{\partial \tilde{\mathcal{L}}}{\partial \bar{q}_i} = -\frac{\partial \tilde{\mathcal{L}}}{\partial \bar{q}} + \bar{\mathcal{Q}}, \tag{6.35}$$

$$\Sigma_c: \ \frac{\mathrm{d}}{\mathrm{d}t}\frac{\partial \tilde{\mathcal{L}}}{\partial \dot{q}_{cj}} - \frac{\partial \tilde{\mathcal{L}}}{\partial q_{cj}} = -\frac{\partial \tilde{\mathcal{L}}}{\partial q_{cj}} + \bar{\mathcal{Q}}. \tag{6.36}$$

From Corollary (5.5.1), we know that

$$\frac{\mathrm{d}}{\mathrm{d}t}\mathcal{H}(\bar{\boldsymbol{q}}, \dot{\bar{\boldsymbol{q}}}) = (\bar{u}_i + \bar{\mathcal{Q}}_i')\dot{\bar{q}}_i. \tag{6.37}$$

For the controller subsystem Σ_c, we have that

$$\frac{\mathrm{d}}{\mathrm{d}t}\mathcal{L}_c = \sum_j \left[\frac{\partial \mathcal{L}_c}{\partial \dot{q}_{cj}}\ddot{q}_{cj} + \frac{\partial \mathcal{L}_c}{\partial q_{cj}}\dot{q}_{cj} + \frac{\partial \mathcal{L}_c}{\partial t}\right] + \sum_i \frac{\partial \mathcal{L}_c}{\partial \bar{q}_i}\dot{\bar{q}}_i \tag{6.38}$$

Making use of the EL equations (6.34) and the time-invariance of $\mathcal{L}_c$, we can rewrite (6.38) as

$$\frac{\mathrm{d}}{\mathrm{d}t}\mathcal{L}_c = \sum_j \left\{\left[\frac{\mathrm{d}}{\mathrm{d}t}\frac{\partial \mathcal{L}_c}{\partial \dot{q}_{cj}} - \mathcal{Q}_{cj}\right]\dot{q}_{cj} + \frac{\partial \mathcal{L}_c}{\partial \dot{q}_{cj}}\ddot{q}_{cj}\right\} + \sum_i \frac{\partial \mathcal{L}_c}{\partial \bar{q}_i}\dot{\bar{q}}_i, \tag{6.39}$$

or

$$\frac{\mathrm{d}}{\mathrm{d}t}\mathcal{L}_c = \sum_j \frac{\mathrm{d}}{\mathrm{d}t}\left[\frac{\partial \mathcal{L}_c}{\partial \dot{q}_{cj}}\dot{q}_{cj}\right] - \sum_j \mathcal{Q}_{cj}\dot{q}_{cj} + \sum_i \frac{\partial \mathcal{L}_c}{\partial \bar{q}_i}\dot{\bar{q}}_i. \tag{6.40}$$

It follows that

$$\frac{\mathrm{d}}{\mathrm{d}t}\left[\sum_j \frac{\partial \mathcal{L}_c}{\partial \dot{q}_{cj}} - \mathcal{L}_c\right] = \sum_j \mathcal{Q}_{cj}\dot{q}_{cj} - \frac{\partial \mathcal{L}_c}{\partial \bar{q}_i}\dot{\bar{q}}_i. \tag{6.41}$$

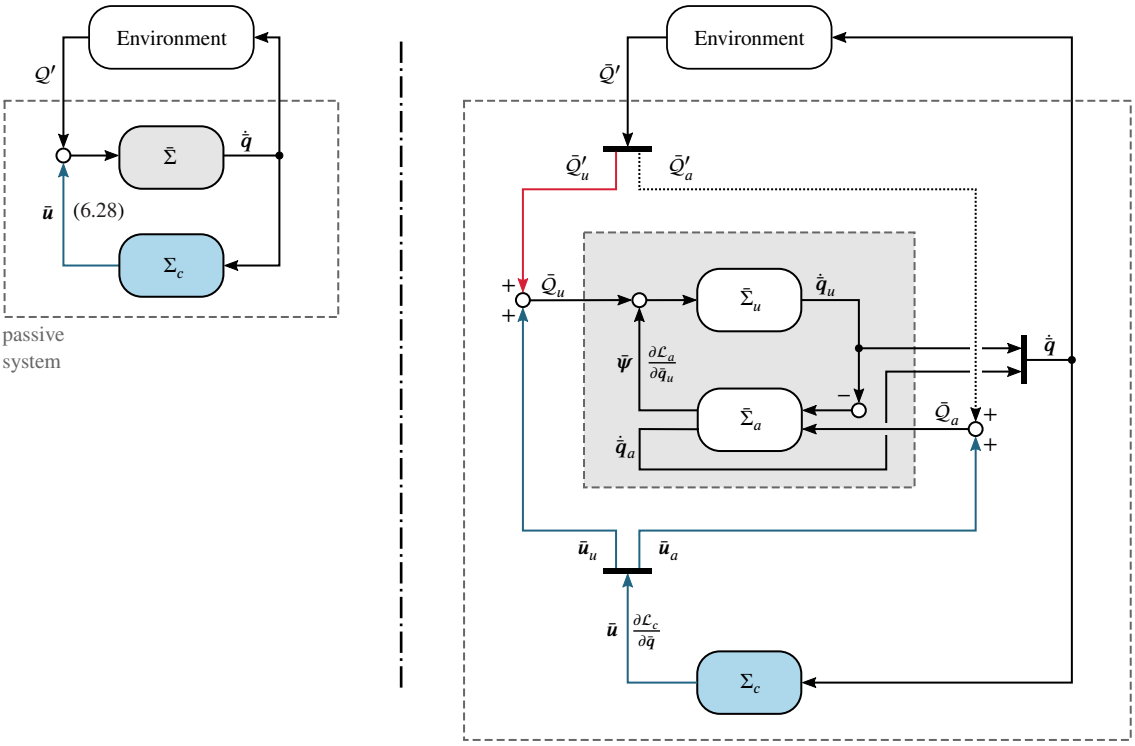

Figure 6.5: (**Left**): Feedback interconnection of two passive EL systems, $\bar{\Sigma}$ and Σ_c. (**Right**): Subsystem $\bar{\Sigma}$ can be represented as the negative feedback interconnection of the two passive EL subsystems, $\bar{\Sigma}_u$ and $\bar{\Sigma}_a$.

Identifying the LHS with $\frac{\mathrm{d}}{\mathrm{d}t}\mathcal{H}_c$ establishes the second energy balance equation

$$\frac{\mathrm{d}}{\mathrm{d}t}\mathcal{H}_c = \sum_j \mathcal{Q}_{cj}^{\mathrm{T}} \dot{q}_{cj} - \sum_i \frac{\partial \mathcal{L}_c}{\partial \bar{q}_i} \dot{\bar{q}}_i. \tag{6.42}$$

From Corollary 5.5.1, and the energy balances (6.37) and (6.42) it is clear that the closed-loop system $\tilde{\bar{\Sigma}}$ can be represented as the feedback interconnection of the three passive subsystems Σ_u, Σ_a and Σ_c as depicted in Fig. 6.5 (right).

6.3.2 Discussion

Input (6.28) establishes a feedback interaction between the plant EL system $\bar{\Sigma}$, (5.95), and the controller EL system, (6.29). The dynamic extension injects damping through $\mathcal{F}_c(\dot{\boldsymbol{q}}_c)$, while $\mathcal{T}_c(\boldsymbol{q}_c, \dot{\boldsymbol{q}}_c)$ and $\mathcal{V}_c(\boldsymbol{q}_c, \bar{\boldsymbol{q}})$ shape the systems Lagrangian. The resulting EL closed-loop system is shown in Fig. 6.5, where the virtual dynamics of the plant define the operator $\bar{\Sigma} : \bar{\boldsymbol{u}} \mapsto \bar{\boldsymbol{q}}$, and the passive operator $\Sigma_c : \bar{\boldsymbol{q}} \mapsto \bar{\boldsymbol{u}}$ is determined by (6.28)–(6.29). In contrast, in the original formulation of EL controllers [137], the feedback interconnection between plant Σ and controller

$$\Sigma_c : \boldsymbol{M}_c(\boldsymbol{q}_c)\ddot{\boldsymbol{q}}_c + \boldsymbol{C}_c(\boldsymbol{q}_c, \dot{\boldsymbol{q}}_c)\dot{\boldsymbol{q}}_c + \frac{\partial \mathcal{V}_c(\boldsymbol{q}_c, \boldsymbol{q}_a)}{\partial \boldsymbol{q}_c} + \frac{\partial \mathcal{F}_c(\dot{\boldsymbol{q}}_c)}{\partial \dot{\boldsymbol{q}}_c} = \boldsymbol{0}, \tag{6.43}$$

[137]: Ortega et al. (1994), "On passivity-based output feedback global stabilization of Euler-Lagrange systems"

is established by

$$\boldsymbol{u} = -\frac{\partial \mathcal{V}_c(\boldsymbol{q}_c, \boldsymbol{q}_a)}{\partial \boldsymbol{q}_a}. \tag{6.44}$$

A crucial difference to the proposed scheme is that the controller potential energy in (6.43) depends on only the collocated coordinates $\boldsymbol{q}_a$. In this way, only $\boldsymbol{q}_a$ enters into the controller via the term $\partial_{\boldsymbol{q}_a}\mathcal{V}_c$. This restriction on the potential energy of the controller imposes clear limitations on the achievable desired Lagrangian functions. Proposition 6.3.1 removes this restriction. In (6.28), we see that the entire set of coordinates $\bar{\boldsymbol{q}}$ enters the controller via the term $\partial_{\bar{\boldsymbol{q}}}\mathcal{V}_c$. Inspecting the controller dynamics (6.29), we further observe that the potential energy of the controller depends on the noncollacated outputs $\boldsymbol{q}_u$, providing fundamentally more freedom in modifying the potential energy, and thus the interaction behavior, of the EL plant. Although Theorem 3.1 in [137] is more limited in its scope of shaping the potential energy compared to the proposed extension reported in Proposition 6.3.1, it should be remarked, that the former result applies to a more general class of EL systems. In particular Assumption 5.1.1 is not required.

6.4 Shaping the Interaction with the Physical World

This section reports an adoption of classic impedance control to the class of underactuated EL systems specified in Chapter 5. The developments are based on the seminal works [68–70] by Hogan that established the concept of impedance control. Since there are fundamental physical reasons to refrain from shaping the inertia of the non-actuated subsystem[1], the focus is set on the special case where the inertial properties are preserved. This special case of impedance control is also known as compliance control.

Let us start with the static analysis of system $\bar{\Sigma}$. The potential energy $\mathcal{V}$ is a function only of position and the Lagrangian does not include the time explicitly. The system is said to be in equilibrium when the generalized forces acting on the system vanish, i.e.

$$\left(\frac{\partial \mathcal{V}}{\partial \bar{\boldsymbol{q}}}\right)_0 + \bar{\boldsymbol{u}} + \bar{\mathcal{Q}}' = \boldsymbol{0}. \tag{6.45}$$

Suppose that $\bar{u}_i = 0$. Let $\bar{\boldsymbol{q}}^0$ be the solution to

$$\left(\frac{\partial \mathcal{V}}{\partial \bar{\boldsymbol{q}}}\right)_0 = \bar{\mathcal{Q}}', \tag{6.46}$$

then, the potential energy has an extremum at this equilibrium configuration. The stiffness matrix of system $\bar{\Sigma}$ describes the change of the external force $\bar{\mathcal{Q}}'$ with the change of the position in the configuration space. By deriving (6.46) with respect to $\bar{\boldsymbol{q}}$, we obtain

$$\frac{\partial^2 \mathcal{V}}{\partial \bar{\boldsymbol{q}}^2} = \frac{\partial \bar{\mathcal{Q}}'}{\partial \bar{\boldsymbol{q}}}, \tag{6.47}$$

where the familiar Hessian on the LHS is the *stiffness matrix*. It is important to underline that (6.47) applies only locally for infinitesimal displacement

[68]: Hogan (1985), "Impedance control: An approach to manipulation: Part I—Theory"
[69]: Hogan (1985), "Impedance control: An approach to manipulation: Part II—Implementation"
[70]: Hogan (1985), "Impedance control: An approach to manipulation: Part III—Applications"

1: Discussing the underlying reasons would go beyond the focus of this work. Loosely speaking, such an approach would require feedback of $\mathcal{Q}'_u$ up to it's second time derivative. For the same reasons as discussed in Chapter 9, such feedback is likely to cause input saturation at the moment of hard impacts.

from the equilibrium $\bar{\boldsymbol{q}}_0$. Further, the form of the stiffness matrix depends on the choice of the generalized coordinates. Sometimes the stiffness matrix is used to describe the interaction behavior of a system, however, due to its local nature it allows only relating an infinitesimal deflection with an external force. In this section, we are rather interested in the global relation between a system's deflection from the equilibrium and an external force. Let us sharpen this objective. Suppose that we have a system with a unique equilibrium in absence of external forces. Now given some external force $\mathcal{Q}'_u$ on Σ_u, we would like to know whether the system Σ assumes a new unique equilibrium position. If such equilibrium position existed for any $\mathcal{Q}'_u$, we would also want to know how it is related to the magnitude and direction of $\mathcal{Q}'_u$. The proposition developed in this section allows imposing such a relation on the considered systems.

Let us decompose the potential energy function as

$$\mathcal{V} = \mathcal{V}_1(\bar{\boldsymbol{q}}_u) + \mathcal{V}_2(\bar{\boldsymbol{q}}) + \mathcal{V}_3(\bar{\boldsymbol{q}}_a). \tag{6.48}$$

Considering an ASR as exemplary system, then $\mathcal{V}_1$ would encode the gravity potential acting on the rigid body dynamics and possibly elastic elements that couple the links, $\mathcal{V}_2$ would gives rise to the potential force that couples the subsystems $\bar{\Sigma}_u$ and $\bar{\Sigma}_a$, and $\mathcal{V}_3$ would, e.g. encode elastic coupling on the motor side. In order to simplify the analysis in the following, let us make the following assumption.

Assumption 6.4.1 *Let $n_u = n_a$ and the potential function $\mathcal{V}_2$ satisfies*

$$\begin{aligned} \frac{\partial \mathcal{V}_2}{\partial \bar{\boldsymbol{q}}_a} = \boldsymbol{0} \;\Rightarrow\; \frac{\partial \mathcal{V}_2}{\partial \bar{\boldsymbol{q}}_u} = \boldsymbol{0} \;\Rightarrow\; \bar{\boldsymbol{q}}_u = \bar{\boldsymbol{q}}_a, \\ \mathcal{V}_2(\bar{\boldsymbol{q}}) > \boldsymbol{0} \text{ for } \bar{\boldsymbol{q}}_u \neq \bar{\boldsymbol{q}}_a, \\ \bar{\boldsymbol{q}}_u = \bar{\boldsymbol{q}}_a \;\Rightarrow\; \mathcal{V}_2(\bar{\boldsymbol{q}}) = \boldsymbol{0}, \end{aligned}$$

In other words, we assume that the vanishing of the coupling force acting on subsystem $\bar{\Sigma}_a$ implies the vanishing of the coupling force acting on subsystem $\bar{\Sigma}_u$. In this case, a natural choice for a controller achieving a compliant behavior on subsystem $\bar{\Sigma}_u$, and thus on $\bar{\Sigma}_u$, is summarized in the following proposition. In essence, the effects of $\mathcal{V}_1$ and $\mathcal{V}_3$ are canceled, and a spring behavior is added on $\bar{\Sigma}_u$.

Proposition 6.4.1 (Impedance control) *Let Σ be an EL system satisfying Assumption 5.1.1 and 5.1.2. Then, in absence of external forces, i.e. $\mathcal{Q}' = \boldsymbol{0}$, the controller*

$$\bar{\boldsymbol{u}} = -\boldsymbol{\mathcal{K}}_v \dot{\bar{\boldsymbol{q}}} - \boldsymbol{\mathcal{K}}_p(\bar{\boldsymbol{q}} - \bar{\boldsymbol{q}}^*) + \frac{\partial \mathcal{V}_1}{\partial \bar{\boldsymbol{q}}_u} + \frac{\partial \mathcal{V}_3}{\partial \bar{\boldsymbol{q}}_a}, \tag{6.49}$$

with $\boldsymbol{\mathcal{K}}_v > 0 \in \mathbb{R}^n$ and $\boldsymbol{\mathcal{K}}_p = \operatorname{diag}(\boldsymbol{K}_{pu}, \boldsymbol{0}_{n_a})$, $\boldsymbol{K}_{pu} > 0$ renders the equilibrium $(\bar{\boldsymbol{q}}, \dot{\bar{\boldsymbol{q}}}) = (\bar{\boldsymbol{q}}^*, \boldsymbol{0})$ globally asymptotically stable. In the presence of a constant external force $\mathcal{Q}' = \left(\mathcal{Q}'_u, \boldsymbol{0}\right)$, the shifted equilibrium $(\bar{\boldsymbol{q}}, \dot{\bar{\boldsymbol{q}}}) = (\bar{\boldsymbol{q}}^0, \boldsymbol{0})$, $\bar{\boldsymbol{q}}^0 = (\bar{\boldsymbol{q}}^0_u, \bar{\boldsymbol{q}}^0_u)$, is globally asymptotically stable, where $\bar{\boldsymbol{q}}^0_u$ is the solution to

$$\boldsymbol{\mathcal{K}}_{pu}(\bar{\boldsymbol{q}}_u - \bar{\boldsymbol{q}}^*_u) = \mathcal{Q}'_u. \tag{6.50}$$

Proof. The following proof is based on LaSalle's Theorem (see Theorem C.1.1 in Appendix C). In order to invoke this theorem, we must first construct the compact and positively invariant set Ω. We shall follow the common procedure (see, e.g., [95, p. 128]) of constructing the function $V(\boldsymbol{x})$ such that it itself guarantees the existence of a set $\Omega\}$. If $\Omega_c = \left\{\boldsymbol{x} \in \mathbb{R}^{2n} | V(\boldsymbol{x}) \leq c\right\}$ is bounded and $\dot{V}(\boldsymbol{x}) \leq 0$ in Ω_c, then we can take $\Omega = \Omega_c$. When $V(\boldsymbol{x})$ is positive definite, then Ω_c is bounded and for sufficiently small $c > 0$. Let us derive a Hamiltonian $\tilde{\mathcal{H}}$ exhibiting these features such that it qualifies as the function V. To this end, we will apply the change of coordinates

$$\tilde{\boldsymbol{q}} = \bar{\boldsymbol{q}} - \boldsymbol{q}^*. \tag{6.51}$$

to shift the minimum of the closed-loop potential energy to the origin (analogous to the proof of Proposition 6.2.1). Considering the decomposition of the potential energy of $\bar{\Sigma}$ in (6.48), we can write the dynamics of $\bar{\Sigma}$ under (6.49) as

$$\Sigma^*: \frac{\mathrm{d}}{\mathrm{d}t}\frac{\partial \mathcal{T}}{\partial \dot{\bar{\boldsymbol{q}}}} - \frac{\partial \mathcal{T}}{\partial \bar{\boldsymbol{q}}} = -\frac{\partial \mathcal{V}_2}{\partial \bar{\boldsymbol{q}}} - \mathcal{K}_p(\bar{\boldsymbol{q}} - \bar{\boldsymbol{q}}^*) - \mathcal{K}_v\dot{\bar{\boldsymbol{q}}} + \bar{\mathcal{Q}}'. \tag{6.52}$$

Introducing the generalized force $\bar{\mathcal{Q}}^* \triangleq \bar{\mathcal{Q}}' - \mathcal{K}_v\dot{\bar{\boldsymbol{q}}}$, and the functions

$$\mathcal{V}_p \triangleq \frac{1}{2}\left(\bar{\boldsymbol{q}} - \bar{\boldsymbol{q}}^*\right)^{\mathrm{T}}\mathcal{K}_p\left(\bar{\boldsymbol{q}} - \bar{\boldsymbol{q}}^*\right), \tag{6.53}$$

$$\mathcal{L}^*(\bar{\boldsymbol{q}}) \triangleq \mathcal{T}(\bar{\boldsymbol{q}}, \dot{\bar{\boldsymbol{q}}}) - \mathcal{V}^*(\bar{\boldsymbol{q}}) \tag{6.54}$$

$$\mathcal{V}^*(\bar{\boldsymbol{q}}) \triangleq \mathcal{V}_2(\bar{\boldsymbol{q}}) + \mathcal{V}_p(\bar{\boldsymbol{q}}_u), \tag{6.55}$$

we can rewrite (6.52) as

$$\Sigma^*: \frac{\mathrm{d}}{\mathrm{d}t}\frac{\partial \mathcal{L}^*}{\partial \dot{\bar{\boldsymbol{q}}}} - \frac{\partial \mathcal{L}^*}{\partial \bar{\boldsymbol{q}}} = \bar{\mathcal{Q}}^*. \tag{6.56}$$

Applying the point transformation (6.51) to (6.56), we obtain:

$$\Sigma^*: \frac{\mathrm{d}}{\mathrm{d}t}\frac{\partial \mathcal{L}^*}{\partial \dot{\tilde{\boldsymbol{q}}}} - \frac{\partial \mathcal{L}^*}{\partial \tilde{\boldsymbol{q}}} = \bar{\mathcal{Q}}^*, \tag{6.57}$$

where the Lagrangian is expressed as a function of $(\tilde{\boldsymbol{q}}, \dot{\tilde{\boldsymbol{q}}})$ through the transforming equations (6.51). As desired, the transformed system, (6.57), has an unique equilibrium point at the origin. Introducing

$$\tilde{\mathcal{L}}\left(\tilde{\boldsymbol{q}}, \dot{\tilde{\boldsymbol{q}}}\right) = \tilde{\mathcal{T}}\left(\tilde{\boldsymbol{q}}, \dot{\tilde{\boldsymbol{q}}}\right) - \tilde{\mathcal{V}}\left(\tilde{\boldsymbol{q}}\right) \triangleq \mathcal{T}\left(\bar{\boldsymbol{q}}(\tilde{\boldsymbol{q}}), \dot{\bar{\boldsymbol{q}}}(\tilde{\boldsymbol{q}})\right) - \mathcal{V}^*\left(\bar{\boldsymbol{q}}(\tilde{\boldsymbol{q}})\right), \tag{6.58}$$

we can rewrite the closed-loop dynamics as

$$\tilde{\Sigma}: \frac{\mathrm{d}}{\mathrm{d}t}\frac{\partial \tilde{\mathcal{L}}}{\partial \dot{\tilde{\boldsymbol{q}}}} - \frac{\partial \tilde{\mathcal{L}}}{\partial \tilde{\boldsymbol{q}}} = \bar{\mathcal{Q}}^*, \tag{6.59}$$

with the associated Hamiltonian $\tilde{\mathcal{H}} = \sum_i \dot{\tilde{q}}_i \frac{\partial \tilde{\mathcal{L}}}{\partial \dot{\tilde{q}}_i} - \tilde{\mathcal{L}}$. From Assumption 5.1.1 and the fact that $\mathcal{V}^*\left(\bar{\boldsymbol{q}}(\boldsymbol{0})\right) = 0$ is a unique minimum follows that $\tilde{\mathcal{H}}$ is positive definite. Further, we have that

$$\frac{\mathrm{d}}{\mathrm{d}t}\tilde{\mathcal{H}} = \dot{\tilde{\boldsymbol{q}}}^{\mathrm{T}}\bar{\mathcal{Q}}^* = \dot{\tilde{\boldsymbol{q}}}^{\mathrm{T}}\left(\bar{\mathcal{Q}}' - \mathcal{K}_v\dot{\tilde{\boldsymbol{q}}}\right). \tag{6.60}$$

Hence, $\tilde{\mathcal{H}}$ qualifies as the function V. Let us take $V = \tilde{\mathcal{H}}$ and verify that the conditions of LaSalle's theorem are satisfied for the case $\mathcal{Q}' = \boldsymbol{0}$. The

positive definiteness of V w.r.t. $(\tilde{\boldsymbol{q}}, \dot{\tilde{\boldsymbol{q}}})$ guarantees the existence of a bounded set $\Omega_c = \left\{(\tilde{\boldsymbol{q}}, \dot{\tilde{\boldsymbol{q}}}) \in \mathbb{R}^{2n} | V(\tilde{\boldsymbol{q}}, \dot{\tilde{\boldsymbol{q}}}) \leq c\right\}$ and we have that $\dot{V}(\tilde{\boldsymbol{q}}, \dot{\tilde{\boldsymbol{q}}}) \leq 0$ in Ω_c. Thus, taking $\Omega = \Omega_c$ ensures that the first condition of LaSalle's theorem is met. To find $S = \left\{(\tilde{\boldsymbol{q}}, \dot{\tilde{\boldsymbol{q}}}) \in \mathbb{R}^{2n} | \dot{V}(\tilde{\boldsymbol{q}}, \dot{\tilde{\boldsymbol{q}}}) = 0\right\}$, note that $\dot{V} = 0 \Rightarrow \dot{\tilde{\boldsymbol{q}}} = \boldsymbol{0}$. Hence, $S = \left\{(\tilde{\boldsymbol{q}}, \dot{\tilde{\boldsymbol{q}}}) \in \mathbb{R}^{2n} | \dot{\tilde{\boldsymbol{q}}} = 0\right\}$. To determine the largest invariant set, $\boldsymbol{M}$, in S, let $\left(\tilde{\boldsymbol{q}}(t), \dot{\tilde{\boldsymbol{q}}}(t)\right)$ be a solution that belongs identically to S:

$$\dot{\tilde{\boldsymbol{q}}}(t) \equiv \boldsymbol{0} \Rightarrow \ddot{\tilde{\boldsymbol{q}}}(t) \equiv \boldsymbol{0} \Rightarrow \frac{\mathrm{d}}{\mathrm{d}t}\frac{\partial \tilde{\mathcal{T}}}{\partial \dot{\tilde{\boldsymbol{q}}}} - \frac{\partial \tilde{\mathcal{T}}}{\partial \tilde{\boldsymbol{q}}} \equiv \boldsymbol{0} \Rightarrow \frac{\partial \mathcal{V}^*}{\partial \tilde{\boldsymbol{q}}} \equiv \boldsymbol{0} \Rightarrow \tilde{\boldsymbol{q}} \equiv \boldsymbol{0}, \tag{6.61}$$

where the last implication is due to Assumption 6.4.1. Hence the only solution that can stay identically in S is the trivial solution $(\tilde{\boldsymbol{q}}, \dot{\tilde{\boldsymbol{q}}}) = (\boldsymbol{0}, \boldsymbol{0})$ and, thus, the origin is asymptotically stable. Since the generalized coordinates $\tilde{\boldsymbol{q}}$ and $\bar{\boldsymbol{q}}$ are in a one-to-one correspondence, we can conclude GAS of the equilibrium point $\bar{\boldsymbol{q}} = \bar{\boldsymbol{q}}^*$. Moreover, since the generalized coordinates $\boldsymbol{q}$ and $\bar{\boldsymbol{q}}$, are in a one-to-one correspondence (as pointed out in Lemma 5.3.1 and 5.4.1), we can conclude GAS of the corresponding equilibrium point for Σ, which is implicitly defined through the coordinate transforming equations, as shown in Lemma 5.3.1 and 5.4.1. See proof of Proposition 6.2.1 for detailed argument concerning the latter statement. This completes the proof of the first statement.

In the presence of a constant external force $\bar{\mathcal{Q}}' = \left(\bar{\mathcal{Q}}'_u, \boldsymbol{0}\right)$, the equilibrium condition for the closed-loop system (6.59) is

$$\frac{\partial \mathcal{V}^*}{\partial \bar{\boldsymbol{q}}} = \bar{\mathcal{Q}}' \Rightarrow \frac{\partial \mathcal{V}^*}{\partial \bar{\boldsymbol{q}}_a} = \boldsymbol{0} \Rightarrow \bar{\boldsymbol{q}}_u = \bar{\boldsymbol{q}}_a \Rightarrow \mathcal{K}_{pu}(\bar{\boldsymbol{q}}_u - \bar{\boldsymbol{q}}_u^*) = \mathcal{Q}'_u \tag{6.62}$$

Applying the point transformation to (6.56)

$$\bar{\boldsymbol{q}}_u = \tilde{\boldsymbol{q}}_u + \bar{\boldsymbol{q}}_u^* + \mathcal{K}_{pu}^{-1}\mathcal{Q}'_u, \tag{6.63}$$

$$\bar{\boldsymbol{q}}_a = \tilde{\boldsymbol{q}}_a + \bar{\boldsymbol{q}}_a^*, \tag{6.64}$$

shifts the coordinate origin such that at the equilibrium position $\tilde{\boldsymbol{q}} = \boldsymbol{0}$. We can now proceed mutatis mutandis to the stability argument above and show global asymptotic stability of the new equilibrium point uniquely defined by (6.62). How to complete the remaining proof is reported step-by-step in Appendix B.

■

6.5 Choosing the "Right" Set of Coordinates (Task Space Formulation)

For the design and analysis of control schemes it can be advantageous to formulate the system dynamics in terms of generalized coordinates different from $\bar{\boldsymbol{q}}$ [97]. Let $\boldsymbol{x} = (x_1, \ldots, x_n)$ be a set of generalized coordinates such that we can express the $\bar{\boldsymbol{q}}$'s in terms of the $\bar{\boldsymbol{x}}$'s via the transforming equations

$$\bar{\boldsymbol{q}} = \bar{\boldsymbol{q}}(\bar{\boldsymbol{x}}), \tag{6.65}$$

which are assumed to be sufficiently smooth. Further, suppose that the virtual

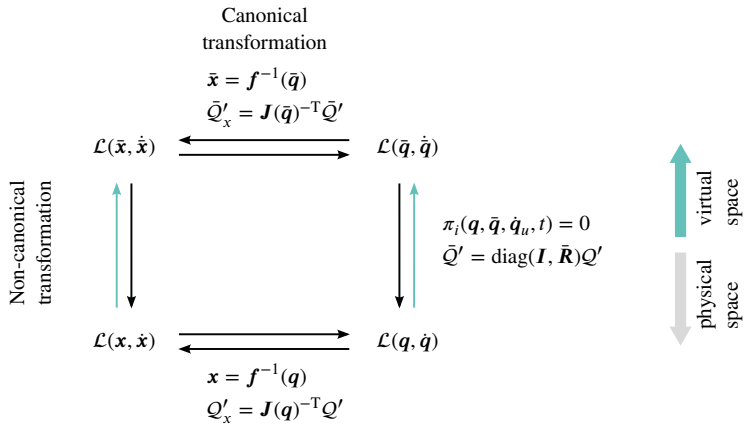

Figure 6.6: Canonical and non-canonical transformations.

displacements are related by the Jacobian $\boldsymbol{J}(\bar{\boldsymbol{q}})$ in the form

$$\delta\bar{\boldsymbol{x}} = \boldsymbol{J}(\bar{\boldsymbol{q}})\delta\bar{\boldsymbol{q}}, \tag{6.66}$$

so that, using the invertibility of $\boldsymbol{J}$,

$$\delta\bar{q}_i = \sum_j \frac{\partial\bar{q}_i}{\partial\bar{x}_j}\delta\bar{x}_j = \sum_j \left(\boldsymbol{J}^{-1}\right)_{ij}\delta\bar{x}_j. \tag{6.67}$$

Considering Corollary 2.5.6, the EL equations of $\bar{\Sigma}$ transform under (6.65) to

$$\frac{\mathrm{d}}{\mathrm{d}t}\frac{\partial\mathcal{L}}{\partial\dot{\bar{x}}_j} - \frac{\partial\mathcal{L}}{\partial\bar{x}_j} = \sum_i \left[\bar{Q}_i \frac{\partial\bar{q}_i}{\partial\bar{x}_j}\right]. \tag{6.68}$$

Introducing $\bar{\boldsymbol{v}} = \boldsymbol{J}^{-T}\bar{\boldsymbol{u}}$ and $\bar{Q}_x = \boldsymbol{J}^{-T}\bar{Q}'$, and using (6.67), we observe that

$$\sum_i \left[\bar{Q}_i \frac{\partial\bar{q}_i}{\partial\bar{x}_j}\right] = \boldsymbol{J}^{-T}\bar{Q} = \boldsymbol{v} + \bar{Q}_x, \tag{6.69}$$

which allows us to rewrite (6.68) in vector form as

$$\bar{\Sigma}_x : \ \frac{\mathrm{d}}{\mathrm{d}t}\left[\frac{\partial\mathcal{L}}{\partial\dot{\bar{\boldsymbol{x}}}}\right]^T - \left[\frac{\partial\mathcal{L}}{\partial\bar{\boldsymbol{x}}}\right]^T = \boldsymbol{J}^{-T}\bar{Q} = \boldsymbol{v} + \bar{Q}_x. \tag{6.70}$$

Considering that both input signals $\bar{\boldsymbol{u}}$ and $\bar{\boldsymbol{v}}$, and both sets of coordinates $\bar{\boldsymbol{q}}$ and $\bar{\boldsymbol{x}}$ are in a one-to-one correspondence, and given that (6.70) are just regular EL equations, the control developments in this chapter can be equally applied considering the transformed system $\bar{\Sigma}_x$ instead of $\bar{\Sigma}$.

In some scenarios, it can be advantageous to transform from the $\boldsymbol{q}$'s to some new coordinates $\boldsymbol{x}$'s first, and then apply the input and coordinate transforming equations that produce the QFA form. This route will be exploited in Chapter 7 to solve the end effector motion tracking problem for ASR. The solution relies on transforming the dynamics from the link and motor positions space to the task and joint deflection space first, before transforming the model into its QFA form.

6.6 Conclusions

This chapter reported the adoption of popular *energy-based* control designs through the QFA representation of the plant. The resulting designs share the following characteristics: a *physically intuitive and passive closed-loop dynamics*, aiming at *minimizing the shaping of the plant dynamics*.

[178]: Takegaki et al. (1981), "A new feedback method for dynamic control of manipulators"

The energy shaping and damping injection scheme by [178] was originally designed for fully actuated systems, and the adoption through the QFA representation allowed extending its range of application to a class of underactuated EL systems. This comes at the price of new constraints on the achievable potential functions and damping behavior (see also the discussion in Section 6.2.2). It is worth remarking that Proposition 6.2.1 can be considered as extension of Proposition 3.1 in [133], which summarizes the results on energy shaping and damping injection by [178].

[133]: Ortega (1998), *Passivity-Based Control of Euler-Lagrange Systems: Mechanical, Electrical, and Electromechanical Applications*

Furthermore, an extension to the EL controllers proposed by [137] was presented. The new approach allows more freedom in specifying the potential energy of the controller. It should be remarked, however, that Theorem 3.1 in [137] applies to a more general class of EL systems compared to the proposed extension in Proposition 6.3.1. In particular Assumption 5.1.1 and 5.1.2 are not required in the original formulation.

[137]: Ortega et al. (1994), "On passivity-based output feedback global stabilization of Euler-Lagrange systems"

An interesting aspect of the presented concepts is the fact they impose no limitations on the controller gains. In particular, the closed-loop stiffness of an ASR can be increased above the system's intrinsic stiffness, as demonstrated in Experiment 3 reported in Chapter 11. In practice, however, limits are to be faced due to finite actuation forces, signal delays, sensor quantization, non-modeled dynamics, and so forth. The performance limits imposed by bounds on the available actuator torques are discussed in Chapter 9 on the basis of an ASR implemented with SEAs.

Elastic Structure Preserving Control of Articulated Soft Robots

7

To understand is to know what to do.

— Ludwig Wittgenstein

The desire for robust and high performance from ASR spurred the development of the Elastic Structure Preserving (ESP) control framework. The procedure stabilizes ASRs while shaping the intrinsic dynamics only to a minimal extent. In particular, ESP-based designs preserve the EL structure of the plant. The ESP control concept was first introduced in [89] and inspired a series of follow-up developments [60, 77, 86, 89–91, 94, 114, 115]. This chapter demonstrates the application of the QFA formulation from Chapter 5 to re-derive the ESP controllers [86, 89–91, 94] in a unifying way. Using Theorem 5.6.1, is will be shown that the aforementioned control designs can be obtained by adjusting only the actuated subsystem Lagrangian of the QFA system.

The chapter is organized as follows. We start with a brief recapitulation of the considered ASR model. Section 7.2 presents solutions to the joint/task space set-point regulation and motion tracking problems for monoarticular ASRs; the latter is solved by adopting rigid body controllers (namely, the Slotine & Li and PD+ controllers) through the QFA formulation. Section 7.3 reports the application of the ESP concept to multiarticular ASRs. Section 7.4 applies the ESP design idea to robots with visco-elastic actuators. The proofs of the main stability and passivity results are presented in Section 7.5. Experiments highlighting the performance and viability of the presented concepts are reported in Chapter 11.

7.1 Recent Developments

To put the developments of this chapter into perspective, the following section summarizes recent ESP control developments and discusses the underlying motivations. An in-depth comparison with state of the art concepts is provided in Chapter 8. In order to increase the mechanical robustness against impacts and unknown contact forces, robot design has evolved from rigid toward compliant actuators. While mechanical compliance provides many benefits it also comes at a price:

- (**C1**) The plant dynamics is *underactuated* as the number of dimensions of the configuration space is greater than the number of dimensions of the control input space.
- (**C2**) To improve energy storing capabilities and efficiency in general, compliant actuators are often designed such that damping and friction in parallel to the spring is negligible. The *intrinsic oscillatory dynamics* can be exploited for cyclic tasks like locomotion, hammering, or drumming, etc. For positioning tasks, however, unwanted oscillations must be addressed by suitable control to achieve a positioning performance that can compete with that of a rigid manipulator.

[60]: Harder et al. (2022), "Simultaneous motion tracking and joint stiffness control of bidirectional antagonistic variable-stiffness actuators"
[77]: Iskandar et al. (2020), "Joint-level control of the DLR lightweight robot SARA"
[86]: Keppler et al. (2018), "Elastic structure preserving (ESP) control for compliantly actuated robots"
[89]: Keppler et al. (2016), "A passivity-based approach for trajectory tracking and link-side damping of compliantly actuated robots"
[90]: Keppler et al. (2016), "A passivity-based controller for motion tracking and damping assignment for compliantly actuated robots"
[91]: Keppler et al. (2021), "Analyzing the performance limits of articulated soft robots based on the ESPi framework: Applications to damping and impedance control"
[94]: Keppler et al. (2018), "Visco-elastic structure preserving impedance (VESPi) control for compliantly actuated robots"
[114]: Meng et al. (2021), "Elastic structure preserving impedance control of bidirectional antagonistic variable stiffness actuation"
[115]: Mengacci et al. (2021), "Elastic Structure Preserving control for compliant robots driven by agonistic-antagonistic actuators (ESPaa)"

Moreover, many variable stiffness robots feature nonlinear elasticities. These issues make control of the link configuration variables a challenging task.

Regulation controllers for the link configuration variables of flexible joint robots have been proposed in [134, 141, 183, 196] and a generalization to the case of nonlinear joint elasticities (often appearing in variable stiffness actuators (VSA) [190]) has been proposed in [7]. The above controllers consider feedback of only control-input-collocated variables. Therefore, the damping performance of these approaches is lower compared to the regulation controllers reported in [5, 147, 158], which feedback also control input non-collocated variables. While [5] provides a comprehensive stability analysis for constant controller gains, the closed-loop dynamics of [147] and [158] are not accompanied by a rigorous stability proof.

Tracking controllers for the link configuration variables of robots with elastic transmissions are reported in the pioneering works [107, 127, 168]. Further solutions to the tracking problem have been reported that are based on cascaded structures [139], integrator backstepping [129, 140] extensions of the well-known controller by Slotine and Weiping [165, 169], feedback linearization [31, 145, 168], and integral manifold control [168]. All of the tracking controllers above, [31, 107, 127, 129, 139, 140, 165, 168], are formulated for linear elasticities with one exception: The method of [145] also applies to robots with nonlinear elasticities. Most of the tracking controllers above have been verified only in computer simulations.

Motivation Triggered by the following observations:

- (**O1**) Motor vibration damping, in combination with joint torque feedback, showed good performance on robots with rather stiff joints [6, 142, 183], but it is not sufficient to achieve well-damped links of highly elastic ASRs such as DLR *David*; see also Video 2.
- (**O2**) A lack of robustness intrinsic with schemes based on canceling nonlinearities [19].
- (**O3**) The higher the joint compliance the lower joint torque control bandwidth compared to that of a rigid robot [91, 153].
- (**O4**) Singular perturbation-based approaches are theoretically and practically limited to systems with high joint stiffness values; this renders them unsuitable for ASRs [6].
- (**O5**) Extensive hands-on experience on DLR *David* indicates that control approaches changing its dynamics to a "high" degree are prone to suffer from instability in practice—albeit being theoretically sound.

We initiated a series of control developments [86, 89, 90]—coined *Elastic Structure Preserving* (ESP) control. The primary objective was to develop a control scheme that simultaneously achieves motion tracking and a desired damping/compliance behavior in terms of the link configuration variables. Moreover it should be theoretically well founded (uniform global asymptotic stability), practically feasible and achieving satisfactory performance in practice. The development was guided by the design principles stated in Chapter 6 (see Fig. 6.2) combined with a fourth design principle: inject link-side damping to deal with (**C2**). The design principles, as summarized in Fig. 7.2, originated from the observations above and reflect the core philosophy of the ESP control are summarized in Fig. 7.1. Their choice is further motivated below:

[134]: Ortega et al. (1995), "A semiglobally stable output feedback PI^{2}D regulator for robot manipulators"
[141]: Ott et al. (2004), "A passivity based cartesian impedance controller for flexible joint robots-part I: Torque feedback and gravity compensation"
[183]: Tomei (1991), "A simple PD controller for robots with elastic joints"
[196]: Zollo et al. (2004), "Regulation with on-line gravity compensation for robots with elastic joints"
[190]: Vanderborght et al. (2013), "Variable impedance actuators: A review"
[7]: Albu-Schäffer et al. (2012), "Constructive energy shaping control for a class of Euler-Lagrange Systems"
[5]: Albu-Schäffer et al. (2001), "A globally stable state feedback controller for flexible joint robots"
[147]: Petit et al. (2011), "State feedback damping control for A multi DOF variable stiffness robot arm"
[158]: Sardellitti et al. (2013), "Gain scheduling control for a class of variable stiffness actuators based on lever mechanisms"
[107]: Loria et al. (1995), "On tracking control of rigid and flexible joints robots"
[127]: Nicosia et al. (1993), "Design of global tracking controllers for flexible-joint robots"
[168]: Spong (1987), "Modeling and control of elastic joint robots"

[139]: Ott et al. (2003), "Decoupling based Cartesian impedance control of flexible joint robots"
[129]: Oh et al. (1999), "Control of flexible joint robot system by backstepping design approach"
[140]: Ott (2008), *Cartesian Impedance Control of Redundant and Flexible-Joint Robots*
[165]: Slotine et al. (1988), "Adaptive manipulator control: A case study"
[169]: Spong (1989), "Adaptive control of flexible joint manipulators"

[31]: De Luca et al. (1998), "A general algorithm for dynamic feedback linearization of robots with elastic joints"
[145]: Palli et al. (2008), "On the feedback linearization of robots with variable joint stiffness"
[168]: Spong (1987), "Modeling and control of elastic joint robots"

[19]: Brogliato et al. (1995), "Global tracking controllers for Flexible-joint manipulators: a comparative study"

[91]: Keppler et al. (2021), "Analyzing the performance limits of articulated soft robots based on the ESPi framework: Applications to damping and impedance control"
[153]: Pratt et al. (1995), "Series elastic actuators"

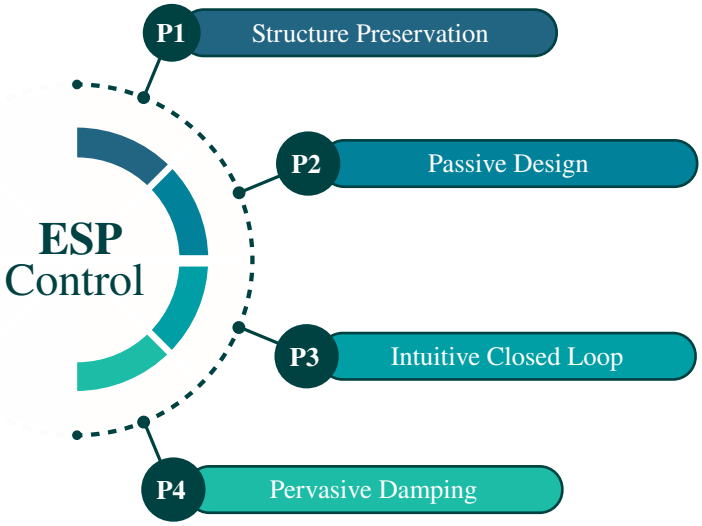

Figure 7.1: Design procedure to obtain a QFA form.

(**P1**) The goal is to achieve natural motions in the sense of [98], with the underlying hope that minimizing the system shaping, and having a closed-loop dynamics match in some way the intrinsic structure of the robot will award high performance with little control effort. Further, control designs that minimize the system shaping usually result in low gain designs, which is favorable with regard to robustness.

(**P2**) Passivity Based Control (PBC) is a structure preserving design approach which handles nonlinearities in a natural way. It is known for originating robust controllers. Moreover, the storage function often qualifies as Lyapunov function.

(**P3**) A physically intuitive closed-loop dynamics allows the operator to anticipate the interaction behavior of the robot with the environment. This is of immense value during the design and tuning phase. Moreover, control gains that are physically interpretable in terms of springs of dampers allows taking the limited joint torque control bandwidth into account during the design stage. Roughly speaking, it can be expected that imposing a link stiffness significantly above the intrinsic one requires high control actions.

(**P4**) The feedback of the control input noncollocated link variables enables good link-side damping performance. Achieving a closed-loop system that is output strictly passively (OSP) is desirable from the robustness point of view, since OSP implies L2-gain stability [188].

[98]: Koditschek (1984), "Natural motion for robot arms"

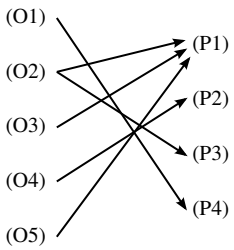

Figure 7.2: Relations between observations (O1)–(O5) and (P1)–(P4).

[188]: van der Schaft (1999), *L2-Gain and Passivity in Nonlinear Control*

Recent Developments The ESP concept was first introduced in [89]. The work [90] extended the concept to avoiding the scaling of the motor inertia to constant values in the new coordinates, which is a non passive control action for itself. We refer to this approach as ESP+ control. Both designs result in a passive closed loop and solve the joint-space global asymptotic tracking problem. A comparison and an extensive passivity and stability analysis is reported in [86]. In [92], we extended the ESP approach from link side damping to full Cartesian impedance control (referred to as ESPi control). The ESP design reported in [77] achieves damping in parallel to the joint spring. The resulting full state feedback controller uses link positions and joint torques, and the associated time-derivatives, as states to solve the output regu-

[89]: Keppler et al. (2016), "A passivity-based approach for trajectory tracking and link-side damping of compliantly actuated robots"

[90]: Keppler et al. (2016), "A passivity-based controller for motion tracking and damping assignment for compliantly actuated robots"

[86]: Keppler et al. (2018), "Elastic structure preserving (ESP) control for compliantly actuated robots"

[92]: Keppler et al. (2018), "Elastic structure preserving impedance (ESPi) control for compliantly actuated robots"

[77]: Iskandar et al. (2020), "Joint-level control of the DLR lightweight robot SARA"

lation problem; thereby, it exploit the high torque sensing resolution of recent lightweight robots. Later developments [114, 115] treated the application of the ESP concept to agonistic-antagonistic actuators to solve the global output regulation problem, while simultaneously allowing to adjust the passive joint stiffness through co-contraction. The work [151] treats the extension to tendon driven systems and reports novel constraint equations for the coordinates transformation into virtual coordinates. The design in [60] achieves simultaneous motion tracking and joint stiffness control on bidirectional antagonistic variable-stiffness actuators. Finally, we address robust stabilization of ASRs by combining ESP and PID control in [88]. A key feature of the controller is that it combines excellent positioning accuracy in free motion with compliant manipulation in contact with the environment. The experimental results highlight that elastic robots may achieve a positioning accuracy comparable to rigid joint robots.

[114]: Meng et al. (2021), "Elastic structure preserving impedance control of bidirectional antagonistic variable stiffness actuation"
[115]: Mengacci et al. (2021), "Elastic Structure Preserving control for compliant robots driven by agonistic-antagonistic actuators (ESPaa)"
[151]: Pollayil et al. (2021), "Elastic structure preserving impedance controlfor nonlinearly coupled tendon-driven systems"
[60]: Harder et al. (2022), "Simultaneous motion tracking and joint stiffness control of bidirectional antagonistic variable-stiffness actuators"

The works most closely related to ESP control are [32, 33, 140]. The former two use the *equivalence principle* [76] to derive control laws that combine gravity cancellation with motor-side PD terms to achieve set-point regulation. Similarly to the ESP approaches [86, 89, 90], the PD terms are formulated in terms of new motor coordinates that encode the desired link-side modifications. Interestingly, using the QFA representation of the Spong's model to cancel the effect of gravity and add motor-side regulation terms produces controllers equal to [32, 33] and (7.98)–(7.100) in [140]. The works [6, 142] report passivity based control designs that aim at preserving the intrinsic compliant dynamics. However, in contrast to the ESP concept, these designs do now allow for direct link-side damping and exact cancellation of gravity.

[32]: De Luca et al. (2011), "A PD-type regulator with exact gravity cancellation for robots with flexible joints"
[33]: De Luca et al. (2010), "Dynamic gravity cancellation in robots with flexible transmissions"
[140]: Ott (2008), *Cartesian Impedance Control of Redundant and Flexible-Joint Robots*
[76]: Isidori (1995), *Nonlinear Control Systems*
[86]: Keppler et al. (2018), "Elastic structure preserving (ESP) control for compliantly actuated robots"
[89]: Keppler et al. (2016), "A passivity-based approach for trajectory tracking and link-side damping of compliantly actuated robots"
[90]: Keppler et al. (2016), "A passivity-based controller for motion tracking and damping assignment for compliantly actuated robots"
[6]: Albu-Schäffer et al. (2007), "A Unified Passivity-based control framework for position, torque and impedance control of flexible joint robots"
[142]: Ott et al. (2008), "On the passivity-based impedance control of flexible joint robots"

In the following, we shall use the following abbreviations:

- ESP: inject link-side damping to suppress link vibrations away from the reference trajectory.
- ESPi: impose a link compliance behavior to adjust the interaction behavior and the convergence rate towards the reference trajectory.

7.1.1 Model Recapitulation

For ease of reference, we recall from (3.24) in Chapter 3 that the simplified model of an n-link ASR is determined by its kinetic and potential energies

$$\mathcal{T}(\boldsymbol{q}, \dot{\boldsymbol{q}}) = \tfrac{1}{2}\dot{\boldsymbol{q}}^{\mathrm{T}} \mathcal{M} \dot{\boldsymbol{q}}, \tag{7.1}$$

$$\mathcal{V}(\boldsymbol{q}) = \mathcal{V}_g(\boldsymbol{q}_u) + \mathcal{V}_e(\boldsymbol{q}), \tag{7.2}$$

with

$$\mathcal{M}(\boldsymbol{q}_u) = \operatorname{diag}\big(\boldsymbol{M}(\boldsymbol{q}_u), \boldsymbol{B}\big). \tag{7.3}$$

The associated EL equations are

$$\Sigma: \ \mathcal{M}(\boldsymbol{q}_u)\ddot{\boldsymbol{q}} + \mathcal{C}(\boldsymbol{q}_u, \dot{\boldsymbol{q}}_u)\dot{\boldsymbol{q}}_u + \left[\frac{\partial \mathcal{V}}{\partial \boldsymbol{q}}\right]^{\mathrm{T}} = \boldsymbol{u} + \mathcal{Q}'. \tag{7.4}$$

For the developments of this chapter, we shall assume that the elastic potential function $\mathcal{V}_e$ satisfies Assumption 5.1.2 such that (7.4) can be transformed

into its QFA form. The following structural properties regarding the QFA representation of (7.4) are most relevant for the control developments of the present chapter:

Property 4. Suppose that $\bar{\boldsymbol{u}}_u$ satisfies the conditions of either Theorem 5.3.6, 5.4.2, or 5.6.1. Then, we can treat the QFA representation of (7.4) as if there is an independent control input for each degree of freedom.

Property 5. The QFA representation of (7.4) defines a passive mapping $\bar{\boldsymbol{u}} \mapsto \dot{\bar{\boldsymbol{q}}}$ between the virtual input forces and the link velocities.

Property 6. The matrix $\dot{\mathcal{M}}(\bar{\boldsymbol{q}}) - 2\mathcal{C}(\bar{\boldsymbol{q}}, \dot{\bar{\boldsymbol{q}}})$ is skew symmetric for any $\boldsymbol{q}, \dot{\boldsymbol{q}} \in \mathbb{R}^n$.

In addition to Assumption 5.1.1 the following is assumed for the inertia matrix.

Assumption 7.1.1 *The maximum singular value of $\mathcal{M}$ is bounded.*

Task Coordinates

The goal of Cartesian impedance control is to establish a desired relationship between the motion of the robot's end effector and the external forces. Let $\boldsymbol{x} = x_1, \dots, x_{n_u}$ be a set of independent task coordinates for a non-redundant robot. Suppose that we can transform from the link configuration coordinates $\boldsymbol{q} = q_1, \dots, q_{n_u}$ to the task coordinates by means of transforming equations of the form

$$x_{ui} = h_{ui}(\boldsymbol{q}_u), \quad i = 1, \dots, n_u. \tag{7.5}$$

It is always assumed that we can transform back from the $\boldsymbol{x}_u$ to the $\boldsymbol{q}_u$. Invertibility of the functions h_i means that the Jacobian of the transformation

$$\boldsymbol{J}_u(\boldsymbol{q}_u) = \frac{\partial \boldsymbol{x}_u}{\partial \boldsymbol{q}_u}, \tag{7.6}$$

is nonsingular. Assume further that the h_i are at least three times continuously differentiable functions, because link jerks will lead to third order derivatives. In conclusion, by employing appropriate singularity avoidance strategies, we can use $\boldsymbol{q}_u$ and $\boldsymbol{x}_u$ as equivalent representations of the link-side configuration.

7.2 Monoarticular Articulated Soft Robots

This section focuses on ASRs driven by monoarticular actuators, i.e. where each motor drives a single link such that we have an equal number of actuated and unactuated coordinates ($n_u = n_a = n/2$). Let us assume that the potential energy of an ASR is given by

$$\mathcal{V}(\boldsymbol{q}) = \mathcal{V}_g(\boldsymbol{q}_u) + \mathcal{V}_e(\boldsymbol{\varphi}) = \mathcal{V}_g(\boldsymbol{q}_u) + \sum_i \mathcal{V}_{ei}(\varphi_i), \quad i = 1, \dots n, \tag{7.7}$$

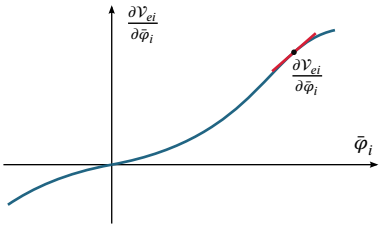

Figure 7.3: A valid generalized elastic force deflection profile.

where φ_i is the ith component of the vector of joint deflections

$$\boldsymbol{\varphi} \triangleq \boldsymbol{q}_a - \boldsymbol{q}_u. \tag{7.8}$$

The functions $\mathcal{V}_g$ and $\mathcal{V}_e$ denote the potential energies due to the gravitational and elastic forces, with the component $\mathcal{V}_{ei}$ being the elastic potential energy of the ith joint, which satisfies the two assumptions below.

Assumption 7.2.1 *The elastic potential functions $\mathcal{V}_{ei}(\varphi) \in C^k$, $k \geq 3$, are strongly convex, radially unbounded, and positive definite for all $\varphi_i \in \mathbb{R}^n$, i.e. $\mathcal{V}_i(\varphi_i) = 0 \implies \varphi_i = 0$.*

Assumption 7.2.2 *The components ψ_i of the generalized elastic force $\boldsymbol{\psi}$ are determined by*

$$\psi_i(\varphi_i) = \frac{\partial \mathcal{V}_{ei}}{\partial \varphi_i}. \tag{7.9}$$

The strong convexity of $\mathcal{V}_{ei}$ ensures the existence of constants $c_i > 0$ such that

$$\frac{\partial^2 \mathcal{V}_{ei}}{\partial \varphi_i^2} = \frac{\partial \psi_i}{\partial \varphi_i} > c_i, \quad i = 1, \dots n/2. \tag{7.10}$$

In other words, ψ_i is strictly monotonic increasing in its argument with a slope strictly greater than zero as visualized in Fig. 7.3. We conclude that ψ_i is a C^{k-1}, $k \geq 3$, diffeomorphism from the the set of joint deflections to the generalized elastic forces. Considering Assumption 7.2.2, we observe that the generalized elastic forces in (7.4) are of the form

$$\frac{\partial \mathcal{V}_e}{\partial \boldsymbol{q}} = \left[\frac{\partial \mathcal{V}_e}{\partial \boldsymbol{q}_u}, \frac{\partial \mathcal{V}_e}{\partial \boldsymbol{q}_a}\right] = \left[-\frac{\partial \mathcal{V}_e}{\partial \boldsymbol{\varphi}}, \frac{\partial \mathcal{V}_e}{\partial \boldsymbol{\varphi}}\right] = \left[\boldsymbol{\psi}(\boldsymbol{\varphi}), -\boldsymbol{\psi}(\boldsymbol{\varphi})\right], \tag{7.11}$$

$$\frac{\partial \mathcal{V}_g}{\partial \boldsymbol{q}} = \left[\frac{\partial \mathcal{V}_g}{\partial \boldsymbol{q}_u}, \boldsymbol{0}\right]. \tag{7.12}$$

Introducing

$$\boldsymbol{\Psi}(\boldsymbol{\varphi}) = \left[\frac{\partial \mathcal{V}_e}{\partial \boldsymbol{q}}\right]^{\mathrm{T}}, \quad \boldsymbol{g}(\boldsymbol{q}_u) = \left[\frac{\partial \mathcal{V}_g}{\partial \boldsymbol{q}}\right]^{\mathrm{T}}, \tag{7.13}$$

we can rewrite (7.4) as

$$\Sigma: \ \mathcal{M}(\boldsymbol{q}_u)\ddot{\boldsymbol{q}} + C(\boldsymbol{q}_u, \dot{\boldsymbol{q}}_u) + \boldsymbol{g}(\boldsymbol{q}_u) + \boldsymbol{\Psi}(\boldsymbol{\varphi}) = \boldsymbol{u}. \tag{7.14}$$

7.2.1 A Quasi-Fully Actuated Representation

Let us use Theorem 5.3.6 to transform the ASR model defined above into its equivalent QFA form. First, however, we have to check whether the model satisfies Assumption 5.1.1 and 5.1.2. From (7.1)–(7.3), we see that the former one is trivially satisfied. Knowing that

$$\frac{\partial \boldsymbol{\varphi}}{\partial \boldsymbol{q}_a} = -\frac{\partial \boldsymbol{\varphi}}{\partial \boldsymbol{q}_u} = \boldsymbol{I}, \tag{7.15}$$

$$\frac{\partial \mathcal{V}_e}{\partial \boldsymbol{q}_u} = \frac{\partial \mathcal{V}_e}{\partial \boldsymbol{\varphi}} \frac{\partial \boldsymbol{\varphi}}{\partial \boldsymbol{q}_u} = -\frac{\partial \mathcal{V}_e}{\partial \boldsymbol{\varphi}}, \tag{7.16}$$

$$\frac{\partial \mathcal{L}_a}{\partial \boldsymbol{q}_u} = -\frac{\partial \mathcal{V}}{\partial \boldsymbol{q}_u} = -\frac{\partial}{\partial \boldsymbol{q}_u}\left(\mathcal{V}_g + \mathcal{V}_e\right) = -\frac{\partial \mathcal{V}_g}{\partial \boldsymbol{q}_u} + \frac{\partial \mathcal{V}_e}{\partial \boldsymbol{\varphi}}, \tag{7.17}$$

$$\frac{\partial^2 \mathcal{L}_a}{\partial \boldsymbol{q}_a \partial \boldsymbol{q}_u} = \frac{\partial}{\partial \boldsymbol{q}_a} \frac{\partial \mathcal{V}_e}{\partial \boldsymbol{\varphi}} = \frac{\partial^2 \mathcal{V}_e}{\partial \boldsymbol{\varphi}^2} \frac{\partial \boldsymbol{\varphi}}{\partial \boldsymbol{q}_a} = \frac{\partial^2 \mathcal{V}_e}{\partial \boldsymbol{\varphi}^2} \tag{7.18}$$

and using (7.7), it follows that

$$\frac{\partial^2 \mathcal{L}_a}{\partial \boldsymbol{q}_a \partial \boldsymbol{q}_u} = \operatorname{diag}\left(\frac{\partial^2 \mathcal{V}_{e1}}{\partial \varphi_1^2}, \dots, \frac{\partial^2 \mathcal{V}_{en}}{\partial \varphi_n^2}\right). \tag{7.19}$$

From (7.10) and (7.19), we can conclude that Assumption 5.1.2 is satisfied as well. Since the conditions of Theorem 5.3.6 are met, we can proceed with applying the coordinate and input transformations (5.29) and (5.57) to obtain the QFA representation of (7.4):

$$\bar{\Sigma}: \ \frac{\mathrm{d}}{\mathrm{d}t}\frac{\partial \mathcal{L}}{\partial \dot{\bar{\boldsymbol{q}}}} - \frac{\partial \mathcal{L}}{\partial \bar{\boldsymbol{q}}} = \bar{\mathcal{Q}}, \tag{7.20}$$

or equivalently in matrix form

$$\bar{\Sigma}: \ \mathcal{M}(\bar{\boldsymbol{q}}_u)\ddot{\bar{\boldsymbol{q}}} + \mathcal{C}(\bar{\boldsymbol{q}}_u, \dot{\bar{\boldsymbol{q}}}_u) + \left[\frac{\partial \mathcal{V}}{\partial \bar{\boldsymbol{q}}}\right]^{\mathrm{T}} = \bar{\mathcal{Q}}, \tag{7.21}$$

with $\bar{\mathcal{Q}} = \bar{\boldsymbol{u}} + \bar{\mathcal{Q}}'$. Introducing

$$\bar{\boldsymbol{\varphi}} = \bar{\boldsymbol{q}}_a - \bar{\boldsymbol{q}}_u, \tag{7.22}$$

and using (7.17), we get for the transforming equations (5.29a)–(5.29b)

$$\left[\frac{\partial \mathcal{V}_e}{\partial \boldsymbol{\varphi}}\right]_q - \left[\frac{\partial \mathcal{V}_e}{\partial \bar{\boldsymbol{\varphi}}}\right]_{\bar{q}} - \bar{\boldsymbol{u}}_u = \boldsymbol{0}, \tag{7.23}$$

$$\boldsymbol{q}_u - \bar{\boldsymbol{q}}_u = \boldsymbol{0}. \tag{7.24}$$

Using (7.9), (7.23) can be written compactly as

$$\boldsymbol{\psi}(\boldsymbol{\varphi}) = \boldsymbol{\psi}(\bar{\boldsymbol{\varphi}}) + \bar{\boldsymbol{u}}_u. \tag{7.25}$$

Evaluating the definitions (5.52), (5.53)–(5.56), we get

$$\frac{\partial \mathcal{L}_a}{\partial \boldsymbol{q}_a} = -\frac{\partial \mathcal{V}_e}{\partial \boldsymbol{\varphi}} \frac{\partial \boldsymbol{\varphi}}{\partial \boldsymbol{q}_a} = -\frac{\partial \mathcal{V}_e}{\partial \boldsymbol{\varphi}}, \tag{7.26}$$

$$\boldsymbol{X} = -\frac{\partial^2 \mathcal{V}_g}{\partial \boldsymbol{q}_u^2} - \frac{\partial^2 \mathcal{V}_e}{\partial \boldsymbol{\varphi}^2}, \tag{7.27}$$

$$\boldsymbol{Y} = \frac{\partial^2 \mathcal{V}_e}{\partial \boldsymbol{\varphi}^2}, \tag{7.28}$$

$$\boldsymbol{A} = \left[\frac{\partial^2 \mathcal{V}_e}{\partial \boldsymbol{\varphi}^2}\right]_q^{-1} \left[\frac{\partial^2 \mathcal{V}_e}{\partial \bar{\boldsymbol{\varphi}}^2}\right]_{\bar{q}}, \tag{7.29}$$

$$\boldsymbol{R} = \boldsymbol{A}^{-1}, \tag{7.30}$$

$$\boldsymbol{\mu}_1 = \big(\boldsymbol{I} - \boldsymbol{A}\big)\dot{\bar{\boldsymbol{q}}}_u + \left[\frac{\partial^2 \mathcal{V}_e}{\partial \boldsymbol{\varphi}^2}\right]_q^{-1} \dot{\bar{\boldsymbol{u}}}_u, \tag{7.31}$$

$$\boldsymbol{\mu}_a = \boldsymbol{B}\big(\dot{\boldsymbol{A}}\dot{\bar{\boldsymbol{q}}}_a + \dot{\boldsymbol{\mu}}_1\big). \tag{7.32}$$

Deriving (7.23)–(7.24) with respect to time gives a relation between the two sets of velocities

$$\dot{\boldsymbol{q}} = \begin{bmatrix} \boldsymbol{A} & \boldsymbol{0} \\ \boldsymbol{0} & \boldsymbol{I} \end{bmatrix} \dot{\bar{\boldsymbol{q}}} + \begin{bmatrix} \boldsymbol{\mu}_1 \\ \boldsymbol{0} \end{bmatrix}. \tag{7.33}$$

Using (7.9) and (7.26)–(7.32), the input transforming equations, (5.57), evaluate to

$$\boldsymbol{u}_a = \boldsymbol{\mu}_a + \boldsymbol{\psi}(\boldsymbol{\varphi}) + \boldsymbol{A}\big[\bar{\boldsymbol{u}}_a - \boldsymbol{\psi}(\bar{\boldsymbol{\varphi}})\big]. \tag{7.34}$$

Theorem 5.3.6 guarantees that we can always express the $\bar{\boldsymbol{q}}$'s in terms of the $\bar{\boldsymbol{q}}$'s. Thus, we may equivalently express the $\bar{\boldsymbol{\varphi}}$'s in terms of the $\boldsymbol{\varphi}$'s such that

$$\boldsymbol{A}(\boldsymbol{\varphi}, \bar{\boldsymbol{\varphi}}) = \boldsymbol{A}\big(\boldsymbol{\varphi}, \bar{\boldsymbol{\varphi}}(\boldsymbol{\varphi})\big). \tag{7.35}$$

Using (7.25), (7.33), (7.32) and (7.35), we can write the input transformation, (7.34), purely in terms of the measurable coordinates, $\boldsymbol{q}$, and the virtual inputs

$$\boldsymbol{u} = \boldsymbol{B}\Big\{ \dot{\boldsymbol{A}}\left[\boldsymbol{A}^{-1}(\dot{\boldsymbol{q}}_a - \boldsymbol{\mu}_1)\right] + \dot{\boldsymbol{\mu}}_1 \Big\} + (\boldsymbol{I} - \boldsymbol{A})\boldsymbol{\psi}(\boldsymbol{\varphi}) + \boldsymbol{A}\big[\bar{\boldsymbol{u}}_a + \bar{\boldsymbol{u}}_u\big]. \tag{7.36}$$

The transforming process is summarized in Fig. 7.4.

The Special Case of Linear Springs

For monoarticular ASRs with linear elastic elements the transforming equations simplify significantly. Let $k_i > 0$ be the joint stiffness of the ith joint. Then, the elastic potential energy and its associated forces are given by

$$\boldsymbol{K} = \mathrm{diag}(k_1, \dots, k_{n_u}), \tag{7.37}$$

$$\mathcal{V}_e = \tfrac{1}{2}\boldsymbol{\varphi}^{\mathrm{T}}\boldsymbol{K}\boldsymbol{\varphi}, \tag{7.38}$$

$$\boldsymbol{\psi} = \boldsymbol{K}\boldsymbol{\varphi}. \tag{7.39}$$

The coordinate and input transforming equations (7.23) and (7.36) simplify to

$$\boldsymbol{q}_a = \bar{\boldsymbol{q}}_a + \boldsymbol{K}^{-1}\bar{\boldsymbol{u}}_u, \tag{7.40}$$

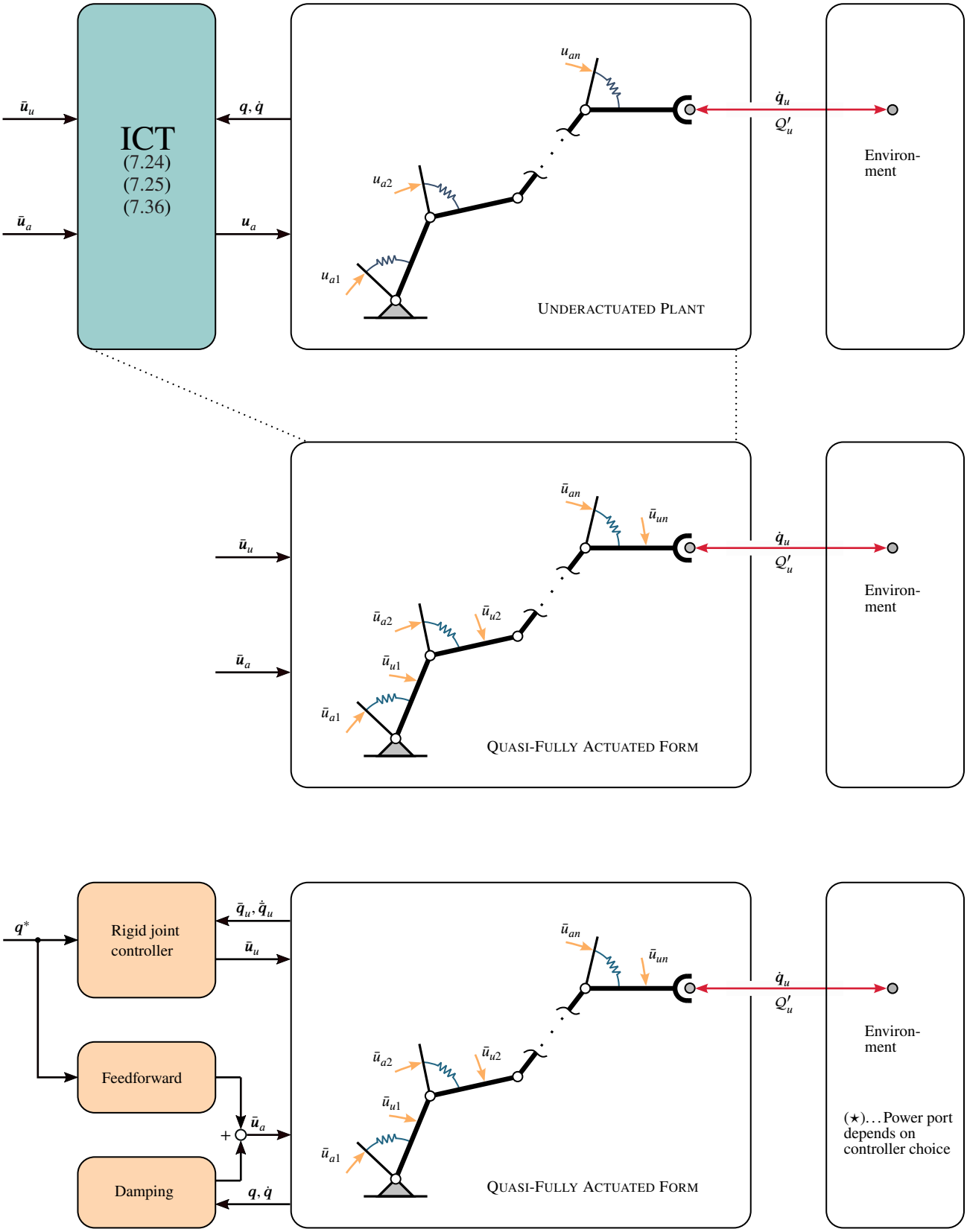

Figure 7.4: Open loop: through the input and coordinate transforming equations (ICT), the ASR can be treated as quasi-fully actuated. Closed-loop: the QFA form enables a straightforward adoption of rigid joint controllers.

and

$$\boldsymbol{u} = \boldsymbol{B}\boldsymbol{K}^{-1}\ddot{\bar{\boldsymbol{u}}}_u + \bar{\boldsymbol{u}}_u + \bar{\boldsymbol{u}}_a. \tag{7.41}$$

Task Space Formulation

An elegant solution to the task space regulation and motion tracking problems can be found by introducing a point transformation for the QFA model (7.20) that separates the moving forces into rigid robot (gravitational) and elastic forces. Let us switch from the generalized link and motor coordinates, $\bar{\boldsymbol{q}}$, to the new set of coordinates

$$\bar{\boldsymbol{x}} = (\bar{\boldsymbol{x}}_u, \bar{\boldsymbol{x}}_a) = (\bar{x}_1, \dots, \bar{x}_{n/2}, \bar{x}_{n/2+1}, \dots, \bar{x}_n) \tag{7.42}$$

where $\bar{\boldsymbol{x}}_u$ and $\bar{\boldsymbol{x}}_a$ denote the task and virtual joint deflections coordinates, respectively, such that

$$\bar{\boldsymbol{x}}_u = \boldsymbol{h}_u(\bar{\boldsymbol{q}}_u), \quad \bar{\boldsymbol{x}}_a = \bar{\boldsymbol{\varphi}} = \bar{\boldsymbol{q}}_a - \bar{\boldsymbol{q}}_u. \tag{7.43}$$

Applying (7.43) to the potential energy $\mathcal{V}$, (7.7),

$$\mathcal{V}\big(\bar{\boldsymbol{q}}(\bar{\boldsymbol{x}})\big) = \mathcal{V}_e(\bar{\boldsymbol{x}}_a) + \mathcal{V}_g\big(\boldsymbol{h}_u^{-1}(\bar{\boldsymbol{x}}_u)\big), \tag{7.44}$$

we see the desired separation into rigid robot (gravitational) and elastic potential energies. Moreover, the transformed elastic potential function $\mathcal{V}_e$ has the crucial properties that it has a unique minimum at $\bar{\boldsymbol{x}}_a = \boldsymbol{0}$, which is convenient for applying classic stability results, since they are usually concerned with the stabilization of the origin. Considering the invertibility of $\boldsymbol{J}_u$ and observing that $\partial \boldsymbol{x}_u / \partial \boldsymbol{q}_u = \partial \bar{\boldsymbol{x}}_u / \partial \bar{\boldsymbol{q}}_u$, it is easy to see that the Jacobian of the transformation (7.43),

$$\boldsymbol{J} = \frac{\partial \bar{\boldsymbol{x}}}{\partial \bar{\boldsymbol{q}}} = \begin{bmatrix} \boldsymbol{J}_u & \boldsymbol{0} \\ -\boldsymbol{I} & \boldsymbol{I} \end{bmatrix}, \tag{7.45}$$

is non singular. From the properties of task space coordinates reported in Section 7.1.1, we can further conclude the existence of the inverse coordinate transformation. Applying the point transformation (7.43) to $\bar{\Sigma}$, (7.20), give (as pointed out in Section 6.5)

$$\bar{\Sigma}_x : \ \frac{\mathrm{d}}{\mathrm{d}t}\frac{\partial \mathcal{L}}{\partial \dot{\bar{\boldsymbol{x}}}} - \frac{\partial \mathcal{L}}{\partial \bar{\boldsymbol{x}}} = \bar{\mathcal{Q}}_x, \tag{7.46}$$

or—equivalently—using the transformation rules from Section 2.5.6

$$\bar{\Sigma}_x : \ \mathcal{M}_x \ddot{\bar{\boldsymbol{x}}} + \mathcal{C}_x \dot{\bar{\boldsymbol{x}}} + \boldsymbol{J}^{-\mathrm{T}} \left[\frac{\partial \mathcal{V}}{\partial \bar{\boldsymbol{q}}}\right]^{\mathrm{T}} = \bar{\mathcal{Q}}_x, \tag{7.47}$$

where all terms are according to the definitions in Section 6.5

$$\mathcal{M}_x = \begin{bmatrix} \boldsymbol{J}^{-\mathrm{T}}(\boldsymbol{q}_u)\big[\boldsymbol{M}(\boldsymbol{q}_u) + \boldsymbol{B}\big]\boldsymbol{J}^{-1}(\boldsymbol{q}_u) & \boldsymbol{J}^{-\mathrm{T}}(\boldsymbol{q}_u)\boldsymbol{B} \\ \boldsymbol{B}\boldsymbol{J}^{-1}(\boldsymbol{q}_u) & \boldsymbol{B} \end{bmatrix} \tag{7.48}$$

$$\mathcal{C}_x = \begin{bmatrix} \boldsymbol{J}_u^{-\mathrm{T}}(\boldsymbol{q}_u)\big[\boldsymbol{M}(\boldsymbol{q}_u) + \boldsymbol{B}\big]\dot{\boldsymbol{J}}_u{}^{-1}(\boldsymbol{q}_u) + \boldsymbol{J}_u^{-\mathrm{T}}(\boldsymbol{q}_u)\boldsymbol{C}(\boldsymbol{q}_u, \dot{\boldsymbol{q}}_u)\boldsymbol{J}_u^{-1}(\boldsymbol{q}_u) & \boldsymbol{0} \\ \boldsymbol{B}\dot{\boldsymbol{J}}_u{}^{-1} & \boldsymbol{0} \end{bmatrix}. \tag{7.49}$$

In these expressions, we can identify the transformed rigid robot inertia and Coriolis/centrifugal matrices

$$\boldsymbol{M}_x = \boldsymbol{J}_u^{-\mathrm{T}}(\boldsymbol{q}_u)\boldsymbol{M}(\boldsymbol{q}_u)\boldsymbol{J}_u^{-1} \tag{7.50}$$

$$\boldsymbol{C}_x = \boldsymbol{J}^{-\mathrm{T}}(\boldsymbol{q}_u)\boldsymbol{M}(\boldsymbol{q}_u)\dot{\boldsymbol{J}}_u^{-1}(\boldsymbol{q}_u) + \boldsymbol{J}_u^{-\mathrm{T}}(\boldsymbol{q}_u)\boldsymbol{C}(\boldsymbol{q}_u, \dot{\boldsymbol{q}}_u)\boldsymbol{J}_u^{-1}(\boldsymbol{q}_u). \tag{7.51}$$

For the covariantly transforming generalized forces, we get

$$\boldsymbol{J}^{-\mathrm{T}}\left[\frac{\partial \mathcal{V}}{\partial \bar{\boldsymbol{q}}}\right]^{\mathrm{T}} = \begin{bmatrix} \boldsymbol{J}_u^{-\mathrm{T}} & \boldsymbol{J}_u^{-\mathrm{T}} \\ \boldsymbol{0} & \boldsymbol{I} \end{bmatrix} \left[\frac{\partial \mathcal{V}}{\partial \bar{\boldsymbol{q}}}\right]^{\mathrm{T}} = \begin{bmatrix} \boldsymbol{J}_u^{-\mathrm{T}} \frac{\partial \mathcal{V}_g}{\partial \bar{\boldsymbol{q}}_u} \\ \frac{\partial \mathcal{V}_e}{\partial \bar{\boldsymbol{\varphi}}} \end{bmatrix} \tag{7.52}$$

$$\bar{\mathcal{Q}}_x = \boldsymbol{J}^{-\mathrm{T}}\bar{\mathcal{Q}}. \tag{7.53}$$

From (7.52), we see that the potential forces are indeed split as desired. For later developments, it is convenient to introduce symbols for the components of (7.53)

$$\boldsymbol{v} = \boldsymbol{J}^{-\mathrm{T}}\bar{\boldsymbol{u}}, \quad \bar{\mathcal{Q}}'_x = \boldsymbol{J}^{-\mathrm{T}}\bar{\mathcal{Q}}'. \tag{7.54}$$

such that $\bar{\mathcal{Q}}_x = \boldsymbol{v} + \bar{\mathcal{Q}}'_x$.

7.2.2 Joint Space Regulation

Suppose that the control objective is to stabilize the considered ASR model at a constant equilibrium such that the outputs $\boldsymbol{q}_u$ approach a constant desired value $\boldsymbol{q}_u^*$ for $t \to \infty$. Let solve this problem using Proposition 6.2.1. Knowing that a minimum of the potential energy corresponds to a stable equilibrium point, let us choose a closed-loop potential energy function $\mathcal{V}^*$ with a unique global minimum at the desired position. In the following, two natural candidates are presented. First, we can cancel the effect of the gravity potential $\mathcal{V}_g(\bar{\boldsymbol{q}}_u)$ and replace it with a radially unbounded potential function in $\bar{\boldsymbol{q}}_u$ that has a unique minimum at $\boldsymbol{q}_u^*$. Second, we can dominate the effect of the gravity potential [178, 183]. It is widely believed that dominating instead of canceling nonlinear terms enhances robustness of the system vis-à-vis uncertainties [133].

[178]: Takegaki et al. (1981), "A new feedback method for dynamic control of manipulators"
[183]: Tomei (1991), "A simple PD controller for robots with elastic joints"
[133]: Ortega (1998), *Passivity-Based Control of Euler-Lagrange Systems: Mechanical, Electrical, and Electromechanical Applications*

Let $\tilde{\boldsymbol{q}} = \bar{\boldsymbol{q}} - \bar{\boldsymbol{q}}^*$, with $\boldsymbol{q}^* = (\boldsymbol{q}_u^*, \boldsymbol{q}_a^*)$ and $\boldsymbol{q}_u^* = \boldsymbol{q}_a^*$, be the control error. Then, a desired potential energy function for the first option may be of the form

$$\mathcal{V}^*(\bar{\boldsymbol{q}}) = \mathcal{V}_e(\bar{\boldsymbol{q}}_a - \bar{\boldsymbol{q}}_u) + \tfrac{1}{2}\tilde{\boldsymbol{q}}^{\mathrm{T}}\mathcal{K}_p\tilde{\boldsymbol{q}}, \tag{7.55}$$

where $\mathcal{K}_p = \mathcal{K}_p^{\mathrm{T}} = \mathrm{diag}(\boldsymbol{K}_{pu}, \boldsymbol{K}_{pa}) \succ 0$. It is straightforward to see that $\mathcal{V}^*$ has an unique global minimum at $\tilde{\boldsymbol{q}} = \boldsymbol{0}$ and that it is radially unbounded with respect to $\tilde{\boldsymbol{q}}$. Hence, $\mathcal{V}^*$ satisfies condition (ii) of Proposition 6.2.1. To render the equilibrium asymptotically stable, let us inject pervasive damping. Choosing the controller

$$\bar{\boldsymbol{u}} = -\left[\frac{\partial}{\partial \bar{\boldsymbol{q}}}\left\{\mathcal{V}^*(\bar{\boldsymbol{q}}) - \mathcal{V}(\bar{\boldsymbol{q}})\right\}\right]^{\mathrm{T}} - \mathcal{K}_v\dot{\tilde{\boldsymbol{q}}} = \boldsymbol{g}(\boldsymbol{q}_u) - \mathcal{K}_p\tilde{\boldsymbol{q}} - \mathcal{K}_v\dot{\tilde{\boldsymbol{q}}}, \tag{7.56}$$

where $\mathcal{K}_v = \mathrm{diag}(\boldsymbol{K}_{vu}, \boldsymbol{K}_{va}) \succ 0$, renders the equilibrium point $\tilde{\boldsymbol{q}} = \boldsymbol{0}$ globally asymptotic stability, which follows directly from invoking Proposition 6.2.1.

Regarding the second option, we can choose a desired potential energy function of the form [88]

$$\mathcal{V}^* = \mathcal{V}(\bar{\boldsymbol{q}}) - \mathcal{V}(\boldsymbol{q}^*) - \left[\frac{\partial \mathcal{V}}{\partial \bar{\boldsymbol{q}}}(\boldsymbol{q}^*)\right](\bar{\boldsymbol{q}} - \boldsymbol{q}^*) + \tfrac{1}{2}\tilde{\boldsymbol{q}}^{\mathrm{T}}\mathcal{K}_P\tilde{\boldsymbol{q}}, \tag{7.57}$$

[88]: Keppler et al. (2022), "From underactuation to quasi-full actuation: Aiming at a unifying control framework for articulated soft robots"

where $\mathcal{K}_p$ is a positive definite and symmetric matrix that can be chosen such that $\mathcal{V}^*$ becomes a strictly convex function and has a global unique minimum $\mathcal{V}^*(\bar{\boldsymbol{q}}) = 0$ at $\tilde{\boldsymbol{q}} = \boldsymbol{0}$. The proof of this statement can be found in [178]. Combining (7.56) with (7.57) globally asymptotically stabilizes the equilibrium point $\tilde{\boldsymbol{q}} = \boldsymbol{0}$, which follows directly from invoking Proposition 6.2.1. It is straightforward to verify that the resulting control signal satisfies the conditions of Theorem 5.3.6.

[178]: Takegaki et al. (1981), "A new feedback method for dynamic control of manipulators"

7.2.3 Task Space Regulation

Consider the problem of stabilizing an ASR at a constant equilibrium such that the outputs $\boldsymbol{x}_u$ approach a constant desired value $\boldsymbol{x}_u^*$ for $t \to \infty$. Knowing that a minimum of the potential energy corresponds to a stable equilibrium point, let us choose a closed-loop potential energy function $\mathcal{V}^*$ that has a unique global minimum at the desired position. To solve this problem, we shall make use of Theorem 6.2.1 and the transformation properties of the EL equations reported in Section 6.5. An elegant solution can be found by switching from the generalized link and motor coordinates, $\bar{\boldsymbol{q}}$, to the set of coordinates $\bar{\boldsymbol{x}} = (\bar{\boldsymbol{x}}_u, \bar{\boldsymbol{x}}_a)$, with $\bar{\boldsymbol{x}}_u, \bar{\boldsymbol{x}}_a \in \mathbb{R}^{n_u}$, where $\bar{\boldsymbol{x}}_u$ denotes the end effector position and the $\bar{\boldsymbol{x}}_a$ the virtual joint deflections such that

$$\bar{\boldsymbol{x}} = \bar{\boldsymbol{x}}(\bar{\boldsymbol{q}}) = \begin{bmatrix} \boldsymbol{h}_u(\bar{\boldsymbol{q}}_u) \\ \bar{\boldsymbol{q}}_a - \bar{\boldsymbol{q}}_u \end{bmatrix}, \tag{7.58}$$

where $\boldsymbol{h}_u$ is the forwards kinematic mapping (7.5). This transformation step separates the potential forces into rigid robot (gravitational) and elastic forces. Moreover, the transformed elastic potential function $\mathcal{V}_e$ has the crucial property that it has a unique minimum at $\bar{\boldsymbol{x}}_a = \boldsymbol{0}$, which is convenient for the application of classic stability results, since they are usually concerned with the stabilization of the origin.

Considering the invertibility of $\boldsymbol{J}_u$ and observing that $\partial \boldsymbol{x}_u / \partial \boldsymbol{q}_u = \partial \bar{\boldsymbol{x}}_u / \partial \bar{\boldsymbol{q}}_u$, it is easy to see that the Jacobian of the transformation (7.58),

$$\boldsymbol{J}(\bar{\boldsymbol{q}}) = \frac{\partial \bar{\boldsymbol{x}}}{\partial \bar{\boldsymbol{q}}} = \begin{bmatrix} \boldsymbol{J}_u & \boldsymbol{0} \\ -\boldsymbol{I} & \boldsymbol{I} \end{bmatrix}, \tag{7.59}$$

is non singular. Making use of the inverse coordinate transformation, we get

$$\bar{\boldsymbol{q}} = \bar{\boldsymbol{q}}(\bar{\boldsymbol{x}}) = \begin{bmatrix} \boldsymbol{h}_u^{-1}(\bar{\boldsymbol{q}}_u) \\ \boldsymbol{h}_u^{-1}(\bar{\boldsymbol{q}}_u) + \bar{\boldsymbol{x}}_a \end{bmatrix}. \tag{7.60}$$

As pointed out in Section 2.5.5, applying such transformation to $\bar{\Sigma}$, (7.20), we get

$$\bar{\Sigma}_x : \ \frac{\mathrm{d}}{\mathrm{d}t}\frac{\partial \mathcal{L}}{\partial \dot{\bar{\boldsymbol{x}}}} - \frac{\partial \mathcal{L}}{\partial \bar{\boldsymbol{x}}} = \boldsymbol{\nu} + \bar{\mathcal{Q}}'_x, \tag{7.61}$$

where

$$\boldsymbol{v} = \boldsymbol{J}^{-\mathrm{T}}\bar{\boldsymbol{u}}, \quad \mathcal{Q}'_x = \boldsymbol{J}^{-\mathrm{T}}\mathcal{Q}'. \tag{7.62}$$

For the potential energy

$$\mathcal{V}\big(\bar{\boldsymbol{q}}(\bar{\boldsymbol{x}})\big) = \mathcal{V}_e(\bar{\boldsymbol{x}}_a) + \mathcal{V}_g\big(\boldsymbol{h}_u^{-1}(\bar{\boldsymbol{x}}_u)\big), \tag{7.63}$$

we have the desired separation into rigid robot (gravitational) and elastic potential energies. Following the idea of minimizing the system shaping, and preserving the system structure, (**P4**), the separation of the potential energies allows us to identify moving forces that we want to preserve, namely the subsystem coupling forces $\frac{\partial \mathcal{V}_e}{\partial \bar{\boldsymbol{\varphi}}}$, and those, we want to cancel or dominate, that is to say the gravitational forces $\frac{\partial \mathcal{V}_g}{\partial \bar{\boldsymbol{q}}}$ that would cause a divergence of the links from the desired equilibrium. Implementing this idea and opting for the cancellation of the gravitational forces, a natural choice for the desired potential energy is

$$\mathcal{V}^*\big(\bar{\boldsymbol{q}}(\bar{\boldsymbol{x}})\big) = \mathcal{V}_e(\bar{\boldsymbol{x}}_a) + \tfrac{1}{2}(\bar{\boldsymbol{x}}_u - \boldsymbol{x}_u^*)^{\mathrm{T}}\mathcal{K}_p(\bar{\boldsymbol{x}}_u - \boldsymbol{x}_u^*). \tag{7.64}$$

where $\mathcal{K}_p = \mathcal{K}_p^{\mathrm{T}} \succ 0$. Comparing (7.63) and (7.64), it is clear that only the influence of gravity is canceled. By adding a positive definite quadratic form in the output error, we obtain a potential function that has a unique and global minimum at $\bar{\boldsymbol{x}} = (\boldsymbol{x}_u^*, \boldsymbol{0})$. To render the equilibrium asymptotically stable, let us inject damping characterized by the Rayleigh dissipation function

$$\mathcal{V}_R = \tfrac{1}{2}\Big(\dot{\bar{\boldsymbol{x}}}_u^{\mathrm{T}}\boldsymbol{K}_{vu}\dot{\bar{\boldsymbol{x}}}_u + \dot{\bar{\boldsymbol{q}}}_a^{\mathrm{T}}\boldsymbol{K}_{va}\dot{\bar{\boldsymbol{q}}}_a\Big); \quad \boldsymbol{K}_{vu}, \boldsymbol{K}_{va} \succ 0 \tag{7.65}$$

It is worth remarking that (7.61) obtained by a series of transformation from the plant model (3.22) which did not modify its dynamics. Following Proposition 6.2.1, let us now shape the system behavior

$$\boldsymbol{v} = -\left[\frac{\partial \mathcal{V}_c}{\partial \bar{\boldsymbol{x}}} + \frac{\partial \mathcal{V}_R}{\partial \dot{\bar{\boldsymbol{x}}}}\right]^{\mathrm{T}} = -\left[\frac{\partial \mathcal{V}_c}{\partial \bar{\boldsymbol{x}}}\right]^{\mathrm{T}} - \mathcal{K}_v\dot{\bar{\boldsymbol{x}}}, \tag{7.66}$$

to achieve our control objective. Recall that $\mathcal{V}_c = \mathcal{V}^* - \mathcal{V}$. The damping matrix, $\mathcal{K}_v$, associated with the Rayleigh dissipation function (7.65) can be obtained easily by applying the congruence transformation connected with the coordinate transformation $(\bar{\boldsymbol{x}}_u, \bar{\boldsymbol{q}}_a) \to (\bar{\boldsymbol{x}})$ to the quadratic form (7.65), we get

$$\mathcal{K}_v = \begin{bmatrix} \boldsymbol{K}_{vu} + \boldsymbol{J}_u^{-\mathrm{T}}\boldsymbol{K}_{va}\boldsymbol{J}_u^{-1} & \boldsymbol{J}^{-\mathrm{T}}\boldsymbol{K}_{va} \\ \boldsymbol{K}_{va}\boldsymbol{J}_u^{-1} & \boldsymbol{K}_{va} \end{bmatrix} \succ 0. \tag{7.67}$$

satisfying $\mathcal{V}_R = \frac{1}{2}\dot{\bar{\boldsymbol{x}}}^{\mathrm{T}}\mathcal{K}_v\dot{\bar{\boldsymbol{x}}}$. It remains to be shown that the resulting control input $\bar{\boldsymbol{u}}$ satisfies the conditions of Theorem 5.3.6. Considering that

$$\mathcal{V}_c = \tfrac{1}{2}(\bar{\boldsymbol{x}}_u - \boldsymbol{x}_u^*)^{\mathrm{T}}\mathcal{K}_p(\bar{\boldsymbol{x}}_u - \boldsymbol{x}_u^*) - \mathcal{V}_g\big(\boldsymbol{h}_u^{-1}(\bar{\boldsymbol{x}}_u)\big), \tag{7.68}$$

$$\frac{\partial \bar{\boldsymbol{q}}_u}{\partial \bar{\boldsymbol{q}}_u} = \frac{\partial \boldsymbol{h}_u^{-1}}{\partial \bar{\boldsymbol{q}}_u} = \frac{\partial \boldsymbol{h}_u^{-1}}{\partial \bar{\boldsymbol{x}}_u}\frac{\partial \bar{\boldsymbol{x}}_u}{\partial \bar{\boldsymbol{q}}_u} = \frac{\partial \boldsymbol{h}_u^{-1}}{\partial \bar{\boldsymbol{x}}_u}\boldsymbol{J}_u = \boldsymbol{I} \;\Rightarrow\; \frac{\partial \boldsymbol{h}_u^{-1}}{\partial \bar{\boldsymbol{x}}_u} = \boldsymbol{J}_u^{-1}, \tag{7.69}$$

$$\frac{\partial \mathcal{V}_c}{\partial \bar{\boldsymbol{x}}_u} = \boldsymbol{K}_{pu}(\bar{\boldsymbol{x}}_u - \boldsymbol{x}_u^*) - \left[\frac{\partial \mathcal{V}_g}{\partial \boldsymbol{h}_u^{-1}}\frac{\partial \boldsymbol{h}_u^{-1}}{\partial \bar{\boldsymbol{x}}_u}\right]^{\mathrm{T}} = \boldsymbol{K}_{pu}(\bar{\boldsymbol{x}}_u - \boldsymbol{x}_u^*) - \boldsymbol{J}_u^{-\mathrm{T}}\left[\frac{\partial \mathcal{V}_g}{\partial \bar{\boldsymbol{q}}_u}\right]^{\mathrm{T}}, \tag{7.70}$$

and from the transforming rule of external forces, (2.91), that

$$\bar{\boldsymbol{u}} = \boldsymbol{J}^{\mathrm{T}}\boldsymbol{v}, \tag{7.71}$$

then making the substitution (7.66) and (7.71), gives

$$\bar{\boldsymbol{u}}_u = \left[\frac{\partial \mathcal{V}_g}{\partial \bar{\boldsymbol{q}}_u}\right]^{\mathrm{T}} - \boldsymbol{J}_u^{\mathrm{T}}\left\{\boldsymbol{K}_{pu}(\bar{\boldsymbol{x}}_u - \boldsymbol{x}_u^*) + \boldsymbol{K}_{vu}\dot{\bar{\boldsymbol{x}}}_u\right\}, \tag{7.72}$$

$$\bar{\boldsymbol{u}}_a = -\boldsymbol{K}_{va}\dot{\bar{\boldsymbol{q}}}_a. \tag{7.73}$$

From (7.72) and (7.73), it is evident that the conditions on the virtual inputs in Theorem 5.3.6 are satisfied. Thus, we may invoke Proposition 6.2.1 to conclude asymptotic stability $\bar{\boldsymbol{x}} = (\boldsymbol{x}_u^*, \boldsymbol{0})$ in the absence of external forces, i.e. $\mathcal{Q}' = \boldsymbol{0}$. Notice that $\bar{\boldsymbol{u}}_u$ is simply a PD plus gravity cancellation controller for rigid robots that is formulated in task coordinates, while $\bar{\boldsymbol{u}}_a$ ensures pervasive damping.

Dominating but Canceling Gravity Terms

Analogous to the joint-space controller in Section 7.2.2, we can dominate but cancel the gravitational forces. The separation of the potential energies into rigid robot and elastic ones in (7.63), simplifies the adoption of the gravity domination controller [178]. Choosing the desired potential energy function

[178]: Takegaki et al. (1981), "A new feedback method for dynamic control of manipulators"

$$\mathcal{V}^*(\bar{\boldsymbol{x}}) = \mathcal{V}(\bar{\boldsymbol{x}}) - \mathcal{V}(\boldsymbol{x}^*) - \left[\frac{\partial \mathcal{V}}{\partial \bar{\boldsymbol{x}}}(\boldsymbol{x}^*)\right](\bar{\boldsymbol{x}} - \boldsymbol{x}^*) + \tfrac{1}{2}\tilde{\boldsymbol{x}}_u^{\mathrm{T}}\boldsymbol{\mathcal{K}}_p\tilde{\boldsymbol{x}}_u, \tag{7.74}$$

gives the desired result. Proposition 6.2.1 guarantees asymptotic stability of the equilibrium $\bar{\boldsymbol{x}} = (\boldsymbol{x}_u^*, \boldsymbol{0})$.

7.2.4 Joint Space Motion Tracking

This section presents a series of control methods, namely ESP, ESP+, ESPi and ESPi+ control, to solve the motion tracking problem for monoarticular ASRs, while simultaneously allowing to

- ESP: inject link-side damping to suppress link vibrations away from the reference trajectory
- ESPi: inject a link compliance behavior to adjust the interaction behavior and the convergence rate towards the reference trajectory.

Uniform global asymptotic stability is shown by invoking a theorem by Matrosov. These approaches were first introduced in [86, 89, 90]. The central idea is to preserve the inertial properties and the elastic structure of the original plant dynamics, hence the name Elastic Structure Preserving (ESP) control. Compared to ESP control, ESP+ control aims at further minimizing the dynamics shaping on the motor side. This is done by avoiding the scaling of the motor inertia to constant values in the new coordinates, which is a non-passive control action for itself. In the following, these controllers are re-derived in an unifying form through Theorem 5.6.1. This theorem allows us to transform the time-independent (autonomous) Lagrangian associated with the open-loop system, $\mathcal{L}$, to a time-dependent (non-autonomous) Lagrangian, $\bar{\mathcal{L}}$, that encodes the structure of the desired closed-loop dynamics. The time-dependency

[86]: Keppler et al. (2018), "Elastic structure preserving (ESP) control for compliantly actuated robots"
[89]: Keppler et al. (2016), "A passivity-based approach for trajectory tracking and link-side damping of compliantly actuated robots"
[90]: Keppler et al. (2016), "A passivity-based controller for motion tracking and damping assignment for compliantly actuated robots"

of the Lagrangian $\bar{\mathcal{L}}$ enters through the time-dependency of the potential function that gives rise to the subsystem coupling force. The explicit time-dependency of the coupling force is crucial for solving the motion tracking problem. Throughout this section, we assume the following.

Assumption 7.2.3 *The desired trajectory $\boldsymbol{q}_u^*(t)$ is bounded and four times continuously differentiable.*

The tracking error is denoted by

$$\tilde{\boldsymbol{q}} = (\tilde{\boldsymbol{q}}_u, \tilde{\boldsymbol{q}}_a); \quad \tilde{\boldsymbol{q}}_u = \bar{\boldsymbol{q}}_u - \boldsymbol{q}_u^*(t); \quad \tilde{\boldsymbol{q}}_a = \bar{\boldsymbol{q}}_a. \tag{7.75}$$

ESP/ESPi Control: Joint Space Formulation

The results presented below are based on [86]. Following the design principles in Fig. 7.1, and inspired by the work [144], which reports an extension of the "natural motion" concept [98] to the motion tracking case, we aim for a PD+ like error dynamics which has been proposed in [86]

$$\mathcal{M}(\boldsymbol{q}_u)\ddot{\tilde{\boldsymbol{q}}} + \left[\mathcal{C}(\boldsymbol{q}_u, \dot{\boldsymbol{q}}_u) + \mathcal{K}_v\right]\dot{\tilde{\boldsymbol{q}}} + \mathcal{K}_p\tilde{\boldsymbol{q}} = \boldsymbol{\Psi}(\bar{\boldsymbol{q}}_a - \tilde{\boldsymbol{q}}_u) + \bar{\mathcal{Q}}, \tag{7.76}$$

with $\mathcal{K}_p = \operatorname{diag}(\boldsymbol{K}_{pu}, \boldsymbol{K}_{pa})$ and $\mathcal{K}_v = \operatorname{diag}(\boldsymbol{K}_{vu}, \boldsymbol{K}_{va}) \succ 0$, where[1]

$$\begin{aligned} \boldsymbol{K}_{pa} &= \boldsymbol{K}_{pa}^{\mathrm{T}} \succ 0, \ \boldsymbol{K}_{pu} = \boldsymbol{0}, \quad \text{for } ESP, \\ \boldsymbol{K}_{pu} &= \boldsymbol{K}_{pu}^{\mathrm{T}} \succ 0, \ \boldsymbol{K}_{pa} = \boldsymbol{0}, \quad \text{for } ESPi. \end{aligned} \tag{7.77}$$

The form of the transformed external force $\bar{\mathcal{Q}}$ is yet to be determined. The central difference compared to the error dynamics in [144] is the additional term $\boldsymbol{\psi}(\bar{\boldsymbol{\varphi}})$. Note that (7.76) matches the open loop system, (7.14), closely. The modifications are: 1) the gravity terms are canceled, 2) PD terms are added, 3) pseudo-feedforward terms are added. The modifications 1) and 2) follow closely the idea of natural motion control, whereas 3) is mandatory to achieve global asymptotic motion tracking.

Let us derive a control input that achieves equivalence of (7.14) and (7.76). To this end, let us start with transforming (7.14) into the QFA form

$$\bar{\Sigma}: \ \mathcal{M}\ddot{\bar{\boldsymbol{q}}} + C\dot{\bar{\boldsymbol{q}}} + \boldsymbol{g}(\boldsymbol{q}_u) - \boldsymbol{\Psi}(\bar{\boldsymbol{q}}_a - \tilde{\boldsymbol{q}}_u) = \bar{\boldsymbol{u}} + \bar{\mathcal{Q}}' \tag{7.78}$$

Notice the explicit time dependency of the subsystem coupling force $\boldsymbol{\psi}$ through $\tilde{\boldsymbol{q}}_u$. Introducing

$$\bar{\boldsymbol{\varphi}} = \bar{\boldsymbol{q}}_a - \tilde{\boldsymbol{q}}_u = \bar{\boldsymbol{q}}_a - [\bar{\boldsymbol{q}}_u - \boldsymbol{q}_u^*(t)], \tag{7.79}$$

$$\bar{\mathcal{V}}(\bar{\boldsymbol{q}}, t) = \bar{\mathcal{V}}_e\big(\bar{\boldsymbol{q}}_a - [\bar{\boldsymbol{q}}_u - \boldsymbol{q}_u^*(t)]\big) + \mathcal{V}_g(\bar{\boldsymbol{q}}_u), \tag{7.80}$$

$$\bar{\mathcal{L}}_a(\bar{\boldsymbol{q}}, \dot{\bar{\boldsymbol{q}}}, t) = \mathcal{T}_a(\bar{\boldsymbol{q}}_a, \dot{\bar{\boldsymbol{q}}}_a) + \bar{\mathcal{V}}(\bar{\boldsymbol{q}}, t), \tag{7.81}$$

we observe that

$$\frac{\partial \bar{\mathcal{V}}_e}{\partial \bar{\boldsymbol{\varphi}}} = \boldsymbol{\psi}^{\mathrm{T}}(\bar{\boldsymbol{\varphi}}), \tag{7.82}$$

$$\frac{\partial \bar{\mathcal{L}}_a}{\partial \bar{\boldsymbol{q}}_u} = -\frac{\partial \bar{\mathcal{V}}}{\partial \bar{\boldsymbol{q}}_u} = -\frac{\partial \bar{\mathcal{V}}_e}{\partial \bar{\boldsymbol{\varphi}}}\frac{\partial \bar{\boldsymbol{\varphi}}}{\partial \bar{\boldsymbol{q}}_u} - \frac{\partial \mathcal{V}_g}{\partial \bar{\boldsymbol{q}}_u} = \left[\boldsymbol{\psi}(\bar{\boldsymbol{\varphi}}) - \boldsymbol{g}(\bar{\boldsymbol{q}}_u)\right]^{\mathrm{T}} \tag{7.83}$$

[86]: Keppler et al. (2018), "Elastic structure preserving (ESP) control for compliantly actuated robots"

[144]: Paden et al. (1988), "Globally asymptotically stable "PD+" controller for robot manipulators"

[98]: Koditschek (1984), "Natural motion for robot arms"

[86]: Keppler et al. (2018), "Elastic structure preserving (ESP) control for compliantly actuated robots"

1: Note that it is also possible to choose both $\boldsymbol{K}_{pa}, \boldsymbol{K}_{pu} \succ 0$. This would result in a closed-loop dynamics that resembles the classical PD+ dynamics even closer.

[144]: Paden et al. (1988), "Globally asymptotically stable "PD+" controller for robot manipulators"

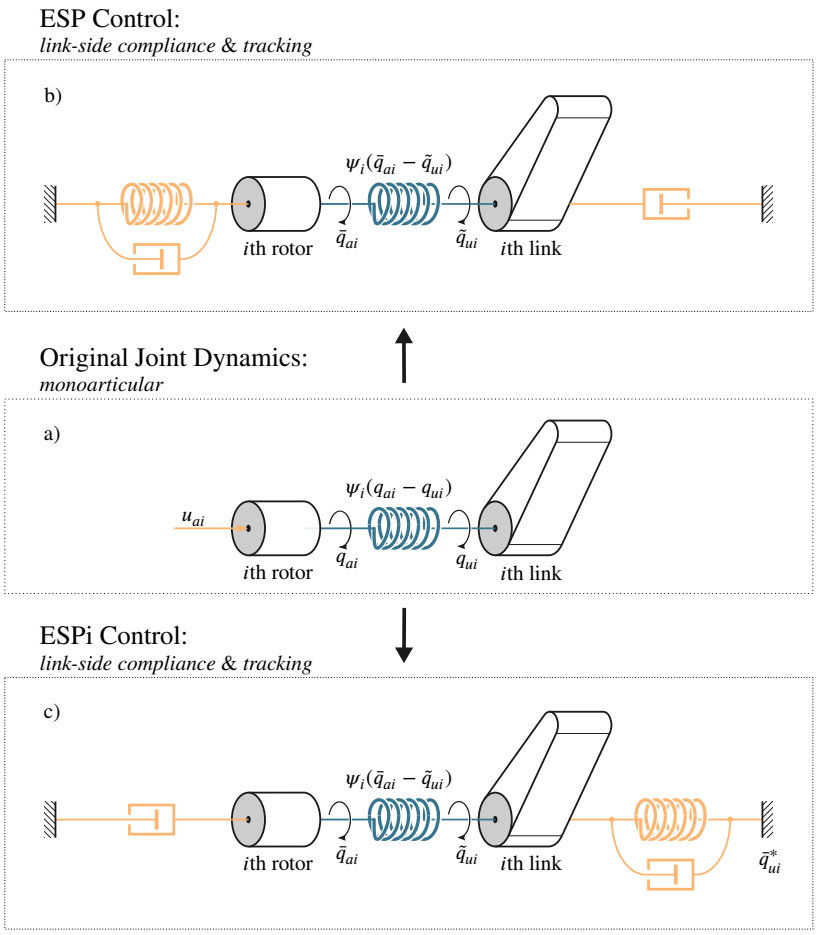

q_{ai} … motor coord. q_{ui} … link coord. q^*_{ui} … desired link position
$\bar{q}_{ai}$ … virtual motor coord. $\bar{q}_{ui}$ … link coord. $\tilde{q}_{ui} \triangleq q_{ui} - q^*_{ui}(t)$ … tracking error

Figure 7.5: Closed loops: the QFA form enables a straightforward adoption of rigid joint controllers.

Seeing that (7.83) produces the potential forces in (7.78), and knowing from Section 2.5.1 that the force of inertia in (7.14) is uniquely determined by the kinetic energy function $\mathcal{T}$, we conclude that the forces of inertia in (7.14) and (7.78) are determined by the same kinetic energy function, $\mathcal{T}$, such that

$$\frac{\mathrm{d}}{\mathrm{d}t}\left[\frac{\partial \mathcal{T}}{\partial \dot{\bar{\boldsymbol{q}}}}\right]^{\mathrm{T}} - \left[\frac{\partial \mathcal{T}}{\partial \bar{\boldsymbol{q}}}\right]^{\mathrm{T}} = \mathcal{M}(\bar{\boldsymbol{q}}_u)\ddot{\bar{\boldsymbol{q}}} + C(\bar{\boldsymbol{q}}_u, \dot{\bar{\boldsymbol{q}}}_u)\dot{\bar{\boldsymbol{q}}}. \tag{7.84}$$

Considering (7.83) and (7.84), it is clear that (7.78) are the EL equations associated with the Lagrangian

$$\bar{\mathcal{L}} = \mathcal{L}_u + \bar{\mathcal{L}}_a. \tag{7.85}$$

and the generalized external forces $\bar{\boldsymbol{u}}$ and $\bar{\mathcal{Q}}'$. Since

$$\frac{\partial^2 \bar{\mathcal{L}}_a}{\partial \dot{\bar{\boldsymbol{q}}}_a^2} = \frac{\partial^2 \mathcal{T}_a}{\partial \dot{\bar{\boldsymbol{q}}}_a^2} = \boldsymbol{B} \succ 0, \tag{7.86}$$

$$\left[\boldsymbol{Y}\right]^{-1}_{\bar{q}} = \left[\frac{\partial^2 \bar{\mathcal{L}}_a}{\partial \bar{\boldsymbol{q}}_a \partial \bar{\boldsymbol{q}}_u}\right] = \frac{\partial}{\partial \bar{\boldsymbol{q}}_a}\boldsymbol{\psi}(\bar{\boldsymbol{\varphi}}) = \frac{\partial \boldsymbol{\psi}}{\partial \boldsymbol{\varphi}} = \frac{\partial^2 \bar{\mathcal{V}}_e}{\partial \bar{\boldsymbol{\varphi}}^2} \succ 0, \tag{7.87}$$

it follows that the Lagrangian $\bar{\mathcal{L}}$ satisfies the conditions of Theorem 5.6.1. Thus, applying the input and coordinate transforming equations (5.155) and (5.136) to (7.14), we obtain (7.76). The transformed external force evaluate

according to (5.153) to

$$\bar{\mathcal{Q}}' = \operatorname{diag}\big(\boldsymbol{I}, \bar{\boldsymbol{R}}\big)\mathcal{Q}'. \tag{7.88}$$

Using (7.79), the coordinate transforming equations (5.136) evaluate to

$$\boldsymbol{\psi}(\boldsymbol{\varphi}) = \boldsymbol{\psi}(\bar{\boldsymbol{\varphi}}) + \bar{\boldsymbol{u}}_u, \tag{7.89}$$

and the components of the input transformation (5.155) are

$$\bar{\boldsymbol{A}} = \big[\boldsymbol{Y}\big]_q^{-1}\big[\bar{\boldsymbol{Y}}\big]_{\bar{q}}, \tag{7.90}$$

$$\bar{\boldsymbol{R}} = \bar{\boldsymbol{A}}^{-1}, \tag{7.91}$$

$$\bar{\boldsymbol{\mu}}_1 = (\boldsymbol{I} - \bar{\boldsymbol{A}})\dot{\bar{\boldsymbol{q}}}_u + \dot{\boldsymbol{q}}_u^* + \left[\frac{\partial^2 \mathcal{V}_e}{\partial \bar{\boldsymbol{\varphi}}^2}\right]_q^{-1} \dot{\bar{\boldsymbol{u}}}_u, \tag{7.92}$$

$$\bar{\boldsymbol{\mu}}_2 = \boldsymbol{B}\big(\bar{\boldsymbol{A}}\dot{\bar{\boldsymbol{q}}}_a + \dot{\bar{\boldsymbol{\mu}}}_1\big), \tag{7.93}$$

After some tedious manipulations, the input transformation (5.155) can be written as

$$\boldsymbol{u}_a = \bar{\boldsymbol{\mu}}_2 + \boldsymbol{\psi}(\boldsymbol{\varphi}) + \bar{\boldsymbol{A}}^{-1}\big[\bar{\boldsymbol{u}}_a - \boldsymbol{\psi}(\bar{\boldsymbol{\varphi}})\big]. \tag{7.94}$$

A detailed derivation of (7.94) is provided in Appendix B.6. Comparing (7.94) with (7.94), we see that only the "pseudo" Jacobian was replaced by the new one $\bar{\boldsymbol{A}}$. Denoting the PD+ controller proposed in [144] by

[144]: Paden et al. (1988), "Globally asymptotically stable "PD+" controller for robot manipulators"

$$\boldsymbol{u}_{\text{PD+}} = \boldsymbol{M}(\bar{\boldsymbol{q}}_u)\ddot{\boldsymbol{q}}_u^* + \boldsymbol{C}(\bar{\boldsymbol{q}}_u, \dot{\bar{\boldsymbol{q}}}_u)\dot{\boldsymbol{q}}_u^* + \boldsymbol{g}_u(\bar{\boldsymbol{q}}_u) - \boldsymbol{K}_{vu}\dot{\bar{\boldsymbol{q}}}_u - \boldsymbol{K}_{pu}\tilde{\boldsymbol{q}}_u, \tag{7.95}$$

we can achieve equivalence of (7.76) and (7.78) with

$$\bar{\boldsymbol{u}}_u = \bar{\boldsymbol{u}}_{\text{PD+}}, \tag{7.96}$$

$$\bar{\boldsymbol{u}}_a = \boldsymbol{B}\ddot{\bar{\boldsymbol{q}}}_a - \boldsymbol{K}_{va}\dot{\bar{\boldsymbol{q}}}_a - \boldsymbol{K}_{pa}\bar{\boldsymbol{q}}_a. \tag{7.97}$$

Notice that depending whether the ESP or ESPi controller shall be implemented, the position gains have to be set according to (7.77). The final controller constituted by (7.77) and (7.94)–(7.97) is the ESP controller introduced in [86], c.f. (46) therein. The ESP controller only injects damping on the subsystem $\bar{\Sigma}_u$ and cancels the effect of gravity. The ESPi controller on the other hands, enables imposing a desired compliance behavior, characterized by $\boldsymbol{K}_{pu}$ and $\boldsymbol{K}_{vu}$, on Σ_u, while also canceling the effect of gravity. The ESPi variant solving the joint-space motion tracking problem has not been published yet. Both controllers achieve GAS of the equilibrium point $(\tilde{\boldsymbol{q}}, \dot{\tilde{\boldsymbol{q}}}) = \boldsymbol{0}$.

[86]: Keppler et al. (2018), "Elastic structure preserving (ESP) control for compliantly actuated robots"

Including Motor Inertia Shaping Scaling the motor inertia to lower values [6] can improve control performance since it also scales down–by an equal factor–disturbances on the actuated subsystem such as friction. Let us replace the inertia matrix and the kinetic energy function in (7.81) with

$$\bar{\boldsymbol{B}} = \alpha \boldsymbol{B};\ \alpha \in \mathbb{R}^+ \setminus \{0\}, \tag{7.98}$$

$$\bar{\mathcal{T}}_a = \bar{\mathcal{T}}_a(\bar{\boldsymbol{q}}_a, \dot{\bar{\boldsymbol{q}}}_a) = \tfrac{1}{2}\dot{\bar{\boldsymbol{q}}}^{\mathrm{T}}\bar{\mathcal{M}}\dot{\bar{\boldsymbol{q}}}. \tag{7.99}$$

such that the inertia matrix of the total system is given by

$$\bar{\mathcal{M}} = \text{diag}\big(\boldsymbol{M}, \bar{\boldsymbol{B}}\big). \tag{7.100}$$

It is straightforward to show that the new Lagrangian

$$\bar{\mathcal{L}} = \mathcal{L}_u + \bar{\mathcal{L}}_a, \tag{7.101}$$

with $\bar{\mathcal{L}}_a = \bar{\mathcal{T}}_a - \bar{\mathcal{V}}$ satisfies the conditions of Theorem 5.6.1, and the QFA representation associated with (7.101) is given by the EL equations

$$\bar{\mathcal{M}}\ddot{\tilde{\boldsymbol{q}}} + \bar{C}\dot{\tilde{\boldsymbol{q}}} + \boldsymbol{g}(\bar{\boldsymbol{q}}_u) = \boldsymbol{\psi}(\bar{\boldsymbol{q}}_a - \tilde{\boldsymbol{q}}_u) + \bar{\boldsymbol{u}} + \bar{\mathcal{Q}}'. \tag{7.102}$$

[6]: Albu-Schäffer et al. (2007), "A Unified Passivity-based control framework for position, torque and impedance control of flexible joint robots"

In conclusion, we can encode the process of shaping the motor inertia [6] directly in the formulation the desired subsystem Lagrangian $\bar{\mathcal{L}}_a$. In contrast to the non-shaping case above, instead of (7.91), we have that

$$\bar{\boldsymbol{R}} = \bar{\boldsymbol{B}}\bar{\boldsymbol{A}}^{-1}\boldsymbol{B}^{-1} = \alpha\bar{\boldsymbol{A}}^{-1}, \tag{7.103}$$

and the input transformation (5.155) evaluates to

$$\boldsymbol{u}_a = \bar{\boldsymbol{\mu}}_2 + \boldsymbol{\psi}(\boldsymbol{\varphi}) + \tfrac{1}{\alpha}\bar{\boldsymbol{A}}\big[\bar{\boldsymbol{u}}_a - \boldsymbol{\psi}(\bar{\boldsymbol{\varphi}})\big]. \tag{7.104}$$

Comparing (7.94) with (7.104), we see that the process of motor inertia shaping scales the last last feedback term by a factor of $1/\alpha$. Modifying (7.97) to consider the shaped motor inertia

$$\bar{\boldsymbol{u}}_a = \bar{\boldsymbol{B}}\ddot{\bar{\boldsymbol{q}}}_a - \boldsymbol{K}_{va}\dot{\bar{\boldsymbol{q}}}_a - \boldsymbol{K}_{pa}\bar{\boldsymbol{q}}_a. \tag{7.105}$$

in the feedforward term, and applying (7.96) and (7.105) to (7.102), we obtain the desired reference dynamics

$$\bar{\mathcal{M}}(\boldsymbol{q}_u)\ddot{\tilde{\boldsymbol{q}}} + \big[\bar{C}(\boldsymbol{q}_u, \dot{\boldsymbol{q}}_u) + \mathcal{K}_v\big]\dot{\tilde{\boldsymbol{q}}} + \mathcal{K}_p\tilde{\boldsymbol{q}} - \boldsymbol{\Psi}(\bar{\boldsymbol{q}}_a - \tilde{\boldsymbol{q}}_u) = \bar{\mathcal{Q}}', \tag{7.106}$$

where $\bar{\mathcal{Q}}'$ are the transform external forces of the form (7.88) with (7.103). The following proposition summarizes the main results of this section.

Proposition 7.2.1 (ESP/ESPi control—joint-space motion tracking) *Consider the system* (7.14) *in closed-loop with the controller* (7.95),(7.96), (7.104) *and* (7.105). *Then*

(i) for $\mathcal{Q}' = \mathbf{0}$, *the equilibrium point* $(\tilde{\boldsymbol{q}}, \dot{\tilde{\boldsymbol{q}}}) = \mathbf{0}$ *of the closed-loop dynamics,* (7.106), *is globally uniformly asymptotically stable;*

(ii) system (7.106) *defines an OSP map* $\bar{\mathcal{Q}}' \mapsto \dot{\tilde{\boldsymbol{q}}}$, *with the transformed external force* $\bar{\mathcal{Q}}'$ *according to* (7.88) *with* (7.103).

Notice that the closed-loop systems (7.76) and (7.106) are equivalent for $\alpha = 1$. Thus, Proposition 7.2.1 also holds for (7.76).

Considering that the closed loop dynamics (7.106) is a special case of the closed loop dyanmics considered in Proposition 7.2.3 (reported later) only a proof for the latter proposition provided.

ESP+ Control—Joint-Space Motion Tracking

The results presented in this section were first presented in [86, 90]. The ESP+ control concept extends the idea of the minimalistic ESP feedback control formulated above. The idea is to avoid scaling the motor inertias to constant values after being transformed into the $\bar{\boldsymbol{q}}$ space. Considering the transforming rules of a point transformation nevertheless, it appears natural to aim for a closed-loop system that is characterized by the inertia matrix

[86]: Keppler et al. (2018), "Elastic structure preserving (ESP) control for compliantly actuated robots"
[90]: Keppler et al. (2016), "A passivity-based controller for motion tracking and damping assignment for compliantly actuated robots"

$$\bar{\mathcal{M}} = \mathcal{A}^{-\mathrm{T}}\mathcal{M}\mathcal{A}^{-1} = \mathrm{diag}\big(\boldsymbol{M}(\bar{\boldsymbol{q}}_u), \bar{\boldsymbol{A}}^{\mathrm{T}}\boldsymbol{B}\bar{\boldsymbol{A}}\big), \tag{7.107}$$

where $\mathcal{A}$ can be identified as a "pseudo" Jacobian. In order to preserve the critical skew-symmetry property reported in Lemma 2.5.8, we know that according to the rules of a point transformation the transformed Coriolis/centrifugal matrix must satisfy, c.f. (2.110),

$$\bar{\mathcal{C}} = \mathcal{A}^{-\mathrm{T}}\big(\mathcal{M}\dot{\mathcal{A}}^{-1} + \mathcal{C}\mathcal{A}^{-1}\big). \tag{7.108}$$

This aspect is critical for the stability proof of Proposition 7.2.3 in Section 7.5.

Lemma 7.2.2 (Skew-symmetry property of the ESP+ error dynamics) *Consider the matrices* (7.107) *and* (7.108)*, then* $\dot{\bar{\mathcal{M}}} - 2\bar{\mathcal{C}}$ *is skew symmetric. Further,* $\bar{\mathcal{M}}$ *is symmetric and positive definite.*

Proof. Introducing

$$\bar{\boldsymbol{B}} = \bar{\boldsymbol{A}}^{\mathrm{T}}\boldsymbol{B}\bar{\boldsymbol{A}}^{-1}; \quad \bar{\boldsymbol{C}}_a = \bar{\boldsymbol{A}}^{\mathrm{T}}\boldsymbol{B}\dot{\bar{\boldsymbol{A}}}, \tag{7.109}$$

such that

$$\bar{\mathcal{M}} = \mathrm{diag}\big(\boldsymbol{M}, \bar{\boldsymbol{B}}\big); \quad \bar{\mathcal{C}} = \mathrm{diag}(\boldsymbol{C}, \bar{\boldsymbol{C}}_a), \tag{7.110}$$

we observe that

$$\boldsymbol{B} = \boldsymbol{B}^{\mathrm{T}} \;\Rightarrow\; \dot{\bar{\boldsymbol{B}}} = \dot{\bar{\boldsymbol{A}}}^{\mathrm{T}}\boldsymbol{B}\bar{\boldsymbol{A}} + \bar{\boldsymbol{A}}^{\mathrm{T}}\boldsymbol{B}\dot{\bar{\boldsymbol{A}}} = \bar{\boldsymbol{C}}_a^{\mathrm{T}} + \bar{\boldsymbol{C}}_a, \tag{7.111}$$

Using (7.111), we can show the skew symmetry of $\dot{\bar{\boldsymbol{B}}} - 2\bar{\boldsymbol{C}}_a$

$$\dot{\bar{\boldsymbol{B}}} - 2\bar{\boldsymbol{C}}_a = \bar{\boldsymbol{C}}_a^{\mathrm{T}} - \bar{\boldsymbol{C}}_a = \big(-\bar{\boldsymbol{C}}_a^{\mathrm{T}} + \bar{\boldsymbol{C}}_a\big)^{\mathrm{T}} = -\big(\bar{\boldsymbol{C}}_a^{\mathrm{T}} - \bar{\boldsymbol{C}}_a\big)^{\mathrm{T}}. \tag{7.112}$$

From Property 6 and (7.120), it follows immediately that $\dot{\bar{\mathcal{M}}} - 2\bar{\mathcal{C}}$ is skew symmetric. Since $\mathcal{M}$ and $\bar{\mathcal{M}}$ are related via a congruence transformation, (7.107), the positive definiteness and symmetry of $\mathcal{M}$ is preserved. Former can be shown establishing a lower bound for the eigenvalues of $\bar{\boldsymbol{B}}$ and $\mathcal{M}$. Concerning the rigid robot inertia matrix $\mathcal{M}$ this is true by Assumption 5.1.1. Knowing that $\boldsymbol{B}$ and $\boldsymbol{A}$ are Hermitian and non-negative, we can write $\bar{\boldsymbol{B}}$ as the product of two positive definite Hermitian matrices and repetitively apply Lemma D.3.3 in Appendix D to obtain

$$\underline{\lambda}(\bar{\boldsymbol{B}}) = \underline{\lambda}\big(\big[\bar{\boldsymbol{A}}^{\mathrm{T}}\boldsymbol{B}^{1/2}\big]\big[\boldsymbol{B}^{1/2}\bar{\boldsymbol{A}}\big]\big) \geq \Big[\underline{\lambda}\big(\bar{\boldsymbol{A}}^{\mathrm{T}}\boldsymbol{B}^{1/2}\big)\Big]^2 \geq \Big[\underline{\lambda}(\bar{\boldsymbol{A}})\underline{\lambda}(\boldsymbol{B}^{1/2})\Big]^2 > 0. \tag{7.113}$$

■

As pointed out in Section 2.5.5, see also (2.91), the generalized external forces transform covariantly under a point transformation. Motivated by the observations so far, let us aim for an error dynamics of the form (first proposed in [86, 90])

[86]: Keppler et al. (2018), "Elastic structure preserving (ESP) control for compliantly actuated robots"
[90]: Keppler et al. (2016), "A passivity-based controller for motion tracking and damping assignment for compliantly actuated robots"

$$\bar{\mathcal{M}}(\boldsymbol{q}_u)\ddot{\tilde{\boldsymbol{q}}} + \left[\bar{C}(\boldsymbol{q}_u, \dot{\boldsymbol{q}}_u) + \mathcal{K}_v\right]\dot{\tilde{\boldsymbol{q}}} + \mathcal{K}_p\tilde{\boldsymbol{q}} - \boldsymbol{\psi}(\bar{\boldsymbol{q}}_a - \tilde{\boldsymbol{q}}_u) = \bar{\mathcal{Q}}', \tag{7.114}$$

with $\mathcal{K}_p = \operatorname{diag}(\boldsymbol{0}, \boldsymbol{K}_{pa})$, $\boldsymbol{K}_{pa} \succ 0$ and $\mathcal{K}_v = \operatorname{diag}(\boldsymbol{K}_{vu}, \boldsymbol{K}_{va}) \succ 0$, and the transformed external force

$$\bar{\mathcal{Q}}' = \mathcal{A}^{-\mathrm{T}}\mathcal{Q}'. \tag{7.115}$$

Introducing the Lagrangian

$$\begin{aligned}
&&(7.116)\\
\bar{\mathcal{T}}_a =& \bar{\mathcal{T}}_a(\bar{\boldsymbol{q}}_a, \dot{\bar{\boldsymbol{q}}}_a) = \tfrac{1}{2}\dot{\bar{\boldsymbol{q}}}_a\bar{\boldsymbol{B}}\dot{\bar{\boldsymbol{q}}}_a, &(7.117)\\
\bar{\mathcal{L}}_a =& \bar{\mathcal{T}}_a - \bar{\mathcal{V}}, &(7.118)\\
\bar{\mathcal{L}} =& \mathcal{L}_u + \bar{\mathcal{L}}_a, &(7.119)
\end{aligned}$$

with $\bar{\mathcal{V}}$ defined as in (7.80), and $\bar{\mathcal{L}}_a$ satisfying Assumption 5.6.1, we can apply the coordinate and input transforming equations (5.136) and (5.155), together with $\bar{\boldsymbol{u}}_u$ and $\bar{\boldsymbol{u}}_a$ as defined in (7.96) and (7.97), to achieve equivalence of (7.14) and (7.114). The input transformation evaluates to

$$\boldsymbol{u}_a = \boldsymbol{B}\boldsymbol{\mu}_1 + \boldsymbol{\psi}(\boldsymbol{\varphi}) + \bar{\boldsymbol{A}}^{-\mathrm{T}}\left(\bar{\boldsymbol{u}}_a - \boldsymbol{\psi}(\bar{\boldsymbol{\varphi}})\right) \tag{7.120}$$

[86]: Keppler et al. (2018), "Elastic structure preserving (ESP) control for compliantly actuated robots"
[90]: Keppler et al. (2016), "A passivity-based controller for motion tracking and damping assignment for compliantly actuated robots"

The resulting input signal $\boldsymbol{u}_a$ is equal to the one presented in [86, 90]. Comparing (7.120) with the previous input transformations (7.34), (7.94), and (7.104), we see that the compensation term $\boldsymbol{B}\bar{\boldsymbol{A}}\dot{\bar{\boldsymbol{q}}}_a$ is missing in the latter one, which confirms our objective for ESP+ control of shaping the motor dynamics less compared to the original ESP formulation. Further notice that the closed-loop EL equations (7.76), (7.106) and (7.114) only differ in their formulation of $\mathcal{T}_a$. The following proposition summarizes the main results of this section.

Proposition 7.2.3 (ESP+/ESPi+ control—joint-space motion tracking) *Consider the system* (7.14) *in closed-loop with the controller* (7.95),(7.96), (7.104) *and* (7.105)*. Then*

(i) for $\mathcal{Q}' = \boldsymbol{0}$, the equilibrium point $(\tilde{\boldsymbol{q}}, \dot{\tilde{\boldsymbol{q}}}) = \boldsymbol{0}$ of the closed-loop dynamics, (7.106)*, is globally uniformly asymptotically stable;*
(ii) system (7.106) *defines an OSP map $\bar{\mathcal{Q}}' \mapsto \ddot{\tilde{\boldsymbol{q}}}$, with the transformed external force $\bar{\mathcal{Q}}'$ according to* (7.88)*.*

A proof for statement (i) is provided in Section 7.5, and statement (ii) is treated below. Notice that the ESP closed-loop dynamics (7.106) can be considered as a special case of the ESP+ control related closed-loop dynamics (7.114) with constant motor inertia $\bar{\boldsymbol{B}} = \alpha\boldsymbol{B}$ and $\bar{\boldsymbol{C}}_a = \boldsymbol{0}$.

Passivity Analysis In the following, a proof of Statement (ii) of Proposition 7.2.1 is presented. Further, it will be shown that the closed-loop system (7.114) can be represented as the negative feedback interconnection of two subsystems $\bar{\Sigma}_u$ (constituted by the link inertias) and $\bar{\Sigma}_a$ (constituted by the

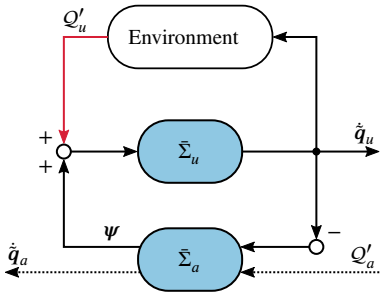

Figure 7.6: Representation of the closed-loop dynamics as the negative feedback interconnection of two passive subsystems.

rotor inertias). Introducing the subsystem storage functions

$$S_u(\tilde{\boldsymbol{q}}_u, \dot{\tilde{\boldsymbol{q}}}_u, t) = \tfrac{1}{2}\dot{\tilde{\boldsymbol{q}}}_u^{\mathrm{T}} \boldsymbol{M} \dot{\tilde{\boldsymbol{q}}}_u, \tag{7.121}$$

$$S_a(\tilde{\boldsymbol{q}}, \dot{\tilde{\boldsymbol{q}}}_a, t) = \tfrac{1}{2}\left(\dot{\bar{\boldsymbol{q}}}_a^{\mathrm{T}} \bar{\boldsymbol{B}} \dot{\bar{\boldsymbol{q}}}_a + \bar{\boldsymbol{q}}_a^{\mathrm{T}} \boldsymbol{K}_{pa} \bar{\boldsymbol{q}}_a\right) + \mathcal{V}_e(\bar{\boldsymbol{q}}_a - \tilde{\boldsymbol{q}}_u), \tag{7.122}$$

and using Property 6, we get for their time derivatives along the solutions of (7.114):[2]

$$\dot{S}_u = -\dot{\tilde{\boldsymbol{q}}}_u^{\mathrm{T}} \boldsymbol{K}_{vu} \dot{\tilde{\boldsymbol{q}}}_u + \dot{\tilde{\boldsymbol{q}}}_u^{\mathrm{T}} \boldsymbol{\psi} + \dot{\tilde{\boldsymbol{q}}}_u^{\mathrm{T}} \bar{\mathcal{Q}}'_u, \tag{7.123}$$

$$\dot{S}_a = -\dot{\bar{\boldsymbol{q}}}_a^{\mathrm{T}} \boldsymbol{K}_{va} \dot{\bar{\boldsymbol{q}}}_a - \dot{\bar{\boldsymbol{q}}}_u^{\mathrm{T}} \boldsymbol{\psi} + \dot{\bar{\boldsymbol{q}}}_a^{\mathrm{T}} \mathcal{Q}'_a. \tag{7.124}$$

2: In the following, the argument of the virtual generalized elastic force, $\boldsymbol{\psi}(\bar{\boldsymbol{q}}_a - \tilde{\boldsymbol{q}}_u)$, is dropped.

We can identify three terms in (7.123). The first one represents the energy dissipation due to the damping assignment on the link side. The latter two terms are interconnection ports. As visualized in Fig. 7.6, the port $\dot{\tilde{\boldsymbol{q}}}_u^{\mathrm{T}} \boldsymbol{\psi}$ interconnects the subsystems $\bar{\Sigma}_u$ and $\bar{\Sigma}_a$, and the port $\dot{\tilde{\boldsymbol{q}}}_u^{\mathrm{T}} \bar{\mathcal{Q}}_u$ represents the energy exchange between the links and the environment. The first term on the RHS of (7.124) can be identified with actuator-side dissipation. As expected, the subsystem interconnection port appears again in (7.124). We conclude that the closed-loop system can be represented as the negative feedback interconnection of two passive subsystems, as shown Fig. 7.6,

$$\bar{\Sigma}_u : \ \left(\boldsymbol{\psi} + \mathcal{Q}'_u\right) \mapsto \dot{\tilde{\boldsymbol{q}}}_u, \tag{7.125}$$

$$\bar{\Sigma}_a : \ \begin{bmatrix} \mathcal{Q}'_a \\ -\dot{\tilde{\boldsymbol{q}}}_a \end{bmatrix} \mapsto \begin{bmatrix} \dot{\tilde{\boldsymbol{q}}}_u \\ \boldsymbol{\psi} \end{bmatrix}. \tag{7.126}$$

The analysis so far motivates the introduction of the storage function

$$S = S_u + S_a. \tag{7.127}$$

Considering (7.123) and (7.124), we get for its time derivative

$$\dot{S} = -\dot{\tilde{\boldsymbol{q}}}_u^{\mathrm{T}} \boldsymbol{K}_{vu} \dot{\tilde{\boldsymbol{q}}}_u - \dot{\bar{\boldsymbol{q}}}_a^{\mathrm{T}} \boldsymbol{K}_{va} \dot{\bar{\boldsymbol{q}}}_a + \dot{\tilde{\boldsymbol{q}}}^{\mathrm{T}} \bar{\mathcal{Q}}' \leq \dot{\tilde{\boldsymbol{q}}}^{\mathrm{T}} \bar{\mathcal{Q}}', \tag{7.128}$$

which completes the proof of Statement (ii) of Proposition 7.2.1.

Remark 7.2.1 From (7.123) it is clear that motions associated with the virtual motors may exchange energy with the environment via the port $\dot{\boldsymbol{q}}_v^{\mathrm{T}} \mathcal{Q}_2$. A closer look on the natural power ports, $\dot{\boldsymbol{q}}_a^{\mathrm{T}} \mathcal{Q}_a$ and $\dot{\boldsymbol{q}}_v^{\mathrm{T}} \mathcal{Q}_a$, reveals that these power flows are connected to the motions of the reflected motor inertias. Considering that these mechanical elements are encapsulated in housings and thus shielded from the environment, we conclude that $\mathcal{Q}'_a$, and consequently $\bar{\mathcal{Q}}'_a$, essentially comprise friction related forces only. In

order to achieve satisfactory performance in practice, it is advisable to compensate friction forces with appropriate observers, e.g. [34]. This point is of particular importance for schemes that shape the intrinsic dynamics to a minimal extend (such as ESP control) and, thus, result in low gain designs. If friction is not compensated, then static friction translates into significant steady-state errors. After this compensation step, we may conclude that all practically meaningful interactions with the environment occur via the mechanical link-side interaction port.
Note that for the regulation case, i.e. $\boldsymbol{q}_u^* = const.$, Proposition 7.2.3 states: the closed-loop system (7.106) defines a passive map $\mathcal{Q}_u \mapsto \dot{\tilde{\boldsymbol{q}}}_u$. Nevertheless, in practice situations may arise where passivity with respect to the power port $(\dot{\tilde{\boldsymbol{q}}}_u, \mathcal{Q}_u)$ will be of importance. More specifically, there exist situations where the environment or the interacting object moves synchronously to the link reference trajectory. One such scenario would be object manipulation on a conveyor belt. In that case, the proposed tracking controlled robot would passively interact with the object.

[34]: De Luca et al. (2006), "Collision detection and safe reaction with the DLR-III lightweight manipulator arm"

Remark 7.2.2 It is worth remarking that the ESP+ design can be easily combined with motor inertia shaping by modifying the motor inertia matrix in the formulation of the kinetic energy $\mathcal{T}_a$ in (7.117) accordingly. See also [86] for a strategy not relying on the QFA representation as intermediary step.

7.2.5 Task Space Motion Tracking

For solving the task space motion tracking problem, we shall proceed similarly to the joint space motion tracking problem reported in Section 7.2.4. Let us start with some observations that will simplify attacking the problem.

Recall that for solving the joint space motion tracking problem, we relied on Theorem 5.6.1 to transform the open-loop system (7.14), characterized by a time-independent (autonomous) Lagrangian function, $\mathcal{L}(\boldsymbol{q}, \dot{\boldsymbol{q}})$, into a QFA representation characterized by a time-dependent (non-autonomous) Lagrangian function $\bar{\mathcal{L}}(\bar{\boldsymbol{q}}, \dot{\bar{\boldsymbol{q}}}, t)$, with the time-dependency entering through the formulation of a time-dependent potential function $\bar{\mathcal{V}}_e$ to facilitate motion tracking of $\bar{\Sigma}_u$. An explicitly time-dependent Lagrangian is usually cumbersome to work with when designing a stabilizing controller (e.g. conservation laws no longer apply [52]). In particular, it can be challenging to find a Lyapunov function for a system with a time-independent elastic potential function. This inconvenience can be resolved by introducing an appropriate change of coordinates. The idea behind such a transformation is captured by the remark below.

[52]: Goldstein et al. (2001), *Classical Mechanics*

Remark 7.2.3 An essential technique for solving difficult problems in Hamiltonian and Lagrangian mechanics is deriving invariants for non-autonomous systems through time-dependent canonical transformations [175]. For example, applying the *time-dependent point transformation*

$$\bar{\boldsymbol{\varphi}} = \bar{\boldsymbol{q}}_a - \left[\bar{\boldsymbol{q}}_u - \bar{\boldsymbol{q}}_u^*(t)\right] \tag{7.129}$$

would transform the time-dependent, (non-autonomous) Lagrangian $\bar{\mathcal{L}}$ in

[175]: Struckmeier et al. (2002), "Canonical transformations and exact invariants for time-dependent Hamiltonian systems"

(7.85), to a time-independent, (autonomous) Lagrangian, since

$$\bar{\mathcal{V}}_e(\tilde{\boldsymbol{q}}, t) = \mathcal{V}_e\big(\bar{\boldsymbol{q}}_a - \big[\bar{\boldsymbol{q}}_u - \bar{\boldsymbol{q}}_u^*(t)\big]\big) = \mathcal{V}_e(\bar{\boldsymbol{\varphi}}). \tag{7.130}$$

In conclusion, by introducing appropriate coordinates, we can avoid introducing a time-dependent potential energy for solving the motion tracking problem.

Following the idea in Remark 7.2.3, we can solve the tracking problem without introducing a time-dependent potential function by applying the change of coordinates (7.43), which is repeated for ease of reference,

$$\bar{\boldsymbol{x}} = (\bar{\boldsymbol{x}}_u, \bar{\boldsymbol{x}}_a); \quad \bar{\boldsymbol{x}}_u = \boldsymbol{h}_u(\bar{\boldsymbol{q}}_u); \quad \bar{\boldsymbol{x}}_a = \bar{\boldsymbol{q}}_a - \bar{\boldsymbol{q}}_u, \tag{7.131}$$

$$\boldsymbol{J} = \begin{bmatrix} \boldsymbol{J}_u & \boldsymbol{0} \\ -\boldsymbol{I} & \boldsymbol{I} \end{bmatrix}, \tag{7.132}$$

$$\dot{\bar{\boldsymbol{x}}} = \boldsymbol{J}(\bar{\boldsymbol{q}})\dot{\bar{\boldsymbol{q}}}, \tag{7.133}$$

to (7.14). The resulting EL equations are (7.46). Let

$$\boldsymbol{x}^*(t) = \big(\boldsymbol{x}_u^*(t), \boldsymbol{x}_a^*(t)\big) = \big(x_{u1}^*(t), \dots, x_{un_u}^*(t), 0, \dots, 0\big), \tag{7.134}$$

$$\tilde{\boldsymbol{x}} \quad = \big(\tilde{\boldsymbol{x}}_u, \tilde{\boldsymbol{x}}_a\big) = \boldsymbol{x} - \boldsymbol{x}^*(t), \tag{7.135}$$

denote the desired trajectory and the tracking error of the QFA system $\bar{\Sigma}_x$ which satisfies the following.

Assumption 7.2.4 *The desired trajectory $\boldsymbol{x}_u^*(t)$ is bounded up to it fourth order time derivative.*

Moreover, it is convenient to introduce the following relations

$$\dot{\tilde{\boldsymbol{q}}}_a \quad = \dot{\tilde{\boldsymbol{x}}}_a \quad + \boldsymbol{J}_u^{-1}\dot{\tilde{\boldsymbol{x}}}_u, \tag{7.136}$$

$$\dot{\tilde{\boldsymbol{q}}}_a^*(t) = \dot{\boldsymbol{x}}_a^*(t) + \boldsymbol{J}_u^{-1}\dot{\boldsymbol{x}}_u^*(t) = \boldsymbol{J}_u^{-1}\dot{\boldsymbol{x}}_u^*(t), \tag{7.137}$$

$$\dot{\tilde{\boldsymbol{q}}}_a \quad = \dot{\tilde{\boldsymbol{q}}}_a \quad - \dot{\tilde{\boldsymbol{q}}}_a^* = \dot{\tilde{\boldsymbol{q}}}_a - \boldsymbol{J}_u^{-1}\dot{\boldsymbol{x}}_u^*(t). \tag{7.138}$$

Before formulating the error dynamics, we shall specify the desired damping behavior.

Damping Injection

Suppose that we want to inject damping on the rigid body and motor dynamics such that the dissipation function is given by

$$\mathcal{V}_D = \tfrac{1}{2}\big(\dot{\tilde{\boldsymbol{x}}}_u^{\mathrm{T}}\boldsymbol{K}_{vu}\dot{\tilde{\boldsymbol{x}}}_u + \dot{\tilde{\boldsymbol{q}}}_a^{\mathrm{T}}\boldsymbol{K}_{va}\dot{\tilde{\boldsymbol{q}}}_a\big); \quad \boldsymbol{K}_{vu}, \boldsymbol{K}_{va} \succ 0. \tag{7.139}$$

The first term represents the energy dissipation of rigid body subsystem as a function of its task space velocity, and the latter term describes the energy loss rate of the motor dynamics in terms of the virtual motor velocities. In order to inject damping according to the dissipation function (7.139), let us establish the damping matrix associated with the $\bar{\boldsymbol{x}}$ coordinates. Using the Jacobians (7.6) and (7.132) associated with the change of coordinates (7.5)

and (7.131), we get

$$\mathcal{V}_D = \tfrac{1}{2}\dot{\tilde{\boldsymbol{q}}}^{\mathrm{T}}\mathrm{diag}(\boldsymbol{J}_u^{\mathrm{T}}, \boldsymbol{I})\mathrm{diag}(\boldsymbol{K}_{vu}, \boldsymbol{K}_{va})\mathrm{diag}(\boldsymbol{J}_u, \boldsymbol{I})\dot{\tilde{\boldsymbol{q}}} \tag{7.140}$$

$$= \tfrac{1}{2}\dot{\tilde{\boldsymbol{x}}}^{\mathrm{T}}\boldsymbol{J}^{-\mathrm{T}}\mathrm{diag}(\boldsymbol{J}_u^{\mathrm{T}}\boldsymbol{K}_{vu}\boldsymbol{J}_u, \boldsymbol{K}_{va})\boldsymbol{J}^{-1}\dot{\tilde{\boldsymbol{x}}} \tag{7.141}$$

which reveals that the quested damping matrix is of the form

$$\mathcal{K}_v = \boldsymbol{J}^{-\mathrm{T}}\begin{bmatrix}\boldsymbol{J}_u^{\mathrm{T}}\boldsymbol{K}_{vu}\boldsymbol{J}_u & \boldsymbol{0}\\ \boldsymbol{0} & \boldsymbol{K}_{va}\end{bmatrix}\boldsymbol{J}^{-1}. \tag{7.142}$$

Since $\mathcal{K}_v$ is related via congruence transformation to the positive definite matrix associated with the quadratic form (7.139), it is positive definite.

ESPi Control: Task Space Formulation

Similar to the joint space case, we aim for a PD+ like error dynamics

$$\mathcal{M}_x\ddot{\tilde{\boldsymbol{x}}} + \big(\mathcal{C}_x + \mathcal{K}_v\big)\dot{\tilde{\boldsymbol{x}}} + \mathcal{K}_p\tilde{\boldsymbol{x}} + \boldsymbol{J}^{-\mathrm{T}}\left[\frac{\partial \mathcal{V}_e}{\partial \bar{\boldsymbol{q}}}\right]^{\mathrm{T}} = \mathcal{Q}'_x, \tag{7.143}$$

as indicated in Fig. 7.7 with $\mathcal{K}_v$ as defined in (7.139) and

$$\mathcal{K}_p = \mathrm{diag}(\boldsymbol{K}_{pu}, \boldsymbol{0}), \quad \boldsymbol{K}_{pu} \succ 0. \tag{7.144}$$

Equivalence of (7.46) and (7.143) is achieved by the control signals

$$\bar{\boldsymbol{u}}_u = \boldsymbol{J}_u^{\mathrm{T}}\big(\boldsymbol{M}_x\ddot{\boldsymbol{x}}_u^* + \boldsymbol{C}_x\dot{\boldsymbol{x}}_u^* - \boldsymbol{K}_{vu}\dot{\tilde{\boldsymbol{x}}}_u - \boldsymbol{K}_{pu}\tilde{\boldsymbol{x}}_u\big) + \frac{\partial \mathcal{V}_g}{\partial \bar{\boldsymbol{q}}_u}, \tag{7.145}$$

$$\bar{\boldsymbol{u}}_a = \boldsymbol{B}\ddot{\bar{\boldsymbol{q}}}_a^* - \boldsymbol{K}_{va}\dot{\bar{\boldsymbol{q}}}_a. \tag{7.146}$$

System (7.143) defines an OSP operator $\bar{\mathcal{Q}}' \mapsto \dot{\tilde{\boldsymbol{x}}}$, which can be shown with the storage function

$$\mathcal{H}_{\mathrm{pd+}} = \tfrac{1}{2}\big(\dot{\tilde{\boldsymbol{x}}}^{\mathrm{T}}\mathcal{M}_x\dot{\tilde{\boldsymbol{x}}} + \tilde{\boldsymbol{x}}^{\mathrm{T}}\mathcal{K}_p\tilde{\boldsymbol{x}}\big) + \mathcal{V}_e(\bar{\boldsymbol{\varphi}}). \tag{7.147}$$

The proof is straightforward. Knowing that $\mathcal{M}_x$ and $\mathcal{C}_x$ satisfy Property 2.5.8, differentiating (7.147) with respect to time along the solutions of (7.143) gives

$$\dot{\mathcal{H}}_{\mathrm{pd+}} = -\dot{\tilde{\boldsymbol{x}}}^{\mathrm{T}}\mathcal{K}_v\dot{\tilde{\boldsymbol{x}}} + \dot{\tilde{\boldsymbol{x}}}^{\mathrm{T}}\bar{\mathcal{Q}}'_x. \tag{7.148}$$

Note that $\bar{\boldsymbol{u}}_u$ is equal to the PD+ control signal solving the tracking problem for the rigid-joint robot case. Control input $\bar{\boldsymbol{u}}_a$ has a clear physical interpretation. The vector $\ddot{\bar{\boldsymbol{q}}}_a^*$ represents the desired task accelerations expressed in joint space. Thus, the first term in $\bar{\boldsymbol{u}}_a$ can be identified as the feedforward term ensuring that the motor inertias accelerate synchronously with the link inertias. The second term adds damping to eliminate any error between the actual and desired motor velocities. In summary, we simply set $\bar{\boldsymbol{u}}_u$ equal to the classic PD+ controller. The second control input $\bar{\boldsymbol{u}}_a$, implements motor-side feedforward forces and injects additional damping to render the closed-loop system fully damped. The following proposition reports the most general passivity and stability result concerning motion tracking via the ESP concept. The following proposition summarizes the main results of this section.

ESPi Control:
Task space compliance & tracking

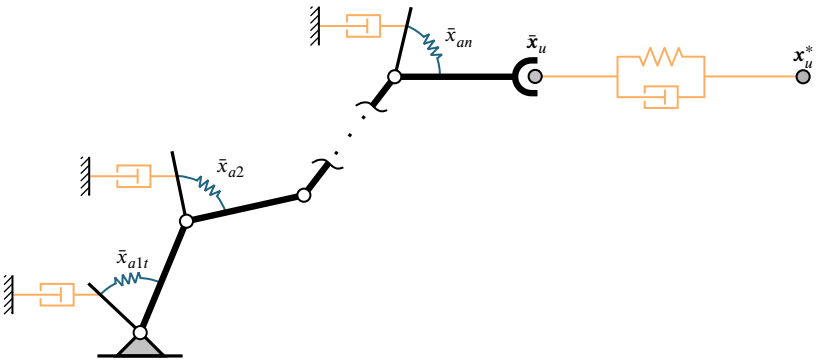

Figure 7.7: ESPi closed-loop dynamics for the task space motion tracking problem.

Proposition 7.2.4 (Task-space tracking via ESP/ESPi control) *Consider the QFA representation* (7.46) *of* (7.14) *in closed-loop with the controller* (7.34), (7.145) *and* (7.146). *Then*

(i) for $\mathcal{Q}' = \mathbf{0}$, *the equilibrium point* $(\tilde{\boldsymbol{x}}, \dot{\tilde{\boldsymbol{x}}}) = \mathbf{0}$ *of the closed-loop dynamics,* (7.106), *is uniformly asymptotically stable;*
(ii) system (7.106) *defines an OSP map* $\bar{\mathcal{Q}}'_x \mapsto \dot{\tilde{\boldsymbol{x}}}$.

A proof is provided in Section 7.5. Notice that the control law above can be easily extended to include motor inertia shaping following the procedure in Section 7.2.4, and using Theorem 5.6.1 with input transformation (7.104) instead of the one associated with Theorem 5.3.6, (7.34). Proposition 7.2.4 equally holds in that case. The proof only needs to be adjusted to account for the shaped motor inertia matrix in the formulation of the Lyapunov function (and storage function).

Adopting the Slotine and Li Controller

Motivated by [165], let us introduce the error signal

[165]: Slotine et al. (1988), "Adaptive manipulator control: A case study"

$$\boldsymbol{s} = \dot{\tilde{\boldsymbol{x}}} + \boldsymbol{\Lambda}\tilde{\boldsymbol{x}}, \tag{7.149}$$

with

$$\tilde{\boldsymbol{x}} = \boldsymbol{x} - \boldsymbol{x}^*(t), \tag{7.150}$$
$$\boldsymbol{x}^* = \big(\boldsymbol{x}_u^*(t), \mathbf{0}\big), \tag{7.151}$$

and aim for a closed-loop dynamics of the form[3]

3: A similar closed-loop dynamics is reported in [133, p. 103], which treats the joint-space motion tracking case.

$$\mathcal{M}_x\dot{\boldsymbol{s}} + \big(\mathcal{C}_x + \mathcal{K}_v\big)\boldsymbol{s} + \boldsymbol{J}^{-\mathrm{T}}\left[\frac{\partial \mathcal{V}_e}{\partial \bar{\boldsymbol{q}}}\right]_{\bar{q}}^{\mathrm{T}} = \bar{\mathcal{Q}}' + \boldsymbol{\Psi}, \tag{7.152}$$

with $\mathcal{K}_v = \mathcal{K}_v^{\mathrm{T}} \succ 0$ as defined in (7.142) and

$$\boldsymbol{\Lambda} = \mathrm{diag}(\boldsymbol{\Lambda}_u, \boldsymbol{\Lambda}_a) \succ 0. \tag{7.153}$$

The key observation here is that (7.152) defines an OSP operator $\boldsymbol{\Psi} + \bar{\mathcal{Q}}' \mapsto \boldsymbol{s}$ [22] with the storage function

[22]: Byrnes et al. (1991), "Passivity, feedback equivalence, and the global stabilization of minimum phase nonlinear systems"

$$\mathcal{H}_s = \tfrac{1}{2}\boldsymbol{s}^{\mathrm{T}}\mathcal{M}_x\boldsymbol{s} + \mathcal{V}_e(\bar{\boldsymbol{\varphi}}). \tag{7.154}$$

The difference to the fully-actuated case is the presence of the subsystem coupling potential energy $\mathcal{V}_e$, which can be shaped (as pointed out in Theorem 5.6.1), but not entirely canceled. Calculating the time derivative of (7.154) along the solutions of (7.152) yields

$$\dot{\mathcal{H}}_s = -\boldsymbol{s}^{\mathrm{T}}\mathcal{K}_v\boldsymbol{s} - \bar{\boldsymbol{\varphi}}^{\mathrm{T}}\boldsymbol{\Lambda}_a\boldsymbol{J}^{-\mathrm{T}}\left[\frac{\partial\mathcal{V}_e}{\partial\bar{\boldsymbol{q}}}\right]^{\mathrm{T}} + \boldsymbol{s}^{\mathrm{T}}\big(\boldsymbol{\Psi} + \bar{\mathcal{Q}}'\big). \tag{7.155}$$

[133]: Ortega (1998), *Passivity-Based Control of Euler-Lagrange Systems: Mechanical, Electrical, and Electromechanical Applications*

Consequently, for $\boldsymbol{\Psi} = \boldsymbol{0}$, we have $\boldsymbol{s} \in \mathcal{L}_2$, c.f. [133]. Introducing the reference positions and velocities

$$\dot{\boldsymbol{x}}_r = \dot{\boldsymbol{x}}^* - \boldsymbol{\Lambda}\tilde{\boldsymbol{x}}, \tag{7.156}$$

a straightforward calculation shows that (7.46) and (7.152) are equivalent if

$$\boldsymbol{\Psi} = \boldsymbol{J}^{-\mathrm{T}}\bar{\boldsymbol{u}} - \left(\mathcal{M}_x\ddot{\boldsymbol{x}}_r + \mathcal{C}_x\dot{\boldsymbol{x}}_r + \boldsymbol{J}^{-\mathrm{T}}\left[\frac{\partial\mathcal{V}_g}{\partial\bar{\boldsymbol{q}}}\right]^{\mathrm{T}} - \mathcal{K}_v\boldsymbol{s}\right). \tag{7.157}$$

[170]: Spong (1990), "Control of flexible joint robots: A survey"

In order to adopt the core idea behind the strict Lyapunov function presented in [170], which relies on diagonal gain matrices, we assume diagonal $\boldsymbol{K}_{vu}$ and $\boldsymbol{K}_{va}$. The control signal setting $\boldsymbol{\Psi} = \boldsymbol{0}$

$$\bar{\boldsymbol{u}} = \boldsymbol{J}^{\mathrm{T}}\big(\mathcal{M}_x\ddot{\boldsymbol{x}}_r + \mathcal{C}_x\dot{\boldsymbol{x}}_r - \mathcal{K}_v\boldsymbol{s}\big) + \left[\frac{\partial\mathcal{V}_g}{\partial\bar{\boldsymbol{q}}}\right]^{\mathrm{T}} \tag{7.158}$$

achieves the desired motion tracking behavior. Let us proceed verifying if the input signal $\bar{\boldsymbol{u}}_u$ satisfies the conditions of Theorem 5.3.6. Knowing that $\dot{\boldsymbol{q}}_a = \boldsymbol{J}_u^{-1}\dot{\boldsymbol{x}}_u + \dot{\boldsymbol{x}}_a$, it is natural to introduce the motor reference velocities

$$\dot{\boldsymbol{q}}_a^r = \boldsymbol{J}_u^{-1}\dot{\boldsymbol{x}}_u^r + \dot{\boldsymbol{x}}_a^r. \tag{7.159}$$

Using (7.159), we observe that

$$\boldsymbol{B}\boldsymbol{J}_u^{-1}\dot{\boldsymbol{x}}_u^r + \dot{\boldsymbol{B}}\dot{\boldsymbol{J}}_u^{-1}\dot{\boldsymbol{x}}_u^r = \boldsymbol{B}\frac{\mathrm{d}}{\mathrm{d}t}\big(\boldsymbol{J}_u^{-1}\dot{\boldsymbol{x}}_u^r\big), \tag{7.160}$$

$$\boldsymbol{B}\frac{\mathrm{d}}{\mathrm{d}t}\big(\boldsymbol{J}_u^{-1}\dot{\boldsymbol{x}}_u^r\big) + \boldsymbol{B}\ddot{\boldsymbol{x}}_a^r = \boldsymbol{B}\ddot{\boldsymbol{q}}_a^r. \tag{7.161}$$

[165]: Slotine et al. (1988), "Adaptive manipulator control: A case study"

Using the notation from 7.2.1, it is convenient to denote the Slotine and Li controller [165] that solves the motion tracking problem for rigid robots by

$$\boldsymbol{u}_r = \boldsymbol{J}^{\mathrm{T}}\big(\boldsymbol{M}_x\ddot{\boldsymbol{x}}_u^r + \boldsymbol{C}_x\dot{\boldsymbol{x}}_u^r - \boldsymbol{K}_{vu}\boldsymbol{s}_u\big) + \boldsymbol{g}(\boldsymbol{q}_u). \tag{7.162}$$

Then, considering (7.159)–(7.161) and the partitioning $\dot{\boldsymbol{x}}_r = (\dot{\boldsymbol{x}}_u^r, \dot{\boldsymbol{x}}_a^r)$, $\dot{\boldsymbol{x}}_u^r, \dot{\boldsymbol{x}}_a^r \in \mathbb{R}^{n_u}$, we can write the components of $\bar{\boldsymbol{u}}$ as

$$\bar{\boldsymbol{u}}_u = \bar{\boldsymbol{u}}_r, \tag{7.163}$$

$$\bar{\boldsymbol{u}}_a = \boldsymbol{B}\ddot{\boldsymbol{x}}_a^r - \boldsymbol{K}_{va}\big(\boldsymbol{J}^{-1}\boldsymbol{s}_u + \boldsymbol{s}_a\big). \tag{7.164}$$

Since $\bar{\boldsymbol{u}}_u$ is only a function of the position and velocity of subsystem Σ_u, it is clear that $\bar{\boldsymbol{u}}_u$ satisfies the conditions of Theorem 5.3.6. The main result of this section is summarized in the following Proposition 7.2.5

Proposition 7.2.5 (Task-space tracking via Slotine & Li Controller) *Consider the system* (7.14) *in closed-loop with the controller* (7.34)*,* (7.158)*. Then, the closed-loop system constituted by* (7.149) *and* (7.152)*, with* $\boldsymbol{\Psi} = \mathbf{0}$*,*

(i) has the trivial equilibrium $(\tilde{\boldsymbol{x}}, \boldsymbol{s}) = \mathbf{0}$ *for* $\mathcal{Q}' = \mathbf{0}$*, which is asymptotically stable;*
(ii) system (7.143) *defines an OSP map* $\bar{\mathcal{Q}}' \mapsto \boldsymbol{s}$*.*

7.3 Multiarticular Articulated Soft Robots

This section studies the application of the QFA transformation, introduced in Chapter 5, to multiarticulated ASRs implemented with bi-antagonistic stiffness variation arrangements. Experimental results concerning the application of ESP control to BAVS actuators (of DLR David) are reported in Chapter 11.

7.3.1 Joint Space Regulation

Consider the set of coordinates

$$\boldsymbol{q} = (\boldsymbol{q}_u, \boldsymbol{q}_a) = (q_{u1}, \dots, q_{un_u}, q_{a11}, \dots, q_{a1n_u}, q_{a21}, \dots, q_{a2n_u}) \tag{7.165}$$

with an obvious partitioning $\boldsymbol{q}_a = (\boldsymbol{q}_{a1}, \boldsymbol{q}_{a2})$, where $\boldsymbol{q}_u$ and $\boldsymbol{q}_a$ represent the link and motor configuration variables. Suppose that there is no inertial coupling between the actuated and unactuated subsystems such that the Lagrangian is of the form:[4]

4: In other words, the system satisfies the Assumption 4.6.1.

$$\mathcal{L} = \mathcal{L}_u(\boldsymbol{q}_u, \dot{\boldsymbol{q}}_u) + \mathcal{L}_a(\boldsymbol{q}, \dot{\boldsymbol{q}}_a), \tag{7.166}$$
$$\mathcal{V} = \mathcal{V}_g(\boldsymbol{q}_u) + \mathcal{V}_e(\boldsymbol{q}), \tag{7.167}$$
$$\mathcal{T} = \mathcal{T}_u(\boldsymbol{q}_u, \dot{\boldsymbol{q}}_u) + \mathcal{T}_a(\boldsymbol{q}_a, \dot{\boldsymbol{q}}_a), \tag{7.168}$$
$$\mathcal{T}_u = \tfrac{1}{2}\dot{\boldsymbol{q}}_u^{\mathrm{T}} \boldsymbol{M} \dot{\boldsymbol{q}}_u, \;\; \mathcal{T}_a = \tfrac{1}{2}\dot{\boldsymbol{q}}_a^{\mathrm{T}} \boldsymbol{B} \dot{\boldsymbol{q}}_a, \tag{7.169}$$

where $\boldsymbol{M}$ denotes the rigid robot inertia matrix, and $\boldsymbol{B}$ is a diagonal matrix containing the reflected motor inertias. Let us further assume the following for the elastic potential energy.

Assumption 7.3.1 *Let* q_{ui}, q_{a1i}, q_{a2i} *be the coordinates associated with the ith joint as depicted in Fig. 7.8, and let the elastic potential energy be given by the radially unbounded functions*

$$\mathcal{V}_{ej}(\boldsymbol{q}_{aj} - \boldsymbol{q}_u) = \sum_{i}^{n_u} \mathcal{V}_{eji}(q_{aji} - q_{ui}), \quad j \in (1, 2) \tag{7.170}$$
$$\mathcal{V}_e(\boldsymbol{q}) = \mathcal{V}_{e1} + \mathcal{V}_{e2}. \tag{7.171}$$

Denoting the joint deflections by $\varphi_j = q_{aji} - q_{ui}$*, we further assume that*

$$\psi_{ji}(\varphi_{ji}) = \frac{\partial \mathcal{V}_{ej}}{\partial \varphi_{ji}} \tag{7.172}$$

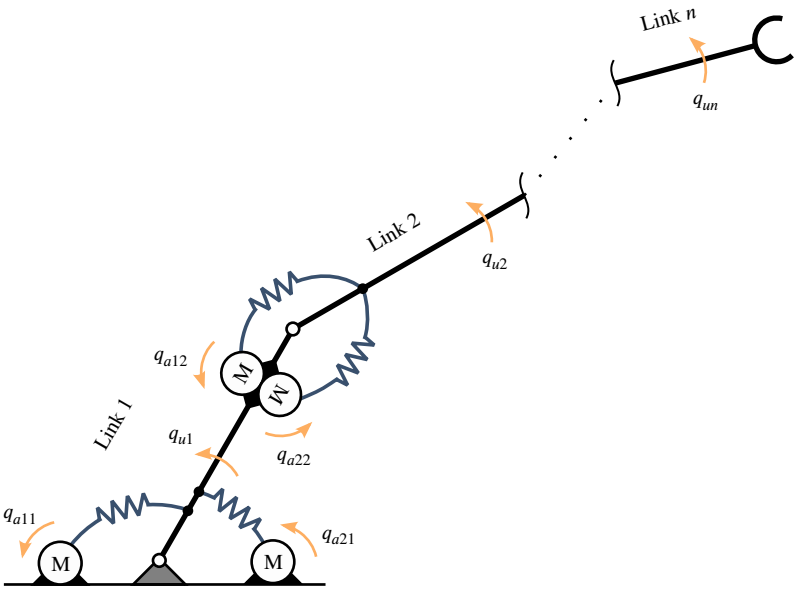

Figure 7.8: A multi-articulated ASR.

are strictly monotonic increasing functions and that

$$\operatorname{rank}\left(\frac{\partial^2 \mathcal{V}_{ej}}{\partial q_{aj}^2}\right) = n_u, \quad j \in (1,2). \tag{7.173}$$

It is clear that (7.166) satisfies Assumption 5.1.1 and 5.1.2, and we conclude that the conditions of Theorem 5.4.2 are satisfied. In fact, an ASRs, as defined above, belongs to the special case of multi-articulated systems discussed in Section 5.4.2. Choosing

$$\boldsymbol{h}(\boldsymbol{q}) = \boldsymbol{\psi}_1(\boldsymbol{q}_u, \boldsymbol{q}_{a1}) - \boldsymbol{\psi}_2(\boldsymbol{q}_u, \boldsymbol{q}_{a2}), \text{ and } \boldsymbol{\nu}_u = \boldsymbol{0}, \tag{7.174}$$

guarantees that Assumption 5.4.2 is satisfied. Consequently, we can apply Theorem 5.3.6 to transform the system into its QFA form

$$\frac{\mathrm{d}}{\mathrm{d}t}\frac{\partial \mathcal{L}}{\partial \dot{\boldsymbol{q}}} - \frac{\partial \mathcal{L}}{\partial \boldsymbol{q}} = \mathcal{Q} \xrightarrow[(5.78),(5.94)]{\text{ICT}} \frac{\mathrm{d}}{\mathrm{d}t}\frac{\partial \mathcal{L}}{\partial \dot{\bar{\boldsymbol{q}}}} - \frac{\partial \mathcal{L}}{\partial \bar{\boldsymbol{q}}} = \bar{\mathcal{Q}}. \tag{7.175}$$

Continuing with (7.175), we can apply any of the controllers introduced in Chapter 6 to solve the output regulation problem. However, it might be desirable to regulate not only the output $\boldsymbol{q}_u$ to its desired position $\boldsymbol{q}_u^*$, but to achieve also a desired joint stiffness pretension at equilibrium. Controllers achieving such behavior are reported in [114, 115]. Let use derive a controller combining the constraint equations (7.174) with an actuator-side offset torque (as reported in [114]) to achieve a desired pretension level.[5] The resulting controller enables the following:

(i) Regulate the links to a desired position, s.t. $(\boldsymbol{q}_u, \dot{\boldsymbol{q}}_u) \to (\boldsymbol{q}_u^*, \boldsymbol{0})$ for $t \to \infty$,
(ii) Impose a desired link-side compliance behavior,
(iii) Achieve a desired passive link stiffness[6] for $t \to \infty$.

[114]: Meng et al. (2021), "Elastic structure preserving impedance control of bidirectional antagonistic variable stiffness actuation"
[115]: Mengacci et al. (2021), "Elastic Structure Preserving control for compliant robots driven by agonistic-antagonistic actuators (ESPaa)"

5: For a symmetric joint arrangement, i.e. $\psi_{1i} = \psi_{2i}$, the constraint equations (7.174) are equal to the ones proposed in [115].

6: With link stiffness, we refer to the Hessian matrix associated with $\mathcal{V}_e$ for fixed motor positions.

Let $\boldsymbol{K}_{pu}, \boldsymbol{K}_{vu}, \boldsymbol{K}_{va}$ be constant matrices, then control objectives (i) and (ii) can be solved with the following controller

$$\bar{\boldsymbol{u}}_u = -\frac{\partial \mathcal{V}_g}{\partial \boldsymbol{q}_u} - \boldsymbol{K}_{vu}\dot{\boldsymbol{q}}_u - \boldsymbol{K}_{pu}\tilde{\boldsymbol{q}}_u, \tag{7.176}$$

$$\bar{\boldsymbol{u}}_{aj} = -\boldsymbol{K}_{vaj}\dot{\tilde{\boldsymbol{q}}}_{aj}. \tag{7.177}$$

Applying (7.176)–(7.177) to the EL system (7.166)–(7.169) shifts the equilibrium to the desired position and renders the system fully damped. The potential energy function of the system is modified to

$$\mathcal{V}^*(\bar{\boldsymbol{q}}) = \mathcal{V} - \mathcal{V}_g + \tfrac{1}{2}\tilde{\boldsymbol{q}}_u^{\mathrm{T}}\boldsymbol{K}_{pu}\tilde{\boldsymbol{q}}_u. \tag{7.178}$$

Using Proposition 6.4.1, we can show that in absence of external forces the equilibrium $(\bar{\boldsymbol{q}}, \dot{\bar{\boldsymbol{q}}}) = (\boldsymbol{q}^*, \boldsymbol{0})$ is globally asymptotically stable.

Regarding control objective (iii), we conclude from

$$\frac{\partial^2 \mathcal{V}_e}{\partial q_{ui}^2} = \frac{\partial \psi}{\partial \varphi_{1i}}(\varphi_{1i}) + \frac{\partial \psi}{\partial \varphi_{1i}}(\varphi_{2i}) \tag{7.179}$$

and Assumption 7.3.1 that increasing joint deflection values φ_{ij} result in increasing link stiffness values. The effect of increasing the link stiffness without shifting the equilibrium position of the link is commonly referred to as *co-contraction*. Let us exploit this effect to achieve a desired (passive) link stiffness modifying (7.177) to include a constant offset torque $\boldsymbol{\tau}^0$ such that

$$\bar{\boldsymbol{u}}_{aj} = (-1)^{\delta_{2j}}\boldsymbol{\tau}^0 - \boldsymbol{K}_{vaj}\dot{\tilde{\boldsymbol{q}}}_{aj}, \tag{7.180}$$

where δ is the Kronecker delta. Applying the controller (7.176) and (7.180) to the EL system (7.166)–(7.169) results in a closed-loop system with the following equilibrium conditions in absence of external forces

$$\frac{\partial \mathcal{V}^*}{\partial \bar{\boldsymbol{q}}_u} = \boldsymbol{0}, \tag{7.181}$$

$$\frac{\partial \mathcal{V}^*}{\partial \bar{\boldsymbol{q}}_{aj}} = (-1)^{\delta_{2j}}\boldsymbol{\tau}^0. \tag{7.182}$$

Considering

$$\frac{\partial \mathcal{V}^*}{\partial \bar{\boldsymbol{q}}_u} = -\sum_j \frac{\partial \mathcal{V}_{ej}}{\partial \bar{\boldsymbol{\varphi}}_j} + \left[\boldsymbol{K}_{pu}\tilde{\boldsymbol{q}}_u\right]^{\mathrm{T}}, \tag{7.183}$$

$$\frac{\partial \mathcal{V}^*}{\partial \bar{\boldsymbol{q}}_{aj}} = \frac{\partial \mathcal{V}_e}{\partial \bar{\boldsymbol{\varphi}}_j}, \tag{7.184}$$

we can rewrite the equilibrium conditions (7.181) and (7.182) as

$$\frac{\partial \mathcal{V}_e}{\partial \bar{\boldsymbol{\varphi}}_j} = (-1)^{\delta_{2j}}\boldsymbol{\tau}^0, \tag{7.185}$$

$$\left[\boldsymbol{K}_{pu}\tilde{\boldsymbol{q}}_u\right]^{\mathrm{T}} = \boldsymbol{0}, \tag{7.186}$$

which implies that $\tilde{\boldsymbol{q}}_u = \boldsymbol{0}$ at equilibrium. Moreover, knowing that the components of $\frac{\partial \mathcal{V}_e}{\partial \varphi_{ji}}$ are strictly monotonic increasing functions of the $\bar{\varphi}_{ji}$, it is clear

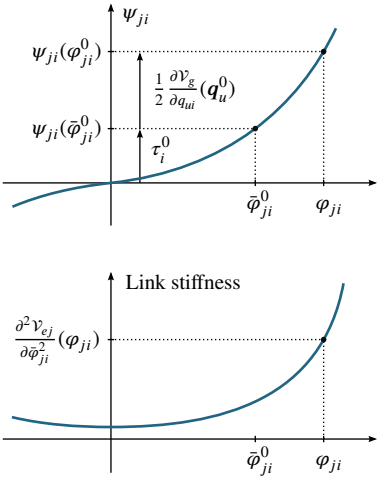

Figure 7.9: Exemplary torque and stiffness profiles.

that the system of n equations

$$\psi_{1i}(\bar{\varphi}_{1i}) = \tau^0_i, \quad \psi_{2i}(\bar{\varphi}_{2i}) = -\tau^0_i \tag{7.187}$$

uniquely determines the n equilibrium joint deflections φ^0_{ji}, see also Fig. 7.9 for a visual argument.

Relation (7.192) tells us the connection between the offset force and the joint deflections at equilibrium. Let use this information to impose a desired passive link stiffness through an appropriate choice of $\boldsymbol{\tau}_0$. The connection between the φ_{ji} and $\bar{\varphi}_{ji}$ is given by the coordinate transforming equations (5.78). Evaluating (5.29b), under the constraint equations (7.174), gives

$$\psi_{1i}(\varphi_{1i}) + \psi_{2i}(\varphi_{2i}) = \psi_{1i}(\bar{\varphi}_{1i}) + \psi_{2i}(\bar{\varphi}_{2i}) + \bar{u}_{ui}, \tag{7.188}$$

$$\psi_{1i}(\varphi_{1i}) - \psi_{2i}(\varphi_{2i}) = \psi_{1i}(\bar{\varphi}_{1i}) - \psi_{2i}(\bar{\varphi}_{2i}). \tag{7.189}$$

Noticing from (7.176) that at equilibrium, we have that $\bar{u}_i = \frac{\partial \mathcal{V}_g}{\partial q_{ui}}(\boldsymbol{q}^0_u)$, such that (7.188)–(7.189), evaluated at the equilibrium, can be rewritten as

$$\psi_{1i}(\varphi^0_{1i}) = \psi_{1i}(\bar{\varphi}^0_{1i}) + \frac{1}{2}\frac{\partial \mathcal{V}_g}{\partial q_{ui}}(\boldsymbol{q}^0_u), \tag{7.190}$$

$$\psi_{2i}(\varphi^0_{2i}) = \psi_{2i}(\bar{\varphi}^0_{2i}) + \frac{1}{2}\frac{\partial \mathcal{V}_g}{\partial q_{ui}}(\boldsymbol{q}^0_u), \tag{7.191}$$

revealing the desired connection between φ^0_{ji} and $\bar{\varphi}^0_{ji}$, as indicated in Fig. 7.9. Knowing that (7.192) must hold at equilibrium, we can rewrite (7.190)–(7.191) as a relation between the φ^0_{1i} and τ^0_i. Knowing that the equilibrium deflections φ^0_{ij} determine the corresponding link stiffness values according to (7.179), we can adjust the τ^0_i to a achieve desired stiffness values.

From Fig. 7.9, it is also clear that we can achieve a desired joint co-contraction by specifying an appropriate $\bar{u}_{ji}$. The equilibrium state is given by

$$\tilde{q}_{ui} = 0; \quad \bar{\varphi}_{ji} = \bar{\varphi}^0_{ji}. \tag{7.192}$$

To show global asymptotic stability of (7.192), we can follow mutatis mutandi the proof of Proposition 6.4.1.

7.4 Visco-Elastic Actuators

This section reports extensions of the ESP design idea to a robot with visco-elastic actuators. We shall refer to the proposed designs as visco-elastic structure perserving (VESP) control. Despite their similarity in the physical structure, SEA and visco-elastic actuators have different control properties. Considering the link side position as an output, the SEA dynamics has a relative degree of 4, while it is at most 3 for a visco-elastic joint [29]. Applying the ESP control concept to a visco-elastic actuator leads, in general, to dynamic state feedback. However, we show that if the generalized elastic force is a linear function of the spring deflections, motion tracking of the link side variables is achievable without dynamic feedback. Similarly to SEA robots, a practical advantage of highly compliant visco-elastically actuated systems

[29]: De Luca et al. (2005), "On the control of robots with visco-elastic joints"

is the mechanical robustness against external impacts, since the system's inherent visco-elastic elements in the power-train act as a low-pass filter on external forces. Thus, at the moment of impact, the system does not suffer from bandwidth limitations of any real controller implementation.

Section 7.4.1 introduces the model under consideration and the corresponding QFA form. Section 7.4.2 reports solutions to joint space motion tracking problem. Experimental evaluation of this new approach on a visco-elastic robot joint is reported in Chapter 11. The desired trajectory is assumed to satisfy the following.

Assumption 7.4.1 *The desired link trajectory $\boldsymbol{q}_u^*(t)$ is bounded and at least three times continuously differentiable.*

7.4.1 Model and Quasi-Fully Actuated Representation

Using the set of coordinates introduced in Section 7.2.1,

$$\boldsymbol{q} = (\boldsymbol{q}_u, \boldsymbol{q}_a) = (q_{u1}, \dots, q_{un_u}, q_{a1}, \dots, q_{an_u}), \tag{7.193}$$

and the axillary variables

$$\boldsymbol{\varphi} = \boldsymbol{q}_a - \boldsymbol{q}_u, \tag{7.194}$$

let us consider the following model of an ASR with visco-elastic joints

$$\Sigma: \ \mathcal{M}(\boldsymbol{q}_u)\ddot{\boldsymbol{q}} + C(\boldsymbol{q}_u, \dot{\boldsymbol{q}}_u) + \boldsymbol{g}(\boldsymbol{q}_u) + \boldsymbol{h}(\boldsymbol{\varphi}, \dot{\boldsymbol{\varphi}}, t) = \boldsymbol{u}. \tag{7.195}$$

Note that compared to the ASR model (7.14), the subsystem coupling force contains a viscous damping term of the form

$$\boldsymbol{h}(\boldsymbol{\varphi}, \dot{\boldsymbol{\varphi}}, t) = \begin{bmatrix} -\boldsymbol{D}(t)\dot{\boldsymbol{\varphi}} \\ \boldsymbol{D}(t)\dot{\boldsymbol{\varphi}} \end{bmatrix}, \tag{7.196}$$

$$\tag{7.197}$$

where $\boldsymbol{D}(t) \in \mathbb{R}^{n_u \times n_u}$, is a diagonal, positive definite matrix which is assumed to be adjustable and thus explicitly time-dependent. In the following, it will be assumed that $\dot{\boldsymbol{D}}(t)$ exists and that it is bounded. Using

$$\boldsymbol{\tau}(\boldsymbol{\varphi}, \dot{\boldsymbol{\varphi}}, t) = \boldsymbol{\psi}(\boldsymbol{\varphi}) + \boldsymbol{D}(t)\dot{\boldsymbol{\varphi}}, \tag{7.198}$$

we can split (7.195) into

$$\Sigma_u: \ \boldsymbol{M}(\boldsymbol{q}_u)\ddot{\boldsymbol{q}}_u + \boldsymbol{C}(\boldsymbol{q}_u, \dot{\boldsymbol{q}}_u)\dot{\boldsymbol{q}}_u + \boldsymbol{g}(\boldsymbol{q}_u) - \boldsymbol{\Psi}(\boldsymbol{\varphi}) - \boldsymbol{h}(\dot{\boldsymbol{\varphi}}, t) = \mathcal{Q}_u, \tag{7.199}$$

$$\Sigma_a: \ \boldsymbol{B}\ddot{\boldsymbol{q}}_a + \boldsymbol{\tau}(\boldsymbol{\varphi}, \dot{\boldsymbol{\varphi}}, t) = \mathcal{Q}_a. \tag{7.200}$$

Consider the new set of coordinates

$$\bar{\boldsymbol{q}} = (\bar{\boldsymbol{q}}_u, \bar{\boldsymbol{q}}_a) = (\bar{q}_{u1}, \dots, \bar{q}_{un_u}, \bar{q}_{a1}, \dots, \bar{q}_{an_u}), \tag{7.201}$$

and auxiliary variables

$$\bar{\boldsymbol{\varphi}} = \bar{\boldsymbol{q}}_a - \bar{\boldsymbol{q}}_u, \tag{7.202}$$

with $\boldsymbol{q}_u \equiv \bar{\boldsymbol{q}}_u$. Now, let us aim for the following QFA representation of (7.193)

$$\mathcal{M}(\bar{\boldsymbol{q}}_u)\ddot{\bar{\boldsymbol{q}}} + C(\bar{\boldsymbol{q}}_u, \dot{\bar{\boldsymbol{q}}}) + \boldsymbol{g}(\bar{\boldsymbol{q}}_u) + \boldsymbol{\Psi}(\bar{\boldsymbol{\varphi}}) = \bar{\mathcal{Q}}, \tag{7.203}$$

with

$$\bar{\mathcal{Q}} = \mathcal{Q}' + \bar{\boldsymbol{u}} = \begin{bmatrix} \mathcal{Q}'_u \\ \mathcal{Q}'_a \end{bmatrix} + \begin{bmatrix} \bar{\boldsymbol{u}}_u \\ \bar{\boldsymbol{u}}_a \end{bmatrix}, \tag{7.204}$$

where $\bar{\boldsymbol{u}}_u$ is assumed to be a sufficiently smooth function of $\boldsymbol{q}_u, \dot{\boldsymbol{q}}_u$ and t. Splitting the dynamics (7.203)

$$\bar{\Sigma}_u : \ \boldsymbol{M}(\bar{\boldsymbol{q}}_u)\ddot{\bar{\boldsymbol{q}}}_u + \boldsymbol{C}(\bar{\boldsymbol{q}}_u, \dot{\bar{\boldsymbol{q}}}_u)\dot{\bar{\boldsymbol{q}}}_u + \boldsymbol{g}(\bar{\boldsymbol{q}}_u) + \boldsymbol{\tau}(\bar{\boldsymbol{\varphi}}, \dot{\bar{\boldsymbol{\varphi}}}, t) = \bar{\mathcal{Q}}_u \tag{7.205}$$

$$\bar{\Sigma}_a : \ \boldsymbol{B}\ddot{\bar{\boldsymbol{q}}}_a + \boldsymbol{\tau}(\bar{\boldsymbol{\varphi}}, \dot{\bar{\boldsymbol{\varphi}}}, t) = \bar{\mathcal{Q}}_a \tag{7.206}$$

and demanding equivalence of the Σ_u and $\bar{\Sigma}_u$ dynamics, we get from comparing (7.199) and (7.205) that

$$\boldsymbol{\tau}(\boldsymbol{\varphi}, \dot{\boldsymbol{\varphi}}, t) = \boldsymbol{\tau}(\bar{\boldsymbol{\varphi}}, \dot{\bar{\boldsymbol{\varphi}}}, t) + \bar{\boldsymbol{u}}_u. \tag{7.207}$$

Since $\boldsymbol{D} > 0$, we can rewrite (7.207) as

$$\begin{aligned} \dot{\boldsymbol{q}}_a &= \dot{\bar{\boldsymbol{q}}}_a + \boldsymbol{\mu}_1, \\ \boldsymbol{\mu}_1 &= \boldsymbol{D}^{-1}\left[\boldsymbol{\psi}(\bar{\boldsymbol{\varphi}}) - \boldsymbol{\psi}(\boldsymbol{\varphi}) + \bar{\boldsymbol{u}}_u\right]. \end{aligned} \tag{7.208}$$

Next, deriving (7.208) with respect to time, we obtain

$$\ddot{\boldsymbol{q}}_a = \ddot{\bar{\boldsymbol{q}}}_a + \frac{\mathrm{d}}{\mathrm{d}t}\boldsymbol{D}^{-1}\left[\boldsymbol{\psi}(\bar{\boldsymbol{\varphi}}) - \boldsymbol{\psi}(\boldsymbol{\varphi}) + \bar{\boldsymbol{u}}_u\right]. \tag{7.209}$$

In general, the differential relation, (7.208), between the original and virtual coordinates cannot be solved in closed-form. In the following, whenever the knowledge of $\bar{\boldsymbol{q}}_a$ is required, we assume it to be computed by numerical integration of (7.208). Eventually, applying the coordinate transformation (7.207) to (7.200) and making the substitutions (7.207)–(7.209) in (7.200), we obtain

$$\boldsymbol{B}\left[\ddot{\bar{\boldsymbol{q}}}_a + \dot{\boldsymbol{\mu}}_1\right] + \boldsymbol{\tau}(\bar{\boldsymbol{\varphi}}, \dot{\bar{\boldsymbol{\varphi}}}, t) + \bar{\boldsymbol{u}}_u = +\mathcal{Q}'_a + \boldsymbol{u}_a, \tag{7.210}$$

and choosing the input transformation

$$\boldsymbol{u}_a = \boldsymbol{B}\dot{\boldsymbol{\mu}}_1 + \bar{\boldsymbol{u}}_u + \bar{\boldsymbol{u}}_a \tag{7.211}$$

we get the desired result (7.205)–(7.206)

7.4.2 Joint Space Motion Tracking

The results presented in this section are based on [94]. It is convenient to denote the tracking error

$$\tilde{\boldsymbol{q}} = (\tilde{\boldsymbol{q}}_u, \tilde{\boldsymbol{q}}_a); \quad \tilde{\boldsymbol{q}}_u = \boldsymbol{q}_u - \boldsymbol{q}^*_u(t); \quad \tilde{\boldsymbol{q}}_a = \bar{\boldsymbol{q}}_a, \tag{7.212}$$

and introduce the additional set of variables

$$\bar{\boldsymbol{\varphi}} = \bar{\boldsymbol{q}}_a - \tilde{\boldsymbol{q}}_u. \tag{7.213}$$

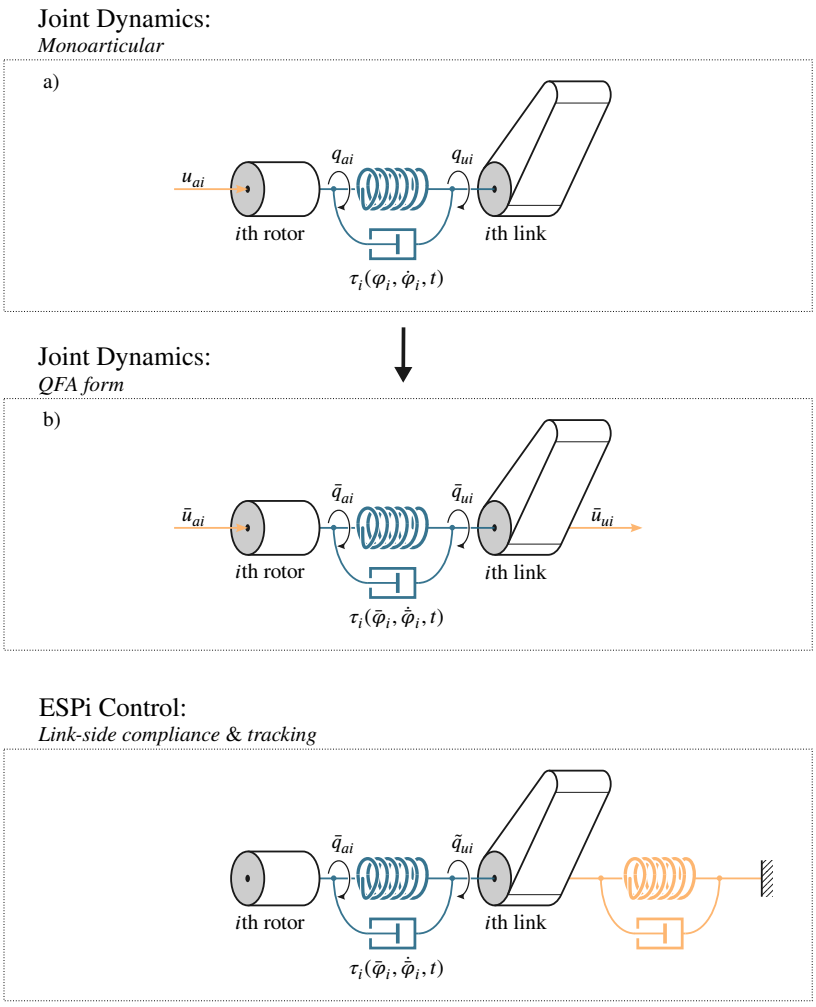

Figure 7.10: The QFA form associated with a visco-elastic joint.

Figure 7.11: Closed-loop: the QFA form enables a straightforward adoption of rigid joint controllers.

Note that for the motion tracking case, we consider virtual deflections as defined in (7.213), which are different from the previous definition in (7.202). Following the design principles in Fig. 7.1, and inspired by the PD+ error dynamics, let us aim for the error dynamics

$$\mathcal{M}(\boldsymbol{q}_u)\ddot{\tilde{\boldsymbol{q}}} + \mathcal{C}(\boldsymbol{q}_u, \dot{\boldsymbol{q}}_u)\dot{\tilde{\boldsymbol{q}}} + \mathcal{D}(t, \bar{\boldsymbol{\varphi}}) + \mathcal{K}_v\dot{\tilde{\boldsymbol{q}}} + \mathcal{K}_p\tilde{\boldsymbol{q}} = \mathcal{Q}', \tag{7.214}$$

with $\mathcal{K}_v = \mathrm{diag}(\boldsymbol{K}_{vu}, \boldsymbol{0}), \mathcal{K}_p = \mathrm{diag}(\boldsymbol{K}_{pu}, \boldsymbol{0}) \in \mathbb{R}^{n\times n}$, where $\boldsymbol{K}_{vu}, \boldsymbol{K}_{pu}$ are constant, symmetric and positive definite matrices. A graphical representation of (7.214) is given in Fig. 7.11. Splitting (7.214) into

$$\bar{\Sigma}_u: \ \boldsymbol{M}(\bar{\boldsymbol{q}}_u)\ddot{\bar{\boldsymbol{q}}}_u + \left[\boldsymbol{C}(\bar{\boldsymbol{q}}_u, \dot{\bar{\boldsymbol{q}}}_u) + \boldsymbol{K}_{vu}\right]\dot{\tilde{\boldsymbol{q}}}_u + \boldsymbol{\tau}(\bar{\boldsymbol{\varphi}}, \dot{\bar{\boldsymbol{\varphi}}}, t) + \boldsymbol{K}_{pu}\tilde{\boldsymbol{q}}_u = \bar{\mathcal{Q}}_u \tag{7.215}$$

$$\bar{\Sigma}_a: \ \boldsymbol{B}\ddot{\bar{\boldsymbol{q}}}_a + \boldsymbol{\tau}(\bar{\boldsymbol{\varphi}}, \dot{\bar{\boldsymbol{\varphi}}}, t) = \bar{\mathcal{Q}}_a \tag{7.216}$$

and considering that $\boldsymbol{q}_u \equiv \bar{\boldsymbol{q}}_u$, it is clear that equivalence of the subsystem dynamics (7.199) and (7.215) is given if

$$\boldsymbol{\tau}(\boldsymbol{\varphi}, \dot{\boldsymbol{\varphi}}, t) = \boldsymbol{\tau}(\bar{\boldsymbol{\varphi}}, \dot{\bar{\boldsymbol{\varphi}}}, t) + \bar{\boldsymbol{u}}_u, \tag{7.217}$$

$$\bar{\boldsymbol{u}}_u = \boldsymbol{M}\dot{\boldsymbol{q}}_u^* + \boldsymbol{C}\dot{\boldsymbol{q}}_u^* + \boldsymbol{g}_u(\boldsymbol{q}_u) - \boldsymbol{K}_{vu}\dot{\tilde{\boldsymbol{q}}}_u - \boldsymbol{K}_{pu}\tilde{\boldsymbol{q}}_u. \tag{7.218}$$

Solving (7.217) for the new velocities $\dot{\bar{\boldsymbol{q}}}_a$, we get

$$\dot{\boldsymbol{q}}_a = \dot{\bar{\boldsymbol{q}}}_a + \boldsymbol{\mu}_1, \tag{7.219}$$

with

$$\boldsymbol{\mu}_1 = \dot{\boldsymbol{q}}_u^* + \boldsymbol{D}^{-1}\big[\boldsymbol{\psi}(\bar{\boldsymbol{\varphi}}) - \boldsymbol{\psi}(\boldsymbol{\varphi}) + \bar{\boldsymbol{u}}_u\big]. \tag{7.220}$$

Finally, making the substitutions (7.200), (7.217) and (7.219), we get

$$\boldsymbol{B}(\ddot{\bar{\boldsymbol{q}}}_a + \dot{\boldsymbol{\mu}}_1) + \boldsymbol{\tau}(\bar{\boldsymbol{\varphi}}, \dot{\bar{\boldsymbol{\varphi}}}, t) + \bar{\boldsymbol{u}}_u = \boldsymbol{u}_a, \tag{7.221}$$

and choosing the control law

$$\boldsymbol{u}_a = \boldsymbol{B}\dot{\boldsymbol{\mu}}_1 + \bar{\boldsymbol{u}}_u, \tag{7.222}$$

gives the desired result (7.216).

Proposition 7.4.1 (Joint-Space Tracking via ESPi Control) *Consider the system* (7.195) *in closed-loop with the controller* (7.222)*. Then* (7.214) *defines an output strictly passive operator* $\mathcal{Q}' \mapsto \dot{\tilde{\boldsymbol{q}}}$*. In absence of external forces* $\mathcal{Q}'$*, the equilibrium point* $\tilde{\boldsymbol{q}} = \boldsymbol{0}$ *is uniformly stable. Further, the velocities* $\dot{\tilde{\boldsymbol{q}}}$ *converge to zero as* $t \to \infty$*.*

The proof follows from Proposition 7.4.3 observing that the closed-loop dynamics (7.214) can be considered as a special case of (7.230)–(7.231) with $\bar{\boldsymbol{D}} = \boldsymbol{D}, \boldsymbol{K}_{va} = \boldsymbol{0}$. Since Proposition 7.4.1 considers the case of nonlinear springs, the storage function (7.247), containing $\mathcal{V}_e$, has to be modified accordingly.

A Simplified Control Law (Part I)

Looking at control law (7.222) the question that may arise whether we can achieve a closed-loop behavior that is similar to (7.214), but without the requiring explicit knowledge of the new motor states $\bar{\boldsymbol{q}}_a, \dot{\bar{\boldsymbol{q}}}_a$. From the implementation point of view, this would no longer require numerical integration of the coordinate transformation (7.219) to obtain $\bar{\boldsymbol{q}}_a$. Considering systems with a subsystem coupling force is of the form

$$\boldsymbol{\tau}(\boldsymbol{\varphi}, \dot{\boldsymbol{\varphi}}, t) = \boldsymbol{D}(t)\dot{\boldsymbol{\varphi}} + \boldsymbol{K}\boldsymbol{\varphi}, \tag{7.223}$$

where $\boldsymbol{K} \in \mathbb{R}^{n_u}$ is a diagonal, constant and positive definite matrix containing the joint stiffness values. Knowing that $\dot{\boldsymbol{D}}^{-1} = -\boldsymbol{D}^{-1}\dot{\boldsymbol{D}}\boldsymbol{D}^{-1}$ and observing that for coupling forces of the form (7.223) the coordinate transformation (7.217) simplifies to

$$\boldsymbol{K}(\bar{\boldsymbol{q}}_a - \boldsymbol{q}_a) + \bar{\boldsymbol{u}}_u = \boldsymbol{D}(t)[\dot{\boldsymbol{q}}_a - \dot{\bar{\boldsymbol{q}}}_a], \tag{7.224}$$

Note that (7.224) allows replacing elastic forces with damper forces and vice versa.

we can separate $\dot{\boldsymbol{\mu}}_1$ as follows

$$\dot{\boldsymbol{\mu}}_1 = \boldsymbol{\mu}_2 + \boldsymbol{K}_{va}\dot{\bar{\boldsymbol{q}}}_a, \tag{7.225}$$

with

$$\boldsymbol{\mu}_2 = \ddot{\boldsymbol{q}}_u^* - \boldsymbol{D}^{-1}\dot{\bar{\boldsymbol{u}}}_u - \boldsymbol{B}^{-1}\boldsymbol{K}_{va}\dot{\boldsymbol{q}}_a, \tag{7.226}$$

$$\boldsymbol{K}_{va} = \boldsymbol{B}\boldsymbol{D}^{-1}\big[\dot{\boldsymbol{D}} + \boldsymbol{K}\big], \tag{7.227}$$

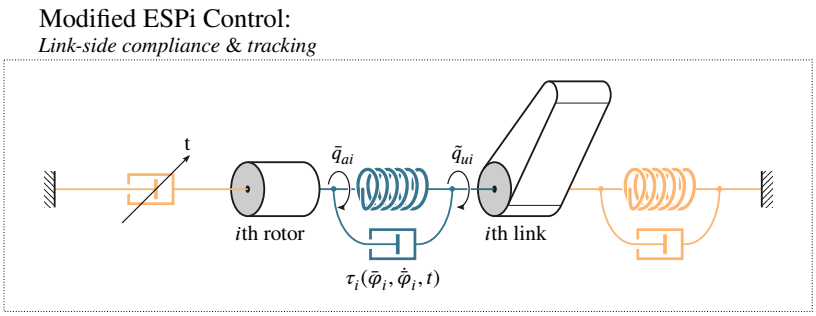

Figure 7.12: Closed-loop dynamics.

where $\boldsymbol{\mu}_2$ is dependent on only the physical coordinates and explicitly on time

Identifying the last term in (7.225) as a possibly favorable damping term suggest the following reduced control law

$$\boldsymbol{u}_a = \boldsymbol{B}\boldsymbol{\mu}_2 + \bar{\boldsymbol{u}}_u, \tag{7.228}$$

Considering (7.225) and continuing from (7.221) it is easy to see that applying control law (7.228) to (7.200) gives

$$\boldsymbol{B}\ddot{\bar{\boldsymbol{q}}}_a + \boldsymbol{K}_{va}\dot{\bar{\boldsymbol{q}}}_a + \boldsymbol{\tau}(\bar{\boldsymbol{\varphi}}, \dot{\bar{\boldsymbol{\varphi}}}, t) = \boldsymbol{0}. \tag{7.229}$$

The final closed-loop system is constituted by (7.215) and (7.229). Comparing the rotor dynamics (7.216) and (7.229), we see that latter contains an additional (explicitly time-varying) damping term acting on the rotor inertias as highlighted in Fig. 7.12. Finally, to ensure that $\boldsymbol{K}_{va}$ is positive definite, we must limit the damping factor rate of change such that $\dot{\boldsymbol{D}} \geq -\boldsymbol{K}$. In summary, we conclude the following.

Proposition 7.4.2 (Simplified Joint-space tracking—restricted damper rate) *Consider the system* (7.195)*, with the subsystem coupling force of the form* (7.223)*, in closed-loop with the controller* (7.228)*. Suppose that* $\dot{\boldsymbol{D}} \geq -\boldsymbol{K}$*, then* (7.215) *and* (7.229) *defines an output strictly passive operator* $\mathcal{Q}' \mapsto \dot{\tilde{\boldsymbol{q}}}$*. In absence of external forces* $\mathcal{Q}'$*, the equilibrium point* $\tilde{\boldsymbol{q}} = \boldsymbol{0}$ *is uniformly stable. Further, the velocities* $\dot{\tilde{\boldsymbol{q}}}$ *converge to zero as* $t \to \infty$*.*

The proof follows from Proposition 7.4.3 observing that the closed-loop dynamics (7.214) can be considered as a special case of (7.230)–(7.231) with $\bar{\boldsymbol{D}} = \boldsymbol{D}$. It it worth remarking that the condition $\dot{\boldsymbol{D}} \geq -\boldsymbol{K}$ can ensured in practice by limiting the damper adjustment rate accordingly.

Remark 7.4.1 An interesting aspect of the controller (7.228) is the absence of new states $\bar{\boldsymbol{q}}_a, \dot{\bar{\boldsymbol{q}}}_a$ in the control law; this significantly simplifies its implementation. However, they appear in the formulation of the closed-loop dynamics, and consequently are used for deriving a stability argument (see proof of Proposition 7.4.3).

A Simplified Control Law (Part II)

This section shows that the restriction on the damper rate $\dot{\boldsymbol{D}}$ in control law (7.222) can be avoided by aiming for a desired closed-loop dynamics with time-

dependent motor inertias and a subsystem coupling force $\bar{\boldsymbol{\tau}}$ that is different from the original one $\boldsymbol{\tau}$ and

$$\boldsymbol{M}(\bar{\boldsymbol{q}}_u)\ddot{\bar{\boldsymbol{q}}}_u + \big[\boldsymbol{C}(\bar{\boldsymbol{q}}_u, \dot{\bar{\boldsymbol{q}}}_u) + \boldsymbol{K}_{vu}\big]\dot{\bar{\boldsymbol{q}}}_u + \boldsymbol{K}_{pu}\tilde{\boldsymbol{q}}_u + \bar{\boldsymbol{\tau}}(\bar{\boldsymbol{\varphi}}, \dot{\bar{\boldsymbol{\varphi}}}, t) = \bar{\mathcal{Q}}'_u, \tag{7.230}$$

$$\bar{\boldsymbol{B}}(t)\ddot{\bar{\boldsymbol{q}}}_a + \big[\bar{\boldsymbol{C}}(t) + \bar{\boldsymbol{K}}_{va}(t)\big]\dot{\bar{\boldsymbol{q}}}_a + \bar{\boldsymbol{\tau}}(\bar{\boldsymbol{\varphi}}, \dot{\bar{\boldsymbol{\varphi}}}, t) = \bar{\mathcal{Q}}'_a, \tag{7.231}$$

with the notation (7.212)–(7.213), $\boldsymbol{\tau}$ defined as in (7.223) and

$$\bar{\boldsymbol{\tau}}(\bar{\boldsymbol{\varphi}}, \dot{\bar{\boldsymbol{\varphi}}}, t) = \bar{\boldsymbol{D}}(t)\dot{\bar{\boldsymbol{\varphi}}} + \boldsymbol{K}\bar{\boldsymbol{\varphi}}, \tag{7.232}$$

$$\boldsymbol{A}(t) = \boldsymbol{D}(t)^{-1}\bar{\boldsymbol{D}}(t), \tag{7.233}$$

$$\bar{\boldsymbol{K}}_{va} = \boldsymbol{B}\boldsymbol{D}^{-1}\big(\dot{\boldsymbol{D}}\boldsymbol{A} + \boldsymbol{K}\big), \tag{7.234}$$

$$\bar{\boldsymbol{B}}(t) = \boldsymbol{A}(t)^{\mathrm{T}}\boldsymbol{B}\boldsymbol{A}(t), \tag{7.235}$$

$$\bar{\boldsymbol{C}}(t) = \boldsymbol{A}(t)^{\mathrm{T}}\boldsymbol{B}\dot{\boldsymbol{A}}(t), \tag{7.236}$$

where $\bar{\boldsymbol{D}}(t) \in \mathbb{R}^{n_u \times n_u}$ is as diagonal and positive definite matrix with a bounded time derivative $\dot{\bar{\boldsymbol{D}}}(t)$, and further satisfying

$$\dot{\boldsymbol{D}}\boldsymbol{D}^{-1}\bar{\boldsymbol{D}} + \boldsymbol{K} > 0 \tag{7.237}$$

It is easy to see that condition (7.237) guarantees positive definiteness of $\boldsymbol{K}_{va}$. Further, notice that

$$\dot{\bar{\boldsymbol{B}}} = \bar{\boldsymbol{C}} + \bar{\boldsymbol{C}}^{\mathrm{T}}. \tag{7.238}$$

Note that (7.238) is equivalent to the statement that $\dot{\boldsymbol{B}} - 2\bar{\boldsymbol{C}}$ is a skew-symmetric matrix.

Next, we can achieve equivalence of (7.199) and (7.230) by modifying the coordinate transformation (7.217) to

$$\boldsymbol{\tau}(\boldsymbol{\varphi}, \dot{\boldsymbol{\varphi}}, t) = \bar{\boldsymbol{\tau}}(\bar{\boldsymbol{\varphi}}, \dot{\bar{\boldsymbol{\varphi}}}, t) + \bar{\boldsymbol{u}}_u, \tag{7.239}$$

Solving (7.217) for the new velocities $\dot{\bar{\boldsymbol{q}}}_a$, we get

$$\dot{\boldsymbol{q}}_a = \boldsymbol{A}\dot{\bar{\boldsymbol{q}}}_a + \boldsymbol{\mu}_1, \tag{7.240}$$

where

$$\bar{\boldsymbol{\mu}}_1 = \boldsymbol{A}\dot{\boldsymbol{q}}_u^* + (\boldsymbol{I} - \boldsymbol{A})\dot{\boldsymbol{q}}_u + \boldsymbol{D}^{-1}\big[\boldsymbol{K}(\bar{\boldsymbol{q}}_a - \boldsymbol{q}_a) + \bar{\boldsymbol{u}}_u\big], \tag{7.241}$$

has additional terms compared to (7.220). Next, substituting (7.240) into (7.200) gives the preliminary dynamics

$$\boldsymbol{B}\boldsymbol{A}\ddot{\bar{\boldsymbol{q}}}_a + \boldsymbol{B}\dot{\boldsymbol{A}}\dot{\bar{\boldsymbol{q}}}_a + \boldsymbol{B}\dot{\boldsymbol{\mu}}_1 + \boldsymbol{\tau}(\boldsymbol{\varphi}, \dot{\boldsymbol{\varphi}}, t) = \boldsymbol{u}_a. \tag{7.242}$$

Considering (7.232)–(7.234) and (7.239), we can be decompose the undesired term $\boldsymbol{\mu}_1$ as follows

$$\begin{aligned}\dot{\bar{\boldsymbol{\mu}}}_1 &= \bar{\boldsymbol{\mu}}_2 + \boldsymbol{B}^{-1}\bar{\boldsymbol{K}}_{va}\dot{\bar{\boldsymbol{q}}}_a,\\ \bar{\boldsymbol{\mu}}_2 &= \frac{\mathrm{d}}{\mathrm{d}t}\big[\boldsymbol{A}\dot{\boldsymbol{q}}_u^* - (\boldsymbol{I} - \boldsymbol{A})\dot{\boldsymbol{q}}_u\big] + \boldsymbol{D}^{-1}\big[\dot{\boldsymbol{D}}(\boldsymbol{I} - \boldsymbol{A})\dot{\boldsymbol{q}}_u + \dot{\bar{\boldsymbol{u}}}_u\big] - \boldsymbol{B}^{-1}\boldsymbol{K}_{va}\dot{\boldsymbol{q}}_a,\end{aligned} \tag{7.243}$$

with $\boldsymbol{K}_{va}$ and $\bar{\boldsymbol{K}}_{va}$ defined as above. Now, pre-multiplying (7.242) with $\boldsymbol{A}^{\mathrm{T}}$, and using (7.243) to factor out the terms containing $\bar{\boldsymbol{q}}_a$ and $\dot{\bar{\boldsymbol{q}}}_a$, we get

$$\bar{\boldsymbol{B}}\ddot{\bar{\boldsymbol{q}}}_a + \big[\bar{\boldsymbol{C}} + \boldsymbol{A}^{\mathrm{T}}\boldsymbol{K}_{va}\big]\dot{\bar{\boldsymbol{q}}}_a = \boldsymbol{A}^{\mathrm{T}}\big[\boldsymbol{u}_a - \boldsymbol{B}\bar{\boldsymbol{\mu}}_2 - \boldsymbol{\tau}(\boldsymbol{\varphi}, \dot{\boldsymbol{\varphi}})\big]. \tag{7.244}$$

Now it is easy to see that using (7.217) and applying the following control input to (7.244)

$$\boldsymbol{u}_a = \boldsymbol{B}\bar{\boldsymbol{\mu}}_2 + \left[\boldsymbol{I} - \boldsymbol{A}^{-\mathrm{T}}\right]\boldsymbol{\tau}(\boldsymbol{\varphi}, \dot{\boldsymbol{\varphi}}, t) + \boldsymbol{A}^{-\mathrm{T}}\bar{\boldsymbol{u}}_u, \tag{7.245}$$

achieves the desired equivalence of (7.200) and (7.231). Making the substitution (7.243) and (7.245) it is clear that the resulting control law is independent of the virtual coordinates $\bar{\boldsymbol{q}}_a$ and $\dot{\bar{\boldsymbol{q}}}_a$. Thus, its implementation does not require dynamic state feedback.

Remark 7.4.2 Compared to (7.228), the controller (7.245) does not impose a constraint on the physical damper rate $\dot{\boldsymbol{D}}$. In fact, the constraint has been shifted to the virtual damper rate $\dot{\bar{\boldsymbol{D}}}$, c.f. (7.237). However, if $\dot{\boldsymbol{D}} \geq -\boldsymbol{K}$, then we can set $\bar{\boldsymbol{D}}(t)$ equal to $\boldsymbol{D}(t)$, which ensures that the structure of the subsystem coupling force is preserved, i.e. $\bar{\boldsymbol{\tau}} = \boldsymbol{\tau}$. Observing that $\boldsymbol{A} = \boldsymbol{I}$ in this case, we see that the control law (7.245) significantly simplifies and feedback of $\ddot{\boldsymbol{q}}_u$ is no longer required. This suggests the following virtual damper variation

$$\begin{aligned} &\bar{\boldsymbol{D}}(t) = \boldsymbol{D}(t), && \text{for } \dot{\boldsymbol{D}} \geq -\boldsymbol{K}; \\ &\bar{\boldsymbol{D}}(t) \text{ such that (7.237)}, && \text{otherwise.} \end{aligned}$$

It is worth noting that in the first case the control law (7.245) degenerates to the one in (7.228). Observing that $\bar{\boldsymbol{D}}(t) \equiv \boldsymbol{D}(t) \implies \boldsymbol{A} = \boldsymbol{I}$ and $\boldsymbol{K}_{va} \equiv \bar{\boldsymbol{K}}_{va}$, it immediately follows that $\boldsymbol{\mu}_2 \equiv \bar{\boldsymbol{\mu}}_2$ and, thus, equivalence of the control laws (7.245) and (7.228).

Remark 7.4.3 The rotor dynamics (7.231) shares some similarity with the rotor dynamics associated with the ESP+ controller, (7.114). In both cases the "pseudo Jacobian" $\boldsymbol{A}$ of the coordinate transforming equations appears in the congruence transformation of the motor inertia matrix, compare (7.235) and (7.109).

The central properties of the closed-loop system (7.230)–(7.231) are summarized in the following.

Proposition 7.4.3 (Simplified Joint-space tracking—unrestricted damper rate) *Consider the system* (7.195)*, with the subsystem coupling force of the form* (7.223)*, in closed-loop with the controller* (7.245)*. Suppose that* (7.237) *is satisfied, then* (7.230)–(7.231) *defines an output strictly passive operator* $\mathcal{Q}' \mapsto \dot{\tilde{\boldsymbol{q}}}$*. In absence of external forces* $\mathcal{Q}'$*, the equilibrium point* $\tilde{\boldsymbol{q}} = \boldsymbol{0}$ *is uniformly stable. Further, the velocities* $\dot{\tilde{\boldsymbol{q}}}$ *converge to zero as* $t \to \infty$*.*

Proof. The physically motivated nature of the closed-loop system (7.230)–(7.231) suggests the following subsystem storage functions

$$S_u = \frac{1}{2}\left[\dot{\tilde{\boldsymbol{q}}}_u \boldsymbol{M}\dot{\tilde{\boldsymbol{q}}}_u + \tilde{\boldsymbol{q}}_u^{\mathrm{T}}\boldsymbol{K}_{pu}\tilde{\boldsymbol{q}}_u\right], \tag{7.246}$$

$$S_a = \frac{1}{2}\dot{\bar{\boldsymbol{q}}}_a^{\mathrm{T}}\bar{\boldsymbol{B}}\dot{\bar{\boldsymbol{q}}}_a + \mathcal{V}_e. \tag{7.247}$$

Computing the time-derivatives of (7.230) and (7.231) along the solutions of

(7.230)–(7.230) gives

$$\dot{S}_u = -\dot{\tilde{\boldsymbol{q}}}_u^{\mathrm{T}} \boldsymbol{K}_{vu} \dot{\tilde{\boldsymbol{q}}}_u + \dot{\tilde{\boldsymbol{q}}}_u^{\mathrm{T}} \big[\bar{\boldsymbol{\tau}}(\bar{\boldsymbol{\varphi}}, \dot{\bar{\boldsymbol{\varphi}}}, t) + \bar{\mathcal{Q}}'_u\big], \tag{7.248}$$

$$\dot{S}_a = -\dot{\tilde{\boldsymbol{q}}}_a^{\mathrm{T}} \boldsymbol{K}_{va} \dot{\tilde{\boldsymbol{q}}}_a - \dot{\tilde{\boldsymbol{q}}}_a^{\mathrm{T}} \big[\bar{\boldsymbol{\tau}}(\bar{\boldsymbol{\varphi}}, \dot{\bar{\boldsymbol{\varphi}}}, t) - \bar{\mathcal{Q}}'_a\big] + \boldsymbol{\psi}^{\mathrm{T}}(\bar{\boldsymbol{\varphi}}) \dot{\bar{\boldsymbol{\varphi}}}, \tag{7.249}$$

which motivates choosing the storage function

$$S = S_u + S_a. \tag{7.250}$$

Combining (7.248) and (7.249), we get

$$\dot{S} = -\dot{\tilde{\boldsymbol{q}}}_u^{\mathrm{T}} \boldsymbol{K}_{vu} \dot{\tilde{\boldsymbol{q}}}_u - \dot{\tilde{\boldsymbol{q}}}_a^{\mathrm{T}} \boldsymbol{K}_{va} \dot{\tilde{\boldsymbol{q}}}_a - \dot{\bar{\boldsymbol{\varphi}}}^{\mathrm{T}} \bar{\boldsymbol{D}} \dot{\bar{\boldsymbol{\varphi}}} + \dot{\tilde{\boldsymbol{q}}}^{\mathrm{T}} \bar{\mathcal{Q}}', \tag{7.251}$$

which shows that (7.230)–(7.231) defines an output strictly passive map $\bar{\mathcal{Q}}' \mapsto \dot{\tilde{\boldsymbol{q}}}_u$ and completes the first part of the proof. Let us continue with demonstrating stability in absence of external forces. Knowing that S is a positive definite function of the states $\tilde{\boldsymbol{q}}, \dot{\tilde{\boldsymbol{q}}}$, and from (7.251) that $\dot{S}$ is a negative semi-definite function, we conclude that S qualifies as Lyapunov function, and subsequently that the closed-loop system is stable. In order to extent the statement to global uniform stability, we further have to show that S is decrescent and radially unbounded. Former is guaranteed to through the following time-invariant function that upper bounds S

$$\begin{aligned} S^* = \frac{1}{2}\Bigg[& \min_{\boldsymbol{q}_u \in \mathbb{R}^{n_u}} \lambda\big(\boldsymbol{M}(\boldsymbol{q}_u)\big) ||\dot{\tilde{\boldsymbol{q}}}_u||^2 + \min_{t \in \mathbb{R}^+} \lambda\big(\bar{\boldsymbol{B}}(t)\big) ||\dot{\tilde{\boldsymbol{q}}}_a||^2 \\ & + \tilde{\boldsymbol{q}}_u^{\mathrm{T}} \boldsymbol{K}_{pu} \tilde{\boldsymbol{q}}_u \Bigg] + \mathcal{V}_e(\bar{\boldsymbol{\varphi}}). \end{aligned} \tag{7.252}$$

The radial unboundedness of S follows directly from the positive definiteness of $\boldsymbol{M}, \bar{\boldsymbol{B}}, \boldsymbol{K}_{pu}$ and the properties of $\mathcal{V}_e$, c.f. Assumption 7.2.1. Further, the boundedness of $\bar{\boldsymbol{B}}$ is ensured by the boundedness of $\dot{\boldsymbol{D}}$ and the positive definiteness of $\boldsymbol{D}$. Note that the coordinate transforming equations (7.239) can be viewed as a stable first-order differential equation in $\boldsymbol{\varphi}$

$$\dot{\boldsymbol{\varphi}} + \boldsymbol{D}^{-1}(t) \boldsymbol{K} \boldsymbol{\varphi} = \boldsymbol{r}; \quad \boldsymbol{r} = \boldsymbol{D}^{-1}(t) \big[\bar{\boldsymbol{D}}(t) \dot{\bar{\boldsymbol{\varphi}}} + \boldsymbol{K} \bar{\boldsymbol{\varphi}} + \bar{\boldsymbol{u}}_u\big], \tag{7.253}$$

with $\boldsymbol{r}$ as an input. For bounded initial conditions, the boundedness of the input $\boldsymbol{r}$ guarantees boundedness of $\dot{\boldsymbol{\varphi}}$ and $\boldsymbol{\varphi}$. In fact, using $1/2 \boldsymbol{\varphi}^{\mathrm{T}} \boldsymbol{K} \boldsymbol{\varphi}$ as storage function, it is easy to see that (7.239) defines an OSP operator $\boldsymbol{r} \mapsto \boldsymbol{\varphi}$ which implies $\mathcal{L}_2$-stability.

Let us continue with showing convergence of the velocity error. First note that

$$\ddot{S} = -2\big(\dot{\tilde{\boldsymbol{q}}}_u^{\mathrm{T}} \boldsymbol{K}_{vu} \ddot{\tilde{\boldsymbol{q}}}_u + \dot{\tilde{\boldsymbol{q}}}_a^{\mathrm{T}} \boldsymbol{K}_{va} \ddot{\tilde{\boldsymbol{q}}}_a + \dot{\bar{\boldsymbol{\varphi}}}^{\mathrm{T}} \dot{\bar{\boldsymbol{D}}} \ddot{\bar{\boldsymbol{\varphi}}}\big) - \dot{\bar{\boldsymbol{\varphi}}}^{\mathrm{T}} \bar{\boldsymbol{D}} \dot{\bar{\boldsymbol{\varphi}}}. \tag{7.254}$$

Knowing that $\tilde{\boldsymbol{q}}, \dot{\tilde{\boldsymbol{q}}}$ are bounded and using the properties of $\boldsymbol{M}, \bar{\boldsymbol{B}}$, we see from (7.230)–(7.231) that $\ddot{\tilde{\boldsymbol{q}}}$ is bounded as well. Concluding that $\ddot{S}$ is bounded, we deduce that $\dot{S}$ is uniformly continuous. Considering (7.251) and that S has a finite limit as $t \to \infty$, we can invoke Barbalat's Lemma to complete the proof. ■

7.5 Stability and Passivity Proofs

This section reports proofs for the main stability and passivity results of this chapter. In the following, when talking about the boundedness of vectors and matrices it is referred to in the sense of bounded Euclidean norms, $||.||$, and bounded eigenvalues, respectively. Let Ω be a domain and I a set. Consider a quadratic matrix $\boldsymbol{A}(t, \boldsymbol{x})$, defined for all $(t, \boldsymbol{x}) \in I \times \Omega$, then $\underline{\lambda}(\boldsymbol{A})$ and $\bar{\lambda}(\boldsymbol{A})$ denote its minimum and maximum eigenvalue such that

$$\underline{\lambda}(\boldsymbol{A}(t, \boldsymbol{x})) \triangleq \inf_{t \in I, \boldsymbol{x} \in \Omega} \lambda(\boldsymbol{A}(t, \boldsymbol{x})), \tag{7.255}$$

$$\bar{\lambda}(\boldsymbol{A}(t, \boldsymbol{x})) \triangleq \sup_{t \in I, \boldsymbol{x} \in \Omega} \lambda(\boldsymbol{A}(t, \boldsymbol{x})). \tag{7.256}$$

Analogously, $\underline{\sigma}(\boldsymbol{A})$ and $\bar{\sigma}(\boldsymbol{A})$ denote the minimum and maximum singular value of $\boldsymbol{A}$, respectively.

Remark 7.5.1 In the the closed-loop dynamics reported in this chapter, the error coordinates $\tilde{\boldsymbol{x}}$ or $\tilde{\boldsymbol{q}}$, and joint coordinate $\bar{\boldsymbol{q}}$ often appear together in the same equation for better readability. Notice that it is straightforward to rewrite the closed-loop dynamics entirely in terms of the error coordinates. Using (7.75), or (7.135) and (7.5), we either have that

$$\mathcal{M}_x(\bar{\boldsymbol{q}}_u) = \mathcal{M}_x\left(\tilde{\boldsymbol{q}}_u + \boldsymbol{q}_u^*(t)\right) \tag{7.257}$$

$$C_x(\bar{\boldsymbol{q}}_u, \dot{\bar{\boldsymbol{q}}}_u) = C_x\left(\tilde{\boldsymbol{q}}_u + \boldsymbol{q}_u^*(t), \dot{\tilde{\boldsymbol{q}}}_u + \dot{\boldsymbol{q}}_u^*(t)\right). \tag{7.258}$$

or

$$\mathcal{M}_x(\bar{\boldsymbol{q}}_u) = \mathcal{M}_x\left(\boldsymbol{h}_u^{-1}\left[\tilde{\boldsymbol{x}}_u + \boldsymbol{x}_u^*(t)\right]\right) \tag{7.259}$$

$$C_x(\bar{\boldsymbol{q}}_u, \dot{\bar{\boldsymbol{q}}}_u) = C_x\left(\boldsymbol{h}_u^{-1}\left[\tilde{\boldsymbol{x}}_u + \boldsymbol{x}_u^*(t)\right], \boldsymbol{J}_u^{-1}\left[\dot{\tilde{\boldsymbol{x}}}_u + \dot{\boldsymbol{x}}_u^*(t)\right]\right). \tag{7.260}$$

Notice that through the explicit time-dependency of the $\mathcal{M}$ and C matrices the closed-loop dynamics are non-autonomous systems. Throughout the proofs of this text, we shall keep a "mixed notation" to improve readability.

Proof of Proposition 7.2.1 and Proposition 7.2.3

The following section provides a proof of Proposition 7.2.1 and 7.2.3. Notice that only the ESP case, that is $\boldsymbol{K}_{pa} \succ 0$, $\boldsymbol{K}_{pu}$, is considered. The ESP+ case can be treated proceeding mutatis mutandis to arguments below, and only requires substituting the potential energy term $\tilde{\boldsymbol{q}}_a^{\mathrm{T}} \boldsymbol{K}_{pa} \tilde{\boldsymbol{q}}_a$ with $\tilde{\boldsymbol{q}}_u^{\mathrm{T}} \boldsymbol{K}_{pu} \tilde{\boldsymbol{q}}_u$ in storage and Lyapunov functions. The following proof evolves around verifying the conditions of Matrosov's Theorem. To verify condition (iv), we shall rely on using Lemma C.1.5. Most of the computations are straight forward, but tedious at times. This is especially true when it comes to checking condition (iv.a) of Lemma C.1.5. In general, the proof relies heavily on the application of the boundedness theorem, Lemma D.3.3 and matrix norm properties.

Matrosov's Theorem and Lemma D.3.3 by Paden and Panja are reprinted in Appendix C.

For better readability, we will neglect the arguments of all system matrices and introduce the state vector $\boldsymbol{x} = (\tilde{\boldsymbol{q}}, \dot{\tilde{\boldsymbol{q}}})$ with the components defined as in (7.75). Let Ω be an open connected region in $\mathbb{R}^{2n}$. Let us consider the storage function (7.127) as an energy-based and time-variant Lyapunov function

candidate $V : [0, \infty) \times \Omega \to \mathbb{R}$

$$V(t, \boldsymbol{x}) = S(\tilde{\boldsymbol{q}}, \dot{\tilde{\boldsymbol{q}}}, t), \tag{7.261}$$

where the set Ω can be chosen arbitrarily large. Clearly, V is lower bounded since $\boldsymbol{M}, \bar{\boldsymbol{B}}, \boldsymbol{K}_{pa}$ and the elastic potential $\mathcal{V}_e$ are positive definite matrices and functions, respectively (cf. Prop. 1, Assumption 7.2.1). Thus, V is positive definite in $\boldsymbol{x}$. Later in the text, V is required to be at least three times continuously differentiable. Knowing from (7.128) that

$$\dot{V}(t, \boldsymbol{x}) = -\dot{\tilde{\boldsymbol{q}}}^{\mathrm{T}} \mathcal{K}_v \dot{\tilde{\boldsymbol{q}}}, \tag{7.262}$$

we conclude from the positive definiteness of $\mathcal{K}_v$ that $\dot{V}$ is negative semi-definite. Thus, V qualifies as a Lyapunov function for the closed-loop system (7.114).

Ad Condition (i) of Matrosov's Theorem. Condition (i) of Matrosov's Theorem can be satisfied by choosing upper and lower bounds for V as follows

$$\alpha(\boldsymbol{x}) = \frac{1}{2}\left(\underline{\lambda}(\boldsymbol{M}) ||\dot{\tilde{\boldsymbol{q}}}_u||^2 + \underline{\lambda}(\bar{\boldsymbol{B}}) ||\dot{\tilde{\boldsymbol{q}}}_a||^2 + \underline{\lambda}(\boldsymbol{K}_{pa}) ||\tilde{\boldsymbol{q}}_a||^2 \right) + U_s(\tilde{\boldsymbol{q}}_a - \tilde{\boldsymbol{q}}_u)$$

$$\beta(\boldsymbol{x}) = \frac{1}{2}\left(\bar{\lambda}(\boldsymbol{M}) ||\dot{\tilde{\boldsymbol{q}}}_u||^2 + \bar{\lambda}(\bar{\boldsymbol{B}}) ||\dot{\tilde{\boldsymbol{q}}}_a||^2 + \bar{\lambda}(\boldsymbol{K}_{pa}) ||\tilde{\boldsymbol{q}}_a||^2 \right) + U_s(\tilde{\boldsymbol{q}}_a - \tilde{\boldsymbol{q}}_u)$$

and invoking [96, Lemma 4.3], which states that there exist class $\mathcal{K}$ functions a and b such that $a(||\boldsymbol{x}||) \leq \alpha(\boldsymbol{x})$ and $b(||\boldsymbol{x}||) \geq \beta(\boldsymbol{x})$. In fact, a and b will be of class $\mathcal{K}_\infty$, since α and β are radially unbounded. Note that $\underline{\lambda}(\bar{\boldsymbol{B}}) > 0$ is guaranteed by Lemma 7.2.2.

Lemma 7.5.1 *The upper and lower bounds on the Lyapunov function* (7.261)*, in form of the class K functions a and b, together with the negative semi-definiteness of* $\dot{V}$*, imply that the closed-loop system* (7.114) *is globally, uniformly stable.*

Ad Condition (ii) of Matrosov's Theorem. In case $\boldsymbol{K}_{vu}$ is time-invariant, we can simply choose $V^*(\boldsymbol{x}) = \dot{V}(t, \boldsymbol{x})$. Otherwise, we can select

$$V^*(\boldsymbol{x}) = -\bar{\lambda}\big(\boldsymbol{K}_{vu}(t, \tilde{\boldsymbol{q}})\big) ||\dot{\tilde{\boldsymbol{q}}}_u||^2 - \dot{\tilde{\boldsymbol{q}}}_a^{\mathrm{T}} \boldsymbol{K}_{va} \dot{\tilde{\boldsymbol{q}}}_a, \tag{7.263}$$

which satisfies Condition (ii). We now can deduce the problematic set where $\dot{V}$ becomes zero, namely $E = \{\boldsymbol{x} \in \Omega \ : \ \dot{\tilde{\boldsymbol{q}}}_u = \dot{\tilde{\boldsymbol{q}}}_a = \boldsymbol{0}\}$.

Ad Condition (iii) of Matrosov's Theorem. We denote the function $W : [0, \infty) \times \Omega \to \mathbb{R}$ as

$$W(t, \boldsymbol{x}) \triangleq \ddot{V}(t, \boldsymbol{x}). \tag{7.264}$$

To ensure that W satisfies Condition (iii) we have to establish the boundedness of $|W(t, \boldsymbol{x})|$. From (7.262) we get

$$W(t, \boldsymbol{x}) = -\big(2\dot{\tilde{\boldsymbol{q}}}_u^{\mathrm{T}} \boldsymbol{K}_{vu} \ddot{\tilde{\boldsymbol{q}}}_u + \dot{\tilde{\boldsymbol{q}}}_u^{\mathrm{T}} \dot{\mathcal{K}}_{vu} \dot{\tilde{\boldsymbol{q}}}_u + 2\dot{\tilde{\boldsymbol{q}}}_a^{\mathrm{T}} \boldsymbol{K}_{va} \ddot{\tilde{\boldsymbol{q}}}_a + \dot{\tilde{\boldsymbol{q}}}_a^{\mathrm{T}} \dot{\boldsymbol{K}}_D \dot{\tilde{\boldsymbol{q}}}_a\big). \tag{7.265}$$

We restrict Ω to be an arbitrarily large, but bounded set. As such, for any starting condition $\boldsymbol{x}(t_0) \in \Omega$, $t_0 \geq 0$, Prop. 7.5.1 implies that $\boldsymbol{x}(t)$ is bounded $\forall t \in [t_0, \infty)$. Thus, we can conclude directly that all RHS terms of (7.265), apart from the one containing $\ddot{\tilde{\boldsymbol{q}}}_u$ and $\ddot{\tilde{\boldsymbol{q}}}_a$, are bounded.

Next, let us show the boundedness of $\ddot{\tilde{\boldsymbol{q}}}_u$ and $\ddot{\tilde{\boldsymbol{q}}}_a$. Since $\boldsymbol{M}$ is continuously differentiable and $\boldsymbol{q}_u$ is bounded, the tensors $\frac{\partial \boldsymbol{M}(\boldsymbol{q}_u)}{\partial \boldsymbol{q}_u}$ and $\frac{\partial^2 \boldsymbol{M}(\boldsymbol{q}_u)}{\partial \boldsymbol{q}_u^2}$ are bounded. We can conclude that $\dot{\boldsymbol{M}}(\boldsymbol{q}_u)$ is bounded.[7] Due to Assumption 5.1.1, $\boldsymbol{M}^{-1}$ exists and is bounded. This, together with the fact that all terms on the RHS of the closed-loop link dynamics

$$\boldsymbol{M}(\boldsymbol{q}_u)\ddot{\tilde{\boldsymbol{q}}}_u = -\big[\boldsymbol{C}(\boldsymbol{q}_u, \dot{\boldsymbol{q}}_u) + \boldsymbol{K}_{vu}(t, \tilde{\boldsymbol{q}})\big]\dot{\tilde{\boldsymbol{q}}}_u + \boldsymbol{\psi}(\tilde{\boldsymbol{q}}_a - \tilde{\boldsymbol{q}}_u), \tag{7.266}$$

are bounded, implies that $\ddot{\tilde{\boldsymbol{q}}}_u$ is bounded.[8]. Boundedness of $\ddot{\boldsymbol{q}}$ follows from Assumption 7.4.1. This again, implies that $\ddot{\boldsymbol{M}}(\boldsymbol{q})$ is bounded.[9] Further, $\ddot{\tilde{\boldsymbol{q}}}_u$ is continuous in $\tilde{\boldsymbol{q}}_u, \dot{\tilde{\boldsymbol{q}}}_u, \tilde{\boldsymbol{q}}_a$ and in t through the bounded functions $\boldsymbol{q}_u^*(t)$ and $\dot{\boldsymbol{q}}_u^*(t)$.

The reasoning for the boundedness of $\ddot{\tilde{\boldsymbol{q}}}_a$ goes along the same lines as for $\ddot{\tilde{\boldsymbol{q}}}_u$. We can write the closed-loop motor dynamics in (7.114) as

$$\bar{\boldsymbol{B}}(t, \tilde{\boldsymbol{q}}, \dot{\tilde{\boldsymbol{q}}}_u)\ddot{\tilde{\boldsymbol{q}}}_a = -\bar{\boldsymbol{C}}_a(t, \tilde{\boldsymbol{q}}, \dot{\tilde{\boldsymbol{q}}})\dot{\tilde{\boldsymbol{q}}}_a - \boldsymbol{\psi}(\tilde{\boldsymbol{q}}_a - \tilde{\boldsymbol{q}}_u) - \boldsymbol{K}_{pa}\tilde{\boldsymbol{q}}_a - \boldsymbol{K}_{va}\dot{\tilde{\boldsymbol{q}}}_a \tag{7.267}$$

From the analysis so far, we can directly conclude the boundedness of the last three terms and upper bound the norm[10] of $\bar{\boldsymbol{C}}_a$

$$||\bar{\boldsymbol{C}}_a|| \leq ||\boldsymbol{A}||\,||\boldsymbol{B}||\,||\dot{\boldsymbol{A}}||. \tag{7.268}$$

Let us analyze each of the RHS terms. From Assumption 7.2.1 and the implicit function theorem D.1.2 follows the continuity of $\big[\boldsymbol{Y}\big]_q^{-1}$, $\big[\dot{\boldsymbol{Y}}\big]_q^{-1}$, $\big[\boldsymbol{Y}\big]_{\bar{q}}$ and $\big[\boldsymbol{Y}\big]_{\bar{q}}$ in the states, and continuity in the time through the bounded functions $\boldsymbol{q}_u^*(t), \dot{\boldsymbol{q}}_u^*(t), \ddot{\boldsymbol{q}}_u^*(t)$. Due to the boundedness of $\boldsymbol{x}$, we know that $\boldsymbol{A}$ is bounded and continuous in time through bounded functions. $\boldsymbol{B}$ is bounded by the assumptions on the model. Knowing that

$$\dot{\boldsymbol{A}} = \big[\dot{\boldsymbol{Y}}\big]_q^{-1}\big[\boldsymbol{Y}\big]_{\bar{q}} + \big[\boldsymbol{Y}\big]_q^{-1}\big[\dot{\boldsymbol{Y}}\big]_{\bar{q}}, \tag{7.269}$$

we can also conclude that $\dot{\boldsymbol{A}}$ is bounded and continuous in time through bounded functions. In the end, we can conclude that $\bar{\boldsymbol{C}}_a$ is continuous in $\boldsymbol{x}$, $\ddot{\tilde{\boldsymbol{q}}}_u$ and t and depends on time through bounded functions $\boldsymbol{q}_u^*(t), \dot{\boldsymbol{q}}_u^*(t), \ddot{\boldsymbol{q}}_u^*(t)$.

From Lemma 7.2.2, we know that the inverse of $\bar{\boldsymbol{B}}$ exists and that it is bounded. This allows us to conclude, that $\ddot{\tilde{\boldsymbol{q}}}_a$ is bounded, continuous in the states $\boldsymbol{x}$, $\ddot{\tilde{\boldsymbol{q}}}_u$ and time t through the bounded functions $\boldsymbol{q}_u^*(t), \dot{\boldsymbol{q}}_u^*(t), \ddot{\boldsymbol{q}}_u^*(t)$.

Ad Condition (iv) of Matrosov's Theorem. To show that W satisfies Condition (iv), we invoke Lemma C.1.5 by B. Paden and R. Panja. Above, we have established that $\ddot{\tilde{\boldsymbol{q}}}_u, \ddot{\tilde{\boldsymbol{q}}}_a$ are continuously in the tracking errors $\boldsymbol{x}$ and depend continuously on time through $\boldsymbol{q}_u^*(t), \dot{\boldsymbol{q}}_u^*(t), \ddot{\boldsymbol{q}}_u^*(t)$, which are bounded. To verify that $\dot{W}$ satisfies condition (iv.a) of Lemma C.1.5, we have yet to show that $\tilde{\boldsymbol{q}}_u^{(3)}, \tilde{\boldsymbol{q}}_a^{(3)}$ are continuous in the tracking errors $\boldsymbol{x}$ and depend continuously on time through a bounded function.

7: Notice that boundedness of $\boldsymbol{x}$, together with Assumption 7.2.3, implies boundedness of $\boldsymbol{q}_u, \dot{\boldsymbol{q}}_u$.

8: Note that $||\boldsymbol{C}(\boldsymbol{q}, \dot{\boldsymbol{q}})|| \leq k_C||\dot{\boldsymbol{q}}||$ for some positive constant k_C.

9: Which is equivalent to the statement that $\dot{\boldsymbol{C}}$ is bounded.

10: Any matrix norm can be used here.

To show that $\tilde{\boldsymbol{q}}_u^{(3)}$ is bounded, we differentiate the link dynamics of (7.114) with respect to time and rearrange some terms

$$\begin{aligned}\boldsymbol{M}(\boldsymbol{q}_u)\frac{\mathrm{d}}{\mathrm{d}t}\left(\dddot{\tilde{\boldsymbol{q}}}_u\right) &= -\dot{\boldsymbol{M}}(\boldsymbol{q}_u)\ddot{\tilde{\boldsymbol{q}}}_u - \boldsymbol{C}(\boldsymbol{q}_u,\dot{\boldsymbol{q}}_u)\ddot{\tilde{\boldsymbol{q}}}_u - \dot{\boldsymbol{C}}(t,\tilde{\boldsymbol{q}},\dot{\tilde{\boldsymbol{q}}}_u)\dot{\tilde{\boldsymbol{q}}}_u \\ &\quad - \dot{\boldsymbol{\mathcal{K}}}_{vu}(t,\tilde{\boldsymbol{q}})\ddot{\tilde{\boldsymbol{q}}}_u - \dot{\boldsymbol{\mathcal{K}}}_{vu}(t,\tilde{\boldsymbol{q}})\dot{\tilde{\boldsymbol{q}}}_u + \boldsymbol{\kappa}(\tilde{\boldsymbol{q}}_a - \tilde{\boldsymbol{q}})(\dot{\tilde{\boldsymbol{q}}}_a - \dot{\tilde{\boldsymbol{q}}}_u).\end{aligned} \tag{7.270}$$

All RHS terms have been shown to be bounded, continuous with respect to the tracking error and depend continuously on time through bounded functions.[11] As $\boldsymbol{M}^{-1}$ is bounded, we can conclude that $\tilde{\boldsymbol{q}}_u^{(3)}$ exists and depends continuously on the tracking error and continuously on time through bounded functions $\boldsymbol{q}_u^*(t), \dot{\boldsymbol{q}}_u^*(t), \ddot{\boldsymbol{q}}_u^*(t)$.

11: See also Assumption 7.1.1.

For $\tilde{\boldsymbol{q}}_a^{(3)}$ we can proceed in analogous fashion. Differentiating the motor dynamics of the closed-loop system (7.114) with respect to time and rearranging some terms gives

$$\begin{aligned}\bar{\boldsymbol{B}}(t,\tilde{\boldsymbol{q}},\dot{\tilde{\boldsymbol{q}}}_u)\frac{\mathrm{d}}{\mathrm{d}t}\left(\dddot{\tilde{\boldsymbol{q}}}_a\right) &= -\dot{\bar{\boldsymbol{B}}}(t,\tilde{\boldsymbol{q}},\dot{\tilde{\boldsymbol{q}}}_u)\ddot{\tilde{\boldsymbol{q}}}_a - \bar{\boldsymbol{C}}_a(t,\tilde{\boldsymbol{q}},\dot{\tilde{\boldsymbol{q}}})\ddot{\tilde{\boldsymbol{q}}}_a - \dot{\bar{\boldsymbol{C}}}_a(t,\tilde{\boldsymbol{q}},\dot{\tilde{\boldsymbol{q}}})\dot{\tilde{\boldsymbol{q}}}_a \\ &\quad - \boldsymbol{\kappa}(\tilde{\boldsymbol{q}}_a - \tilde{\boldsymbol{q}})(\dot{\tilde{\boldsymbol{q}}}_a - \dot{\tilde{\boldsymbol{q}}}_u) - \boldsymbol{K}_{va}\ddot{\tilde{\boldsymbol{q}}}_a - \boldsymbol{K}_{pa}\dot{\tilde{\boldsymbol{q}}}_a.\end{aligned} \tag{7.271}$$

The only terms we still have to analyze are $\dot{\bar{\boldsymbol{B}}}_a$ and $\dot{\bar{\boldsymbol{C}}}_a$. We can use the results from above to argue that $\dot{\boldsymbol{B}}_\eta = 2\boldsymbol{A}^{\mathrm{T}}\boldsymbol{B}\dot{\boldsymbol{A}}$ is continuous in the states $\boldsymbol{x}, \dot{\tilde{\boldsymbol{q}}}$ and in time through bounded functions $\boldsymbol{q}_u^*(t), \ddot{\boldsymbol{q}}_u^*(t), \dddot{\boldsymbol{q}}_u^*(t)$. To obtain an analogous statement for $\dot{\bar{\boldsymbol{C}}}_a = \dot{\boldsymbol{A}}^{\mathrm{T}}\boldsymbol{B}\dot{\boldsymbol{A}} + \boldsymbol{A}^{\mathrm{T}}\boldsymbol{B}\ddot{\boldsymbol{A}}$ we have yet to analyze $\ddot{\boldsymbol{A}}$. The straightforward, but tedious computations, we used to analyze $\dot{\boldsymbol{A}}$ can be extended to show that $\ddot{\boldsymbol{A}}$ is a continuous function in $\boldsymbol{x}$, $\ddot{\tilde{\boldsymbol{q}}}_u, \tilde{\boldsymbol{q}}_u^{(3)}$ and in time through bounded functions $\boldsymbol{q}_u^*(t), \dots, \frac{d^3}{dt^3}\boldsymbol{q}_u^*(t)$. To do so, one only has to the take the continuity and boundedness properties of $\tilde{\boldsymbol{q}}_u^{(3)}$ that we have shown above and the fact that $U_s \in C^4$ additionally into consideration.

To check condition (iv.b) of Lemma C.1.5, we compute the time derivative of W along the solutions of the closed-loop system (7.114) and evaluate $\dot{W}$ on the the critical set E

$$\begin{aligned}\dot{W}(t,\boldsymbol{x}) = &-2\left(\boldsymbol{\psi}(\tilde{\boldsymbol{q}}_a - \tilde{\boldsymbol{q}}_u) + \boldsymbol{K}_{pa}\tilde{\boldsymbol{q}}_a\right)^{\mathrm{T}}\boldsymbol{S}\left(\boldsymbol{\psi}(\tilde{\boldsymbol{q}}_a - \tilde{\boldsymbol{q}}_u) + \boldsymbol{K}_{pa}\tilde{\boldsymbol{q}}_a\right) \\ &+ 2\boldsymbol{\psi}^{\mathrm{T}}(\tilde{\boldsymbol{q}}_a - \tilde{\boldsymbol{q}}_u)^{\mathrm{T}}\boldsymbol{Q}\,\boldsymbol{\psi}(\tilde{\boldsymbol{q}}_a - \tilde{\boldsymbol{q}}_u), \quad \forall \boldsymbol{x} \in E,\end{aligned} \tag{7.272}$$

where

$$\begin{aligned}\boldsymbol{Q} &\triangleq \boldsymbol{M}^{-\mathrm{T}}\boldsymbol{K}_{vu}\boldsymbol{M}^{-1} = \boldsymbol{Q}^{\mathrm{T}}, \\ \boldsymbol{S} &\triangleq \boldsymbol{B}^{-\mathrm{T}}\boldsymbol{K}_{va}\boldsymbol{B}^{-1} = \boldsymbol{S}^{\mathrm{T}}.\end{aligned}$$

Assumption 5.1.1 implies that $\boldsymbol{M}^{-1}$ is non-singular, $\boldsymbol{K}_{vu}$ is a real-symmetric, positive definite matrix, hence, Sylvester's Law of Inertia [118] can be applied to show the positive definiteness of $\boldsymbol{Q}$. Similarly, $\boldsymbol{S}$ can be shown to be positive definite. From the positive definiteness of $\boldsymbol{Q}$ and $\boldsymbol{S}$, follows directly that $\dot{W} \leq \boldsymbol{0}\ \forall (t,\boldsymbol{x}) \in [t_0,\infty) \times E$, whereby equality hold if and only if $\boldsymbol{x} = \boldsymbol{0}$. Let us define

[118]: Meyer (2004), *Matrix Analysis and Applied Linear Algebra*

$$\boldsymbol{P}(t,\boldsymbol{x}) \triangleq \begin{bmatrix}\boldsymbol{Q}+\boldsymbol{S} & \boldsymbol{S}\boldsymbol{K}_{pa} \\ \boldsymbol{K}_{pa}^{\mathrm{T}}\boldsymbol{S} & \boldsymbol{K}_{pa}^{\mathrm{T}}\boldsymbol{S}\boldsymbol{K}_{pa}\end{bmatrix} \in \mathbb{R}^{2n\times 2n},$$

with the following Choleski factorization

$$\begin{bmatrix} \sqrt{\boldsymbol{Q}} & \boldsymbol{S}^{1/2} \\ \boldsymbol{0} & \boldsymbol{K}_{pa}^{\mathrm{T}} \boldsymbol{S}^{1/2} \end{bmatrix}. \tag{7.273}$$

From this follows that $\boldsymbol{P}$ is a positive definite matrix which is state- and explicitly time-dependent.[12] This allows us to write the absolute value of $\dot{W}$ in matrix form

$$|\dot{W}(t,\boldsymbol{x})| = 2 \begin{bmatrix} \boldsymbol{\psi}(\tilde{\boldsymbol{q}}_a - \tilde{\boldsymbol{q}}_u) \\ \tilde{\boldsymbol{q}}_a \end{bmatrix}^{\mathrm{T}} \boldsymbol{P} \begin{bmatrix} \boldsymbol{\psi}(\tilde{\boldsymbol{q}}_a - \tilde{\boldsymbol{q}}_u) \\ \tilde{\boldsymbol{q}}_a \end{bmatrix}, \quad \forall \boldsymbol{x} \in E. \tag{7.274}$$

12: For real-symmetric matrices $\boldsymbol{P}$, the following statements are equivalent: (1) $\boldsymbol{P}$ is positive definite and (2) $\boldsymbol{P} = \boldsymbol{B}\boldsymbol{B}^{\mathrm{T}}$ for some non-singular $\boldsymbol{B}$ [72].

We denote

$$W^*(\boldsymbol{x}) \triangleq \underline{P} \, || \begin{bmatrix} \boldsymbol{\psi}(\tilde{\boldsymbol{q}}_a - \tilde{\boldsymbol{q}}_u) \\ \tilde{\boldsymbol{q}}_a \end{bmatrix} ||^2, \tag{7.275}$$

where

$$\underline{P} \triangleq \inf_{(\boldsymbol{x},t)\in E\times I} \left\{ \lambda(\sqrt{\boldsymbol{Q}}), \underline{\lambda}(\boldsymbol{K}_{pa}) \underline{\lambda} \sqrt{\boldsymbol{S}}) \right\} > 0,$$

which allows us to establish the following inequality

$$|\dot{W}(\boldsymbol{x},t)| \geq W^*(\boldsymbol{x}), \quad \forall \boldsymbol{x} \in E. \tag{7.276}$$

Clearly, W^* is a time-invariant, positive definite function of $\boldsymbol{x}$. According to [96, Lemma 4.3] there exists a function γ of class $\mathcal{K}_\infty$, such that $W^*(\boldsymbol{x}) \geq \gamma(||\boldsymbol{x}||)$. This completes the verification of condition 4(b).

From Prop. 7.5.1 we know already that $\boldsymbol{x}$ is bounded. This, together with the continuity of the RHS of (7.266) and (7.267) in $\boldsymbol{x}$ and in time through $\boldsymbol{q}_u^*(t)$ and its time-derivatives we can conclude that the RHS of (7.266) and (7.267) are bounded for all $(t,\boldsymbol{x}) \in \mathbb{R}^+ \times \Omega$ for bounded Ω. Moreover, $\boldsymbol{M}$ and $\bar{\boldsymbol{B}}$ are bounded (see Assumption 7.1.1). Thus, $\boldsymbol{f}$, which is implicitly defined in (7.266)–(7.267), is bounded on $\mathbb{R}^+ \times \Omega$ for bounded Ω and the last condition of Matrosov's Theorem is fulfilled.

So far all conditions of Matrosov's Theorem have been shown to be satisfied. In addition we can use the first inequality of Condition (i) to determine the region of attraction. For any initial condition $\boldsymbol{x}_0 \in \mathbb{R}^{4n}$ we can find an appropriate α and Ω via Condition (i) such that $\boldsymbol{x}_0$ is element of $V_{t,\alpha}^{-1}$. Thus, according to Matrosov's Theorem, the origin $(\tilde{\boldsymbol{q}}, \dot{\tilde{\boldsymbol{q}}}) = \boldsymbol{0}$ is an uniformly globally asymptotically stable equilibrium point of the closed-loop system (7.114). ■

7.5.1 Proof of Proposition 7.2.4

The proof relies on Theorem C.1.4 by Matrosov and Lemma C.1.5 by Paden and Panja. This technique was first reported in [144] for a fully actuated robot. The storage function (7.147) will be used as Lyapunov function. In [86], we reported the application of Matrosov's theorem to solve the joint space motion tracking problem for ASRs. Here, we highlight only the key steps and adjustments required compared to [86], respectively the proof in Section 7.5. The main challenge lies in verifying Condition (iv) of Theorem C.1.4. Thus, Condition (i) is at the center of focus in the proof below.

[144]: Paden et al. (1988), "Globally asymptotically stable "PD+" controller for robot manipulators"

Proof. Let us consider the storage function in (7.147) as a Lyapunov function candidate $\mathcal{H} : \big([0,\infty)\times\Omega\big) \to \mathbb{R}$, and the error vector $\boldsymbol{e} = \big[\tilde{\boldsymbol{x}}^{\mathrm{T}}, \dot{\tilde{\boldsymbol{x}}}^{\mathrm{T}}\big]^{\mathrm{T}}$. For now, Ω ca be chosen arbitrarily large. Setting $\mathcal{Q}' = \boldsymbol{0}$, then evaluating the time derivative of $\mathcal{H}$ along the solutions of (7.143) gives, c.f. (7.148),

$$\dot{\mathcal{H}} = -\dot{\tilde{\boldsymbol{x}}}^{\mathrm{T}}\mathcal{K}_v\dot{\tilde{\boldsymbol{x}}}, \tag{7.277}$$

which is a negative semi-definite function of the states. Thus, $\mathcal{H}$ qualifies as Lyapunov function. Let us continue with verify Condition (i) of Matrosov's by establish upper and lower bounds on $\mathcal{H}$ through functions of class $\mathcal{K}$. Taking into account Remark 7.5.1, consider the state-dependent bounding functions

$$\alpha(\boldsymbol{e}) = \frac{1}{2}\Big[\inf_{t\in I, e\in\Omega} \lambda\big\{\mathcal{M}_x\big(\tilde{\boldsymbol{x}} + \boldsymbol{x}^*(t)\big)\big\}||\dot{\tilde{\boldsymbol{x}}}||^2 + \inf\lambda\big\{\boldsymbol{K}_{pu}\big\}||\tilde{\boldsymbol{x}}_u||^2\Big] + \mathcal{V}_e(\bar{\boldsymbol{x}}_a), \tag{7.278}$$

$$\beta(\boldsymbol{e}) = \frac{1}{2}\Big[\sup_{t\in I, e\in\Omega} \lambda\big\{\mathcal{M}_x\big(\tilde{\boldsymbol{x}} + \boldsymbol{x}^*(t)\big)\big\}||\dot{\tilde{\boldsymbol{x}}}||^2 + \sup\lambda\big\{\boldsymbol{K}_{pu}\big\}||\tilde{\boldsymbol{x}}_u||^2\Big] + \mathcal{V}_e(\bar{\boldsymbol{x}}_a), \tag{7.279}$$

where $\inf\lambda(.)$ and $\sup\lambda(.)$ denote the minimal and maximal eigenvalues of (.). Invoking Lemma 4.3 in [95], we can conclude the existence of class $\mathcal{K}$ function a and b such that $a(||\tilde{\boldsymbol{x}}||) \leq \alpha(\boldsymbol{e})$ and $b(||\boldsymbol{e}||) \geq \beta(\boldsymbol{e})$. In fact, a and b are of class $\mathcal{K}_\infty$ since α and β are radially unbounded. This allows us to conclude uniform stability of the origin of system (7.143) and that Condition (i) of Matrosov's theorem is satisfied.

The central idea of Matrosov's theorem relies on the appealing usage of bounded auxiliary function that ensures that the system cannot get stuck in the problematic set, $E = \big\{\boldsymbol{e}\in\Omega : \dot{\tilde{\boldsymbol{x}}} = \boldsymbol{0}\big\}$, where the time derivative of the Lyapunov function is zero. Consider the auxiliary function $W : [0,\infty)\times\Omega \to \mathbb{R}$

$$W(t,\boldsymbol{e}) = \ddot{\mathcal{H}}, \tag{7.280}$$

and restrict Ω to be an arbitrarily large, but bounded set. Exploiting the fact that the origin is stable, and applying the same arguments as reported in [86], see also Section 7.5, we can show that (iii) is satisfied. Consider that

$$\tilde{\boldsymbol{x}}_a = \bar{\boldsymbol{x}}_a = \bar{\boldsymbol{q}}_a - \bar{\boldsymbol{q}}_u, \tag{7.281}$$

$$\boldsymbol{J}^{-\mathrm{T}}\begin{bmatrix}\frac{\partial\mathcal{V}_e}{\partial\bar{\boldsymbol{q}}}\end{bmatrix}^{\mathrm{T}} = \begin{bmatrix}\boldsymbol{0}\\ \frac{\partial\mathcal{V}_e}{\partial\bar{\boldsymbol{x}}_a}\end{bmatrix} = \begin{bmatrix}\boldsymbol{0}\\ \frac{\partial\mathcal{V}_e}{\partial\tilde{\boldsymbol{x}}_a}\end{bmatrix}, \tag{7.282}$$

$$\boldsymbol{\psi}(\tilde{\boldsymbol{x}}_a) = \frac{\partial\mathcal{V}_e}{\partial\tilde{\boldsymbol{x}}_a}(\tilde{\boldsymbol{x}}_a), \tag{7.283}$$

so that computing the time derivative of W along the solutions of (7.143), and evaluating the result on the critical set E gives

$$\dot{W}(t,\boldsymbol{e}) = -\begin{bmatrix}\tilde{\boldsymbol{x}}_u\\ \boldsymbol{\psi}(\tilde{\boldsymbol{x}}_a)\end{bmatrix}^{\mathrm{T}}\boldsymbol{P}(t,\boldsymbol{e})\begin{bmatrix}\tilde{\boldsymbol{x}}_u\\ \boldsymbol{\psi}(\tilde{\boldsymbol{x}}_a)\end{bmatrix}, \text{ with} \tag{7.284}$$

$$\boldsymbol{P}(t,\tilde{\boldsymbol{x}}_u) = \mathrm{diag}(\boldsymbol{K}_{pu}^{\mathrm{T}}, \boldsymbol{I})\mathcal{M}_x^{-\mathrm{T}}\mathcal{K}_v\mathcal{M}_x^{-1}\mathrm{diag}(\boldsymbol{K}_{pu}, \boldsymbol{I}). \tag{7.285}$$

The positive definiteness of $\mathcal{M}_x, \mathcal{K}_v, \boldsymbol{K}_{pu}$ and the symmetry of $\mathcal{M}_x, \boldsymbol{K}_{pu}$ implies that $\boldsymbol{P}$ is a positive definite matrix, which is state and explicitly time-

dependent. Introducing

$$W^*(\boldsymbol{e}) = \inf_{t\in I, \boldsymbol{e}\in\Omega} \lambda\big(\boldsymbol{P}(t,\tilde{\boldsymbol{x}}_u)\big)|| \begin{bmatrix} \tilde{\boldsymbol{x}}_u \\ \boldsymbol{\psi}(\tilde{\boldsymbol{x}}_a) \end{bmatrix} ||^2, \tag{7.286}$$

which is a positive definite function of the states, allows us to establish the inequality

$$|W(t,\boldsymbol{e})| \geq W^*(\boldsymbol{e}), \quad \forall \boldsymbol{e} \in E. \tag{7.287}$$

Lemma 4.3 in [96], guarantees the existence of a class $\mathcal{K}_\infty$ function $\boldsymbol{\gamma}$ such that $W^*(\boldsymbol{e}) \geq \boldsymbol{\gamma}\big(||\boldsymbol{e}||\big)$. Putting everything together, we conclude that

$$|\dot{W}(\boldsymbol{e})| \geq \boldsymbol{\gamma}(||\boldsymbol{e}||), \forall \boldsymbol{e} \in E \text{ and } t \in [0,\infty). \tag{7.288}$$

We can conclude that condition (iv.b) of Lemma C.1.5 is satisfied, and invoke this lemma to show that the critical Condition (iv) of Matrosov's Theorem is satisfied. The fulfillment of Condition (v) can be shown in a straightforward manner, e.g. as pointed out in [92]. This completes the proof. ■

7.5.2 Proof of Proposition 7.2.5

The closed-loop dynamics (7.149)–(7.152) closely resembles the one of the rigid robot case [167]. The crucial difference is the presence of the generalized elastic force. Due to the conservative nature of this force, we can adapt the techniques proposed in [170] by including the potential energy function $\mathcal{V}_e$ in the Lyapunov function. A similar approach is applied in the work [133], which considers linear elastic elements and joint space motion tracking though.

Proof. The proof relies on Lyapunov's direct method. Let us consider the Lyapunov function candidate

$$\mathcal{V} = \tfrac{1}{2}\boldsymbol{s}^{\mathrm{T}}\mathcal{M}_x\boldsymbol{s} + \tilde{\boldsymbol{x}}_u^{\mathrm{T}}\boldsymbol{\Lambda}_u\mathcal{K}_{vu}\tilde{\boldsymbol{x}}_u + \mathcal{V}_e(\tilde{\boldsymbol{x}}_a). \tag{7.289}$$

which contains a positive definite quadratic form in $\tilde{\boldsymbol{x}}_u$ compared to the storage function (7.154). The positive definiteness of this term follows directly from the fact that $\boldsymbol{\Lambda}_u$ and $\boldsymbol{\Lambda}_u$ are diagonal and positive definite. This ensures that (7.289) qualifies as Lyapunov function candidate since it is a globally positive function [57]. In the following, we shall repetitively make use of the fact that $\boldsymbol{K}_{vu}, \boldsymbol{K}_{va}, \boldsymbol{\Lambda}_u, \boldsymbol{\Lambda}_a$ are diagonal matrices without explicitly mentioning. Using the skew-symmetry from Lemma 2.5.8, we obtain for the time derivative of (7.289) along the solutions of (7.149)–(7.152)

$$\dot{\mathcal{V}} = -\boldsymbol{s}^{\mathrm{T}}\mathcal{K}_v\boldsymbol{s} - \tilde{\boldsymbol{x}}_a^{\mathrm{T}}\boldsymbol{\Lambda}_a\boldsymbol{\psi}(\tilde{\boldsymbol{x}}_a) + 2\tilde{\boldsymbol{x}}_u^{\mathrm{T}}\boldsymbol{\Lambda}_u\mathcal{K}_{va}\dot{\tilde{\boldsymbol{x}}}_u. \tag{7.290}$$

With an obvious partitioning $\boldsymbol{s} = (\boldsymbol{s}_u, \boldsymbol{s}_a)$, and using the definition of $\mathcal{K}_v$ in (7.142), we can rewrite the first term in (7.290) as

$$\boldsymbol{s}^{\mathrm{T}}\mathcal{K}_v\boldsymbol{s} = \begin{bmatrix} \boldsymbol{J}_u^{-1}\boldsymbol{s}_u \\ \boldsymbol{J}_u^{-1}\boldsymbol{s}_u + \boldsymbol{s}_a \end{bmatrix}^{\mathrm{T}} \begin{bmatrix} \boldsymbol{J}_u^{\mathrm{T}}\boldsymbol{K}_{vu}\boldsymbol{J}_u & \boldsymbol{0} \\ \boldsymbol{0} & \boldsymbol{K}_{va} \end{bmatrix} \begin{bmatrix} \boldsymbol{J}_u^{-1}\boldsymbol{s}_u \\ \boldsymbol{J}_u^{-1}\boldsymbol{s}_u + \boldsymbol{s}_a \end{bmatrix}, \tag{7.291}$$

$$= -\dot{\tilde{\boldsymbol{x}}}_u^{\mathrm{T}}\boldsymbol{K}_{vu}\dot{\tilde{\boldsymbol{x}}}_u - \tilde{\boldsymbol{x}}_u\boldsymbol{\Lambda}_u\boldsymbol{K}_{vu}\boldsymbol{\Lambda}_u + 2\tilde{\boldsymbol{x}}_u^{\mathrm{T}}\boldsymbol{\Lambda}_u\boldsymbol{K}_{vu}\dot{\tilde{\boldsymbol{x}}}_u \tag{7.292}$$

$$+ \big(\boldsymbol{J}_u^{-1}\boldsymbol{s}_u + \boldsymbol{s}_a\big)^{\mathrm{T}}\boldsymbol{K}_{va}\big(\boldsymbol{J}^{-1}\boldsymbol{s}_u + \boldsymbol{s}_a\big). \tag{7.293}$$

Making the substitution (7.290) and (7.291) gives

$$\dot{\mathcal{V}} = -\dot{\tilde{\boldsymbol{x}}}_u^{\mathrm{T}} \boldsymbol{K}_{vu} \dot{\tilde{\boldsymbol{x}}}_u - \tilde{\boldsymbol{x}}_u^{\mathrm{T}} \boldsymbol{\Lambda}_u \boldsymbol{K}_{vu} \boldsymbol{\Lambda}_u \tilde{\boldsymbol{x}}_u - \tilde{\boldsymbol{x}}_a^{\mathrm{T}} \boldsymbol{\Lambda}_a \boldsymbol{\psi}(\tilde{\boldsymbol{x}}_a) \tag{7.294}$$

$$- \left(\boldsymbol{J}_u^{-1} \boldsymbol{s}_u + \boldsymbol{s}_a\right)^{\mathrm{T}} \boldsymbol{K}_{va} \left(\boldsymbol{J}^{-1} \boldsymbol{s}_u + \boldsymbol{s}_a\right). \tag{7.295}$$

It follows from (7.294) and Assumption 7.2.2 that $\dot{\mathcal{V}}$ is a globally negative definite function of the states, $(\tilde{\boldsymbol{x}}, \dot{\tilde{\boldsymbol{x}}})$, which assures global asymptotic stability. To guarantee uniform stability, it needs to be shown that V is also decrescent, that is, bounded from above by a class $\mathcal{K}$ function with the norm of the states as argument. Considering Property 2.5.7 and (7.259), introducing the bounding function

$$V \leq \frac{1}{2} \inf_{t \in \boldsymbol{I}, \tilde{\boldsymbol{x}} \in \mathbb{R}^n} \lambda\{\mathcal{M}_x\} ||\boldsymbol{s}||^2 + \inf \lambda\{\boldsymbol{\Lambda}_u \boldsymbol{K}_{vu}\} ||\tilde{\boldsymbol{x}}_u||^2 + \mathcal{V}_e(\tilde{\boldsymbol{x}}_a), \tag{7.296}$$

and invoking Lemma 4.3 from [96], we can guarantee the existence of the desired bounding class $\mathcal{K}$ function, which completes the proof.

■

7.6 Conclusions

This chapter considered the application of the QFA formulation from Chapter 5 to re-derive the ESP controllers [86, 89–91, 94, 114, 115] in a unifying way. Using Theorem 5.6.1, it has been be shown that the different formulations can be obtained by adjusting only the actuated subsystem Lagrangian of the QFA system.

Moreover, an extension of the ESP concept to ASRs with visco-elastic joints has been reported. The presence of damping in visco-elastic joints has the important consequence that, in general, the virtual motor coordinates cannot be computed through algebraic operations since they are related to the original coordinate in terms of differential equations. Consequently, the controller is a dynamic state feedback, in contrast to static state feedback for purely elastic ASRs. It has been shown, however, that by modifying the controller, we can avoid dynamic state feedback by accepting an additional (time-dependent) motor-side damping term. It is worth remarking that the statements of Proposition 7.4.1, 7.4.2 and 7.4.3 can be strengthened to uniform GAS of the equilibrium point $(\tilde{\boldsymbol{q}}_u, \dot{\tilde{\boldsymbol{q}}}_u) = (\boldsymbol{0}, \boldsymbol{0})$ using techniques for the proofs of Proposition 7.2.1 and 7.2.3.

All ESP designs have in common that the closed-dynamics are characterized by EL equations, which allowed formulating energy-based Lyapunov and storage functions. Figure 7.13 compares the closed-loop dynamics resulting from applying ESP/ESPi control and PD control to a compliant manipulator for the regulation case. In particular, it highlights the physically intuitive nature of the resulting designs.

Extensive experimental evaluation of the ESP concept on the anthropomorphic humanoid DLR *David* is reported in Chapter 11. Moreover, Chapter 12 discusses the integration of ESP designs into a higher-level control framework, and presents several applications. Figure 7.13 compares the closed-loop dynamics resulting from applying ESP, ESPi and PD control to a compliant manipulator for the regulation case.

[86]: Keppler et al. (2018), "Elastic structure preserving (ESP) control for compliantly actuated robots"
[89]: Keppler et al. (2016), "A passivity-based approach for trajectory tracking and link-side damping of compliantly actuated robots"
[90]: Keppler et al. (2016), "A passivity-based controller for motion tracking and damping assignment for compliantly actuated robots"
[91]: Keppler et al. (2021), "Analyzing the performance limits of articulated soft robots based on the ESPi framework: Applications to damping and impedance control"
[94]: Keppler et al. (2018), "Visco-elastic structure preserving impedance (VESPi) control for compliantly actuated robots"
[114]: Meng et al. (2021), "Elastic structure preserving impedance control of bidirectional antagonistic variable stiffness actuation"
[115]: Mengacci et al. (2021), "Elastic Structure Preserving control for compliant robots driven by agonistic-antagonistic actuators (ESPaa)"

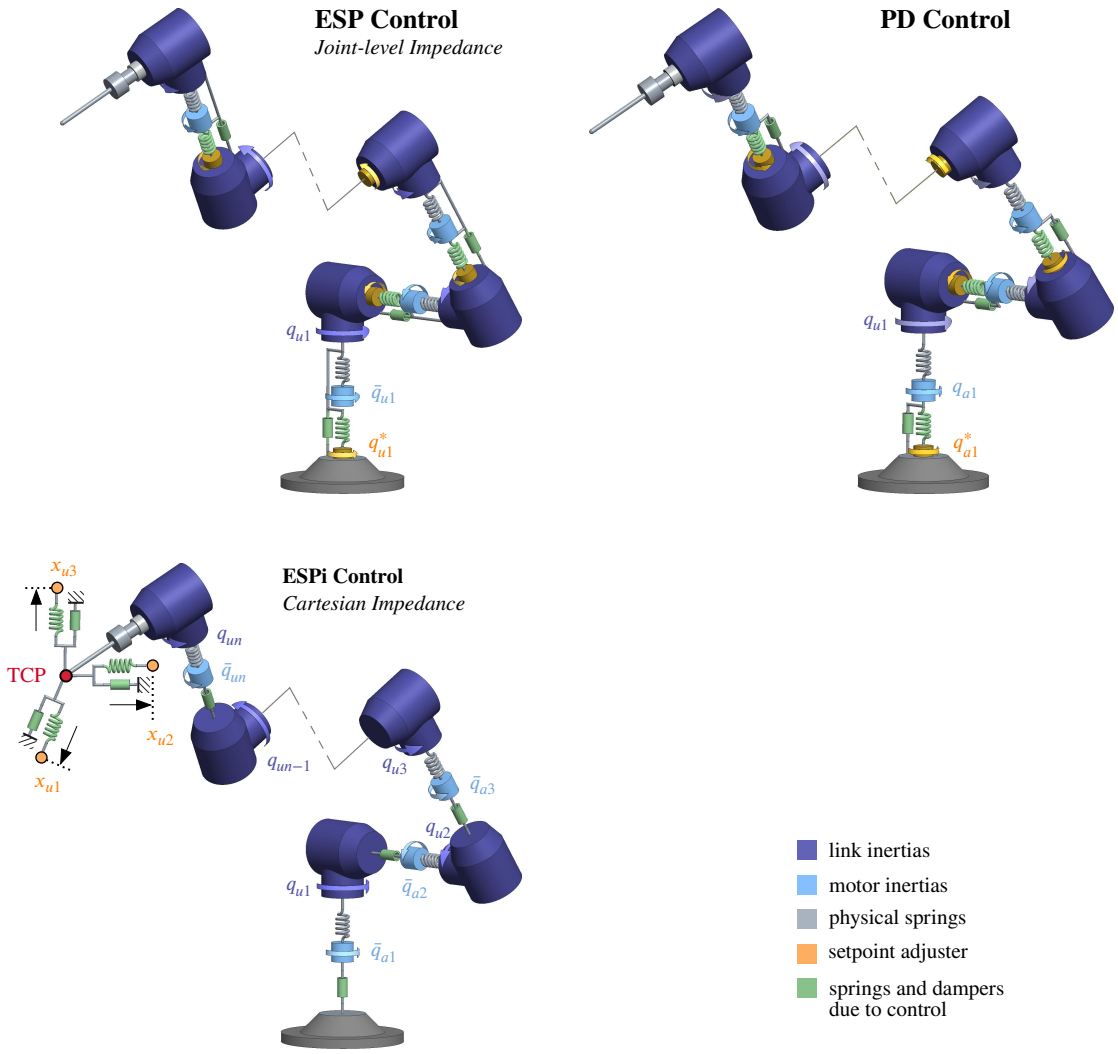

Figure 7.13: ESP, ESPi and PD control closed-loop behavior for a compliant manipulator (regulation case).

Comparison of Nonlinear Controllers for Flexible Joint Manipulators

8

Theories of the known, which are described by different physical ideas may be equivalent in all their predictions and are hence scientifically indistinguishable. However, they are not psychologically identical when trying to move from that base into the unknown. For different views suggest different kinds of modifications which might be made and hence are not equivalent in the hypotheses one generates from them in ones attempt to understand what is not yet understood.

– Richard P. Feynman

Several controller design techniques addressing the problem of global trajectory tracking of nonlinear systems have been reported that can be applied to flexible joint robots (FJRs). Popular representatives are decoupling-based schemes, backstepping-based schemes and passivity-based schemes. Naturally, the question arises how these schemes compare with regard to performance and robustness. This is still an open research problem. The work [20] investigates the connection between the three aforementioned control schemes as applied to FJRs, and analyzes the performance with regard to the following parameters: continuity vis-à-vis the joint stiffness, availability of adaptive implementations when the robot parameters are unknown, and robustness to "energy-preserving" (i.e. passive) unmodeled effects. This section extends this analysis by including two ESP-based designs and the decoupling-based controller reported in [140]. The ESP-based controllers under consideration have been first reported in [86] and [92], and are investigated for the SEA case.

[20]: Brogliato et al. (1998), "Experimental comparison of nonlinear controllers for flexible joint manipulators"

[140]: Ott (2008), *Cartesian Impedance Control of Redundant and Flexible-Joint Robots*

[86]: Keppler et al. (2018), "Elastic structure preserving (ESP) control for compliantly actuated robots"

[92]: Keppler et al. (2018), "Elastic structure preserving impedance (ESPi) control for compliantly actuated robots"

8.1 Control Schemes

This chapter considers the Spong model [168] with the elastic potential energy $\mathcal{V}_e = \frac{1}{2}(\boldsymbol{q}_a - \boldsymbol{q}_u)^{\mathrm{T}} \boldsymbol{K} (\boldsymbol{q}_a - \boldsymbol{q}_u)$, where $\boldsymbol{K}$ is a diagonal positive definite matrix. Let $\boldsymbol{q}_u^*$ be the desired output (link) trajectory. In the following, the subscripts u and a indicate link-side and motor-side quantities, and the superscript $(.)^*$ indicates desired trajectories. To allow for a comparison with the results in [19], we shall rewrite the control laws with a unifying notation:

[168]: Spong (1987), "Modeling and control of elastic joint robots"

[19]: Brogliato et al. (1995), "Global tracking controllers for Flexible-joint manipulators: a comparative study"

$$\boldsymbol{q} = (\boldsymbol{q}_u, \boldsymbol{q}_a) = (q_1, \dots, q_{n_u}, q_{n_u+1}, \dots, q_n), \quad (8.1)$$

$$\boldsymbol{q}^* = (\boldsymbol{q}_u^*, \boldsymbol{q}_a^*) = (q_1^*, \dots, q_{n_u}^*, q_{n_u+1}^*, \dots, q_n^*), \quad (8.2)$$

$$\tilde{\boldsymbol{q}} = (\tilde{\boldsymbol{q}}_u, \tilde{\boldsymbol{q}}_a) = \boldsymbol{q} - \boldsymbol{q}^*, \quad (8.3)$$

$$\boldsymbol{s} = (\boldsymbol{s}_u, \boldsymbol{s}_a) = \dot{\tilde{\boldsymbol{q}}} + \boldsymbol{\Lambda}\tilde{\boldsymbol{q}}, \quad (8.4)$$

$$\boldsymbol{\Lambda} = \mathrm{diag}(\boldsymbol{\Lambda}_u, \boldsymbol{\Lambda}_a) > 0 \text{ and diagonal}, \quad (8.5)$$

where desired motor position signal $\boldsymbol{q}_a^*$ can be interpreted as follows. The rational by Brogliato was to make $\boldsymbol{q}_a$ converge to some function $\boldsymbol{q}_a^*$, that if applied as input to the link dynamics, will drive $\boldsymbol{q}_u$ towards $\boldsymbol{q}_u^*$. In the following,

$\boldsymbol{u}_r$ denotes the control law for the rigid robot dynamics (i.e., the unactuated subsystem Σ_u). That is for the considered controllers, we have:

$$\boldsymbol{u}_r = \begin{cases} \boldsymbol{M}\ddot{\boldsymbol{q}}_u^* + \boldsymbol{C}\dot{\boldsymbol{q}}_u^* + \boldsymbol{g}(\boldsymbol{q}_u) - \boldsymbol{K}_{vu}\boldsymbol{s}_u, & \text{for Controller 2–5} \\ \boldsymbol{M}\ddot{\boldsymbol{q}}_u^* + \boldsymbol{C}\dot{\boldsymbol{q}}_u^* + \boldsymbol{g}(\boldsymbol{q}_u) - \boldsymbol{K}_{vu}\dot{\tilde{\boldsymbol{q}}}_u, & \text{for Controller 6} \\ \boldsymbol{M}\ddot{\boldsymbol{q}}_u^* + \boldsymbol{C}\dot{\boldsymbol{q}}_u^* + \boldsymbol{g}(\boldsymbol{q}_u) - \boldsymbol{K}_{vu}\dot{\tilde{\boldsymbol{q}}}_u - \boldsymbol{K}_{pu}\tilde{\boldsymbol{q}}_u, & \text{for Controller 1, 7} \end{cases} \tag{8.6}$$

with $\boldsymbol{K}_{pu}, \boldsymbol{K}_{vu} > 0$. Considering the Spong model for ASR, and using the notation (8.6), we can summarize the controllers from [20], the decoupling-based controller from [140] and the ESP controllers from [86] and [92] in a unified form:

[140]: Ott (2008), *Cartesian Impedance Control of Redundant and Flexible-Joint Robots*

Controller 1: Decoupling-based control [140]

$$\begin{aligned} \boldsymbol{u}_a &= \boldsymbol{B}\left[\ddot{\boldsymbol{q}}_a^* - \boldsymbol{K}_v\dot{\tilde{\boldsymbol{q}}}_a - \boldsymbol{K}_p\tilde{\boldsymbol{q}}_a\right] + \boldsymbol{K}(\boldsymbol{q}_a^* - \boldsymbol{q}_u) \\ \boldsymbol{q}_a^* &= \boldsymbol{K}^{-1}\boldsymbol{u}_r + \boldsymbol{q}_u \end{aligned} \tag{8.7}$$

[19]: Brogliato et al. (1995), "Global tracking controllers for Flexible-joint manipulators: a comparative study"

Controller 2: Decoupling-based control [19], with $\boldsymbol{K}_1, \boldsymbol{K}_2 > 0$

$$\begin{aligned} \boldsymbol{u}_a &= \boldsymbol{B}\ddot{\boldsymbol{q}}_a^* - \boldsymbol{K}_2\dot{\tilde{\boldsymbol{q}}}_a - \boldsymbol{K}_1\tilde{\boldsymbol{q}}_a + \boldsymbol{K}(\boldsymbol{q}_a - \boldsymbol{q}_u) \\ \boldsymbol{q}_a^* &= \boldsymbol{K}^{-1}\boldsymbol{u}_r + \boldsymbol{q}_u \end{aligned} \tag{8.8}$$

Controller 3: Backstepping-based control [19]

$$\begin{aligned} \boldsymbol{u}_a &= \boldsymbol{B}\left[\ddot{\boldsymbol{q}}_a^* - 2\dot{\tilde{\boldsymbol{q}}}_a - 2\tilde{\boldsymbol{q}}_a - \boldsymbol{K}(\dot{\boldsymbol{s}}_u + \boldsymbol{s}_u)\right] + \boldsymbol{K}(\boldsymbol{q}_a - \boldsymbol{q}_u) \\ \boldsymbol{q}_a^* &= \boldsymbol{K}^{-1}\boldsymbol{u}_r + \boldsymbol{q}_u \\ \boldsymbol{s}_u &= \dot{\tilde{\boldsymbol{q}}}_u + \boldsymbol{\Lambda}_u\tilde{\boldsymbol{q}}_u \end{aligned} \tag{8.9}$$

Controller 4: Robustified backstepping-based control [19]

$$\begin{aligned} \boldsymbol{u}_a &= \boldsymbol{B}\left[\ddot{\boldsymbol{q}}_a^* - 2\dot{\tilde{\boldsymbol{q}}}_a - 2\tilde{\boldsymbol{q}}_a - (\dot{\boldsymbol{s}}_u + \boldsymbol{s}_u)\right] + \boldsymbol{K}(\boldsymbol{q}_a - \boldsymbol{q}_u) \\ \boldsymbol{q}_a^* &= \boldsymbol{K}^{-1}\boldsymbol{u}_r + \boldsymbol{q}_u \\ \boldsymbol{s}_u &= \dot{\tilde{\boldsymbol{q}}}_u + \boldsymbol{\Lambda}_a\tilde{\boldsymbol{q}}_u \end{aligned} \tag{8.10}$$

Controller 5: Passivity-based control [19]

$$\begin{aligned} \boldsymbol{u}_a &= \boldsymbol{B}\left(\ddot{\boldsymbol{q}}_a^* - \boldsymbol{\Lambda}_a\dot{\tilde{\boldsymbol{q}}}_a\right) + \boldsymbol{K}(\boldsymbol{q}_a^* - \boldsymbol{q}_u^*) - \boldsymbol{K}_a\boldsymbol{s}_a \\ \boldsymbol{q}_a^* &= \boldsymbol{K}^{-1}\boldsymbol{u}_r + \boldsymbol{q}_u^* \\ \boldsymbol{s}_a &= \dot{\tilde{\boldsymbol{q}}}_a + \boldsymbol{\Lambda}_a\tilde{\boldsymbol{q}}_a \end{aligned} \tag{8.11}$$

[86]: Keppler et al. (2018), "Elastic structure preserving (ESP) control for compliantly actuated robots"

Controller 6: ESP-based control [86]

$$\begin{aligned} \boldsymbol{u}_a &= \boldsymbol{B}\ddot{\boldsymbol{q}}_a^* + \boldsymbol{K}\boldsymbol{q}_a^* - \boldsymbol{K}_{va}\dot{\tilde{\boldsymbol{q}}}_a - \boldsymbol{K}_{pa}\tilde{\boldsymbol{q}}_a \\ \boldsymbol{q}_a^* &= \boldsymbol{K}^{-1}\boldsymbol{u}_r + \boldsymbol{q}_u^* \end{aligned} \tag{8.12}$$

[92]: Keppler et al. (2018), "Elastic structure preserving impedance (ESPi) control for compliantly actuated robots"

Controller 7: ESPi-based control [92]

$$\begin{aligned} \boldsymbol{u}_a &= \boldsymbol{B}\ddot{\boldsymbol{q}}_a^* + \boldsymbol{K}\boldsymbol{q}_a^* - \boldsymbol{K}_{va}\dot{\tilde{\boldsymbol{q}}}_a \\ \boldsymbol{q}_a^* &= \boldsymbol{K}^{-1}\boldsymbol{u}_r + \boldsymbol{q}_u^* \end{aligned} \tag{8.13}$$

The controllers under investigation originated from the following design techniques:

[159]: Seibert et al. (1990), "Global stabilization of nonlinear cascade systems"

- Stabilization of cascaded nonlinear system [159] for Controller 1–2.

- Backstepping [81] for Controller 3–4.
- Passivity-based methods [165, 178] for Controller 5–7.

[81]: Kanellakopoulos et al. (1991), "Systematic design of adaptive controllers for feedback linearizable systems"

[165]: Slotine et al. (1988), "Adaptive manipulator control: A case study"

[178]: Takegaki et al. (1981), "A new feedback method for dynamic control of manipulators"

The theoretical aspects of the controllers are not recalled. The interested reader is referred to the cited works.

Remark 8.1.1 It is worth mentioning that the follow-up work [20] of [19] includes also singular perturbation-based designs [51, 169] that exploit the two-time scale behavior in systems with relatively large joint stiffness. In this work, however, we are primarily interested in systems that have deliberately incorporated highly elastic elements into the drive train with a stiffness low enough to exploit these elements as energy storage. Clearly, for these kind of systems the two-time scale assumption of singular perturbation-based design does not hold and are not included in the comparison.

[20]: Brogliato et al. (1998), "Experimental comparison of nonlinear controllers for flexible joint manipulators"

[19]: Brogliato et al. (1995), "Global tracking controllers for Flexible-joint manipulators: a comparative study"

[51]: Ghorbel et al. (1989), "Adaptive control of flexible-joint manipulators"

[169]: Spong (1989), "Adaptive control of flexible joint manipulators"

Comparing (8.6)–(8.13), we can make the following observations:

- All controllers require state feedback, i.e. measurement of $\boldsymbol{q}$ and $\dot{\boldsymbol{q}}$, and knowledge of the model parameters.
- Controllers 2–4 compensate the joint torques $\boldsymbol{K}(\boldsymbol{q}_a - \boldsymbol{q}_u)$. The absence of this drawback in the passivity-based designs is noteworthy. Controller 1 is unique in this regard as it compensates $\boldsymbol{K}(\boldsymbol{q}_a^* - \boldsymbol{q}_u)$.
- All controllers use the rigid robot control signal $\boldsymbol{u}_r$ to formulate a desired motor trajectory $\boldsymbol{q}_a^*$; we see that Controller 6 uses the most minimalist one.
- Controller 1–4 require feedback of the output $\boldsymbol{q}_u$ to formulate the desired motor trajectory $\boldsymbol{q}_a^*$. This results in dynamics cancellation of the form $\boldsymbol{B}\ddot{\boldsymbol{q}}_u$, which is undesirable from the robustness point of view. On the other hand, Controller 5–7: require only the desired output trajectory $\boldsymbol{q}_u^*$ for formulating $\boldsymbol{q}_a^*$.
- Controller 6 stands out by the absence of feeding into the loop the output error signal $\tilde{\boldsymbol{q}}_u$.
- Controller 7 stands out by the absence of feeding into the loop the motor error signal $\tilde{\boldsymbol{q}}_a$.
- Outview: The input signals of Controller 6–7 can be physically interpreted as representing the dynamics of a driven spring-mass-damper system, as pointed out in Chapter A. This geometrical point of view reveals ways for avoiding the feedback necessity of the link jerk signals.
- As $\boldsymbol{K}$ grows unbounded, the Controller 5–7 converge to the rigid robot controller. This is not the case for the Controller 1–4 due to the partial motor dynamics cancellation via the term $\boldsymbol{B}\ddot{\boldsymbol{q}}_u$. Moreover, Controller 3 becomes a high-gain design because of the term $\boldsymbol{K}(\dot{\boldsymbol{s}}_u + \boldsymbol{s}_u)$.
- While all controllers require feedback of the acceleration and link jerk signals[1], they do so for two fundamentally different reasons: 1) partial *cancellation* of the motor dynamics, 2) *gravity compensation*, 3) *add* energy dissipation term. Note that only Controller 1–4 require operation 1). It is commonly expected that designs that refrain from dynamics cancellation yield more robust designs. On the contrary, operation 3) can be expected to have a stabilizing effect. Moreover, operation 3) produces an OSP closed loop for Controller 5–7; since OSP implies L2-gain stability [188] this can be considered a desirable operation from the robustness point of view.

1: We recall that $\boldsymbol{q}_u^{(3)}$ can computed without numerical differentiation, as discussed in Section B.2 in Appendix B)

[188]: van der Schaft (1999), *L2-Gain and Passivity in Nonlinear Control*

Based on the observations above, we conclude that the ESP-based controllers are most closely related to the passivity-based approach by [19].

8.1.1 Closed-Loop Passivity

Let us analyze the possibility of representing the closed-loops as two passive operators interconnected in negative feedback. The closed loops of Controller 2–5 can be interpreted as the interconnection of passive subsystems as demonstrated in [19]. In [140] it has been shown that Controller 1 defines a passive map $\mathcal{Q}'_u \mapsto \dot{\boldsymbol{q}}_u$. An interpretation of this scheme as an interconnection of passive subsystems is not provided. For the sake of briefness, only the passivity properties of the passivity-based Controller 5 [19] are recalled and compared to ESP-based controllers since these are most closely related. The closed-loop equations associated with Controller 5 are

$$\begin{aligned}\boldsymbol{\Lambda} =& \operatorname{diag}(\boldsymbol{\Lambda}_u, \boldsymbol{\Lambda}_a),\\ \mathbf{0} =& \mathcal{M}\dot{\boldsymbol{s}} + \left(C + \boldsymbol{K}_v\right)\boldsymbol{s} + \mathcal{K}\tilde{\boldsymbol{q}},\\ \dot{\tilde{\boldsymbol{q}}} =& \boldsymbol{s} + \boldsymbol{\Lambda}\tilde{\boldsymbol{q}}.\end{aligned} \tag{8.14}$$

This error dynamics and can be represented as the negative feedback interconnection of the following two passive subsystems (as shown in Fig. 8.1)

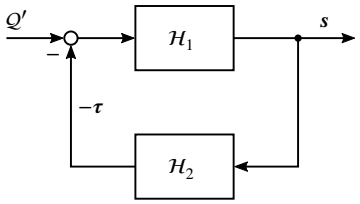

Figure 8.1: Passive subsystem decomposition of the closed loop resulting from the Slotine and Li controller.

$$\boldsymbol{\tau} = \left[\boldsymbol{\psi}^{\mathrm{T}}, -\boldsymbol{\psi}^{\mathrm{T}}\right], \tag{8.15}$$

$$\Sigma_u : \ \boldsymbol{s} \mapsto \left(\boldsymbol{\tau} + \mathcal{Q}'\right), \tag{8.16}$$

$$\Sigma_a : \ \boldsymbol{s} \mapsto -\boldsymbol{\tau}, \tag{8.17}$$

with storage functions

$$\mathcal{H}_1 = \tfrac{1}{2}\boldsymbol{s}^{\mathrm{T}}\operatorname{diag}(\boldsymbol{M}, \boldsymbol{B})\boldsymbol{s}, \tag{8.18}$$

$$\mathcal{H}_2 = \tfrac{1}{2}\tilde{\boldsymbol{q}}^{\mathrm{T}}\mathcal{K}\tilde{\boldsymbol{q}}. \tag{8.19}$$

The following analysis is easier to appreciate if we first recall the passive subsystem decomposition property of flexible joint manipulators. We extend the analysis in [19] by considering link and motor-side disturbance forces $\mathcal{Q}'_u$ and $\mathcal{Q}'_a$. According to Proposition 6.1.1, a flexible joint robot satisfying Spong's model can be represented as the negative feedback interconnection of two passive subsystems as show in Fig. 8.2

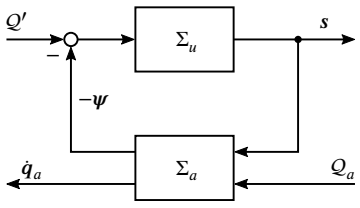

Figure 8.2: Passive subsystem decomposition of an SEA-based manipulator.

$$\Sigma_u : \ \left(\boldsymbol{\psi} + \mathcal{Q}'_u\right) \mapsto \dot{\boldsymbol{q}}_u, \tag{8.20}$$

$$\Sigma_a : \ \begin{bmatrix}-\boldsymbol{\psi}\\ \mathcal{Q}_a\end{bmatrix} \ \mapsto \begin{bmatrix}\dot{\boldsymbol{q}}_u\\ \dot{\boldsymbol{q}}_a\end{bmatrix}, \tag{8.21}$$

where the function $\boldsymbol{\psi} : \mathbb{R}^n \to \mathbb{R}^n$

$$\boldsymbol{\psi} = \boldsymbol{K}(\boldsymbol{q}_a - \boldsymbol{q}_u), \tag{8.22}$$

denotes the subsystem coupling signal, and $\mathcal{Q}_a = \mathcal{Q}'_a + \boldsymbol{u}_a$. The structure of the closed-loop dynamics resulting from applying the ESP-based Controller 6 and 7 mirrors that of the open-loop dynamics. Naturally, the open

loop passivity properties are reflected in the closed-loop system. Knowing that applying

$$\bar{\boldsymbol{u}}_u = \boldsymbol{u}_r + \boldsymbol{K}\boldsymbol{q}_u^* = \boldsymbol{K}\boldsymbol{q}_a^*, \tag{8.23}$$

to QFA Spong model (9.3) achieves the desired ESP/ESPi control error dynamics (see also Fig. 7.5), and observing that the coordinate transformation (9.5) can be written as

$$\bar{\boldsymbol{q}}_a = \boldsymbol{q}_a - \boldsymbol{K}^{-1}\bar{\boldsymbol{u}}_u = \boldsymbol{q}_a - \boldsymbol{q}_a^* = \tilde{\boldsymbol{q}}_a, \tag{8.24}$$

we see that the virtual motor coordinates can be interpreted as the motor position errors. As pointed out in Proposition 7.2.3, the closed-loop system associated with an ESP-based joint space motion tracking controller can be represented as the negative feedback interconnection of two passive subsystems (as shown in Fig. 8.3)

$$\bar{\Sigma}_u : \left(\boldsymbol{\psi} + \mathcal{Q}_u'\right) \mapsto \dot{\tilde{\boldsymbol{q}}}_u, \tag{8.25}$$

$$\bar{\Sigma}_a : \begin{bmatrix} -\boldsymbol{\psi} \\ \mathcal{Q}_a' \end{bmatrix} \mapsto \begin{bmatrix} \dot{\tilde{\boldsymbol{q}}}_u \\ \dot{\tilde{\boldsymbol{q}}}_a \end{bmatrix}, \tag{8.26}$$

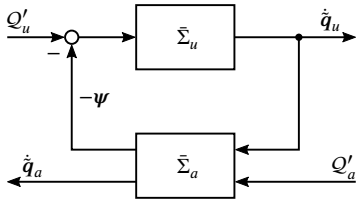

Figure 8.3: Passive subsystem decomposition of an ESP-based closed loop.

with the subsystem coupling signal evaluating for the considered model (9.2) to

$$\boldsymbol{\psi} = \boldsymbol{K}(\tilde{\boldsymbol{q}}_a - \tilde{\boldsymbol{q}}_u). \tag{8.27}$$

Comparing Fig. 8.2 and Fig. 8.3, we observe that ESP-based designs have the remarkable property of preserving the passive subsystem interconnection structure of the open-loop system. Moreover, for ESP-based designs the Hamiltonian of the plant can be usually extended by the energy storing elements added through control to obtain an appropriate storage function, see also Chapter 7. It is worth noting that this property of ESP-based concepts hold for *any* design choice for the virtual inputs $\bar{\boldsymbol{u}}_u$ and, thus, also holds for the dynamic extension-based designs proposed in Chapter 9.

The backstepping-based schemes do possess some closed-loop passivity properties, however, as pointed out in [19], they are formulated in terms of transformed coordinates. We observe from (8.16) that the same is true for the Slotine and Li controller, which defines a passive map $\boldsymbol{s} \mapsto \mathcal{Q}_u'$. In contrast, the closed loops associated with Controller 1, 7 and 8 define a passive map $\mathcal{Q}_u' \mapsto \dot{\tilde{\boldsymbol{q}}}_u$ in terms of the output (error) coordinates. In fact, Controller 7 and 8 define a passive map $\mathcal{Q}' \mapsto \dot{\tilde{\boldsymbol{q}}}$.

8.2 Conclusions

This section extends the comparison of nonlinear controllers for flexible joint manipulators [19, 20] by including two ESP-based designs and a decoupling scheme [140]. Most importantly, it was shown that ESP-based closed loops preserve the passive subsystem decomposition property of the open loop. Further, it was demonstrated that when the joint stiffness grows unbounded (i.e., the rigid robot model is retrieved), an ESP-based scheme converges to the rigid control law.

It is hard to draw a definite conclusion about the performance and robustness of the different controllers from the theoretical observations made in this chapter. It is widely believed that passivity-based designs that incorporate the physical structure of the system and avoid cancellation of nonlinearities yield robust designs. In this regard, we can expect passivity-based ESP schemes to have particularly favorable robustness properties. This intuition is strongly confirmed by the experimental results reported in Chapter 11 and Chapter 12. However, while confirmed by numerous experiments—to the best of the author's knowledge—this robustness hypothesis has not been proven yet.

The experimental comparison in [20] concluded that it is worth taking the joint flexibilities into account in control design. This allows achieving acceptable performance with a fixed set of feedback gains. It is worth noting that the aforementioned study focused on a manipulator with rather large joint stiffness values. Considering that the joint stiffness parameters play a crucial role for the controller performance, and given that articulated soft robots have a significantly higher joint flexibility compared to the manipulator studied in [20], it seems worth extending this comparison study to concern highly elastic manipulators. Furthermore, the work [20] showed that controllers, which seem very close to each other, either by their design approach or by their final form, can yield very different results when applied to actual hardware. In this regard, and considering that the ESP scheme has been derived specifically with highly compliant systems in mind, future studies should also concern ESP-based designs.

On the Performance Limits of Articulated Soft Robots

9

Today's scientists have substituted mathematics for experiments, and they wander off through equation after equation, and eventually build a structure which has no relation to reality.

– Nikola Tesla

In situations of harsh impacts, damping injection directly on the link of an articulated soft robot is challenging and usually requires high actuator torques at the moment of impact. This chapter discusses the underlying reasons and analyzes the performance limitations arising in the implementation of basic impedance elements, such as springs and dampers, through the QFA representation of Spong's model [168]. Using the insights obtained, we present a method for designing impedance controllers with a damping layout based on dynamic extensions. Inspired by the design of shock absorbers and the muscle-tendon model, the presented damping layout requires substantially smaller actuator torques in situations where the robot is subject to harsh impacts. The implementation is facilitated through the virtual inputs of the QFA model and results in a physically intuitive impedance design. The resulting closed-loop system can be interpreted as an interconnection of passive Euler Lagrange systems, which again, yields a passive system. The design's passive nature ensures stability in the free motion case and enables the robot to interact robustly and safely with its environment. We focus on robotic systems with no inertial coupling between the motor and link dynamics. Experimental results, obtained with the presented design on a dedicated series elastic actuator (SEA) test bed, are reported and discussed. A majority of this chapter has been published already in [91].

[168]: Spong (1987), "Modeling and control of elastic joint robots"

[91]: Keppler et al. (2021), "Analyzing the performance limits of articulated soft robots based on the ESPi framework: Applications to damping and impedance control"

9.1 Motivation

Chapter 5 introduced the concept of quasi-full actuation that enables the direct adoption of impedance control techniques to underactuated articulated soft robots [54, 74, 153, 190]. The availability of a virtual link-side control input fueled the development of the ESP scheme in Chapter 7. All the ESP controllers presented achieve a pervasively closed loop through link-side damping injection, which results in a well-damped disturbance rejection behavior, as highlighted by experimental results reported in [86, 92] and shown in Video 2 (Section 12.6).

[54]: Grebenstein et al. (2011), "The DLR hand arm system"
[74]: Hutter et al. (2016), "Anymal-a highly mobile and dynamic quadrupedal robot"
[153]: Pratt et al. (1995), "Series elastic actuators"
[190]: Vanderborght et al. (2013), "Variable impedance actuators: A review"

Situations may arise, however, where an ASR is subject to hard and/or fast impacts, and in these scenarios, the implementation of a damping term directly on the link can be challenging since the actuators easily run into torque saturations at the moment of impact. Motivated by this observation, we analyze the performance limits of ASRs concerning the implementation of basic impedance elements such as springs and dampers through the ESPi framework. Using the insights gained, we present enhanced damping designs, based on dynamic extensions, which significantly reduce the risk of input

[86]: Keppler et al. (2018), "Elastic structure preserving (ESP) control for compliantly actuated robots"
[92]: Keppler et al. (2018), "Elastic structure preserving impedance (ESPi) control for compliantly actuated robots"

saturation in the moment of a harsh impact. The inspiration for these damping designs was drawn from shock absorbers and the muscle-tendon system, which are required to showcase a smooth force variation at the moment of impact. Dynamic extension is a familiar concept in control. In [83, 137, 173] dynamic extensions were used to create artificial damping without the need for velocity measurements. Further, [137, 173] report elegant solutions to deal with actuator torque limits. However, such dynamic extensions have not yet been used in the context of enhancing the damping behavior of an ASR. The gain design required for our purpose is diametrical to what is recommended in [44, 173]. Roughly speaking, in [137, 173], and for the implementation of "dirty derivatives" (filtered derivatives) [83], the spring that decouples the damper is usually chosen as stiff as possible. However, for reducing the control effort during impacts the opposite is favorable as argued in this paper. The work [107] reports a tracking controller for ASRs using a filtered derivative to avoid feedback of the link jerk signals. In contrast to [107], the proposed controllers preserve the intrinsic system structure and result in a physically intuitive closed-loop behavior. In fact, the resulting closed-loop systems can be interpreted as the negative feedback interconnection of two passive Euler Lagrange systems, which again, results in a passive system.

[83]: Kelly (1993), "A simple set-point robot controller by using only position measurements"
[137]: Ortega et al. (1994), "On passivity-based output feedback global stabilization of Euler-Lagrange systems"
[173]: Stramigioli (1996), "Creating artificial damping by means of damping injection"
[137]: Ortega et al. (1994), "On passivity-based output feedback global stabilization of Euler-Lagrange systems"
[173]: Stramigioli (1996), "Creating artificial damping by means of damping injection"
[44]: Folkertsma et al. (2017), *Energy in Robotics*
[173]: Stramigioli (1996), "Creating artificial damping by means of damping injection"
[137]: Ortega et al. (1994), "On passivity-based output feedback global stabilization of Euler-Lagrange systems"
[173]: Stramigioli (1996), "Creating artificial damping by means of damping injection"
[83]: Kelly (1993), "A simple set-point robot controller by using only position measurements"
[107]: Loria et al. (1995), "On tracking control of rigid and flexible joints robots"
[107]: Loria et al. (1995), "On tracking control of rigid and flexible joints robots"

A physically motivated design allows the operator to anticipate the robot's interaction behavior with the environment (another physical system). Loosely speaking, the interaction between two physical systems visualizable in terms of real mechanical elements is easier to comprehend and anticipate than the interaction between a set of differential equations and the environment. This fact can hardly be overestimated when it comes to the commissioning stage since physical intuition is of immense value for tuning the controller. In addition, having a physically intuitive closed-loop behavior provides—to some extent—a feeling for the extent of system shaping imposed by a particular controller choice. The presented concept imposes no limitations on the achievable closed-loop stiffness and, in particular, it can be increased above the system's intrinsic stiffness. However, on a real system with motor saturation, limits obviously exist.

This chapter is organized as follows. In Section 9.2, we establish a link-side interconnection port. Section 9.3 discusses the challenges of link-side damping injection. In Section 9.4, we analyze the performance limits of ASRs based on the ESPi framework. Based on the insights, enhanced damping designs are presented in Section 9.5. A presentation and discussion of experimental results that have been obtained on a SEA test bed are reported in Chapter 11.

9.1.1 Model Assumptions

Let us again consider the Spong model introduced in [168], where the angular part of the kinetic energy of each rotor is considered due only to its own rotation. In order to simplify the analysis, we shall focus on systems characterized by positive definite elastic potential functions of the form

$$\mathcal{V}_e = \frac{1}{2}\boldsymbol{q}^{\mathrm{T}}\mathcal{K}\boldsymbol{q}; \quad \mathcal{K} = \begin{bmatrix} \boldsymbol{K} & -\boldsymbol{K} \\ -\boldsymbol{K} & \boldsymbol{K} \end{bmatrix}, \tag{9.1}$$

[168]: Spong (1987), "Modeling and control of elastic joint robots"

where $\boldsymbol{K} = \mathrm{diag}(k_1, \dots, k_n)$ is a constant diagonal matrix containing the joint stiffness values, such that the equations of motion (7.4) reduce to

$$\Sigma : \ \mathcal{M}(\boldsymbol{q}_u)\ddot{\boldsymbol{q}} + \mathcal{C}(\boldsymbol{q}_u, \dot{\boldsymbol{q}}_u)\dot{\boldsymbol{q}} + \mathcal{K}\boldsymbol{q} + \boldsymbol{g}(\boldsymbol{q}_u) = \boldsymbol{u} + \mathcal{Q}'. \tag{9.2}$$

As we will see shortly, Σ defines a passive operator from the applied actuator torques to motor shaft velocities, though it is not passive from the applied actuator torques to the link velocities.

9.2 Shaping the Interaction with the Physical World

Using the results from Chapter 5, we can use Theorem 5.3.6 to established a *link-side interconnection port* by transforming (9.2) into its QFA form

$$\Sigma_{\bar{q}} : \ \mathcal{M}(\bar{\boldsymbol{q}}_u)\ddot{\bar{\boldsymbol{q}}} + \mathcal{C}(\bar{\boldsymbol{q}}_u, \dot{\bar{\boldsymbol{q}}}_u)\dot{\bar{\boldsymbol{q}}} + \mathcal{K}\bar{\boldsymbol{q}} + \boldsymbol{G}(\bar{\boldsymbol{q}}_u) = \bar{\boldsymbol{u}} + \mathcal{Q}', \tag{9.3}$$

with the input and coordinate transforming equations (9.5) and (9.6) evaluating to

$$\boldsymbol{q}_u = \bar{\boldsymbol{q}}_u, \tag{9.4}$$

$$\boldsymbol{q}_a = \bar{\boldsymbol{q}}_a + \boldsymbol{K}^{-1}\bar{\boldsymbol{u}}_u, \tag{9.5}$$

$$\boldsymbol{u} = \boldsymbol{B}\boldsymbol{K}^{-1}\ddot{\bar{\boldsymbol{u}}}_u + \dot{\bar{\boldsymbol{u}}}_u + \bar{\boldsymbol{u}}_a, \tag{9.6}$$

and $\mathcal{Q} = \mathcal{Q}'$. In this chapter, we will study the implementation of impedance control through this interconnection port. Intuitively, we can think of the virtual motor coordinates $\bar{\boldsymbol{q}}_a$ being formed by shifting the original motor coordinates $\boldsymbol{q}_a$. The magnitude of this shift is directly proportional to the input $\bar{\boldsymbol{u}}_u$ with the factor of proportionality being the joint compliance $\boldsymbol{K}^{-1}$. Note that (9.5)–(9.6) comprise n independent[1] scalar equations each since, both the stiffness and motor inertia matrix are diagonal. The following assumption guarantees that the input conditions of Theorem 5.3.6 are satisfied.

1: Independent in the sense that each of the n scalar state and input transformation equations can be solved separately.

Assumption 9.2.1 *The inputs $\bar{u}_{ui}$ are sufficiently smooth such that $\dot{\bar{u}}_{ui}, \ddot{\bar{u}}_{ui}$ exist, and contain feedback of $\bar{\boldsymbol{q}}_u, \dot{\bar{\boldsymbol{q}}}_u$ and t only.*

Remark 9.2.1 The smoothness constraint on the virtual input defined in Assumption 9.2.1 is not specific to the ESPi framework. Indeed, it is a manifestation of the physical fact that the link-side torque bandwidth of ASRs is fundamentally reduced compared to directly actuated systems.

A closer examination of the input transformation (9.6) reveals an interesting connection to the natural frequencies of the individual mass-spring systems which are constituted by the motor inertias and joint springs

$$\omega_{ni} \triangleq \sqrt{k_i / b_i}. \tag{9.7}$$

Introducing

$$\boldsymbol{\Omega}^{-2} = \boldsymbol{B}\boldsymbol{K}^{-1} = \mathrm{diag}(\omega_{n1}^{-2}, \dots, \omega_{nn}^{-2}), \tag{9.8}$$

allows us to rewrite the input transformation (9.6) as

$$\boldsymbol{u} = \boldsymbol{\Omega}^{-2}\ddot{\bar{\boldsymbol{u}}}_u + \bar{\boldsymbol{u}}_u + \bar{\boldsymbol{u}}_a. \tag{9.9}$$

The input transformation (9.6) has important implications for the design of elastic robots, since it reveals the fundamental connection between the system's inherent natural eigenfrequencies ω_i and the achievable link-side torque control bandwidth. This matter is discussed in detail in Section 9.4.

The interaction of an ASR with its environment is characterized by the way energy is exchanged. This energy exchange can be computed by taking the time derivative of the robot's Hamiltonian $\mathcal{H}$. Recalling Proposition 6.1.1, we have for Σ

$$\dot{\mathcal{H}}(\boldsymbol{q}, \dot{\boldsymbol{q}}) = \dot{\boldsymbol{q}}^{\mathrm{T}} \left(\boldsymbol{u} + \mathcal{Q}' \right) \tag{9.10}$$

and time integration from 0 to T establishes the key energy balance equation

$$\begin{aligned} &\mathcal{H}\big(\boldsymbol{q}(T), \dot{\boldsymbol{q}}(T)\big) - \mathcal{H}\big(\boldsymbol{q}(0), \dot{\boldsymbol{q}}(0)\big) = \\ &\underbrace{\int_0^T \left(\dot{\boldsymbol{q}}_u^{\mathrm{T}} \mathcal{Q}'_u \right) dt}_{\text{natural exchange}} + \underbrace{\int_0^T \left(\dot{\boldsymbol{q}}_a^{\mathrm{T}} \mathcal{Q}'_a \right) dt}_{\text{friction losses}} + \underbrace{\int_0^T \dot{\boldsymbol{q}}_a^{\mathrm{T}} \boldsymbol{u}_a dt}_{\text{supplied}}. \end{aligned} \tag{9.11}$$

Considering Corollary 6.1.2, we have for the QFA model

$$\dot{\bar{\mathcal{H}}}(\bar{\boldsymbol{q}}, \dot{\bar{\boldsymbol{q}}}) = \dot{\bar{\boldsymbol{q}}}^{\mathrm{T}} \left(\bar{\boldsymbol{u}} + \mathcal{Q}' \right), \tag{9.12}$$

and after time integration

$$\begin{aligned} &\mathcal{H}\big(\bar{\boldsymbol{q}}(T), \dot{\bar{\boldsymbol{q}}}(T)\big) - \mathcal{H}\big(\bar{\boldsymbol{q}}(0), \dot{\bar{\boldsymbol{q}}}(0)\big) = \\ &\underbrace{\int_0^T \left(\dot{\bar{\boldsymbol{q}}}_u^{\mathrm{T}} \mathcal{Q}'_u \right) dt}_{\text{natural exchange}} + \underbrace{\int_0^T \left(\dot{\bar{\boldsymbol{q}}}_a^{\mathrm{T}} \mathcal{Q}'_a \right) dt}_{\text{indeterminate}} + \underbrace{\int_0^T \left(\dot{\bar{\boldsymbol{q}}}_u^{\mathrm{T}} \bar{\boldsymbol{u}}_u + \dot{\bar{\boldsymbol{q}}}_a^{\mathrm{T}} \bar{\boldsymbol{u}}_a \right) dt}_{\text{supplied}}. \end{aligned} \tag{9.13}$$

In either case, we can identify three types of power flows, see also Fig. 9.1. The first terms on the RHS of (9.11) and (9.13) denote the respective system's natural exchange of energy with its environment. The third term on the RHS represents the artificial supply rate imposed by a particular controller. The second term in (9.11) mostly comprises friction losses, and thus can be considered as strengthening the passivity of Σ, whereas the second term in (9.13) is indeterminate in the sense that it can either add or remove energy from the system. When it comes to ASR, we are interested primarily in the energy exchange via the port $(\dot{\boldsymbol{q}}'_u, \mathcal{Q}_u)$ since this port's behavior dictates the interaction behavior with the environment. Unfortunately, our control input is non-collocated with the output $\boldsymbol{q}_u$, which complicates shaping this port behavior. However, observing the equivalence of the power flows $(\dot{\boldsymbol{q}}'_u, \mathcal{Q}_u)$ and $(\dot{\bar{\boldsymbol{q}}}'_u, \bar{\mathcal{Q}}_u)$ of Σ and $\bar{\Sigma}$, it is clear that we simplify this task by using controllable port $(\dot{\bar{\boldsymbol{q}}}', \bar{\mathcal{Q}})$ of the QFA system $\bar{\Sigma}$ instead.

Remark 9.2.2 In practice ASR, motions associated with the motor-side inertias exchange energy with the environment as well (via the port $(\dot{\boldsymbol{q}}_a, \mathcal{Q}'_a)$). However, a closer look reveals that their influence on the interaction behav-

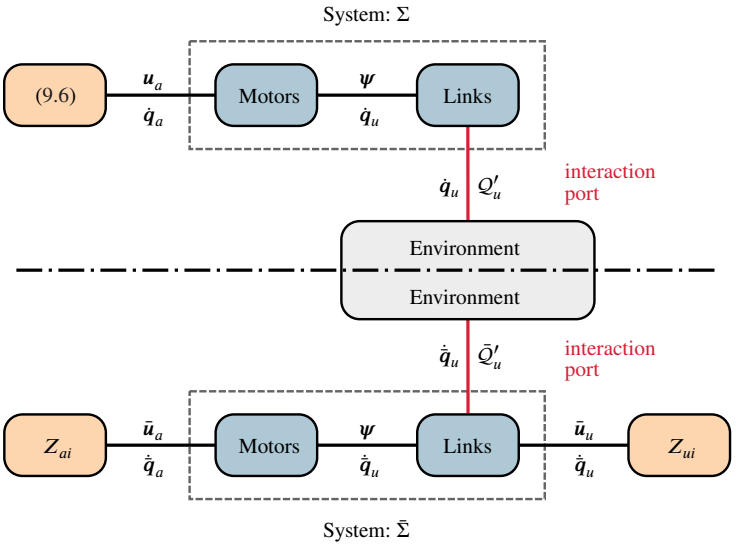

Figure 9.1: Energy flows of the original, Σ, and transformed system, $\bar{\Sigma}$, which are equivalent representations of the same system. The control signal $\boldsymbol{u}_a$ on Σ realizes the interconnection of the virtual system $\bar{\Sigma}$ with the impedances Z_{ai} and Z_{ui}.

ior is negligible, since all parts constituting the reflected motor inertias are encapsulated in housings and thus shielded from the environment. As such, we can think of $\mathcal{Q}'_a$ essentially comprising friction related forces only. From the practical performance point of view, however, it is clearly advisable to compensate friction forces with e.g appropriate observers [34]. After this step, we may assume that all practically meaningful interactions with the environment occur via the mechanical link-side interaction port. For this reason, we shall assume that $\mathcal{Q}_a = \mathbf{0}$ in the following.

[34]: De Luca et al. (2006), "Collision detection and safe reaction with the DLR-III lightweight manipulator arm"

Remark 9.2.3 Calculating the Hamiltonian, using the definition of $\mathcal{H}$ as the Legendre transformation of $\mathcal{L}$, then it corresponds to the total energy of the system $\mathcal{H} = \sum_i \dot{q}_i \frac{\partial \mathcal{L}}{\partial \dot{q}_i} - \mathcal{L} = \mathcal{T} + \mathcal{V}$. Comparing (9.2) and (9.3), it is clear that systems Σ_q and $\Sigma_{\bar{q}}$ are characterized by the same Lagrangian and Hamiltonian functions. However, as pointed out in Section 5.7.1, it is worth remarking that in general the Hamiltonian function does not evaluate to the same values for Σ and $\bar{\Sigma}$

$$\mathcal{H}(\boldsymbol{q}, \dot{\boldsymbol{q}}) = \mathcal{H}(\bar{\boldsymbol{q}}, \dot{\bar{\boldsymbol{q}}}) + \Delta\mathcal{H}, \tag{9.14}$$

$$\Delta\mathcal{H} \triangleq \tfrac{1}{2}\left[\dot{\boldsymbol{q}}_a^{\mathrm{T}} \boldsymbol{B} \dot{\boldsymbol{q}}_a - \dot{\bar{\boldsymbol{q}}}_a^{\mathrm{T}} \boldsymbol{B} \dot{\bar{\boldsymbol{q}}}_a + \mathcal{V}_e(\boldsymbol{q}_a - \boldsymbol{q}_u) - \mathcal{V}_e(\bar{\boldsymbol{q}}_a - \boldsymbol{q}_u)\right]. \tag{9.15}$$

From (9.11) it is clear that Hamiltonian $\mathcal{H}$ suits as a storage function for showing that $\Sigma_{\bar{q}}$ defines a passive operator $(\bar{\boldsymbol{u}} + \mathcal{Q}') \mapsto \dot{\bar{\boldsymbol{q}}}$. The fact that the port $(\dot{\boldsymbol{q}}_u, \mathcal{Q}'_u)$ is preserved under the transformations (9.5)–(9.6) is key for the developments in this chapter. Using this interconnection port to interconnect impedance elements allows us to shape the interaction behavior of an ASR. Throughout this chapter, Z_{ui} and Z_{ai} denote impedances interconnected with the ith link and virtual motor, respectively, c.f. Fig. 9.1. The control structure that results from such interconnections is shown in Fig. 9.2.

An important aspect of impedance control is the superposition principle, which facilitates the understanding of complex interconnected systems. As highlighted by Hogan in [68]: if the dynamics is dissected into a set of component impedances, these may be reassembled by simple addition even when the behavior of any or all of the components is nonlinear (known as the superposition principle for impedances). The underlying reason being

[68]: Hogan (1985), "Impedance control: An approach to manipulation: Part I—Theory"

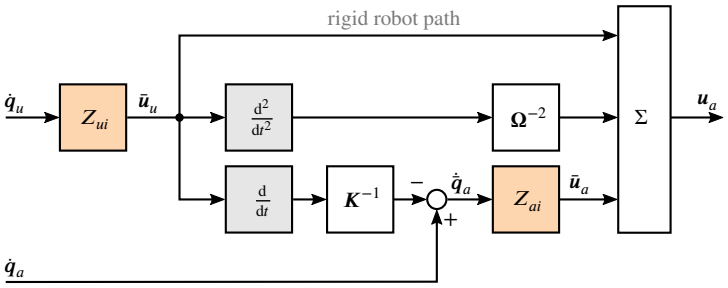

Figure 9.2: Block diagram of the input transformation. The resulting control input $\boldsymbol{u}_a$ realizes the interconnection of the impedance elements, Z_{ui} and Z_{ai} with the transformed system $\bar{\Sigma}$.

that an environment acting as an admittance sums the forces applied to it and determines its motions in response. Thus, the environment also sums any impedances connected to it.

9.3 Challenges of Link-Side Damping Injection

This section discusses the challenges regarding link-side damping injection on ASR, which has been identified as a desirable design objective in Section 7.1. Based on the insights obtained, we formulate enhanced damping designs in Section 9.4. The challenges arise from the fact that implementation of a damping term, that acts directly on a link, requires feedback of the link jerks. This fact is easily revealed within the ESPi control framework. We can use input $\bar{\boldsymbol{u}}_u$ to interconnect a viscous damper with each link

$$\bar{u}_{ui} = -d_{qi}\dot{q}_{ui}, \tag{9.16}$$

where d_{qi} is the damping coefficient for the ith link. Making the substitutions (5.57) and (9.16), it is clear that the implementation requires feedback of the jerk signals $q_{ui}^{(3)}$. A fundamental property of the model (9.2) is that these quantities can be derived from the dynamics equations without numerical differentiation, see Appendix. However, (B.11) reveals that the link jerk magnitudes are related to the rate of change of the external forces $\mathcal{Q}_1$ and, in fact, grow unbounded for impact forces approaching a step-like variation. As a consequence, the feedback of jerk signals can potentially lead to input saturation during harsh impacts with the environment. Notice that deactivation of active damping during impacts is no viable option, as it would require non-smooth joint torque variations which are physically impossible. Unless the system is at rest, such switching would cause a non-smooth variation of $\bar{\boldsymbol{u}}_u$, which would violate Assumption 9.2.1. What defines a harsh impact? Let us assume a sine-like force excitation of constant amplitude A and frequency ω on the ith joint of the form $\mathcal{Q}_{ui}(t) = A\sin(\omega t)$, then the magnitude of $\dot{\mathcal{Q}}_{ui}$ rises linearly with ω. Hence, for the limit case $\omega \to \infty$, we have $\dot{\mathcal{Q}}_{ui} \to \infty$ and, thus, $q_{ui}^{(3)} \to \infty$. In conclusion, in impact situations where the impact force signal contains substantial high frequency content, the implementation of direct link damping requires large actuator torques. Note that jerk signals are contained in the feedback terms $\ddot{\bar{u}}_{ui}$ which are scaled with ω_{ni}^{-2}. We conclude, the softer the joint, the harder the challenge of direct damping injection on the links. In practice, the "harshness" of an impact depends significantly on the relative speed and hardness of the collision partners.

It is important to notice that the challenge regarding link-side damping injection does not arise from limitations of the ESPi framework, we used for analysis here. In fact, these limitations are a manifestation of the mechanical

bandwidth limitation of an elastic joint [153]. To support this statement, let us consider one of the most straightforward ways to implement a link-side damping term of the form (9.16). Implementation with a classic joint torque tracking controller[2] [140]

$$\boldsymbol{u} = \boldsymbol{\Omega}^2 \ddot{\bar{\boldsymbol{u}}}_u + \bar{\boldsymbol{u}}_u - \boldsymbol{\Omega}^2 \left(\boldsymbol{D}_e \dot{\boldsymbol{e}} + \boldsymbol{K}_e \boldsymbol{e} \right) + \boldsymbol{B} \ddot{\boldsymbol{q}}, \tag{9.17}$$

$$\boldsymbol{e} \triangleq \boldsymbol{\psi} - \bar{\boldsymbol{u}}_u, \tag{9.18}$$

reveals the feedback necessity of the link jerks through the same term, $\boldsymbol{\Omega}^{-2} \ddot{\bar{\boldsymbol{u}}}_u$, as the damping implementation via (5.57). We conclude that in order to reduce the actuator torque requirements in situations of harsh impacts, we have to avoid link jerk signals in the feedback path.

[153]: Pratt et al. (1995), "Series elastic actuators"

2: Considering $\bar{\boldsymbol{u}}_u$ as the desired joint torque, the controller achieves global asymptotic convergence $\boldsymbol{\psi} \to \bar{\boldsymbol{u}}_u$ for $t \to \infty$.

[140]: Ott (2008), *Cartesian Impedance Control of Redundant and Flexible-Joint Robots*

Remark 9.3.1 Notice that deactivation of active damping during impacts is no viable option. Unless the system is at rest, such switching would cause a non-smooth variation of $\bar{\boldsymbol{u}}_u$, which would violate Assumption 9.2.1. If link-side damping is injected via a joint torque tracking approach [140], such switching would require non-smooth joint torque variations which are physically impossible.

[140]: Ott (2008), *Cartesian Impedance Control of Redundant and Flexible-Joint Robots*

9.4 Performance Limitations

Let us analyze the actuator torques required for interconnecting basic link impedances through the link-side port established above. The insights obtained are crucial for the layout of the enhanced damping designs presented in Section 9.5. Since the transformation equations (9.5) and (9.6) are constituted by n independent scalar equations, the performance analysis for a multi-joint manipulator can be conducted by analyzing each joint individually. Setting $\bar{\boldsymbol{u}}_2 = \boldsymbol{0}$ and performing a Laplace transform on the input transformation (5.57) yields:

$$U_i = \bar{U}_i + \left(\omega_{ni}^{-1} s \right)^2 \bar{U}_i, \tag{9.19}$$

which expresses the ith motor torque in terms of the ith link-side input. The first, $\bar{U}_i$, is the torque transmitted through the elastic element to the link. The second, $\left(\omega_{ni}^{-1} s \right)^2 \bar{U}_i$, is the torque required to accelerate the motor's mass so as to track the deformation of the elastic element [153]. Only the latter is unique to elastic robots.

[153]: Pratt et al. (1995), "Series elastic actuators"

Ignoring motor velocity saturation, we can compute performance limits by imposing a symmetric bound on the magnitude of each actuator torque $|u_i| \leq u_{max,i}$. Introducing

$$G_{\mathrm{ESP},i}(s) \triangleq \frac{U_i(s)}{\bar{U}_i(s)} = 1 + (\omega_{ni}^{-1} s)^2, \tag{9.20}$$

which maps link-side torques to actuator torques, substituting $s = j\omega$ and analyzing its magnitude over ω, provides valuable insight into the performance characteristics of an elastic joint, see Fig. 9.3 (top). Interestingly, the important performance characteristic $G_{\mathrm{ESP},i}$ is independent of the link inertias or masses. Suppose, we want to interconnect a link impedance $Z_{ui} = \bar{U}_i / V_i$ with the ith link. Assuming that the environment acts as an admittance and imposes a link

velocity V_i on the ith joint, then the corresponding control effort is determined by:

$$\frac{U_i(s)}{V_i(s)} = G_{\mathrm{ESP},i}(s) Z_{ui}(s). \tag{9.21}$$

3: When speaking of the rigid robot counterpart, we refer to the limit case where the joint stiffness values approach infinity.

In comparison, the control effort for the rigid robot counterpart[3], to interconnect a link impedance Z_{ui}, is simply given by Z_{ui} itself. Comparing (9.21) with Z_{ui} allows for the following conclusion. In the frequency range $0 < \omega < \sqrt{2}\omega_n$, where $|G_{\mathrm{ESP}}| < 1$, the elastic system is superior to the rigid counterpart, in the sense that it requires less control effort to interconnect a link impedance $Z_{ui} = \bar{U}_i / V_i$ on the ith link. This property is independent of the particular link impedance choice. This important fact becomes clear considering that the multiplication of two transfer functions, c.f. (9.21), translates into an addition of their magnitudes responses. A closer inspection of G_{ESP} reveals that the superiority of the elastic system is maximal for imposed link velocities with a frequency of $\omega = \omega_n$. For $\omega > \sqrt{2}\omega_n$, the slope of $|G_{\mathrm{ESP}}|$ is 40 db/decade and, thus, the elastic system becomes vastly inferior in this frequency range. It is for this reason, that in order to maximize the operational frequency range of an elastic system, it is paramount to minimize the amplitude of Z_{ui} beyond $\sqrt{2}\omega_n$. This aspect is particularly important whenever the environmental admittance imposes velocities with a high frequency content on the ith link.

It is important to underline that the performance analysis results obtained via the ESPi transformation are of general nature and not specific to this particular framework. The 40 dB rise, in the red zone of Fig. 9.3, is a manifestation of the fact that the joint elasticity acts as a low-pass filter on the actuator output, as highlighted by Pratt in his fundamental work on SEA [153].

[153]: Pratt et al. (1995), "Series elastic actuators"

9.4.1 Implementing Basic Impedance Elements

Let us compute the control effort required to interconnect linear spring and damper elements to obtain further insights into the performance limits of an ASR. For the ith motor inertia and joint stiffness, we assume the test bed parameters reported in Table 11.6. Suppose, we want to interconnect a spring element, with spring constant k_{qi}, with the ith link, then $\bar{u}_{1,i} = -k_{qi} q_{ui}$ and for the ith link impedance, we have $Z_{ui} = k_{qi}/s$. The corresponding frequency responses of $G_{\mathrm{ESP},i} Z_{ui}$ and Z_{ui} are reported in Fig. 9.3 (mid) for the stiffness values $k_{qi} = \{k_i/2, k_i, 2k_i\}$. Doubling/halving the stiffness k_{qi} translates into rising/lowering the magnitude of $G_{\mathrm{ESP},i} Z_{ui}$ by 6 dB as indicated by the dashed lines. This becomes immediately clear by inspecting the transfer function. When implementing an additional damper $d_{q,i} = 2\xi_q \sqrt{k_i b_i}$, where ξ_q denotes the damping ratio, then, according to the superposition principle, we can simply add up the individual impedances s.t. $Z_{ui} = k_{qi}/s + d_{q,i}$. The resulting frequency responses of $G_{\mathrm{ESP},i} Z_{ui}$ and Z_{ui} are reported in Fig. 9.3, with $\xi_q = 0.7$ and $k_{qi} = \{k_i/2, k_i, 2k_i\}$ as above. Clearly, the actuator torque required to implement an additional link-side damper is significantly increased compared to a pure spring implementation in the high frequency regime, where the damper dominates over the spring. Again, the dashed lines indicate a doubling/halving of the imposed stiffness k_{qi} (the damping factors change accordingly). Inspecting the transfer functions $G_{\mathrm{ESP},i} Z_{ui}$ and Z_{ui}, it is straightforward to verify that doubling/halving the stiffness k_{qi} moves the magnitude

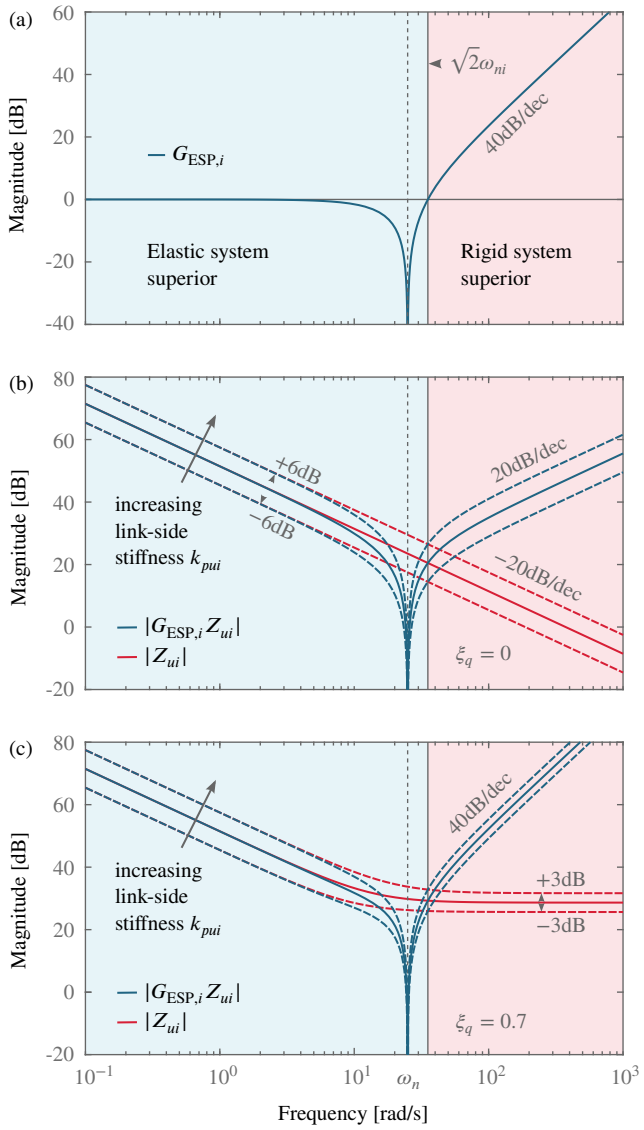

Figure 9.3: (**a**) G_{ESP} maps the link-side torques to the actuator torques. (**b**)–(**c**) Frequency responses of the control effort transfer functions $G_{\mathrm{ESP}}Z_{ui}$ and Z_{ui}, which map the ith link velocity to the ith control torque in case of an ASR and rigid robot case, respectively. (**b**) Implementation of a linear spring. (**c**) Implementation of a linear spring and damper.

plots up/down by 6 dB in the low frequency domain (spring-like behavior) and up/down by ±3 dB in the high frequency domain (damper-like behavior), c.f. Figure 9.3.

9.5 Improved Disturbance Rejection via Dynamic Extensions

Building on the insights of the previous two sections, we can formulate damping designs that reduce the control effort in case of an environmental disturbance with high frequency content. Inspired by the design of shock absorbers and considering the observations above, it appears natural to decouple the damper element with a spring-like element to low-pass filter shock loads, thereby greatly reducing the peaks of the interconnection torques $\bar{u}_i$ at the moment of impact, see Fig. 9.4 for examples. In fact, choosing a link impedance Z_{ui} with such a decoupled damper reduces the slope of $|G_{\mathrm{ESP},i}Z_{ui}|$ from 40 dB/dec to 20 dB/dec in the high frequency regime $\omega > \sqrt{2}\omega_{ni}$, c.f. Figure 9.3 (mid) with Figure 9.3 (bottom). This is a direct consequence of the fact

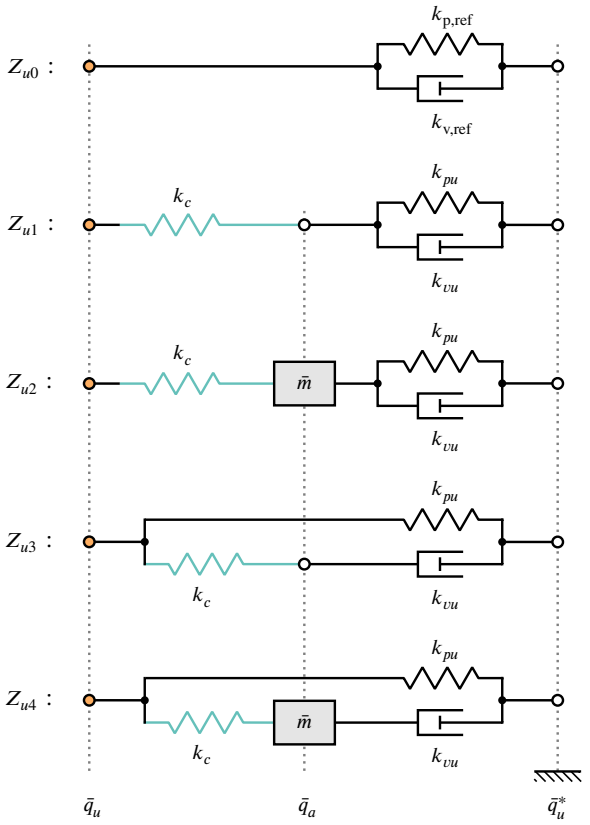

Figure 9.4: Mechanical impedance candidates with enhanced damping properties. For Variant 1, the PD element is decoupled via an additional elastic element. In Variant 2, the additional (small) mass guarantees that the dynamic extension represents an actual physical system. Variants 3–4 differ in the sense that only the damper is decoupled via an additional elastic element, thus, the stiffness is uniquely determined by k_u analogous to k_{ref} of the reference impedance Z_{u0}.

that the interconnection of such elements, via input $\bar{u}_{1,i}$, no longer requires velocity feedback. Consequently, the implementation of (5.57) no longer requires the critical jerk signals. Impedance elements Z_{u1} to Z_{u4} have in common that the damper is decoupled via a spring element (orange), which results in a dynamics extension with one (Variants 1 & 3) or two additional states (Variants 2 & 4). Importantly, interconnecting these elements via (5.57) results in a closed-loop system that can be interpreted as an interconnection of passive Euler Lagrange systems, which again, yields a passive system, see [133] for details.

The dynamic extension Z_{u3} can be interpreted as the mechanical realization of the popular "dirty derivatives" filter [83], Z_{u2} has been initially introduced in [137, 173] and Z_{u1} can be conceived as Hill's muscle model [64]. However, the motivations for these dynamic extensions were different, and thus the recommended gain layouts differ. In case of the dirty derivative filter, the gain k_c is usually chosen as high as possible with the intention of approximating the real velocities reasonably well. In [44, 173] the gains are chosen s.t. $k_c >> k_q$ and $\bar{m} << m$, where m is the link inertia, based on the intuitive reasoning that in this case the two masses tend to become one and the "felt" stiffness will become k_q [113, 173]. In other words, the impedance behavior $Z_{u,2}$ can be well approximated by the black spring/damper part in Fig. 9.4. When it comes to reducing the actuator torque magnitudes in the moment of a harsh impact, a diametrical layout is desirable. Physical intuition suggests: the lower the coupling stiffness k_c the lower the required actuator torque magnitude.

[133]: Ortega (1998), *Passivity-Based Control of Euler-Lagrange Systems: Mechanical, Electrical, and Electromechanical Applications*

[83]: Kelly (1993), "A simple set-point robot controller by using only position measurements"

[137]: Ortega et al. (1994), "On passivity-based output feedback global stabilization of Euler-Lagrange systems"

[173]: Stramigioli (1996), "Creating artificial damping by means of damping injection"

[64]: Hill (1938), "The heat of shortening and the dynamic constants of muscle"

[44]: Folkertsma et al. (2017), *Energy in Robotics*

[173]: Stramigioli (1996), "Creating artificial damping by means of damping injection"

[113]: Melchiorri et al. (1999), "Using damping injection and passivity in robotic manipulation"

[173]: Stramigioli (1996), "Creating artificial damping by means of damping injection"

9.5.1 Interpretation as Euler-Lagrange Controllers

Interpreting the dynamic extensions in Fig. 9.4 as EL systems, it is clear that the controllers achieving the interconnection with $\bar{\Sigma}$ belong to the class of EL controllers.

As an example, let us treat the interconnection of Z_{u2}-elements with each link of the QFA system (9.3). The controller dynamics associated with Z_{u2} of the ith link is

$$\Sigma_c : \bar{m}_i \ddot{q}_{ci} + k_{vui}\dot{q}_{ci} + k_{ci}(q_{ci} - \bar{q}_{ui}) + k_{pui}(q_{ci} + \bar{q}^*_{ui}) = 0, \tag{9.22}$$

with the controller Lagrangian

$$\mathcal{L}_c = \mathcal{T}_c - \mathcal{V}_c; \tag{9.23}$$

being composed of

$$\mathcal{T}_c = \sum_i^{n_u} \tfrac{1}{2}\bar{m}_i \dot{q}^2_{ci}, \tag{9.24}$$

$$\mathcal{V}_c = \sum_i^{n_u} \tfrac{1}{2}\left[k_{ci}(q_{ci} - \bar{q}_{ui}) + k_{pu}(q_{ci} - \bar{q}^*_{ui})\right]. \tag{9.25}$$

Let $\mathcal{L}(\bar{\boldsymbol{q}}, \dot{\bar{\boldsymbol{q}}})$ be the Lagrangian of the plant in its QFA form. Then, following Proposition 2.5.5, the feedback interconnection between the QFA model, (9.3), and controller, (9.22) is established by

$$\bar{\boldsymbol{u}} = -\frac{\partial \mathcal{V}_c}{\partial \bar{\boldsymbol{q}}}. \tag{9.26}$$

and according to Proposition 2.5.5 the resulting closed-loop system is an EL system with the Lagrangian

$$\mathcal{L}_{cl}(\bar{\boldsymbol{q}}, \boldsymbol{q}_c, \dot{\bar{\boldsymbol{q}}}, \dot{\boldsymbol{q}}_c) = \mathcal{L}(\bar{\boldsymbol{q}}, \dot{\bar{\boldsymbol{q}}}) + \mathcal{L}_c(\bar{\boldsymbol{q}}, \boldsymbol{q}_c, \dot{\bar{\boldsymbol{q}}}, \dot{\boldsymbol{q}}_c). \tag{9.27}$$

9.5.2 Parameter Optimization

In [192], we propose a H_∞ based optimization procedure for the gain layout of the dynamic extensions shown in Fig. 9.4 with respect to the following three objectives:

- minimize the actuator force magnitudes during impacts by minimizing the the H_∞ norm of the disturbance transfer function from $\mathcal{Q}_u$ to u_a,
- minimize the H_∞ norm of noise transfer function from q_u to u_a,
- the magnitude of the resulting manipulator impedance, $\mathcal{Q}_1/V$, which defines the interaction behavior, must lie withing an epsilon band of the reference impedance Z_{u0}. For the results in Fig. 11.19 and the experiments reported in Chapter 11 (see also Fig. 11.21) the band was chosen to be ± 6 dB.

[192]: Wandinger (2020), "Enhancing classical impedance control concepts while ensuring transferability to flexible joint robots"

Figure 11.19 compares the frequency responses of the link-side impedance candidates from Fig. 9.4 for two different layout approaches. Figure 11.19 (**top**) reports the parameter layout according to the suggestion by [173], and Figure 11.19 (**bottom**) reports the parameters layout based on the optimization procedure reported in [192]. From Fig. 9.3, we know that the interconnection

[173]: Stramigioli (1996), "Creating artificial damping by means of damping injection"
[192]: Wandinger (2020), "Enhancing classical impedance control concepts while ensuring transferability to flexible joint robots"

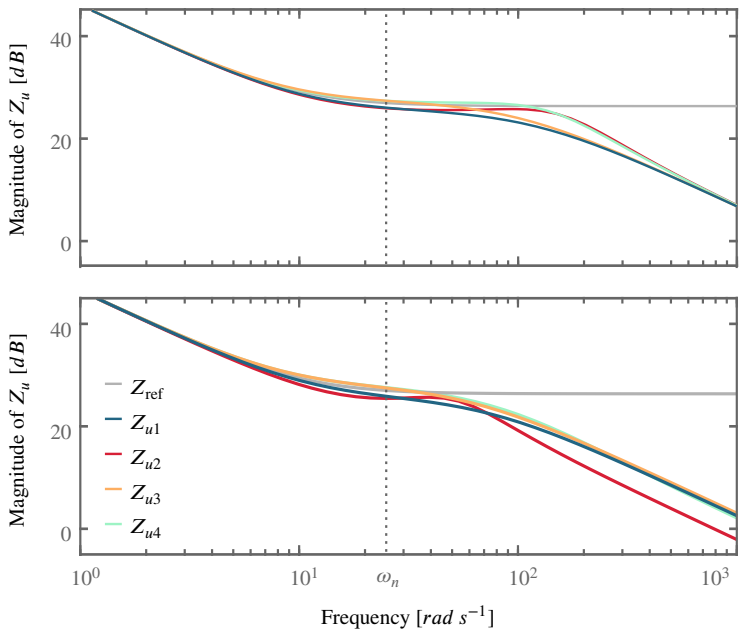

Figure 9.5: Frequency responses of the link-side impedance candidates. (**top**) Parameter layout according to the suggestions by [173]. (**bottom**) Optimized parameters.

of an link-side impedance Z_{ui} with high magnitudes $|Z_{ui}|$ for $\omega > \omega_n$ requires high actuation torques. In harmony with these insights, the optimization shifts the cutoff frequencies of the impedance candidates towards ω_n.

9.6 Conclusions

Using the ESPi control framework for ASRs, we analyzed the performance limits arising in the implementation of link-side impedance elements and discussed the challenges concerning link-side damping injection in impact scenarios. These challenges are fundamentally linked to the feedback necessity of the link jerks. Based on the insights obtained, we presented impedance controllers with an enhanced damping design that is based on dynamic extensions. These impedance controllers require fundamentally smaller actuator torques at the moment of impact. The experimental results reported in Chapter 11 confirm this favorable behavior compared to classical impedance controllers with a direct damping implementation (see also Video 5 in 12.6). As demonstrated on a dedicated test bed, the new impedance designs combine this advantage with the set-point regulation performance of classical impedance controllers. Since the presented impedance controllers are implemented using the idea of quasi-full actuation, the system's intrinsic structure is preserved and the resulting closed-loop dynamics are passive and physically intuitive. In fact, the reported dynamic extensions can be interpreted as Euler-Lagrange controllers, which allows applying the results from Section 6.3 to show GAS and passivity of the resulting closed loop.

On Time-Optimal Control of Elastic Joints with Bounded Input

10

Nature uses as little as possible of anything.

— Johannes Kepler

This chapter presents a complete synthesis method for time-optimal rest-to-rest motions of an elastic joint system with bounded torque input. An equivalence with the two-body problem in classical mechanics is highlighted, allowing to introduce a change of coordinates that reduces the problem to a pair of decoupled one-body problems. In place of the original coupled fourth-order dynamics, the motion of two equivalent masses has to be synchronized in separate phase spaces. The solution is provided in closed form by following purely geometric arguments, and verifies the standard optimality conditions. The obtained control is a bang-bang policy with either one or three switchings, depending on the dynamic parameters and the required displacement. One-switching solutions are called *natural motions* for the system: given a set of dynamic parameters, they cover the displacement space in a sparse way. Natural motions are the only instances when minimum-time solutions for the elastic and the equivalent rigid joint system match, whereas the rigid system is faster for all other optimal rest-to-rest motions. The results of this chapter have been first published in [87].

[87]: Keppler et al. (2020), "On time-optimal control of elastic joints under input constraints"

10.1 Motivation

For many robotic applications, fast motion along a given path is crucial. It requires the exploitation of the maximal allowable actuator torques. Therefore, it is natural to aim at time-optimal solutions along a predefined path. The minimum-time optimization problem for rigid manipulators was treated first in [15, 161]. These methods rely on projecting the robot dynamics on the predefined path. Using the parametric position and velocity along the path allows an elegant treatment of the problem in the phase plane. Unfortunately, these algorithms cannot be applied in the presence of elastic joints. Other methods have been proposed to solve the time-optimal control problem for robots with (linear or nonlinear) flexible joints. In [18], a constrained optimal control problem is formulated to obtain an optimal motor trajectory. The problem of reaching a desired state in minimum time for visco-elastic joints under limited deflection has been treated in [109]. However, in order to simplify the analysis, these works contemplate a simplified model by considering the motors as ideal velocity sources. The time-optimal control problem for the complete elastic joint model was addressed also in [27], but only in a numerical way.

[15]: Bobrow et al. (1985), "Time-optimal control of robotic manipulators along specified paths"
[161]: Shin et al. (1985), "Minimum-time control of robotic manipulators with geometric path constraints"
[18]: Braun et al. (2013), "Robots driven by compliant actuators: Optimal control under actuation constraints"
[109]: Mansfeld et al. (2014), "Reaching desired states time-optimally from equilibrium and vice versa for visco-elastic joint robots with limited elastic deflection"
[27]: Dahl (1992), "Path constrained robot control"

In this chapter, we consider a system of two masses m and b connected by an elastic joint of stiffness k, as shown in Fig. 10.1 (top). The corresponding

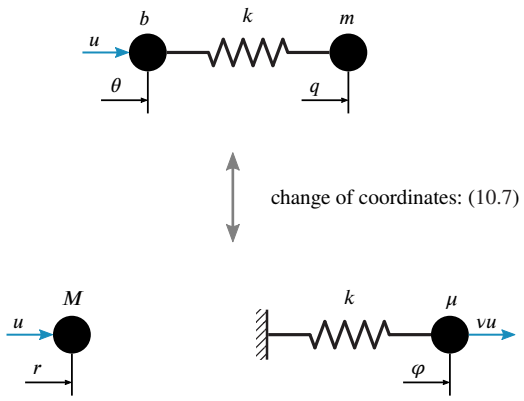

Figure 10.1: The proposed change of coordinates reduces the two-body problem in eqs. (10.1–10.2) to a pair of one-body problems. With this transformation, the control input will act on both masses, although in a scaled fashion in one case.

dynamic model is

$$m\ddot{q} + k(q - \theta) = 0 \tag{10.1}$$

$$b\ddot{\theta} + k(\theta - q) = u, \tag{10.2}$$

where θ and q are the positions of the two masses, relative to some inertial reference frame, and u is the control input force. We assume a symmetric bound on the input

$$|u| \leq \hat{u}. \tag{10.3}$$

Note that this model (with masses in translation) is equivalent to that of a robot joint (with rigid bodies in rotation), where the control torque u acts on the motor inertia b, driving the link inertia m through an elastic transmission of finite stiffness k. In this case, θ and q are the motor and link position, respectively.

We will present a new method that simplifies the generation and analysis of optimal bang-bang control policies for the elastic system (10.1–10.2) under the input bound (10.3). Time-optimal rest-to-rest (RTR) solutions are derived in closed form by means of pure geometric considerations, providing thus valuable insight into the RTR motion problem. With respect to existing works, our method does not suffer from numerical robustness issues nor does it require an offline processing/optimization phase.

At its core, our method relies on exploiting translational and time symmetries of the elastic system. In particular, we showcase the equivalence between the motion of the elastic system and the two-body problem in classical mechanics, introducing thus a change of coordinates that reduces the two-body problem to a pair of decoupled one-body problems. In contrast to a two-body problem in classical mechanics, additional external forces are exerted on each mass. These forces are directly related to our control input. This approach allows to extend the idea of phase-plane based optimization [15, 161] to the presence of elastic joints. However, instead of working with the projected dynamics in a single phase-space diagram, we face the problem of synchronizing the motion of two bodies in two separate phase planes. In this framework, we derive conditions under which the elastic joint system achieves time-optimal motion for a RTR problem in a total time equal to that of a rigid joint (i.e., when $k \to \infty$). Further, in all other situations the optimal solution for the elastic case will be slower than that of the rigid case. As a result, an elastic joint matches the performance of a rigid system only in special cases that we define as *natural motions*. Interestingly enough, this analysis may be used also

to optimize the mechanical design of an elastic transmission.

The rest of the chapter is organized as follows. In Section 10.2, we introduce the change of coordinates that decouples the dynamics of the elastic joint system. Section 10.3 presents the concept of natural motions, and the associated bang-bang solution to the minimum time problem with a single control switch. In Section 10.4, we generalize the solution to a generic RTR motion, synthesizing the time-optimal bang-bang policy with three control switchings. Numerical results are reported in Section 10.5.

10.2 Equivalence Transformation

In classical mechanics, the two-body problem predicts the motion of two masses, each exerting a force on the other. One of the prominent examples is the gravitational case, also known as Kepler problem [84, 85], which arises in orbital mechanics for predicting the orbits of two bodies in a binary system[1]. This problem can be treated in an elegant fashion by reducing it to a pair of one-body problems. Substituting Newton's law of universal gravitation [125] with Hooke's law, we can treat the elastic joint system (10.1–10.2) as a two-body problem that evolves in one dimension, allowing to apply the techniques that simplified the analysis of the Kepler problem.

[84]: Kepler (1621), *Epitome Astronomiae Copernicanae*
[85]: Kepler (1609), *Astronomia Nova*

1: In the simplest case, each of the two bodies exert a conservative, central force on the other, with no other external force being present.

[125]: Newton (1687), *Philosophiae Naturalis Principia Mathematica*

In our elastic system, each body exerts a conservative central force on the other (Figure 10.1). In addition, one of the two bodies is subject to an external force which represents our control input. The force of interaction is the elastic force $k(q_a - q_u)$. This suggests that we may conveniently use the relative position as one of the generalized coordinates

$$\varphi \triangleq q_a - q_u, \tag{10.4}$$

letting the potential energy of the system take the simple form

$$\mathcal{V} = \tfrac{1}{2} k \left(q_a - q_u\right)^2 = \tfrac{1}{2} k \varphi^2. \tag{10.5}$$

A good choice for the second generalized coordinate turns out to be the position of the center of mass (CoM) of the system.

$$r \triangleq \frac{m q_u + b q_a}{M}, \tag{10.6}$$

where $M \triangleq m + b$ is the total mass of the two bodies. The original set of coordinates is related to the introduced one by the inverse transformation

$$q_u = r - \frac{b}{M}\varphi; \quad q_a = r + \frac{m}{M}\varphi. \tag{10.7}$$

Thus, we can rewrite the kinetic energy of the system as

$$\mathcal{T} = \tfrac{1}{2}\left(m\dot{q}_u^2 + b\dot{q}_a^2\right) = \tfrac{1}{2}\left(M\dot{r}^2 + \mu\dot{\varphi}^2\right), \tag{10.8}$$

with the *reduced mass* $\mu \triangleq \frac{mb}{m+b} < \min(m, b)$, see also [181]. The kinetic energy of the system is thus equal to that of two virtual particles, one of total mass M moving with the speed of the CoM, and the other of reduced mass μ moving with the speed of the relative position. The total energy of the

[181]: Taylor (2005), *Classical Mechanics*

system,

$$\mathcal{H} = \tfrac{1}{2} M \dot{r}^2 + \tfrac{1}{2} \left(\mu \dot{\varphi}^2 + k \varphi^2 \right) \triangleq \mathcal{H}_{\text{com}} + \mathcal{H}_{\text{rel}}, \tag{10.9}$$

shows the decoupled nature of the two one-body problems. This structure significantly simplifies matters. The equations of motion in the new coordinates are in fact

$$M \ddot{r} = u, \qquad \text{(rigid)} \tag{10.10}$$

$$\mu \ddot{\varphi} + k \varphi = \nu u, \qquad \text{(flexible)} \tag{10.11}$$

with the dimensionless parameter $\nu \triangleq m/M$. As predicted (see also the bottom of Figure 10.1), equation (10.10) is precisely that of a free floating particle of mass M driven by u, while (10.11) represents a mass μ oscillating about a fixed center while subject to the external force u scaled by the constant factor ν. We note also that, given a constant input, the elastic joint system is invariant to time reversal, i.e., under the operation $T : t \mapsto -t$. Intuitively speaking, this is due to the conservation of entropy. This property will turn out to be extremely useful later in this chapter.

10.2.1 Solution of the Decoupled Systems

Since we are interested in bang-bang control policies, we assume that u is piece-wise constant. In this case, the solution to the equation of motion (10.10) is trivial

$$r(t) = \frac{u}{2M} t^2 + C_1 t + C_2, \tag{10.12}$$

with C_1 being the initial velocity and C_2 being the initial position. Since we are interested in RTR motions we can assume, without loss of generality[2], that $C_1 = 0$ and $C_2 = 0$. The general solution of (10.11) is

2: We can always choose the inertial frame so that $r(t)|_{t=0} = 0$.

$$\varphi(t) = A \cos(\omega t + \delta) + \bar{u}, \tag{10.13}$$

with oscillation amplitude A, *angular frequency* $\omega \triangleq \sqrt{k/\mu}$, phase shift δ, and *static response*

$$\bar{u} \triangleq \nu u / k. \tag{10.14}$$

The amplitude and phase shift depend on the initial conditions. The corresponding velocity is given by

$$\dot{\varphi}(t) = -A\omega \sin(\omega t + \delta). \tag{10.15}$$

We can represent the phase space trajectory of system (10.11) in a useful way by moving into the complex plane. To this end, we express (10.13) and (10.15) in terms of complex exponentials. The system state will be a single point in the complex plane, i.e., the complex plane serves as phase plane. To this end, let

$$z(t) \triangleq \bar{u} + \varphi(t) + i\dot{\varphi}(t) = \bar{u} + A_1 e^{i(\omega t + \delta)} + A_2 e^{-i(\omega t + \delta)}, \tag{10.16}$$

with $A_1 \triangleq \frac{A}{2}(1 - \omega)$ and $A_2 \triangleq \frac{A}{2}(1 + \omega)$. As the reduced mass oscillates back

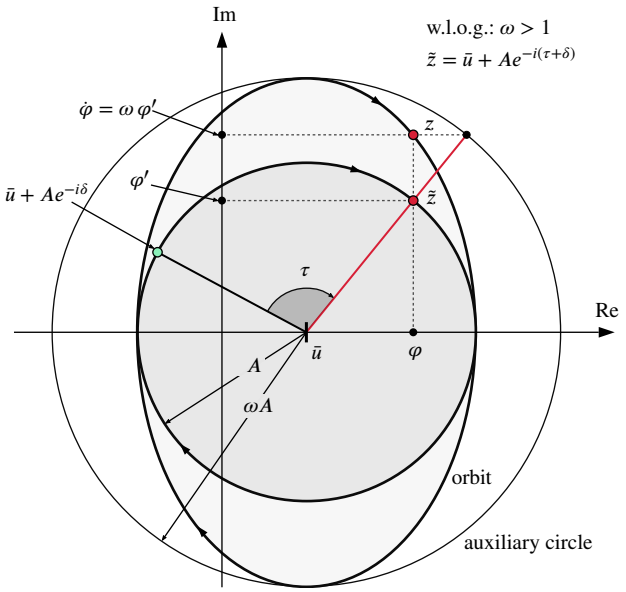

Figure 10.2: The position $(\varphi, i\varphi')$ of the normalized system is given by the complex pointer $Ae^{i(\tau+\delta)}$ whose origin is offset along the real axis by $\bar{u}$. As the reduced mass oscillates back and forth, this point moves in clockwise orientation on an inscribed circle with radius A that is centered at $\bar{u}$. The elliptic orbit of the reduced mass $(\varphi, \dot{\varphi})$ can be obtained by scaling the imaginary part of $\tilde{z}$, *i. e.* φ', by ω.

and forth, point z moves on an ellipse centered at $\bar{u}$ in clockwise orientation. This result is illustrated in Figure 10.2. The exact shape will become clear in a moment.

Observe that the state trajectory becomes particularly simple for $\omega = 1$, when the ellipse in the phase plane degenerates to a circle. Exploiting this fact to simplify matters, we rewrite (10.13)–(10.15) in terms of the scaled time

$$\tau = \omega t, \tag{10.17}$$

that we shall refer to as *natural time* (which is system specific, as the scaling factor is its angular frequency). Using the chain rule $d(\cdot)/dt = \omega\, d(\cdot)/d\tau$, we have

$$\varphi(t) = \varphi(\tau/\omega), \tag{10.18a}$$
$$\dot{\varphi}(t) = \omega\varphi'(\tau/\omega), \tag{10.18b}$$

with the natural time as parameter, and having denoted by $(\cdot)' \triangleq d(\cdot)/d\tau$ the new differential operator. We note that (φ, φ') are equivalent to the analytical solution of a clamped spring-mass system with natural frequency $\omega = 1$. The scaled trajectory

$$\tilde{z}(\tau) = \bar{u} + \varphi(\tau) + i\varphi'(\tau) = \bar{u} + Ae^{i(\tau+\delta)}, \tag{10.19}$$

then corresponds to the solution of a spring-mass system with a unitary angular frequency. Thus, a phase plane trajectory z can be obtained from the trajectory $\tilde{z}$ by scaling the imaginary part of $\tilde{z}$ by the constant factor ω.

If we know the trajectory $\tilde{z}(\tau/\omega)$ in the complex plane, we obtain $z(t)$ by stretching ($\omega > 1$) or squeezing ($\omega < 1$) the imaginary part of $\tilde{z}$ by the angular frequency factor. It is straightforward to see that $\tilde{z}$ defines a point that moves in the clockwise direction on a circle centered at $\bar{u}$ and having radius A. Hence, z will trace an ellipse centered at $\bar{u}$, with axes parallel to the coordinate axes, semi-major axis ($\omega > 1$) of length ωA and semi-minor axis of length A.

Note finally that the natural time τ, with δ as an offset, corresponds to the polar angular coordinate of $\tilde{z}$, but not to the polar angular coordinate of

z. However, the parameter pair τ and δ can be interpreted as the eccentric anomaly [36] of a point z that moves on an elliptic orbit, a popular concept in astronomy. The geometric meaning of the eccentric anomaly becomes clear in the point construction method of an ellipse by La Hire. Given a trajectory $\tilde{z}(\tau/\omega)$, this construction method allows to derive the corresponding trajectory $z(t)$, and vice versa, in a purely geometric way, see Figure 10.2.

[36]: De Ruiter et al. (2012), *Spacecraft Dynamics and Control: An Introduction*

10.3 Natural Motions

We preliminarily recap the rest-to-rest motion in minimum time of the total mass M made by the two individual masses m and b connected by a rigid joint ($k \to \infty$). We then transfer these insights to the case of an elastic joint and introduce the concept of *natural motions*. When a natural motion applies, this associated rest-to-rest command is time optimal. Further, natural motions are the only cases when an elastic joint matches the fastest RTR motion performance of a rigid joint.

10.3.1 Rigid Joint Case

Consider (10.10) as the dynamics of the rigid joint case. The minimum time control problem to displace by a desired amount r_f the total mass M from rest to rest, under the constraint (10.3), reduces to a minimum time problem for a double integrator with constant bounds on the acceleration input $\ddot{r}$. From (10.3), the upper and lower bounds for the acceleration are $\ddot{r}_{\max} = \hat{u}/M$ and $\ddot{r}_{\min} = -\hat{u}/M$. Throughout this paper we assume, w.l.o.g, that $r_f > 0$.[3] The solution to the optimal control problem is a bang-bang input [11]. Due to the symmetry of the constraints (10.3) and the time symmetry of (10.10) under constant inputs, the rest-to-rest solution will also be symmetric with respect to time and has the form

3: The solutions for $r_f < 0$ are simply obtained by inverting the input signs.

[11]: Athans et al. (2006), *Optimal Control: An Introduction to the Theory and Its Applications*

$$\ddot{r} = \begin{cases} \ddot{r}_{\max}, & \text{for } 0 \le t \le t_s \\ \ddot{r}_{\min}, & \text{for } t_s < t \le t_f, \end{cases} \tag{10.20}$$

where t_f denotes the final time and $t_s \triangleq t_f/2$ the instant of command switching. Obviously, this corresponds to the control law

$$u = \begin{cases} \hat{u}, & \text{for } 0 \le t \le t_s \\ -\hat{u}, & \text{for } t_s < t \le t_f, \end{cases} \tag{10.21}$$

which yields the system response

$$r(t) = \begin{cases} \frac{\hat{u}}{2M} t^2, & \text{for } 0 \le t \le t_s \\ -\frac{\hat{u}}{2M}(t^2 - 4t_s t + 2t_s^2), & \text{for } t_s < t \le t_f \end{cases} \tag{10.22}$$

and

$$\dot{r}(t) = \begin{cases} \frac{\hat{u}}{M} t, & \text{for } 0 \le t \le t_s \\ -\frac{\hat{u}}{M}(t - 2t_s), & \text{for } t_s < t \le t_f. \end{cases} \tag{10.23}$$

The response to a bang-bang input (10.21) is shown in Fig. 10.3.

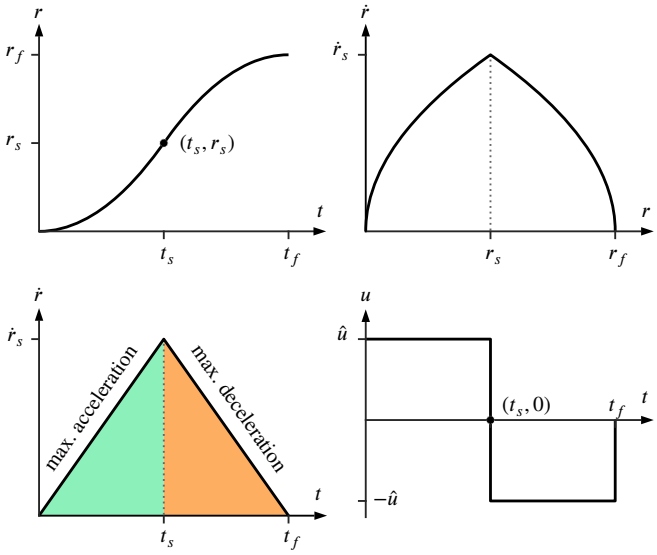

Figure 10.3: A typical time-optimal RTR motion profile for a rigid joint. We have points and lines of symmetry. The total area under the velocity profile is equal to the total displacement $r_f > 0$. The CoM trajectory of an elastic joint has the same form for the natural motion case.

10.3.2 Elastic Joint Case

We know that the class of bang-bang inputs (10.21) solve the time-optimal control problem in the rigid joint case. We are interested in whether such solutions exist and are optimal also for the elastic case, when the task is to move the entire system (10.10)–(10.11) from rest to rest, with initial and final positions

$$r(t) = \begin{cases} 0, & \text{for } t = 0 \\ r_f > 0, & \text{for } t = t_f \end{cases}, \quad \varphi(t) = \begin{cases} 0, & \text{for } t = 0 \\ 0, & \text{for } t = t_f. \end{cases} \tag{10.24}$$

The result for the rigid case allows to conclude that a bang-bang input yields the time-optimal rest-to-rest motion for the CoM of the flexible joint system. The solution is equivalent to the one shown in Fig. 10.3. However, since we are interested in moving the entire system from rest to rest (and with zero final deformation), we have to ensure that our control input induces a synchronized motion for the CoM and the reduced mass μ. The acceleration of the reduced mass subject to the bang-bang input (10.21) is

$$\ddot{\varphi}(t) = \omega^2 \varphi''(\tau/\omega) = \begin{cases} f(\varphi, \hat{u}), & \text{for } 0 \le t \le t_s \\ f(\varphi, -\hat{u}), & \text{for } t_s \le t \le t_f \end{cases} \tag{10.25}$$

where $f(\varphi, u) \triangleq \mu^{-1}(\nu u - k\varphi)$. In order to simplify the notation, let $h(\varphi, u) \triangleq \omega^{-2} f(\varphi, u)$ such that $\varphi''(\tau/\omega) = h(\varphi, u)$. Also, denote for compactness $\bar{u}_{\max} \triangleq \nu\hat{u}/k$.

As we prove below, there exist indeed bang-bang inputs of the form (10.21) that yield synchronized RTR motions satisfying the boundary conditions (10.24). The most intuitive approach to find the switching position is to build the switching curve in the $(\varphi, i\varphi')$ phase plane. We start with maximum acceleration and solve $\varphi'' = f(\varphi, \hat{u})$ forward in time from the initial point $\varphi = \varphi' = 0$. From (10.19), we know that for a constant input u all solutions are circles centered at $\bar{u}$ which are traced in the clockwise direction. As such, a system that starts from the origin, under $u = \hat{u}$, moves clockwise on the orbit o_+ with radius $A = \bar{u}_{\max}$. This behavior is shown in Fig. 10.4, as well as on the left in Fig. 10.6 (where the natural time τ corresponds to the blue angle

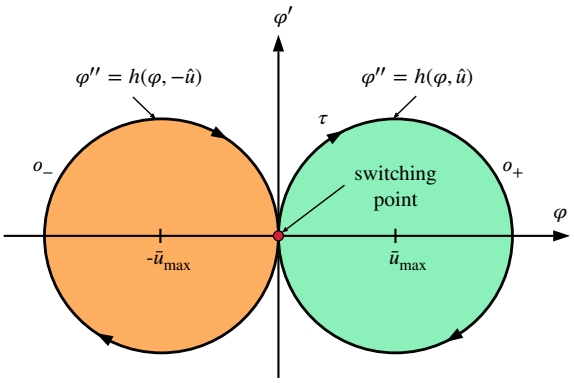

Figure 10.4: A natural motion trajectory of the reduced mass with one switching event. The orbit o_+ (o_-) is the locus of all points (φ, φ') which can be transferred to the origin by the control $u = \hat{u}$ ($u = -\hat{u}$).

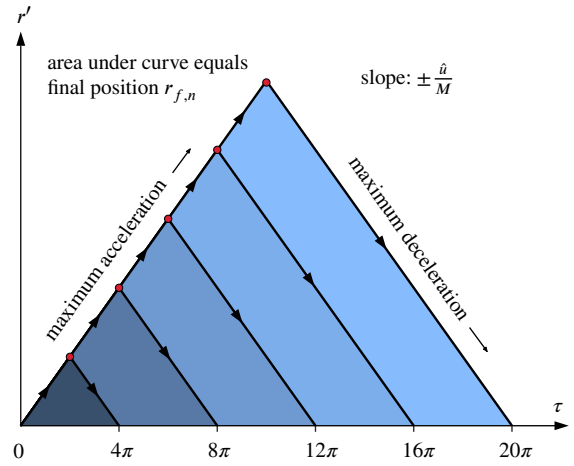

Figure 10.5: Typical natural motion velocity profiles for the CoM. The red dots indicate the switching events for $n = 1, 2, \ldots$ full acceleration/deceleration cycles. This construction process can be continued ad infinum by adding further acceleration and deceleration orbits.

that is being covered).

Next, we solve $\varphi'' = f(\varphi, -\hat{u})$ backward in time from the final point $\varphi = \varphi' = 0$, yielding the circular orbit o_-. Since system (10.10–10.11) under a constant input is invariant to time reversal, forward and backward integration are equivalent operations when starting from a given system state. Therefore, we don't need to solve the system dynamics backwards in time: due to the control policy (10.21), forward and backward trajectories are just mirror images with respect to the imaginary axis.

We note also that the two trajectories are tangent at the origin of the phase plane. Since no other point of tangency or intersection exists, transfer between the two orbits may occur only at the origin. The phase plane trajectory that emerges from solving $\varphi'' = h(\varphi, -\hat{u})$ backwards in time from $\varphi = \varphi' = 0$ is the switching curve for this scenario. The optimal control policy is to apply maximum acceleration $\varphi'' = h(\varphi, \hat{u})$ until the trajectory intersects the origin, and then switch to maximum deceleration $\varphi'' = h(\varphi, -\hat{u})$.

The acceleration and deceleration phases are in the time intervals $0 < \tau \leq 2\pi$ and $2\pi < \tau \leq 4\pi$, respectively. Hence, we spend half of the time applying $u = \hat{u}$ and the remaining half applying $u = -\hat{u}$. Since this strategy is time optimal for the RTR motion of the CoM, we conclude that this control policy moves the entire system (10.10)–(10.11) from rest to rest in a time-optimal way[4].

We can immediately see that there exists an infinite number of such solutions. In fact, we may cover n orbits with maximum acceleration and n orbits with maximum deceleration. We refer to all these instances as natural

4: Recall that we have two decoupled systems. As such, the minimum possible time for moving both systems synchronously has to be greater or equal to the minimum times for moving the individual systems.

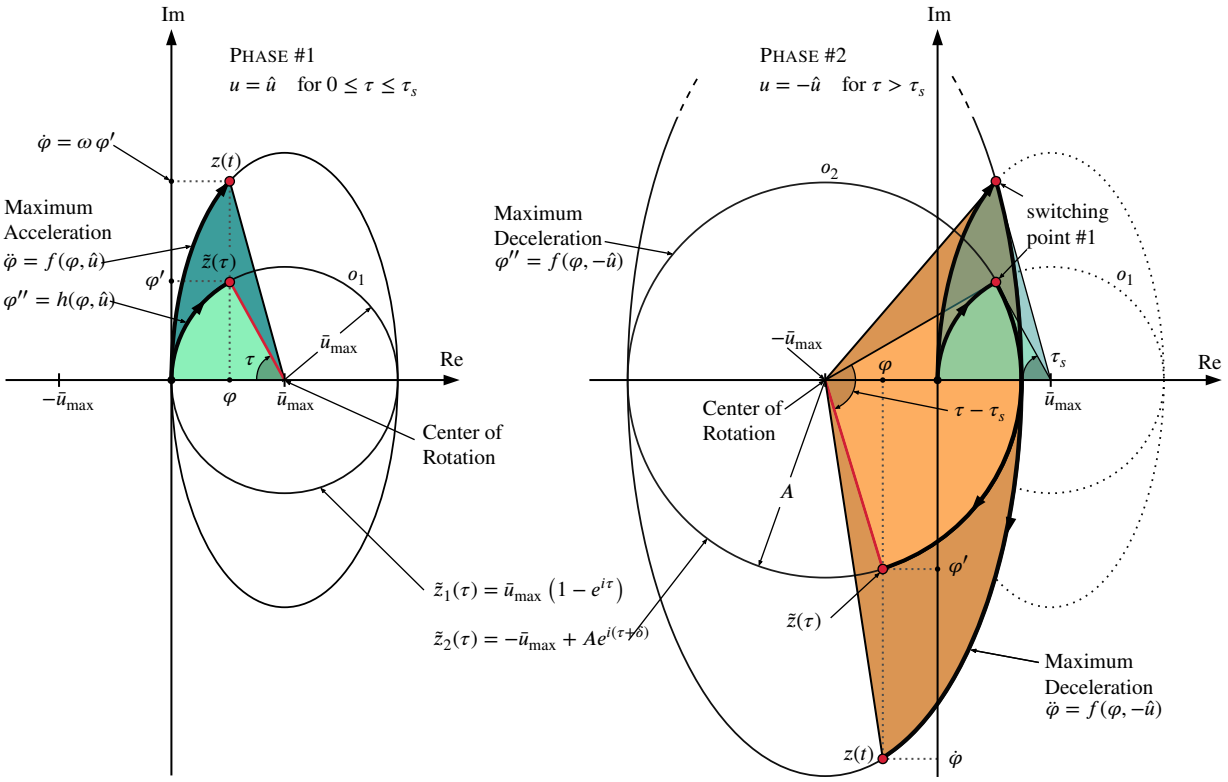

Figure 10.6: Geometry of the phase-space trajectories for multiple switching incidents.

motions. All natural RTR motions of system (10.1–10.2) emerge from the control policy

$$u = \begin{cases} \hat{u}, & \text{for } 0 \le \tau \le \tau_{s,n} \\ -\hat{u}, & \text{for } \tau_{s,n} < \tau \le \tau_{f,n}, \end{cases} \tag{10.26}$$

with $\tau_{f,n} = 4n\pi$ and $\tau_{s,n} = \tau_{f,n}/2$, for $n \in \mathbb{N}$. Furthermore, each natural motion is a time-optimal solution to a specific RTR motion problem for the elastic joint system.

The velocity profile of the CoM mass subject to the control (10.26) is piece-wise linear, as shown in Fig. 10.5. The geometric relation between the CoM velocity r' and the corresponding final positions r_f is given by

$$r_f = \int_0^{t_f} \dot{r}\, dt = \int_0^{\tau_f} r'\, d\tau. \tag{10.27}$$

Thus, the final position $r_{f,n}$ is equal to the area under the corresponding velocity profile in Fig. 10.5. From (10.23), we know that the peak velocity at the switching point n is given by $\dot{r}(t_{s,n}) = (\hat{u}/M)(\tau_{s,n}/\omega)$. Applying basic geometry allows to determine the final reached position as[5]

$$r_{f,n} = \frac{\hat{u}}{M}\left(\frac{\tau_{s,n}}{\omega}\right)^2 = \frac{\hat{u}}{M}\left(\frac{2n\pi}{\omega}\right)^2. \tag{10.28}$$

Indeed, the achievable final positions are countable and do not cover the entire set $\mathbb{R}^+$. We may only reach (infinitely many) discrete points for a given set of system parameters. In the following section, we present the class of bang-bang solutions that allows to cover the entire set of real numbers.

5: Note that we cover half of the distance in half of the time.

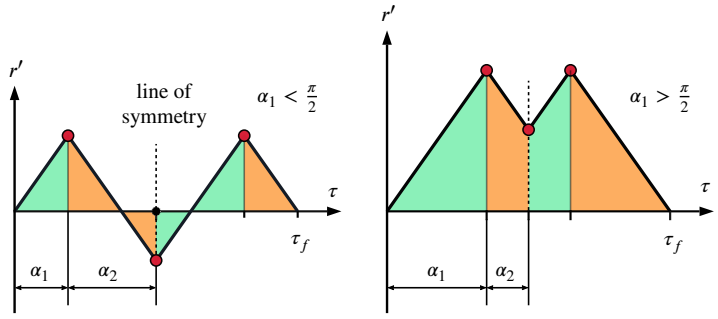

Figure 10.7: Typical CoM velocity profiles for the three-switchings solution. By purely geometrical reasoning we may conclude that the CoM velocity assumes negative values if and only if $\alpha_1 < \pi/2$.

10.4 Reaching any Distance

In this section, we synthesize a three-switching bang-bang control strategy that achieves RTR motions in minimum time for arbitrary final positions .

10.4.1 The Synchronization Problem

By introducing three switching points, we will show that one can reach any desired position for the CoM as well. Again, we synchronize the motion of the CoM with the motion of the reduced mass so that the boundary conditions (10.24) are all satisfied. From the time-symmetry of the dynamics, we observe that any time-optimal control strategy must be symmetric with respect to the half motion time. Thus, we only consider three-switching strategies that satisfy this condition. Therefore, a policy including three control switches (for $r_f > 0$) must be of the form

$$u = 3\begin{cases} \hat{u}, & \text{for } 0 \le \tau \le \alpha_1 \\ -\hat{u}, & \text{for } \alpha_1 < \tau \le \alpha_1 + \alpha_2 \\ \hat{u}, & \text{for } \alpha_1 + \alpha_2 < \tau \le \alpha_1 + 2\alpha_2 \\ -\hat{u}, & \text{for } \alpha_1 + 2\alpha_2 < \tau \le 2\left(\alpha_1 + \alpha_2\right). \end{cases} \tag{10.29}$$

When applying an input torque $\hat{u}$ to system (10.10)–(10.11), and starting from the origin, we know that the resulting trajectory for $\tilde{z}$ is a circular orbit o_1 centered at $\bar{u}_{\max}$ —see the left side of Figure 10.6. Switching to an input $-\hat{u}$ after some time $\tau_{s1,n}$ transfers $\tilde{z}$ to a circular orbit o_2 with its center at $-\bar{u}_{\max}$. The continuity of the solution (φ, φ') implies that these two circular orbits intersect at the switching time τ_s. This uniquely defines the radius of orbit o_2. At the time-point of switching, the amplitude A in (10.19) assumes the radius of o_2. In a switching event, we can think of an amplitude A and angular offset δ adaptation such that continuity of the solution for (φ, φ') is ensured. This construction is illustrated on the right side of Figure 10.6. We remark that a continuous solution in (φ, φ') implies a continuous solution in $(\varphi, \dot{\varphi})$. Also, since we require the CoM to complete the motion at rest, the total intervals of maximum acceleration and of maximum deceleration must be equal. This is visualized in Figure 10.7.

We are now in the position to derive a control policy with three switches that allows us to achieve any final rest position for the CoM, while simultaneously moving the reduced mass from rest to rest. We shall build the phase plane trajectory of the reduced mass that corresponds to a three-switching

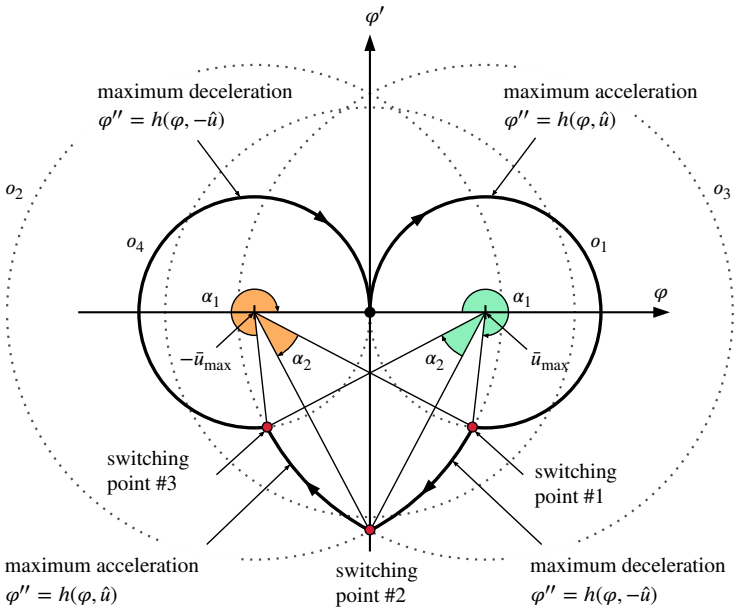

Figure 10.8: A symmetric three-switchings trajectory for the reduced mass. Note that it is possible to cover the maximum acceleration orbit o_1 multiple times before transferring to orbit o_2. However, symmetry demands that for n maximum acceleration cycles on orbit o_1 we enter n maximum deceleration cycles on orbit o_4.

control policy, as shown in Figure 10.7. A typical trajectory of this type is shown in Figure 10.8.

The first two phases of maximum and minimum acceleration yield orbit o_1 and the transfer to orbit o_2. The time spent on orbit o_1 corresponds to the polar angle α_1. The actual time span is related to the scaled one by the relation $t = \omega^{-1}\tau$. In a similar way, the polar angle α_2 corresponds to the time spent on the deceleration orbit o_2. Imagine now to perform the same procedure of trajectory construction backward in time. We know that our final position shall be the origin. Thus, we start by integrating $\varphi'' = f(\varphi, -\hat{u})$ backward in time from the origin of the phase plane, which yields orbit o_4. After some time α_1, we switch to full acceleration and obtain orbit o_3. We observe that by choosing α_1 and then α_2 wisely, we will have the second command switching exactly where the orbits o_2 and o_3 intersect for the first time. Recall now that forward and backward integration for our system are equivalent operations. Thus, the forward and backward trajectories, due to the above control policy, must be mirror images with respect to the imaginary axis. This implies that the switching must happen where the phase plane trajectory intersects the imaginary axis (i.e., when $\varphi = 0$).

We conclude that this geometric construction yields cyclic trajectories for the reduced mass, moving it from rest to rest. Further, due to our assumptions above, the same control policy yields also rest-to-rest motions for the CoM. We show next that we can reach any distance (in particular, between two natural motions) by adjusting the value of α_1.

10.4.2 Solution by Phase Space Geometry

Let us start with some geometric observations. Clearly, the radius of the first orbit o_1 is $R_1 = \bar{u}_{\max}$. The relation between the first switching angle α_1 and the radius of the second orbit o_2, as shown in Figure 10.9, is given by

$$R_2 = \bar{u}_{\max}\sqrt{5 - 4\cos(\alpha_1)}. \tag{10.30}$$

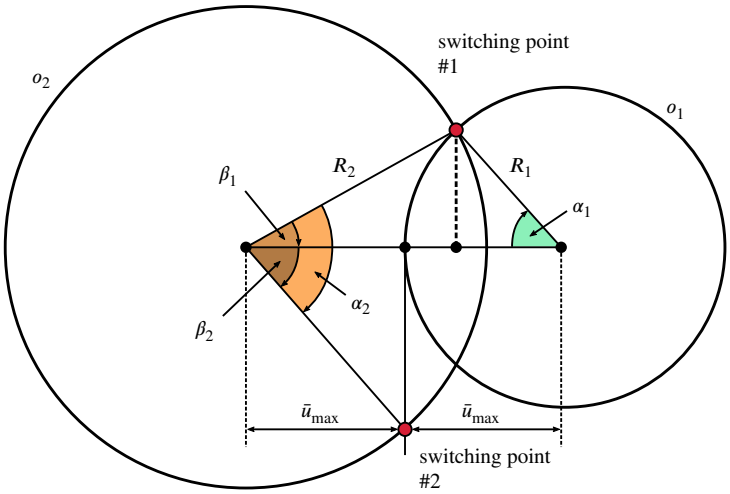

Figure 10.9: Geometric derivation of the dependence of α_2 on α_1.

We simplify the derivation of the angle α_2 by introducing two intermediary angles β_1 and β_2, which are defined in Figure 10.9. For these two angles we can derive the following relations

$$\beta_1 = \arcsin\left(\frac{R_1}{R_2}\sin(\alpha_1)\right) = \arcsin\left(\frac{\sin(\alpha_1)}{\sqrt{5-4\cos(\alpha_1)}}\right)$$
$$\beta_2 = \arccos\left(\frac{\hat{u}}{R_2}\right) = \arccos\left(\frac{1}{\sqrt{5-4\cos(\alpha_1)}}\right).$$

Note that both intermediary angles are solely a function of the first switching time point α_1. In turn, this implies that α_2 is a function of α_1. We have

$$\alpha_2 = \beta_1 + \beta_2, \tag{10.31}$$

which is zero if and only if $\alpha_1 = 2\pi n$, as expected. Recall that the final position is given by (10.27). The integral corresponds to the area under the curves in Figure 10.7 on the right. This area can be derived through purely geometric reasoning, and is equal to

$$r_f(\alpha_1) = \frac{\hat{u}}{M\omega^2}\left(2\alpha_1^2 - \left(\alpha_1 - \alpha_2\right)^2\right). \tag{10.32}$$

The corresponding natural time required to reach $r_f > 0$ is

$$\tau_f(\alpha_1) = 2\left(\alpha_1 + \alpha_2\right). \tag{10.33}$$

Is it easy to verify that, for the degenerate case of $\alpha_2 = 0$, we obtain just one of the natural motion solutions (10.28).

Finally, Figure 10.10 shows the mapping between the final (natural) motion time τ_f and the desired motion displacement $r_f > 0$, as a result of relations (10.31) to (10.33). One can immediately see that, for all but the natural motion cases, the minimum time needed for a RTR motion realizing a desired displacement r_f of the CoM is always larger in the flexible case in comparison to the rigid case. Importantly, the differences tend to vanish for longer displacements (as well as for increasing values of the joint stiffness k).

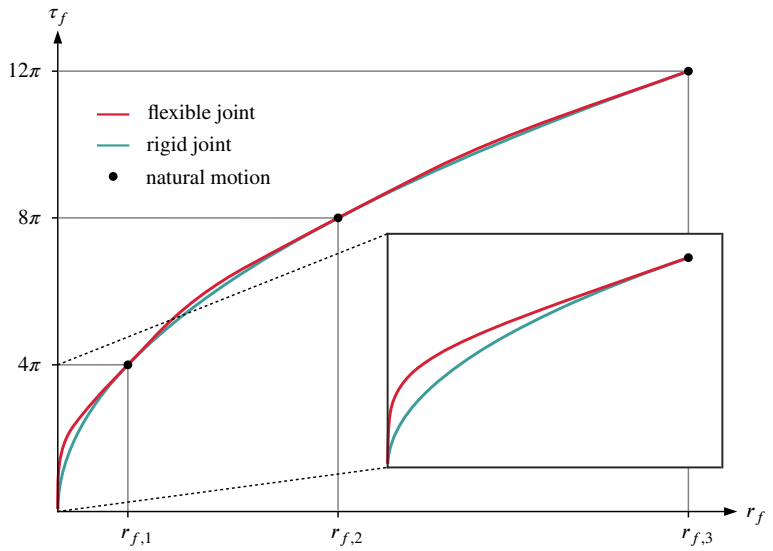

Figure 10.10: A comparison of the three-switching control policy, including natural motion solutions, versus the time-optimal RTR solutions for a rigid joint. Note, the natural motion solutions of a flexible joint match the time-optimal solutions for a rigid joint. Otherwise, a flexible joint is always inferior for RTR motions. However, for motions that take longer than 4π this mismatch, in relation to the total time τ_f, becomes negligible.

10.4.3 Optimality Result

We conclude this section with the following proposition.

Proposition 10.4.1 *Given the initial and desired final positions of the form (10.24) for system (10.1–10.2), the three-switching bang-bang control policy (10.29) provides the time-optimal solution for rest-to-rest motions. If the final position satisfies condition (10.28), the control policy (10.29) degenerates to a single switching bang-bang input which results in a natural motion.*

We sketch here the verification of the time-optimality of the three-switching strategy, based on a procedure that uses Pontryagin's minimum principle [11]. For our linear, single-input, time-invariant, and controllable system, we deal with a *normal* time-optimal problem, and therefore singular arcs in the optimal solution can be ruled out. Pontryagin's minimum principle provides then the optimal control as a piece-wise constant function of time, which is always in saturation (i.e., bang-bang) except in isolated instants of switching. The sign of the control law $u^*(t)$ is determined by the sign of the switching function $s(t)$, which in our case depends on the evolution of two components of the optimal costate vector $\lambda(t) \in \mathbb{R}^4$. We impose then equality to zero of the Hamiltonian $\mathcal{H}(t)$ at the initial and final times, $t = 0$ and $t = t_f$, using the known boundary conditions of the problem, the optimal values of our control profile, $u^*(0)$ and $u^*(t_f)$, and the final time t_f obtained from our geometric approach. Similarly, we impose in two out of the three instants of control switching, namely $t_1 = \alpha_1/\omega$ and $t_2 = t_f/2$ (both obtained from our geometric computations), the vanishing of the switching function, $s(t_1) = s(t_2) = 0$. In this way, we set up a well-defined linear system of equations that allows us to determine the four initial costate values, i.e., $\lambda_i(0)$, $i = 1, \ldots, 4$. With these, we integrate forward the necessary conditions of optimality and obtain analytically the unique expression of the optimal costate $\lambda^*(t)$ and of the associated switching function $s^*(t)$. We verify then that the crossing of zero of this function occurs only at the switching instants of our control policy and that the sign of $s^*(t)$ elsewhere is always opposite to the sign of our $u^*(t)$. Moreover, using forward integration of the state equations driven by our optimal control, we obtained also the optimal state evolution

[11]: Athans et al. (2006), *Optimal Control: An Introduction to the Theory and Its Applications*

$\boldsymbol{x}^*(t)$. With all these values plugged into the Hamiltonian, we finally verify that $\mathcal{H}(t) = 0$ at any time $t \in [0, t_f]$. Therefore, our solution satisfies the minimum principle of Pontryagin and the necessary conditions of optimality.

10.5 Numerical results

[27]: Dahl (1992), "Path constrained robot control"

As reference motions, we have considered the three examples presented by Dahl in [27]. The parameters of the considered two-mass system are $m = b = 0.5$ [kg], whereas the bound on the input force is $\hat{u} = 1$ [N]. The results are summarized in Table 10.1. We refer to the three sets of system parameters (for different values of the stiffness k) as Case 1 to Case 3.

[27]: Dahl (1992), "Path constrained robot control"

Our geometric control policy (10.29) yields exactly the same solutions presented by [27]. It important to remark that those optimal solutions were obtained through numerical optimization. In contrast, we provide a closed-form solution to the problem.

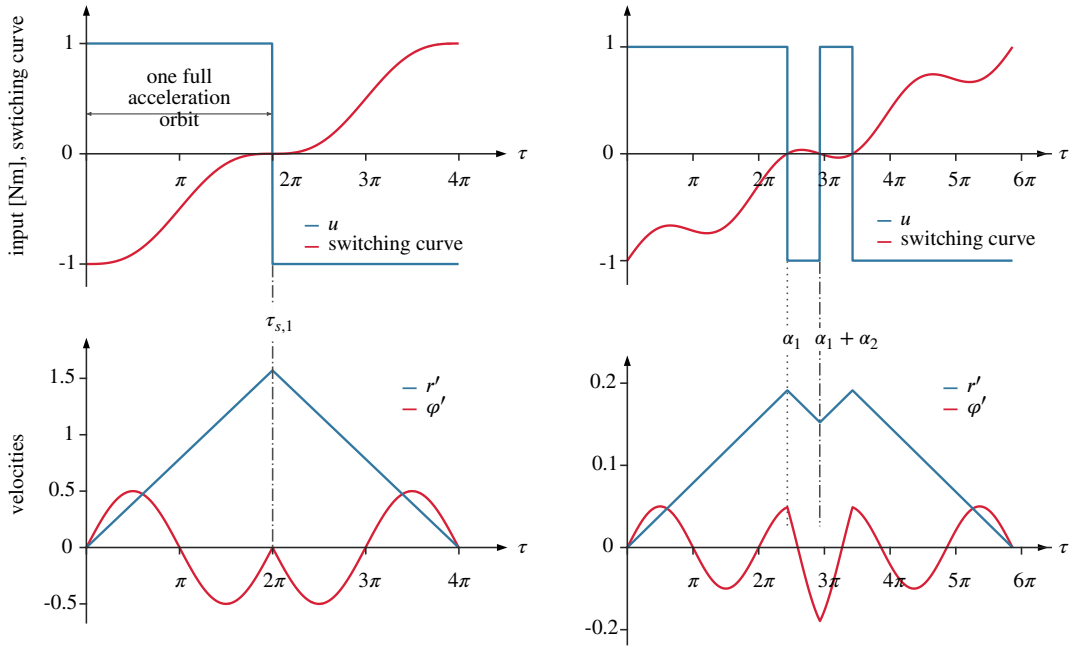

Figure 10.11: (**left**) The first natural motion for Case 1: $r_f = \pi^2$ m, $\tau_f = 4\pi$ rad. (**right**) Three-switchings solution for Case 2: $r_f = 2$ m, $\tau_f = 5.86\pi$ rad.

In Fig. 10.11 (left), we show the time-optimal bang-bang control for the first natural motion in Case 1 ($k = 1$ N m^{-1}). The final position, as given by (10.28) with $n = 1$, is $r_f = \pi^2$. In the top part, we have plotted also the optimal switching function.

Figure 10.11 (right) shows the time-optimal control law with three switchings, the optimal switching function, and the two state velocities that result

Table 10.1: Three time-optimal motions.

k [N/m]	ω [rad/s]	α_1 [rad]	α_2 [rad]	r_f [m]	τ_f [rad]	t_f [s]
1	2	2.032	1.528	2	2.27π	3.56
10	6.325	7.653	1.558	2	5.86π	2.91
100	20	26.803	1.567	2	18.08π	2.84

from control policy (10.29) in Case 2 ($k = 10\ \mathrm{N\,m^{-1}}$). The zero crossings of the switching function match the switching instants of our control policy (10.29). This confirms the conclusion about the achieved time-optimality with our geometric approach.

10.6 Conclusion

In this chapter, we highlighted the connection between a two-mass system with an elastic joint and the two-body problem in classical mechanics. Based on this insight, we introduced a change of coordinates that decouples the complete dynamics into a pair of single-body problems. This simplification allowed us to apply pure geometrical reasoning to generate and analyze minimum-time bang-bang solutions to the rest-to-rest (RTR) motion problem under actuator torque bounds. All solutions are provided in closed form. Further, we introduced the concept of natural motions which are time-optimal solutions to the RTR motion problem. These are the only RTR solutions where the minimum-time performance of an elastic joint system matches that of a rigid joint.

The insight obtained from the natural motion analysis, can be exploited to optimize the design of an elastic robot joint. In fact, it is desirable that the natural motion of an elastic joint matches its nominal motion. Only in this case, the RTR motion in the elastic case can reach the motion time performance of a rigid joint. Our framework can be easily extended to account for limitations on joint deflections and motor velocities. The natural motion concept could be extended to include periodic motions, like in pick-and-place robotic tasks. These issues will be the subject of future investigations.

11 Evaluation

It doesn't matter how beautiful your theory is, it doesn't matter how smart you are. If it doesn't agree with experiment, it's wrong.

— Richard P. Feynman

This chapter reports simulation and experimental validation of the different ESP controllers presented in Chapter 7, 9 and Appendix A. The various experiments emphasize the remarkable damping performance and robustness of the proposed ESP concept. We will study the performance of the proposed controllers on two different systems. The first is a dedicated SEA testbed, and the second, DLR *David* [54] is an ASR. Note that the applicability of the developed controller is not limited to these two systems, but rather extends to all systems satisfying the central model assumptions in Chapter 5.

Hardware Setup Critical system parameters of DLR *David* and the SEA testbed are summarized in Table 11.1. For either system, we employed a fourth-order derivative filter with a cut-off frequency of 80 Hz to obtain velocity signals. For compensating motor-side friction and estimating link-side disturbances, we used the momentum observer [34]. For all simulations and experiments the link acceleration and possibly jerk signals are computed via the method reported in Section B.2 in Appendix B if not explicitly stated otherwise as for some cases in Experiment 5. Furthermore, we followed the damping design reported in [86] and $\boldsymbol{\xi}_u$ and $\boldsymbol{\xi}_a$ refer to the link- and motor-side modal damping factors.

DLR *David* [54], as shown in Fig. 3.1, is an ASR implemented with variable impedance actuators (VSAs) in all its joints. For the experiments, we considered the first four or five main axes, namely the elbow, the three shoulder joints, which are implemented with FSJs [194] and the underarm rotation, which is realized by a bidirectional antagonistic variable stiffness

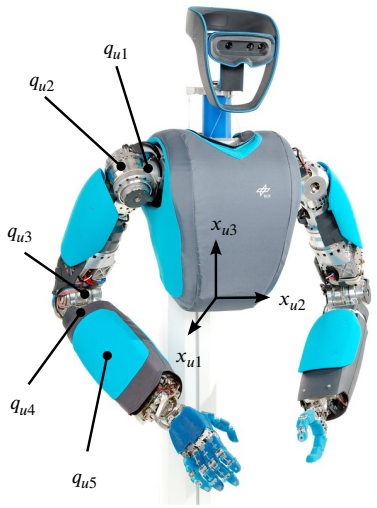

Figure 11.1: DLR *David*: A soft robot with variable stiffness actuators [54].

[54]: Grebenstein et al. (2011), "The DLR hand arm system"

[34]: De Luca et al. (2006), "Collision detection and safe reaction with the DLR-III lightweight manipulator arm"

[86]: Keppler et al. (2018), "Elastic structure preserving (ESP) control for compliantly actuated robots"

[194]: Wolf et al. (2011), "The DLR FSJ: Energy based design of a variable stiffness joint"

Table 11.1: System and control parameters

	David	Testbed
Link inertia	n.a.	$1\,\mathrm{kg\,m^2}$
Motor inertia	$0.3117\,\mathrm{kg\,m^2}$	$0.6\,\mathrm{kg\,m^2}$
Joint stiffness	$52.4\text{–}826\,\mathrm{N\,m\,rad^{-1}}$	$362\,\mathrm{N\,m\,rad^{-1}}$
Actuator limits	$\pm 67\,\mathrm{N\,m}$	$\pm 100\,\mathrm{N\,m}$
Link sensor resolution	16 bit / 271°	23 bit / revolution
Controller rate	3000 Hz	3000 Hz

(BAVS) joint [47]. The applied stiffness settings, indicated by the variables σ_i, correspond to the stiffness profiles shown in Fig. 3.1. More technical details on *David* are reported in Section 3.1.

[47]: Friedl et al. (2011), "Wrist and forearm rotation of the DLR hand arm system: Mechanical design, shape analysis and experimental validation"

The SEA testbed is constituted by a LWR III motor unit and elastic elements from DLR C-Runner, and moves in the horizontal plane, is depicted in Fig. 11.2. See [91] for details. This basic setup is intended to demonstrate what control performance can be achieved in a scenario where the dynamics of the actual hardware matches the considered model closely.

[91]: Keppler et al. (2021), "Analyzing the performance limits of articulated soft robots based on the ESPi framework: Applications to damping and impedance control"

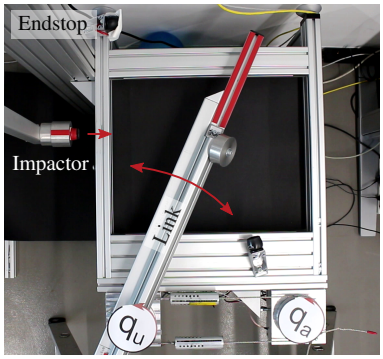

Figure 11.2: Series elastic actuator testbed with impactor.

[154]: Ray et al. (1993), "A Monte Carlo approach to the analysis of control system robustness"

Overview The chapter is structured as follows. Section 11.1, 11.2, and 11.3 evaluate the ESP schemes reported in Chapter 7 on DLR *David*. Experiment 1 and 2 highlight the motion tracking performance and robustness, whereas Experiment 3 and 4 evaluate joint and task space impedance control implementations. Section 11.4 reports experimental evaluation of the dynamic extensions proposed in Chapter 9 on the SEA testbed. Section 11.7 compares the adoption of the PD+ and Slotine & Li controllers through the QFA formulation and presents a Monet-Carlo based robustness analysis [154]. Section 11.8 reports a gain analysis that compares ESP control in full state feedback (FSF) form with feedback-linearization-based FSF control. Section 11.9 analyzes the stead-state error resulting from parameter uncertainties for regular and dynamic extension based ESP schemes; see also Chapter 9.

11.1 Experiment 1: Motion Tracking

The first experiment evaluates the motion tracking performance of the ESP and ESP+ controllers reported in Section 7.2.4 in free motion (Case 1) and during disturbances (Case 2). Note that the controllers developed in Section 7.2.4 consider a monoarticular ASR. However, by exploiting the symmetric setup of the BAVS actuator in the fifth axis of DLR *David*, it is possible to treat this joint as if monoarticular by "combining" the two motor inertias and elastic elements.[1] The controller settings for the subsequent experiment are summarized in Table 11.2. For the design of the damping matrices, $\boldsymbol{K}_{vu}$ and $\boldsymbol{K}_{va}$, the modal-damping-based reported in [86] was applied with the damping factors reported in Table 11.2. The controller gains were manually tuned such that the control input obeyed the maximal motor torques of 65 Nm for the FSJ and 4 Nm for the BAVS joint. The joint pretension was set to $\sigma_i = 5$ deg, $i = 1, \ldots, 4$, for the FSJ and to middle stiffness setting for the BAVS joint. Due to some technical sensor issues regarding the second joint, the corresponding control inputs show significantly increased noise levels. No friction compensation was active during the experiments. Consequently, viscous friction deteriorates the transient tracking performance and static friction leads to nonzero steady-state errors. In particular the harmonic drives

1: Note that recent ESP control developments in [60, 114, 151] not longer require such symmetry assumption.

	Link-side	Motor-side
Stiffness [N m rad^{-1}]	-	$\boldsymbol{K}_{pa} = \text{diag}(1000, 900, 750, 750, 750)$
Damping	$\xi_{ui} = 0.5$	$\xi_{ai} = 0.7$
Motor friction compensation		no
Motor inertia shaping		no

Table 11.2: Experiment 1. ESP/ESP+ controller settings.

are significantly affected by friction. For low stiffness values, $\boldsymbol{K}_{pa}$, static friction such as stiction significantly impacts the steady-state error. Position sensor uncertainties result in elastic torque uncertainties causing imperfect motion tracking and steady-state errors.

11.1.1 Case 1: Free Motion

Figure 11.3 shows the tracking performance in the absence of disturbances. The commanded link trajectories are shown in the top row as dashed lines with peak link velocities of $\max(\dot{\boldsymbol{q}}_u) = (218, 79, 117, 128, 329)$ deg/s. As expected, the magnitude of the tracking error correlates with the link velocities. The underlying reasons are discussed in the beginning of this chapter. Video 1 and Video 2 in Section 12.6.1 show experiments of the considered case.

11.1.2 Case 2: Disturbance Rejection

Figure 11.5 demonstrates the performance of the ESP/ESP+ controllers to reject disturbances while the system moves along a commanded trajectory. In the highlighted area, external forces are imposed on the system through the interaction with a human subject. During the motion the robot is pushed in the direction opposite to the nominal motion. The experimental setup is shown in Fig. 11.4. The magnitudes of disturbance forces roughly correlate with the peaks in corresponding joint torque plots. From the results in Fig. 11.5, we see that the ESP/ESP+ controllers show remarkable disturbance rejection performances even when the system is in motion. Within approximately 0.3 s the disturbance are rejected and the robot returns to the commanded trajectory. From joint torque plots in Fig. 11.5, it clear that the ESP+ shows slightly less overshooting. Video 1 and Video 2 in Section 12.6.1 show experiments of the considered case.

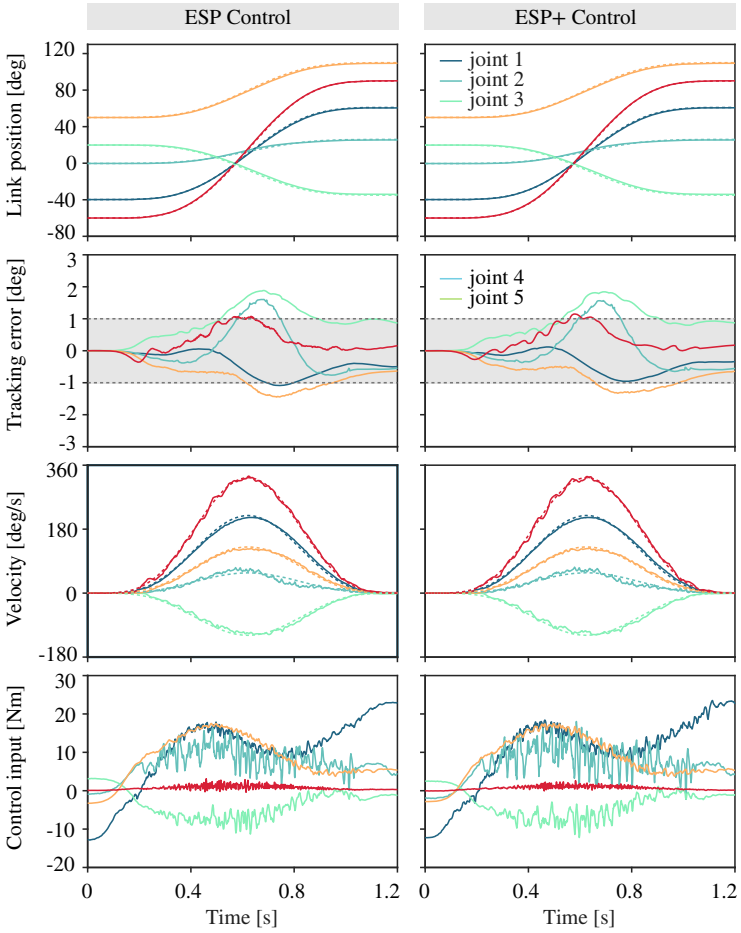

Figure 11.3: Experiment 1, Case 1. Tracking performance of the EPS/ESP+ controllers in free motion.

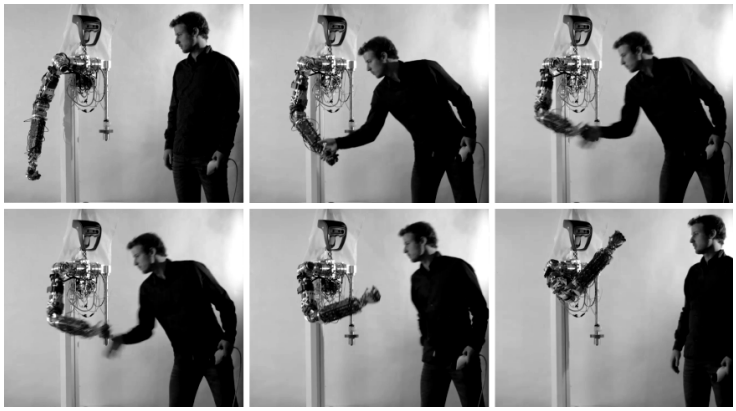

Figure 11.4: Setup for Experiment 2. The disturbance during Case 2 is shown.

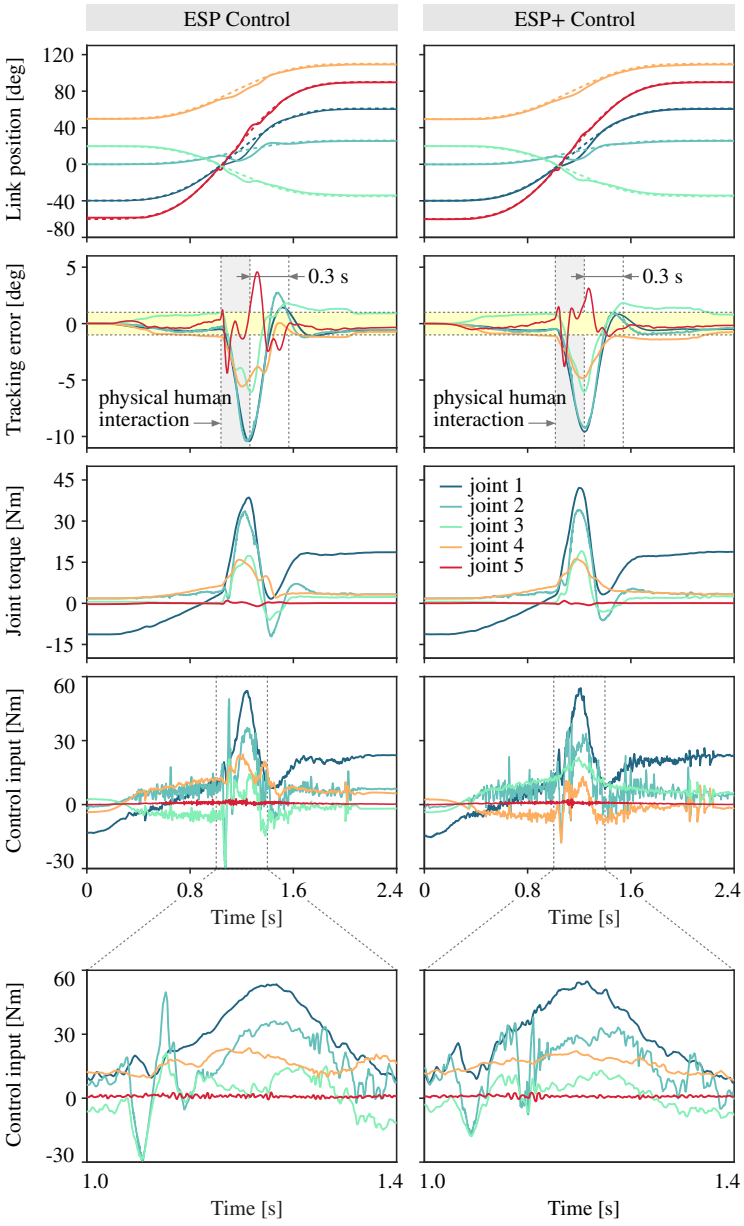

Figure 11.5: Experiment 1, Case 2. Tracking performance of the EPS/ESP+ controllers in the presence of disturbances imposed through an interacting human.

11.2 Experiment 2: Disturbance Rejection

The following experiment compares the disturbance rejection performance of ESP/ESP+ joint space motion tracking controllers introduced in Section 7.2.4 on DLR *David*. The corresponding closed-loop dynamics are stated in Proposition 7.2.1 and 7.2.3, respectively. Considering that both controllers achieve globally asymptotic motion tracking, the same behavior is to be expected in the nominal motion tracking case (any given link trajectory uniquely defines the required variation of the input forces). For this reason, the subsequent experiment compares the disturbance rejection behavior for constant setpoints, where ESP and ESP+ controllers are expected produce different results. A motor PD controller serves as reference. Figure 11.6 shows the experimental setup with the 3 kg medicine ball attached with a rope to the ceiling. During each run it is released such that it impacts, in a reproducible manner, with the arm of DLR *David*, which is commanded to hold its pre-impact position.

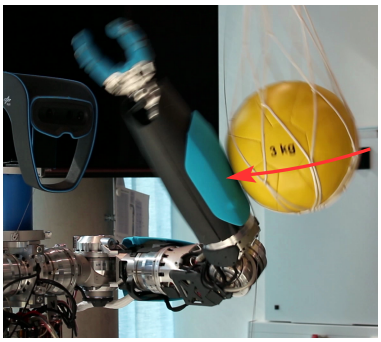

Figure 11.6: Series elastic actuator testbed with impactor.

In order to analyze the effect of the intrinsic joint stiffness setting on the disturbance rejection behavior, the experimented has been performed for the minimum ($\sigma_i = 0$), medium ($\sigma_i = 5$ deg) and highest ($\sigma_i = 10$ deg) stiffness setting. The joint characteristics corresponding with these settings are given by the outer, center and inner curves of Fig. 3.1(d–e). The results of this impact experiment are summarized in Fig. 11.7 and 11.8. Clearly, the convergence rate increases with increasing joint stiffness settings. Considering the visualization of the closed-loop dynamics in Fig. 7.5 this behavior becomes intuitively clear. The resulting closed-loop stiffness is determined by the series interconnection of the controller springs ($\boldsymbol{K}_{pa}$) with the intrinsic elastic elements. Consequently, the higher the stiffness setting, the higher the closed-loop stiffness. Moreover, considering the modal damping layout, the damping parameters increase online with increasing joint stiffness values; thus stiffness settings are expected to result in higher convergence rates. However, due to the nonlinear and load-dependent stiffness of the elastic elements, the differences in the convergence rates are smaller than one might expect. Observing Fig. 11.8, we see that for example joint 4, which faces the highest external load, reaches high stiffness values for all experiments irrespectively of the stiffness setting. The results for the PD controller [183] highlight the system's intrinsic oscillatory nature and the need for elaborate damping control concepts.

[183]: Tomei (1991), "A simple PD controller for robots with elastic joints"

It is worth remarking that for the softest stiffness setting the control inputs for the ESP/ESP+ controllers were saturated for an extended period. Despite these input saturations, the stability of the closed-loop system is not impaired. Further, both controllers show impressive damping and disturbance rejection performances in spite of these saturations. This is one of the impressive features of ESP/ESP+ control. The same controller gains have been used for all stiffness settings in order to show how the ESP/ESP+ perform over a vast joint stiffness range (approximately on order of magnitude variation) with equal gains. Notice that the ESP controller suffers less from sensor noise compared to the ESP+ controller. However, at the moment of impact and shortly thereafter, the ESP+ controller commands lower actuator torques. In addition, the EPS+

Table 11.3: ESP and ESP+ control parameters for Experiment 3.

Joint stiffness in $\mathrm{N\,m\,rad^{-1}}$								Pretension
q_{u1}	q_{u2}	q_{u3}	q_{u4}	q_{u5}	ξ_u	ξ_a	β	$\sigma_{i=1\ldots4}$
1000	900	750	750	750	0.5	0.7	1	5

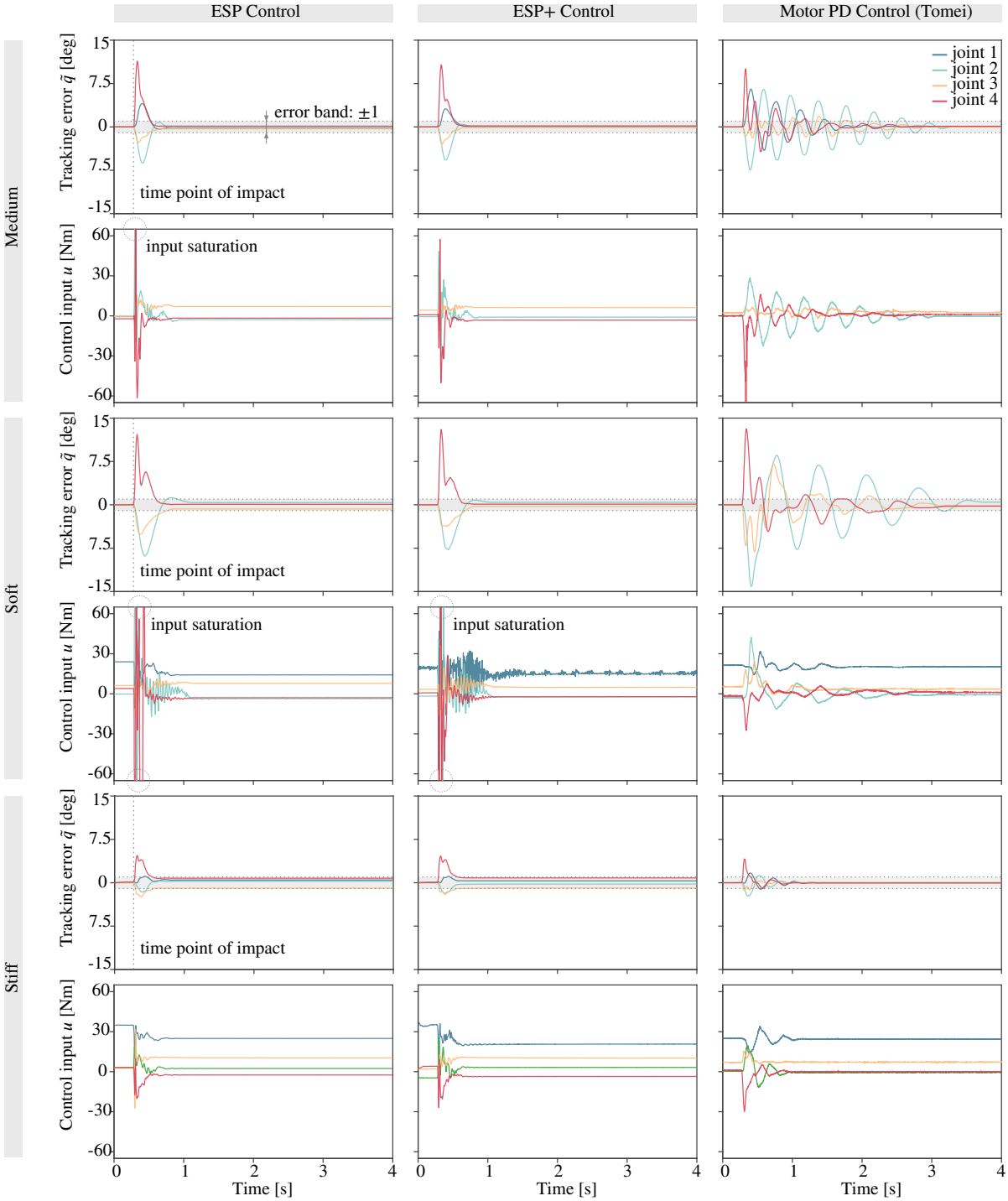

Figure 11.7: Experiment 2. Impact experiments comparing ESP and EPS+ control. The arm of DLR *David* is hit, in a reproducible manner, with a medicine ball of 3 kg swinging on a rope; see also Fig. 11.6. During the experiment the robot is commanded to hold its position. The performances of the ESP controller (left column), the ESP+ controller (center column) and the PD controller by Tomei [183] are shown in comparison. Three different stiffness settings for the VSAs were used (soft, medium, stiff). Under ESP/ESP+ control (medium stiffness) the links return into a ±1° error band within 0.25 s post impact. Reprinted from [86]

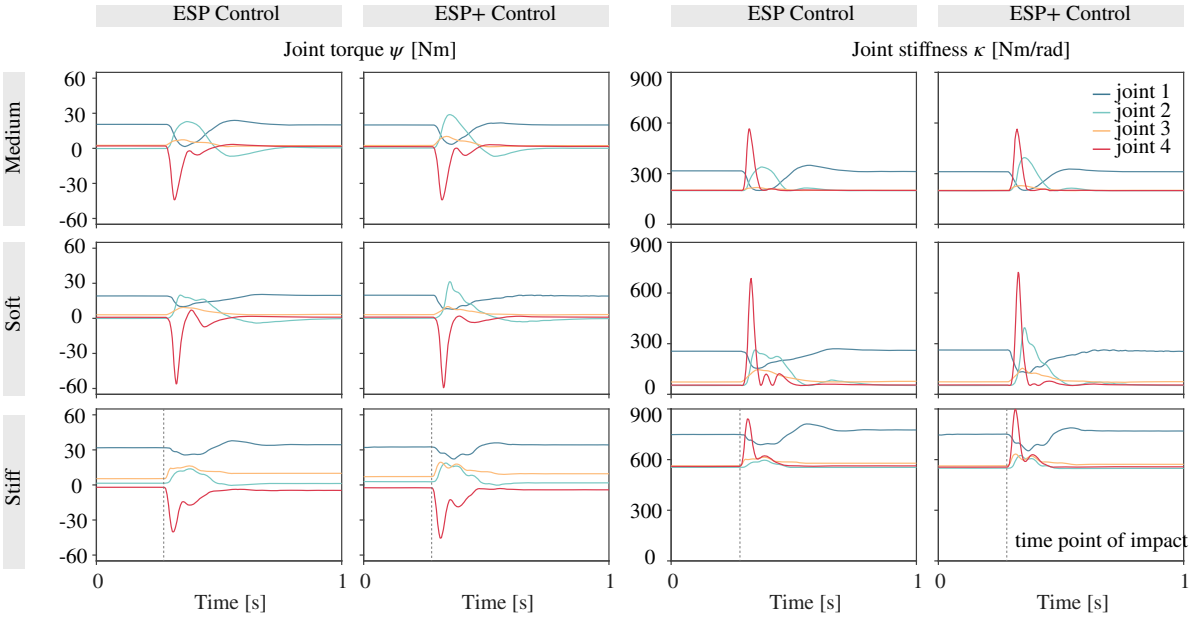

Figure 11.8: Experiment 2. Continuation of the impact experiment results. Notice that the joint stiffness values vary continuously throughout the course of each experiment, which is due to the fact that the joint stiffness values increase with rising external loads. Reprinted from [86]

controller shows slightly less overshooting. In conclusion, despite the joint stiffness values varying over a vast range, the ESP and ESP+ controllers perform excellently without gain adaption. Video 2 in Section 12.6.1 shows the considered impact experiment.

11.3 Experiment 3: Impedance Control

Experiment 3 evaluates the performance of the joint and task space impedance controllers (ESPi) reported Section 7.2.4 and 7.2.5. The controllers and associated closed-loop dynamics are summarized in Proposition 7.2.1 and 7.2.4, respectively. The commanded stiffness values, damping parameters and motor inertia shaping factors are reported in Table 11.4 (Case 1 and 2) and Table 11.5 (Case 3 and 4). For the damping design the method from [86] is applied resulting in a damping matrix that adapts online to the robot's varying joint stiffness values and inertia matrix. Throughout all experiments the motor inertia was scaled down by a factor of $\alpha = 0.3$. The forces exerted on the robot's TCP were estimated by a momentum observer [34]. The estimated forces $\mathcal{Q}'_{xu}$ and torques $\mathcal{Q}'_{u}$ were used for validation purposes only, and we filtered these signals with a Butterworth filter with a -3 dB cut-off frequency at 10 Hz. Video 4 linked in Section 12.6 demonstrates the performance of ESPi control on DLR *David*.

[34]: De Luca et al. (2006), "Collision detection and safe reaction with the DLR-III lightweight manipulator arm"

Table 11.4: Experiment 3, Case 1 and 4. ESPi control parameters.

	Joint stiffness in N m rad^{-1}							Pretension
	q_{u1}	q_{u2}	q_{u3}	q_{u4}	ξ_u	ξ_a	β	$\sigma_{i=1\ldots4}$
Case 1	1000	500	150	50	0.1	0.05	0.3	5
Case 4	800	800	800	800	0.6	0.05	0.3	5

	Stiffness in N m^{-1}						Pretension
	x_{u1}	x_{u2}	x_{u3}	ξ_u	ξ_a	β	$\sigma_{i=1\ldots4}$
Case 2	0	60	3000	0	0	0.3	5
Case 3	1500	600	1500	0.6	0.05	0.3	5
Case 3	1500	600	1500	0	0.05	0.3	5

Table 11.5: ESPi control parameters for Case 2 and 3 of Experiment 3.

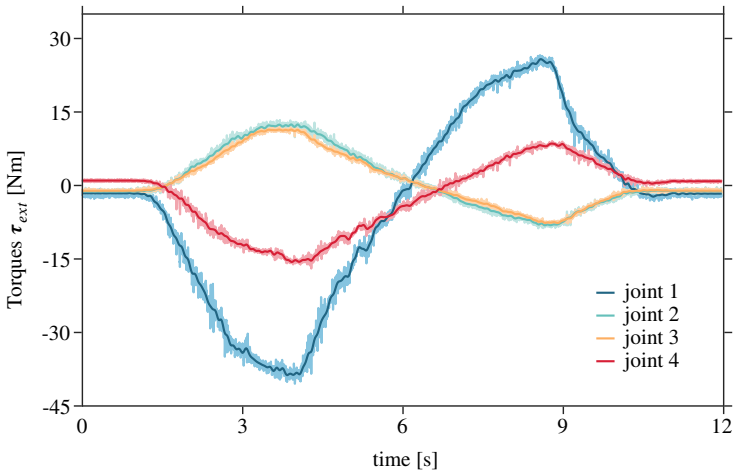

Figure 11.9: Experiment 3, Case 1: The raw and filtered signals of the external torque observer are shown.

11.3.1 Case 1: Joint Space Interaction Behavior

During the experiment a human user applies forces on the end effector by pushing and pulling on the robot's hand. The time variation of the interaction forces are reported in Fig. 11.9. Figure 11.10 reports the torque-deflection relation for the first four joints together with the desired steady-state behavior (dashed line). We can see that the results closely approximate the desired steady-state behavior. It should be remarked that the implemented closed-loop behavior is that of an impedance (relating forces with velocities). The dashed line only represent the desired dynamic behavior in the quasi-static case. During motions, the interaction behavior of the end effectorector is dictated by an interplay of inertial, elastic and damping forces resulting in an ellipse shaped force-deflection characteristics. Deviations from the nominal closed-loop behavior result from model errors, sensor inaccuracies, joint torque errors, uncompensated link-side and motor-side friction, inaccuracies in the estimation of the external disturbances etc. Figure 11.11 shows the local joint stiffness values of the physical springs, i.e., $\frac{\partial^2 \mathcal{V}_e}{\partial \boldsymbol{\varphi}^2}$. For comparison, the commanded link-side stiffness values $\boldsymbol{K}_{vu}$ are shown as well. For this particular experiment, the commanded—and achieved link-side stiffnesses (c.f. Fig. 11.10)—are up to 5 times higher than the physical joint stiffnesses.

11.3.2 Case 2: Task Space Interaction Behavior

Case 2 analyzes the interaction behavior of the Cartesian ESPi controller. A human user applies forces on the end effectorector by pushing and pulling on the robot's hand. The forces exerted on the robot's TCP are reported in Fig. 11.12. The raw and (offline) filtered values are given. The corresponding end effectorector deflections are shown in Fig. 11.13. Figure 11.14 reports

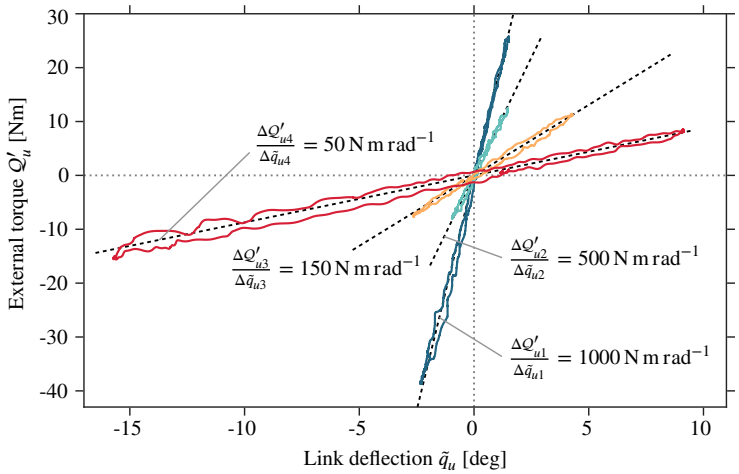

Figure 11.10: Experiment 3 (Case 1): Link deflections for the first four joints. The dashed lines represent the desired quasi-static behavior.

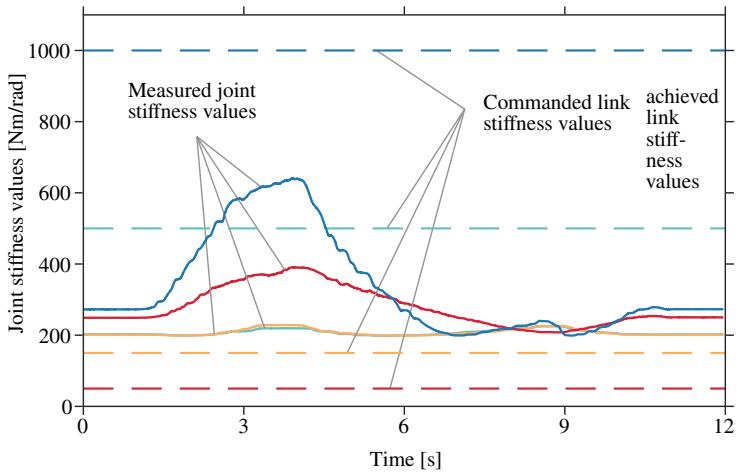

Figure 11.11: Experiment 3, Case 1: Joint torques and stiffnesses for the first four joints. The dashed lines represent the commanded link stiffness values.

the force-position relation for the y- and z-direction together with the desired steady-state behavior (dashed line). We can see that the results closely approximate the desired steady-state behavior. It should be remarked that the implemented closed-loop behavior is that of an impedance (relating forces with velocities). The dashed line only represent the desired dynamic behavior in the quasi-static case. During motions, the interaction behavior of the end effector is dictated by an interplay of inertial, elastic and damping forces resulting in an ellipse shaped force-deflection characteristics. Deviations from the nominal closed-loop behavior result from model errors, sensor inaccuracies, joint torque errors, uncompensated link-side and motor-side friction, inaccuracies in the estimation of the external disturbances etc. Notice from Fig. 11.12 that the static error of the external force observer is up to 8 N.

11.3.3 Case 3: Disturbance Rejection Behavior

In Case 3, we study the disturbance rejection performance for two different end effector damping settings ($\xi_u = 0$ and $\xi_u = 0$), and compare the results with the behavior of the PD controller proposed by Tomei [183]. The end effector is manually deflected from its equilibrium position and then quickly released. The results are reported in Fig. 11.15, with the release times being indicated by dotted lines. For the well-damped case the deflection of approximately 9 cm is rejected within 0.28 s with basically no overshooting. In the absence of link-side damping, we observe an oscillatory behavior as expected. Notice

[183]: Tomei (1991), "A simple PD controller for robots with elastic joints"

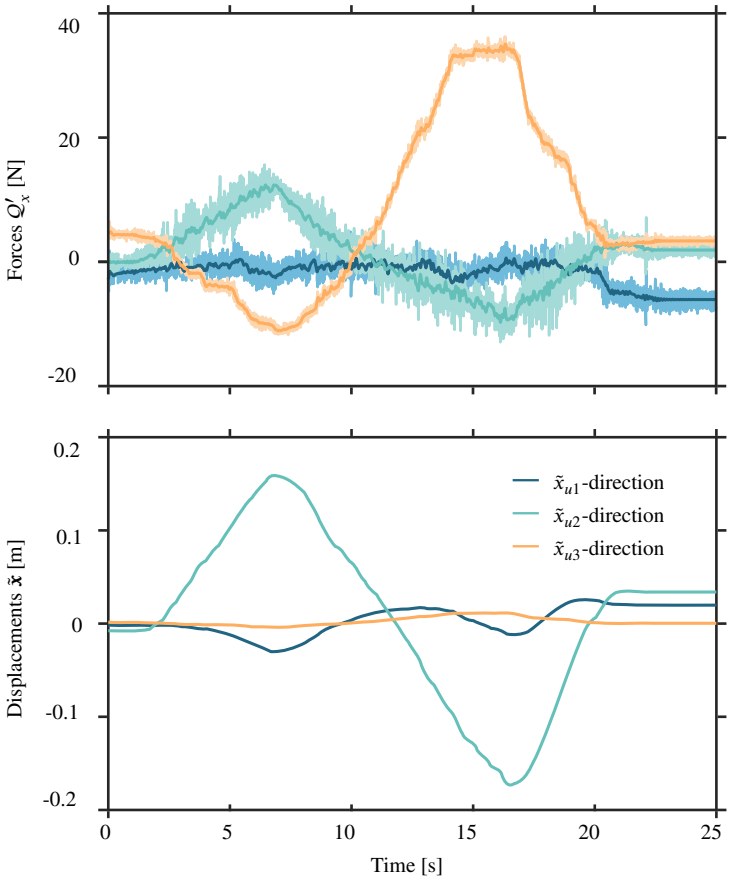

Figure 11.12: Experiment 3, Case 2: Estimated TCP interaction forces; the raw and filtered signals are shown.

Figure 11.13: Experiment 3, Case 2: End effector displacements.

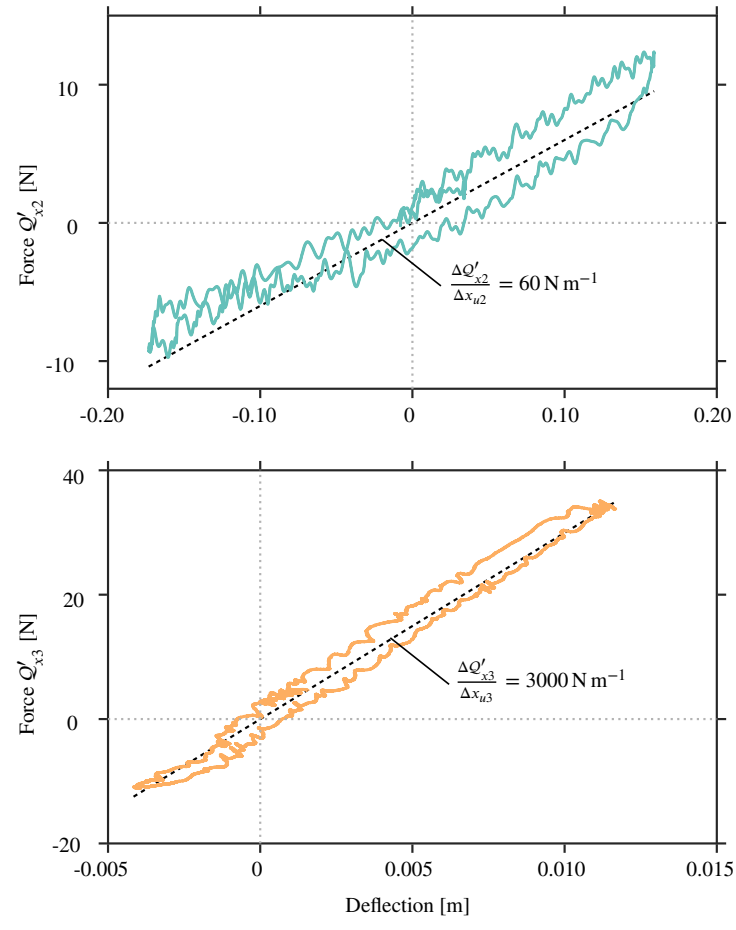

Figure 11.14: Experiment 3, Case 2: The dashed line represents the desired quasi-static behavior. (**top**) Deflection and force in y-direction during. (**bottom**) Deflection and force in y-direction.

that some damping is injected through the presence of the damping terms on the virtual motors ($\xi = 0.05$) resulting in a gradual decay of the motion. The results for the PD controller [183] emphasize the system's intrinsic oscillatory nature and the need for elaborate damping control concepts.

11.3.4 Case 4: Input Saturation

Case 4 analyzes the robustness of the ESPi control with regard to input saturation. The controller gains are given in the Table 11.4 and the results are reported in Fig. 11.16. The experiment shows that a satisfactory link convergence behavior can be achieved in spite of input saturation—highlighting also the robustness of the ESPi controller.

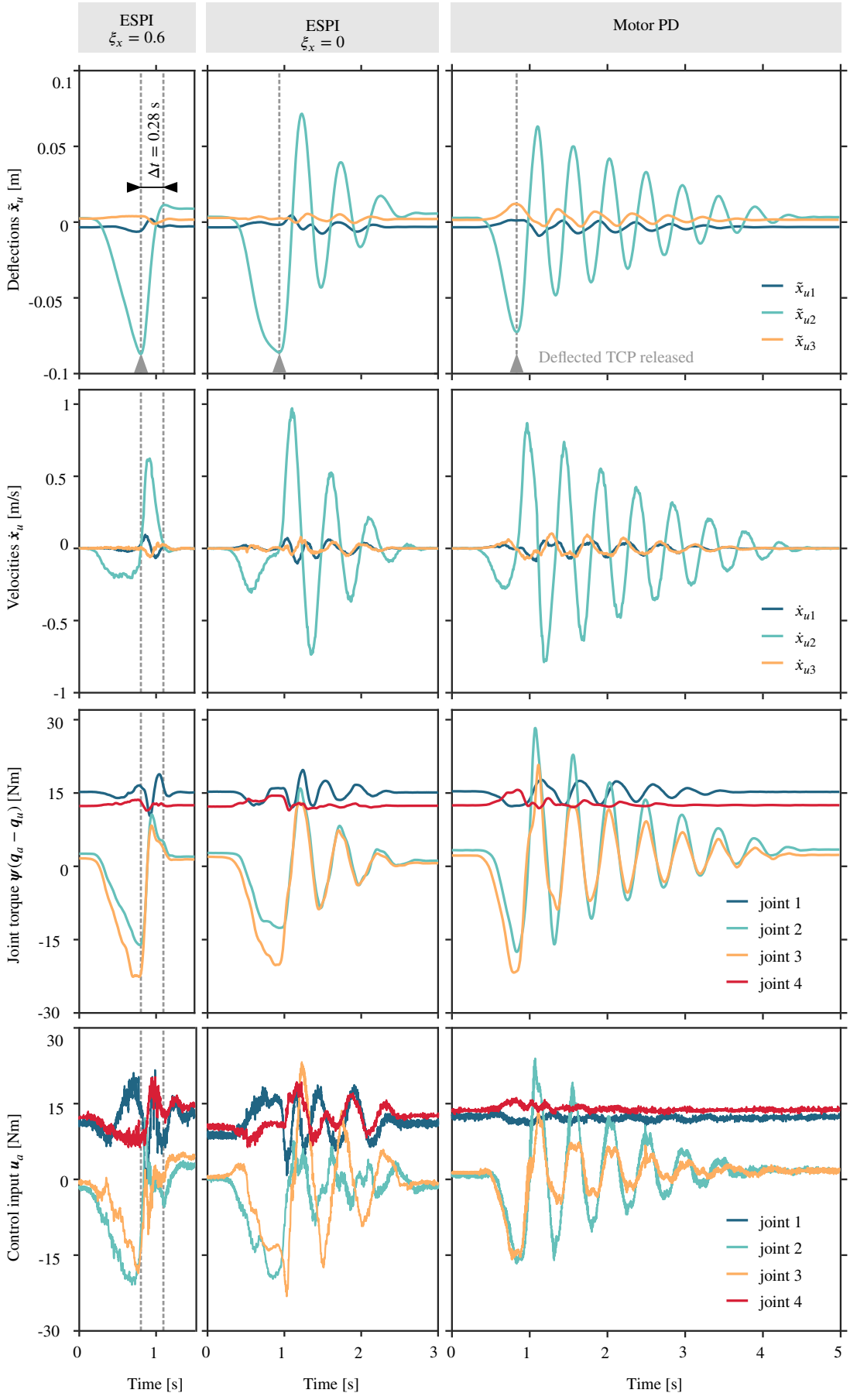

Figure 11.15: Experiment 3, Case 3: The disturbance rejection performance of the ESPi controller for two different modal damping factors is shown. As reference, and in order to show the 'natural' oscillatory behavior of the system, the performance of the well known motor PD controller by Tomei is shown [25].

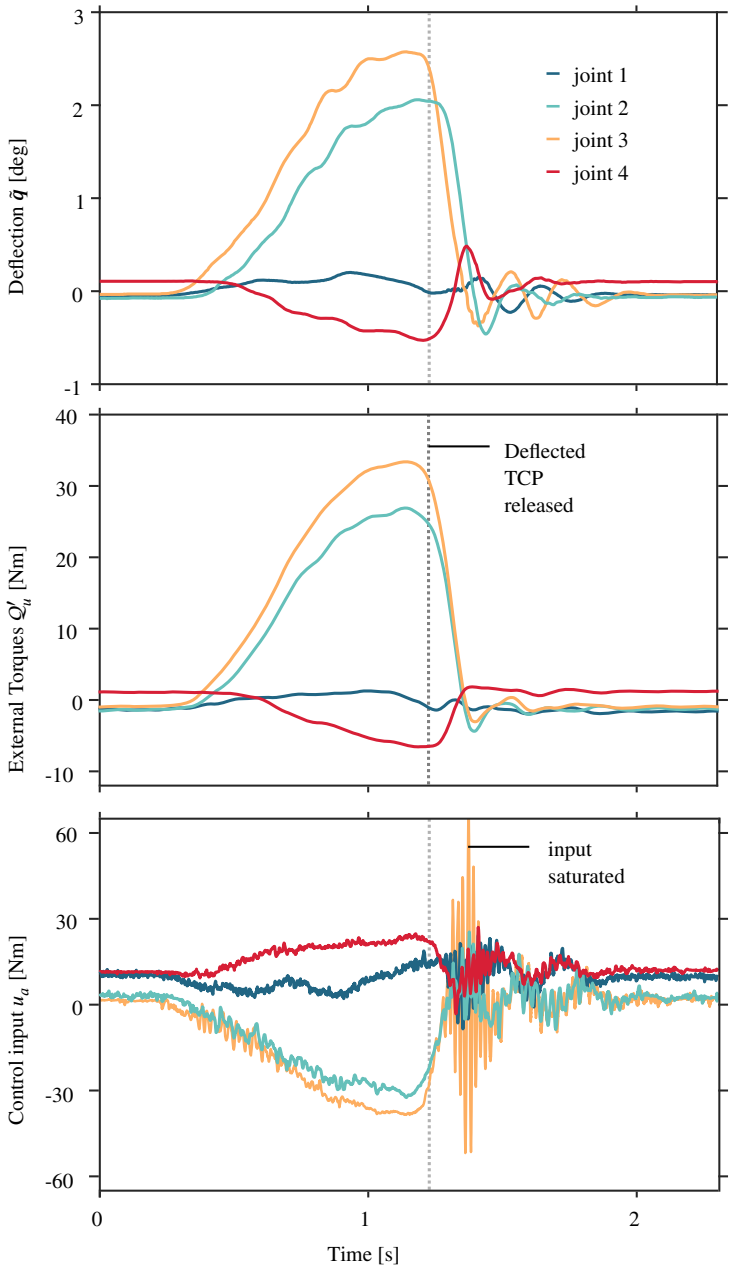

Figure 11.16: Experiment 3, Case 2: The ESPi controller shows satisfactory performance and remains stable even in case of control input saturations.

11.4 Experiment 4: Dynamics Extensions

A dedicated single joint setup has been used to compare the performance of the enhanced damping design Z_{u2} to the "standard" approach Z_{u0}, c.f. Fig. 9.4. For ease of reference, the considered closed-loop dynamics are visualized in Fig. 11.18. Figure 11.17 shows the setup, which consists of a DLR LWR III [66] motor unit in series with a compliant element from DLR C-Runner [106] and a horizontally moving link. The system's dynamics is that of a single elastic joint with a linear spring. To evaluate the closed-loop interaction behavior, the link is equipped with a force sensor (ME KD40s). The link and motor positions are measured with an optical Heidenhain rotary encoder (ECN1023 with 23 bit resolution) and the default LWR III motor sensor. Velocity signals were computed with a standard fourth-order derivative filter with a cut-off frequency of 80 Hz. Link acceleration and jerk signals were computed as discussed in the Appendix. The test bed parameters are summarized in Table 11.6 and the controller parameters are reported in Table 11.8. The virtual motor was interconnected with a damper, $\bar{u}_a = -k_{va}\dot{q}_v$, with $k_{va} = 2\xi_a\sqrt{bk}$. A factor of $\alpha = 1/5$ in Table 11.8 indicates a reduction of the motor inertia to one fifth of its original value. The motor inertia shaping employed is elaborated in [86]. The dynamic extension parameters were computed with the optimization procedure presented in [192].[2] The results obtained, c.f. Table 11.8, minimize the H_∞ norm of the disturbance transfer function U/Q'_u under the following constraint: the manipulator impedance, Q'_u/V, must approximate the reference manipulator impedance defined by the mass-spring-damper system $Z_{\text{ref}} = ms + d_{\text{ref}} + k_{\text{ref}}/s$ with a maximal deviation of ± 6 dB, where m is the link inertia, $d_{\text{ref}} = 2\xi_a\sqrt{bk_{\text{ref}}}$, $k_{\text{ref}} = 200\,\text{N m rad}^{-1}$. The link impedance obtained from this optimization is plotted in Fig. 11.19 and the parameters are reported in Table 11.8. For comparison, Z^*_{u2} with the mass and stiffness ratios $m/m_c = 10$ and $k/k_c = 10$ used by [173] is plotted as well. Clearly, the optimization results deviate from the recommendation $m >> \bar{m}$ and $k >> k_c$ [173]. The reason for this deviation is intuitive, following the arguments from Section 9.5, we know that in order to reduce the control effort the link impedance should fall after $\sqrt{2}\omega_n$. The reason why it does not drop immediately after $\sqrt{2}\omega_n$ is due to the constraint that the resulting closed-loop behavior must approximate the reference manipulator impedance within ± 6 dB.

[66]: Hirzinger et al. (2002), "DLR's torque-controlled light weight robot III-are we reaching the technological limits now?"

[106]: Loeffl et al. (2016), "The DLR C-runner: Concept, design and experiments"

[86]: Keppler et al. (2018), "Elastic structure preserving (ESP) control for compliantly actuated robots"

[192]: Wandinger (2020), "Enhancing classical impedance control concepts while ensuring transferability to flexible joint robots"

2: Please see Section 9.5.2 in Appendix B for additional information.

[173]: Stramigioli (1996), "Creating artificial damping by means of damping injection"

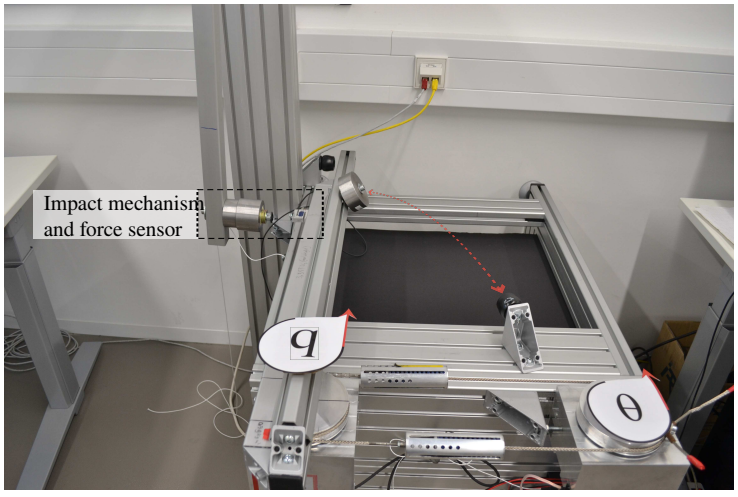

Figure 11.17: Experiment 4. Setup.

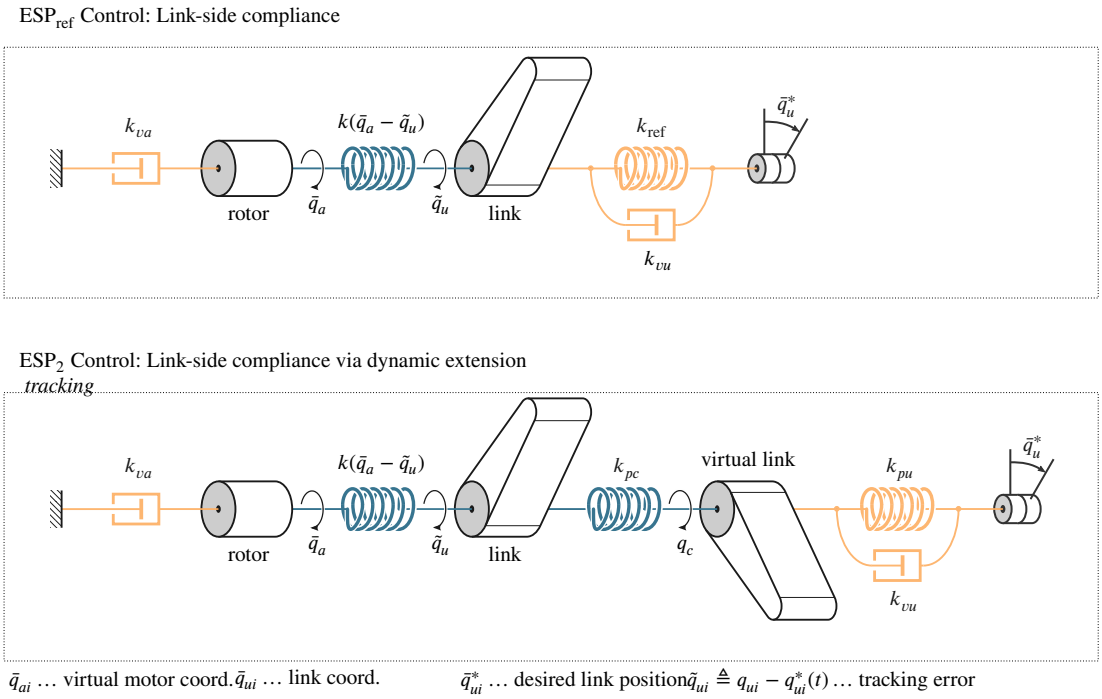

$\bar{q}_{ai}$ … virtual motor coord. $\bar{q}_{ui}$ … link coord. $\bar{q}_{ui}^*$ … desired link position $\tilde{q}_{ui} \triangleq q_{ui} - q_{ui}^*(t)$ … tracking error

Figure 11.18: Considered closed-loop dynamics.

Table 11.6: System and control parameters

System parameters		Force sensor/control parameters	
Link inertia	1 kg m^2	Sensor accuracy	0.1 %
Motor inertia	0.6 kg m^2	Sensor range	±500 N
Joint stiffness	374 N m rad^{-1}	Sensor sample rate	375 Hz
Actuator limits	±100 N m	Controller sample rate	3000 Hz

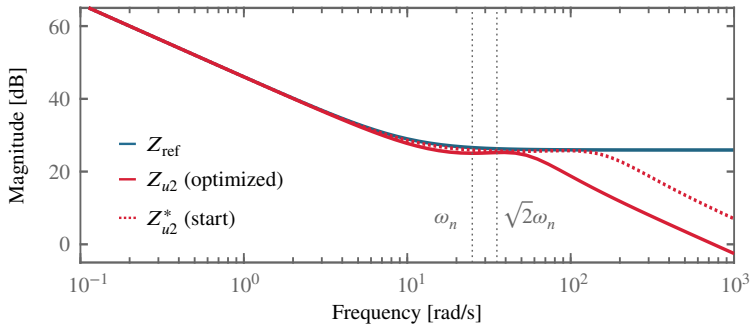

Figure 11.19: Frequency responses of the link-side impedance candidates.

Table 11.7: Experiment 4. Controller configurations

Controller	Link Impedance	Motor Impedance	α	k_{ref}	k_u	k_c	ξ_u	ξ_a	$\bar{m}$
				[N m rad^{-1}]					[kg]
ESP$_{\text{ref}}$	Z_{u0}	Z_v	1	200	-	-	0.7	0.3	-
ESP$_{\text{ref}}^*$	Z_{u0}	Z_v	1/5	200	-	-	0.7	0.3	-
ESP$_2$	Z_{u2}	Z_v	1	-	273	745	0.7	0.3	0.39
ESP$_2^*$	Z_{u2}	Z_v	1/5	-	273	745	0.7	0.3	0.39

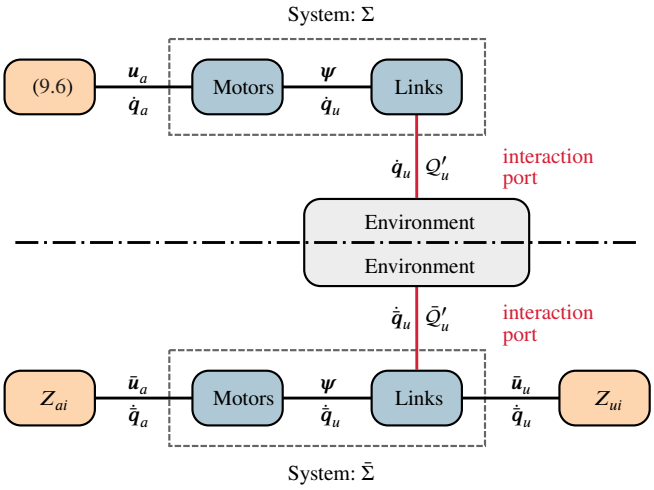

Figure 11.20: The structure of the original and the transformed system. The controller interconnected with the physical system, realizes the interconnected link- and motor-side impedances on the virtual system.

In the following, three types of experiments are presented. The first one is concerned with the identification of the closed-loop manipulator impedance, $\mathcal{Q}'_u/V$, and the control effort transfer functions U/V and $U/\mathcal{Q}'_u$, cf. (9.21). The second one refers to the set-point regulation performance of the control loops. The last one illustrates the performance of the schemes in a basic manipulation task.

Remark 11.4.1 It is worth remarking that motor friction compensation is of particular importance for control designs that shape the intrinsic dynamics to a minimal extend and thus resulting in low gain results. If friction wasn't compensated, then static friction would translate into significant steady-state errors. For this reasons all experiments reported in the following have been performed with motor-side friction compensation.

11.4.1 Case 1: Identification of Interaction Behavior

In this test, a 4 kg impactor generated a impulse-like excitation of the link, which was followed by a frequency analysis to obtain the frequency responses of the manipulator impedance $\mathcal{Q}'_u/V$, and the control efforts U/V and $U/\mathcal{Q}'_u$, see Fig. 11.21 from top to bottom. Clearly, the resulting manipulator impedances for ESP_2 and ESP_2^* satisfy the tuning goal of lying within a ± 6 dB band (green) of the reference impedance Z_{ref} (dashed grey curve). Figure 11.21 further reveals the increase in control effort due to motor inertia shaping.

The effect of the dynamic extension in reducing the control effort in case of high frequency disturbances is clearly visible in the critical frequency range ($\omega > \sqrt{2}\omega_n$). As predicted by the performance analysis in Section 9.4, for controllers with a direct damping injection, $\mathrm{ESP}_{\mathrm{ref}}$ and $\mathrm{ESP}^*_{\mathrm{ref}}$, $|U/V|$ exhibits a slope of 40 dB/dec, whereas for controllers with indirect damping injection, ESP_2 and ESP_2^*, $|U/V|$ exhibits a slope of 20 dB/dec, see Fig. 11.21 (mid). To check whether these results transfer to the case of external forces $\mathcal{Q}'_u$ as disturbance input, we identified the frequency response that relates external forces to the control effort, $U/\mathcal{Q}'_u$, see Fig. 11.21 (bottom). Again, the structural difference between a direct damper and a dynamically decoupled damper implementation is clearly visible past $\omega = \sqrt{2}\omega_n$.

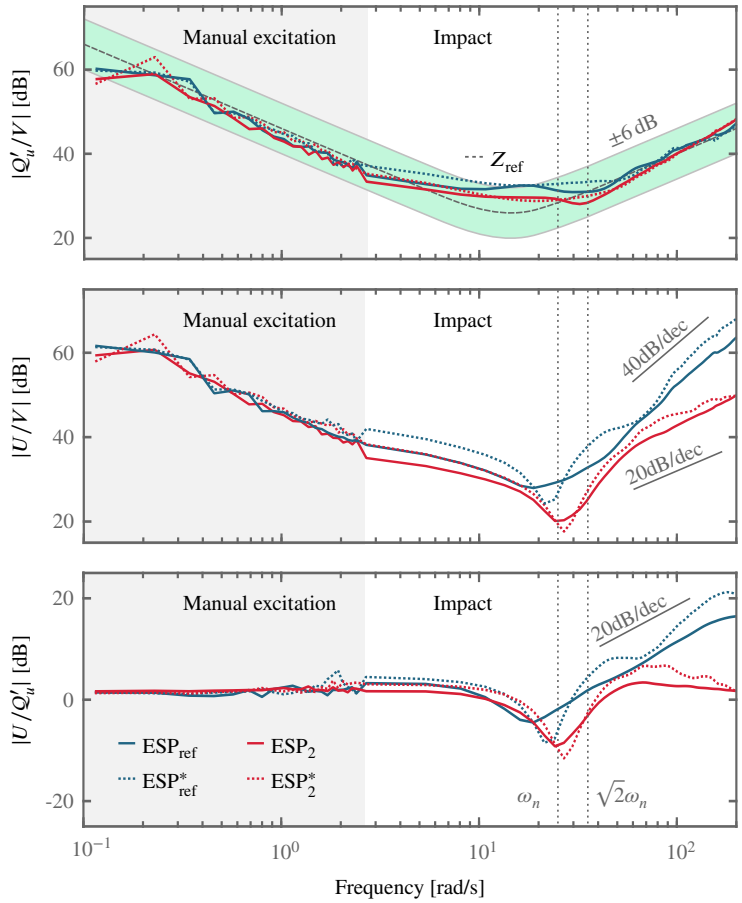

Figure 11.21: Experiment 4, Case 1. From top to bottom: frequency response of the manipulator impedance $\mathcal{Q}'_u/V$, the control efforts U/V and $U/\mathcal{Q}'_u$.

11.4.2 Case 2: Set-Point Regulation

This experiment is concerned with the analysis of the step response behavior and the results are reported in Fig. 11.22. The new controllers were evaluated without (blue curve) and with motor inertia shaping (red curve). To eliminate the (slight) overshooting of ESP_2 and ESP^*_2, we increased the motor damping ratio to $\xi_a = 0.4$ for this experiment. The performance of the motor PD controller demonstrates the necessity for link-side damping for a system with low intrinsic damping. The marginal steady state error is mostly due to Coulomb friction acting on the link and the elastic mechanism. The slight asymmetry of the steady state error suggests a minor sensor calibration inaccuracy and/or some hysteresis effect. The reduction of the motor inertia reduces the overshooting as physical intuition suggests. Even though link kinetic energy is dissipated only indirectly in the dynamic extension case (underdamped closed-loop system), satisfactory point regulation behaviors can be achieved.

11.4.3 Case 3: A Simple Manipulation Task

Figure 11.23 reports an experiment involving the interaction of the link with the environment. The desired motion $q^*_u(t)$ follows a sinusoidal trajectory, leading to an unplanned contact with an obstacle. To analyze the worst case contact impact scenario, the link was commanded to impact with a rigid obstacle (end stop). Thus, both impact partners had negligible intrinsic damping properties. The course of the real link position indicates that a transition from a free-space

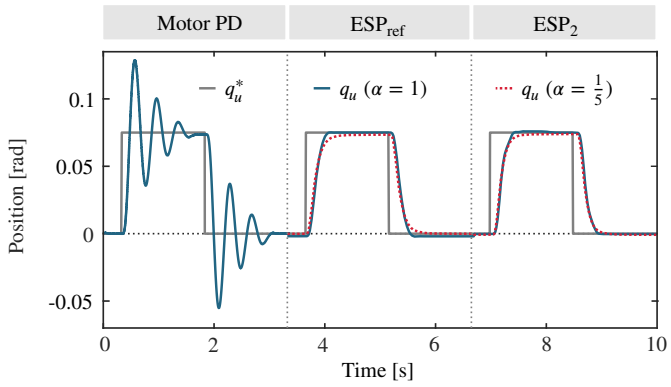

Figure 11.22: Experiment 4, Case 2. Set-point regulation behavior.

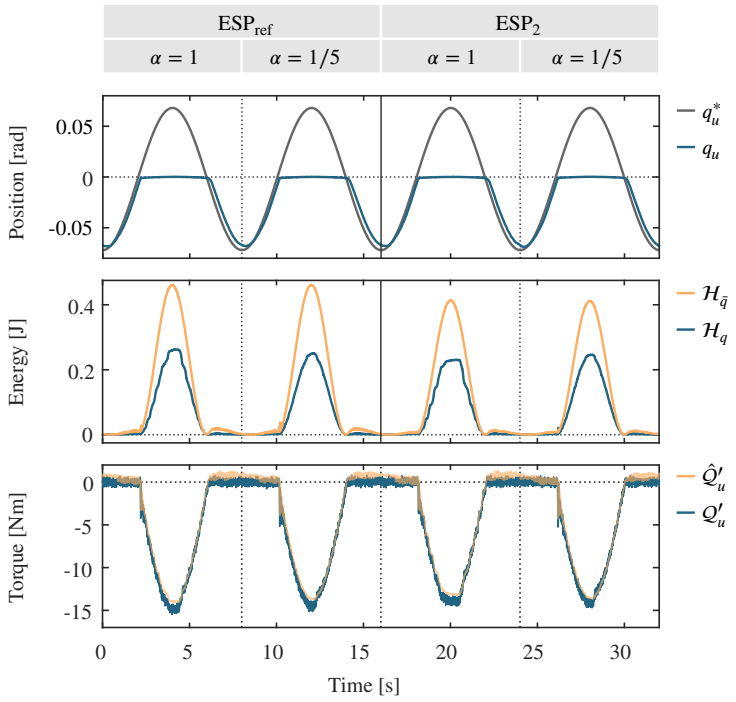

Figure 11.23: Experiment 4, Case 3. (**top**) desired and real position of the link. (**mid**) real total energy and virtual closed-loop energy. (**bottom**) measured and estimated external torques $\mathcal{Q}'_u$ and $\hat{\mathcal{Q}}_u$, respectively.

motion to a contact does not cause any stability issue. The energy is properly dissipated and the system is stable in free motion and passive during the entire motion. The total energy of the physical and the virtual (closed-loop) system is reported in Fig. 11.23, cf. $\mathcal{H}_q$ and $\mathcal{H}_{\bar{q}}$. In the latter case, the total energy can be considered as a storage function for the respective closed-loop system and was obtained by summing up all kinetic and potential energies of the virtual system.

Remark 11.4.2 In general, no force sensors are implemented in ASRs and in order to reflect a realistic scenario, we used a momentum based observer [34] instead to estimate the external force to compute link acceleration and jerk signals, via (B.10) and (B.11) for Case 3. The sensor was only used to report the interaction force.

[34]: De Luca et al. (2006), "Collision detection and safe reaction with the DLR-III lightweight manipulator arm"

Table 11.8: Experiment 5. Controller configurations

Controller	Link Impedance	Motor Impedance	α	k_{ref}	k_u	k_c [N m rad^{-1}]	ξ_u	ξ_a	$\bar{m}$ [kg]
ESP_{ref}	Z_{u0}	Z_v	1	200	-	-	0.7	0.3	-
ESP_{ref}	Z_{u0}	Z_v	1/5	200	-	-	0.7	0.3	-
ESP_2	Z_{u2}	Z_v	1	-	273	745	0.7	0.3	0.39
ESP_2	Z_{u2}	Z_v	1/5	-	273	745	0.7	0.3	0.39

Table 11.9: Experiment 5. Observer parameters

Observer	Gain [Hz]	S_1 [Hz^2]	S_2 [Hz^2]	T_1 [Hz]	T_2 [Hz]
Momentum observer: friction	150	-	-	-	-
Momentum observer: input	1000	-	-	-	-
Sliding mode observer: input	-	100	1000	16	2000

11.5 Experiment 5: A Momentum-based Input Observer

Based on the theoretical results reported in Section A, we compare three different implementations of the input transforming equations (A.14):

- Direct implementation of the control input u_{ai} via (A.2).
- Estimating u_{ai} through a momentum observer [34].
- Estimating u_{ai} through a sliding mode observer [48].

[34]: De Luca et al. (2006), "Collision detection and safe reaction with the DLR-III lightweight manipulator arm"

[48]: Garofalo et al. (2019), "Sliding mode momentum observers for estimation of external torques and joint acceleration"

The dedicated single joint setup introduced in Section 11.4 has been used to compare the performance of the ESP_{ref} and ESP_2 closed-loop dynamics, see also Fig. 11.18. These controllers are implemented through the different input transformation implementations above. The employed testbed is shown in Fig. 11.2 and its parameters are summarized in Table 11.6. The gains for the controllers, friction and input observers are summarized in Table 11.8 and Table 11.9, respectively.

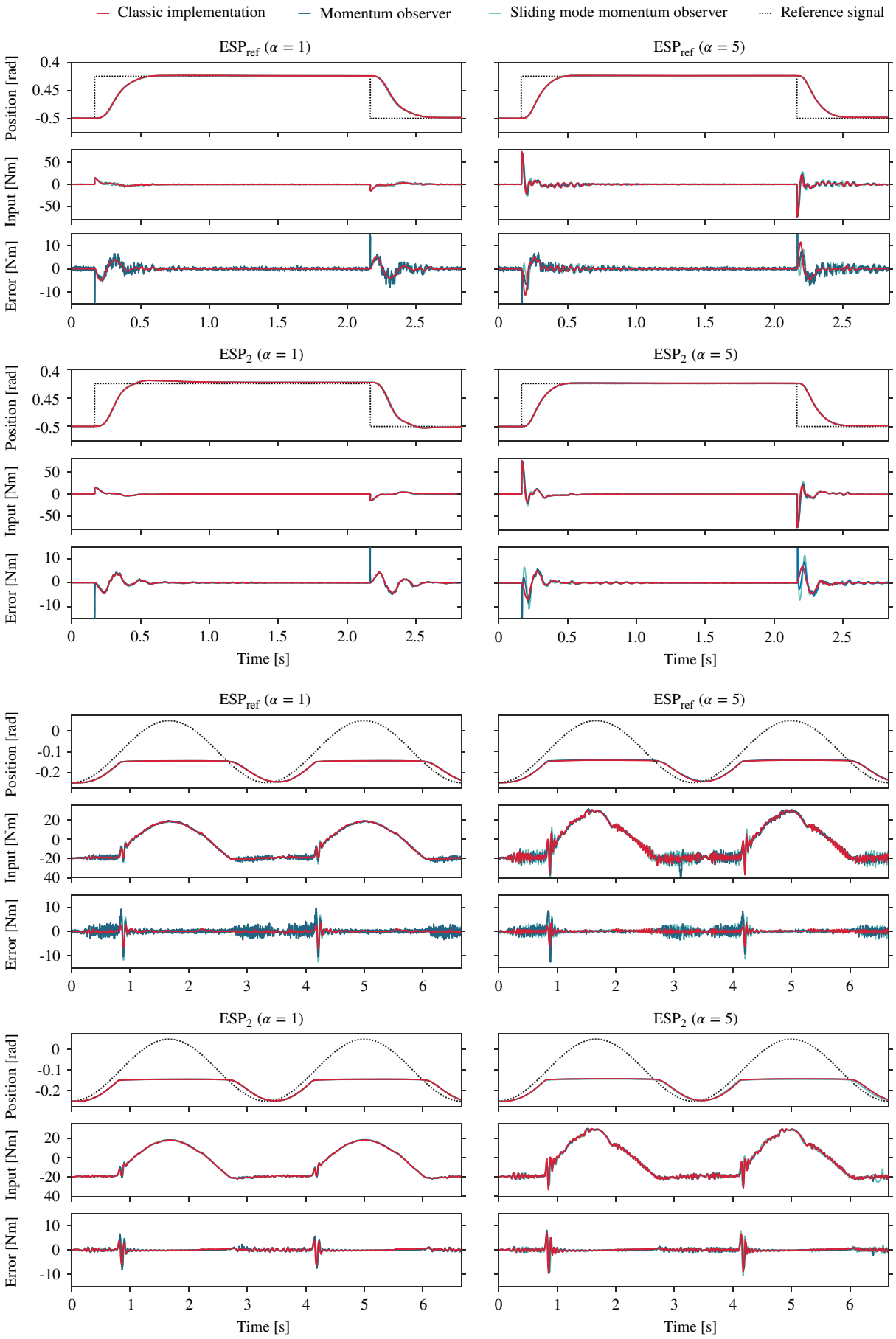

Figure 11.24: Experiment 5. Direct implementation of the input transformation versus an observer-based estimation of the control input.

11.6 Actual versus Nominal Behavior

Deviations from the nominal closed-loop behavior commonly result from model errors, sensor inaccuracies, joint torque errors, uncompensated link-side and motor-side friction, inaccuracies in the estimation of the external disturbances, round-trip delay in the feedback loop etc.

- *Model* errors: the plant model used for the control design is always just an approximation of the actual physical system with varying degrees of accuracy. Concerning the employed Spong model the following prominent effects are neglected: 1) non-modeled dynamics such as structural elasticities of the links, sensor mountings, gears, 2) parameter inaccuracies, 3) round-trip delay in the feedback loop.
- *Feedforward terms*: Parameter uncertainties regarding the mass (Coriolis/centrifugal matrices) play a role for trajectories with high link-side accelerations (velocities).
- *Friction*: Static friction affects the steady-state positioning accuracy, dynamic (viscous) friction deteriorates the tracking performance during high-velocity motions.
- *External force estimation*: Estimation errors cause inaccuracies in the computation of the link acceleration and jerk signals, as pointed out in Section B.2. It is worth noting that this issue is completely resolved for the control design proposed in Chapter A.
- *Motor inertia shaping*: It is easy to see that motor inertia scaling also scales—by the same factor—disturbance forces acting on the motor dynamics. However, there is a downside with motor inertia shaping. As pointed out later in Section 11.9, inaccuracies in the joint torque measurements/estimations cause steady-state errors.

11.7 Simulation 1: Adoption of Rigid Robot Controllers

This section reports simulation results verifying the stability and performance characteristics of two passivity-based rigid robot controllers adapted through the QFA formulation: 1) Slotine & Li controller[165], 2) PD+ control [98, 144]. The considered control laws are (7.145)–(7.146) and (7.158) with the input transformation (7.34) in Section 7.2.5. We consider a 2R manipulator composed of two identical links that is carrying a load, as indicated in Fig. 11.25 (left). At each joint, a series elastic actuator (SEA) is mounted with a torque characteristics modeled by a third-order polynomial

$$\psi_i(\varphi) \triangleq a_{i,1}\varphi + a_{i,2}\varphi^3, \tag{11.1}$$

with coefficients $a_{i,1} = 200\ \mathrm{N\,rad^{-1}}$, $a_{i,2} = 2000\ \mathrm{N\,rad^{-3}}$. The parameters are chosen such that the resulting torque characteristics resemble roughly the one of the floating spring joint (FSJ) featured in the DLR Hand Arm System introduced in [54]. The mechanical properties of the robot are summarized in Table 11.10. The motor inertia of each SEA is denoted by b. At each link of length l a mass m is located at the center. In addition, an external load of mass m_{load} is located at the tip (TCP) of the distal link. A maximal motor torque of $u_i \leq 60\ \mathrm{N\,m}$ was assumed for each SEA, which is approximately three times

[165]: Slotine et al. (1988), “Adaptive manipulator control: A case study”

[98]: Koditschek (1984), “Natural motion for robot arms”

[144]: Paden et al. (1988), “Globally asymptotically stable "PD+" controller for robot manipulators”

[54]: Grebenstein et al. (2011), “The DLR hand arm system”

m [kg]	m_{load} [kg]	b [kg m^{-2}]	l [m]
1	1	0.2	0.5

Table 11.10: Parameters of the considered compliant planar two-link robot.

	Link-side gains	Motor-side gains
PD+	$\boldsymbol{K}_{pu} = \text{diag}(500, 500)$ $\boldsymbol{K}_{vu} = \text{diag}(47.5, 37.5)$	- $\boldsymbol{K}_{va} = \text{diag}(5, 5)$
Slotine & Li	$\boldsymbol{\Lambda}_u = \text{diag}(15, 15)$ $\boldsymbol{K}_{vu} = \text{diag}(15, 15)$	$\boldsymbol{\Lambda}_a = \text{diag}(10, 10)$ $\boldsymbol{K}_{va} = \text{diag}(10, 10)$

Table 11.11: Control parameters.

the maximum torque required for the nominal motion. The manually tuned controller gains are summarized in Table 11.11. In order to make the results comparable, a maximal motor torque $u_{ai} \leq 60$ Nm was assumed.

The robot's TCP is required to move back and forth along a straight trajectory starting at $(x, y) = (0, 0.3)$ m and ending at $(x, y) = (0.2, 0.7)$ m with a frequency of one cycle per second. The parameterization of the desired trajectory $\boldsymbol{x}_d$ is

$$x_i^* = A_i \sin\left(\omega t + p_i\right) + c_i, \tag{11.2}$$

with $\omega = 2\pi$ rad s^{-1}, $A_1 = 0.1$ m, $A_2 = 0.2$ m, $p_1 = p_2 = 3\pi/2$, $c_1 = 0.1$ m and $c_2 = 0.5$ m. Two cases are considered:

Case 1: For evaluating the nominal performance it is assumed that all model parameters are exactly known.

Case 2: For analyzing the robustness against parameter uncertainties a Monte-Carlo analysis is performed.

For the subsequent simulations it is assumed that all required position and velocity measurements are available. Notice that despite "perfect" position and velocity signals the computations of the link acceleration and jerk signals are deteriorated in Case 2 due to parameter uncertainties.

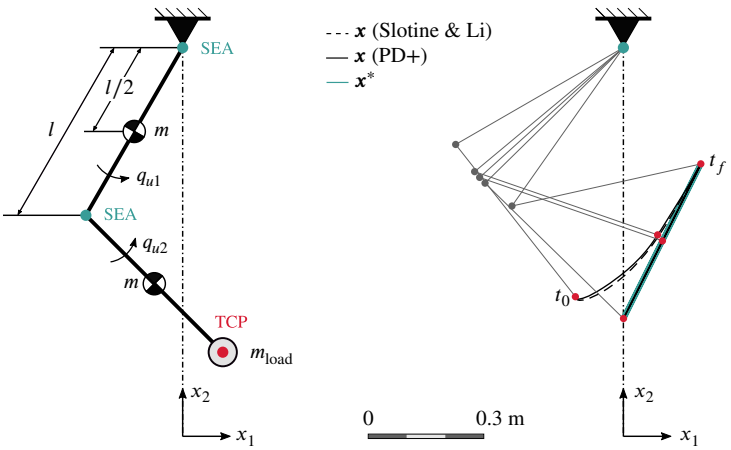

Figure 11.25: (**left**) Robot model considered for simulation. A compliant two-link planar robot with nonlinear joint springs carrying a load. (**right**) The desired trajectory (blue), and the actual TCP trajectories for PD+ (solid) and Slotine & Li (dashed) controllers are shown. Starting with the initial configuration, the robot poses are shown in 0.25 s intervals (PD+).

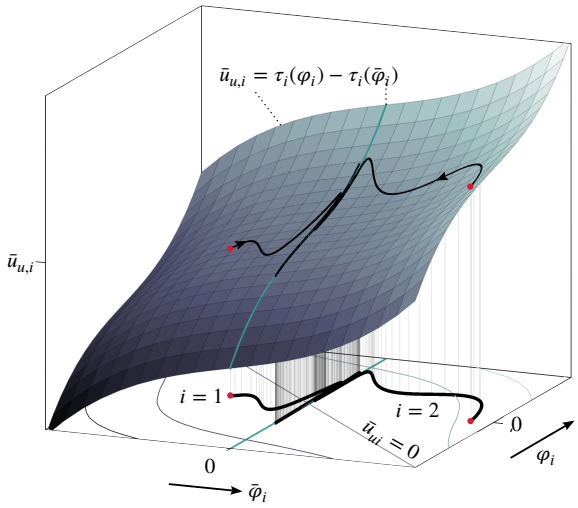

Figure 11.26: Each of the transforming equations (7.25) defines a hypersurface whose shape is uniquely determined by the joint torque functions τ_i. Its contour lines are projected on the bottom. In contrast to joints with linear springs, these are no longer straight lines, cf. Fig. 4.11. In order to draw the time trajectories of two configuration points on one hypersurface, we assumed w.l.o.g that $\psi_1 = \psi_2$, c.f. (11.1). The trajectories shown are exemplary motions of a two-link planar manipulator under adopted PD+ control, see Chapter 7.

11.7.1 Case 1: Nominal Performance

At each run the robot is initialized (at time $t = t_0$) with the configuration $(q_{u1}, q_{u2}) = (q_{a1}, q_{a2}) = (-\pi/3, 6\pi/11)$ rad. Fig. 11.27 summarizes the simulation results for the PD+ (Slotine & Li) controller plotted in solid (dashed) lines. Fig. 11.27 (e) shows the evolution of the actual and virtual joint deflections on the hyperplane denoted by (7.25), where the contour lines $\bar{u}_{ui} = const.$ are projected projected into the $(\varphi_i, \bar{\varphi}_i)$-plane, c.f. Fig. 11.26. Notice that the robot system is initialized with zero joint deflections ($\boldsymbol{\varphi} = \mathbf{0}$) and thus zero elastic torques ($\boldsymbol{\psi} = \mathbf{0}$), which is no static equilibrium state since gravity is not compensated by the elastic elements. The initial states are marked with an "x". Interestingly, since the PD+ and Slotine & Li controller initiate with different input values $\bar{\boldsymbol{u}}_u$, we have differing initial deflection errors $\tilde{\boldsymbol{\varphi}}$.

Notice from Fig. 11.27 (d) that the PD+ and Slotine & Li controllers initiate with differing virtual input values $\bar{u}_{ui}$, and thus differing initial deflection errors $\tilde{\boldsymbol{\varphi}}$ which implies that the virtual subsystems $\bar{\Sigma}_a$ also initiate at different locations. As anticipated from our stability analysis the subset $\left\{\bar{\varphi}_i \in \mathbb{R} \mid \bar{\varphi}_i = 0\right\}$ is attractive. As such, for $t \to \infty$, the point defined by the triplet $(\varphi_i, \bar{\varphi}_i, \bar{u}_i)$ slides along a one-dimensional submanifold on the hyperplane defined by (7.25). We observe that the Slotine & Li controller starts with slightly lower deflection errors and shows a smoother convergence behavior. This is a general trend we observed in simulations. Fig. 11.27 (a-d) shows the tracking errors and control input as well as the system energies for the two controllers. As anticipated from Proposition 7.2.4 and 7.2.5, the control errors converge to zero, see Fig. 11.27 (a).

Both controllers inject similar levels of energy into the system and show comparable convergence rates. The total physical energy of the robot is denoted by $\mathcal{H}_{phy}$, see Fig. 11.27 (b). The closed-loop storage functions (7.147) and (7.154) are denoted by $\mathcal{H}_{\text{pd+}}$ and $\mathcal{H}_s$, respectively. Interestingly, albeit the control input $\boldsymbol{u}_a$ varying similarly with time, the (virtual) inputs $\bar{\boldsymbol{u}}_u$ and $\bar{\boldsymbol{u}}_a$ to the quasi-fully actuated systems show quite a different behavior during convergence, cf. Fig. 11.27 (c) and Fig. 11.27 (d).

11.7.2 Case 2: Monte-Carlo Analysis

In order to analyze the robustness of the adopted controllers against model parameter uncertainties, we performed a Monte Carlo simulation. The load mass m_{load}, the motor inertia values, and the torque profile parameters $\alpha_{i,1}$ and $\alpha_{i,2}$ of the robot were randomly sampled in an interval of $\pm 20\%$ around the nominal values given above. We repeated the random sampling 100 times and analyzed the control performance of the PD+ and Slotine & Li controllers each time. The robot was commanded to follow the same desired trajectory as above, see (11.2), and starts from the same initial configuration. All results are combined in Fig. 11.27 (f-g) showing: (f) the tracking performance, and (g) the control inputs. The Slotine & Li controllers appears to have a slightly better tracking performance. However, on average, both controllers result in a root mean square error for $\tilde{\boldsymbol{x}}$ of 0.03 m. In both cases, the control input magnitudes deviate only slightly from the nominal ones.

11.7.3 Discussion

It is very difficult to derive a definite conclusion about performance differences of different controllers. The original rigid robot controllers are both passivity-based designs and derived from fundamental energy-based considerations, yielding designs with enhanced robustness properties that do not need cancellation of nonlinearities [98, 164]. The simulation results demonstrate that rigid robot controllers that are expected to show a similar performance on rigid robots also show a similar performance when adopted through the QFA formulation. From the practical point of view, it seems worth mentioning that the PD+ controller allows for non-diagonal gain matrices, and thus, permitting modal decomposition based damping designs that adapt the gain layout online to the varying robot inertia and joint stiffnesses, see [86] for details. In both cases, no lower or upper bounds on the controller gains are imposed. In particular, the link-side stiffness that characterizes the interaction of the robot with environment can be increased above the intrinsic stiffness of the robot.

[98]: Koditschek (1984), "Natural motion for robot arms"
[164]: Slotine (1988), "Putting physics in control-the example of robotics"

[86]: Keppler et al. (2018), "Elastic structure preserving (ESP) control for compliantly actuated robots"

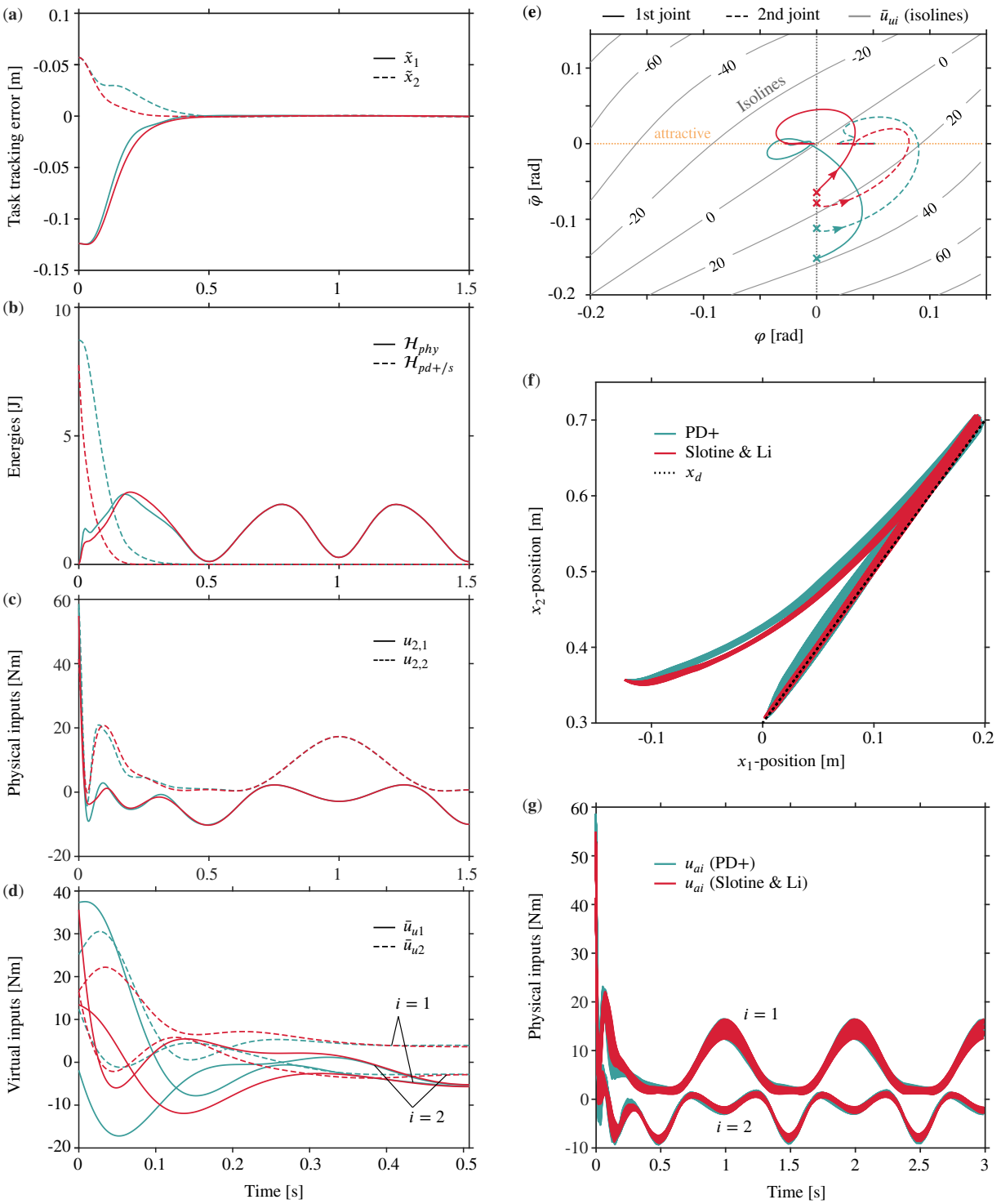

Figure 11.27: Simulation 1. (**a-d**) Adopted PD+ (blue lines) and Slotine & Li (red lines) control. (**a**) TCP tracking error (cf. Fig. 11.25 (right)). (**b**) Physical energies $\mathcal{H}_{phy}$ and storage functions (7.147) and (7.154), respectively, (**c**). Control inputs acting on the actual robot. (**d**) Inputs acting on the quasi-fully actuated system (note the scaling of the time axis for better readability), cf. Fig. 7.4 (right) for input definitions. (**e**) Actual and virtual joint deflections for PD+ (solid) and Slotine & Li (dashed) controllers. The contour lines of the link-side input $\bar{u}_{1,i}$ as a function of the joint deflections φ_i and $\bar{\varphi}_i$, defined via the state transformation (7.25), are shown in black. (**f-g**) Monte Carlo simulation: (**f**) tracking performance, (**g**) control inputs.

11.8 Simulation 2: ESP Control vs. Feedback Linearization

This section reports a gain analysis comparing ESP control in full state feedback (FSF) form with feedback-linearization-based FSF control. This analysis considers DLR *David* as an exemplary system. Its inertia is highly configuration dependent and varies significantly throughout its workspace. Let us consider the first five joints of the right arm. The first joint faces an inertia, $\boldsymbol{M}$, that depends on the configuration of the distal joints as visualized in Fig. 11.29, and ranges from $m_{min} = 0.01\ \mathrm{kg\,m^2}$ (left pose) to $m_{max} = 1.1\ \mathrm{kg\,m^2}$ (right pose).

Similarly, depending on the stiffness setting σ and the external load, the stiffness k of the first joint (cf. Fig. 11.29) varies between $k_{min} = 40\ \mathrm{Nm\,rad^{-1}}$ and $k_{max} = 900\ \mathrm{Nm\,rad^{-1}}$. The subsequent analysis considers a single robotic joint as shown in Fig. 11.28. The corresponding model is given by (4.10)

$$m\ddot{q}_u + k(q_u - q_a) = 0, \tag{11.3}$$
$$b\ddot{q}_a + k(q_a - q_a) = u. \tag{11.4}$$

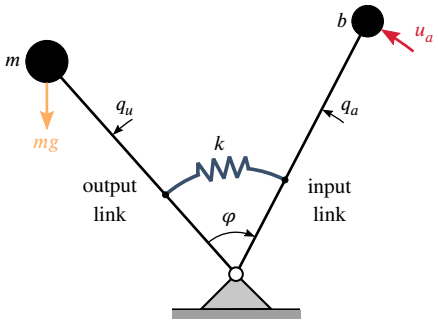

Figure 11.28: An elastic joint with control input u_a.

Suppose that the link inertia and joint stiffness can take a range of values: $m \in [m_{min}, m_{max}]$ and $k \in [k_{min}, k_{max}]$, as it would be the case for the first axis of DLR *David*. As discussed in Section 4.1, the coordinate and input transformations (4.14) and (4.17) allow rewriting the considered model, (4.10), in its QFA representation and are repeated below for convenience

$$q_a = \bar{q}_a + k^{-1}\bar{u}_u, \tag{11.5}$$
$$u_a = bk^{-1}\ddot{\bar{u}}_u + \bar{u}_u + \bar{u}_a. \tag{11.6}$$

For the gravity-free regulation case, we can write the ESP controller [86]

$$\bar{u}_u = -k_{vu}\dot{q}_u, \quad \bar{u}_a = -k_{va}\dot{\bar{q}}_a - k_{pa}\bar{q}_a \tag{11.7}$$

in full state feedback (FSF) form with state vector $\boldsymbol{x} = [q_u\ \dot{q}_u\ \ddot{q}_u\ q_u^{(3)}]$. Considering that we can use the link dynamics (11.3) to express q_a in terms of q_u and $\ddot{q}_u$, we can substitute the resulting relation in (11.5) to obtain $\bar{q}_a$ in terms of only q_u and its time-derivatives

$$\bar{q}_a = k^{-1}m\ddot{q}_u + k^{-1}k_{vu}\dot{q}_u + q_u. \tag{11.8}$$

[86]: Keppler et al. (2018), "Elastic structure preserving (ESP) control for compliantly actuated robots"

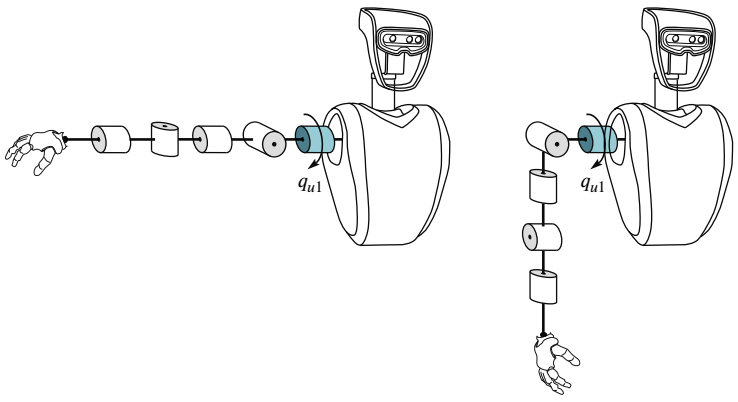

Figure 11.29: The minimum and maximum inertia configurations with respect to the first joint of the DLR Hand Arm System are shown.

Making the substitution (11.6), (11.7) and (11.8) gives the ESP controller in full state feedback form. Without loss of generality, let us assume that $\bar{q}_a^* = q_u^* = 0$, and choose the damping coefficients as: $D = 2\xi_u\sqrt{mk}$, and $k_{va} = 2\xi_a\sqrt{bk_{pa}}$, with $\xi_u = \xi_a = 0.7$, resulting in the FSF ESP controller

$$u_a = -\boldsymbol{k}^d \boldsymbol{x}, \tag{11.9}$$

where $\boldsymbol{k}_d$ is the gain matrix with the following components

$$k_1^d = k_{pa}, \tag{11.10}$$

$$k_2^d = 2\xi_u\sqrt{mk}\left(1 + \frac{k_{pa}}{k}\right) + 2\xi_a\sqrt{bk}, \tag{11.11}$$

$$k_3^d = 4\frac{\xi_a\xi_u}{k}\sqrt{mk}\sqrt{bk_{pa}} + \frac{k_{pa}}{k}m, \tag{11.12}$$

$$k_4^d = 2\xi_u\frac{b}{k}\sqrt{mk} + 2\frac{m}{k}\xi_a\sqrt{bk_{pa}}. \tag{11.13}$$

Let us now derive a feedback-linearization-based FSF controller for the elastic joint. Solving the motor dynamics (11.4) with respect to $\ddot{\theta}$ and substituting it in the second time derivative of the link dynamics (11.3), we can re-write system (11.4)–(11.3) as a 4th order system

$$q_u^{(4)} = \frac{k}{bm}u_a - k\left(\frac{1}{b} + \frac{1}{m}\right)\ddot{q}_u. \tag{11.14}$$

In order to input-state linearize the system, let us choose the control input[3]

$$u^f = \frac{bm}{k}v + (b+m)\ddot{q}, \tag{11.15}$$

such that making the substitution u^f and u_a results in the linear controllability canonical form

$$\dot{\boldsymbol{x}} = \begin{bmatrix} \boldsymbol{0}_{3\times1} & \boldsymbol{I}_{3\times3} \\ 0 & \boldsymbol{0}_{1\times3} \end{bmatrix}\boldsymbol{x} + \begin{bmatrix} \boldsymbol{0}_{3\times1} \\ 1 \end{bmatrix} v, \tag{11.16}$$

where $\boldsymbol{x}$ denotes the new state vector and v the new control input. Choosing full state feedback control

$$v = -\boldsymbol{k}\boldsymbol{x}, \tag{11.17}$$

with $\boldsymbol{k} = [\, k_1\ k_2\ k_3\ k_4\,]$, and making the substitution (11.17) and (11.15) gives the final controller

$$u_f = -\boldsymbol{k}^f\boldsymbol{x} = -\frac{bm}{k}\begin{bmatrix} k_1 & k_2 & k_3 - \frac{k}{bm}(b+m) & k_4 \end{bmatrix}\boldsymbol{x}, \tag{11.18}$$

with $\boldsymbol{k}^f = [\, k_1^f\ k_2^f\ k_3^f\ k_4^f\,]$. Now let us choose $k_1, \ldots, k_4$ such that $k_i^d = k_i^f$ for the case that the link inertia and joint stiffness assume the reference values: $m_{ref} = 0.1\,\mathrm{kg\,m^2}$ and $k_{ref} = 200\,\mathrm{Nm/rad}$, that is $k_1 = k_{pa}k_{ref}/(b\,m_{ref})$ etc. The reference values are chosen such that they are located magnitude-wise in the center of their respective range. Consequently, for the reference case $m = m_{ref}$ and $k = k_{ref}$, both controllers are identical, and thus achieve the same closed-loop behavior. Starting from this reference point we are now interested in how the gains $\boldsymbol{k}^d$ and $\boldsymbol{k}^f$ change if the link inertia and joint stiffness deviate from their respective reference values. Figure 11.30 shows the results of this analysis. The white spheres mark the reference cases, where

3: To assure controllability, we must have that $k > 0$ and $bm < \infty$.

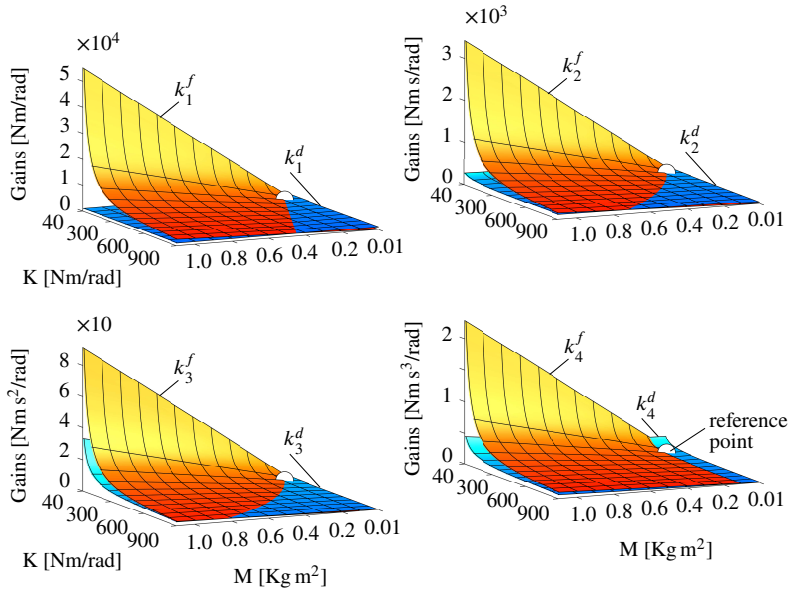

Figure 11.30: Simulation 2. The gains $\boldsymbol{k}^d$ and $\boldsymbol{k}^f$ as a function of the link inertia m and joint stiffness k. The feedback linearization gains $\boldsymbol{k}^f$ vary significantly stronger with changing inertia and stiffness values compared to the ESP gains $\boldsymbol{k}^d$. Reprinted from [86].

m and k assume their reference values and $\boldsymbol{k}^d$ and $\boldsymbol{k}^f$ coincide. Clearly, the elements of $\boldsymbol{k}^f$ vary significantly stronger than those of $\boldsymbol{k}^d$. This has several theoretical and practical implications. Compared to feedback linearization, ESP control is less susceptible to input saturation and shows less sensor noise amplification. Moreover, from experience we know that gains on q_u and $\dot{q}_u$ as high as 5×10^4 N m/rad and 3×10^3 N m/rad, respectively, are not realizable on the Hand Arm System. It is also clear that uncertainties in k and m have a much larger impact on the gains for feedback linearization than for ESP control. These findings allow the conclusion that ESP control shapes the plant dynamics significantly less than feedback linearization.

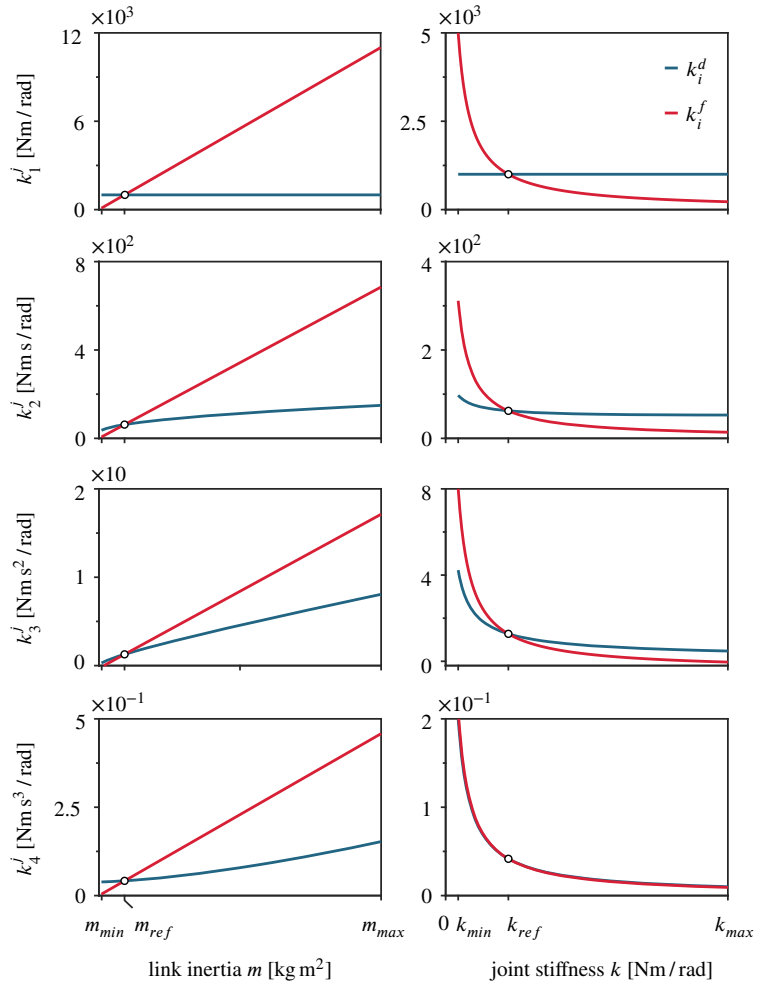

Figure 11.31: Simulation 2. The gains $\boldsymbol{k}^d$ and $\boldsymbol{k}^f$ as a function of the link inertia m and joint stiffness k, respectively. The plots show planar, vertical cuts of Fig. 11.30 that run parallel to the m and k axis, respectively, and intersect the reference point. Reprinted from [86].

11.9 Simulation 3: Steady-State Error Analysis

[154]: Ray et al. (1993), "A Monte Carlo approach to the analysis of control system robustness"

[91]: Keppler et al. (2021), "Analyzing the performance limits of articulated soft robots based on the ESPi framework: Applications to damping and impedance control"

[154]: Ray et al. (1993), "A Monte Carlo approach to the analysis of control system robustness"

This section reports a Monte Carlo simulation [154] to evaluate the robustness of the control designs reported in Chapter 9 with respect to parameter uncertainties and analyzes the resulting stead-state errors. The results have been first published in [91]. We simulated a single joint with the same parameters reported in Table 11.6 and considered the same scenario as reported in Case 2 of Experiment 5, with the addition of a step-like force disturbance of -11 N m at $t = 2$ s. A uniform probability density function models the parameter uncertainties, with variations between $\pm 5\%$ of the nominal values for the link and motor inertias, m and b, and $\pm 10\%$ for the joint stiffness k, which is a very pessimistic uncertainty set, c.f. [154]. The control parameters were set as reported in Table 11.8 (Chapter 9), with only ξ_q changed to 1 since the lack of link-side friction in the simulation necessitates a higher damping ratio to avoid overshooting. The result of 500 runs is plotted in Fig. 11.32. Analyzing the equilibrium conditions for the nominal case, we have that $\bar{q}_u - \bar{q}_u^* = Q_u / k_r$,

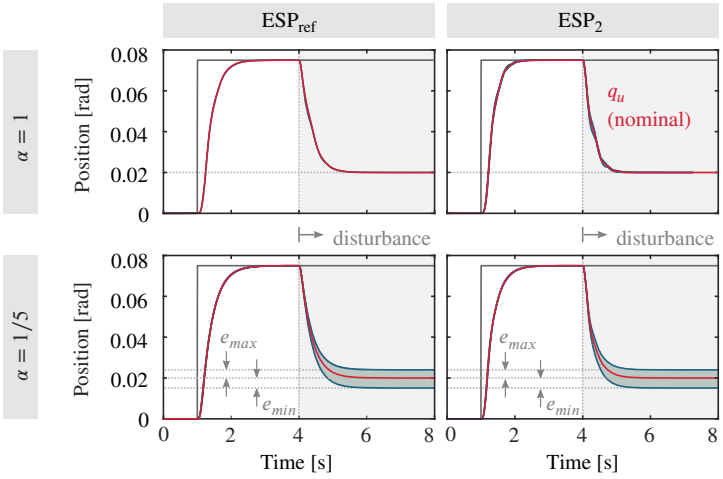

Figure 11.32: Simulation 3. Monte Carlo simulation: step-response and disturbance rejection. Reprinted from [91]

where k_r is the resultant closed-loop stiffness, i.e.

$$k_r = \begin{cases} k_{\text{ref}} & \text{for ESP}_{\text{ref}} \\ \left(\frac{1}{k_u} + \frac{1}{k_c}\right)^{-1} & \text{for ESP}_{1\text{–}2} \\ k_u & \text{for ESP}_{3\text{–}4} \end{cases} \tag{11.19}$$

k_{ref} for ESP_{ref}, $\left(\frac{1}{k_u} + \frac{1}{k_c}\right)^{-1}$ for $\text{ESP}_{1\text{–}2}$, and k_u for $\text{ESP}_{3\text{–}4}$. Let us assume the model parameters are not known exactly, and let $\hat{m}, \hat{b}$ and $\hat{k}$ be the estimates of m, b and k used for the controller implementation. Introducing $\beta \triangleq \hat{k}/k$ and analyzing the equilibrium conditions gives the following relation for the deviation of the equilibrium position from the nominal one:

$$e = \frac{Q_u}{k_r}(1-\alpha)(1-\beta), \tag{11.20}$$

which matches the result from the Monte-Carlo simulation, c.f. Fig. 11.32. Evaluating (11.20) for the worst case scenario of $\beta = 1.1$ and $\beta = 0.9$ gives steady-state errors of 4×10^{-3} rad and -4.9×10^{-3} rad. From (11.20), we observe that e is non-zero only if $\alpha \neq 1$ and $\beta \neq 1$. Uncertainties in either m or b have no influence on the equilibrium position. The arguments above are no substitute for an in-depth robustness analysis of the proposed designs, and further investigations regarding the stability of an n degree of freedom ASR in the presence of parameter uncertainties are required in future work.

From the input transformation (4.17) it is clear that model uncertainties in $\boldsymbol{B}$ and $\boldsymbol{K}$ affect only the "dynamic" part, $\boldsymbol{B}\boldsymbol{K}^{-1}\ddot{\boldsymbol{u}}_u$, of the input transformation. Uncertainties in the rigid-body (link) parameters enter the input transformation (4.17) only through the model-based computation of $\ddot{\boldsymbol{q}}$ for $\text{ESP}_{1\text{–}4}$, and additionally $\boldsymbol{q}^{(3)}$ for ESP_{ref}; see Section B.2 in Appendix C.1. Thus, if $\ddot{\boldsymbol{q}}$ was obtained via an acceleration sensor the implementation of $\text{ESP}_{1\text{–}4}$ would be completely unaffected from model uncertainties concerning the rigid-body dynamics. The implementation of motor inertia shaping (see [86]) requires feedback of the joint torques $\boldsymbol{K}(\boldsymbol{\theta} - \boldsymbol{q})$. As a consequence, parameter errors associated with $\boldsymbol{K}$ affect the equilibrium behavior. This intuition is confirmed by (11.20) and the bottom plots of Fig. 11.32.

[86]: Keppler et al. (2018), "Elastic structure preserving (ESP) control for compliantly actuated robots"

EPILOGUE

12 Applications

Today's scientists have substituted mathematics for experiments, and they wander off through equation after equation, and eventually build a structure which has no relation to reality.

– Nikola Tesla

This chapter presents a variety of applications in which the ESP control framework is used to facilitate motions on the anthropomorphic robot DLR *David*. These applications demonstrate that using the ESP concept to implement the joint control for a compliant robot enables the execution of advanced manipulation tasks. Realizing these demos was a team effort by many people involved in the development, maintenance and operation of *David*. Special credit goes to Martin Pfanne who's contributions were key for realizing many of the demonstrations. Figure 12.3 gives an overview of the control architecture for *David* which has been developed in the course of this work; with ESP control at its center. Please note that most figures are collectively provided at the end of this chapter.

12.1 Human-Robot Interaction

The task-space ESPi controller reported in Section 7.2.5 enables modulating the robot's interaction behavior in an intuitive manner. To match the task requirements, we can directly specify the end effector compliance in terms of stiffness and damping parameters. For example, in typical service or medical robot scenarios, we can command very soft behaviors, whereas in a shared workspace cobot scenario, we can increase the robot's stiffness even above the intrinsic one to facilitate high precision manipulation.

The passive ESP control guarantees safe interaction between humans and robots. As pointed out in Chapter 7, the closed-loop system is output strictly passive with the power port constituted by the link velocities and disturbances. Consequently, during an interaction, the energy increase of the system is at most the energy injected by the interacting agent. In absence of external contacts, the closed-loop energy is steadily decreasing. In the handshake scenario shown in Fig. 12.1, the energy injection is determined by the power port constituted by the wrench (force, torque) applied to the robot's hand and the resulting twist (linear and angular velocity). When it comes to human robot interaction, safety is a critical concern. From the control point of view, a key aspect with regard to safety is the robustness of the controller. Knowing that OSP implies L2-gain stability [191], we can expect favorable robustness properties of an OSP ESP controller. The experiments in Section 11.2 confirm this intuition, highlighting the ESP concept's robustness concerning input saturation, disturbances (friction, impacts, human-robot interaction), and model uncertainties.

[191]: van Schaft (2017), *L2-Gain and Passivity Techniques in Nonlinear Control*

While keeping harm away from the human is a primary concern when endowing a robot with dexterous physical motion capabilities, we must not

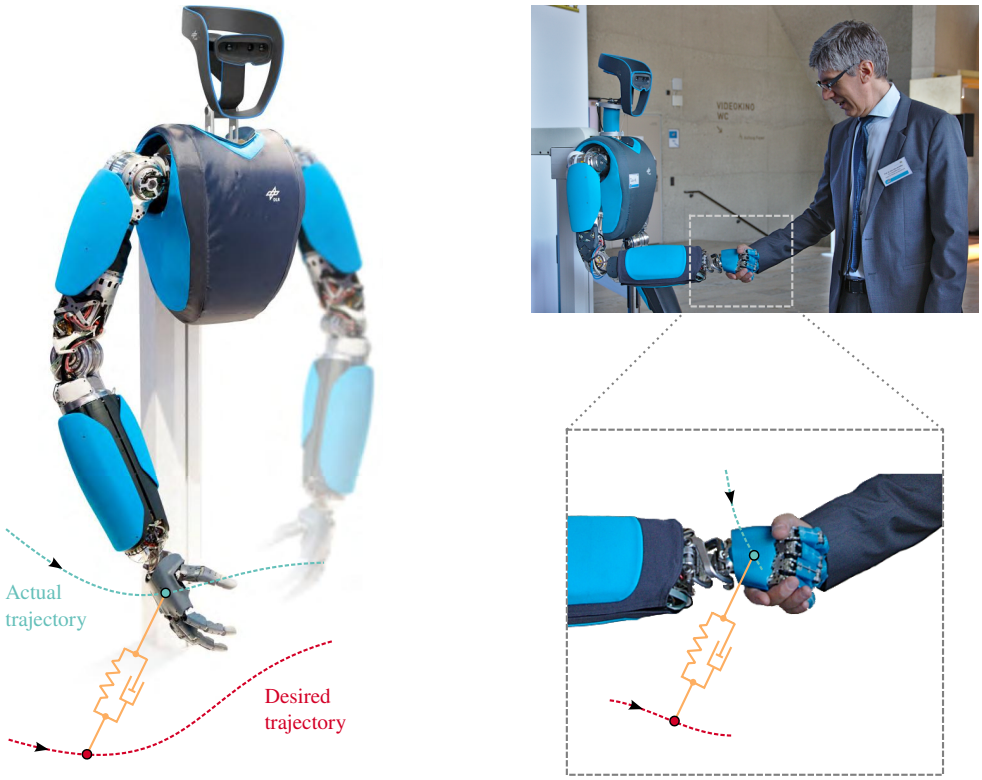

Figure 12.1: Natural and safe human-robot interaction facilitated through ESP control.

neglect teaching the robot to protect itself from damage. A broken robot neither can be deemed safe nor useful. The physical joint compliance significantly increases the mechanical robustness of an ASR; however, it can still break by overloading its elastic elements or by running into its endstops. For this reason, the ESP controller is integrated into an overarching control architecture that makes use of the robot's perception capabilities to avoid such a damaging scenario. An overview of David's high-level control architecture, with a focus on the damage avoidance logic, is shown in Fig. 12.2. The safety block in Fig. 12.3 can override the nominal control input by switching to a joint protection controller. We use the momentum observer proposed in [34] for collision detection and external wrench estimation. If an unplanned contact exerts a wrench that surpasses a specified threshold, a "safety controller" is activated. Usually, we employ a zero-gravity or motor PD controller for this role. By setting all position gains to zero, the ESP controllers degenerate to pure gravity compensation controllers (c.f. [32, 33]) with damping injection. Latter ensures the dissipation of all kinetic energy post an impact. Considering that any state with $\dot{\boldsymbol{q}} = \mathbf{0}$ is an equilibrium point of the closed-loop system, the human can easily push the robot arm away post collision; see also Video 12.6.1 for a demonstration. Thus, the robot cannot possibly clamp a human, or any object (even in case of a power failure; due to the intrinsic joint compliance the robot can always be pushed away). A joint protection controller is activated if contact with an endstop or overloading of an elastic element is imminent. If any link moves within a threshold band of the endstop it is being pushed away by the controller. In case the elastic energy of any joint approaches its maximal allowable value, the controller aims to keep the energy below this threshold. The object tracking and in-hand localization algorithms, which are essential for many applications, are based on the works [25, 150, 172].

[34]: De Luca et al. (2006), "Collision detection and safe reaction with the DLR-III lightweight manipulator arm"

[32]: De Luca et al. (2011), "A PD-type regulator with exact gravity cancellation for robots with flexible joints"
[33]: De Luca et al. (2010), "Dynamic gravity cancellation in robots with flexible transmissions"

[25]: Chalon et al. (2013), "Online in-hand object localization"
[150]: Pfanne et al. (2018), "Fusing Joint Measurements and Visual Features for In-Hand Object Pose Estimation"
[172]: Stoiber et al. (2020), "A sparse gaussian approach to region-based 6dof object tracking"

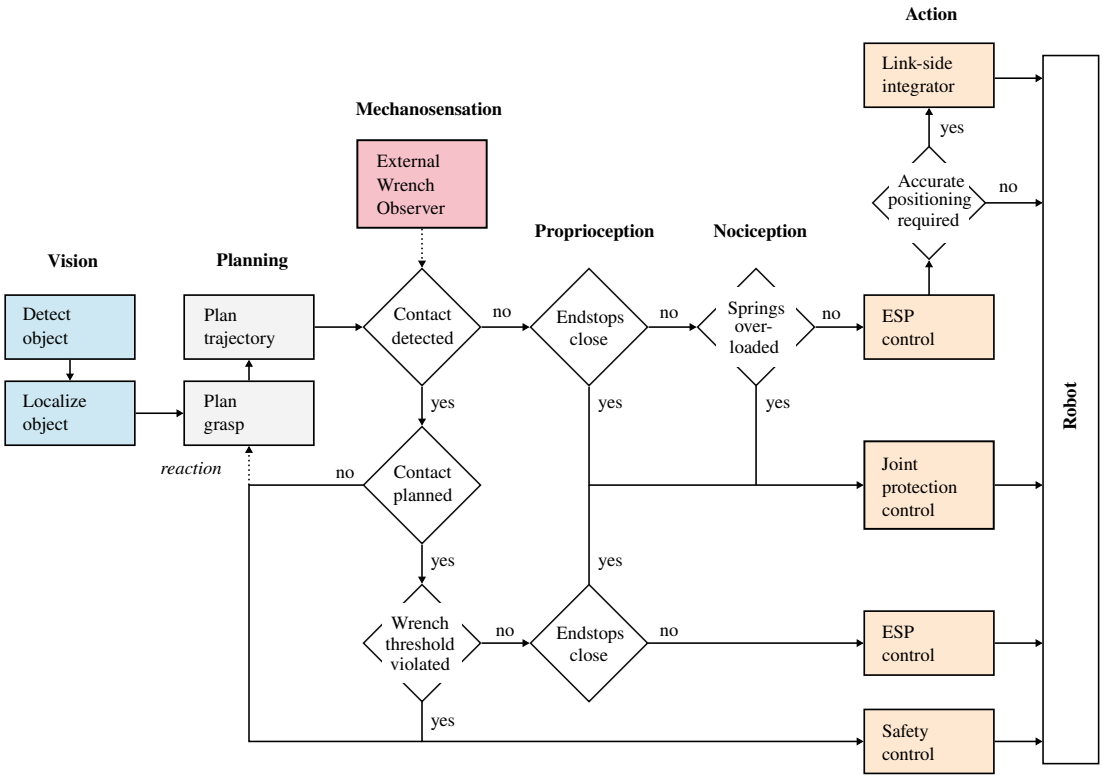

Figure 12.2: Safety logic for *David*.

12.2 Drill-Hammering

In this demonstration, the robot is tasked to use a drill hammer to bore a hole into a plate of concrete. The setup is shown in Fig. 12.4 a. In order to succeed, the robot must first pick up and position the vacuum cleaner and drill hammer on the plate with a certain pretension. Then, by spanning a virtual spring from the drill tip to a point behind the plate—with the line connecting both points intersecting the wall perpendicularly—the robot pushes the running drill hammer through the stone. Moving the equilibrium position of the virtual spring in front of the plate initiates the drill retraction. The demonstration ends with the robot returning the vacuum cleaner handle and the drill hammer to their initial positions. Figure 12.3 shows a high-level overview of *David*'s control architecture with a focus on the modules critical for the drill-hammering demonstration reported in this Section.

The robot is able to track objects using its on-board cameras. The system is capable of 6-DOF region-based object tracking implemented through an efficient sparse approach requiring only a monocular RGB camera and the 3D object model [172]. Experiments demonstrating the performance of this method can be watched on YouTube.[1] A common reality during pick and place operations with a humanoid hand is the relative motion between object and palm during the grasp acquisition phase resulting in a grasp execution differently as planned. In order to achieve robust manipulation, this relative motion has to be observed and take account of during object placement. To this end, we employ an online in-hand object localization algorithm [25] that exploits the contact sensing capabilities of *David* to provide an object pose estimation even when object occlusion is high. As soon as the visual perpection of the robot's environment is completed, the control framework

[172]: Stoiber et al. (2020), "A sparse gaussian approach to region-based 6dof object tracking"

1: https://youtu.be/lwhxSRpwn3Y

[25]: Chalon et al. (2013), "Online in-hand object localization"

enters the planning phase.

A non-collocated integrator activates whenever precise positioning of the manipulators is required. The integrator is activated multi times throughout the scene. Basically, whenever there is contact detected and the motion of the robot is below some threshold. Critical activation are during the following sequences: (b) placing the hand to grasp the vacuum cleaner, (c)–(d) placing the hand to grasp the the drill hammer, (e) precise placement of the drill on the stone plate, (f) returning the vacuum cleaner, (g) placing the drill hammer on the table.

12.3 Teleoperation

Teleoperation is concerned with the remote operation of robotic machines and typically encountered in research and technical environments such as: space and deep sea exploration, emergency response, law enforcement, handling of radioactive material and remote surgery.

2: Kinfinity is a spin-off from the German Aerospace Center (DLR); for more info visit `https://kinfinity.eu/`.

[24]: Chalon et al. (2014), "Backstepping experimentally applied to an antagonistically driven finger with flexible tendons"

This section reports the teleoperation of *David* via a human-machine interface developed by Kinfinity[2]. The Kinfinity suit and glove—shown in Fig. 12.5—enable programming a robot by demonstration, and teleoperating it from a distance. The Kinifity motion suite senses the movement of the human operator. A software algorithm translates this sensor data in real-time into a trajectory for the robot. Using the motion tracking capabilities of the ESP controller allows *David* to mirror the arm motion of the human operator. The mirroring of the finger motions is realized by the controller presented in [24]. Figure 12.5 shows three sequential photos from a live demonstration during the *Hannover Messe 2018*. A brief demonstration of *David* being teleoperated via the motion suite can be found on YouTube; see Video 6 in Section 12.6 for the link.

12.4 Pipette Grasping and Handling

Combining link-side (non-collocated) integral action with ESP control, as proposed in [93], enables to position the arm of *David* with a link-side accuracy of 72 µrad. This is the maximum achievable accuracy, as this value is exactly the sensor resolution of the link position sensors (16 bit/271°). In the following demo, *David* grasps and operates an adjustable pipette. Especially, the picking up, positioning over the Petri dish and the returning of the pipette require high precision. See Video 7 in Section 12.6 for a recorded demonstration.

12.5 Opening and Unloading a Dishwasher

Emptying a dishwasher, as shown in Fig. 12.7, is a complex task that involves multiple consecutive sub-tasks. From a control perspective, it is essential to achieve precise positioning of the arm and fingers, while navigating alternating forceful and delicate interactions with various objects in a robust and compliant manner. Notably, the initial opening of the dishwasher presents a significant challenge, as the robot must overcome a substantial force threshold to unlock the door. This application essentially relies on the controller proposed in [93], which achieves compliant interaction in contact and remarkable positioning accuracy in free motion.

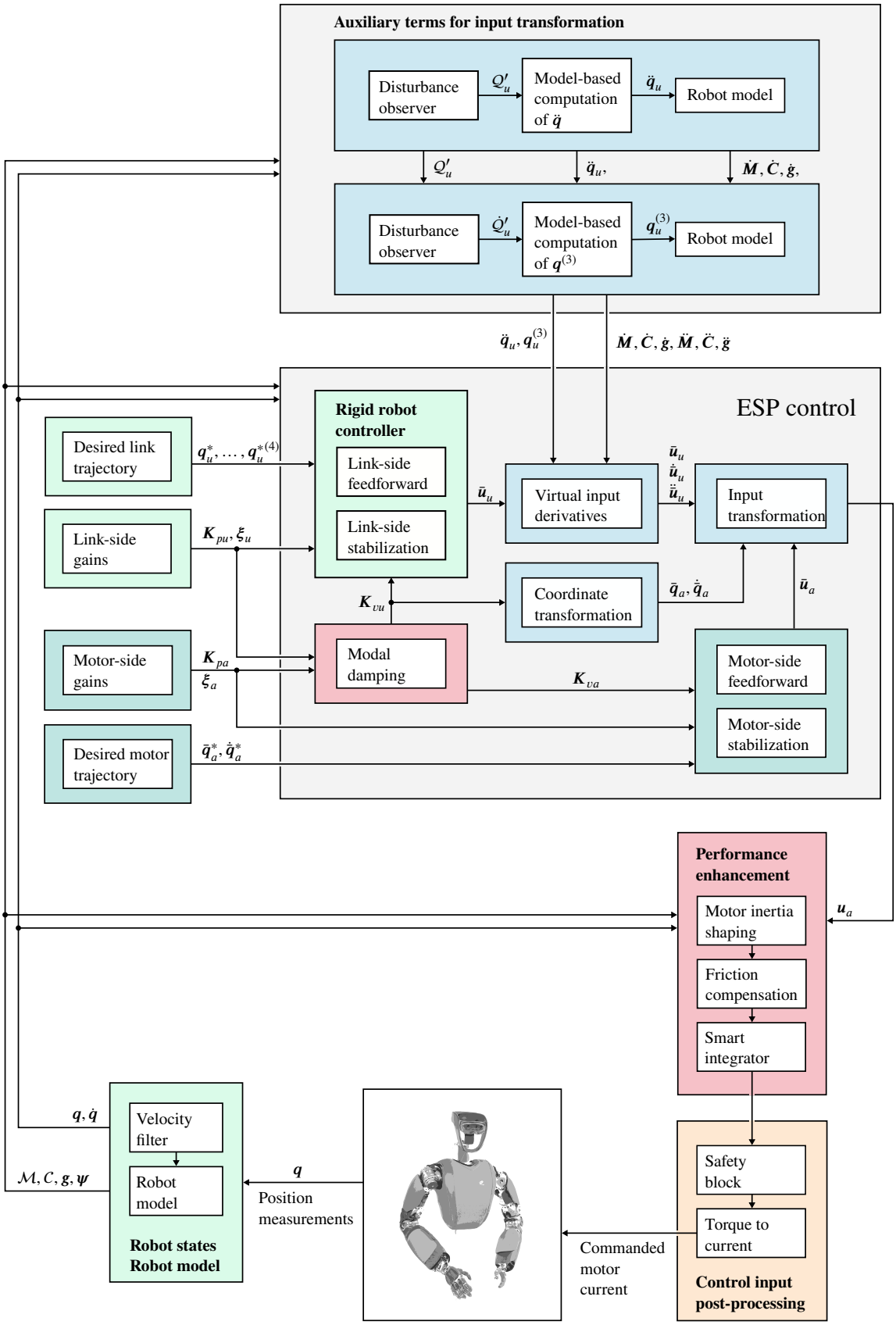

Figure 12.3: Control architecture for *David* based on ESP control.

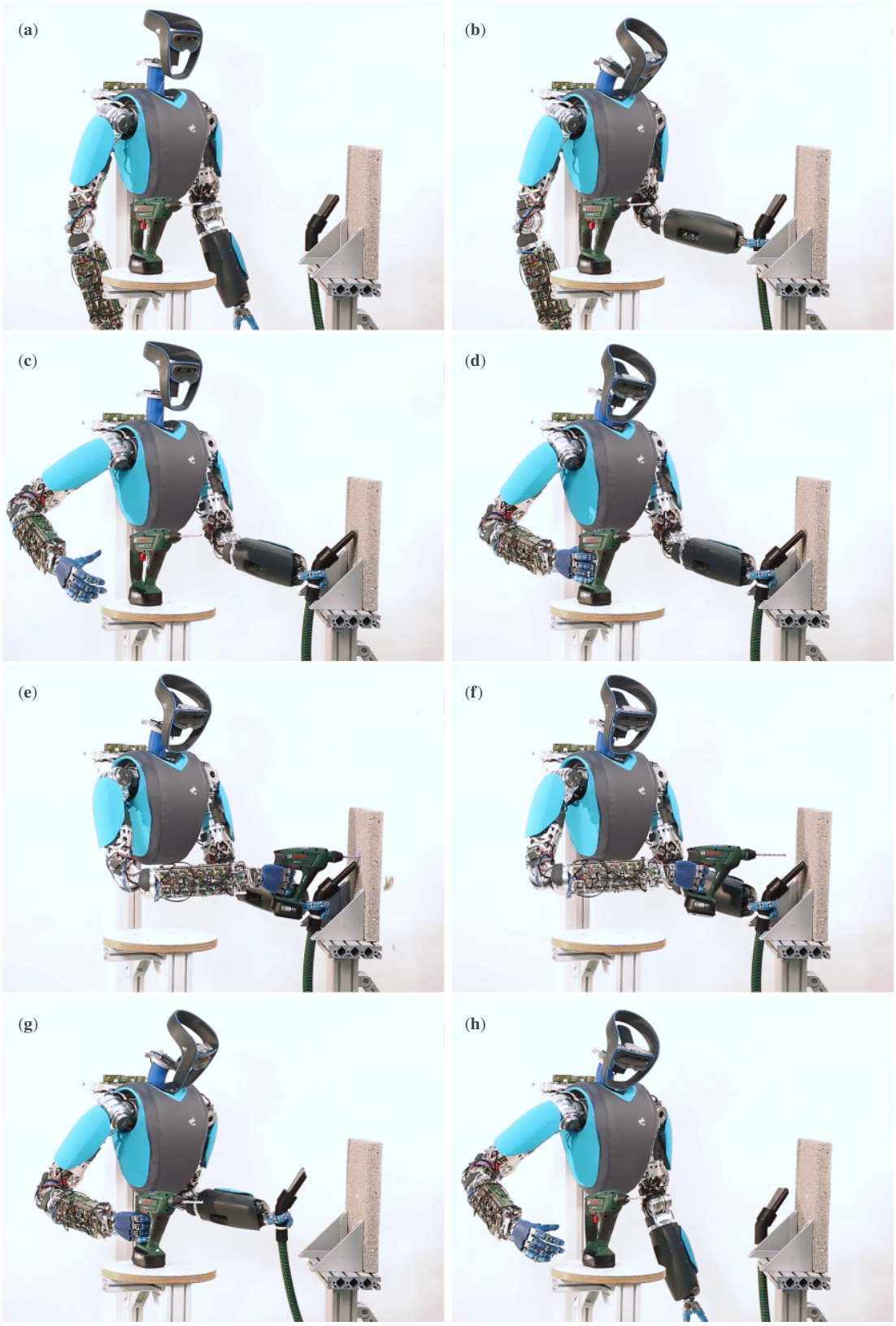

Figure 12.4: Drill hammering into concrete with an ASR. (**a**) Initial configuration. (**b**) end effector tracking with the head-mounted camera enables two finger grasp of vacuum cleaner. (**c**) Placing vacuum cleaner with pretension against the stone plate. Initiate grasping motion for the right arm. (**d**) Force controlled closure of the right hand around the drill handle. ESP controller adapts to account for added tool mass. (**e**) Positioning drill on stone, pulling the trigger, commanding a set-point behind the plate, initiate drilling, detecting break via external wrench observer. (**f**) Shift set-point to a location in front of the plate to initiate extracting the drill. (**g**) Releasing tool and resetting tool mass adaption. Returning vacuum cleaner. (**h**) Releasing vacuum cleaner. Arms returning to the initial configurations.

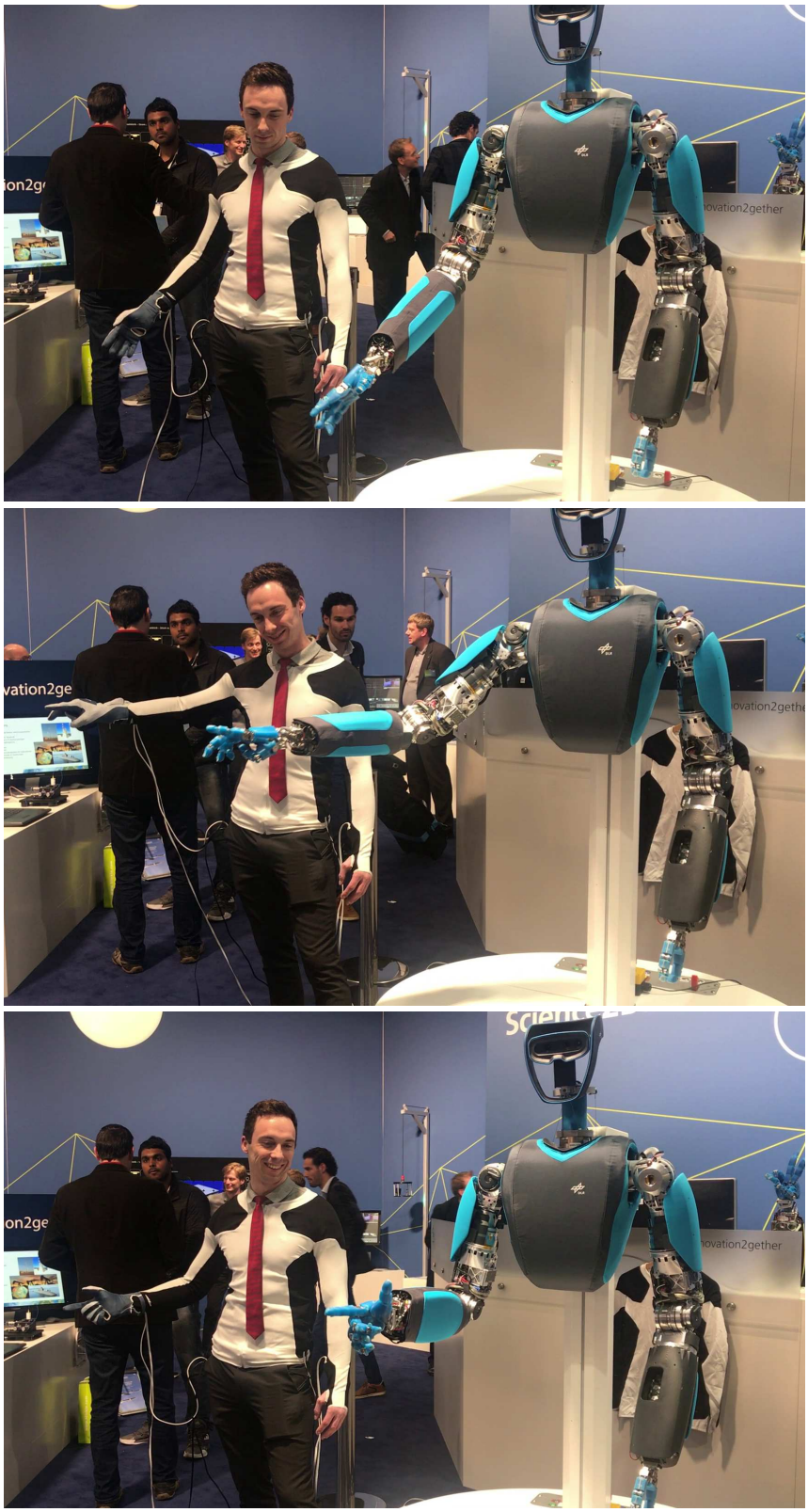

Figure 12.5: Teleoperation of an ASR. *David* mirroring the motion of a human operator wearing a Kinfinity suit and glove.

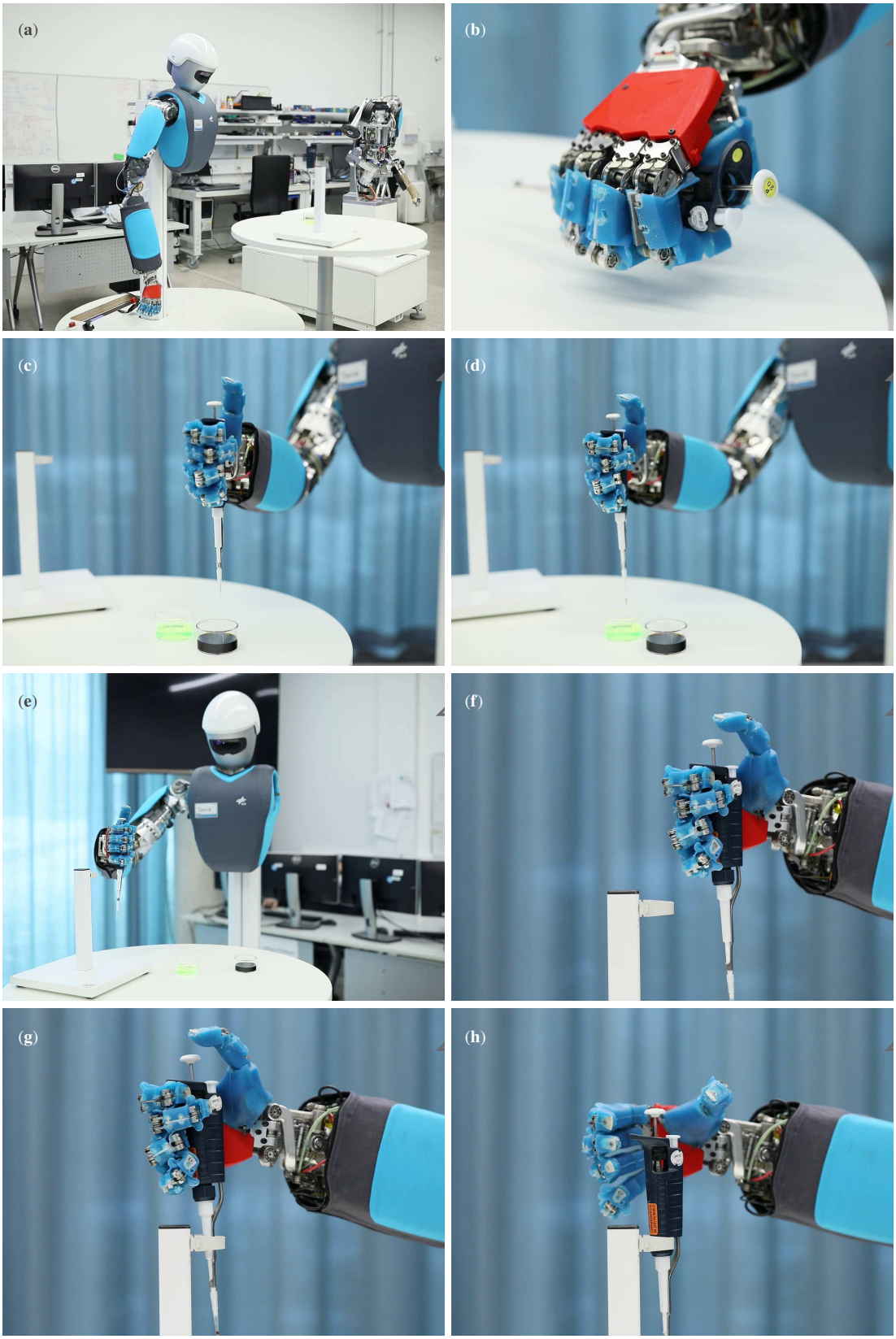

Figure 12.6: Grasping and operating a pipette with DLR *David*. (**a**) Initial configuration. (**b**) Grasping and picking up the pipette. (**c**–**d**) Placing the pipette over the Petri dishes. (**e**–**h**) Returning the pipette to the rack.

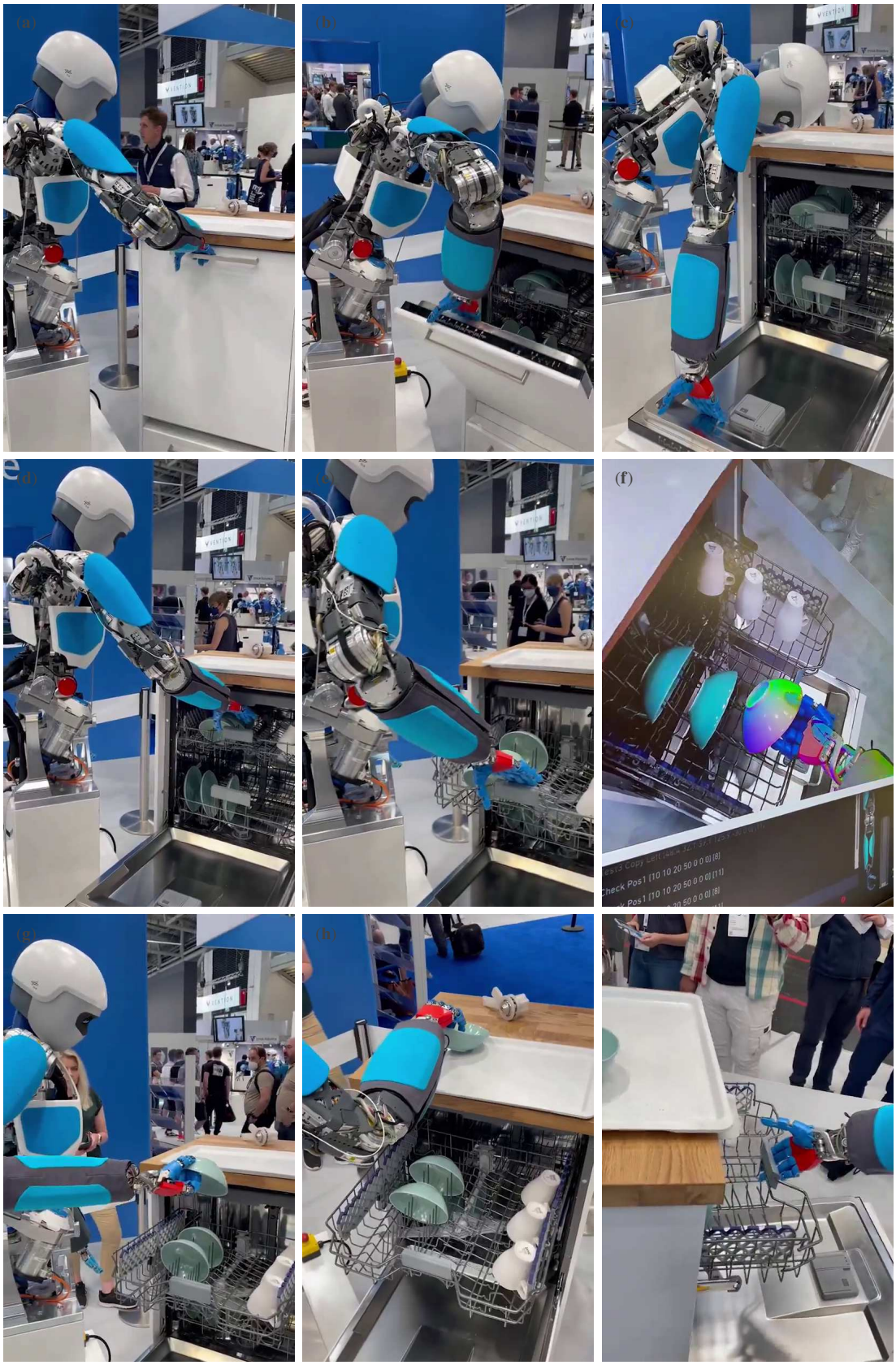

Figure 12.7: Opening and unloading a dishwasher with DLR *David*. (**a**–**b**) The dishwasher is opened by grasping the door handle and pulling it back and downward around the hinge axis. (**c**) To fully open the door, the handle is released, and the door is pushed downward using the fingertips. (**d**–**e**) The tray is pulled out of the dishwasher with the fingertips hooked behind the handle. (**f**–**g**) Localization and tracking of the desired object, such as a plate, as well as Davids forearm and wrist, are performed. This enables relative planning and execution of motions between the hand and the plate. The tracking algorithm is designed to be robust against partial occlusions caused by David's own fingers. (**h**) The plate is released and placed on top of the dishwasher, with contact forces compensated for by the intrinsic and controlled elasticity of the fingers and arm. (**i**) Closing the dishwasher and completes the task (partially shown).

12.6 Multimedia Material

12.6.1 Videos

This work focuses on the fundamental aspects of the presented framework and how it simplifies the control design for underactuated compliant robots. However, extensive experimental results on the anthropomorphic DLR Robot *David* with Variable Stiffness Actuators (VSA) confirm the practical applicability of the framework. In [86, 90] we introduced a globally asymptotically stable joint-space motion tracking approach. Motion tracking and impact experiments can be found here:

- Video 1 (Motion tracking and disturbance rejection):
  https://rmc.dlr.de/rm/de/staff/extcms/images/rmc/2016_ICRA_Keppler.mp4

- Video 2 (Motion tracking and impact experiments):
  https://youtu.be/PATvv47QfQs

The robustness of this approach is highlighted in a demo where *David* drills into a block of concrete. This task requires both precise positioning of the tool center point and vibration damping, see:

- Video 3 (Drill hammering):
  https://youtu.be/JVdufPRK4NI

In [92], we present an asymptotically stable Cartesian impedance regulation controller with remarkable stiffness and damping range. Experiments showing task-space human-robot interaction and disturbance rejection behavior are shown here:

- Video 4 (Cartesian impedance control and human-robot interaction):
  https://youtu.be/sbhiNNIxMNQ

- Video 5 (Enhanced damping designs based on dynamic extensions):
  https://youtu.be/O9Cx3H1Jal4

All these passivity-based concepts can be unified and elegantly expressed in the presented framework. However, importantly, through the presented adoption of e.g. the PD+ and Slotine and Li controllers we were able achieve asymptotically stable tasks-space motion tracking. To the best of our knowledge, these are the first PBC approaches that enable task-space motion tracking for compliant robots with nonlinear spring characteristics. The PD+ adoption can be considered a tasks-space impedance control with tracking behavior. It allows to specify a compliant behavior of the robot TCP with respect to a reference trajectory thereby enabling a compliant and passive interaction with moving objects.

- **Video 6** (Teleoperation via Kinfinity motion suite):
  https://youtu.be/KmPZxiUB0Vc

- **Video 7** (Advanced manipulation of a pipette):
  https://youtu.be/_kj1RgdIkfk

12.6.2 Coverage on IEEE Spectrum and News

Video Friday: normal and headliner

- IEEE Video Friday headline:
  https://spectrum.ieee.org/automaton/robotics/robotics-hardware/video-friday-soft-robot-impedance-control-autonomous-rescue-drone-robosimian-skating
- IEEE Video Friday:
  https://spectrum.ieee.org/video-friday-dogs-that-code-robotic-football-self-driving-bicycle
- ETF Trends:
  https://www.etftrends.com/robotics-ai-channel/impedance-control-for-soft-robots/

13 Summary and Outlook

This thesis treats the nonlinear control of a class of underactuated Euler-Lagrange systems. A fundamental property connected with this class of systems is the decomposability into passive subsystems. A challenge inherent with the control of underactuated system is the lack of input channels. A popular representative of this class are articulated soft robots which are in the focus of this work.

The objective of this work is twofold. On the one hand, it aims to advance the field of nonlinear control of underactuated systems, and on the other hand, it aims to demonstrate that ASRs can indeed be considered a viable alternative to classic rigid robots. Guided by energy considerations and experience in control application in the lab, the reported developments are tailored for application on robotic hardware. The physically intuitive closed loops of the proposed designs enable the operator to anticipate the interaction behavior of the robot with the environment, i.e., another physical system. Clearly, the interaction between two physical systems that are visualizable in terms of real physical elements is fundamentally easier to comprehend and anticipate than the interaction between a set of (partial) differential equations and the environment. In addition, having a physical intuitive closed-loop behavior provides—to some extent—a feeling for the extent of system shaping imposed by a particular control design. This enables the operator to provide an ad-hoc estimate of the maximal achievable gains and, thus, expected performance. This fact can hardly be overestimated when it comes to the commissioning stage since physical intuiting is of immense value for tuning a controller.

The main theoretical contribution is reported in Chapter 5. In the Lagrangian picture of mechanics, we can represent a system evolving in time by the motion of a single point P through its configuration space $\mathcal{C}$. The *principle of stationary action* tells us that the path taken by P through $\mathcal{C}$ between times t_0 and t_1 and two fixed points in $\mathcal{C}$ is the one for which the action is stationary. Guided by this Lagrangian picture of mechanics, this work proposes a new approach to treat the stabilization of a class of underactuated Euler-Lagrange systems. A fundamental property connected with this class of systems is the *decomposability* into passive subsystems. Exploiting this property, we can decompose such a system into an actuated Σ_a and unactuated subsystem Σ_u. Instead of thinking in terms of a single point P moving through $\mathcal{C}$, it is rewarding to think of two points P_u and P_a—representing the configurations of Σ_u and Σ_a—moving through two subspace of $\mathcal{C}$. The only source of interaction is the forces arising from the potential field $\mathcal{V}$ that permeates $\mathcal{C}$. The shape of this potential field—and consequently the magnitude and direction of the arising coupling force—is dictated by the relative position of Σ_u and Σ_a. Consequently, the only option to impose a desired motion on the unactuated subsystem Σ_u is to adjust the variation of the coupling force by adjusting the motion of the actuated subsystem through the input force $\boldsymbol{u}_a$

Using this geometrical view, we introduced a partial change of coordinates $(q_{ui}, q_{ai}) \rightarrow (\bar{q}_{ui}, \bar{q}_{ai})$ with $q_{ui} \equiv \bar{q}_{ui}$, and a transformation of the input forces $u_i \rightarrow \bar{u}_i$, such that EL system Σ is transformed into an *equivalent* EL system $\bar{\Sigma}$ that can be treated as *quasi-fully actuated*. Equivalence of Σ and $\bar{\Sigma}$ is to be understood in the sense that the solutions of both systems are in a

one-to-one correspondence (as pointed out in Lemma 5.4.1) and, thus, both systems describe the *same* physical reality. Therefore, instead of studying and controlling the behavior of Σ, one can equivalently study and control the behavior of $\bar{\Sigma}$. Since the virtual inputs $\bar{u}_i$ on the unactuated subsystem cannot be chosen completely freely, the transformed system is being referred to as quasi-fully actuated. The structural properties of the QFA system that are most notable from the control point of view are:

- Even though the transformation is a non point transformation, the structure of the Euler-Lagrange equations is preserved.
- For each degree of freedom there is a virtual input.
- The QFA system (4.18) defines a passive mapping $\bar{\boldsymbol{u}} \rightarrow \dot{\bar{\boldsymbol{q}}}$ between the virtual input forces and the velocities.

The central results of Chapter 5 are summarized in Theorem 5.3.6, 5.4.2 and 5.6.1, and serve as basis for all subsequent chapters, but Chapter 10.

The equilibria of an EL system are determined by the critical points of its potential function. If the potential energy is at a local minimum and suitable damping is present then the associated equilibrium point is asymptotically stable. These two fundamental properties were first exploited in [178]. Takegaki and Arimoto translated the dynamic control of manipulators into a problem of shaping its potential energy and injecting damping. Using the concept of QFA, Proposition 6.2.1 in Chapter 6 reports an extension to the energy shaping and damping injection scheme to the class of underactuated EL systems specified in Chapter 6. Moreover, Proposition 6.3.1 in Chapter 6 proposes an extension of the concept of EL controllers [133]. Compared to the original scheme, the new result allows for more freedom in formulating the controller EL equations by allowing the associated potential and kinetic energies to be formulated in terms of non-collocated coordinates. Finally, Chapter 6 treats the adoption of impedance control [68–70] through the QFA representation of.

[178]: Takegaki et al. (1981), "A new feedback method for dynamic control of manipulators"

[133]: Ortega (1998), *Passivity-Based Control of Euler-Lagrange Systems: Mechanical, Electrical, and Electromechanical Applications*

[68]: Hogan (1985), "Impedance control: An approach to manipulation: Part I—Theory"
[69]: Hogan (1985), "Impedance control: An approach to manipulation: Part II—Implementation"
[70]: Hogan (1985), "Impedance control: An approach to manipulation: Part III—Applications"

Based on the theoretical results in Chapter 5, Chapter 7 developed a series of passivity-based control schemes tailored for ASRs with elastic or visco-elastic joints that aim at natural motions by minimizing the systems shaping. These schemes are collectively referred to as ESP designs and share the following properties: 1) preservation of the EL structure of the plant, 2) output strict passivity, 3) intuitive closed-loop behavior, 4) pervasive damping. The underlying hope is that minimizing the system shaping, and having a closed-loop dynamics match in some way the intrinsic structure of the robot will award high performance with little control effort. Further, control designs that minimize the system shaping usually result in low gain designs, which is favorable with regard to robustness.

Chapter 8 compares several design techniques that achieve global asymptotic motion tracking for SEA-based robots including the ESP designs developed in Chapter 7.

Chapter 9 exploits the QFA representation of a SEA-based robot to analyze its performance limits. Moreover, enhanced damping designs are proposed that significantly reduce the actuator torque requirements at the moment of an impact compared to classic damping implementations in Chapter 7. In addition, the sensitivity regarding link position measurement noise is reduced by 20 dB/dec by avoiding feedback of the link jerk signals. This, however,

comes at the price of sacrificing the pervasive damping, and thus global output strict passivity, of the ESP designs in Chapter 7.

Chapter 10 presents a complete synthesis method for time-optimal rest-to-rest motions of an elastic joint system with bounded torque input. The solution is provided in closed form by following purely geometric arguments, and verifies the standard optimality conditions. Further, we introduced the concept of natural motions which are time-optimal solutions to the RTR motion problem. These are the only RTR solutions where the minimum-time performance of an elastic joint system matches that of a rigid joint. In future works, it is worth investigating how the insights obtained from the natural motion analysis can be exploited to optimize the design of an elastic robot joint.

The experiment results in Chapter 11 and 12 highlight the performance of the proposed ESP concept. Videos of the reported experiments are linked in Section 12.6. Summarizing the experimental demonstrations, the ESP concept achieves:

- Dexterous, robust and passive interaction with the (unknown) environment, as demonstrated in all experiments and videos.
- Excellent link-side damping with minimal over-shooting in motion tracking and setpoint regulation; see Experiment 1 and 2 and Video 1 and 2.
- Precise stiffness control in joint and Cartesian space; see Experiment 3 and Video 4.
- The link-side stiffness can be substantially increased over the system's natural one, while preserving passivity of the closed loop; see Experiment 3.
- The system remains stable even in the case of control input saturation.
- By setting all gains to zero, the robot can be moved freely in gravity compensation mode; see Video 4.
- Despite the joint stiffness values varying over a vast range, the ESP/ESP+ controllers achieve excellent performance without gain adaption; see Experiment 2.
- A desired link compliance can be imposed without requiring feedback of link acceleration and jerk signals; see Experiment 5.

In recent years we have seen a surge in the application of robotic manipulators in new areas that require a dynamic interaction with the environment, e.g., shared work spaces with humans, health care, Industry 4.0. In order to facilitate these interactions in a safe manner, and to increase the mechanical robustness of robots against impacts, robot design evolved from rigid toward compliant actuators, i.e., soft robots. The intrinsic oscillatory dynamics can be exploited, for cyclic tasks such as locomotion, hammering, or drumming. For positioning tasks, however, these oscillatory dynamics require elaborate control concepts [28] to achieve positioning performance that come close to that of rigid manipulators. In many cases, ASRs were limited in their performance by control technology which matured on robotic arms where joint elasticity was considered a parasitic effect that must be avoided since it introduces unwanted oscillatory dynamics into the system. The extensive experimental results in Chapter 11 and the applications in Chapter 12 on the anthropomorphic robot DLR *David* demonstrate that these challenges can be overcome.[1]

[28]: De Luca et al. (2016), "Robots with Flexible Elements"

Although many challenges in soft robotics remain ahead, this work advanced the state of the art by developing control schemes that combine tra-

1: Contrary to popular believe in the robotics community, the reported experiments clearly demonstrate that high performance and robust designs can be achieved despite feedback of acceleration and jerk signals. The author believes that the robustness of a control design equally suffers from extensive dynamics shaping as from feedback of acceleration and jerks signals.

jectory tracking in free motion with robust and compliant manipulation in contact. Experimental evaluations of the proposed ESP concept highlight the link-side damping performance and demonstrate the robustness in challenging situations such as hard impacts. “Do as little as possible.” These words may summarize the ESP design philosophy best. Finally, using the proposed ESP concept enabled us to demonstrate the practical viability of ASRs in various real-world scenarios, including pick and place, teleoperation, and drill-hammering; see videos in Section 12.6. In conclusion, when it comes to commercial applications, it is safe to say that articulated soft robots can indeed be considered a viable alternative to classic rigid robots.

APPENDIX

A

A Geometric Point of View

Studying mathematics as symbol manipulation is like studying music without ever hearing a note. [112, 124]

– Tristan Needham

This chapter considers systems where the elastic potential assumes a quadratic form. The following discourse has two objectives. First, to facilitate an intuitive understanding of the system shaping imposed through a particular design choice for the virtual control inputs, a geometric interpretation of the input transformation is derived (Section A.1). Second, it reports an alternative derivation of the QFA representation based on purely geometric considerations. More precisely, it will be shown that by introducing a non-inertial reference frame to describe the motions of the actuated subsystem, the QFA representation emerges naturally (Section A.3). The result shows that the virtual coordinates are actually observable and measurable quantities.

A.1 Revisiting the Input Transformation

The following text connects a geometrical picture with the input transforming equations derived in Chapter 5 for the case where the elastic potential function is a quadratic form.

A.1.1 Series Elastic Actuators

Consider an ASR implemented with SEA satisfying Spong's model. Chapter 9, demonstrated that we can bring such a system into a QFA form through the coordinate and input transforming equations (7.40) and (7.41), which are repeated for convenience:

$$\boldsymbol{q}_a = \bar{\boldsymbol{q}}_a + \boldsymbol{K}^{-1}\bar{\boldsymbol{u}}_u, \tag{A.1}$$

$$\boldsymbol{u}_a = \boldsymbol{B}\boldsymbol{K}^{-1}\ddot{\bar{\boldsymbol{u}}}_u + \bar{\boldsymbol{u}}_u + \bar{\boldsymbol{u}}_a, \tag{A.2}$$

where $\boldsymbol{B} = \mathrm{diag}(b_1, \ldots, b_{n_a})$ and $\boldsymbol{K} = \mathrm{diag}(k_1, \ldots, k_{n_a})$. Introducing the auxiliary coordinates and forces

$$\boldsymbol{r} = \boldsymbol{K}^{-1}\bar{\boldsymbol{u}}_u = (r_{a1}, \ldots, r_{na}), \tag{A.3}$$

$$\tilde{\boldsymbol{u}} = \boldsymbol{u}_a - \bar{\boldsymbol{u}}_a = (\tilde{u}_{a1}, \ldots, \tilde{u}_{na}) \tag{A.4}$$

and making the substitutions (A.2) and (A.3)–(A.4) yields

$$\boldsymbol{B}\ddot{\boldsymbol{r}} + \boldsymbol{K}\boldsymbol{r} = \tilde{\boldsymbol{u}}_a. \tag{A.5}$$

Inspecting the Euler-Lagrange equations (A.5) reveals a striking geometric interpretation. Consider a system of n_a independent harmonic oscillators. Let b_i and k_i denote the mass and stiffness of the ith oscillator, and let r_i denote its deflection, as sketched in Fig. A.1. Then the corresponding EL equations are just (A.5). Observing that the components of the virtual control input, $\bar{u}_{ui}$, are in a linear one-to-one correspondence with the deflections r_i through (A.3), we conclude that whenever the variation of the $\bar{u}_{ui}$ corresponds to an unforced motion of the associated harmonic oscillator, the control forces, $\tilde{u}_i$, are zero by definition.

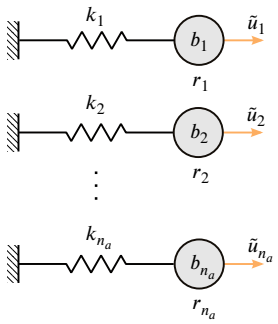

Figure A.1: Interpreting the time evolution of each control signal as the evolution of a driven harmonic oscillator.

We can modify this picture to obtain a direct connection between the motion of the harmonic oscillators and the actual control forces u_{ai}. Introducing

$$\boldsymbol{s} = -\boldsymbol{K}^{-1}\bar{\boldsymbol{u}}_a = (s_{a1}, \dots, s_{na}), \tag{A.6}$$

and making the substitution (A.5) and (A.6), we get

$$\boldsymbol{B}\ddot{\boldsymbol{r}} + \boldsymbol{K}(\boldsymbol{r} - \boldsymbol{s}) = \boldsymbol{u}_a. \tag{A.7}$$

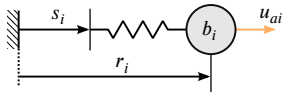

Figure A.2: Interpreting the time evolution of each control signal as the evolution of a driven harmonic oscillator.

From (A.7), we see that s_i determines the equilibrium position and u_{ai} the driving force of the ith harmonic oscillator. In conclusion, the stronger the ith harmonic oscillator deviates from its unforced motion the higher the control forces u_{ai}, and the higher the system shaping imposed on the ASR; of course, given that the magnitudes of the control forces u_{ai} qualify as a measure of system shaping. An alternative measure would be the power injected through the port (q_{ai}, u_{ai}). However, analyzing the latter goes beyond the scope of this work.

A.1.2 Linear Elastic Couplings

Consider an ASR with linear elastic coupling, such that the potential energy $\mathcal{V}_e$ is a positive definite quadratic form

$$\mathcal{V}_e = \tfrac{1}{2}\begin{bmatrix}\boldsymbol{q}_u\\ \boldsymbol{q}_a\end{bmatrix}^{\mathrm{T}}\begin{bmatrix}\boldsymbol{K}_u & -\boldsymbol{K}_{ua}\\ -\boldsymbol{K}_{ua}^{\mathrm{T}} & \boldsymbol{K}_a\end{bmatrix}\begin{bmatrix}\boldsymbol{q}_u\\ \boldsymbol{q}_a\end{bmatrix}. \tag{A.8}$$

Notice that Assumption 5.1.2 translates into $\boldsymbol{K}_{ua} \succ 0$. The coordinate and input transforming equations, (5.29a) and (5.57), evaluate to

$$\boldsymbol{q}_a = \bar{\boldsymbol{q}}_a + \boldsymbol{K}_{ua}^{-1}\bar{\boldsymbol{u}}_u, \tag{A.9}$$

$$\boldsymbol{u}_a = \boldsymbol{B}\boldsymbol{K}_{ua}^{-1}\ddot{\bar{\boldsymbol{u}}}_u + \boldsymbol{K}_a\boldsymbol{K}_{ua}^{-1}\bar{\boldsymbol{u}}_u + \bar{\boldsymbol{u}}_a. \tag{A.10}$$

Introducing the auxiliary coordinates

$$\boldsymbol{r} = \boldsymbol{K}_{ua}^{-1}\bar{\boldsymbol{u}}_u, \tag{A.11}$$

considering (A.4) and the Lagrangian

$$\mathcal{L}_r = \tfrac{1}{2}\big(\dot{\boldsymbol{r}}^{\mathrm{T}}\boldsymbol{B}\dot{\boldsymbol{r}} + \boldsymbol{r}^{\mathrm{T}}\boldsymbol{K}_a\boldsymbol{r}\big), \tag{A.12}$$

we observe that (A.10) are just the EL equations

$$\left(\frac{\mathrm{d}}{\mathrm{d}t}\frac{\partial}{\partial \dot{\boldsymbol{r}}} - \frac{\partial}{\partial \boldsymbol{r}}\right)\mathcal{L}_r = \tilde{\boldsymbol{u}}_a, \tag{A.13}$$

which evaluate to

$$\boldsymbol{B}\ddot{\boldsymbol{r}} + \boldsymbol{K}_a\boldsymbol{r} = \tilde{\boldsymbol{u}}_a. \tag{A.14}$$

Considering (A.8), we can think of (A.14) as the EL equations associated with a coupled spring-mass system with n_a degrees of freedom driven by the forces $\tilde{u}_{ai}$, as sketched in Fig. A.3.

Modifying the Lagrangian to include the control forces $\bar{\boldsymbol{u}}_a$

$$\mathcal{L}_r^* = \mathcal{L}_r + \boldsymbol{r}^{\mathrm{T}}\bar{\boldsymbol{u}}_a, \tag{A.15}$$

we can rewrite the input transforming equations as the EL equations

$$\left(\frac{\mathrm{d}}{\mathrm{d}t}\frac{\partial}{\partial \dot{\boldsymbol{r}}} - \frac{\partial}{\partial \boldsymbol{r}}\right)\mathcal{L}_r^* = \boldsymbol{u}_a. \tag{A.16}$$

In summary, imposing the virtual input forces $\bar{\boldsymbol{u}}_u$ and $\bar{\boldsymbol{u}}_a$ on $\bar{\Sigma}$ translates into applying on Σ the control force $\boldsymbol{u}_a$ defined by EL equations (A.16). This remarkable result allows representing all the ESP schemes for ASRs with elastic couplings of the form (A.8) in a unified way through the formulation of a single quantity; the Lagrangian $\mathcal{L}_r^*$. Notice that the form of the Lagrangian is invariant.

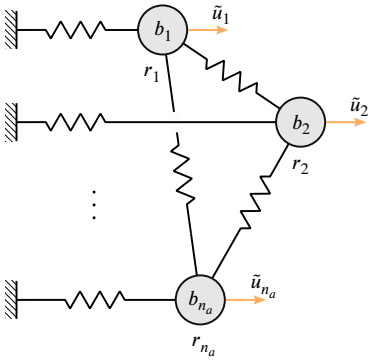

Figure A.3: Interpreting the time evolution of the control signals as the evolution of a coupled spring-mass system.

A.2 A Control Input Observer

This section exploits the mechanical interpretation of the input transforming equations developed above to reduce the computational effort for implementing these equations. The following discussion considers the case treated in Section A.1.2.

In practice, a major challenge concerning the implementation of the input transforming equations (A.10) is the required knowledge of $\ddot{\bar{\boldsymbol{u}}}_u$. For the linear spring case this fact is immediately clear from (A.2). Let us use the insight that the transforming equations can be viewed as the EL equations of a driven spring-mass system to avoid feedback $\ddot{\bar{\boldsymbol{u}}}_u$. The idea is as follows. Considering (A.12), we can think of (A.13) as a system of point masses driven by the generalized forces $\frac{\partial \mathcal{L}_r}{\partial \boldsymbol{r}}$ and $\tilde{\boldsymbol{u}}_a = \boldsymbol{u}_a - \bar{\boldsymbol{u}}_a$. Suppose that all but $\boldsymbol{u}_a$ are known. Then, using the generalized momentum associated with the EL equations (A.14)

$$\boldsymbol{p} = \frac{\partial \mathcal{L}_r}{\partial \dot{\boldsymbol{r}}}, \tag{A.17}$$

we can obtain an estimate of $\boldsymbol{u}_a$ by employing a momentum-based disturbance [34, 48]. The implementation of such an observer requires knowledge of only the generalized momentum and the generalized forces $\bar{\boldsymbol{u}}_a$ and $\frac{\partial \mathcal{L}_r}{\partial \boldsymbol{r}}$. Thus, implementing an estimate $\hat{\boldsymbol{u}}_a$ of $\boldsymbol{u}_a$ instead of $\boldsymbol{u}_a$ itself no longer requires feedback of $\ddot{\boldsymbol{r}}$, and thus $\ddot{\bar{\boldsymbol{u}}}_u$.

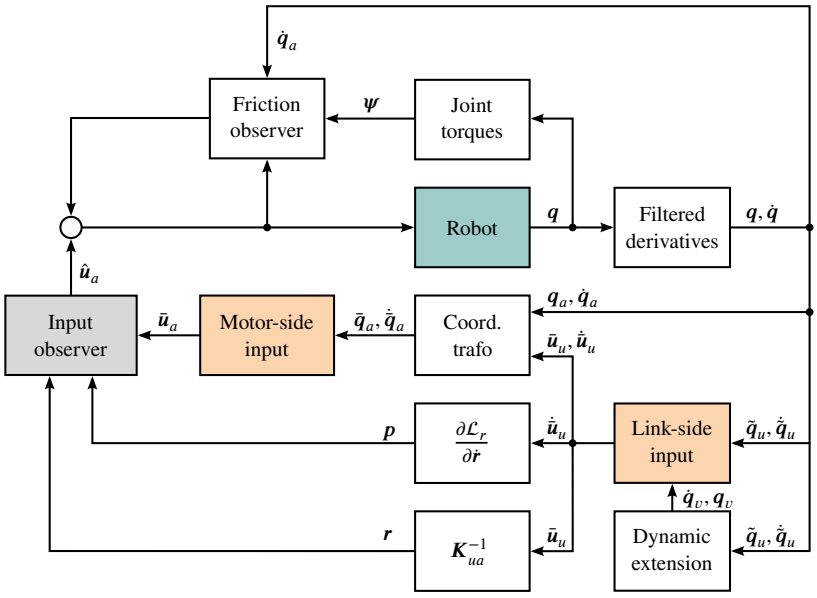

Figure A.4: Using a momentum observer to reduce the computational effort for implementing the input transformation.

Combining this observer based approach for estimating $\boldsymbol{u}_a$ with the dynamic extensions proposed in Chapter 9, results in controllers requiring measurements of only the positions and velocities $\boldsymbol{q}, \dot{\boldsymbol{q}}$. This is a significant advantage, since the model-based computation of $\ddot{\boldsymbol{q}}_u$ (and possibly $\boldsymbol{q}_u^{(3)}$), as introduced in Appendix B.2, is no longer required. Consequently, estimating the external forces $\mathcal{Q}_u'$ and $\dot{\mathcal{Q}}_u'$ becomes superfluous which greatly reduces the implementation effort of the input transformation. Block diagram in Fig. A.4 shows the implementation of the dynamics extension based designs in Chapter 9. Ironically, we circumvented the observer for $\mathcal{Q}_u'$ by introducing an observer for $\boldsymbol{u}_a$.

In order to test the applicability of the concept summarized in Fig. A.4, several experiments have been performed on a SEA testbed. The results reported in Chapter 11 confirm that the presented procedure is a valid strategy and produces satisfactory results in practice. Apart from the reduced computational effort, the presented procedure is particularly helpful when feedback of the acceleration and jerk must be avoided. Consider, for example, robotic systems with extremely low link inertias such as fingers or lightweight legs. In such case, the model based computation method reported in Appendix B.2 fails due to badly conditioned inertia matrices.

Remark A.2.1 If the original Lagrangian is not explicitly time-dependent. Explicit time dependency usually enters the Lagrangian in two ways: 1) if the system is subject to explicitly time-dependent constraints or 2) time-dependent forces.

A.3 Are the Virtual Coordinates not so Virtual After All?

This section introduces an interpretation of the virtual coordinates as non-inertial coordinates. The following discussion requires a comparison between reference systems (observers). Let S be an inertial reference frame and $\bar{S}$ a

non-inertial frame that is accelerating relative to S. Let us use the following convention: all quantities measured from $\bar{S}$ will be denoted by the same letters as the quantities measured in the inertial frame, but with a "bar". Consider the motion of two point masses m and b whose motions are constrained to one dimension. Let q_u and q_a denote their positions relative to S, and let F_u and F_a be the net forces on the masses m and b, respectively.

$$m\ddot{q}_u = F_u, \tag{A.18}$$

$$b\ddot{q}_a = F_a. \tag{A.19}$$

Suppose that $\bar{S}$ moves with velocity $\dot{r}$ and acceleration $\ddot{r}$ relative to S. The position of mass b in $\bar{S}$ is $\bar{q}_a$. Using the velocity addition rules of classical mechanics, the velocities of mass b observed from S and $\bar{S}$ are related by

$$\dot{q}_a = \dot{\bar{q}}_a + \dot{r}. \tag{A.20}$$

Differentiating with respect to time, we get

$$\ddot{q}_a = \ddot{\bar{q}}_a + \ddot{r}. \tag{A.21}$$

Multiplying both sides of (A.21) with b and replacing $b\ddot{q}_a$ with F_a gives

$$b\ddot{\bar{q}}_a = F_a - b\ddot{r}. \tag{A.22}$$

We see that the motion of mass b in an accelerating frame follows Newton's second law if we add an extra force $-b\ddot{r}$. This additional force is often referred to as an *apparent* or *fictitious* force. It is the same force that pushes us back in the driver seat when stepping on the gas.

Now suppose that the two masses m and b are interconnected by a spring satisfying Hook's law. Such scenario is indicated in Fig. A.5. Assume that both masses experience no other impressed force, but the spring force.

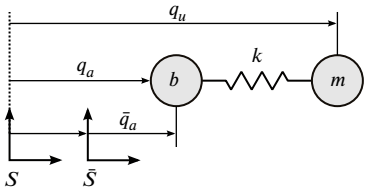

Figure A.5: Describing the motions of two points relative to an inertial reference frame with origin O and relative to an non-inertia reference frame with origin $\bar{O}$ which is in purely translational motion.

Then according to observer S the force acting on mass m evaluates to

$$F_u = k(q_a - q_u), \tag{A.23}$$

and according to observer $\bar{S}$ the force on mass b is

$$F_a = -k(\bar{q}_a + r - q_u). \tag{A.24}$$

Knowing that the forces on both ends of a massless spring are equal and in opposite directions, it follows that

$$F_u + F_a = 0. \tag{A.25}$$

Using (A.23)–(A.25) to replace the impressed forces in (A.18)–(A.19) gives

$$m\ddot{q}_u = \quad k(\bar{q}_a - q_u) + kr, \tag{A.26}$$

$$m\ddot{\bar{q}}_a = -k(\bar{q}_a - q_u) - b\ddot{r} - kr. \tag{A.27}$$

Now assume an extra impressed force u_a acting on mass b, then its equation of motion (A.27) becomes

$$m\ddot{\bar{q}}_a = -k(\bar{q}_a - q_u) - b\ddot{r} - kr + u_a. \tag{A.28}$$

Suppose that u_a is a control force that can be varied freely. Then, we can cancel the extra forces arising from observing the motion of mass b from an non-inertial frame and add a new control force $\bar{u}_a$ such that

$$u_a = b\ddot{r} + kr + \bar{u}_a, \tag{A.29}$$

and obtain

$$m\ddot{\bar{q}}_a = -k(\bar{q}_a - q_u) + \bar{u}_a. \tag{A.30}$$

Observing (A.26) and (A.30), we see that these equations have the form of Newton's second law, except for the additional force kr in (A.26) and for the fact that $\bar{q}_a$ is measured from a non-inertial frame.

Remark A.3.1 The cancellation of the forces $b\ddot{r}$ and kr through u_a means that any non-inertial observer residing with mass b will not experience any apparent forces. Canceling these two forces makes this observer feel the "same" force as if he was an inertial observer.

It is convenient to denote the extra force on mass m by

$$\bar{u}_u = kr. \tag{A.31}$$

Notice that no assumption on the relative motion between S and $\bar{S}$ has been made, apart from that $\bar{S}$ accelerates relative to S with acceleration $\ddot{r}$. Observing from (A.31) the one-to-one correspondence between the distance of S and $\bar{S}$ and the force $\bar{u}_u$, we will define $\ddot{r}$ as follows. Exploiting this property and observing from (A.23)–(A.25) that

$$F_u = \bar{u}_u + k(\bar{q}_a - q_u), \tag{A.32}$$

let us interpret (A.32) as a decomposition of F_u into a desired and undesired component such that

$$\begin{aligned} \bar{u}_u &\ldots \text{desired component of} F_u \\ k(\bar{q}_a - q_u) &\ldots \text{undesired compenent of } F_u \end{aligned}$$

Suppose that the desired component of F_u is well defined at any point in time, then this decomposition fixes the trajectory of $\bar{S}$ relative to S. It is worth remarking that the force error, $k(\bar{q}_a - q_u)$ would naturally tend to zero in the presence of dissipation, since both masses are rendered attracted by the spring.

In conclusion, we derived a quasi-fully actuated representation of a SEA by introducing a non-inertial reference frame $\bar{S}$ to describe the motion of the actuated mass b. The relative distance between S and $\bar{S}$ encodes the undesired component of the elastic force. The input transformation can be interpreted as cancellation of the apparent forces arising from the introduction of a non-inertial observer.

A.3.1 A Generalization to n Dimensions

For a SEA-based manipulator with n degrees of freedom—satisfying Spong's model—the motor inertias can be though of as $n/2$ *independent* point masses

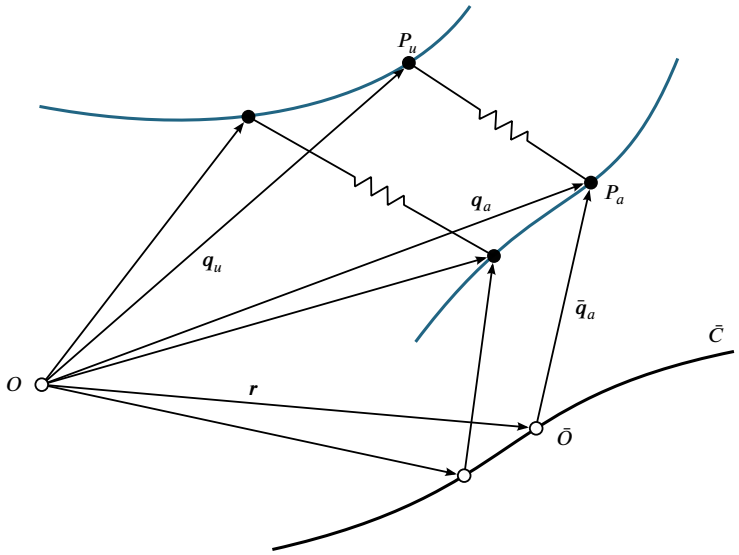

Figure A.6: Describing the motions of two points relative to an inertial reference frame with origin O and relative to an non-inertial reference frame with origin $\bar{O}$ which is in purely translational motion.

moving along one dimension each. However, there is a more elegant view based on geometric/kinematic considerations similar to the one dimensional case requiring the introduction of only one non-inertial reference frame.

Let us introduce the three kinematical quantities: the radius vector $\boldsymbol{q}_a$, the velocity $\dot{\boldsymbol{q}}_a$ and the acceleration $\ddot{\boldsymbol{q}}_a$ of a moving particle P_a with mass b, measured in an inertial and non-inertial frame S and $\bar{S}$, respectively. Now, assume that $\bar{S}$ is in purely translational motion. Following Lanczos [103], the translational motion of a reference frame can be characterized as follows. The origin $\bar{O}$ of a reference frame $\bar{S}$ moves along some given curve $\bar{C}$, traced out by the vector $\boldsymbol{r}$ originating in the origin O of S, as indicated in Fig. A.6. The radius vector $\boldsymbol{q}_a$ measured in S and the radius vector $\bar{\boldsymbol{q}}_a$ measured in $\bar{S}$ are in the following relation to each other

[103]: Lanczos (2020), *The Variational Principles of Mechanics*

$$\boldsymbol{q}_a = \boldsymbol{r} + \bar{\boldsymbol{q}}_a. \tag{A.33}$$

Differentiating (A.33) twice with respect to time, we obtain

$$\ddot{\boldsymbol{q}}_a = \ddot{\boldsymbol{r}} + \ddot{\bar{\boldsymbol{q}}}_a. \tag{A.34}$$

Without loss of generality, let us assume that $\boldsymbol{B} = \operatorname{diag}(b, \dots, b) > 0$.[1] Then, multiplying both sides with $\boldsymbol{B}$ gives

1: The justification is given in Remark A.3.2 below.

$$b\ddot{\boldsymbol{q}}_a = b\ddot{\boldsymbol{r}} + b\ddot{\bar{\boldsymbol{q}}}_a \tag{A.35}$$

Similarly to the case above, we see that whenever measurements are made relative to an non-inertial reference frame $\bar{S}$, the force of inertia is composed of two parts: the relative force of inertia $b\ddot{\bar{\boldsymbol{q}}}_a$ and the apparent force $b\ddot{\boldsymbol{r}}$.

Analogous to the single joint example above, we can now introduce a spring that connects the particle P_a with a point P_u with radius vector $\boldsymbol{q}_u$, see also Fig. A.6. According to Hook's law, the force exerted on P_a is

$$\boldsymbol{F}_a = -\boldsymbol{K}(\boldsymbol{q}_a - \boldsymbol{q}_u), \tag{A.36}$$

where $\boldsymbol{K}$ is some diagonal matrix containing the joint stiffness values. According to D'Alembert's principle the total virtual work of the impressed forces, augmented by the inertial forces vanishes for reversible displacements.

Applying this principle to the mass particle b subject to the impressed force $\boldsymbol{F}_a$, and considering that the "true" force of inertia and the force of inertia measured from $\bar{S}$ are related via (A.35), we get

$$b\ddot{\bar{\boldsymbol{q}}}_a = \boldsymbol{F}_a - b\ddot{\boldsymbol{r}}, \tag{A.37}$$

with the impressed force measured from $\bar{S}$ evaluating to

$$\boldsymbol{F}_a = -\boldsymbol{K}(\bar{\boldsymbol{q}}_a - \boldsymbol{q}_u) - \boldsymbol{K}\boldsymbol{r}. \tag{A.38}$$

We notice that the motion of our reference system $\bar{S}$ creates the forces $b\ddot{\boldsymbol{r}}$ and $\boldsymbol{K}\boldsymbol{r}$. The former is part of the inertia force (often referred to as apparent force) and the latter is part of the impressed force.

Now, suppose that P_u is the configuration point of the unactuated subsystem Σ_u of a SEA manipulator. It is worth remarking, that $\boldsymbol{F}_a$ is still well defined in this case since both radii vectors $\boldsymbol{q}_u$ and $\boldsymbol{q}_a$ are elements of the same $n/2$ dimensional vector space. As pointed out in Section 2.5.1, the force of inertia for Σ_u is

$$\boldsymbol{I}_u^\star = \frac{\mathrm{d}}{\mathrm{d}t}\frac{\partial \mathcal{T}_u}{\partial \dot{\boldsymbol{q}}_u} - \frac{\partial \mathcal{T}_u}{\partial \boldsymbol{q}_u}, \tag{A.39}$$

with the kinetic energy $\mathcal{T}_u$ as defined in (3.23). Thus, the equations of motion are.

$$\boldsymbol{I}_u^\star = -\boldsymbol{F}_a \tag{A.40}$$

Suppose that Σ_a is subject to an additional impressed force $\boldsymbol{u}_a$ with $n/2$ independent components. This allows canceling the forces arising from the motion of our reference system $\bar{S}$ with

$$\boldsymbol{u}_a = b\ddot{\boldsymbol{r}} + \boldsymbol{K}\boldsymbol{r} + \bar{\boldsymbol{u}}_a, \tag{A.41}$$

where $\bar{\boldsymbol{u}}_a$ can be considered as new control force. Introducing $\boldsymbol{I}_a^\star = b\dot{\bar{\boldsymbol{q}}}_a$ and $\bar{\boldsymbol{u}}_u = \boldsymbol{K}\boldsymbol{r}$, allows summarizing the resulting dynamics as

$$\boldsymbol{I}_u^\star = \quad \boldsymbol{K}(\bar{\boldsymbol{q}}_a - \boldsymbol{q}_u) + \bar{\boldsymbol{u}}_u, \tag{A.42}$$

$$\boldsymbol{I}_a^\star = -\boldsymbol{K}(\bar{\boldsymbol{q}}_a - \boldsymbol{q}_u) + \bar{\boldsymbol{u}}_a, \tag{A.43}$$

which is the familiar QFA representation of the original system.

Remark A.3.2 The assumption that P_a is a particle of mass b might appear difficult to bring in harmony with the observation that the motor inertias of a SEA manipulator can differ from joint to joint. This issue can be remedied by scaling the coordinates q_{ai} accordingly. In fact, without loss of generality, we can even assume that $b = 1$. Let the motor inertia matrix be $\boldsymbol{B} = \mathrm{diag}(b_1, \ldots, b_{n/2}) > 0$, then the $n/2$ generalized coordinates $\boldsymbol{\mu}_2$ univocally defined by $\boldsymbol{q}_a^{\mathrm{T}}\boldsymbol{B}\boldsymbol{q}_a = \boldsymbol{\mu}_a^{\mathrm{T}}\boldsymbol{\mu}_a$ have the desired property.

A.4 Conclusions

This chapter introduced a mechanical interpretation of the input transforming equations. Based on interpreting these equations as the EL equation of a multi-dimensional spring mass a system momentum observer was suggested to obtain an estimate of the actual control. This avoids feedback of the second order time derivative of the virtual link-side inputs which is required to implement the input transforming equations.

Moreover, it has been shown that by introducing a non-inertial reference frame to describe the motions of the non-actuated subsystem, the QFA representation emerges naturally (Section A.3). From this point of view, the input transforming equations can be interpreted as the cancellation of the *apparent* forces arising from introducing a non-inertial observer. This result shows that the virtual coordinates are observable and measurable quantities at least theoretically.

B

Supplementary Proofs and Arguments

B.1 On the Local Differential Flatness of the Considered Euler-Lagrange Systems

This section proofs that the class of systems specified in Section 5.1 is locally differentially flat for the special case $n_u = n_a$. This result is summarized in the corollary below.

Corollary B.1.1 (Local Differential Flatness of EL systems) *Consider an Euler-Lagrange system* (5.1) *satisfying Assumption 5.1.1 and 5.1.2. Then for the case $n_u = n_a$ it is locally differentially flat.*

We recall that a system is differentially flat if there exists a set of outputs (equal in number to the inputs) such that all states and inputs can be expressed in terms of these outputs and a finite number of their derivatives. Formally, a system with states $\boldsymbol{x} \in \mathbb{R}^n$, and inputs $\boldsymbol{u} \in \mathbb{R}^m$, is flat if there exist outputs $\boldsymbol{y} \in \mathbb{R}^m$ of them form [123]

[123]: Murray et al. (1995), "Differential flatness of mechanical control systems: A catalog of prototype systems"

$$\boldsymbol{y} = \boldsymbol{y}\left(\boldsymbol{x}, \boldsymbol{u}, \dot{\boldsymbol{u}}, \dots, \boldsymbol{u}^{(p)}\right), \tag{B.1}$$

such that

$$\boldsymbol{x} = \boldsymbol{x}\left(\boldsymbol{y}, \dot{\boldsymbol{y}}, \dots, \boldsymbol{y}^{(p)}\right), \tag{B.2}$$

$$\boldsymbol{u} = \boldsymbol{u}\left(\boldsymbol{y}, \dot{\boldsymbol{y}}, \dots, \boldsymbol{y}^{(p)}\right). \tag{B.3}$$

Proof of Corollary B.1.1. Introducing n_u functions $\Psi_i(\boldsymbol{q}_u, \dot{\boldsymbol{q}}_u, \ddot{\boldsymbol{q}}_u, \boldsymbol{q}_a)$, of $3n_u + n_a$ variables, we may write the dynamics of the primary subsystem (5.1) compactly as

$$\Psi_i(\boldsymbol{q}_u, \dot{\boldsymbol{q}}_u, \ddot{\boldsymbol{q}}_u, \boldsymbol{q}_a) = \frac{\mathrm{d}}{\mathrm{d}t}\frac{\partial \mathcal{T}_u}{\partial \dot{q}_{ui}} - \frac{\partial \mathcal{T}_u}{\partial q_{ui}} + \frac{\partial \mathcal{V}}{\partial q_{ui}} = \boldsymbol{0}, \quad i = 1, \dots, n_u. \tag{B.4}$$

Considering Assumption 5.1.2, the implicit function theorem assures that locally, near any point $\left(\boldsymbol{q}_u^0, \dot{\boldsymbol{q}}_u^0, \ddot{\boldsymbol{q}}_u^0, \boldsymbol{q}_a^0\right) \in \mathbb{R}^{3n_u+n_a}$, we may solve (B.4) for the q_{ai} in terms of the q_{ui} and their time derivatives

$$q_{ai} = h_i(\boldsymbol{q}_u, \dot{\boldsymbol{q}}_u, \ddot{\boldsymbol{q}}_u). \tag{B.5}$$

Further, the implicit function theorem assures that the functions h_i are two times continuously differentiable. Hence, we have that

$$\dot{q}_{a,i} = \sum_j \left[\frac{\partial h_i}{\partial q_{u,j}}\dot{q}_{u,j} + \frac{\partial h_i}{\partial \dot{q}_{u,j}}\ddot{q}_{u,j} + \frac{\partial h_i}{\partial \ddot{q}_{u,j}}q_{u,j}^{(3)}\right] \tag{B.6}$$

and

$$\ddot{q}_{a,i} = \sum_k \sum_j \Bigg(\frac{\partial}{\partial q_{u,k}} \left[\frac{\partial h_i}{\partial q_{u,j}} \right] \dot{q}_{u,j} \dot{q}_{u,k} + \frac{\partial}{\partial \dot{q}_{u,k}} \left[\frac{\partial h_i}{\partial q_{u,j}} \right] \dot{q}_{u,j} \ddot{q}_{u,k} + \frac{\partial}{\partial \ddot{q}_{u,k}} \left[\frac{\partial h_i}{\partial q_{u,j}} \right] \dot{q}_{u,j} q^{(3)}_{u,k} + \frac{\partial h_i}{\partial q_{u,j}} \ddot{q}_{u,j} + \cdots + \frac{\partial}{\partial \ddot{q}_{u,k}} \left[\frac{\partial h_i}{\partial \ddot{q}_{u,j}} \right] q^{(3)}_{u,j} q^{(3)}_{u,k} + \frac{\partial h_i}{\partial \ddot{q}_{u,j}} q^{(4)}_{u,j} \Bigg), \tag{B.7}$$

which shows that all states can be expressed in terms of the outputs and its derivatives. For convenience we repeat the dynamics of the secondary subsystem

$$\frac{\mathrm{d}}{\mathrm{d}t} \frac{\partial \mathcal{T}_a}{\partial \dot{q}_{ai}} - \frac{\partial \mathcal{T}_a}{\partial q_{ai}} + \frac{\partial \mathcal{V}}{\partial q_{ai}} = u_{ai}(t), \quad i = 1, \dots, n_a. \tag{B.8}$$

Clearly, by making the substitutions (B.5)–(B.7) and (B.8), the input $\boldsymbol{u}_a$ can be written in terms of the outputs and its derivatives, which completes the proof. ■

B.2 On the Acceleration and Jerk Signals of the Unactuated Subsystem

Many the presented concepts rely on the availability of the acceleration (and jerk) of the non-actuated subsystem Σ_u. This section discusses the drawbacks and challenges connected with providing these signals. Considering the class of EL systems specified in Section 5.1, we can split the equations of motions (5.1) into (5.65) and (5.66). Knowing that

$$\frac{\mathrm{d}}{\mathrm{d}t} \left[\frac{\partial \mathcal{L}_u}{\partial \dot{\boldsymbol{q}}_u} \right] = \left[\frac{\partial^2 \mathcal{L}_u}{\partial \dot{\boldsymbol{q}}_u^2} \right] \ddot{\boldsymbol{q}}_u + \left[\frac{\partial^2 \mathcal{L}_u}{\partial \boldsymbol{q}_u \partial \dot{\boldsymbol{q}}_u} \right] \dot{\boldsymbol{q}}_u, \tag{B.9}$$

we can make the substitution (5.65) and (B.9) to obtain

$$\begin{aligned} \ddot{\boldsymbol{q}}_u &= \left[\frac{\partial^2 \mathcal{L}_u}{\partial \dot{\boldsymbol{q}}_u^2} \right]^{-1} \boldsymbol{\gamma}(\boldsymbol{q}, \dot{\boldsymbol{q}}), \\ \gamma &= \left\{ \frac{\partial \mathcal{L}_u}{\partial \boldsymbol{q}_u} + \frac{\partial \mathcal{L}_a}{\partial \boldsymbol{q}_u} - \left[\frac{\partial^2 \mathcal{L}_u}{\partial \boldsymbol{q}_u \partial \dot{\boldsymbol{q}}_u} \right] \dot{\boldsymbol{q}}_u + \mathcal{Q}'_u \right\}, \end{aligned} \tag{B.10}$$

where the invertibility of the inertia matrix is ensured by Assumption 5.1.1. Deriving (B.10) with respect to time gives

$$\boldsymbol{q}_u^{(3)} = \left[\frac{\partial^2 \mathcal{L}_u}{\partial \dot{\boldsymbol{q}}_u^2} \right]^{-1} \dot{\boldsymbol{\gamma}}(\boldsymbol{q}, \dot{\boldsymbol{q}}) + \frac{\mathrm{d}}{\mathrm{d}t} \left[\frac{\partial^2 \mathcal{L}_u}{\partial \dot{\boldsymbol{q}}_u^2} \right]^{-1} \boldsymbol{\gamma}(\boldsymbol{q}, \dot{\boldsymbol{q}}). \tag{B.11}$$

From (B.10) and (B.11) it is clear that computing the acceleration and jerk signal requires only knowledge of $(\boldsymbol{q}, \dot{\boldsymbol{q}})$ and $\mathcal{Q}'_u$.[1]

1: Notice that making the substitution (B.10) and (B.11) removes the acceleration dependency of the RHS expression of (B.11).

Given that the inertia matrix $\partial^2 \mathcal{L}_u / \partial \dot{\boldsymbol{q}}_u^2$ is at least twice continuously differentiable and given that $\boldsymbol{q}_u$ is bounded, the tensors $D_{\boldsymbol{q}_u}(\partial^2 \mathcal{L}_u / \partial \dot{\boldsymbol{q}}_u^2)$ and $D^2_{\boldsymbol{q}_u}(\partial^2 \mathcal{L}_u / \partial \dot{\boldsymbol{q}}_u^2)$ are bounded. In addition, the minimum singular value of

$\partial^2 \mathcal{L}_u / \partial \dot{\boldsymbol{q}}_u^2$ is bounded away from zero. Further, given that the potential energy $\mathcal{V}(\boldsymbol{q})$ is twice continuously differentiable and suppose that $\mathcal{Q}_u, \dot{\mathcal{Q}}_u$ are bounded, then $\ddot{\boldsymbol{q}}_u, \boldsymbol{q}_u^{(3)}$ are continuous functions of $\boldsymbol{q}, \dot{\boldsymbol{q}}$ and, according to the boundedness theorem, bounded for bounded $\boldsymbol{q}, \dot{\boldsymbol{q}}$.

It is worth remarking that $\boldsymbol{q}_u^{(3)}$ grows unbounded for external disturbance signals $\mathcal{Q}_u'$ approaching a step-like time behavior. More precisely, if $\dot{\mathcal{Q}}_u$ grows unbounded so will $\boldsymbol{q}_u^{(3)}$. Thus, in situations where Σ_u is subject to harsh impacts the feedback of the jerk signals easily causes input saturation. This aspect is of particular importance for robots with low natural frequencies ω_i since the jerk feedback contained in $\ddot{\tilde{\boldsymbol{u}}}_i$ is scaled by ω_i^2. This matter is analyzed in detail in Chapter 9.

Remark B.2.1 On most robotic systems, only (angular) positions are directly measured through sensors. Velocity signals are usually computed via a derivative filters. For DLR David, e.g., we employ a standard fourth order derivative filter with a cut-off frequency at 80 Hz to obtain motor and link velocity signals. Using these position and velocity signals allows the computation of the link acceleration and jerk signals via (B.10) and (B.11). At the DLR, we utilize this method for implementing the ESP controllers [86, 92, 94, 114] on David, Bert and C-Runner. Concerning the implementation of ESPi controllers, we improve the fidelity of these calculations by employing a momentum based observer [34] to estimate the external torques, $\mathcal{Q}_u$, and their time-derivatives. This aspect is critical for the following reason. The equilibrium position of Σ is determined by the interplay of $\mathcal{Q}_u$ and the implemented link-side stiffness $\mathcal{K}_{pu}$. The implementation of a link-side spring, however, requires the feedback of the terms $\mathcal{K}_{pu}\tilde{\boldsymbol{q}}$ and $\mathcal{K}_{pu}\ddot{\tilde{\boldsymbol{q}}}$. This fact is particularly obvious for ASRs with linear elastic elements as discussed in Section B.5. Thus, the fidelity of the link acceleration signals affects the equilibrium of the closed-loop system.

[86]: Keppler et al. (2018), "Elastic structure preserving (ESP) control for compliantly actuated robots"
[92]: Keppler et al. (2018), "Elastic structure preserving impedance (ESPi) control for compliantly actuated robots"
[94]: Keppler et al. (2018), "Visco-elastic structure preserving impedance (VESPi) control for compliantly actuated robots"
[114]: Meng et al. (2021), "Elastic structure preserving impedance control of bidirectional antagonistic variable stiffness actuation"

B.3 A One-to-one Correspondance

$$D\boldsymbol{\alpha}(\boldsymbol{x}) = \frac{\partial \alpha_i}{\partial x_j} = \left[\begin{array}{c|c|c|c|c} \frac{\partial \boldsymbol{q}_u}{\partial \boldsymbol{q}_u} & \frac{\partial \boldsymbol{q}_u}{\partial \boldsymbol{q}_a} & \frac{\partial \boldsymbol{q}_u}{\partial \dot{\boldsymbol{q}}_u} & \frac{\partial \boldsymbol{q}_u}{\partial \dot{\boldsymbol{q}}_a} & \frac{\partial \boldsymbol{q}_u}{\partial t} \\ \frac{\partial \boldsymbol{\psi}}{\partial \boldsymbol{q}_u} & \frac{\partial \boldsymbol{\psi}}{\partial \boldsymbol{q}_a} & \frac{\partial \boldsymbol{\psi}}{\partial \dot{\boldsymbol{q}}_u} & \frac{\partial \boldsymbol{\psi}}{\partial \dot{\boldsymbol{q}}_a} & \frac{\partial \boldsymbol{\psi}}{\partial t} \\ \hline \frac{\partial \dot{\boldsymbol{q}}_u}{\partial \boldsymbol{q}_u} & \frac{\partial \dot{\boldsymbol{q}}_u}{\partial \boldsymbol{q}_a} & \frac{\partial \dot{\boldsymbol{q}}_u}{\partial \dot{\boldsymbol{q}}_u} & \frac{\partial \dot{\boldsymbol{q}}_u}{\partial \dot{\boldsymbol{q}}_a} & \frac{\partial \dot{\boldsymbol{q}}_u}{\partial t} \\ \frac{\partial \dot{\boldsymbol{\psi}}}{\partial \boldsymbol{q}_u} & \frac{\partial \dot{\boldsymbol{\psi}}}{\partial \boldsymbol{q}_a} & \frac{\partial \dot{\boldsymbol{\psi}}}{\partial \dot{\boldsymbol{q}}_u} & \frac{\partial \dot{\boldsymbol{\psi}}}{\partial \dot{\boldsymbol{q}}_a} & \frac{\partial \dot{\boldsymbol{\psi}}}{\partial t} \\ \hline \frac{\partial t}{\partial \boldsymbol{q}_u} & \frac{\partial t}{\partial \boldsymbol{q}_a} & \frac{\partial t}{\partial \dot{\boldsymbol{q}}_u} & \frac{\partial t}{\partial \dot{\boldsymbol{q}}_u} & \frac{\partial t}{\partial t} \end{array}\right],$$

$$|D\boldsymbol{\alpha}(\boldsymbol{x})| = \begin{vmatrix} \boldsymbol{I} & \boldsymbol{0} & \boldsymbol{0} \\ \frac{\partial \boldsymbol{\psi}}{\partial \boldsymbol{q}_u} & \frac{\partial \boldsymbol{\psi}}{\partial \boldsymbol{q}_a} & \boldsymbol{0} \\ \boldsymbol{0} & \boldsymbol{0} & 1 \end{vmatrix} \begin{vmatrix} \boldsymbol{I} & \boldsymbol{0} \\ \frac{\partial \boldsymbol{\psi}}{\partial \boldsymbol{q}_u} & \frac{\partial \boldsymbol{\psi}}{\partial \boldsymbol{q}_a} \end{vmatrix} = \begin{vmatrix} \boldsymbol{I} & \boldsymbol{0} \\ \frac{\partial \boldsymbol{\psi}}{\partial \boldsymbol{q}_a} & \frac{\partial \boldsymbol{\psi}}{\partial \boldsymbol{q}_u} \end{vmatrix}^2 = \left| \frac{\partial \boldsymbol{\psi}}{\partial \boldsymbol{q}_a} \right|^2 \tag{B.12}$$

where the last equality can be shown through repeated cofactor expansion along the first row. Proceeding analogously to the steps above, and further

considering that $\partial_{\dot{\boldsymbol{q}}_a}\boldsymbol{\delta} = \mathbf{0}$, we obtain

$$
\begin{aligned}
D\boldsymbol{\beta}(\boldsymbol{x}) = \frac{\partial \beta_i}{\partial x_j} &= \left[\begin{array}{c|c} \boldsymbol{A} & \boldsymbol{B} \\ \hline \boldsymbol{C} & \boldsymbol{D} \end{array}\right] \\
&= \left[\begin{array}{ccc|cc}
\frac{\partial \boldsymbol{q}_u}{\partial \boldsymbol{q}_u} & \frac{\partial \boldsymbol{q}_u}{\partial \boldsymbol{q}_a} & \frac{\partial \boldsymbol{q}_u}{\partial \dot{\boldsymbol{q}}_u} & \frac{\partial \boldsymbol{q}_u}{\partial \dot{\boldsymbol{q}}_a} & \frac{\partial \boldsymbol{q}_u}{\partial t} \\
\partial_{\boldsymbol{q}_u}(\boldsymbol{\psi} - \bar{\boldsymbol{u}}_u) & \frac{\partial \boldsymbol{\psi}}{\partial \boldsymbol{q}_a} & \partial_{\dot{\boldsymbol{q}}_u}(\boldsymbol{\psi} - \bar{\boldsymbol{u}}_u) & \frac{\partial \boldsymbol{\psi}}{\partial \dot{\boldsymbol{q}}_a} & \partial_t(\boldsymbol{\psi} - \bar{\boldsymbol{u}}_u) \\
\frac{\partial \dot{\boldsymbol{q}}_u}{\partial \boldsymbol{q}_u} & \frac{\partial \dot{\boldsymbol{q}}_u}{\partial \boldsymbol{q}_a} & \frac{\partial \dot{\boldsymbol{q}}_u}{\partial \dot{\boldsymbol{q}}_u} & \frac{\partial \dot{\boldsymbol{q}}_u}{\partial \dot{\boldsymbol{q}}_a} & \frac{\partial \dot{\boldsymbol{q}}_u}{\partial t} \\
\hline
\partial_{\boldsymbol{q}_u}(\dot{\boldsymbol{\psi}} - \boldsymbol{\delta}) & \partial_{\boldsymbol{q}_a}(\dot{\boldsymbol{\psi}} - \boldsymbol{\delta}) & \partial_{\dot{\boldsymbol{q}}_u}(\dot{\boldsymbol{\psi}} - \boldsymbol{\delta}) & \partial_{\dot{\boldsymbol{q}}_a}(\dot{\boldsymbol{\psi}} - \boldsymbol{\delta}) & \partial_t(\dot{\boldsymbol{\psi}} - \boldsymbol{\delta}) \\
\frac{\partial t}{\partial \boldsymbol{q}_u} & \frac{\partial t}{\partial \boldsymbol{q}_a} & \frac{\partial t}{\partial \dot{\boldsymbol{q}}_u} & \frac{\partial t}{\partial \dot{\boldsymbol{q}}_u} & \frac{\partial t}{\partial t}
\end{array}\right] \\
&= \left[\begin{array}{ccc|cc}
\boldsymbol{I} & \mathbf{0} & \frac{\partial \boldsymbol{q}_u}{\partial \dot{\boldsymbol{q}}_u} & \mathbf{0} & \mathbf{0} \\
\partial_{\boldsymbol{q}_u}(\boldsymbol{\psi} - \bar{\boldsymbol{u}}_u) & \frac{\partial \boldsymbol{\psi}}{\partial \boldsymbol{q}_a} & \partial_{\dot{\boldsymbol{q}}_u}(\boldsymbol{\psi} - \bar{\boldsymbol{u}}_u) & \mathbf{0} & \partial_t(\boldsymbol{\psi} - \bar{\boldsymbol{u}}_u) \\
\mathbf{0} & \mathbf{0} & \boldsymbol{I} & \mathbf{0} & \mathbf{0} \\
\hline
\partial_{\boldsymbol{q}_u}(\dot{\boldsymbol{\psi}} - \boldsymbol{\delta}) & \partial_{\boldsymbol{q}_a}(\dot{\boldsymbol{\psi}} - \boldsymbol{\delta}) & \partial_{\dot{\boldsymbol{q}}_u}(\dot{\boldsymbol{\psi}} - \boldsymbol{\delta}) & \partial_{\dot{\boldsymbol{q}}_a}(\dot{\boldsymbol{\psi}} - \boldsymbol{\delta}) & \partial_t(\dot{\boldsymbol{\psi}} - \boldsymbol{\delta}) \\
\mathbf{0} & \mathbf{0} & \mathbf{0} & \mathbf{0} & 1
\end{array}\right],
\end{aligned}
$$

According to Schur's determinant identity, we have that

$$|D\boldsymbol{\beta}(\boldsymbol{x})| = |\boldsymbol{D}|\,|\boldsymbol{A} - \boldsymbol{B}\boldsymbol{D}^{-1}\boldsymbol{C}|,$$

where

$$\boldsymbol{D}^{-1} = \begin{bmatrix} \frac{\partial \boldsymbol{\psi}}{\partial \boldsymbol{q}_a}^{-1} & -\frac{\partial \boldsymbol{\psi}}{\partial \boldsymbol{q}_a}\partial_t(\dot{\boldsymbol{\psi}} - \boldsymbol{\delta}) \\ \mathbf{0} & 1 \end{bmatrix}, \tag{B.13}$$

Using (B.13), it is straightforward to show that $\boldsymbol{B}\boldsymbol{D}^{-1}\boldsymbol{C} = \mathbf{0}$ such that

$$|D\boldsymbol{\beta}(\boldsymbol{x})| = |\boldsymbol{D}|\,|\boldsymbol{A}|,$$

where

$$|\boldsymbol{D}| = |\partial_{\dot{\boldsymbol{q}}_a}(\dot{\boldsymbol{\psi}} - \boldsymbol{\delta})|\,|1| = |\partial_{\boldsymbol{q}_a}\boldsymbol{\psi}|,$$

and after repeated cofactor expansion along the first row, we get after n_u steps

$$|\partial_{\dot{\boldsymbol{q}}_a}(\dot{\boldsymbol{\psi}} - \boldsymbol{\delta})|\,|1| = |\partial_{\boldsymbol{q}_a}\boldsymbol{\psi}|.$$

Repeated cofactor expansion along the first row of the remaining matrix gives after n_u steps

$$|\boldsymbol{A}| = \begin{vmatrix} \boldsymbol{I} & \mathbf{0} & \mathbf{0} \\ \partial_{\boldsymbol{q}_u}(\boldsymbol{\psi} - \bar{\boldsymbol{u}}_u) & \frac{\partial \boldsymbol{\psi}}{\partial \boldsymbol{q}_a} & \mathbf{0} \\ \mathbf{0} & \mathbf{0} & \boldsymbol{I} \end{vmatrix} = \begin{vmatrix} \boldsymbol{I} & \mathbf{0} \\ \partial_{\boldsymbol{q}_u}(\boldsymbol{\psi} - \bar{\boldsymbol{u}}_u) & \frac{\partial \boldsymbol{\psi}}{\partial \boldsymbol{q}_a} \end{vmatrix} = \underbrace{1 \cdot \ldots \cdot 1}_{n_u} \cdot \left|\frac{\partial \boldsymbol{\psi}}{\partial \boldsymbol{q}_a}\right| = \left|\frac{\partial \boldsymbol{\psi}}{\partial \boldsymbol{q}_a}\right|.$$

$$|D\boldsymbol{\beta}(\boldsymbol{x})| = |\boldsymbol{D}|\,|\boldsymbol{A}| = \left|\frac{\partial \boldsymbol{\psi}}{\partial \boldsymbol{q}_a}\right|^2. \tag{B.14}$$

B.4 Proof ad Impedance Control

The closed-loop dynamics is

$$\Sigma^*: \frac{\mathrm{d}}{\mathrm{d}t}\frac{\partial \mathcal{T}}{\partial \dot{\bar{\boldsymbol{q}}}} - \frac{\partial \mathcal{T}}{\partial \bar{\boldsymbol{q}}} = -\frac{\partial \mathcal{V}_2}{\partial \bar{\boldsymbol{q}}} - \mathcal{K}_p(\bar{\boldsymbol{q}} - \bar{\boldsymbol{q}}^*) - \mathcal{K}_v\dot{\bar{\boldsymbol{q}}} + \bar{\mathcal{Q}}' = -\frac{\partial \mathcal{V}^*}{\partial \bar{\boldsymbol{q}}} + \bar{\mathcal{Q}}^* \tag{B.15}$$

with $\mathcal{V}^*(\bar{\boldsymbol{q}}) \triangleq \mathcal{V}_2(\bar{\boldsymbol{q}}_u - \bar{\boldsymbol{q}}_a) + \mathcal{V}_p(\boldsymbol{q}_u - \boldsymbol{q}_u^*)$, $\mathcal{Q}^* \triangleq -\mathcal{K}_v\dot{\bar{\boldsymbol{q}}} + \bar{\mathcal{Q}}'$. Introducing $\mathcal{L}^*(\bar{\boldsymbol{q}}, \dot{\bar{\boldsymbol{q}}}) \triangleq \mathcal{T}(\bar{\boldsymbol{q}}, \dot{\bar{\boldsymbol{q}}}) - \mathcal{V}^*(\bar{\boldsymbol{q}})$, we can rewrite

$$\frac{\mathrm{d}}{\mathrm{d}t}\frac{\partial \mathcal{L}^*}{\partial \dot{\bar{\boldsymbol{q}}}} - \frac{\partial \mathcal{L}^*}{\partial \bar{\boldsymbol{q}}} = -\mathcal{K}_v\dot{\bar{\boldsymbol{q}}} + \bar{\mathcal{Q}}', \tag{B.16}$$

Using

$$\mathcal{V}^0(\bar{\boldsymbol{q}}) \triangleq \mathcal{V}^*(\bar{\boldsymbol{q}}) + \bar{\boldsymbol{q}}^{\mathrm{T}}\bar{\mathcal{Q}}', \tag{B.17}$$

then (B.15) becomes

$$\frac{\mathrm{d}}{\mathrm{d}t}\frac{\partial \mathcal{T}}{\partial \dot{\bar{\boldsymbol{q}}}} - \frac{\partial \mathcal{T}}{\partial \bar{\boldsymbol{q}}} = -\frac{\partial \mathcal{V}^0}{\partial \bar{\boldsymbol{q}}} - \mathcal{K}_v\dot{\bar{\boldsymbol{q}}} \equiv \frac{\mathrm{d}}{\mathrm{d}t}\frac{\partial \mathcal{L}^0}{\partial \dot{\bar{\boldsymbol{q}}}} - \frac{\partial \mathcal{L}^0}{\partial \bar{\boldsymbol{q}}} = -\mathcal{K}_v\dot{\bar{\boldsymbol{q}}}. \tag{B.18}$$

Let $\bar{\boldsymbol{q}}^0 = (\bar{\boldsymbol{q}}_u^0, \bar{\boldsymbol{q}}_a^0)$ be the solution to

$$\frac{\partial \mathcal{V}_0}{\partial \bar{\boldsymbol{q}}} = \begin{bmatrix} \frac{\partial \mathcal{V}^0}{\partial \bar{\boldsymbol{q}}_u} \\ \frac{\partial \mathcal{V}^0}{\partial \bar{\boldsymbol{q}}_a} \end{bmatrix} = \begin{bmatrix} \frac{\partial \mathcal{V}^*}{\partial \bar{\boldsymbol{q}}_u} - \bar{\mathcal{Q}}'_u \\ \frac{\partial \mathcal{V}^*}{\partial \bar{\boldsymbol{q}}_a} - \bar{\mathcal{Q}}'_a \end{bmatrix} = \begin{bmatrix} \frac{\partial \mathcal{V}_2}{\partial \bar{\boldsymbol{q}}_u} + \frac{\partial \mathcal{V}_p}{\partial \bar{\boldsymbol{q}}} - \mathcal{Q}'_u \\ \frac{\partial \mathcal{V}_2}{\partial \bar{\boldsymbol{q}}_a} \end{bmatrix} = 0. \tag{B.19}$$

The last n_a rows of (B.19) imply that

$$\begin{aligned} \frac{\partial \mathcal{V}_2}{\partial \bar{\boldsymbol{q}}_a} = \boldsymbol{0} \Rightarrow \frac{\partial \mathcal{V}_2}{\partial \bar{\boldsymbol{q}}_u} = \boldsymbol{0} \Rightarrow \frac{\partial \mathcal{V}_p}{\partial \bar{\boldsymbol{q}}_u} - \mathcal{Q}'_u = \mathcal{K}_{pu}\left(\bar{\boldsymbol{q}}_u - \bar{\boldsymbol{q}}_u^*\right) - \mathcal{Q}'_u \\ \iff \mathcal{K}_{pu}\left(\bar{\boldsymbol{q}}_u - \bar{\boldsymbol{q}}_u^*\right) = \mathcal{Q}'_u \\ \iff \bar{\boldsymbol{q}}_u = \bar{\boldsymbol{q}}_u^* + \mathcal{K}_{pu}^{-1}\mathcal{Q}'_u = \bar{\boldsymbol{q}}_u^0 = \bar{\boldsymbol{q}}_a^0 \end{aligned} \tag{B.20}$$

Introduce deflection from equilibrium position $\bar{\boldsymbol{q}}^0$

$$\tilde{\boldsymbol{q}} \triangleq \bar{\boldsymbol{q}} - \bar{\boldsymbol{q}}^0 \tag{B.21}$$

and applying (B.21) to (B.18) yields

$$\frac{\mathrm{d}}{\mathrm{d}t}\frac{\partial \mathcal{L}^0}{\partial \dot{\tilde{\boldsymbol{q}}}} - \frac{\partial \mathcal{L}^0}{\partial \tilde{\boldsymbol{q}}} = -\mathcal{K}_v\dot{\tilde{\boldsymbol{q}}}, \tag{B.22}$$

where $\mathcal{L}^0$ is evaluated as a function of $(\tilde{\boldsymbol{q}}, \dot{\tilde{\boldsymbol{q}}})$ through (B.8), i.e. $\mathcal{L}^0\left(\bar{\boldsymbol{q}}(\tilde{\boldsymbol{q}}), \dot{\bar{\boldsymbol{q}}}(\tilde{\boldsymbol{q}})\right)$. Introducing the Lagrangian function

$$\tilde{\mathcal{L}}\left(\tilde{\boldsymbol{q}}, \dot{\tilde{\boldsymbol{q}}}\right) = \tilde{\mathcal{T}}(\tilde{\boldsymbol{q}}, \dot{\tilde{\boldsymbol{q}}}) - \tilde{\mathcal{V}}(\tilde{\boldsymbol{q}}) = \mathcal{L}^0\left(\bar{\boldsymbol{q}}(\tilde{\boldsymbol{q}}), \dot{\bar{\boldsymbol{q}}}(\tilde{\boldsymbol{q}})\right), \tag{B.23}$$

where the new potential function

$$\tilde{\mathcal{V}}(\tilde{\boldsymbol{q}}) = \mathcal{V}^0\left(\bar{\boldsymbol{q}}(\tilde{\boldsymbol{q}})\right) = \mathcal{V}^0(\tilde{\boldsymbol{q}} + \boldsymbol{q}^0), \tag{B.24}$$

is positive definite w.r.t. $\tilde{\boldsymbol{q}}$. Considering Corollary 6.1.2, it is clear that $\tilde{\mathcal{H}}(\tilde{\boldsymbol{q}}, \dot{\tilde{\boldsymbol{q}}}) \triangleq \sum_i \dot{\tilde{q}}_i \frac{\partial \tilde{\mathcal{L}}}{\partial \dot{\tilde{q}}_i} - \tilde{\mathcal{L}}$ qualifies as the function V since

$$\frac{\mathrm{d}}{\mathrm{d}t}\tilde{\mathcal{H}} = -\dot{\tilde{\boldsymbol{q}}}^{\mathrm{T}} \mathcal{K}_v \dot{\tilde{\boldsymbol{q}}}. \tag{B.25}$$

B.5 On the Smoothness Condition on the Virtual Inputs

It is important to notice that the challenge regarding link-side damping injection does not arise from limitations of the ESPi framework, we used for analysis here. In fact, these limitations are a manifestation of the mechanical bandwidth limitation of an elastic joint [153]. To support this statement, let us consider one of the most straightforward ways to implement a link-side damping term on an flexible joint robot satisfying the Spong model. Let $\bar{\boldsymbol{u}}_u$ be the desired elastic joint torque and $\boldsymbol{e} \triangleq \boldsymbol{\psi} - \bar{\boldsymbol{u}}_u$ the joint torque error. Then, choosing $\bar{\boldsymbol{u}}_u = \boldsymbol{K}_{vu}\dot{\boldsymbol{q}}_u$ the joint torque tracking controller [140]

$$\boldsymbol{u} = \boldsymbol{\Omega}^{-2}\ddot{\bar{\boldsymbol{u}}}_u + \bar{\boldsymbol{u}}_u - \boldsymbol{\Omega}^{-2}\left(\boldsymbol{D}_e\dot{\boldsymbol{e}} + \boldsymbol{K}_e\boldsymbol{e}\right) + \boldsymbol{B}\ddot{\boldsymbol{q}}, \tag{B.26}$$

achieves global asymptotic convergence $\boldsymbol{\psi} \to \bar{\boldsymbol{u}}_u$ for $t \to \infty$ and a link-side damping behavior. Notice that (B.26) reveals the feedback necessity of the link jerks.[2]. The joint torque bandwidth limitations of a soft actuators requires that the desired joint torque is sufficiently smooth such that $\boldsymbol{u}$ is bounded, which is equivalent to requiring that the virtual input $\bar{\boldsymbol{u}}_u$ and $\ddot{\bar{\boldsymbol{u}}}_u$ are bounded. In conclusion, the smoothness constraint on the virtual input arises naturally from the physical limitations of an ASR.

2: Interestingly, the jerk signal enters the controller through the same term, $\boldsymbol{\Omega}^{-2}\ddot{\bar{\boldsymbol{u}}}_u$, as is the case for the ESP based controllers reported in Chapter 9.

B.6 The Input Transformation for Monoarticular ASRs

In the following, we shall evaluate the components of the input transformation (5.155) in detail. Using

$$\left[\boldsymbol{Y}\right]_q = \frac{\partial^2 \mathcal{L}_a}{\partial \boldsymbol{q}_a \partial \boldsymbol{q}_u} = -\frac{\partial^2}{\partial \boldsymbol{q}_a \partial \boldsymbol{q}_u}\left[\mathcal{V}_g + \mathcal{V}_e\right] = -\frac{\partial}{\partial \boldsymbol{q}_a}\left[\frac{\partial \mathcal{V}_e}{\partial \boldsymbol{\varphi}}\frac{\partial \boldsymbol{\varphi}}{\partial \boldsymbol{q}_u}\right] = \frac{\partial^2 \mathcal{V}_e}{\partial \boldsymbol{\varphi}^2}, \tag{B.27}$$

$$\left[\bar{\boldsymbol{Y}}\right]_{\bar{q}} = \frac{\partial^2 \bar{\mathcal{L}}_a}{\partial \bar{\boldsymbol{q}}_a \partial \bar{\boldsymbol{q}}_u} = -\frac{\partial^2}{\partial \bar{\boldsymbol{q}}_a \partial \bar{\boldsymbol{q}}_u}\left[\mathcal{V}_g + \bar{\mathcal{V}}_e\right] = -\frac{\partial}{\partial \bar{\boldsymbol{q}}_a}\left[\frac{\partial \bar{\mathcal{V}}_e}{\partial \bar{\boldsymbol{\varphi}}}\frac{\partial \bar{\boldsymbol{\varphi}}}{\partial \bar{\boldsymbol{q}}_u}\right] = \frac{\partial^2 \bar{\mathcal{V}}_e}{\partial \bar{\boldsymbol{\varphi}}^2}, \tag{B.28}$$

$$\left[\boldsymbol{X}\right]_q = \frac{\partial^2 \mathcal{L}_a}{\partial \boldsymbol{q}_u^2} = -\frac{\partial^2}{\partial \boldsymbol{q}_u^2}\left[\mathcal{V}_g + \mathcal{V}_e\right] = -\frac{\partial^2 \mathcal{V}_g}{\partial \boldsymbol{q}_u^2} - \frac{\partial^2 \mathcal{V}_e}{\partial \boldsymbol{\varphi}^2}, \tag{B.29}$$

$$\left[\bar{\boldsymbol{X}}\right]_{\bar{q}} = \frac{\partial^2 \bar{\mathcal{L}}_a}{\partial \bar{\boldsymbol{q}}_u^2} = -\frac{\partial^2}{\partial \bar{\boldsymbol{q}}_u^2}\left[\mathcal{V}_g + \bar{\mathcal{V}}_e\right] = -\frac{\partial^2 \mathcal{V}_g}{\partial \bar{\boldsymbol{q}}_u^2} - \frac{\partial^2 \bar{\mathcal{V}}_e}{\partial \bar{\boldsymbol{\varphi}}^2}, \tag{B.30}$$

and

$$\begin{aligned}
\frac{\partial}{\partial t}\left[\frac{\partial \bar{\mathcal{V}}}{\partial \bar{\boldsymbol{q}}_u}\right]_{\bar{q}} =& \frac{\partial}{\partial t}\left[\frac{\partial \bar{\mathcal{V}}_e}{\partial \bar{\boldsymbol{\varphi}}}\frac{\partial \bar{\boldsymbol{\varphi}}}{\partial \bar{\boldsymbol{q}}_u}\right] = -\frac{\partial}{\partial t}\boldsymbol{\psi}\left(\bar{\boldsymbol{q}}_a - \bar{\boldsymbol{q}}_u + \boldsymbol{q}_u^*(t)\right) = \frac{\partial \boldsymbol{\psi}}{\partial \bar{\boldsymbol{\varphi}}}\frac{\partial \bar{\boldsymbol{\varphi}}}{\partial t},\\
=& \frac{\partial \boldsymbol{\psi}}{\partial \bar{\boldsymbol{\varphi}}}\frac{\partial \bar{\boldsymbol{\varphi}}}{\partial \boldsymbol{q}_u^*}\frac{\partial \boldsymbol{q}_u^*}{\partial t} = \frac{\partial^2 \boldsymbol{\psi}}{\partial \bar{\boldsymbol{\varphi}}^2}\dot{\boldsymbol{q}}_u^* = \frac{\partial^2 \bar{\mathcal{V}}_e}{\partial \bar{\boldsymbol{\varphi}}^2}\dot{\boldsymbol{q}}_u^*,\\
\left[\frac{\partial^2 \mathcal{L}_a}{\partial \dot{\boldsymbol{q}}_a^2}\right]_q =& \boldsymbol{B},\\
\left[\frac{\partial^2 \bar{\mathcal{L}}_a}{\partial \dot{\bar{\boldsymbol{q}}}_a^2}\right]_q =& \boldsymbol{B},\\
\left[\frac{\partial^2 \mathcal{L}_a}{\partial \boldsymbol{q}_a \partial \dot{\boldsymbol{q}}_a}\right]_q =& \boldsymbol{0},
\end{aligned}$$

we get for the components of input transformation (5.155)

$$\begin{aligned}
\bar{\boldsymbol{R}} =& \bar{\boldsymbol{A}}^{-1}\\
\bar{\boldsymbol{\mu}}_1 =& \left[\frac{\partial^2 \mathcal{V}_e}{\partial \boldsymbol{\varphi}^2}\right]_q^{-1}\left\{\left[-\frac{\partial^2 \bar{\mathcal{V}}_e}{\partial \bar{\boldsymbol{\varphi}}^2} + \frac{\partial^2 \mathcal{V}_e}{\partial \boldsymbol{\varphi}^2}\right]\dot{\bar{\boldsymbol{q}}}_u + \frac{\partial^2 \bar{\mathcal{V}}_e}{\partial \bar{\boldsymbol{\varphi}}^2}\dot{\boldsymbol{q}}_u^* + \dot{\bar{\boldsymbol{u}}}_u\right\}\\
=& \left[\frac{\partial^2 \mathcal{V}_e}{\partial \boldsymbol{\varphi}^2}\right]_q^{-1}\left\{\frac{\partial^2 \mathcal{V}_e}{\partial \boldsymbol{\varphi}^2}\dot{\bar{\boldsymbol{q}}}_u - \frac{\partial^2 \bar{\mathcal{V}}_e}{\partial \bar{\boldsymbol{\varphi}}^2}\dot{\bar{\boldsymbol{q}}}_u + \dot{\bar{\boldsymbol{u}}}_u\right\} \qquad \text{(B.31)}\\
=& \dot{\bar{\boldsymbol{q}}}_u + \left[\frac{\partial^2 \mathcal{V}_e}{\partial \boldsymbol{\varphi}^2}\right]_q^{-1}\left\{\dot{\bar{\boldsymbol{u}}}_u - \frac{\partial^2 \bar{\mathcal{V}}_e}{\partial \bar{\boldsymbol{\varphi}}^2}\dot{\bar{\boldsymbol{q}}}_u\right\}\\
=& \left(\boldsymbol{I} - \bar{\boldsymbol{A}}\right)\dot{\bar{\boldsymbol{q}}}_u + \dot{\boldsymbol{q}}_u^* + \left[\frac{\partial^2 \mathcal{V}_e}{\partial \boldsymbol{\varphi}^2}\right]_q^{-1}\dot{\bar{\boldsymbol{u}}}_u,\\
\bar{\boldsymbol{\mu}}_2 =& \boldsymbol{B}\left(\bar{\boldsymbol{A}}\dot{\bar{\boldsymbol{q}}}_a + \dot{\boldsymbol{\mu}}_1\right), \qquad \text{(B.32)}
\end{aligned}$$

where the first equality is due to $\boldsymbol{B}$ and $\bar{\boldsymbol{A}}$ being diagonal. Knowing that

$$\left[\frac{\partial \mathcal{L}_a}{\partial \boldsymbol{q}_a}\right]_q = -\left[\frac{\partial \mathcal{V}_a}{\partial \boldsymbol{q}_a}\right]_q = -\left[\frac{\partial \mathcal{V}_e}{\partial \boldsymbol{\varphi}}\frac{\partial \boldsymbol{\varphi}}{\partial \boldsymbol{q}_a}\right]_q = -\boldsymbol{\psi}(\boldsymbol{\varphi}), \qquad \text{(B.33)}$$

$$\left[\frac{\partial \mathcal{L}_a}{\partial \bar{\boldsymbol{q}}_a}\right]_{\bar{q}} = -\left[\frac{\partial \bar{\mathcal{V}}_a}{\partial \bar{\boldsymbol{q}}_a}\right]_{\bar{q}} = -\left[\frac{\partial \bar{\mathcal{V}}_e}{\partial \boldsymbol{\varphi}}\frac{\partial \boldsymbol{\varphi}}{\partial \bar{\boldsymbol{q}}_a}\right]_{\bar{q}} = -\boldsymbol{\psi}(\bar{\boldsymbol{\varphi}}), \qquad \text{(B.34)}$$

we obtain for the final control law

$$\boldsymbol{u}_a = \bar{\boldsymbol{\mu}}_2 + \boldsymbol{\psi}(\boldsymbol{\varphi}) + \bar{\boldsymbol{R}}^{-1}\left[\bar{\boldsymbol{u}}_a - \boldsymbol{\psi}(\bar{\boldsymbol{\varphi}})\right]. \qquad \text{(B.35)}$$

B.6.1 Important Relations and Definitions

The original inertia matrix $\mathcal{M}$ and Coriolis/centrifugal matrix $\mathcal{C}$ transformed into the deflection space are of the form

$$\mathcal{M}_z(\boldsymbol{q}_u) = \begin{bmatrix} \boldsymbol{M}(\boldsymbol{q}_u) + \boldsymbol{B} & \boldsymbol{B} \\ \boldsymbol{B} & \boldsymbol{B} \end{bmatrix},\ \mathcal{C}_z(\boldsymbol{q}_u, \dot{\boldsymbol{q}}_u) = \begin{bmatrix} \boldsymbol{C}(\boldsymbol{q}_u, \dot{\boldsymbol{q}}_u) & \boldsymbol{0} \\ \boldsymbol{0} & \boldsymbol{0} \end{bmatrix}$$

Their transformations into the task space are given by

$$\begin{aligned}\mathcal{M}_x =& \boldsymbol{T}_x^{-\mathrm{T}}\boldsymbol{T}_z^{-\mathrm{T}}\begin{bmatrix}\boldsymbol{M} & \boldsymbol{0}\\ \boldsymbol{0} & \boldsymbol{B}\end{bmatrix}\boldsymbol{T}_z^{-1}\boldsymbol{T}_x^{-1}\\ =& \begin{bmatrix}\boldsymbol{J}^{-\mathrm{T}}(\boldsymbol{q}_u)\big(\boldsymbol{M}(\boldsymbol{q}_u)+\boldsymbol{B}\big)\boldsymbol{J}^{-1}(\boldsymbol{q}_u) & \boldsymbol{J}^{-\mathrm{T}}(\boldsymbol{q}_u)\boldsymbol{B}\\ \boldsymbol{B}\boldsymbol{J}^{-1}(\boldsymbol{q}_u) & \boldsymbol{B}\end{bmatrix}\end{aligned}$$

and

$$C_x \triangleq \begin{bmatrix}\boldsymbol{J}^{-\mathrm{T}}(\boldsymbol{q}_u)\big(\boldsymbol{M}(\boldsymbol{q}_u)+\boldsymbol{B}\big)\dot{\boldsymbol{J}}^{-1}(\boldsymbol{q}_u)+\boldsymbol{J}^{-\mathrm{T}}(\boldsymbol{q}_u)\boldsymbol{C}(\boldsymbol{q}_u,\dot{\boldsymbol{q}}_u)\boldsymbol{J}^{-1}(\boldsymbol{q}_u) & \boldsymbol{0}\\ \boldsymbol{B}\dot{\boldsymbol{J}}^{-1} & \boldsymbol{0}\end{bmatrix}.$$

In these expressions we can identify the transformed link-side intertia and Coriolis/centrifugal matrices

$$\boldsymbol{J}^{-\mathrm{T}}(\boldsymbol{q}_u)\boldsymbol{M}(\boldsymbol{q}_u)\boldsymbol{J}^{-1}(\boldsymbol{q}_u) \tag{B.36}$$

and

$$\boldsymbol{J}^{-\mathrm{T}}(\boldsymbol{q}_u)\boldsymbol{M}(\boldsymbol{q}_u)\dot{\boldsymbol{J}}^{-1}(\boldsymbol{q}_u)+\boldsymbol{J}^{-\mathrm{T}}(\boldsymbol{q}_u)\boldsymbol{C}(\boldsymbol{q}_u,\dot{\boldsymbol{q}}_u)\boldsymbol{J}^{-1}(\boldsymbol{q}_u). \tag{B.37}$$

The original and transformed generalized external forces are related as follows

$$\bar{\mathcal{Q}}' = \begin{bmatrix}\boldsymbol{I} & \boldsymbol{0}\\ \boldsymbol{0} & \boldsymbol{A}^{-1}\end{bmatrix}\mathcal{Q}'. \tag{B.38}$$

Transformation and Input Matrices

$$\boldsymbol{T}_z = \begin{bmatrix}\boldsymbol{I} & \boldsymbol{0}\\ -\boldsymbol{I} & \boldsymbol{I}\end{bmatrix}; \qquad \boldsymbol{T}_z^{-1} = \begin{bmatrix}\boldsymbol{I} & \boldsymbol{0}\\ \boldsymbol{I} & \boldsymbol{I}\end{bmatrix};$$

$$\boldsymbol{T}_x = \begin{bmatrix}\boldsymbol{J}(\boldsymbol{q}_u) & \boldsymbol{0}\\ \boldsymbol{0} & \boldsymbol{I}\end{bmatrix}; \qquad \boldsymbol{T}_x^{-1} = \begin{bmatrix}\boldsymbol{J}^{-1}(\boldsymbol{q}_u) & \boldsymbol{0}\\ \boldsymbol{0} & \boldsymbol{I}\end{bmatrix};$$

$$\mathcal{N}_z = \begin{bmatrix}\boldsymbol{0} & \boldsymbol{0}\\ \boldsymbol{0} & \boldsymbol{I}\end{bmatrix};$$

$$\mathcal{N}_{\tilde{z}} = \boldsymbol{T}_z^{-\mathrm{T}} = \begin{bmatrix}\boldsymbol{I} & \boldsymbol{I}\\ \boldsymbol{0} & \boldsymbol{I}\end{bmatrix}; \qquad \mathcal{N}_{\tilde{z}}^{-1} = \begin{bmatrix}\boldsymbol{I} & -\boldsymbol{I}\\ \boldsymbol{0} & \boldsymbol{I}\end{bmatrix};$$

$$\mathcal{N}_x = \boldsymbol{T}_x^{-\mathrm{T}}\boldsymbol{T}_z^{-\mathrm{T}} = \begin{bmatrix}\boldsymbol{J}^{-\mathrm{T}}(\boldsymbol{q}_u) & \boldsymbol{J}^{-\mathrm{T}}(\boldsymbol{q}_u)\\ \boldsymbol{0} & \boldsymbol{I}\end{bmatrix}; \mathcal{N}_x^{-1} = \begin{bmatrix}\boldsymbol{J}^{\mathrm{T}}(\boldsymbol{q}_u) & -\boldsymbol{I}\\ \boldsymbol{0} & \boldsymbol{I}\end{bmatrix}$$

Gain Matrices

Expression (7.67) can be expanded as

$$\begin{aligned}\mathcal{K}_v(\boldsymbol{q}_u) =& \boldsymbol{T}_x^{-\mathrm{T}}\boldsymbol{T}_z^{-\mathrm{T}}\boldsymbol{T}_x^{\mathrm{T}}\begin{bmatrix}\mathcal{K}_{v,1} & \boldsymbol{0}\\ \boldsymbol{0} & \mathcal{K}_{v,2}\end{bmatrix}\boldsymbol{T}_x\boldsymbol{T}_z^{-1}\boldsymbol{T}_x^{-1}\\ =& \begin{bmatrix}\mathcal{K}_{v,1}+\boldsymbol{J}^{-\mathrm{T}}(\boldsymbol{q}_u)\mathcal{K}_{v,2}\boldsymbol{J}^{-1}(\boldsymbol{q}_u) & \boldsymbol{J}^{-\mathrm{T}}(\boldsymbol{q}_u)\mathcal{K}_{v,2}\\ \mathcal{K}_{v,2}\boldsymbol{J}^{-1}(\boldsymbol{q}_u) & \mathcal{K}_{v,2}\end{bmatrix}\end{aligned}$$

Note the structural analogy to how the original inertia matrix transforms into task space, cf. $\mathcal{M}_x$. Note that we defined the gain matrix $\mathcal{K}_{v,1}$ for the rigid coordinates already in task space.

This chapter reports several fundamental stability and passivity results that are used in this work. It is important to be familiar with the presented definitions to follow the material developed in this work.

C

Stability and Passivity Fundamentals

C.1 Stability in the Sense of Lyapunov

This section reports several fundamental results regarding the stability of equilibrium points which are used throughout this work. In the following, stability is treated in the sense of Lyapunov. An equilibrium point is considered *stable* if all solutions starting in a neighborhood stay nearby. It is considered *asymptotically stable* if all solutions starting in a neighborhood not only remain in a neighborhood, but gravitate to the equilibrium point as time approaches infinity. These concepts are summarized formally in the definition below.

First, let us consider the *autonomous* system

$$\dot{\boldsymbol{x}} = \boldsymbol{f}(\boldsymbol{x}), \tag{C.1}$$

where $f : D \to \mathbb{R}^n$ is a locally Lipschitz map from a domain $D \subset \mathbb{R}^n$ into $\mathbb{R}^n$. The following theorems are stated for the case when the equilibrium point is at the origin of $\mathbb{R}^n$. This is no loss of generality as we can always introduce a change of coordinates that shifts any equilibrium point to the origin.

It is often difficult and time consuming to find Lyapunov functions with negative definite time derivatives. The following theorems by J.P La'Salle [104], E. A. Barbashin [12] and N. N. Krasovski [100] allow to prove asymptotic stability, local as well as global, using $V(\boldsymbol{x})$ whose time derivative is only smaller than or equal to zero. Such a situation is commonly found when V is derived from physical energy considerations. The relaxation concerning the properties V is compensated by a new hypothesis, namely that the set E where $\dot{V}(\boldsymbol{x}) = 0$ contains no complete trajectory.

[104]: LaSalle (1960), "Some extensions of Lyapunov's second method"

[12]: Barbashin et al. (1961), *On stability of motion in the large*

[100]: Krasovskii (1963), "Problems of the theory of stability of motion"

Theorem C.1.1 (LaSalle's Invariance Principle [95, p. 128]) *Let $\Omega \subset D \subset \mathbb{R}^n$ be a compactly positively invariant set with respect to the system dynamics* (C.1)*. Let $V : D \to \mathbb{R}$ be a continuously differentiable function such that $\dot{V}(\boldsymbol{x}(t)) \leq 0$ in Ω. Let $E \subset \Omega$ be the set of all points where $\dot{V}(\boldsymbol{x}) = 0$. Let $M \subset E$ be the largest invariant set in E. Then every solution starting in Ω approaches M as $t \to \infty$.*

Notice that the inclusion of the sets in LaSalle's Theorem is: $M \subset E \subset \Omega \subset D \subset \mathbb{R}^n$.

Theorem C.1.2 (Barbashin's Theorem [95, p. 128]) *Let $\boldsymbol{x} = \boldsymbol{0}$ be an equilibrium point for* (C.1)*. Let $V : D \to \mathbb{R}$ be a continuously differentiable positive definite function on a domain $D \subset \mathbb{R}^n$ containing the origin such that $\dot{V}(\boldsymbol{x}(t)) \leq 0$ in D. Let $E = \left\{\boldsymbol{x} \in D : \dot{V}(\boldsymbol{x}) = 0\right\}$ and suppose that no other solution can stay in E, other than the trivial solution $\boldsymbol{x}(t) \equiv \boldsymbol{0}$. Then*

the origin is locally asymptotically stable. If, in addition, $V(\boldsymbol{x})$ is radially unbounded then the origin is globally asymptotically stable.

Theorem C.1.3 (Krasovskii's Theorem [95, p. 129]) *Let $\boldsymbol{x} = \mathbf{0}$ be an equilibrium point for* (C.1)*. Let $V : \mathbb{R}^n \to \mathbb{R}$ be a continuously differentiable radially unbounded, positive definite function on a domain $D \subset \mathbb{R}^n$ containing the origin such that $\dot{V}(\boldsymbol{x}(t)) \leq 0$ in D. Let $E = \left\{\boldsymbol{x} \in \mathbb{R}^n : \dot{V}(\boldsymbol{x}) = 0\right\}$ and suppose that no other solution can stay in E, other than the trivial solution $\boldsymbol{x}(t) \equiv \mathbf{0}$. Then the origin is locally asymptotically stable.*

Consider the *nonautonomous* system

$$\dot{\boldsymbol{x}} = \boldsymbol{f}(\boldsymbol{x}, t), \tag{C.2}$$

where $\boldsymbol{x} \in \mathbb{R}^n$, $t \in \mathbb{R}$ is the time and $\boldsymbol{f}$ is a continuous function $\boldsymbol{f} : I \times \Omega \to \mathbb{R}^n$, where $I = [t_0, \infty)$ for some $t_0 \in \mathbb{R}$ and Ω is an open connected set in $\mathbb{R}^n$, containing the origin. We assume that $\boldsymbol{f}(t, \mathbf{0}) = \mathbf{0} \quad \forall t \in I$, so that the origin is an equilibrium point for the differential equation (C.2).

Definition C.1.1 *The equilibrium point $\boldsymbol{x} = \mathbf{0}$ of* (C.2) *is*

- *stable if, for each $\epsilon > 0$ there exists a $\delta(\epsilon, t_0) > 0$ such that*

$$\|\boldsymbol{x}(t_0)\| < \delta \implies \|\boldsymbol{x}(t)\| < 0, \textit{for all} t \geq t_0 \geq 0. \tag{C.3}$$

- *uniformly stable, if for each ϵ, there is a $\delta(\epsilon) > 0$ such that* (C.3) *is satisfied.*
- *unstable if not stable*
- *asymptotically stable if is stable and there exists a positive constant $c = c(t_0)$ such that $\boldsymbol{x}(t) \to 0$ as $t \to \infty$, for all $\|\boldsymbol{x}(t_0)\| < c$.*
- *globally uniformly stable if is uniformly stable and there is a positive constant c, independent of t_0, such that for all $\|\boldsymbol{x}(t_0)\|$, $\boldsymbol{x}(t) \to 0$ for $t \to \infty$, uniformly in t_0, that is, for each $\eta > 0$, there is a $T = T(\eta) > 0$ such that*

The following result by Matrosov deals with the general class of nonautonmous systems. The crucial condition that the set E where $\dot{V}(\boldsymbol{x}, t) = 0$ contains no complete semi-trajectory can longer be used [155]. This issue is remedied through the introduction of a second auxiliary function defined in some appropriate neighborhood of M and possessing properties guaranteeing that the solutions cannot stay forever close to E.

[155]: Rouche et al. (1977), *Stability Theory by Liapunov's Direct Method*

Theorem C.1.4 (Matrosov's theorem [155, p. 62]) *Let there there exist two C^1 functions $V : I \times \Omega \to \mathbb{R}$, $W : I \times \Omega \to \mathbb{R}$, a C^0 function $V^* : \Omega \to \mathbb{R}$, three functions a, b, c of class $\mathcal{K}$ and two constants $S > 0$ and $T > 0$ such that, for every $(t, x) \in I \times \Omega$*

(i) $a(\|\boldsymbol{x}\|) \leq V(t, \boldsymbol{x}) \leq b(\|\boldsymbol{x}\|)$;
(ii) $\dot{V}(t, \boldsymbol{x}) \leq V^*(\boldsymbol{x}) \leq 0$; $E \triangleq \{\boldsymbol{x} \in \Omega : V^*(\boldsymbol{x}) = 0\}$;
(iii) $|W(t, \boldsymbol{x})| < S$;
(iv) $\max(d(\boldsymbol{x}, E), |\dot{W}(t, \boldsymbol{x})|) \geq c(\|\boldsymbol{x}\|)$;
(v) $\|\boldsymbol{f}(t, \boldsymbol{x})| < T$;

choosing $\alpha > 0$ such that $\bar{B}_\alpha \subset \Omega$, let us put for every $t \in I$

$$V_{t,\alpha}^{-1} = \boldsymbol{x} \in \Omega : V(t, \boldsymbol{x}) \leq a(\alpha). \tag{C.4}$$

Then

(i) for any $t_0 \in I$ and any $\boldsymbol{x}_0 \in V_{t_0,\alpha}^{-1}$, any solution $\boldsymbol{x}(t)$ of (C.2)*, passing through $(\boldsymbol{x}_0, t_0) \in I \times \Omega$, tends to zero uniformly in t_0 and $\boldsymbol{x}_0$, as $t \to \infty$.*

(ii) the origin is uniformly asymptotically stable.

Above, $d(\boldsymbol{x}, E)$ denotes the minimum distance of point $\boldsymbol{x}$ to set E, i.e. $\inf_{y \in E}(\|\boldsymbol{x} - \boldsymbol{y}\|)$. In order to facilitate the verification of Matrosov's condition (iv), we apply the following lemma by Paden and Panja:

Lemma C.1.5 ([144]) *Condition* (iv) *of Matrosov's theorem is satisfied if conditions below are satisfied.*

(iv.a) $\dot{W}(\boldsymbol{x}, t)$ is continuous in both arguments and depends on time in the following way. $\dot{W}(\boldsymbol{x}, t) = g(\boldsymbol{x}, \beta(t))$ where g is continuous in both of its arguments. $\beta(t)$ is also continuous and its image lies in a bounded set K_1. (For simplicity, we assume that $\dot{W}(\boldsymbol{x}, t)$ depends on time continuously through a bounded function.)

(iv.b) There exists a class $\mathcal{K}$ function, k, such that $|\dot{W}(\boldsymbol{x}, t)| \geq k(\|\boldsymbol{x}\|) \forall \boldsymbol{x} \in E$ and $t \geq t_0$.

C.2 Definitions

Definition C.2.1 *A continuous function $V : \mathbb{R}^n \to \mathbb{R}^+$ is said to be positive definite if*

$$V(\mathbf{0}) = 0, \quad V(\boldsymbol{x}) \neq \mathbf{0} \text{ for } \boldsymbol{x} \neq \mathbf{0}. \tag{C.5}$$

If V satisfies the weaker condition

$$V(\mathbf{0}) = 0, \quad V(\boldsymbol{x}) \geq 0, \forall \boldsymbol{x} \neq \mathbf{0}, \tag{C.6}$$

it is said to be positive semidefinite. A function V is said to be negative definite if $-V$ is positive definite. A time-varying function $V : \mathbb{R}^n \times \mathbb{R}^+ \to \mathbb{R}$ is said to be positive definite if

$$V(\boldsymbol{x}, t) \geq W(\boldsymbol{x}), \tag{C.7}$$

for some positive definite function $W : \mathbb{R}^n \to \mathbb{R}^+$.

Definition C.2.2 *A continuous function $V : \mathbb{R}^n \times \mathbb{R}^+ \to \mathbb{R}$ is decrescent if for some $\epsilon > 0$ and some continuous, strictly increasing function $\beta : \mathbb{R}^+ \to \mathbb{R}$,*

$$V(\boldsymbol{x}, t) \leq \beta(||\boldsymbol{x}||), \quad \forall \boldsymbol{x} \in B_\epsilon, \forall t \geq 0. \tag{C.8}$$

Definition C.2.3 *A set $M \subset \mathbb{R}^n$ is said to be:*

- *an invariant set with respect to* (C.2) *if:*
  $\boldsymbol{x}(0) \in M \implies \boldsymbol{x}(t) \in M, \forall t \in \mathfrak{R}$
- *a positively invariant set with respect to* (C.2) *if:*
  $\boldsymbol{x}(0) \in M \implies \boldsymbol{x}(t) \in M, \forall t \geq 0$

C.3 Passivity

Let us consider state-space systems of the form:

$$\Sigma: \begin{cases} \dot{\boldsymbol{x}} = \boldsymbol{f}(\boldsymbol{x}, \boldsymbol{y}), & \boldsymbol{u} \in U \\ \boldsymbol{y} = \boldsymbol{h}(\boldsymbol{x}, \boldsymbol{u}), & \boldsymbol{y} \in Y \end{cases} \tag{C.9}$$

with state $\boldsymbol{x} \in \mathbb{R}^n$, and U and Y are space of dimension m, respectively p. On the combined space $U \times Y$ of inputs and outputs and consider a function

$$s: U \times Y \to \mathbb{R}, \tag{C.10}$$

called the *supply rate*.

Definition C.3.1 (Dissipativity [191, p. 34]) *A state space system Σ is said to be dissipative with respect to the supply rate s if there exists a function $S: U \to \mathbb{R}^+$, called the storage function, such that for all initial conditions $x(t_0) = x_0 \in U$ at any time t_0, and for all allowed input functions $u(.)$ and all $t_1 \geq t_0$ the following inequality holds*

$$S\big(x(t_1)\big) \leq S\big(x(t_0)\big) + \int_{t_0}^{t_1} s\big(u(t), y(t)\big) \tag{C.11}$$

If (C.11) *holds with equality for all x_0, $t_1 \geq t_0$, and all $u(\cdot)$, then Σ is conservative with respect to s.*

The dissipative inequality expresses the fact that the stored energy at any point in time t_1 of Σ is at most equal to the stored energy at any past time t_0, plus the total supplied energy during the time elapsed.

Definition C.3.2 (Passivity [191, p. 34]) *A system Σ with $U = Y = \mathbb{R}^m$ is passive if it is dissipative with respect to the supply rate $s(\boldsymbol{u}, \boldsymbol{y}) = \boldsymbol{u}^T\boldsymbol{y}$. The system Σ is called input strictly passive if there exists $\delta > 0$ such that Σ is dissipative with respect to $s(\boldsymbol{u}, \boldsymbol{y}) = \boldsymbol{u}^T\boldsymbol{y} - \delta||\boldsymbol{u}||^2$. The system Σ is output strictly passive if there exists $\epsilon > 0$ such that Σ is dissipative with respect to $s(\boldsymbol{u}, \boldsymbol{y}) = \boldsymbol{u}^T\boldsymbol{y} - \epsilon||\boldsymbol{y}||^2$. Finally, Σ is lossless if it is conservative with respect to $s(\boldsymbol{u}, \boldsymbol{y}) = \boldsymbol{u}^T\boldsymbol{y}$.*

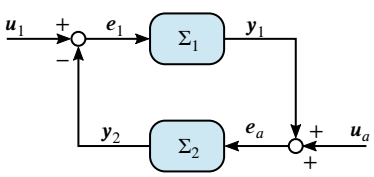

Figure C.1: Feedback interconnection of passive systems.

The following proposition reports a well-known result concerning the feedback interconnection of two passive subsystems as depicted in Fig. C.1. Each subsystem $\Sigma_k, k = u, a$, is of the form (C.9).

Proposition C.3.1 (Invariance of passivity [133, p. 479]) *Consider the input-output system depicted in Fig. C.1. If Σ_1 and Σ_2 are both passive then*

$\Sigma: \boldsymbol{u} \mapsto \boldsymbol{y}$ *is also passive. If furthermore they are OSP then* $\Sigma: \boldsymbol{u} \mapsto \boldsymbol{y}$ *with* $\boldsymbol{u} = (\boldsymbol{u}_1, \boldsymbol{u}_2)$ *and* $\boldsymbol{y} = (\boldsymbol{y}_1, \boldsymbol{y}_2)$ *is also OSP.*

Definition C.3.3 *A state-space system* Σ *with* $\boldsymbol{y} = \boldsymbol{h}(\boldsymbol{x})$ *is zero-state observable, if for all initial conditions* $\boldsymbol{x}(t_0) \in \mathbb{R}^n$*, we have that* $\boldsymbol{u}(t) \equiv \boldsymbol{0}, \boldsymbol{y}(t) \equiv \boldsymbol{0} \implies \boldsymbol{x}(t) \equiv \boldsymbol{0}$ *for* $t \geq t_0$*. It is zero-state detectable if* $\boldsymbol{u}(t) \equiv \boldsymbol{0}, \boldsymbol{y}(t) \equiv \boldsymbol{0}$ *for* $t \geq t_0 \implies \lim_{t\to\infty} \boldsymbol{x}(t) = \boldsymbol{0}$.

Using this definition allows summarizing one of the main results in [65] as follows.

[65]: Hill et al. (1976), "The stability of nonlinear dissipative systems"

Proposition C.3.2 *Let* Σ *be OSP and zero-state observable with a positive definite storage function, then the origin of the system is asymptotically stable. Furthermore, suppose the storage function is radially unbounded, then the origin is globally asymptotically stable.*

Theorem C.3.3 (Theorem 2.2.13 of [191, p. 21]) *Let* Σ *be* ϵ*-output strictly passive, then its has* L_2*-gain* $\leq \frac{1}{\epsilon}$.

Definition C.3.4 (L_2-gain [191, p. 199]) *A state space system* Σ *has* L_2*-gain*$\leq \gamma$ *if it is dissipative with respect to the supply rate* $s(\boldsymbol{u}, \boldsymbol{y}) = \frac{1}{2}\gamma^2||\boldsymbol{u}||^2 - \frac{1}{2}||\boldsymbol{y}||^2$*; that is there exists a storage function satisfying*

$$S\big(\boldsymbol{x}(t_1)\big) - S\big(\boldsymbol{x}(t_0)\big) \leq \frac{1}{2}\int_{t_0}^{t_1} \big(\gamma^2||\boldsymbol{u}(t)||^2 - ||\boldsymbol{y}(t)||^2\big)dt. \tag{C.12}$$

One way to interpret OSP and L_2-gain is as follows. An OSP system is a passive system for which a small amount of positive feedback does not destroy the passivity property. The actual amount is quantified by the parameter ϵ and, thus, can be interpreted as some measure of robustness. The relation between ϵ and the L_2-gain is given by Theorem C.3.3.

Definition C.3.5 (Passive mapping [191]) *Consider the set* χ *of all measurable real valued n-dimensional functions of time* $f(t): \mathbb{R}^+ \to \mathbb{R}^n$*. Introduce the extended space*

$$L_{2e} \triangleq \Big\{\boldsymbol{x} \in \chi \Big| \int_0^T ||\boldsymbol{f}(t)||^2 dt < \infty, \forall T\Big\}. \tag{C.13}$$

Define the inner product[1]

$$< \boldsymbol{u}, \boldsymbol{y} >_T = \int_0^T \boldsymbol{u}(t)^T \boldsymbol{y}(t) dt. \tag{C.14}$$

1: If the product $< \boldsymbol{u}(t), \boldsymbol{y}(t) >$ has the dimension of power, then the inner product (C.14) denotes the externally supplied energy during the time interval $[0, T]$.

A system $\Sigma: L_{2e} \to L_{2e}: \boldsymbol{u} \mapsto \boldsymbol{y}$ *defines a passive map if and only if there exists some constant* $\beta > 0$ *such that*

$$< \boldsymbol{u}, \boldsymbol{y} >_T \geq \beta, \tag{C.15}$$

for all $T \geq 0$.

Note that we can interpret (C.15) as stating that the *maximally extractable*

energy is finite. In other words, a system Σ is passive if and only if a *finite amount* of energy can be extracted from it.

D

Mathematical Fundamentals

This thesis is written for readers with a basic knowledge of linear algebra, multivariable calculus, real analysis and differential equations. This appendix, reports the most important definitions and results that are prerequisites for reading this work. For details on most of the ideas presented here, the interested reader can consult [72, 156].

[72]: Horn et al. (2012), *Matrix Analysis*
[156]: Rudin (1976), *Principles of Mathematical Analysis*

D.1 Calculus and Real Analysis

Definition D.1.1 ([193]) *Let $U \subset \mathbb{R}^d$ be open, and let $f : U \to \mathbb{R}^n$. We say that f is differentiable of class $\mathbb{C}^k$ on U (or simply that $f \in \mathbb{C}^k$, if the derivatives $f', f'', \dots, f^{(k)}$ exist and are continuous on U. The function f is said to be class $\mathbb{C}^\infty$, infinitely differentiable, or smooth if it is $\mathbb{C}^k$ for all $k \geq 0$.*

Corollary D.1.1 *Let $\boldsymbol{A}$ be open in $\mathbb{R}^n$ and $\boldsymbol{f} : \boldsymbol{A} \to \mathbb{R}^n$ be a diffeomorphism. Then $\boldsymbol{f}^{-1}$ is a diffeomorphism from $\boldsymbol{f}(\boldsymbol{A})$ onto $\boldsymbol{A}$.*

The implicit function plays a central role in this work for deriving the concept of quasi-full actuation.

Theorem D.1.2 (Implicit function theorem [99, p. 43]) *Let*

$$\Phi(x) = \Phi(x_1, \dots, x_N) \equiv \big(\varphi_1(x_1, \dots, x_N), \dots, \varphi_M(x_1, \dots, x_N)\big)$$

be a mapping of class C^k, $k \geq 1$, defined on an open set $U \subset \mathbb{R}^N$ and taking values in $\mathbb{R}^M$. We assume that $1 \leq M < N$. Set $Q = N - M$. Let $x^0 = (x_1^0, \dots, x_N^0)$ be a fixed point of U. Of course we let $x = (x_1, \dots, x_N)$ be any point of U. Set

$$x_a = (x_1, \dots, x_Q) \quad \text{and} \quad x_a^0 = (x_1^0, \dots, x_Q^0). \tag{D.1}$$

We suppose that

$$\frac{\partial(\varphi_1, \dots, \varphi_M)}{\partial(x_{Q+1}, \dots, x_N)}(x^0) \neq 0. \tag{D.2}$$

Then there exists a neighborhood $\tilde{U}$ of x^0, and open set $W \subset \mathbb{R}^Q$ containing x_a^0, and functions $f_1, \dots, f_M$ of class C^k on W such that

$$\Phi\big(x_1, \dots, x_Q, f_1(x_a), \dots, f_M(x_a)\big) = 0 \quad \text{for every } x_a \in W. \tag{D.3}$$

Furthermore $f_1, \dots, f_M$ are the unique functions satisfying

$$\{x \in \tilde{U} : \Phi(x) = 0\} =$$
$$\{x \in \tilde{U} : x_a \in W, x_{Q+l} = f_l(x_a) \text{ for } l = 1, \dots, M\}.$$

It is worth remarking that the implicit function theorem is usually formulated in terms of implicit mappings of class C_1. However, for the developments in Chapter 5 it is crucial to guarantee that whenever a mapping Φ is of class C^k, $k \geq 2$, and satisfies the conditions of the implicit function theorem, then also the functions $f_1, \dots, f_M$ are of class C_k, $k \geq 2$.

D.2 Interchange Property of Partial and Ordinary Derivatives

The following interchange property of partial and ordinary differentiation is often used in modern works on Lagrangian mechanics. Let f be a function of the independent scalar variables $(q_1, \dots, q_n)$ such that their time-derivatives and time, t,

$$f = f\left(q_1, \dots, q_n, \dot{q}_1, \dots, \dot{q}_n, \dots, q_1^{(p)}, \dots, q_n^{(p)}, t\right). \tag{D.4}$$

Let q_i, $i = 1, \dots, n$ denote one the independent variables and $\dot{y}$ denote a kth time-derivative of q_i, $k = 0, \dots, p$ of q_i, then we have that

$$\frac{\partial}{\partial \dot{y}}\left(\frac{df}{dt}\right) = \frac{\mathrm{d}}{\mathrm{d}t}\left(\frac{\partial f}{\partial \dot{y}}\right), \quad \dot{y} = q_i, \tag{D.5}$$

and

$$\frac{\partial}{\partial \dot{y}}\left(\frac{\partial f}{\partial t}\right) = \frac{\mathrm{d}}{\mathrm{d}t}\left(\frac{\partial f}{\partial \dot{y}}\right) + \frac{\partial f}{\partial x}, \quad \dot{y} \neq q_i. \tag{D.6}$$

The following proof is a straightforward extension of the result reported in [120]. The total derivative of f with respect to t is

$$\frac{df}{dt} = \frac{\partial f}{\partial q_1}\dot{q}_1 + \cdots + \frac{\partial f}{\partial q_n}\dot{q}_n + \frac{\partial f}{\partial \dot{q}_1}\ddot{q}_1 + \cdots + \frac{\partial f}{\partial q_n^{(p)}}q_n^{(p+1)} + \frac{\partial f}{\partial t}, \tag{D.7}$$

The partial derivative of (D.7) with respect to $\dot{y}$ is

$$\begin{aligned}\frac{\partial}{\partial \dot{y}}\left(\frac{df}{dt}\right) =& \frac{\partial^2 f}{\partial \dot{y}\partial q_1}\dot{q}_1 + \cdots + \frac{\partial^2 f}{\partial \dot{y}\partial q_n}\dot{q}_n + \\ & \frac{\partial^2 f}{\partial \dot{y}\partial \dot{q}_1}\ddot{q}_1 + \cdots + \frac{\partial^2 f}{\partial \dot{y}\partial q_n^{(p)}}q_n^{(p+1)} + \frac{\partial^2 f}{\partial \dot{y}\partial t} + \frac{\partial f}{\partial y},\end{aligned} \tag{D.8}$$

where the last term vanishes if $\dot{y}$ is one of the variables $(q_1, \dots, q_n)$. Considering that f is a function of the variables q_i, their time-derivatives up to order p, and t, its partial derivative is in general also a function of q_i, their time-derivatives up order p, and t, that is

$$\frac{\partial f}{\partial \dot{y}} = \frac{\partial f}{\partial \dot{y}}\left(q_1, \dots, q_n, \dot{q}_1, \dots, q_n^{(p-1)}, q_1^{(p)}, \dots, q_n^{(p)}\right). \tag{D.9}$$

The time-derivative of (D.9) is

$$\frac{\mathrm{d}}{\mathrm{d}t}\left(\frac{\partial f}{\partial \dot{y}}\right) = \frac{\partial^2 f}{\partial q_1 \partial \dot{y}}\dot{q}_1 + \cdots + \frac{\partial^2 f}{\partial q_n \partial \dot{y}}\dot{q}_n + \tag{D.10}$$

$$\frac{\partial^2 f}{\partial \dot{q}_1 \partial \dot{y}}\ddot{q}_1 + \cdots + \frac{\partial^2 f}{\partial q^{(p)} \partial \dot{y}}q^{(p+1)} + \frac{\partial^2 f}{\partial t \partial \dot{y}}. \tag{D.11}$$

Considering that mixed partial derivatives are equal, the desired results (D.7) follows immediately from comparing (D.8) with (D.10), and the special case (D.5) follows when $\dot{y} = q_i$.

D.3 Linear Algebra

The following theorems by Silvester [163] and Schur [72] about determinants of block matrices are used frequently throughout the text.

Theorem D.3.1 (Determinants of 2×2 block matrices) *If* $\boldsymbol{M} = \begin{bmatrix} \boldsymbol{A} & \boldsymbol{B} \\ \boldsymbol{C} & \boldsymbol{D} \end{bmatrix}$, *where* $\boldsymbol{A}, \boldsymbol{B}, \boldsymbol{C}, \boldsymbol{D} \in {}^{n}F^{n}$ *and* $\boldsymbol{C}\boldsymbol{D} = \boldsymbol{D}\boldsymbol{C}$, *then*

$$\det_{F} \boldsymbol{M} = \det\left(\boldsymbol{A}\boldsymbol{D} - \boldsymbol{B}\boldsymbol{C}\right). \tag{D.12}$$

Theorem D.3.2 (Schur's determinant identity) *If* $\boldsymbol{M} = \begin{bmatrix} \boldsymbol{A} & \boldsymbol{B} \\ \boldsymbol{C} & \boldsymbol{D} \end{bmatrix}$, *where* $\boldsymbol{A}, \boldsymbol{B}, \boldsymbol{C}$ *and* $\boldsymbol{D}$ *are matrices of dimension* $n \times n, n \times m, m \times n$ *and* $m \times m$, *respectively. Then, if either* $\boldsymbol{D}$ *or* $\boldsymbol{A}$ *are invertible*

$$\det \boldsymbol{M} = \det \boldsymbol{D} \det\left(\boldsymbol{A} - \boldsymbol{B}\boldsymbol{D}^{-1}\boldsymbol{C}\right), \tag{D.13}$$

and

$$\det \boldsymbol{M} = \det \boldsymbol{A} \det\left(\boldsymbol{D} - \boldsymbol{C}\boldsymbol{A}^{-1}\boldsymbol{B}\right), \tag{D.14}$$

respectively.

The following determinant properties are frequently used throughout the text without explicit mentioning:

- $|\boldsymbol{A}\boldsymbol{B}| = |\boldsymbol{A}|\,|\boldsymbol{B}|$,
- $|\boldsymbol{A}^{-1}| = |\boldsymbol{A}|^{-1}$.

The following Lemma allows under- and overestimating the eigenvalues of a matrix product based on the eigenvalues of the single matrices.

If $\boldsymbol{A}$ *and* $\boldsymbol{B}$ *are Hermitian and nonnegative definite matrices of appropriate dimensions, then we can both underestimate and overestimate eigenvalues of* $\boldsymbol{A}\boldsymbol{B}$ *by using the eigenvalues of* $\boldsymbol{A}$ *and* $\boldsymbol{B}$

$$\lambda_i(\boldsymbol{A})\lambda_{\min}(\boldsymbol{B}) \leq \lambda_i(\boldsymbol{A}\boldsymbol{B}) \leq \lambda_i(\boldsymbol{A})\lambda_{\max}(\boldsymbol{B}). \tag{D.15}$$

Bibliography

The references are listed in alphabetical order.

[1] R. Abraham and J. E. Marsden. *Foundations of Mechanics*. 364. American Mathematical Soc., 2008 (cit. on pp. 13, 19).

[2] A. Ailon and R. Ortega. "An observer-based set-point controller for robot manipulators with flexible joints". In: *Systems & Control Letters* 21.4 (1993), pp. 329–335 (cit. on p. 110).

[3] R. Alami et al. "Safe and dependable physical human-robot interaction in anthropic domains: State of the art and challenges". In: *2006 IEEE/RSJ International Conference on Intelligent Robots and Systems*. 2006, pp. 1–16 (cit. on p. 3).

[4] A. Albu-Schäffer, C. Ott, and G. Hirzinger. "Constructive energy shaping based impedance control for a class of underactuated Euler-Lagrange systems". In: *2005 IEEE International Conference on Robotics and Automation*. Institute of Electrical & Electronics Engineers (IEEE), 2005 (cit. on p. 111).

[5] A. Albu-Schäffer and G. Hirzinger. "A globally stable state feedback controller for flexible joint robots". In: *Advanced Robotics* 15.8 (2001), pp. 799–814 (cit. on p. 130).

[6] A. Albu-Schäffer, C. Ott, and G. Hirzinger. "A Unified Passivity-based control framework for position, torque and impedance control of flexible joint robots". In: *The International Journal of Robotics Research* 26.1 (2007), pp. 23–39 (cit. on pp. 3, 5, 6, 110, 130, 132, 145, 146).

[7] A. Albu-Schäffer, C. Ott, and F. Petit. "Constructive energy shaping control for a class of Euler-Lagrange Systems". In: *10th int. IFAC symposium on robot control*. 2012 (cit. on pp. 110, 111, 130).

[8] A. Albu-Schäffer et al. "Dynamic modelling and control of variable stiffness actuators". In: *IEEE International Conference on Robotics and Automation*. 2010 (cit. on pp. 44, 69).

[9] G. Alici and B. Shirinzadeh. "Enhanced stiffness modeling, identification and characterization for robot manipulators". In: *IEEE Transactions on Robotics* 21.4 (2005), pp. 554–564 (cit. on p. 4).

[10] V. I. Arnol'd. *Mathematical Methods of Classical Mechanics*. Vol. 60. Springer Science & Business Media, 2013 (cit. on p. 13).

[11] M. Athans and P. L. Falb. *Optimal Control: An Introduction to the Theory and Its Applications*. McGraw-Hill, 2006 (cit. on pp. 200, 207).

[12] E. A. Barbashin and N. N. Krasovskii. *On stability of motion in the large*. TRW Space Technology Labs Los Angeles California, 1961 (cit. on p. 283).

[13] A. K. Bejczy. *Robot arm dynamics and control*. manual. Jet Propulsion Lab., California Inst. of Tech. Pasadena, 1974 (cit. on p. 5).

[14] A. Bicchi et al. "Variable stiffness actuators for fast and safe motion control". In: *Robotics research. The eleventh international symposium*. Springer, 2005, pp. 527–536 (cit. on p. 66).

[15] J. E. Bobrow, S. Dubowsky, and J. S. Gibson. "Time-optimal control of robotic manipulators along specified paths". In: *The International Journal of Robotics Research* 4.3 (1985), pp. 3–17 (cit. on pp. 195, 196).

[16] K. Bodie, C. D. Bellicoso, and M. Hutter. "ANYpulator: Design and control of a safe robotic arm". In: *2016 IEEE/RSJ International Conference on Intelligent Robots and Systems*. 2016, pp. 1119–1125 (cit. on p. 4).

[17] D. J. Braun, M. Howard, and S. Vijayakumar. "Exploiting variable stiffness in explosive movement tasks". In: *Robotics: Science and systems*. 2011 (cit. on p. 110).

[18] D. J. Braun et al. "Robots driven by compliant actuators: Optimal control under actuation constraints". In: *IEEE Trans. on Robotics* 29.5 (2013), pp. 1085–1101 (cit. on p. 195).

[19] B. Brogliato, R. Ortega, and R. Lozano. "Global tracking controllers for Flexible-joint manipulators: a comparative study". In: *Automatica* 31.7 (July 1995), pp. 941–956 (cit. on pp. 60, 130, 177–181).

[20] B. Brogliato et al. “Experimental comparison of nonlinear controllers for flexible joint manipulators”. In: *The International Journal of Robotics Research* 17.3 (1998), pp. 260–281 (cit. on pp. 177–179, 181, 182).

[21] H. D. Bui. “Duality and symmetry lost in solid mechanics”. In: *Comptes Rendus Mécanique* 336.1-2 (2008), pp. 12–23 (cit. on p. 54).

[22] C. I. Byrnes, A. Isidori, and J. C. Willems. “Passivity, feedback equivalence, and the global stabilization of minimum phase nonlinear systems”. In: *IEEE Transactions on automatic control* 36.11 (1991), pp. 1228–1240 (cit. on p. 153).

[23] G. Cesareo and R. Marino. “On the controllability properties of elastic robots”. In: *Analysis and optimization of systems*. Ed. by A. Bensoussan and J. L. Lions. Springer Berlin Heidelberg, 1984, pp. 352–363 (cit. on p. 5).

[24] M. Chalon and B. d’Andréa-Novel. “Backstepping experimentally applied to an antagonistically driven finger with flexible tendons”. In: *IFAC Proceedings Volumes* 47.3 (2014), pp. 217–223 (cit. on p. 248).

[25] M. Chalon, J. Reinecke, and M. Pfanne. “Online in-hand object localization”. In: *2013 IEEE/RSJ International Conference on Intelligent Robots and Systems* (2013), pp. 2977–2984 (cit. on pp. 246, 247).

[26] J.-B. l. R. D’Alembert. *Traité de Dynamique*. 1743 (cit. on p. 21).

[27] O. Dahl. “Path constrained robot control”. PhD thesis. Lund University, 1992 (cit. on pp. 195, 208).

[28] A. De Luca and W. Book. “Robots with Flexible Elements”. In: *Springer Handbook of Robotics*. Ed. by B. Siciliano and O. Khatib. 2nd ed. Springer, 2016, pp. 243–282 (cit. on p. 259).

[29] A. De Luca, R. Farina, and P. Lucibello. “On the control of robots with visco-elastic joints”. In: *2005 IEEE International Conference on Robotics and Automation*. IEEE, 2005 (cit. on p. 158).

[30] A. De Luca and L. Lanari. “Robots with elastic joints are linearizable via dynamic feedback”. In: *34th IEEE Conference on Decision and Control*. Vol. 4. Dec. 1995, 3895–3897 vol.4 (cit. on p. 5).

[31] A. De Luca and P. Lucibello. “A general algorithm for dynamic feedback linearization of robots with elastic joints”. In: *1998 IEEE International Conference on Robotics and Automation*. Vol. 1. May 1998, 504–510 vol.1 (cit. on pp. 5, 6, 47, 130).

[32] A. De Luca and F. Flacco. “A PD-type regulator with exact gravity cancellation for robots with flexible joints”. In: *2011 IEEE International Conference on Robotics and Automation*. 2011, pp. 317–323 (cit. on pp. 6, 132, 246).

[33] A. De Luca and F. Flacco. “Dynamic gravity cancellation in robots with flexible transmissions”. In: *49th IEEE Conference on Decision and Control*. IEEE, 2010, pp. 288–295 (cit. on pp. 6, 132, 246).

[34] A. De Luca et al. “Collision detection and safe reaction with the DLR-III lightweight manipulator arm”. In: *2006 IEEE/RSJ International Conference on Intelligent Robots and Systems*. IEEE, 2006, pp. 1623–1630 (cit. on pp. 150, 187, 211, 218, 229, 230, 246, 265, 275).

[35] G. De Marco, G. Gorni, and G. Zampieri. “Global inversion of functions: an introduction”. In: *Nonlinear Differential Equations and Applications NoDEA* 1.3 (1994), pp. 229–248 (cit. on p. 84).

[36] A. H. De Ruiter, C. Damaren, and J. R. Forbes. *Spacecraft Dynamics and Control: An Introduction*. John Wiley & Sons, 2012 (cit. on p. 200).

[37] H. Dekker. “Classical and quantum mechanics of the damped harmonic oscillator”. In: *Physics Reports* 80.1 (1981), pp. 1–110 (cit. on pp. 25, 107).

[38] M. A. Diftler et al. “Robonaut 2 - The first humanoid robot in space”. In: *2011 IEEE International Conference on Robotics and Automation*. May 2011, pp. 2178–2183 (cit. on p. 4).

[39] P. A. Dirac et al. “Lectures on quantum field theory”. In: (1966) (cit. on p. 75).

[40] C. Dumas et al. “Joint stiffness identification of six-revolute industrial serial robots”. In: *Robotics and Computer-Integrated Manufacturing* 27.4 (2011), pp. 881–888 (cit. on p. 4).

[41] O. Eiberger et al. “On joint design with intrinsic variable compliance: Derivation of the DLR QA-joint”. In: *2010 IEEE International Conference on Robotics and Automation*. IEEE, 2010, pp. 1687–1694 (cit. on p. 47).

[42] C. Ferrario and A. Passerini. “Transformation properties of the Lagrange function”. In: *Revista Brasileira de Ensino de Física* 30.3 (2008), pp. 3306–1 (cit. on pp. 35, 106).

[43] A. Ficola, R. Marino, and S. Nicosia. “A singular perturbation approach to the control of elastic robots”. In: *Proc. of IEEE Int. Conf. Rob. Automat., Philadelphia, PA, USA, pp.324-329 (1983)* (1983) (cit. on p. 5).

[44] G. A. Folkertsma, S. Stramigioli, et al. *Energy in Robotics*. Now Publishers, 2017 (cit. on pp. 31, 184, 192).

[45] T. Frankel. *The Geometry of Physics: An Introduction*. 2nd ed. Cambridge University Press, 2003 (cit. on p. 19).

[46] W. Friedl et al. “FAS A flexible antagonistic spring element for a high performance over”. In: *2011 IEEE/RSJ International Conference on Intelligent Robots and Systems*. IEEE, 2011, pp. 1366–1372 (cit. on p. 5).

[47] W. Friedl et al. “Wrist and forearm rotation of the DLR hand arm system: Mechanical design, shape analysis and experimental validation”. In: *2011 IEEE/RSJ International Conference on Intelligent Robots and Systems*. IEEE, 2011, pp. 1836–1842 (cit. on pp. 5, 41, 42, 212).

[48] G. Garofalo et al. “Sliding mode momentum observers for estimation of external torques and joint acceleration”. In: *2019 IEEE International Conference on Robotics and Automation*. IEEE, 2019, pp. 6117–6123 (cit. on pp. 230, 265).

[49] I. M. Gelfand, R. A. Silverman, et al. *Calculus of Variations*. Courier Corporation, 2000 (cit. on pp. 27, 107).

[50] F. Ghorbel and M. W. Spong. “Integral manifolds of singularly perturbed Systems with application to rigid-link flexible-joint multibody systems”. In: *International Journal of Nonlinear Mechanics, Vol. 35, No. 1, pp. 133-155* (2000) (cit. on p. 5).

[51] F. Ghorbel, J. Y. Hung, and M. W. Spong. “Adaptive control of flexible-joint manipulators”. In: *IEEE Control Systems Magazine* 9.7 (1989), pp. 9–13 (cit. on p. 179).

[52] H. Goldstein, C. Poole, and J. Safko. *Classical Mechanics*. American Association of Physics Teachers, 2001 (cit. on pp. 13, 24–26, 57, 79, 105, 106, 150).

[53] W. B. Gordon. “On the diffeomorphisms of euclidean space”. In: *American Mathematical Monthly* 79 (1972), pp. 755–759 (cit. on p. 84).

[54] M. Grebenstein et al. “The DLR hand arm system”. In: *2011 IEEE International Conference on Robotics and Automation*. 2011, pp. 3175–3182 (cit. on pp. 3, 4, 41, 46, 110, 183, 211, 232).

[55] M. Grebenstein and P. van der Smagt. “Antagonism for a highly anthropomorphic hand-arm system”. In: *Advanced Robotics* 22.1 (2008), pp. 39–55 (cit. on p. 41).

[56] J. Hadamard. “Sur les transformations ponctuelles”. In: *Bulletin de la Société Mathématique de France* 34 (1906), pp. 71–84 (cit. on p. 84).

[57] W. Hahn. *Stability of Motion*. Berlin, Heidelberg: Springer Berlin Heidelberg, 1967 (cit. on p. 173).

[58] D. W. Haldane, J. K. Yim, and R. S. Fearing. “Repetitive extreme-acceleration (14-g) spatial jumping with Salto-1P”. In: *2017 IEEE/RSJ International Conference on Intelligent Robots and Systems*. 2017, pp. 3345–3351 (cit. on p. 4).

[59] W. R. Hamilton. “XV. On a general method in dynamics; by which the study of the motions of all free systems of attracting or repelling points is reduced to the search and differentiation of one central relation, or characteristic function”. In: *Philosophical Transactions of the Royal Society of London* 124 (1834), pp. 247–308 (cit. on p. 13).

[60] M. Harder et al. “Simultaneous motion tracking and joint stiffness control of bidirectional antagonistic variable-stiffness actuators”. In: *IEEE Robotics and Automation Letters* 7.3 (2022), pp. 6614–6621 (cit. on pp. 94, 129, 132, 212).

[61] F. Harmanni. “Higher Order Lagrangians for classical mechanics and scalar fields”. PhD thesis. Faculty of Science and Engineering, 2016 (cit. on pp. 25, 27, 107).

[62] N. Hashemia et al. “Generalization in the learning of mathematics”. In: *MB ali (president). Second international seminar on quality and affordable education (ISQAE). Universiti teknologi malaysia, johor bahru, malaysia. Recuperado de https://educ. utm. my/wp-content/uploads/2013/11/291. pdf*. 2013 (cit. on p. 74).

[63] P. Havas. “The range of application of the lagrange formalism — I”. In: *Il Nuovo Cimento* 5.S3 (Oct. 1957), pp. 363–388 (cit. on pp. 25, 107).

[64] A. V. Hill. “The heat of shortening and the dynamic constants of muscle”. In: *Proc. R. Soc. Lond. B126136–195* (1938), pp. 126–195 (cit. on p. 192).

[65] D. Hill and P. Moylan. “The stability of nonlinear dissipative systems”. In: *IEEE Transactions on Automatic Control* 21.5 (1976), pp. 708–711 (cit. on p. 287).

[66] G. Hirzinger et al. “DLR’s torque-controlled light weight robot III-are we reaching the technological limits now?” In: *2002 IEEE International Conference on Robotics and Automation*. Vol. 2. May 2002, 1710–1716 vol.2 (cit. on pp. 3, 225).

[67] G. Hirzinger et al. “On a new generation of torque controlled light-weight robots”. In: *2001 IEEE International Conference on Robotics and Automation*. Vol. 4. IEEE, 2001, pp. 3356–3363 (cit. on p. 6).

[68] N. Hogan. “Impedance control: An approach to manipulation: Part I—Theory”. In: *Journal of Dynamic Systems, Measurement, and Control* 107.1 (Mar. 1985), pp. 1–7 (cit. on pp. 5, 109, 122, 187, 258).

[69] N. Hogan. “Impedance control: An approach to manipulation: Part II—Implementation”. In: *Journal of Dynamic Systems, Measurement, and Control* 107.1 (Mar. 1985), pp. 8–16 (cit. on pp. 109, 122, 258).

[70] N. Hogan. “Impedance control: An approach to manipulation: Part III—Applications”. In: *Journal of Dynamic Systems, Measurement, and Control* 107.1 (Mar. 1985), pp. 17–24 (cit. on pp. 109, 122, 258).

[71] Y. P. Hong and C.-T. Pan. “A lower bound for the smallest singular value”. In: *Linear Algebra and its Applications* 172 (1992), pp. 27–32 (cit. on p. 85).

[72] R. A. Horn and C. R. Johnson. *Matrix Analysis*. Cambridge University Press, 2012 (cit. on pp. 171, 289, 291).

[73] W. Huang et al. “Dynamic simulation of articulated soft robots”. In: *Nature Communications* 11.1 (2020), pp. 1–9 (cit. on p. 41).

[74] M. Hutter et al. “Anymal-a highly mobile and dynamic quadrupedal robot”. In: *2016 IEEE/RSJ International Conference on Intelligent Robots and Systems*. IEEE, 2016, pp. 38–44 (cit. on pp. 4, 110, 183).

[75] C. A. Ibáñez, O. O. G. Frías, and M. S. S. Castañón. “Lyapunov-based controller for the inverted pendulum cart system”. In: *Nonlinear Dynamics* 40 (2005), pp. 367–374 (cit. on p. 39).

[76] A. Isidori. *Nonlinear Control Systems*. Berlin New York: Springer, 1995 (cit. on p. 132).

[77] M. Iskandar et al. “Joint-level control of the DLR lightweight robot SARA”. In: *2020 IEEE/RSJ International Conference on Intelligent Robots and Systems*. 2020, pp. 8903–8910 (cit. on pp. 129, 131).

[78] H. Iwata and S. Sugano. “Design of human symbiotic robot TWENDY-ONE”. In: *2009 IEEE International Conference on Robotics and Automation*. Proceedings - IEEE international conference on robotics and automation. Nov. 2, 2009, pp. 580–586 (cit. on p. 4).

[79] S. Jörg et al. “The computing and communication architecture of the DLR hand arm system”. In: *2011 IEEE/RSJ International Conference on Intelligent Robots and Systems*. IEEE, 2011, pp. 1055–1062 (cit. on p. 47).

[80] J. V. José and E. J. Saletan. *Classical dynamics: A contemporary approach*. 1998 (cit. on p. 75).

[81] I. Kanellakopoulos, P. Kokotovic, and A. Morse. “Systematic design of adaptive controllers for feedback linearizable systems”. In: *IEEE Transactions on Automatic Control* 36.11 (1991), pp. 1241–1253 (cit. on p. 179).

[82] R. E. Kass and P. W. Vos. *Geometrical Foundations of Asymptotic Inference*. John Wiley & Sons, 2011 (cit. on pp. 84–86, 95).

[83] R. Kelly. “A simple set-point robot controller by using only position measurements”. In: *IFAC Proceedings Volumes* 26.2 (1993), pp. 527–530 (cit. on pp. 184, 192).

[84] J. Kepler. *Epitome Astronomiae Copernicanae*. 1621 (cit. on pp. 14, 197).

[85] J. Kepler. *Astronomia Nova*. 1609 (cit. on pp. 14, 197).

[86] M. Keppler et al. “Elastic structure preserving (ESP) control for compliantly actuated robots”. In: *IEEE Transactions on Robotics* 34.2 (2018), pp. 317–335 (cit. on pp. 6, 54, 129–132, 142, 143, 145, 147, 148, 150, 171, 172, 174, 177, 178, 183, 211, 212, 217, 218, 225, 235, 237, 239–241, 254, 275).

[87] M. Keppler and A. De Luca. “On time-optimal control of elastic joints under input constraints”. In: *59th IEEE Conference on Decision and Control* (2020), pp. 4149–4156 (cit. on pp. 14, 56, 195).

[88] M. Keppler, C. Ott, and A. Albu-Schäffer. “From underactuation to quasi-full actuation: Aiming at a unifying control framework for articulated soft robots”. In: *International Journal of Robust and Nonlinear Control* 32.9 (2022), pp. 5453–5484 (cit. on pp. 132, 140).

[89] M. Keppler et al. “A passivity-based approach for trajectory tracking and link-side damping of compliantly actuated robots”. In: *2016 IEEE International Conference on Robotics and Automation*. IEEE, 2016, pp. 1079–1086 (cit. on pp. 111, 129–132, 142, 174).

[90] M. Keppler et al. “A passivity-based controller for motion tracking and damping assignment for compliantly actuated robots”. In: *55th IEEE Conference on Decision and Control*. IEEE, 2016, pp. 1521–1528 (cit. on pp. 129–132, 142, 147, 148, 174, 254).

[91] M. Keppler et al. “Analyzing the performance limits of articulated soft robots based on the ESPi framework: Applications to damping and impedance control”. In: *IEEE Robotics and Automation Letters* 6.4 (2021), pp. 7121–7128 (cit. on pp. 111, 129, 130, 174, 183, 212, 240, 241).

[92] M. Keppler et al. “Elastic structure preserving impedance (ESPi) control for compliantly actuated robots”. In: *2018 IEEE/RSJ International Conference on Intelligent Robots and Systems* (2018), pp. 5861–5868 (cit. on pp. 6, 131, 173, 177, 178, 183, 254, 275).

[93] M. Keppler et al. “Robust stabilization of elastic joint robots by ESP and PID control: Theory and experiments”. In: *IEEE Robotics and Automation Letters* 7.3 (2022), pp. 8283–8290 (cit. on p. 248).

[94] M. Keppler et al. “Visco-elastic structure preserving impedance (VESPi) control for compliantly actuated robots”. In: *2018 European Control Conference* (2018), pp. 255–260 (cit. on pp. 129, 160, 174, 275).

[95] H. K. Khalil. *Nonlinear Systems*. 3rd ed. Prentice Hall, 2001 (cit. on pp. 5, 124, 172, 283, 284).

[96] W. Khalil and E. Dombre. *Modeling, Identification and Control of Robots*. 3rd. Bristol, PA, USA: Taylor & Francis, Inc., 2002 (cit. on pp. 168, 171, 173, 174).

[97] O. Khatib. “A unified approach for motion and force control of robot manipulators: The operational space formulation”. In: *IEEE Journal on Robotics and Automation* 3.1 (Feb. 1987), pp. 43–53 (cit. on pp. 5, 37, 125).

[98] D. Koditschek. “Natural motion for robot arms”. In: *The* (Dec. 1984) (cit. on pp. 5, 56, 131, 143, 232, 235).

[99] S. G. Krantz and H. R. Parks. *The Implicit Function Theorem: History, Theory, and Applications*. Springer Science & Business Media, 2012 (cit. on p. 289).

[100] N. N. Krasovskii. “Problems of the theory of stability of motion”. In: *(Russian), 1959 English translation: Stanford University Press* (1963) (cit. on p. 283).

[101] J. L. Lagrange. *Mécanique Analytique*. Vol. 1. Mallet-Bachelier, 1853 (cit. on p. 27).

[102] D. Lakatos, F. Petit, and A. Albu-Schäffer. “Nonlinear oscillations for cyclic movements in human and robotic arms”. In: *IEEE Transactions on Robotics* 30.4 (2014), pp. 865–879 (cit. on p. 111).

[103] C. Lanczos. *The Variational Principles of Mechanics*. University of Toronto press, 2020 (cit. on pp. 13, 17, 18, 22, 26, 78, 79, 106, 269).

[104] J. LaSalle. “Some extensions of Lyapunov’s second method”. In: *IRE Transactions on Circuit Theory* 7.4 (1960), pp. 520–527 (cit. on p. 283).

[105] C. Lessig. “A Primer on geometric mechanics”. 2012 (cit. on p. 19).

[106] F. Loeffl et al. “The DLR C-runner: Concept, design and experiments”. In: *2016 IEEE-RAS 16th International Conference on Humanoid Robots*. 2016, pp. 758–765 (cit. on p. 225).

[107] A. Loria and R. Ortega. “On tracking control of rigid and flexible joints robots”. In: *Appl. Math. Comput. Sci* 5.2 (1995), pp. 101–113 (cit. on pp. 6, 130, 184).

[108] J. Lützen. “Interactions between mechanics and differential geometry in the 19th century”. In: *Archive for History of Exact Sciences* 49.1 (1995), pp. 1–72 (cit. on p. 19).

[109] N. Mansfeld and S. Haddadin. “Reaching desired states time-optimally from equilibrium and vice versa for visco-elastic joint robots with limited elastic deflection”. In: *2014 IEEE/RSJ International Conference on Intelligent Robots and Systems*. 2014, pp. 3904–3911 (cit. on p. 195).

[110] R. Marino and S. Nicosia. “Singular perturbation techniques in the adaptive control of elastic robots”. In: *IFAC Proceedings Volumes* 18.16 (1985), pp. 95–100 (cit. on p. 5).

[111] M. T. Mason. *Mechanics of robotic manipulation*. 2001 (cit. on p. 16).

[112] J. L. McClelland et al. “A parallel-distributed processing approach to mathematical cognition”. In: *Manuscript, Stanford University* (2016) (cit. on p. 263).

[113] C. Melchiorri, S. Stramigoli, and S. Andreotti. “Using damping injection and passivity in robotic manipulation”. In: *1999 IEEE/ASM International Conference on Advanced Intelligent Mechatronics*. 1999, pp. 979–984 (cit. on p. 192).

[114] X. Meng, M. Keppler, and C. Ott. “Elastic structure preserving impedance control of bidirectional antagonistic variable stiffness actuation”. In: *European Control Conference 2020, ECC 2021* (2021), pp. 263–269 (cit. on pp. 68, 94, 99, 129, 132, 156, 174, 212, 275).

[115] R. Mengacci et al. “Elastic Structure Preserving control for compliant robots driven by agonistic-antagonistic actuators (ESPaa)”. In: *IEEE Robotics and Automation Letters* 6.2 (2021), pp. 879–886 (cit. on pp. 68, 94, 99, 129, 132, 156, 174).

[116] J. K. Merikoski and R. Kumar. “Inequalities for spreads of matrix sums and products.” In: *Applied Mathematics E-Notes* 4 (2004), pp. 150–159.

[117] D. R. Merkin. *Introduction to the Theory of Stability*. Vol. 24. Springer-Verlag New York, Inc., 1997 (cit. on p. 30).

[118] C. D. Meyer. *Matrix Analysis and Applied Linear Algebra*. Philadelphia, PA: Society for Industrial and Applied Mathematics, 2004 (cit. on p. 170).

[119] J. Miller. “Some global inverse function theorems”. In: *Journal of Mathematical Analysis and Applications* 100 (1984), pp. 375–384 (cit. on p. 84).

[120] P. Mitiguy and B. Heyneman. *Interchange property of partial and ordinary derivatives*. 2021. URL: https://web.stanford.edu/class/me331b/documents/InterchangePropertyOfPartialAndOrdinaryDerivative.pdf (visited on 10/30/2021) (cit. on p. 290).

[121] T. Morita, H. Iwata, and S. Sugano. “Development of human symbiotic robot: WENDY”. In: *1999 IEEE International Conference on Robotics and Automation*. Vol. 4. 1999, 3183–3188 vol.4 (cit. on p. 4).

[122] F. L. Moro, N. G. Tsagarakis, and D. G. Caldwell. “A human-like walking for the COmpliant huMANoid COMAN based on CoM trajectory reconstruction from kinematic Motion Primitives”. In: *2011 IEEE-RAS International Conference on Humanoid Robots*. IEEE, 2011, pp. 364–370 (cit. on p. 4).

[123] R. M. Murray, M. Rathinam, and W. Sluis. “Differential flatness of mechanical control systems: A catalog of prototype systems”. In: *Proceedings of the 1995 ASME international congress and exposition*. 1995 (cit. on p. 273).

[124] T. Needham. *Visual Complex Analysis*. 1997 (cit. on p. 263).

[125] I. Newton. *Philosophiae Naturalis Principia Mathematica*. 1687 (cit. on p. 197).

[126] S. Nicosia and P. Tomei. “A method to design adaptive controllers for flexible joint robots”. In: *1992 IEEE International Conference on Robotics and Automation*. Nice, France: IEEE, 1992, 701–706 vol.1 (cit. on p. 57).

[127] S. Nicosia and P. Tomei. “Design of global tracking controllers for flexible-joint robots”. In: *Journal of robotic systems* 10.6 (1993), pp. 835–846 (cit. on p. 130).

[128] E. Noethers. “Invariante variationsprobleme”. In: *Nachrichten der Göttinger Gesellschaft der Wissenschaften* (1918) (cit. on p. 14).

[129] J. H. Oh and J. S. Lee. “Control of flexible joint robot system by backstepping design approach”. In: *Intelligent Automation & Soft Computing* 5.4 (1999), pp. 267–278 (cit. on p. 130).

[130] J. M. Ortega and W. C. Rheinboldt. *Iterative Solution of Nonlinear Equations in Several Variables*. SIAM, 2000 (cit. on p. 84).

[131] R. Ortega and M. W. Spong. “Adaptive motion control of rigid robots: a tutorial”. In: *27th IEEE Conference on Decision and Control* (1988), 1575–1584 vol.2 (cit. on pp. 29, 30).

[132] R. Ortega et al. “Stabilization of a class of underactuated mechanical systems via interconnection and damping assignment”. In: *IEEE Transactions on Automatic Control* 47.8 (2002), pp. 1218–1233 (cit. on p. 109).

[133] R. Ortega. *Passivity-Based Control of Euler-Lagrange Systems: Mechanical, Electrical, and Electromechanical Applications*. London New York: Springer, 1998 (cit. on pp. 30–32, 39, 48, 51, 77, 109, 110, 116, 118, 127, 139, 153, 154, 173, 192, 258, 286).

[134] R. Ortega, A. Loria, and R. Kelly. “A semiglobally stable output feedback PI^2D regulator for robot manipulators”. In: *IEEE Trans. on Automatic Control* 40 (1995), pp. 1432–1436 (cit. on pp. 32, 130).

[135] R. Ortega et al. “Control by interconnection and standard passivity-based control of port-Hamiltonian systems”. In: *IEEE Transactions on Automatic control* 53.11 (2008), pp. 2527–2542 (cit. on p. 109).

[136] R. Ortega et al. “Interconnection and damping assignment passivity-based control of port-controlled Hamiltonian systems”. In: *Automatica* 38.4 (2002), pp. 585–596 (cit. on pp. 56, 109).

[137] R. Ortega et al. “On passivity-based output feedback global stabilization of Euler-Lagrange systems”. In: *33rd IEEE Conference on Decision and Control*. Vol. 1. IEEE, 1994, pp. 381–386 (cit. on pp. 121, 122, 127, 184, 192).

[138] R. Ortega et al. “On passivity-based output feedback global stabilization of euler-lagrange systems”. In: *International Journal of Robust and Nonlinear Control* 5.4 (1995), pp. 313–323 (cit. on p. 32).

[139] C. Ott et al. “Decoupling based Cartesian impedance control of flexible joint robots”. In: *2003 IEEE International Conference on Robotics and Automation*. Vol. 3. 2003, 3101–3107 vol.3 (cit. on pp. 6, 130).

[140] C. Ott. *Cartesian Impedance Control of Redundant and Flexible-Joint Robots*. Springer, 2008 (cit. on pp. 6, 130, 132, 177, 178, 180, 181, 189, 278).

[141] C. Ott et al. “A passivity based cartesian impedance controller for flexible joint robots-part I: Torque feedback and gravity compensation”. In: *2004 IEEE International Conference on Robotics and Automation*. 2004 (cit. on pp. 110, 130).

[142] C. Ott et al. “On the passivity-based impedance control of flexible joint robots”. In: *Robotics, IEEE Transactions on* 24.2 (2008), pp. 416–429 (cit. on pp. 130, 132).

[143] S. Ozgoli and H. D. Taghirad. “A survey on the control of flexible joint robots”. In: *Asian Journal of Control* 8.4 (2006), pp. 332–344 (cit. on pp. 4, 5, 47).

[144] B. Paden and R. Panja. “Globally asymptotically stable "PD+" controller for robot manipulators”. In: *International Journal of Control* 47.6 (1988), pp. 1697–1712 (cit. on pp. 5, 143, 145, 171, 232, 285).

[145] G. Palli, C. Melchiorri, and A. De Luca. “On the feedback linearization of robots with variable joint stiffness”. In: *2008 IEEE International Conference on Robotics and Automation*. 2008, pp. 1753–1759 (cit. on p. 130).

[146] R. Penrose. *The Emperor’s New Mind: Concerning Computers, Minds, and the Laws of Physics*. USA: Oxford University Press, Inc., 1989 (cit. on p. 18).

[147] F. Petit and A. Albu-Schäffer. “State feedback damping control for A multi DOF variable stiffness robot arm”. In: *2011 IEEE International Conference on Robotics and Automation*. 2011 (cit. on p. 130).

[148] F. Petit et al. “Bidirectional antagonistic variable stiffness actuation: Analysis, design & implementation”. In: *2010 IEEE International Conference on Robotics and Automation*. IEEE, 2010, pp. 4189–4196 (cit. on pp. 41, 99).

[149] F. P. Petit. “Analysis and control of variable stiffness robots”. PhD thesis. ETH Zurich / Technical University of Munich, 2014 (cit. on p. 43).

[150] M. Pfanne et al. “Fusing Joint Measurements and Visual Features for In-Hand Object Pose Estimation”. In: *IEEE Robotics and Automation Letters* 3.4 (Oct. 2018), pp. 3497–3504 (cit. on p. 246).

[151] G. J. Pollayil et al. “Elastic structure preserving impedance controlfor nonlinearly coupled tendon-driven systems”. In: *IEEE Control Systems Letters* (2021) (cit. on pp. 94, 132, 212).

[152] G. K. Pozharitskii. “On asymptotic stability of equilibria and stationary motions of mechanical systems with partial dissipation”. In: *Journal of Applied Mathematics and Mechanics* 25.4 (1961), pp. 979–993 (cit. on p. 51).

[153] G. A. Pratt and M. M. Williamson. “Series elastic actuators”. In: *1995 IEEE/RSJ International Conference on Intelligent Robots and Systems* 1 (1995), 399–406 vol.1 (cit. on pp. 3, 110, 130, 183, 189, 190, 278).

[154] L. R. Ray and R. F. Stengel. “A Monte Carlo approach to the analysis of control system robustness”. In: *Automatica* 29.1 (1993), pp. 229–236 (cit. on pp. 212, 240).

[155] N. Rouche, P. Habets, and M. Laloy. *Stability Theory by Liapunov’s Direct Method*. Springer New York, 1977 (cit. on p. 284).

[156] W. Rudin. *Principles of Mathematical Analysis*. International series in pure and applied mathematics. McGraw-Hill, 1976 (cit. on p. 289).

[157] J.-C. Samin. “Criteria for pervasive damping of mechanical systems with first integrals of motion”. In: *ZAMM-Journal of Applied Mathematics and Mechanics/Zeitschrift für Angewandte Mathematik und Mechanik* 55.7-8 (1975), pp. 381–385 (cit. on p. 31).

[158] I. Sardellitti et al. “Gain scheduling control for a class of variable stiffness actuators based on lever mechanisms”. In: *Robotics, IEEE Transactions on* 29.3 (June 2013), pp. 791–798 (cit. on p. 130).

[159] P. Seibert and R. Suarez. “Global stabilization of nonlinear cascade systems”. In: *Systems & Control Letters* 14.4 (1990), pp. 347–352 (cit. on p. 178).

[160] Y. Yi-Sheng and G. Dun-He. “A note on a lower bound for the smallest singular value”. In: *Linear algebra and its applications* 253.1-3 (1997), pp. 25–38 (cit. on p. 85).

[161] K. G. Shin and N. McKay. “Minimum-time control of robotic manipulators with geometric path constraints”. In: *IEEE Trans. on Automatic Control* 30.6 (1985), pp. 531–541 (cit. on pp. 195, 196).

[162] B. Siciliano and W. J. Book. “A singular perturbation approach to control of lightweight flexible manipulators”. In: *The International Journal of Robotics Research* 7.4 (1988), pp. 79–90 (cit. on p. 5).

[163] J. Silvester. “Determinants of block matrices”. In: *The Mathematical Gazette* 84 (Nov. 2000) (cit. on p. 291).

[164] J.-J. Slotine. “Putting physics in control-the example of robotics”. In: *IEEE Control Systems Magazine* 8.6 (1988), pp. 12–18 (cit. on pp. 56, 235).

[165] J.-J. Slotine and L. Weiping. “Adaptive manipulator control: A case study”. In: *IEEE Transactions on Automatic Control* 33.11 (1988), pp. 995–1003 (cit. on pp. 5, 130, 153, 154, 179, 232).

[166] J.-J. E. Slotine. “Putting Physics Back in Control”. In: *New Trends in Nonlinear Control Theory*. Springer, 1989, pp. 459–473 (cit. on p. 109).

[167] J.-J. E. Slotine and W. Li. “On the adaptive control of robot manipulators”. In: *The International Journal of Robotics Research* 6.3 (1987), pp. 49–59 (cit. on p. 173).

[168] M. W. Spong. “Modeling and control of elastic joint robots”. In: *Transactions of the ASME: Journal of Dynamic Systems, Measurement, and Control* 109 (1987), pp. 310–319 (cit. on pp. 5, 46, 47, 57, 68, 69, 101, 130, 177, 183, 184).

[169] M. W. Spong. “Adaptive control of flexible joint manipulators”. In: *Systems & Control Letters* 13.1 (1989), pp. 15–21 (cit. on pp. 130, 179).

[170] M. W. Spong. “Control of flexible joint robots: A survey”. In: *Coordinated Science Laboratory Report no. UILU-ENG-90-2203, DC-116* (1990) (cit. on pp. 4, 5, 154, 173).

[171] M. W. Spong and M. Vidyasagar. *Robot Dynamics and Control*. Wiley, 1989 (cit. on p. 29).

[172] M. Stoiber et al. “A sparse gaussian approach to region-based 6dof object tracking”. In: *Proceedings of the Asian Conference on Computer Vision* (2020) (cit. on pp. 246, 247).

[173] S. Stramigioli. “Creating artificial damping by means of damping injection”. In: *In proceedings of the ASME dynamic systems and control division*. Citeseer, 1996 (cit. on pp. 184, 192–194, 225).

[174] S. Stramigioli. “Energy-Aware Robotics”. In: *Mathematical Control Theory I*. Springer, 2015, pp. 37–50 (cit. on p. 109).

[175] J. Struckmeier and C. Riedel. “Canonical transformations and exact invariants for time-dependent Hamiltonian systems”. In: *Annalen der Physik* 11.1 (2002), pp. 15–38 (cit. on p. 150).

[176] G. J. Sussman and J. Wisdom. *Structure and Interpretation of Classical Mechanics*. The MIT Press, 2015 (cit. on p. 106).

[177] L. M. Sweet and M. C. Good. “Re-definition of the robot motion control problem: Effects of plant dynamics, drive system constraints, and user requirements”. In: *23rd IEEE Conference on Decision and Control* (1984), pp. 724–732 (cit. on p. 5).

[178] M. Takegaki and S. Arimoto. “A new feedback method for dynamic control of manipulators”. In: *Journal of Dynamic Systems, Measurement, and Control* 103.2 (1981), p. 119 (cit. on pp. 5, 51, 56, 58, 109, 110, 114, 116, 118, 127, 139, 140, 142, 179, 258).

[179] D. A. V. I. D. Tall. “Looking for the bigger picture”. In: *For the Learning of Mathematics* 31.2 (2011), pp. 17–18 (cit. on p. 74).

[180] T. Tao. *There’s more to mathematics than rigour and proofs*. 2021. URL: https://terrytao.wordpress.com/career-advice/theres-more-to-mathematics-than-rigour-and-proofs/ (cit. on p. 51).

[181] J. R. Taylor. *Classical Mechanics*. University Science Books, 2005 (cit. on pp. 13, 16, 25, 106, 197).

[182] R. Tedrake. “Online notes for MAT237: Multivariable calculus, 2018-9”. In: *Course Notes for MIT 6.832*. (2020) (cit. on p. 38).

[183] P. Tomei. “A simple PD controller for robots with elastic joints”. In: *IEEE Transactions on Automatic Control* 36.10 (Oct. 1991), pp. 1208–1213 (cit. on pp. 46, 110, 130, 139, 216, 217, 220, 222).

[184] G. Tonietti, R. Schiavi, and A. Bicchi. “Design and control of a variable stiffness actuator for safe and fast physical Human/Robot interaction”. In: *2005 IEEE International Conference on Robotics and Automation*. Apr. 2005, pp. 526–531 (cit. on p. 3).

[185] T. D. Tuttle and W. P. Seering. “A nonlinear model of a harmonic drive gear transmission”. In: *IEEE Transactions on Robotics and Automation* 12.3 (1996), pp. 368–374 (cit. on p. 47).

[186] T. D. Tuttle. “Understanding and modeling the behavior of a harmonic drive gear transmission”. PhD thesis. Massachusetts Institute of Technology, 1992 (cit. on p. 47).

[187] M. Uebel, I. Minis, and K. Cleary. “Improved computed torque control for industrial robots”. In: *1992 IEEE International Conference on Robotics and Automation*. 1992, pp. 528–533 (cit. on p. 5).

[188] A. van der Schaft. *L2-Gain and Passivity in Nonlinear Control*. Springer-Verlag New York, Inc., 1999 (cit. on pp. 131, 179).

[189] R. Van Ham et al. “MACCEPA, the mechanically adjustable compliance and controllable equilibrium position actuator: Design and implementation in a biped robot”. In: *Robotics and Autonomous Systems* 55.10 (2007), pp. 761–768 (cit. on p. 47).

[190] B. Vanderborght et al. “Variable impedance actuators: A review”. In: *Robotics and Autonomous Systems* 61.12 (2013), pp. 1601–1614 (cit. on pp. 3, 110, 130, 183).

[191] A. van Schaft. *L2-Gain and Passivity Techniques in Nonlinear Control*. London New York: Springer, 2017 (cit. on pp. 47, 51, 245, 286, 287).

[192] D. Wandinger. “Enhancing classical impedance control concepts while ensuring transferability to flexible joint robots”. BA thesis. Technical University of Munich / University of Applied Sciences Munich, Sept. 2020 (cit. on pp. 193, 225).

[193] F. W. Warner. *Lie groups*. 1983 (cit. on p. 289).

[194] S. Wolf, O. Eiberger, and G. Hirzinger. “The DLR FSJ: Energy based design of a variable stiffness joint”. In: *2011 IEEE International Conference on Robotics and Automation*. May 2011, pp. 5082–5089 (cit. on pp. 4, 41, 42, 211).

[195] S. Wolf et al. “Variable stiffness actuators: Review on design and components”. In: *IEEE/ASME Transactions on Mechatronics* 21.5 (2015), pp. 2418–2430 (cit. on p. 66).

[196] L. Zollo, A. De Luca, and B. Siciliano. “Regulation with on-line gravity compensation for robots with elastic joints”. In: *2004 IEEE International Conference on Robotics and Automation*. Vol. 3. Apr. 2004, pp. 2687–2692 (cit. on p. 130).

Alphabetical Index

V

Z